Editor's preface

Volume 41-Advances in Physical Organic Chemistry

The capacity for chemists to work and make progress has arguably remained constant through the years. However, the scope of the research programs of individual chemists is in general contracting in comparison to the rapidly expanding field of chemistry. At the same time, our work is becoming increasingly focused on making progress in well-developed areas of research, and on intractable problems that have escaped solution over the years. All of this has been accompanied by an increase in the linkage between the seemingly diverse research projects that we study. Physical organic chemistry suffers when the research of its proponents becomes overly focused and of restricted interest. The health of the field requires an awareness of the links between research on seemingly unrelated problems, and the fostering of interactions between chemists with related interests in structure, kinetics and mechanism. The chapters in this volume represent the great diversity of interests of their authors, which range from organic, inorganic and organometallic reaction mechanisms, to the mechanism for enzyme catalysis. This willingness of these authors to contribute to this monograph reflects well on the breadth of physical organic chemistry. This editor has great admiration for readers with the capacity he lacks of easily grasping all of the concepts presented in these chapters. He does hope that each of these chapters has something to offer to all of our readers.

John P. Richard
University at Buffalo

Contributors to Volume 41

Lisa Berreau Department of Chemistry and Biochemistry, Utah State University, 0300 Old Main Hill, Logan, UT 84322-0300, USA

Rudi van Eldik Institut für Anorganische Chemie, Universität Erlangen-Nürnberg, Egerlandstraße 1, D-91058 Erlangen, Germany

Nicole Horenstein Department of Chemistry, University of Florida, Gainesville, Florida, 32611-7200, USA

Colin Hubbard Institut für Anorganische Chemie, Universität Erlangen-Nürnberg, Egerlandstraße 1, D-91058 Erlangen, Germany

Steve Nelsen Department of Chemistry, University of Wisconsin, Madison, Wisconsin, 53706-1396, USA

Stephen F. Schwartz Department of Biophysics and Biochemistry, Albert Einstein College of Medicine, USA

Ken Westaway Department of Chemistry, Laurentian University, Sudbury, Ontario P3E 2C6, Canada

AUTHOR INDEX

SUBJECT INDEX

Cumulative Index of Authors

Cumulative Index of Titles

Effect of enzyme dynamics on catalytic activity

DIMITRI ANTONIOU, JODI BASNER, SARA NÚÑEZ and STEVEN D. SCHWARTZ

Department of Biophysics, Albert Einstein College of Medicine, Bronx, New York, USA

1 Introduction

It is widely accepted that the catalytic properties of enzymes are a consequence of binding energy differences between reactants and transition state (TS), arising from the arrangement of residues in the active site. There are two versions of this concept, both of which have experimental support. In the TS binding picture,[1] the configuration that binds most strongly to the enzyme is assumed to be at the top of the uncatalyzed barrier to reaction. This binding releases energy that stabilizes the TS, lowering the energetic barrier to reaction. In the ground state destabilization picture[2] the role of the enzyme is to make the reactants less stable, leading again to a lower barrier to reaction.

In the last few years it has been suggested by us and other groups that enzyme dynamics may play a role in catalysis. We do not claim that these dynamical effects contribute more to catalysis than the standard binding energy effects, but that they should be taken into account in the interpretation of, for example, kinetic isotope effects (KIE) measurements[3] and that they may provide insight to some puzzling data. In particular, our work on the relation between catalysis and enzyme dynamics originated in the effort to understand some unusual properties of the

ADVANCES IN PHYSICAL ORGANIC CHEMISTRY
VOLUME 41 ISSN 0065-3160 DOI: 10.1016/S0065-3160(06)41006-6

following three systems:

1. It is now widely accepted that for some enzymes (e.g., liver alcohol dehydrogenase, thermophilic alcohol dehydrogenase, etc.) proton transfer proceeds through quantum tunneling. The high activation barriers in these systems were consistent with tunneling. However, the KIE were modest, when tunneling would seem to imply high KIE.
2. The enzyme lactate dehydrogenase (LDH) catalyzes the interconversion of lactate to pyruvate. There are two isoforms in the body to accommodate different substrates. Despite the fact that the active site is identical in these two isoforms, one favors the production of lactate and the other production of pyruvate.
3. Crystal structures of human purine nucleoside phosphorylase with several TS analogs showed an unusual geometric arrangement of three oxygens, lying in a close stack. One may question whether this geometry serves a catalytic purpose.

We will show that the answers to all the three of these puzzles involve the dynamics of the enzyme. There has recently been a disagreement among some authors regarding the meaning of the term ''dynamical'', with some suggesting that the term should be reserved for non-equilibrium motions, while others would use it for equilibrium motions. For clarity, we will define the meaning we give to the term ''dynamical'' in this review.

Let us assume that a variable $A(t)$ is coupled to the reaction coordinate and that (A) is its mean value. If a measurement of some property P depends on (A), but not on the particular details of the time dependence of $A(t)$, then we will call it a ''statistical'' dependence. If the property P depends on particular details of the dynamics of $A(t)$ we will call it a ''dynamical'' dependence. Note that in this definition it is not the mode $A(t)$ alone that causes dynamical effects, but it also depends on the timescale of the measured property P. Promoting vibrations (to be discussed in Sections 2–4) are a ''dynamic'' effect in this sense, since their dynamics is coupled to the reaction coordinate and have similar timescales. Conformation fluctuations that enhance tunneling (to be discussed in Section 5) are a ''statistical'' effect: the reaction rate is the sum of transition state theory (TST) rates for barriers corresponding to some configuration, weighted by the probability that the system reaches that configuration. This distinction between dynamic and statistical phenomena in proteins was first made in the classic paper of Agmon and Hopfield.[4]

We will discuss three kinds of motions:

1. ''Rate-promoting'' quasi-harmonic motions, a fast sub-ps effect we and other have proposed (Section 3).
2. Other kinds of sub-ps motions that involve correlated motions of several residues (Section 4).
3. Conformation fluctuations (Section 5).

The structure of this review is as follows. In Section 2 we will review the concept of ''rate-promoting'' vibrations. We will first need to review briefly the theory of

quantum hydrogen/hydride transfer, because it is the large proton mass (relative to an electron) that makes the reaction rate very sensitive to motions that modulate its transfer distance. We will then identify the experimental and computational signatures of these promoting vibrations. We will close with investigating some objections to the possibility of existence of such promoting vibrations. In Section 3 we will apply the theory of Section 2 to the three enzymatic systems that we mentioned earlier in the Introduction.

In Section 4 we will use two theoretical techniques (transition path sampling (TPS) and essential dynamics (ED)) to analyze molecular dynamics trajectories. We will explain how we were able to identify in atomic detail collective motions that affect catalysis.

Finally, in Section 5 we will briefly discuss recent work by Truhlar, Brooks, and Hammes-Schiffer on the relation of conformation fluctuations and catalysis in dihydrofolate reductase (DHFR) and we will propose a new method for studying much slower motions (such as conformation fluctuations) that may affect catalysis.

This review is not meant to be comprehensive of all work on enzyme dynamics and catalysis. The emphasis will be on the work done by our group, mainly on fast sub-ps enzyme motions, while other groups have studied mostly conformational fluctuations. When necessary, we will provide brief descriptions and references to the current work by other groups.

2 Proton transfer and rate-promoting vibrations

We first identified rate-promoting vibrations in enzymatic systems where proton transfer proceeds via quantum tunneling (in this theoretical section, we will use the terms hydrogen, hydride, proton as if they were equivalent). In order to understand why systems with proton tunneling are good candidates for identifying promoting vibrations, we must review the modern theory of quantum charge transfer in condensed phase, which will be the subject of this section.

Excellent recent reviews of the experimental work in tunneling in enzymes have been written by Scrutton,[5] Romesberg and Schowen,[6] and Kohen.[7]

QUANTUM THEORY OF PROTON TRANSFER

The reaction rate of proton transfer in condensed phases depends on several parameters: temperature, potential barrier height, transfer distance, reactant frequency, strength of coupling to the environment. For different values of these parameters, different physical mechanisms dominate which have been described by different theoretical models, in the chronological order they were studied, the parameter regions were:

Region I: The dynamics is over the barrier (as described by TST) or just below the barrier (small quantum corrections).

Region II: The dynamics takes place by tunneling from excited energy states in the reactant well (moderate to large quantum effects).

Region III: The dynamics takes place by tunneling from the ground state in the reactant well (large quantum effects).

Special care must be taken if one attempts to draw conclusions from the temperature dependence of the rate, because the rate has Arrhenius form in all the three regions, but the activation energy has different meaning in each regime.

Region I: Small quantum corrections

This region is often studied with the methods described in the book by Bell,[8] even though it is not really correct to use gas-phase approaches in condensed phase reactions. An assumption is made that there are several energy levels below the top of the barrier and that over the barrier transfer is described by classical dynamics. The TST result for the transfer rate is:

$$k = \frac{k_B T}{2\pi} \frac{1}{Z_0} e^{-\beta V} \tag{1}$$

where $\beta = 1/k_B T$ is the inverse temperature and Z_0 is the partition function for an oscillator of frequency ω_H. If we describe the motion at the reactant well quantum mechanically (QM), then

$$\frac{1}{Z_0} = 2\sinh\left(\frac{\beta\omega_H}{2}\right) \tag{2}$$

If $\beta\omega_H/2 \ll 1$, one arrives at the familiar textbook TST result for the transfer rate, $k = (\omega_H/2\pi)\ \exp(-\beta V)$. However, a typical frequency for a proton–carbon bond vibration is $3000\,cm^{-1}$, so in the present case the opposite limit $\beta\omega_H/2 \gg 1$ is relevant. In this limit $1/Z_0 \simeq \exp(\beta\omega_H/2)$ and the semiclassical result for the rate is obtained by:

$$k = A_H e^{-\beta(V-\omega_H/2)} \tag{3}$$

Equation (3) predicts a KIE (assuming $A_H = A_D$):

$$\ln\frac{k_H}{k_D} = \frac{\beta}{2}(\omega_H - \omega_D) = \frac{\beta}{2}\left(1 - \sqrt{\frac{m_H}{m_D}}\right)\omega_H \tag{4}$$

For C–H bond cleavage, Equation (4) predicts a KIE equal to $k_H/k_D \sim 7$ at room temperature. In the limit where the semiclassical theory is valid, experimentalists measure the Schaad–Swain exponent, $\ln(k_H/k_T)/\ln(k_D/k_T)$. In the special case that the pre-Arrhenius factor A_L is the same for all isotopes (which is not true in most cases) then semiclassical theory predicts for this exponent a value 3.26. Deviations from this value are often interpreted as signs of increased tunneling, but in our opinion this line of argument is based on an oversimplified model of quantum transfer in condensed phases. Note that in tunneling reactions where the ratio $A_H/A_D \neq 1$, the semiclassical theory predicts an exponent that is *not* equal to 3.26 and is temperature dependent.

Region III: Large quantum effects

When the energetic barrier is very high, tunneling takes place from the ground state. In this limit, the Marcus–Levich–Dogonadze theory[9] has been used in the

study of electron transfer in solution and biomolecules. It is assumed that the environment can be described by a 1-dimensional (1-D) coordinate (a questionable assumption when details of environment dynamics are important) and one exploits the fact that in the deep tunneling limit the tunneling matrix element Δ can be used as a small parameter in a perturbative approach and find a transfer rate equal to:

$$k \sim \Delta^2 e^{-\beta(E_r+\varepsilon)^2/4E_r} \tag{5}$$

where E_r is the reorganization energy of the *environment*, ε is the exothermicity and Δ is the tunneling matrix element. Note that the quantum result Equation (5) predicts an Arrhenius form for the rate, similarly to the TST result. In this theory, the KIE is equal to $k_H/k_D \sim \Delta_H^2/\Delta_D^2$, which in the deep tunneling limit has a value of the order 10^3–10^4, much larger than the measured KIE in biological systems. However, we will see later in this section that the Marcus theory approach, while valid for electron transfer, has to be modified for proton transfer.

Region II: Moderate quantum effects

This is the case when tunneling takes place from excited states, but not close to the barrier top, and had eluded solution for decades because there is no small parameter available (as in the previous two cases). Finally, this problems was numerically solved in the mid 1990s[10] and the solution was analytically verified with a different method by our group.[11]

It is instructive to have a feeling for when and how the semiclassical theory fails. In Table 1 we compare some exact results[10] with the predictions of the semiclassical model Equation (3). There is a range of values for the exact result, because the rate depends on friction (an effect that cannot be captured in the semiclassical model). We note that when the reactant frequency becomes large, the semiclassical theory of the rate fails (we should note that despite the failure in predicting the rate, the semiclassical model gives reasonably good prediction for the KIE).

We will briefly describe how it became possible in the 1990s to describe QM this region of moderate quantum effects. One *assumes* that the classical charge transfer problem is adequately described by the Langevin equation:[12]

$$m\ddot{s} = -\frac{\mathrm{d}V(s)}{\mathrm{d}s} - \int_0^t \mathrm{d}t'\gamma(t-t')\dot{s} + F_{\mathrm{env}}(t) \tag{6}$$

where s is the reaction coordinate and $V(s)$ is the potential energy surface (PES). The influence of the enzymatic environment in Equation (6) is represented by the random force $F_{\mathrm{env}}(t)$, which is related to the friction $\gamma(t)$ through the fluctuation–dissipation theorem.[13]

Table 1 The ratio of rates $k_{\mathrm{exact}}/k_{\mathrm{semiclassical}}$

$\omega/_R/k_BT$	Exact	Semiclassical
3.2	0.8–1.8	1.5
4.8	2.0–3.8	2.3
9.6	30–1000	12.9

A most important result in rate theory was the proof[14] that the classical dynamics of s governed by the Hamiltonian equation:

$$H = \frac{p_s^2}{2m_s} + V(s) + \sum_k \frac{P_k^2}{2m_k} + \sum_k \frac{1}{2} m_k \omega_k^2 \left(q_k - \frac{c_k s}{m_k \omega_k^2} \right)^2 \tag{7}$$

is described by Equation (6). The harmonic oscillators ω_k constitute a fictitious effective environment that is constructed to generate the correct friction kernel $\gamma(t)$. We must emphasize that there is no approximation in using harmonic oscillators to describe an anharmonic environment, since these oscillators are an effective medium that is really a Fourier decomposition of the friction kernel $\gamma(t)$, and are only indirectly related to protein dynamics. The approximation lies in assuming that the Langevin equation is a good approximation for describing the classical charge transfer. The advantage of casting the problem in terms of the Hamiltonian Equation (7) is that there are many tools for solving quantum Hamiltonians that have harmonic terms, while there are no methods for solving the quantum version of the Langevin equation.

The beautiful point of this formulation is that the Marcus–Levich–Dogonadze result Equation (5) is the solution of the Hamiltonian Equation (7) in the deep tunneling limit. In addition, the solution of the Hamiltonian Equation (7) in the classical limit reproduces the TST result, corrected for recrossings of the barrier and for memory effects.[12] These results mean that the Zwanzig Hamiltonian provides a unified description of proton transfer reactions in all the three parameter regions defined earlier in this section.

Finally, we should mention that the approach described above is not the only possible for studying quantum proton transfer in condensed phases. Truhlar and coworkers have followed a different methodology, based on variational TST, summarized in detail recently by Truhlar.[15] An advantage of that methodology is that its inputs are related naturally to quantities that are obtained in quantum chemistry calculations. On the other hand, because of its phenomenological character, one cannot easily understand when its approximations are justified.

RATE-PROMOTING VIBRATIONS

The theory outlined in the previous subsection is appropriate for electron transfer, but has to be modified for proton transfer. In this section we will describe the physical justification and mathematical formalism that incorporates these effects.

Hynes' theory of promoting vibrations

In the early 1990s, in their studies of proton transfer in solution using Marcus' rate theory Equation (5), Hynes and coworkers[16,17] noticed the following limitation. If Q is the tunneling distance, it can be shown that the tunneling matrix element that appears in Equation (5) has the form $\Delta \sim e^{-\alpha Q}$. For typical electron transfer reactions

$\alpha \simeq 1\,\text{Å}^{-1}$, while for typical proton transfer reactions $\alpha \simeq 30\,\text{Å}^{-1}$. This means that while electron transfer rates are insensitive to variations of the tunneling distance Q, proton transfer rates, because of the large value of α, depend strongly on motions that possibly reduce the transfer distance Q.

Hynes assumed that the deviation δQ of the transfer distance from its equilibrium value has a harmonic time dependence, $\delta Q = \delta Q_0 \cos(\Omega_{pv} t)$, and calculated the rate using Fermi's golden rule (i.e. the same level of approximation as Marcus' theory). He found for the rate:

$$k = \Delta_0^2 \; e^{-\beta E_M} \; e^{2\alpha^2/\beta M_{pv}\Omega_{pv}^2} \tag{8}$$

where Δ_0 is the tunneling splitting that corresponds to the equilibrium transfer distance, E_M is the activation energy of the ordinary Marcus theory and M_{pv}, Ω_{pv} are, respectively, the mass and frequency of the promoting vibration.

In the previous section we mentioned that Marcus' theory is not a plausible model for describing proton transfer because it predicts a KIE $k_H/k_D = \Delta_H^2/\Delta_D^2$, that is very large, since the tunneling splittings decrease exponentially with the square root of the mass. This problem is remedied by Hynes' work, since the KIE in the presence of a promoting vibration becomes:

$$\frac{k_H}{k_D} = \frac{\Delta_H^2}{\Delta_D^2} \exp\left\{ -\frac{\alpha_D^2 - \alpha_H^2}{\beta M_{pv}\Omega_{pv}^2} \right\} \tag{9}$$

Since α scales like $\sqrt{m}$, the exponential in Equation (9) reduces significantly the KIE. Recently, Hynes reviewed[18] his approach, with emphasis on applications to enzymes.

Benderskii's theory of promoting vibrations

Hynes' formulation is intuitively very appealing, but there are some drawbacks. The environment is described by a 1-D coordinate and the promoting vibration is an artifact that was introduced to modulate the tunneling splitting. In a series of papers on gas-phase proton transfer,[19–21] Benderskii had examined the same effect, tunneling rate modulated by fluctuations of transfer distance, using a Hamiltonian formalism. We will briefly summarize his approach.

Let us assume a symmetric double well PES, $V(s) = as^4 - bs^2$. Its barrier height is $b^2/4a$ and the transfer distance $\sqrt{2b/a}$. Let us assume that a harmonic mode $Q(t)$ is coupled to s through a term cs^2Q. Effectively, the parameter b of the original PES is replaced by $b - cQ(t)$. As $Q(t)$ oscillates, the transfer distance also oscillates around its equilibrium value. In addition, when the transfer distance decreases, the barrier height is lowered. In summary, the simple, symmetric with respect to s, functional form cs^2Q of the coupling reproduces the desired behavior of a PES whose barrier is lowered as the transfer distance decreases.

Benderskii managed to solve this problem in the deep tunneling limit using the instanton method. Roughly speaking, an instanton is the most probable among the

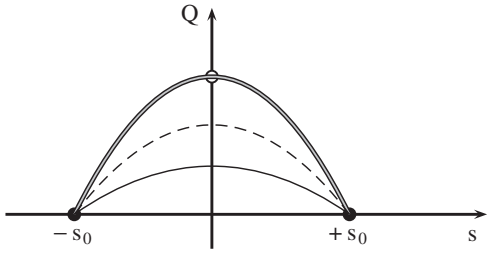

Fig. 1 The PES surface in Benderskii's model. The dark circles are the reactant/product minima and the open circle is the saddle point. The double line is the MEP. The solid line is the instanton tunneling path for H, and the dashed line for D. Because D is heavier, it tunnels closer to the saddle point where the barrier is lower. As a result, the KIE is relatively low, even though the reaction proceeds through tunneling.

possible classical trajectories when one solves the problem QM. We summarize Benderskii's results in Fig. 1.

The double line represents the minimum energy path (MEP), which is the reaction path assumed by TST. The single line represents the instanton trajectory for proton tunneling and the dashed line the instanton trajectory for deuteron tunneling. The heavier deuteron tunnels closer to the MEP, where the barrier is lower. These distinct instanton paths are the reason for the lowering of the KIE by the promoting vibration that we mentioned earlier.

There are other important features in this seemingly simple diagram. The instanton trajectories cross the TS parallel to the *s*-axis, which means that tunneling is happening instantaneously in the timescale of the promoting vibration. But this does not mean that the frequency of the promoting vibration does not play a role! In fact, the result depends on the ratio of the promoting vibration frequency over the barrier frequency Ω_{pv}/ω_b. We have to distinguish between the following limits:[22]

- When $2\Omega_{pv}/\omega_b \ll 1$, we are in the "fast-flip", or "sudden approximation", or "corner-cutting", or "large curvature" limit, where the reaction coordinate follows theMEP, but before it reaches the saddle point it tunnels along the *s* coordinate in a time that is short compared to the timescale of the *Q* vibration.
- When $2\Omega_{pv}/\omega_b \gg 1$, we are in the "slow-flip", or "adiabatic", or "small curvature" limit, where the *Q* vibration adiabatically follows the *s* coordinate and transfer takes place along the MEP path (i.e. at the saddle point).

Therefore very fast promoting vibrations do not affect the rate, and we should expect to see an effect when $2\Omega_{pv}/\omega_b \ll 1$, i.e. when Ω_{pv} is smaller than roughly $500\,cm^{-1}$, which explains why we mentioned earlier that we studied sub-ps motions.

Theory of promoting vibrations in condensed phase

The formulation of promoting vibrations by Benderskii is very satisfactory because it formulated the problem in a Hamiltonian language. On the other hand, the Hynes

formulation, even though it uses an ensatz for the promoting vibration, has the advantage that includes interaction with the environment (with the limitation of the Marcus model, i.e. that the environment is represented by a single degree of freedom). We can incorporate these two theories into the Zwanzig Hamiltonian equation (7) and obtain a theoretically satisfying framework for the description of proton transfer in condensed phases, coupled to a promoting vibration.[22]

We add a term $cs^2Q + \frac{1}{2}M_Q\,\Omega_{\mathrm{pv}}^2$ in Equation (7), to obtain the Hamiltonian:

$$\frac{p_s^2}{2m_s} + V(s) + cs^2Q + \frac{1}{2}M_Q\Omega_{\mathrm{pv}}^2 + \sum_k \frac{P_k^2}{2m_k} + \sum_k \frac{1}{2}m_k\omega_k^2\left(q_k - \frac{c_k s}{m_k\omega_k^2}\right)^2 \tag{10}$$

This incorporates the advantages of Benderskii's and Hynes' ideas, and in addition contains a more realistic description of the environment. One important difference is that Hynes and Benderskii studied systems in which the oscillator Q was a bond vibration, while in Equation (10) Q(t) can be any variable that modulates the PES, for example, it can be a distance between the donor and a nearby residue that changes in time because of equilibrium fluctuations of the enzyme.

To establish a relationship between the Hamiltonian equation (10) and the actual enzymatic system one performs a molecular dynamics simulation to obtain the force $F(t)$ acted upon the reaction coordinate. Then the force autocorrelation function $\langle \mathrm{F(t)F(0)} \rangle$, which is proportional to the friction kernel $\gamma(t)$, is related to the parameters of the fictitious medium of Equation (10) through

$$\gamma(t) = \frac{1}{k_{\mathrm{B}}T}\langle F(t)F(0)\rangle \sim \sum_{k=1}^{N}\frac{c_k^2}{m_k\omega_k^2}\cos(\omega_k t) \tag{11}$$

This equation permits the mapping of the computed force $F(t)$ to the parameters of our Hamiltonian.

To obtain some insight into the behavior of the solutions of the Hamiltonian equation (10), we performed a numerical simulation of a model system:[23] we assumed that $V(s)$ is a symmetric double well, we coupled s to 1000 harmonic oscillators ω_k with frequencies ranging from 10 to 1000 cm^{-1}, and symmetrically to one oscillator Ω_{pv}. Even though the simulation is completely classical, we obtained instructive results that illustrate several of the points we have mentioned in this section.

The next two figures show results for proton transfer in a symmetric double well potential that has barrier height equal to 6 kcal mol^{-1} and transfer distance 1 Å; the proton is coupled symmetrically to an oscillator of frequency 300 cm^{-1}. In Fig. 2 we show the progress of the reaction coordinate from reactants to products. The very fast oscillations are bond oscillations in the reactant/product wells. The slower oscillation that envelopes the bond oscillations is the promoting vibration. Note that the promoting vibration is fast enough that the time the barrier is lowered is not long enough for a reactive event to occur, i.e. it requires several oscillations of the promoting vibration for the charge transfer to occur. Once the crossing over the barrier happens though, it is practically instantaneous in the timescale of the promoting vibration.

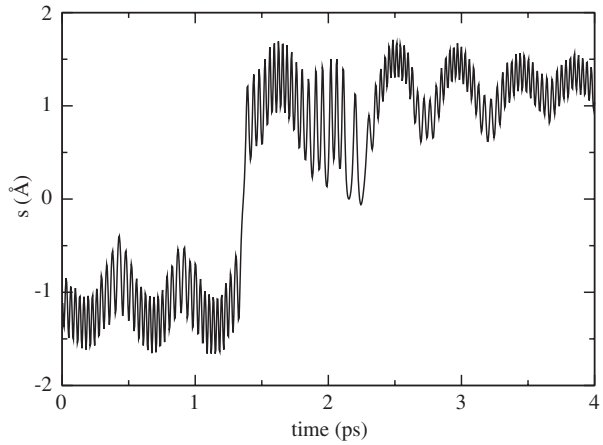

Fig. 2 An example of a reactive trajectory. The TS is at the $s = 0$ line and the reactant/product wells at the $s = \mp 1$ lines.

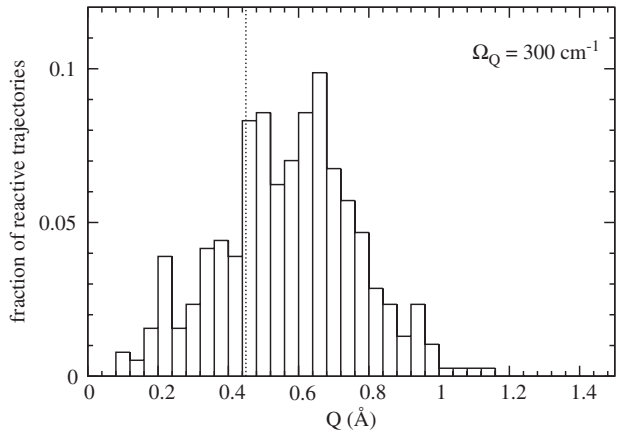

Fig. 3 A histogram of the values of the promoting vibration coordinate Q, as the reactive trajectories cross the TS. The dashed line corresponds to the location of the saddle point.

In Fig. 3 we plot a statistics of the values of the promoting vibration coordinate as the reactive trajectories cross the TS. The saddle point in Fig. 1 corresponds to the value of Q shown with a dashed line in Fig. 3. We note that the reactive trajectories do not pass through the saddle point, but rather through a broad region centered at the saddle point. This picture shows that the dynamics cannot be described by a single TS. The deeper reason for this is that the assumption of separability fails:[24] the promoting vibration is strongly coupled to the reaction coordinate in the TS region and the frequency of the promoting vibration is comparable to the inverted barrier frequency, so there is no separation of timescales.

Finally, in our opinion, there is an open question in quantum theories of proton transfer. The theories we have been discussing use a mean field potential as the PES. This is undoubtedly correct when the environment relaxes quickly in the timescale of the reaction. However, the transfer step in quantum tunneling is very fast, and it is not certain that all the configurations that enter the mean field potential are sampled. This point was first raised by Hynes[25] and implemented in studying proton transfer in solution by Hynes and Wilson.[26]

COMPUTATIONAL SIGNATURE OF PROMOTING VIBRATIONS

In a realistic system there are many other motions present, so there is no guarantee that the effect of the promoting vibration will not be masked by other interactions that are present in an enzyme. We need a diagnostic that when we perform a computer simulation of the dynamics of an enzyme, will allow us to identify whether a promoting vibration is present.

We have found[27] such a computational signature in the framework of the Langevin equation (6). Let us recall that if we compute from a simulation the force $F(t)$ on the reaction coordinate, then the friction kernel $\gamma(t)$ is proportional to the autocorrelation of that force. We have shown that if we add a term $cs^2Q + \frac{1}{2}M_Q\Omega_{\rm pv}^2$ to the Langevin equation, and allowing the promoting vibration to be coupled to the environment with coupling strength ζ, the friction kernel becomes

$$\gamma_{\rm pv}(t) = \gamma(t) + \frac{4c^2}{M\Omega_{\rm pv}^2} s(t)s(0)\left[\cos(\tilde{\Omega}_{\rm pv}t) + \frac{\zeta}{2\tilde{\Omega}_{\rm pv}}\sin(\tilde{\Omega}_{\rm pv}t)\right]e^{-\zeta t/2} \tag{12}$$

Here $\gamma(t)$ is the friction of the original Langevin equation and $\tilde{\Omega}_{\rm pv} = \sqrt{\Omega_{\rm pv}^2 - \zeta^2/4}$ is the effective frequency of the promoting vibration, modified due to its coupling to the environment.

Equation (12) provides the diagnostic we have been looking for. Note that the correction to the friction kernel due to the promoting vibration is proportional to $s(t)s(0)$. Suppose we perform a simulation where we have imposed constraints to keep the transferred proton fixed, so that the correction term is proportional to $s(0)^2$. If we keep the proton fixed near the TS, $s = 0$, the correction term will be very small. If we keep it fixed away from the TS (most simply, at the reactant or product configuration), the correction term will be nonzero. In addition, if we take the Fourier transform of Equation (12), the presence of the trigonometric terms in the correction term will produce large peaks at the frequency of the promoting vibration.

In conclusion, if we perform simulations with the transferred proton fixed near and away the TS, and then take a Fourier transform of the calculated friction kernel, if we see sharp peaks for the latter simulation that are absent when the proton is held fixed near the TS, then we have evidence that a promoting vibration is present, and the position of the peak is an indication of its frequency. In the next section we will discuss examples of enzyme simulations where this diagnostic was successful.

EXPERIMENTAL SIGNATURE OF PROMOTING VIBRATIONS

The discussion in this section has suggested a clear experimental signature for the presence of promoting vibrations. Hynes' formalism, Benderskii's formalism and our quantum calculations using the Hamiltonian equation (10) all predict a low KIE, i.e. much lower than what one would expect for transfer through tunneling. In fact, the initial resistance to accepting that tunneling can occur in enzymes was exactly the low values of KIE. As mentioned earlier, Hynes has recently reviewed[18] the topic of influence of promoting vibrations on KIE, but with a perspective different than ours.

Furthermore, the tunneling rate depends exponentially on the reorganization energy of the environment, which for an enzymatic system depends strongly on the rigidity of the enzyme. This raises some intriguing possibilities for the interpretation of certain experiments on thermophilic enzymes. Thermophilic enzymes show low enzymatic activity at mesophilic temperatures, and the conservation of the active site structure and chemical mechanisms suggests that the same chemical mechanism is present at both thermophilic and mesophilic temperatures. One possible interpretation focuses on the temperature-dependent motions of proteins, because experiments have shown that the rigidity of thermophilic proteins is less at thermophilic rather than at mesophilic temperatures.[28]

The work that is of interest with respect to promoting vibrations is a study[29] of hydrogen tunneling in alcohol dehydrogenase from *Bacillus stearothermophilus*. The unusual features of this system are (i) the activation energy is smaller in the thermophilic regime, which in a naive interpretation would imply that tunneling is enhanced with increasing temperature; (ii) the primary KIE is small and temperature-independent in the thermophilic regime, but larger and temperature-dependent in the mesophilic regime. We have shown[30] that by assuming the presence of a promoting vibration in the thermophilic regime, and assuming that it freezes out in the mesophilic regime, one is able to reproduce all the trends mentioned earlier in this paragraph. Reproducing trends is not definite proof, but at the very least it is a reminder that the presence of a minimal dynamical element makes the problem sufficiently complex, that conclusions derived by studying Arrhenius plots should not be trusted.

Anomalous values of the secondary KIE have been interpreted as indications of tunneling. The reader should consult the arguments regarding secondary KIEs in reviews of experimental literature.[6,7]

FOUR OBJECTIONS TO PROMOTING VIBRATIONS

The real protein dynamics is not harmonic

"Proteins are very anharmonic systems, so what is the justification of modeling the protein environment as a set of harmonic oscillators in Equation (10)?" The real approximation we have made is modeling the proton transfer by the Langevin

equation (6). One expects this to be a good approximation for the short timescales relevant for barrier crossing. Within the Langevin equation, the effect of the environment on the proton is captured through the friction kernel, which is the force autocorrelation function. No approximation is made regarding this friction kernel, it is what is obtained from a simulation. This time-dependent friction kernel can be decomposed into Fourier components, which are the harmonic oscillators appearing in Equation (10). That is, these oscillators are fictitious quantities introduced to reproduce the exact form of the friction kernel, therefore no simplification regarding the protein anharmonic dynamics is made.

The promoting vibration is quickly dephased

"*If we embed a harmonic oscillator in a medium, it will be very quickly dephased. Therefore, the identification in an enzyme of a promoting vibration with a definite frequency is not plausible*." Here, the misunderstanding is that the promoting vibration is not a harmonic oscillator embedded in the enzymatic environment.

The motion of a protein on its PES can be described as anharmonic motions near local minima (i.e. conformations), with rare hops between conformations. While the system executes this motion, we can record, for example, the distance $Q(t)$ between two residues. If the Fourier transform of $Q(t)$ is relatively peaked, then the distance between these residues varied in time like a damped harmonic motion. The quantity $Q(t)$ is not an oscillator with energy levels, that is embedded in the enzyme, rather it is an internal distance of, for example, residues that participate in the equilibrium fluctuations of the enzyme.

In simple model calculations we can mimic this effect by writing a Hamiltonian like Equation (10) in which $Q(t)$ appears as an independent oscillator, but it must be understood that this Hamiltonian is a simplified model designed to produce a fluctuating PES, and $Q(t)$ is a quantity that parametrizes this fluctuation. However, it is true that one cannot assume beforehand that the distance $Q(t)$ is harmonic, one has to calculate it, Fourier transform it and check whether it is peaked at some frequency, as we will do in the examples in the next section.

Parenthetically, we would like to use this opportunity to correct a misunderstanding that is common in enzymatic literature. Highly anharmonic potentials do not necessarily exclude harmonic dynamics! An example is water: the interatomic potential is extremely anharmonic (hard spheres), but water supports harmonic waves (sound). The resolution of the paradox is that the variable that describes sound waves (density) is not the variable that enters the anharmonic interatomic potentials, so it is possible for equilibrium fluctuations, like sound, to have harmonic dynamics.

The promoting vibration is much faster than the turnover rate

"*The turnover rate for enzymes has timescales μs–ns, but the promoting vibration has ps-timescale, therefore they can't be related*." This argument is correct for some gas-phase reactions, but it is not valid for condensed phase reactions.

Let us look at a simple condensed phase reaction, electron transfer in liquids, which is described by Marcus' theory equation (5). As is well known, electron tunneling takes place only when the interaction with the solvent symmetrizes the PES. The reorganization energy required for the solvent to reach its configuration that will symmetrize the PES of the electron, is the activation energy appearing in Equation (5). Once the PES is symmetrized, the probability that the electron will transfer is proportional to the square Δ^2 of the tunneling matrix element. Therefore, even for simple transfer reactions in condensed phases, several events of widely varying timescales contribute to reaction and the turnover rate is not simply related to the timescale of a single event.

The method was designed to identify ps-timescale motions

"*The reason this method identified promoting vibrations for some systems is that by construction it searches only for fast ps motions, and therefore it cannot identify e.g., slower conformational motions that possibly affect the reaction rate.*" This criticism is absolutely correct, if there are conformations that bring donor and acceptor close together thus enhancing tunneling, they are outside the grasp of a method that is based on Langevin equation. In Section 5 we will outline some ideas for searching the conformation space for configurations that affect the reaction rate.

3 Examples of rate-promoting motions in enzymatic systems

We will now present examples of enzymatic systems where we applied the ideas and formalism of the previous section, and we were able to identify rate-promoting vibrations.

HORSE LIVER ALCOHOL DEHYDROGENASE

The first system in which we identified a promoting vibration was horse liver alcohol dehydrogenase (HLADH).[31] The active site and surrounding residues are shown in Fig. 4. The suspicion that dynamics may play a role existed because two specific mutations had been identified, Val203→Ala and Phe93→Trp, which significantly affect enzyme kinetics. Both residues are located at the active site. Val203 impinges directly on the face of the nicotinamide ring in the nicotinamide adenine dinucleotide (NAD) cofactor distal to the alcohol substrate. Additionally, there is evidence from molecular dynamics simulations,[32] that Val203 forces the nicotinamide ring of NAD^+ into closer proximity to the substrate, thus facilitating the hydride transfer to produce the corresponding aldehyde. These facts suggest that motions of these residues may play an important role in catalysis.

In the previous section we found a computational signature for the existence of promoting vibrations: fix the transferred proton at the TS and away from it, and compare the magnitude of the Fourier transform of the forces on the proton, as it is

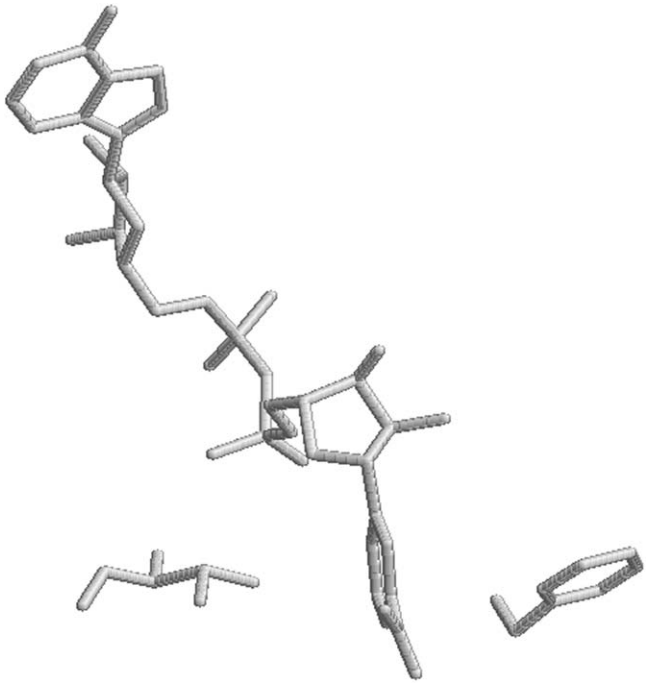

Fig. 4 Active site of HLADH: Val203, the NAD cofactor and the alcohol substrate.

held fixed at different positions. Since the location of the TS is unknown, we tried several intermediate positions and selected the one for which the spectral density is smallest, i.e. a position of minimum coupling.

We shall present results from simulations for three configurations – reactants (R), products (P), and minimal coupling (MC):

- The R configuration consists of NAD^+ and the deprotonated benzyl alcohol ($PhCH_2O^-$).
- The P consists of NADH and benzaldehyde.
- In the third configuration MC, we have NAD^+ and $PhCH_2O^-$ with the pro-R hydrogen restrained so that it is equidistant from the hydroxyl α-carbon (hydride donor) and the C4 carbon (hydride acceptor) in the nicotinamide ring.

We performed a 30-ps simulation and saved the time series for several distances between atoms. In Fig. 5 we plot, for all three configurations, the Fourier transform of the donor–acceptor distance. We see a peak at ca. $100\,cm^{-1}$, common to all three configurations, signifying that the two motions appear to be in resonance.

The Fourier transform of the force on the reaction coordinate is shown in the right panel of Fig. 5. Again, the peak at ca. $100\,cm^{-1}$ is common to both configurations. This is a strong indication that the motion of the transferred proton is

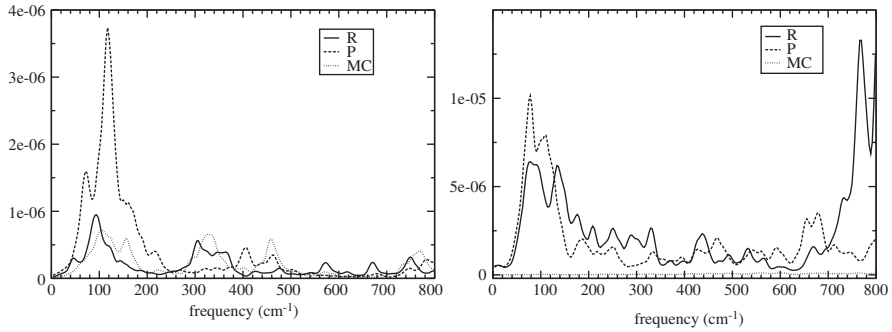

Fig. 5 Left: the spectral density for the donor–acceptor relative motion in the wild type; it monitors the donor–acceptor distance. Right: the spectral density for the reaction coordinate, in the wild type. The three lines represent the reactants configuration (R), the products configuration (P), and the minimal coupling configuration (MC).

coupled to the relative motion between the alcohol and the nicotinamide ring. On the scale of the graph, the spectral density for MC appears as the flat line close to the horizontal axis, which shows that the spectral density is position-dependent, as predicted by Equation (12). Furthermore, if we had shown the MC line in magnification we would see that although the high frequency peaks in the P and C are still present in MC, the peak at ca. $100\,\mathrm{cm}^{-1}$ is almost absent in MC. These results strongly suggest that the reaction coordinate is coupled to an oscillation of frequency ca. $100\,\mathrm{cm}^{-1}$.

In view of our earlier analysis, our results indicate that the reaction coordinate is coupled to the alcohol-NAD motion, which in turn is coupled to Val203, whose side chain impinges directly on the face of the nicotinamide ring. It is thus shown that in HLADH this dynamic coupling is central to the catalytic process. Finally, we should point out that Cui and Karplus[33] used our concept of symmetrically coupled vibrations and performed a simulation on HLADH following a different method, and found results that are in agreement with the results presented here.

LACTATE DEHYDROGENASE

The next system we studied was the isoforms of human LDH. The first part of the calculation was similar to HLADH. However, we encountered interesting complications.

LDH catalyzes the interconversion of lactate and pyruvate with the coenzyme NAD (see Fig. 6). This enzyme plays a fundamental role in respiration, and multiple isozymes have evolved to enable efficient production of substrate in different microenvironments. Two main subunits, referred to as heart and muscle, are combined in the functional enzyme as a tetramer, and subunit combinations range from pure heart to pure muscle. The kinetic properties of the heart and muscle isoforms are

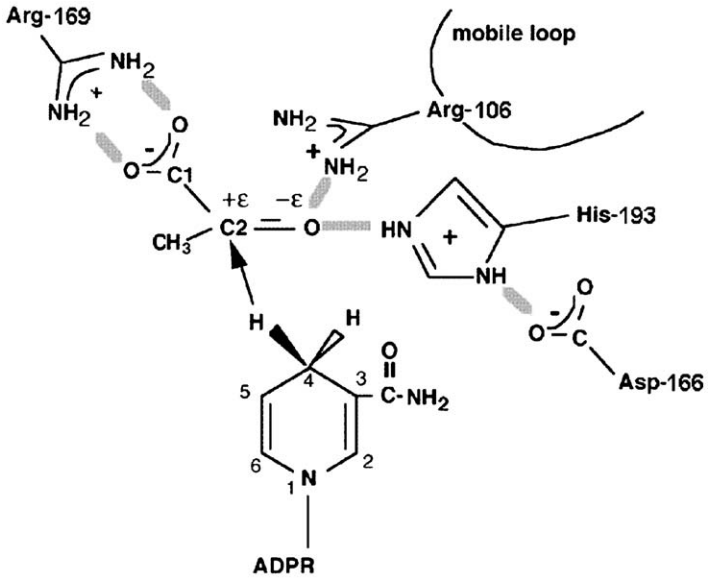

Fig. 6 Diagram of the binding site of LDH with bound NADH and pyruvate showing hydrogen bonds between the substrate and key catalytically important residues of the protein. The catalytic event involves the hydride transfer of the C4 hydrogen of NADH from the pro-R side of the reduced nicotinamide ring to the C2 carbon of pyruvate and protein transfer from the imidazole group of His-193 to pyruvate's keto oxygen.

distinct: the heart favors production of lactate and the muscle of pyruvate. Despite this difference, the domain structure, subunit association, and amino acid content of the active sites of the two isoforms are almost identical, leading to the puzzle of what is the cause of their difference in activity. We propose that placement of the TS, coupled with a promoting vibration, can influence kinetic control of hydride transfer.

Results will be presented for the following configurations: the heart and muscle isoform each with lactate and NAD^+ bound; the heart and muscle isoform each with pyruvate and NADH bound; two simulations of the heart isoform with lactate and NAD^+ bound where the hydride distance was restrained at a point between donor and acceptor carbons. In the following figures, in the language of the previous subsection, the reactant configuration for the heart isoform is the line "lactate" and the product configuration is the line "pyruvate." And vice versa, the reactant configuration for the muscle isoform is the line "pyruvate" and the product configuration is the line "lactate."

In Fig. 7 we show results for the heart LDH isoform: (1) the Fourier transform of the force on the transferred hydride (left); (2) the Fourier transform of the relative motion between the substrate C2 carbon and carbon C4N of the nicotinamide ring of the cofactor NAD^+/NADH (right). In Fig. 8 we show the corresponding figures

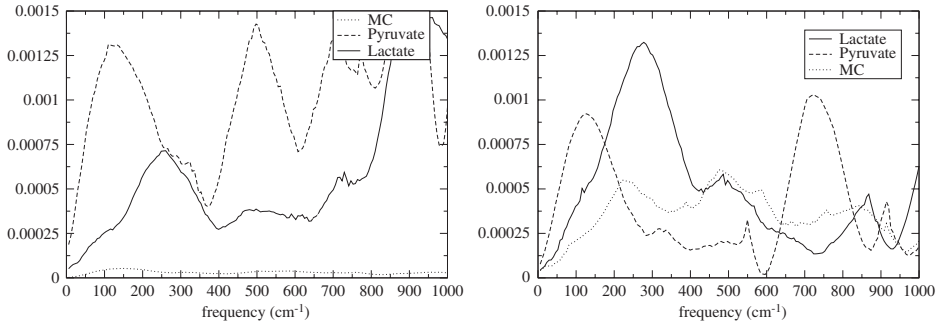

Fig. 7 Wild-type heart LDH isoform: Fourier transform of the force on the reaction coordinate (left) and Fourier transform of relative donor–acceptance distance (right).

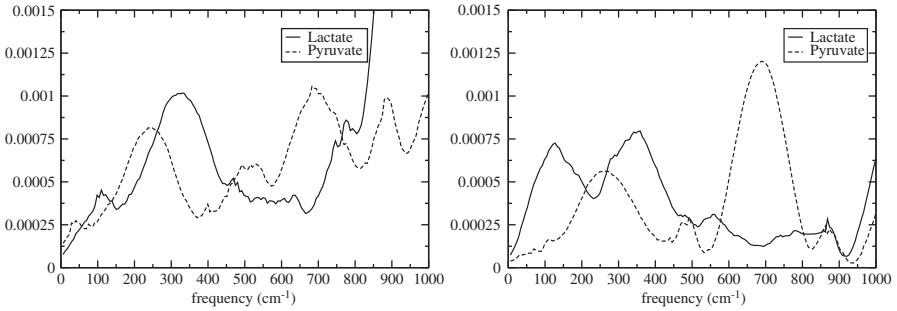

Fig. 8 Wild-type muscle LDH isoform: Fourier transform of the force on the reaction coordinate (left) and Fourier transform of relative donor–acceptance distance (right).

for the muscle LDH isoform. Similarly, to the HLADH simulation we found clear evidence of the presence of a promoting vibration:

(1) The spectral density is much lower when the hydride is near the TS, as predicted by Equation (12) (line MC in the Figure).
(2) The peaks of the Fourier transform of the force on the hydride, are in resonance with the peaks of the Fourier transform of the relative donor–acceptor motion.

These results show strong evidence for the presence of a promoting vibration, but they are symmetric for both isoforms, so they don't resolve the paradox why one isoform favors the production of pyruvate and the other of lactate. However, there is a hint: in the left panels of Figs 7 and 8, the pyruvate peak is higher for the heart isoform and the lactate peak higher for the muscle isoform. Recall that the height of the spectral density is proportional to the force on the reaction coordinate. According to Equation (12), what may lead to bigger force, is bigger $s(t)$, i.e. bigger deviation from the TS. Since the lines "lactate" and "pyruvate" in Figs 7 and 8 correspond to the hydride bound to the donor/acceptor (and vice versa for the other

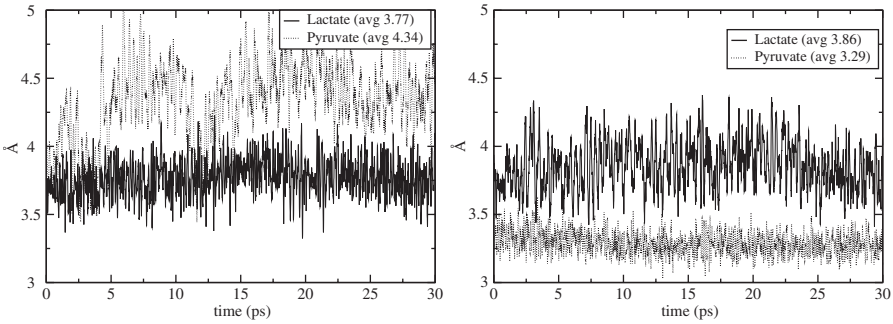

Fig. 9 Donor–acceptor distance for the wild-type human heart LDH isoform (left) and the muscle isoform (right).

isoform), it would be interesting to see what is the average distance of donor–acceptor in the two isoforms.

In Fig. 9 we show the results of a 30-ps simulation for the donor–acceptor distance, i.e. the distance between the C2 carbon of substrate and carbon C4N of the nicotinamide ring of the cofactor NAD^+/NADH. Fig. 9 shows that the average donor–acceptor distance is shorter for the heart isoform when lactate and NAD^+ are bound, and for the muscle isoform when pyruvate and NADH are bound. We propose that the different kinetic activity of the two isoforms is due to the reduced donor–acceptor distance when lactate is bound to the heart isoform and pyruvate is bound to the muscle isoform.

The next question is to identify residues near the active site that may modulate the donor–acceptor distance. In Fig. 10 we show the active site and some nearby residues. In the spirit of the previous results, in order to predict the degree that the motion of these residues is correlated with the donor–acceptor motion, we can calculate the Fourier transform of the autocorrelation of the residue motion, and then order the residues according to the height of the peak of the spectral density.[34] In Fig. 11 we show one result, the spectral densities for the motion, projected first along the residue–donor axis and then along the donor–acceptor direction, of three residues, two of them strongly correlated and one not correlated.

Finally, to bring our argument to its logical conclusion, we can test for the consistency of our interpretation: we substituted residue 31, Valine, with a less bulky one, Alanine. If our interpretation is correct, we expect that the Fourier transform of the force on the hydride would have a higher peak in the wild type than in the mutant, since the bulkier Valine is more efficient in pushing the nicotinamide ring of the NAD^+, and as a result the average donor–acceptor distance would be smaller for the wild type than in the mutant. In Fig. 12, we show the results of the simulation, which are consistent with our prediction. As we mentioned earlier, the peak of the spectral density can be lowered either because the coupling to the reaction coordinate is weaker, or because the reaction coordinate is fixed closer to the TS. The right panel of Fig. 12 shows that the average donor–acceptor distance is larger

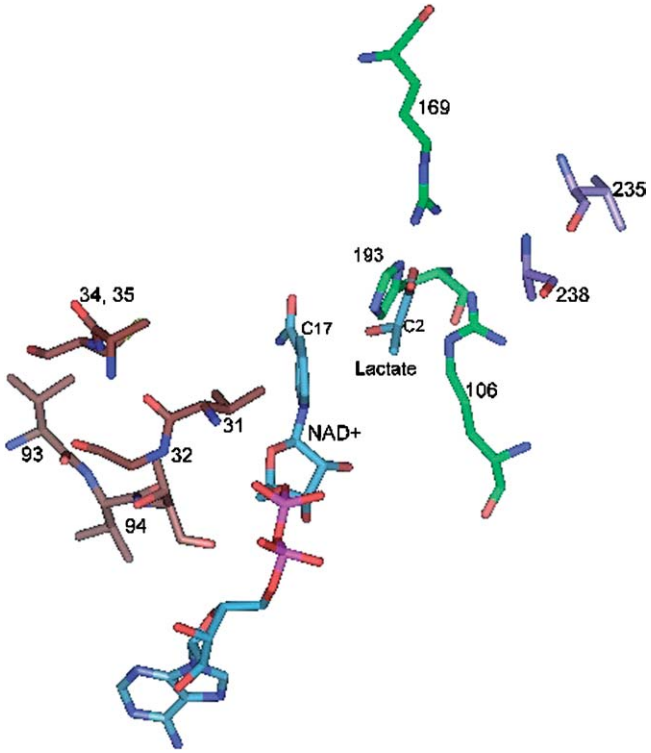

Fig. 10 The structure of the heart isoform with lactate and NAD^+ bound.

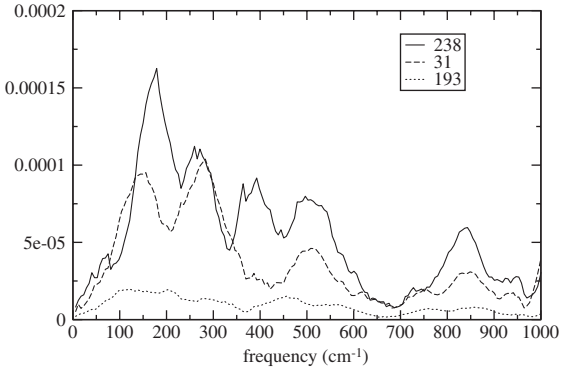

Fig. 11 Spectral density of motion of three residues in the wild-type human heart LDH isoform with lactate and NAD^+ bound: residue 238 is the most strongly correlated residue, 31 is strongly correlated and substituted in the mutagenesis simulation, and residue 193, the essential active site histidine, is poorly correlated.

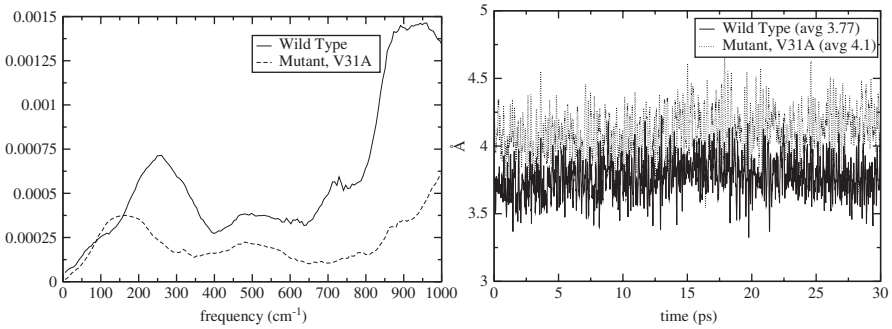

Fig. 12 Left, spectral density for the reaction coordinate in the wild type and mutant human heart LDH isoform with lactate and NAD^+ bound: the solid line is the wild-type configuration where residue 31 is Valine, and the dashed line is the mutant configuration where residue 31 is Alanine. Right, donor–acceptor distance for the wild type and mutant human heart LDH isoform with lactate and NAD^+ bound: the solid line represents the wild-type configuration where residue 31 is Valine and the dashed line represents the mutant configuration where residue 31 is Alanine.

for the mutant result, therefore the lower peak of the spectral density in the left panel necessarily means that the coupling is weaker for the less bulky Alanine.

HUMAN PURINE NUCLEOSIDE PHOSPHORYLASE

Up to this point, all the examples we discussed, concerned protein motions that affect reactions that involve a light particle transfer. However, rate-promoting enzymatic motions can also exist in other types of reactions. For example, we have shown[35] that such motions can influence catalysis by acting through electron density fluctuations caused by geometrical changes. The system we investigated is human purine nucleoside phosphorylase (hPNP), which catalyzes reversible bond cleavage of 6-oxopurine nucleosides to form phosphorylated α-D-ribose products in the presence of phosphate, as seen in Fig. 13.

The cleavage of the C-1′–N-9 ribosidic bond (for atom terminology see Fig. 14) occurs in a dissociative mechanism that forms a TS with a substantial oxycarbenium ion character. The phosphate provides an electrostatic stabilization of this oxycarbenium ion, encouraging TS formation.[36,37] As the N-ribosidic bond is cleaved, electron density is expelled by the oxygen-stack compression towards the purine ring, and improves electrostatic interactions with nearby residues and facilitates the abstraction of a proton from a close-by proton donor, making the purine a better leaving group and accelerating catalysis. In summary, oxycarbenium stabilization, increased phosphate ionization and purine ring activation, contribute in concert to catalytic acceleration. Crystallographic data of several hPNP complexes with TS analogs, showed an unusual geometric arrangement of the atoms O-5′, O-4′, and O_P, lying in a close threeoxygen stack (Fig. 14), which was later corroborated by

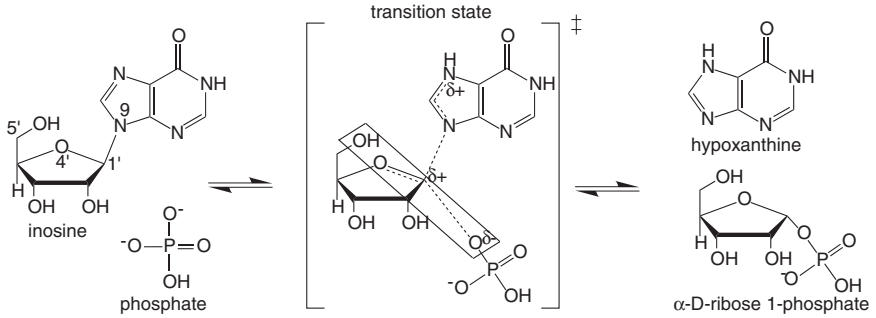

Fig. 13 hPNP-catalyzed phosphorolysis of the purine nucleoside. The guanine leaving group and phosphate nucleophile are well-separated from the oxycarbenium ion, defining a highly dissociative TS. Note the oxygen stacking, indicated by the rectangle, of O5′, O4′, and the phosphate nucleophile O_P.

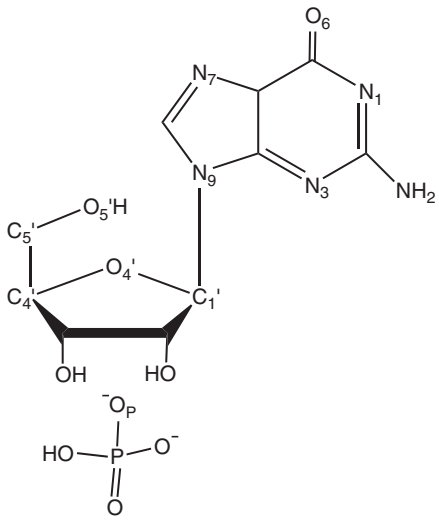

Fig. 14 Atomic nomenclature of the purine nucleoside and phosphate nucleophile.

extensive experimental KIE analysis.[38] We have shown[35] that protein motions in hPNP and its substrates cause the O-5′, O-4′, and O_P oxygens to squeeze together and push electrons towards the purine ring, stabilizing the oxycarbenium character of the TS.

The starting point of our computations was the 2.5 Å resolution structure of hPNP complexed with the TS analog ImmH and phosphate. Following standard computational procedures for enzymes we performed both classical molecular dynamics simulations and hybrid quantum/molecular simulations.[35]

The enzymatic system was divided into two concentric zones. These consisted of the QM region, containing the atoms being treated QM, and the molecular mechanics

(MM) region, in which the atoms were treated with a MM potential. In the case of the simulation of the E···S complex, the QM region contained the substrates guanosine and phosphate, and the conserved catalytic water. For the E···I complex, the QM region contained ImmG, phosphate and a catalytic water. The AM1 semi-empirical Hamiltonian was employed as the QM potential, and the all-atom force field of CHARMM22 was used to describe the atoms in the MM region.

For example, for the E···S complex, we chose the QM/MM model shown schematically in Fig. 15. The residues N243 and E201 are actively involved in catalysis by stabilization of the TS, but since they are not directly involved in the acid catalysis, they were not included in the QM region due to computational limitations of QM/MM methods. However, their contribution to the stabilization of the TS structure is introduced by the QM/MM electrostatic term of the Hamiltonian. We were interested in the last step of the reaction, the cleavage of the N-ribosidic bond and protonation of the purine ring to yield the protonated guanine and phosphorylated α-D-ribose. It is essential that a good reaction coordinate be used in order to represent the enzymatic reaction properly to obtain meaningful PESs. After investigating a variety of reaction coordinates, we found that a suitable reaction coordinate to describe the phosphorolysis reaction was the interatomic C-1′–N-9 and C-1′–O_P distances (Fig. 15).

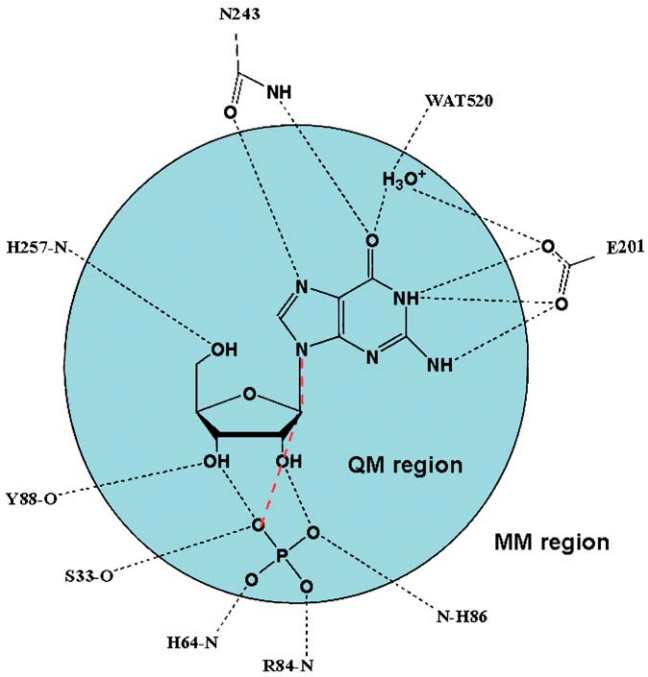

Fig. 15 QM/MM model used to obtain the PES. The reaction coordinate used to produce these surfaces is shown with dashed lines in the figure.

Results: dynamics

During the classical MD simulation we saved the values of the O-5′–O-4′ and O-4′–O_P distances. We found that these distances are quite stable, deviating only up to 0.3 Å from their average value. This implies that the O-5′–C-5′–C-4′–O-4′ dihedral is not rotating freely as it does in aqueous solution, but is restricted by the enzymatic environment. We show the time series for that dihedral in both the enzymatic environment and in aqueous solution in Fig. 16. We note that the mean value in each case is different, and that there is a higher deviation from the mean value in solution, verifying that this dihedral's motion is restricted in the enzyme.

In Table 2 we show the average O-5′–O-4′ and O-4′–O_P distances and standard deviations, for the WT and for several mutants of hPNP complexed with guanosine and phosphate (the maximum fluctuation of the O-5′–O-4′ distance is 0.6 Å, therefore a difference of, for example, 0.2 Å in the average distance is substantial). For each mutation the changes in compression of the oxygen stack were different. For example, we found that for the H257G mutant, the average O-5′–O-4′ distance was considerably higher than that of the WT, meaning that the residue H257 plays a role in keeping the two oxygens compressed.

We now move to a dynamical analysis of the time series for these distances. In the left panel of Fig. 17, we show the Fourier transforms of the O-5′–O-4′ distance autocorrelation function, and of the O-5′–O-4′, O-4′–O_P distance–distance correlation function. The spectra are very similar, indicating that O-5′−O-4′ and O-4′–O_P

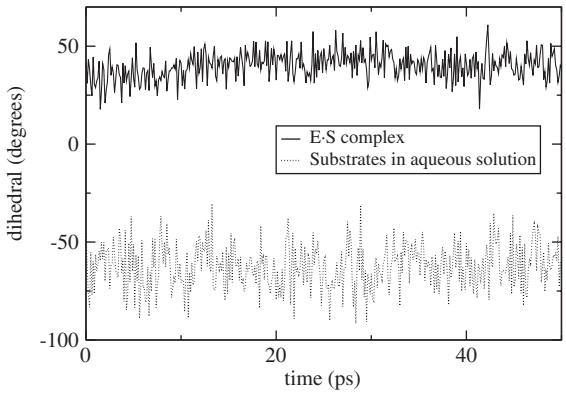

Fig. 16 O-5′−C-5′−C-4′−O-4′ dihedral (degrees) of the ribose ring during the WT classical MD simulation in aqueous solution and in the E···S complex.

Table 2 Average O-5′−O-4′ and O-4′−O_P distances (Å) for the WT and mutated hPNPs

Distance	WT	E201G	V260G	H257G
O-5′−O-4′	2.81 ± 0.08	2.88 ± 0.11	2.78 ± 0.08	3.04 ± 0.08
O-4′−O_P	4.34 ± 0.10	6.58 ± 0.11	3.90 ± 0.11	4.69 ± 0.10

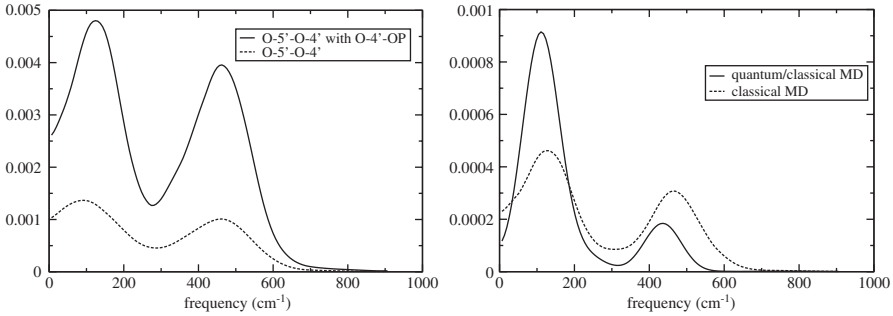

Fig. 17 Left: Comparison of the spectra of the O-5′−O-4′ distance autocorrelation function and the O-5′−O-4′ and O-4′−O_P distance–distance correlation function. Right: The similarity of the spectra of the O-5′−O-4′ distance autocorrelation function for the E···S complex based on the classical and quantum/classical MD simulation, shows an agreement to the classical simulations.

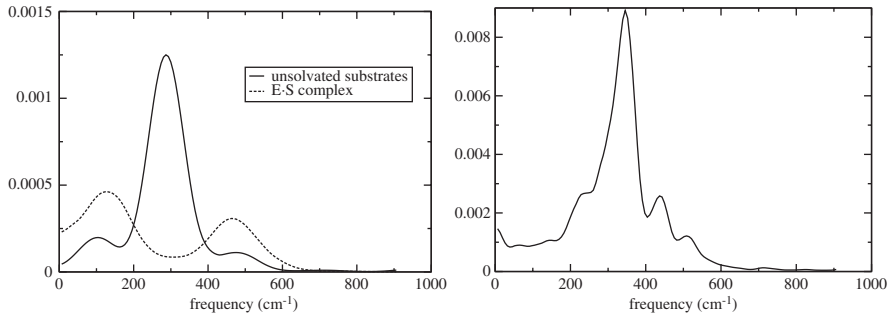

Fig. 18 Left: spectra of the O-5′−O-4′ distance autocorrelation function for hPNP and unsolvated substrates. Note that the natural vibration of the oxygen centers, i.e. 285 cm^{-1}, is altered in the presence of the enzyme. Right: the power spectrum of the H257G mutant of the E···S complex shows a distinct peak at 333 cm^{-1}, very similar to the result for the solvated substrate.

oscillate at the same frequencies: 125 and 465 cm^{-1} in the enzyme environment. In the right panel of Fig. 17, we compare the Fourier transforms of the classical and mixed quantum/classical MD simulations, and find that they are similar.

Next we examine whether these vibrations are unique in the enzymatic environment or they are inherent in the substrates. In the left panel of Fig. 18 we compare the calculation in the enzyme with a simulation of the substrates in aqueous solution, in the absence of hPNP. The spectrum of the O-5′−O-4′ distance autocorrelation function of the classical MD of solvated substrates showed a peak at 330 cm^{-1}, and of the unsolvated substrates at 285 cm^{-1}, i.e. distinct from the peaks in the presence of the enzyme, revealing that hPNP is directly affecting the way in which these oxygens naturally vibrate.

In order to assess the effect of the mutation of nearby residues on the three oxygen stack electronic interaction, we performed classical simulations of mutated hPNPs.

We studied whether changes in protein structure have an influence on the pattern of spectra discussed above for WT hPNP. In particular, we mutated F200G, E201G, H257G, H257A, V260G, and L261G. The spectrum of the O-5′−O-4′ motion for the F200G, E201G, V260G, and L261G mutated hPNPs was very similar to that of the WT. However, as can be seen in the left panel of Fig. 18, the H257G was very similar to that of the unsolvated substrates, giving further evidence that H257 is responsible for modifying the power spectrum in the E···S complex.

Results: energetic barrier

We turn our attention to the coupling of the rate-promoting motion we have been describing, to the reaction coordinate. We used the hybrid QM/MM method described earlier to obtain the PES for the phosphorolysis reaction for various E···S complexes, for a range of O-5′−O-4′ and O-4′–O_P interatomic distances. We have presented elsewhere[35] detailed results for the activation energies (kcal mol^{-1}) as a function of oxygen interatomic distances of the E···S complex and the E···TS complex. This is collection of structures covered a wide range of geometries, with O-5′−O-4′ ranging from 2.78 to 3.64 Å and O-4′−O_P ranging from 3.35 to 4.30 Å. Thus, these structures were sufficient to represent the different E···S geometries that can be found in the PES.

To quantify this correlation between lower activation energy and compression of the oxygen distances, we fitted the results for the activation energies to a function that had up to quadratic terms, as seen in Fig. 19 (a parabolic fitting had smaller χ^2 than the also plausible linear fitting). The parabolic dependence of the activation on energy on distance may have a simple interpretation: as the distances between the oxygen increases the energy rises as carbocation stabilization is lost, but at shorter distances, as we approach distances equal to twice the van der Waals radius, electron–electron repulsion will compete with the stabilization and there is a point where there are no further reduction of the activation energy. From the values of the

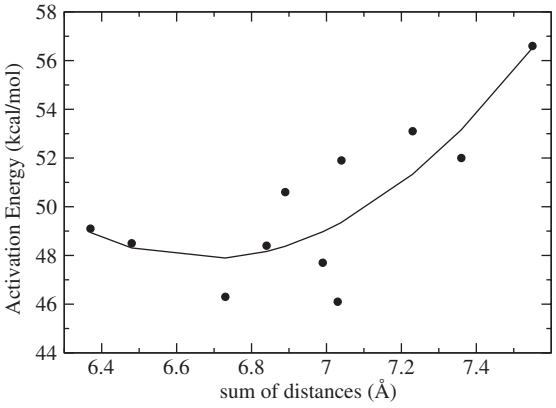

Fig. 19 Activation energies (kcal mol^{-1}) versus the sum of O-5′−O-4′ and O-4′−O_P distances (Å) for the E···S complex.

curvature of the parabolic fittings we can obtain a spring constant, and by using a mass equal to the reduced mass of O−O, we can obtain an effective harmonic frequency associated with the parabolic fittings shown in Fig. 19. This effective frequency was equal to 180 cm^{-1}, in surprising agreement with the position of the peaks of the spectra of the oxygen motions.

In conclusion, the protein motion that compresses the oxygen stack, is one of the factors which makes the reaction possible, leading up to a 20% decrease in barrier height.

Results: charge fluctuations

In addition, we have studied[39] charge fluctuations in the ribose and purine groups of the enzyme-bound ribonucleoside. If these fluctuations are resonant with the oxygen-stack promoting motion, it would further validate the hypothesis that the promoting motion pushes electrons across the ribosidic bond.

Partial charge calculations were employed to follow changes in electron density in the substrate guanosine, using Gaussian98 at the B3LYP level of theory with the 6-31G(d,p) basis set. Partial charges for each atom were calculated using the CHELPG algorithm. Charges for the ribose and purine ring components of the ribonucleoside substrate were calculated by adding up the partial charges of the constituent atoms of each.

We generated time series for the partial charges, and as usual took the Fourier transforms, shown in the left panel of Fig. 20. The two spectra nearly overlap, demonstrating that the charge fluctuations in the ribose are resonant with the charge fluctuations in the purine ring, with a dominant peak at 450 cm^{-1} and a smaller peak at 160 cm^{-1}. Recalling that the spectrum of the oxygen-stack compression motion had peaks 125 and 465 cm^{-1}, we note that the partial charge spectra are clearly resonant with those of the oxygen motion.

In addition, we probed fluctuations across the N9-C1′ ribosidic bond, since this is the bond that is broken in this reaction. The spectra are shown in the right panel of Fig. 20. They are resonant with each other and with the spectra for ribose and purine

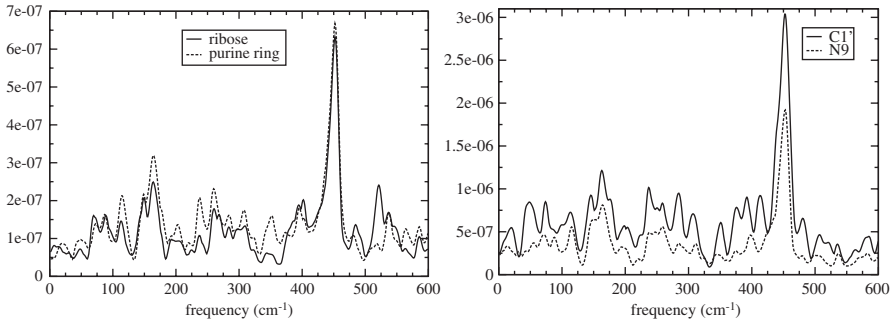

Fig. 20 Left: Power spectra for ribose and purine ring partial charge time series. Right: Power spectra for atoms C1′ and N9 partial charge time series.

ring, and also feature peaks at 160 and 450 cm^{-1}, i.e. they contain the signature peaks of the oxygen-stack compression spectra. These results confirm that the oxygen-stack compression is the cause of these partial charge fluctuations.

4 Description in atomic detail of correlated protein motions

In this section we will examine other kinds of correlated protein motions (with ps- or ns-timescales) and methods that can identify them. The rate-promoting vibrations we examined in the previous section are just one example of correlated protein motions. Because promoting vibrations involve residues in the immediate vicinity of donor and acceptor, it was relatively easy to identify them. In the more general case of extended correlated motions, it would be a challenge to identify residues that take part in them. In this section we describe two methods that have been successfully used for identifying atomic motions of interest, the TPS and the ED method. We will apply them to two enzymes we already studied in the previous section, LDH and PNP.

TRANSITION PATH SAMPLING

TPS was originally developed for studying rare reactive events. The most difficult problem in studying reactive events, which is hidden by the wide acceptance of TST, is to define an appropriate reaction coordinate and find the location of the TS. In addition, if one tries to simulate rare reaction events using a molecular dynamics simulation, most of the trajectories that start from the reactants will not cross to the products, and as a consequence the calculation becomes computationally not feasible, because the time step that must be used in the MD simulation is much smaller than the timescale of interest.

TPS[40,41] addresses these problems by performing a Monte Carlo search in the trajectory space. It can simulate rare events without the knowledge of a reaction coordinate or the TS. TPS needs another algorithm (molecular dynamics) to generate trajectories, while TPS itself is an algorithm for searching the trajectory space. The essence of TPS is that the chaotic nature of classical multi-dimensional systems guarantees a fast Monte Carlo search of the trajectory space.

A brief description of the algorithm follows. Let us assume a transition between R and P (i.e. reactants and products). Since R and P are long-lived states, they can accommodate equilibrium fluctuations, and can be characterized by a variable, called ''order parameter'', which can be used as a criterion for deciding whether the system is localized in R or P. Let us further assume that we somehow know one reactive trajectory that starts from R and ends in P. In the TPS algorithm we randomly select a time slice along this reactive trajectory, we perturb slightly all momenta at that time slice, and starting from that time slice and using the new momenta, we propagate (''shoot'') forward and backward in time, examining whether the new trajectory is reactive or not. In the usual Monte Carlo fashion, the

new trajectory is accepted or not, according to some probability distribution. Because of the ergodicity of classical dynamics, new trajectories are guaranteed to quickly deviate from old ones, leading to a fast sampling of the trajectory space.

An ensemble of reactive trajectories in LDH

We have applied[42] the TPS algorithm to LDH, i.e. to the enzyme in which we identified a rate-promoting vibration, as discussed in the previous section. This work, along with a paper by Schlick[43] were the first that applied the TPS algorithm to a realistic protein. By finding common features in all the harvested trajectories, one can get insights for defining an appropriate reaction coordinate, and for identifying experimental targets for future studies. Recall that LDH catalyzes the interconversion of the hydroxy-acid lactate and the keto-acid pyruvate with the coenzyme NAD. The reaction involves a double transfer: a proton transfer between the active site histidine and the C2 substrate oxygen and a hydride transfer between NC4 of the coenzyme and C2 of the substrate (see Fig. 6). In fact, there was a controversy regarding whether the transfer steps are concerted or sequential, that our study was able to resolve. Since the reaction involves bond cleavage we must use a quantum potential for describing the reactive potential surface. The details of our choice for the quantum description are explained elsewhere.[42] Below we briefly define the variables and concepts that our TPS simulation used.

Definition of the order parameter. The first step in the TPS algorithm is to define an "order parameter," i.e. a variable that describes whether the system is in the reactants, products or in an intermediate region, as shown schematically in Fig. 21. The pyruvate and lactate regions were defined by the values of the appropriate bond lengths.[42]

Decorrelation of trajectories. The goal of TPS is to generate reactive trajectories that span the whole trajectory space. We must ensure that the ensemble of trajectories

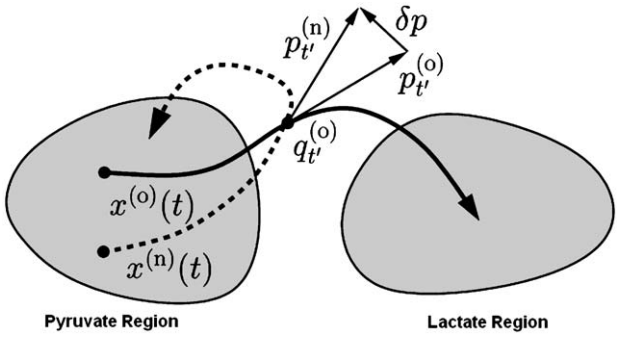

Fig. 21 Schematic representation of the TPS algorithm. The shaded regions are identified by the order parameter as reactants and products. The solid line is a reactive trajectory. A "shooting" move is shown: a time slice was chosen along the reactive trajectory, momenta were perturbed, and then the system was propagated forward and backward in time, resulting in a non-reactive trajectory shown with the dashed line.

we generated do not lie "near each other" in the trajectory space. The variable that monitors this is an autocorrelation function of the appropriate variable. This autocorrelation function is shown in Fig. 22. As can be seen, the trajectories became uncorrelated after about 30 successful iterations of the algorithm.

Results: atomic description of relevant catalytic motions

A compression of residues facilitates catalysis. We have identified a compression–relaxation sequence of residue motions that facilitates catalysis. These are the residues 31 and 65, located behind the cofactor and transferring hydride, and 106 and 195, located on the acceptor side behind the substrate, as seen in Fig. 23.

In Fig. 24 we plot various distances that reveal a compression of several residues that occurs close to the reaction event. These are taken from a trajectory with a concerted hydride and proton transfer. All graphs are plotted in the pyruvate to lactate reaction direction.

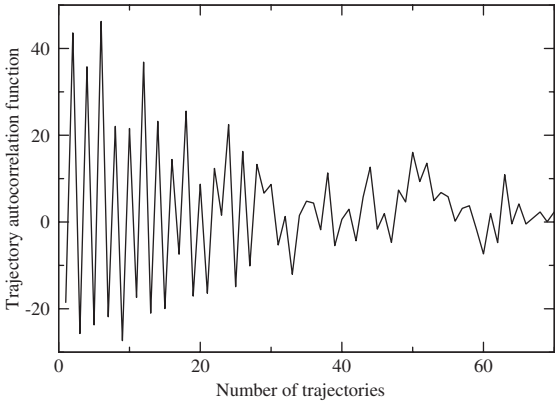

Fig. 22 Autocorrelation function for trajectories, plotted versus the number of reactive trajectories that have been generated after a given trajectory. The figure shows a decorrelation of reactive trajectories generated by TPS.

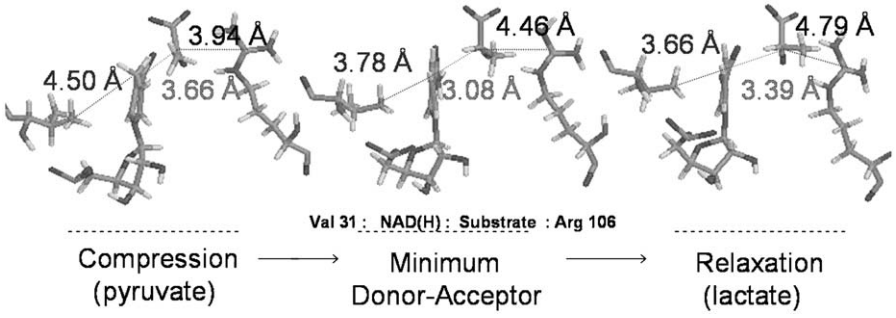

Fig. 23 Three snapshots of the compression of residues that leads to a reactive event.

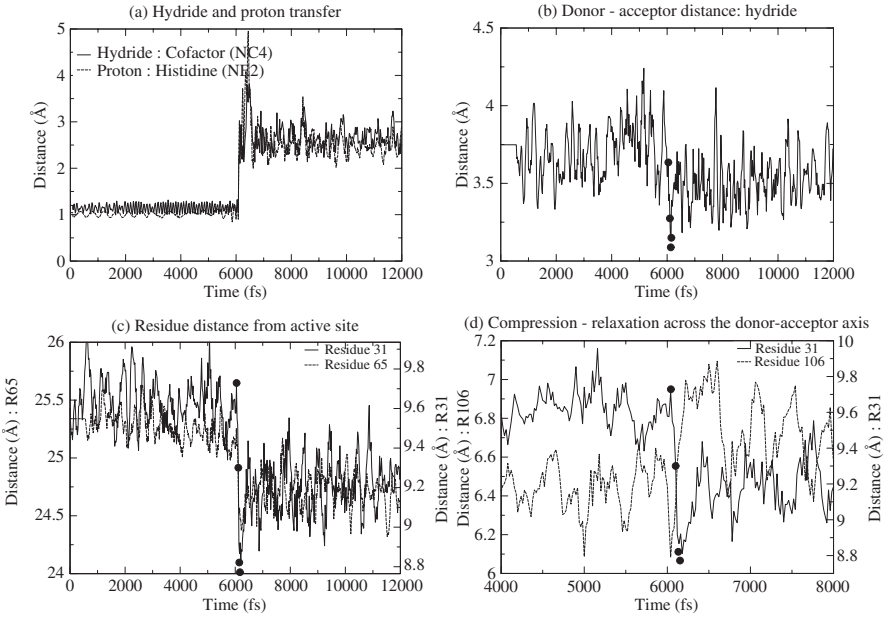

Fig. 24 Comparison of motions of donor–acceptor and surrounding residues reveals a compression-relaxation motion. See text for description of the panels.

The panels of Fig. 24 describe the following:

(a) Plots the distance of the hydride from the cofactor reactive carbon and the distance of the proton from the histidine reactive nitrogen. At time = 6100 fs the atoms begin to transfer to the substrate.
(b) Plots the donor–acceptor distance for the hydride. The minimum distance of the donor–acceptor distance, and the distance of residues Valine 31 and Arginine 106 from the active site are marked by solid circles. The hydride donor–acceptor distance reaches its minimum at time = 6132 fs. A similar plot can be drawn for the proton transfer.
(c) Plots the distance of residues 31 and 65 from the active site. They are located behind the cofactor and transferring hydride.
(d) Plots the distance of residues 31 and 106 from 4 to 8 ps. Residue 106, responsible for polarization of the substrate carbonyl bond via hydrogen bonding, initially compresses towards the active site reaching a minimum distance at 6043 fs (marked by solid circle). By 6153 fs (marked by solid circle) residue 31 has reached its minimal compression towards the active site.

The compression towards the active site revealed in Fig. 24 is what causes the donor–acceptor distances for the hydride and proton transfers to reach their minimum. When they reach their minimum, interactions across the donor, transferring atom, and acceptor are initiated. The events that occur next are critical for

completion of the reaction. The continued compression of the donor side residues towards the active site, are not only involved with bringing the donor–acceptor distance closer together, but also with shifting the entire enzyme. While the donor–acceptor distances increase again, it will be the motion of the surrounding residues that ultimately determine whether the atoms transfer. In particular, the compression of the donor side residues cause the acceptor side residues to relax away and the reaction to complete.

Concerted vs. *stepwise transfers.* We now address the question of whether the hydride and proton transfers are concerted, or whether the hydride transfer precedes the proton in the pyruvate to lactate reaction direction. Our TPS study showed that both mechanisms are possible. In Fig. 25 we show the distribution of the time lag between the hydride and proton transfer for all reactive trajectories. We note that both concerted and sequential transfers are possible, and that 74% of the trajectories have a time lag greater than 10 fs, indicating that the majority of reactive trajectories have sequential transfer steps.

Figure 26 compares two trajectories: one for concerted hydride and proton transfers with one for sequential transfers, as seen in panel (a). In panel (b) we can see that the donor–acceptor distance for the stepwise trajectory reaches its minimum first, due to the earlier combined compression of residues 31 and 106. Why does the proton take longer to transfer? If we look at panel (c) at the distance of residue 31 after it reaches its minimum, it jumps back away from the active site causing a delay in the relaxation of residue 106, as seen in panel (d), and a delay in the increase of the proton donor–acceptor distance. Soon after, panel (d) shows that residue 106 relaxes away from the active site while the donor–acceptor distance increases, completing the reaction.

Perturbation of the donor–acceptor axis and compression reaction coordinate. We will now demonstrate the effects of disrupting the compression–relaxation of the donor–acceptor axis residues close to the reactive event. For the perturbation we used the coordinates and velocities of a time slice 160 fs away from the reactive event

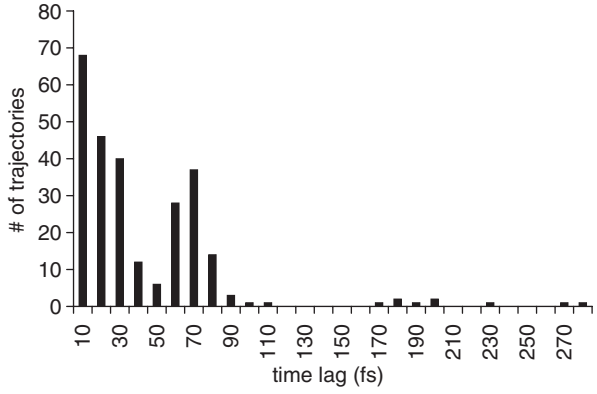

Fig. 25 Distribution of the time lag between the hydride and proton transfer.

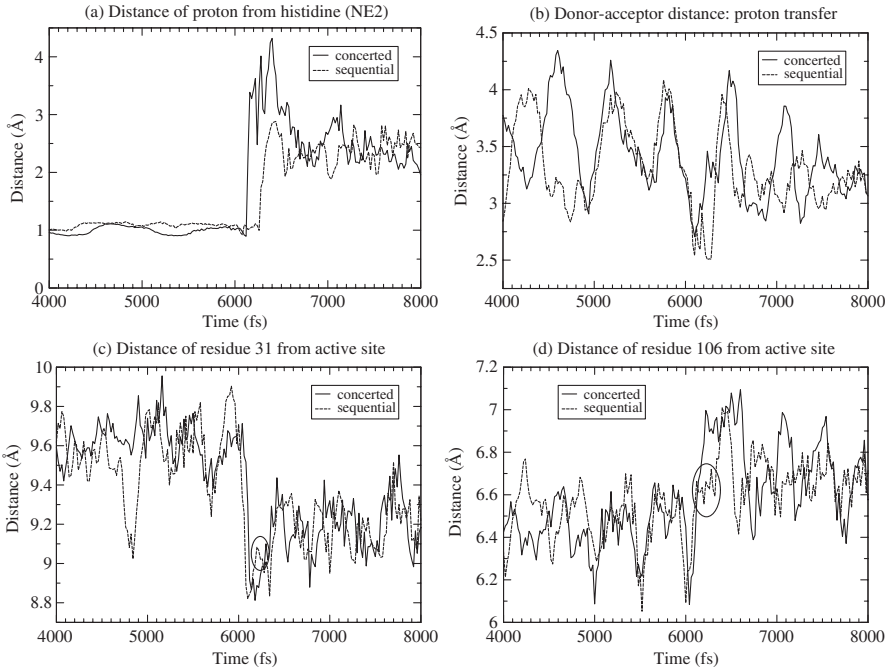

Fig. 26 Comparison of motions of donor–acceptor and surrounding residues reveals when the double transfer is sequential and when it is concerted. See text for description of the panels. The circles in the residue trajectories in the lower panels, highlight the moment the transfer event happens.

of a concerted transfer trajectory. The momenta of residue 31 were perturbed along the residue-active site axis, 1 Å away from the active site.

Figure 27 contrasts the original reactive trajectory to the perturbed one, shown in panel (a). Panel (b) shows that after a delay, the hydride donor–acceptor distance begins to deviate from the original reactive trajectory, unable to reach its minimum without the full compression of the donor side residues, i.e. 65 shown in panel (c) and the perturbed 31 (not shown). Additionally, the absence of the compression prevents the relaxation of the acceptor side residues, for example, of 106 shown in panel (d). The donor–acceptor distance comes closer, since at that time residue 106 is still compressing and the perturbed residue 31 has a weaker, delayed compression. Due to this, the hydride starts to transfer. However, since the compression–relaxation transition does not occur, the reaction is not completed.

ESSENTIAL DYNAMICS

ED (or principal component analysis), is a method commonly used for identifying large scale motions in proteins, e.g., protein folding or substrate binding. A summary of the method follows. Let $\vec{R} = (R_{1,x}, R_{1,y}, \ldots, R_{N,z})$ be the positions of the

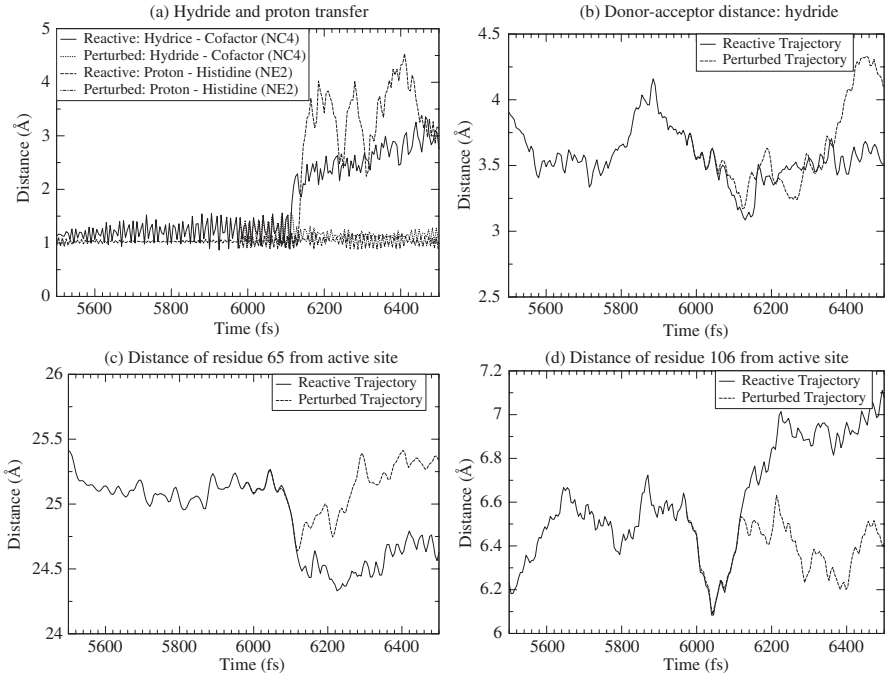

Fig. 27 How perturbation of a residue makes a trajectory nonreactive.

protein atoms. One assumes that the solution of Newton's equation of motion can be written in the following approximate form:

$$\vec{R}(t) \simeq \sum_{m=1}^{3N} a_m(t)\vec{\eta}_m \tag{13}$$

One then tries to find the coefficients and basis functions a_m, $\vec{\eta}_m$ that provide the best approximation (in a least-squares sense) of $\vec{R}(t)$ to the exact solution of Newton's equation of motion. This condition is satisfied by choosing the spatial basis set $\vec{\eta}_m$ to be the eigenfunctions of the covariance matrix

$$C_{ij} = \langle (R_i - \langle R_i \rangle)\ (R_j - \langle R_j \rangle) \rangle \tag{14}$$

where $\langle \cdots \rangle$ denotes time average over the entire MD trajectory. When a few eigenvalues of the covariance matrix are much bigger than the rest, the corresponding eigenvectors dominate the dynamics. When sorted by their eigenvalues, the ED modes are sorted according to their contribution to the total mean-square fluctuation. These few dominant modes are designed to provide a good fitting to the trajectory. In a protein, there may be concerted motions of groups of atoms (e.g., loop motions) which provide a significant number of covariant matrix elements C_{ij}, and therefore dominate the principal eigenvectors of the covariant matrix. In this case, ED separates the conformational space into an *essential subspace* containing

only a few dominant collective modes, and a remaining space which contains random atomic fluctuations.[44,45]

In Section 3, we found that protein motions in hPNP accelerate the chemical step. Now we will present an application of the ED method, used to identify protein motions that increase turnover by creating substrate binding affinity. In particular, we have studied[46] the conformational change in the 241–265 loop, and identify variations in its orientation, which is crucial in determining the substrate accessibility to the active site.

Substrate binding in PNP

As a reference for the discussion below, in Fig. 28 show a plot of the active site of PNP. We will present the experimental reasons that led us to focus our attention on the 241–265 loop. If one assumes that each X-ray crystal structure represents a possible conformation in solution, considering several crystals and their relative atomic B-factors presents an experimental view of the conformational flexibility of the protein at an atomic resolution. The relative B-factors of the C_α atoms of apo hPNP, and hPNP complexed with the TS analog Immucillin-H show that the loop residue E250 is the centroid of highly mobile region, while residues G63 and E183 are centroids of more localized mobile regions. Additionally, from the structural differences between the crystal pairs of apo hPNP–hPNP · guanine (formation of the Michaelis complex), and apo hPNP–hPNP · ImmH (formation of the TS analog

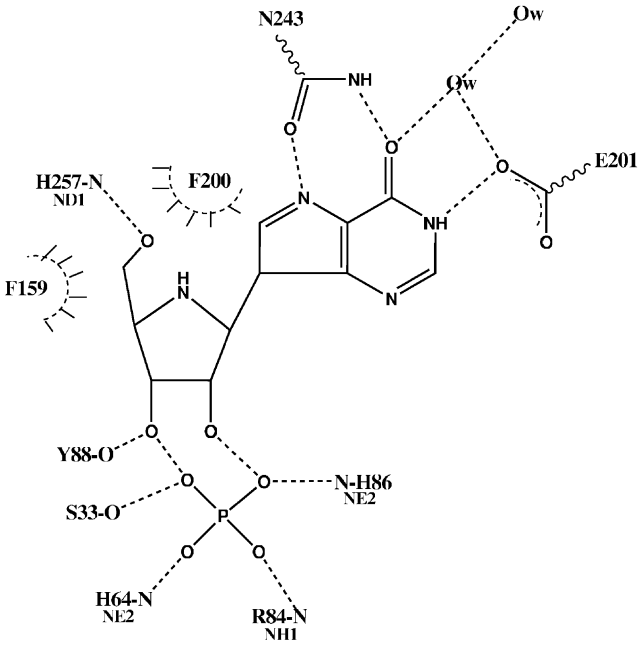

Fig. 28 Active site of hPNP with the TS analog ImmH and the phosphate nucleophile.

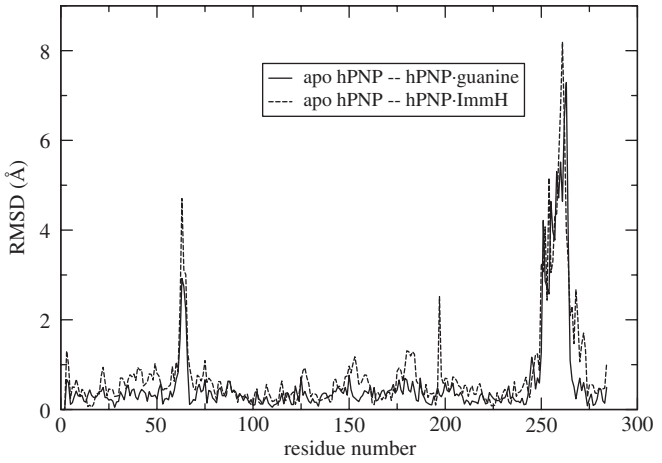

Fig. 29 Detailed root-mean-square displacement (RMSD) Å, per residue, of the geometric difference between the apo hPNP–hPNP···guanine (black), and apo hPNP–hPNP···ImmH (red) crystal structure pairs. The different RMSDs of both pairs of crystals, provide evidence that the TS analog is bound to hPNP much tighter than the substrate analog.

complex), it has been questioned whether correlated motions exist to allow the necessary conformational change of the 241–265 loop for substrate binding and turnover. It is accepted that reorganization of this flexible loop, which makes up part of the active site, is essential for allowing different substrates/inhibitors to enter the active site.[47] The loop displacement is conjectured to push the substrates towards the active center favoring more reactive configurations. In Fig. 29 we show the root-mean-square deviation of the C_α geometric difference between the apo hPNP–hPNP · guanine, and the apo hPNP–hPNP · ImmH pairs. The same geometrical difference trend appears for any combination of two apo hPNP structures with six substrate/TS analogs, confirming the substantial loop rearrangement upon substrate analog/TS analog binding.

We used principal component analysis to identify correlated motions in different forms of hPNP, namely, its apo and complexed forms, and assess whether they facilitate the 241–265 loop rearrangement prior to the subsequent phosphorolysis reaction. We compared the principal components for the apo and complexed hPNP simulations, and examined the different correlated motions for each form of the enzyme, comparing directly to the crystallographic B-factors. Finally, via experimental site-directed mutagenesis, several residues implicated in the correlated motion were mutated, and the kinetic constants k_{cat} and K_M (fingerprints of catalytic efficiency), were measured to weigh the impact of these residues in the phosphorolytic efficiency.

Results: mobile residues in the active site

We performed molecular dynamics simulations for the APO, ES, and EI-APO models. The objective of the EI-APO simulation is to capture putative concerted

motions in hPNP during the loop conformational change taking place upon going from an "E···I geometry" towards an "apo hPNP geometry", which reversibly translates into existing motions in hPNP during substrate binding and TS formation.

For the APO simulations, from the first few eigenvectors, we observed prominent correlated motions in the neighboring residues F159 and P150, adjacent to the purine substrate. Moreover, it is not surprising that G63 and E183 also show strong motions, granted their large B-factors. Additionally, to a lesser extent, the active site residues S33, H84, H86, and F200 display high mobilities. These concerted motions were observed both in a 1-ns vacuum simulation and in a solvated simulation. Overall, the most significant feature of the APO simulations is the correlated motions found in the spatially neighboring F159 and P150 residues.

In the case of the ES simulations, we found that there exist correlated motions around the F200 and E250 residues, the latter being the epicenter of the loop dynamics. To a lesser extent, residues S33 and P150 also showed concerted behavior. It is not surprising that residues H183 and N121 are involved in dynamics granted their high mobilities implied by its high B-factors. We found differences in the concerted motions between the APO and ES models of hPNP: the APO model presents concerted dynamics around the F159 and P150 residues, while for the simulation of the Michaelis complex (ES), concerted motions are mostly found around the active site residue F200 and loop residue E250. This in turn suggested that dynamics in the apo enzyme is concentrated around the residues F159 and P150, though once the substrate enters the active site, these become dormant, and active site residue F200 and loop residue E250 (embracing the purine substrate), come into action.

For the EI-APO simulations, the correlated motions were again found around the neighboring residues F159 and P150, as well as around F200, E250, and S33. This behavior resembles a combination of the APO and ES models. These results suggest these residues are coordinated in the enzyme so that it can successfully accommodate the substrate in the active site and achieve TS formation.

We observe that the three computational models (APO, ES, and EI-APO) present distinct characteristics in their correlated motions. Some similarities are found, for example, in the high mobilities of G63 and E183, in agreement with their high crystallographic B-factors. However, other residues which had not been seen as highly mobile based on their B-factors (namely F159, P150, H230, and F200), have been found to have correlated dynamics. This implies that observation of crystallographic structures alone may not be enough to infer important dynamic behavior in proteins, and that additional MD studies are needed to identify correlated dynamical modes. Finally, we have been able to successfully recognize correlated motions on the 241–265 loop, particularly present in the simulations of the Michaelis complex, and in a lesser extent in the EI-APO simulations. This suggests that the loop may have a favorable role in capturing the substrate *as well as* in the chemical step. Fig. 30 highlights the residues that were identified by the principal component analysis: note the presence of residues F159 and F200, whose involvement in binding was not obvious from B-factors alone.

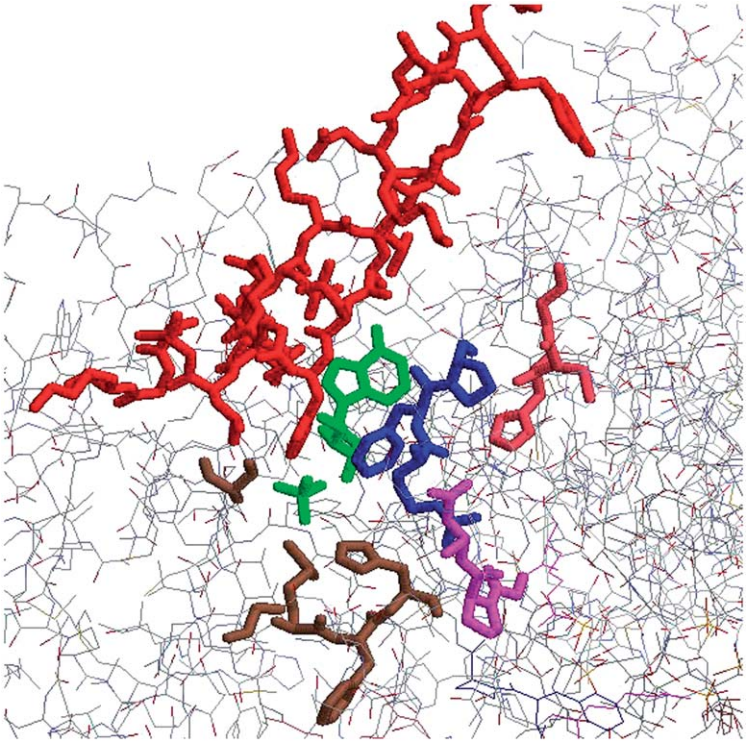

Fig. 30 hPNP with marked residues that show correlated motions: S33 (brown), H64 (brown), H86 (brown), P150 (magenta), F159 (blue), H230 (pink) and 241–265 loop (red).

Table 3 Experimental kinetic parameters for different mutants which show correlated motions in hPNP

Mutant	WT	F200G	F159G	H230G	N121G
K_M (μM)	76.8	1580	2260	145	64.9
k_{cat} (s^{-1})	32.4	3.8	2.3	2.6	33.0
k_{cat}/K_M ($10^5 s^{-1} M^{-1}$)	4.2	0.024	0.01	0.1	5.0

Experimental site-directed mutagenesis

The X-ray crystal structures indicate that all direct contacts between hPNP and the substrates guanosine and phosphate are through amino acid side chains. Our site-directed mutagenesis strategy replaced each residue with glycine in order to assess the contribution of the residue's side chain to substrate binding and/or catalysis. Results from the kinetic studies (Table 3) indicate that substrate binding affinity was most sensitive to the F159G and F200G mutations. In the phosphorolytic direction, an increase of ca. 400-fold in K_M (and modest change in k_{cat}) is observed for the

F159G mutant. Loss of the herringbone-type interaction between the β-face of the ribose and the hydrophobic surface created by this residue is important for substrate binding, thus essential for hPNP activity. Additionally, the H230G mutant showed modest changes in both K_M and k_{cat}, unexpectedly given its long distance from the active site. Finally, the N121G mutant, did not show any relevant change in catalytic efficiency, regardless of proving substantial concerted dynamic behavior during the Michaelis complex simulation.

5 Conformational fluctuations

The motions we examined in the previous sections had ps- or ns-timescales, therefore they were accessible with ordinary molecular dynamic simulations. However, it is well known that conformation fluctuations are sometimes coupled to the reaction coordinate. From a computational point of view, such effects are practically impossible to study directly. To understand the reason, let us recall the shape of the energy landscape of a protein (a description of the modern energy landscape view of biomolecules can be found in the recent textbook of Wales[48]). It consists of a very large number of local minima (conformations), separated by barriers whose height ranges from moderate to high (left panel of Fig. 32). The time evolution of the system in this landscape consists of relatively long periods of oscillations in the local minima, separated by hops between conformations (Fig. 31).

The rate-promoting vibrations we examined earlier are fluctuations within a single conformation. The problem we want to address is, whether there are some conformations which favor catalysis, for example, because in them the average

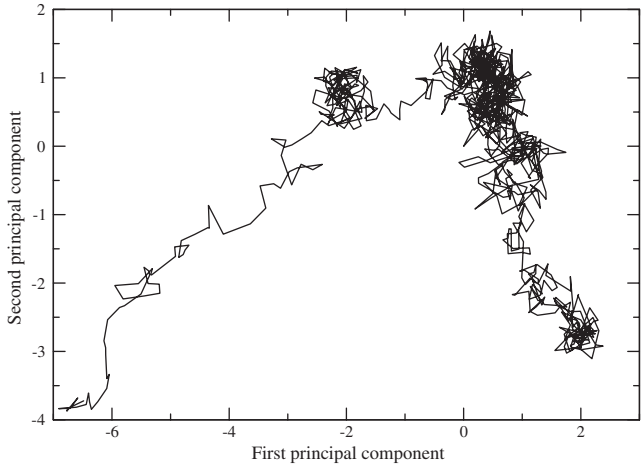

Fig. 31 A 100 ps MD trajectory of PNP, plotted in the plane of the two largest principal components. The two darker regions, where the trajectory fluctuates locally, are two conformations. If we are interested in sampling many conformations, the long time the system spends in local fluctuations in a given conformation, is a waste of resources.

donor–acceptor distance is shorter. To study this problem, we would like to have our molecular dynamics trajectory visit as many conformations as possible. However, the system spends most of its time in fluctuations within a conformation local minimum, and only rarely hops to a different conformation minimum. Therefore, MD simulations may be useful for studying other problems, but they are not a practical tool for searching the conformation space. However, there are other techniques that may be useful. In the rest of this section, we will first briefly review recent work on conformation fluctuations that enhance tunneling in DHFR; we will close with a computational scheme we propose for studying this class of problems.

DIHYDROFOLATE REDUCTASE

DHFR catalyzes the reduction of 7,8-dihydrofolate (DHF) to 5,6,7,8-tetrahydrofolate (THF) through the oxidation of the coenzyme NADPH. DHFR has been studied extensively due to its role in maintaining intracellular pools of THF, which is an important component of several metabolic pathways. The reaction catalyzed by DHFR is thought to involve transfer of a proton followed by a hydride to DHF.

It has been shown through nuclear magnetic resonance (NMR) studies[49,50] that the catalytic cycle involves conformational changes of the M20 loop. This mobile loop is close to the active site and is assumed to play an important role in binding of the cofactor and substrate to DHFR. Also, mutational studies have identified distal residues[51] that affect catalysis. These studies strongly suggest that conformational changes are related to catalysis.

In addition, classical MD simulations[52] have identified correlated domain motions in the reactant DHF complex but not in product complexes, indicating they are related to catalysis. These domains are in the same regions highlighted by the NMR studies.

We will only present a very brief review of theoretical studies on this system and refer to reader to publications of the groups that have studied it.[53–55] Since the catalytic step involves a hydride transfer, a major difficulty is how to treat quantum effects. These works followed different paths.

Truhlar, Gao, and Garcia-Viloca[53] use a geometric reaction coordinate, the difference between acceptor-hydrogen and donor-hydrogen distances. The system is divided into a small primary zone at the active site, and a secondary zone. The results are averaged over several secondary zone configurations. Electronic quantum effects are included with a semi-empirical QM/MM potential that is augmented with a valence bond term, parametrized to fit the experimental free energies. The free energy profile is calculated with an umbrella sampling along the above reaction coordinate. Brooks and Thorpe,[55] also used a semi-empirical QM/MM potential. Only structures from the reactant side were used, and those with donor–acceptor distance smaller than 2.5 Å were used in the QM/MM calculations. For each of these configurations, a QM/MM optimization was performed for a series of fixed hydrogen-acceptor distances. Only atoms within 10 Å from the transferring hydrogen, were allowed to move. Hammes-Schiffer[54] used as a reaction coordinate the

energy difference between reactant and product diabatic states, averaged over the ground state of the vibrational wavefunction of the transferred hydrogen. Electronic quantum effects are included through an EVB potential, parametrized to fit experimental free energies of activation. The free energy profile is generated by sampling over the entire range of that collective reaction coordinate. Once the energy profile is found, they used TST to calculate the reaction rate. Note that in real time the protein dynamics may need e.g., 1 ms to move along the reaction pathway of the reactive coordinate used in these works, so the generation of the energy profile allowed them to describe an event that requires time longer than any feasible molecular dynamics trajectory.

There is a long-standing debate whether approaches that calculate the free energy barrier using a geometric reaction coordinate can sufficiently sample protein conformations and whether methods that use the energy gap as the reaction coordinate are superior. In the present system, it has been shown[53] that the two methods generate equivalent results. In fact both methods produced similar free energy profiles.

Coming back to the work of Truhlar and coworkers,[53] and Hammes-Schiffer,[54] after they generated a free energy profile along their choice of reaction coordinate, the next step was to examine the ensemble of conformations used to generate a point on the energy profile, and generate statistics and comparisons for various geometric characteristics along the energy profile. They both found a correlation of structural changes as the system approaches the TS, which show a tightening of some hydrogen bonds and of the donor–acceptor distance.

We should emphasize that the structural changes found in those works were not motions in real time. Even if it is true that conformational changes affect catalysis, it is not clear if the enhancement of the rate is due to a coupling to the motion of the hydride, or due to different thermodynamic averages, for example, because the transfer distance became shorter. The fact that in the calculations of Thorpe and Brooks,[55] most of the enzyme was held fixed, is an indication that the effect is structural rather than dynamical. In this last work, a wide range of barrier heights was found, which led to questioning whether approaches that are based on mean field potentials can capture the range of protein conformations that led to that range of energy profiles. Various opinions on these questions can be found in the original papers.

To avoid semantic confusion we should clarify that Hammes-Schiffer uses the term ''promoting motion'' to describe an ensemble of conformations that, for example, have a shorter donor–acceptor distance. The ''motion'' in her case is the implied intra-conversion among these conformations. The ''promoting vibration'' we described earlier refers to fluctuations within a single conformation. The two effects are different and occur in separate timescales.

The identification of the way conformation fluctuations in DHFR affect particular distances at the TS, is a significant achievement. There are some details that maybe improved, but we should emphasize that the point we will make this is not a criticism of those works, but rather of the limitations of simulations that are currently possible. These simulations identified distances that change in the TS, but they can't distinguish if they must change in a particular order (e.g., as found with TPS in

LDH). Also, they generated an ensemble of conformations near the TS, but since they have no notion of time, they cannot give details of how the system samples the conformations. In the next section we will propose a scheme that may provide a starting point for a discussion that will address these questions.

A PROPOSED SCHEME FOR SEARCHING THE CONFORMATION SPACE

It would be desirable to have a more systematic method for searching for conformation fluctuations that are coupled to the reaction coordinate. In the rest of this section, we will propose a computational scheme that tries to address this problem. This scheme is unpublished work. It consists of three elements:

(1) The topological structure of the conformation space.
(2) A computational scheme (kinetic Monte Carlo) for describing dynamics in the conformation space.
(3) An algorithm (string method) for calculating energetic barriers between conformations.

The topological structure of conformation space

It is well known that conformations that have similar geometries have similar energies, but the opposite is not true, conformations that are unrelated may accidentally have similar energies. In addition, long MD runs that visit several conformations, sample geometrically similar conformations. The above observations suggest that conformations populate their configuration space in some structured way. The structure of the conformation space was studied by Berry and Kunz,[56] Becker and Karplus,[57] and Becker.[58] They termed it "topological" structure because the key in the description is neither geometrical similarity nor energy, but rather a connectivity concept, i.e. given a conformation, which other conformations are accessible to it, and how many saddle points are crossed by the pathway that connects them.

Their main conclusions are summarized in Fig. 32. In the left panel, we see a free energy profile. At the energy level marked as "–1," the conformations that are

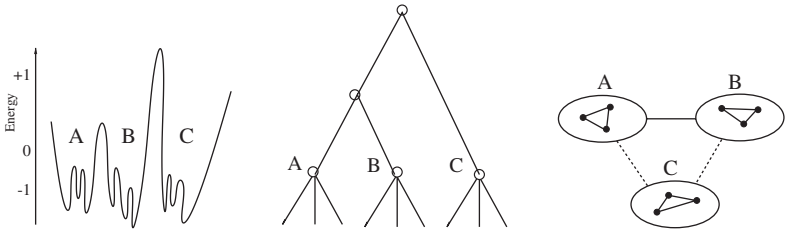

Fig. 32 The topological structure of conformation space. Left: the energetic profile. Middle: the connectivity graph. Right: the clustering of conformations into basins.

clustered under A are accessible to each other by crossing a single saddle point. The same is true for the conformations under B and under C. At the energy level marked as "0," one can go from A to B by crossing one saddle point. A group of conformations like the ones clustered A or B, is called a "basin." There are three basins visible in the diagram: A, B, and C. At the energy level marked as "+1," one can go from A to B, but to go from basin B to basin C, one has to cross another saddle point. We say that A and B belong to the same "superbasin," but C belongs to a different superbasin. The above structure is depicted in the "connectivity graph" shown in the middle panel, that shows how the various conformations and saddle points are connected. An easier to understand schematic picture is shown in the right panel: the solid dots are conformations and they are grouped in their basins. Solid lines represent transitions through a single saddle point, possible either between conformations in the same basin, or between basin A and B. Basins A and B are connected to basin C by a dashed line, in order to signify that they belong to a different superbasin and one has to cross 2 saddle points instead of 1, for a transition to C.

Becker and Karplus[57] classified in this manner all the minima and saddle points of a small peptide, met-enkephalin, and found the topological structure shown in Fig. 32. It should be noted that Frauenfelder and Wolynes,[59] from their analysis of experimental data, had predicted earlier that the energy landscape of proteins would have the topological structure shown in Fig. 32. In addition, they found that conformations that belong to the same basin are separated by low barriers of a few $k_{\mathrm{B}}T$. Basins are separated from each other by a high barrier. That is, a basin consists of geometrically similar conformations that are separated by low barriers, and is separated from another basin by a high barrier. This structure explains the observations mentioned at the beginning of this section. A constellation of basins can have various structures,[48] one of which corresponds to the well-known "funnel" landscape of proteins.[60]

From the dynamic point of view, the system frequently hops among conformations in the same basin, and it rarely hops to a different basin.

Basin hopping in the conformation space

In the beginning of this section we mentioned that even an MD trajectory that is several ns long, can sample only a few conformations. With the help of the basin picture, we now realize that the conformations sampled by MD run, all lie in the same basin. The reason is that, by definition, only these conformations are separated by low barriers, which can be overcome in the timescale accessible to MD runs. A simple corollary is that the MD run would be able to sample more conformations, if it could somehow be able to hop to a neighboring basin.

Now, imagine that we have two conformations that belong to different basins, and that we know the height of the barrier that separates these two conformations. Things become more interesting if we recall that the conformations that belong to the same basin are geometrically and energetically similar to each other, therefore we can pick any conformation as representative of that basin. We can make the

following assumption, first suggested by Berry[56] (he recently applied it to a study of small peptide[61]): each basin is represented by any conformation in it, and hopping among basins can be approximated by transitions among their representative conformations. In our case, one can use TST to describe these transitions.

This is a summary of the proposed scheme for studying dynamics in conformation space:

(1) Generate many protein conformations.
(2) Classify them into basins, and keep one representative conformation for each basin.
(3) Find the energetic barriers between these representative conformations (see next subsection).
(4) Once a set of conformations and the rates of conversions among them have been determined, we can use a standard algorithm (e.g., kinetic Monte Carlo[62]) to describe the dynamics of hopping in the conformation space.

What we gained compared to standard MD simulations, is that the extremely long trajectories required until the system hops to a different basin, have been replaced by a transition described by TST and kinetic Monte Carlo. In this way, one is able to sample many more conformations than with an ordinary MD simulation.

To connect these abstract concepts with the subject of this review paper, let us imagine that in an enzyme where proton is transferred through tunneling, there are some conformations that have donor–acceptor distance that is on average closer than other conformations. Then, conformation fluctuations that bring the protein towards these favorable for reaction conformations, will strongly enhance the rate. Unlike the rate-promoting vibrations we discussed earlier, whose timescale were so fast that several oscillations were needed before the proton is transferred, once the protein reaches a conformation in which donor and acceptor are close, it stays in that conformation for long enough time that tunneling takes place in that configuration of donor–acceptor.

The string method for finding reaction pathways

In order to implement the algorithm suggested in the previous subsection, we need a method for identifying the energetic barrier between two conformations. This is a specific case of a more general problem: given two states that lie in local minima of the energy landscape, find the MEP that connects them. This is a difficult problem that has attracted a lot of activity in the last decade.

The most successful method for identifying the MEP and energetic barrier between two stable states, is the ''nudged elastic band'' method.[63] This elastic band is a collection of system images that connect in configuration space the initial and final stable states. Adjacent system images are connected with fictitious harmonic strings. If this elastic band lies along the MEP, the force on it is equal to zero. If it is displaced from the MEP, then the forces acting on it (arising from the protein potential) will tend to return it towards the MEP. If there were no fictitious springs

that connected the adjacent system images, the images would relax towards either the initial or final stable states, i.e. the function of the springs is to keep the system images well separated. The presence of the fictitious springs guarantees that the elastic band will slide towards the MEP. The computational procedure is conceptually simple (but difficult to implement in practice): interpolate a few images between initial and final states; connect them with fictitious springs; use the protein potential to calculate the forces on the system images; Newton's equations of motion will make the elastic band slide towards the MEP.

The elastic band method has been applied with remarkable success.[63,64] However, it cannot be applied to problems that have rugged energy landscapes, like proteins. Recently, a similar method has been developed, that was designed to be applicable to rugged landscape systems. It is called the "finite-temperature string method".[65]

The difference with respect to the nudged elastic band method is the following: again, a chain of system images that connect the initial and final stable states is formed, but instead of connecting them with fictitious springs, the system images are assumed to be elements of a string of uniform density. Similarly to the elastic band, Newtonian dynamics using the protein potential makes the string slide towards the MEP, and during its descent it stretches, while keeping its property of uniform density.

The advantage of setting up the chain of images as a string rather as an elastic band, is that while for the elastic band the dynamics of the fictitious springs have to be solved explicitly (causing difficulties in rugged landscapes where the springs get stuck), the string dynamics that keeps its density uniform can be implemented with the standard SHAKE algorithm of molecular dynamics.

Recently, the string algorithm was used for finding the transition path in Alanine dipeptide. If one can apply it successfully to a large protein, then this will be the final missing link in the scheme outlined above for studying dynamics in conformation space.

References

1. Pauling, L. (1948). The nature of forces between large molecules of biological interest. *Nature* **161**, 707–709
2. Jencks, W. (1975). Binding energy, specificity, and enzymic catalysis: the Circe effect. *Adv. Enzym.* **43**, 219–310
3. Schramm, V. (2005). Enzymatic transition states: thermodynamics, dynamics and analogue design. *Arch. Biochem. Biophys.* **433**, 13–26
4. Agmon, N. and Hopfield, J. (1983). CO binding to heme proteins: a model for barrier height distributions and slow conformational changes. *J. Chem. Phys.* **79**, 2042–2053
5. Masgrau, L., Basran, J., Hothi, P., Sutclifie, M. and Scrutton, N. (2004). Hydrogen tunneling in quinoproteins. *Arch. Biochem. Biophys.* **428**, 41–51
6. Romesberg, F. and Schowen, R. (2004). Isotope effects and quantum tunneling in enzyme-catalyzed hydrogen transfer. Part I. The experimental basis. *Adv. Phys. Org. Chem.* **39**, 27–77
7. Kohen, A. (2005). Probes for hydrogen tunneling and coupled motion in enzymatic systems. In: Schowen, R., Klinman, J. and Hynes, J. (eds), *Handbook of Hydrogen, Vol. 2: Biological Aspects of Hydrogen Transfer*. Wiley, Weinheim

8. Bell, R.P. (1980). *The Tunnel Effect in Chemistry*. Chapman and Hall, New York
9. Marcus, R.A. and Sutin, N. (1985). Electron transfers in chemistry and biology. *Biochim. Biophys. Acta.* **811**, 265–322
10. Topaler, M. and Makri, N. (1994). Quantum rates for a double well coupled to a dissipative bath: accurate path integral results and comparison with approximate theories. *J. Chem. Phys.* **101**, 7500–7519
11. Schwartz, S.D. (1996). Quantum activated rates: an evolution operator approach. *J. Chem. Phys.* **105**, 6871–6879
12. Hänggi, P., Talkner, P. and Borkovec, M. (1990). Reaction-rate theory: fifty years after Kramers. *Rev. Mod. Phys.* **62**, 251–341
13. Straub, J.E., Borkovec, M. and Berne, B.J. (1987). Calculation of dynamic friction on intramolecular degrees of freedom. *J. Phys. Chem.* **91**, 4995–4998
14. Zwanzig, R. (1973). Nonlinear generalized Langevin equations. *J. Stat. Phys.* **9**, 215–220
15. Truhlar, D. (2005). Variational transition state theory and multidimensional tunneling for simple and complex reactions in the gas phase, solids, liquids, and enzymes. In: Kohen, A. and Limbach, H. (eds), *Isotope Effects in Chemistry and Biology*. Marcel Dekker, New York
16. Borgis, D. and Hynes, J.T. (1989). Proton transfer reactions. In: Cooper, A., Houben, J. and Chien, L. (eds), *The Enzyme Catalysis Process*. Plenum, New York p. 293
17. Borgis, D. and Hynes, J.T. (1991). Molecular dynamics simulation for a model nonadiabatic proton transfer reactions in solution. *J. Chem. Phys.* **94**, 3619–3628
18. Kiefer, P. and Hynes, J. (2004). Kinetic isotope effects for nonadiabatic proton transfer reactions in a polar environment: 1 Interpretation of tunneling kinetic isotopic effects. *J. Phys. Chem. A.* **108**, 11793–11808
19. Benderskii, V., Goldanskii, V. and Makarov, D. (1990). The theory of cryochemical reaction rates in the Leggett formalism. *Chem. Phys. Lett.* **171**, 91–96
20. Benderskii, V., Goldanskii, V. and Makarov, D. (1991). Low-temperature chemical reactions. Effect of symmetrically coupled vibrations in collinear exchange reactions. *Chem. Phys.* **154**, 407–424
21. Benderskii, V., Makarov, D. and Wight, C. (1994). Chemical dynamics at low temperatures. *Adv. Chem. Phys.* **88**, 1–385
22. Antoniou, D. and Schwartz, S.D. (1998). Activated chemistry in the presence of a strongly symmetrically coupled vibration. *J. Chem. Phys.* **108**, 3620–3625
23. Antoniou, D., Abolfath, M.R. and Schwartz, S.D. (2004). Transition path sampling study of classical rate-promoting vibrations. *J. Chem. Phys.* **121**, 6442–6447
24. Miller, W.H. (1976). Importance of nonseparability in quantum mechanical transition state theory. *Acc. Chem. Res.* **9**, 306–312
25. van der Zwan, G. and Hynes, J.T. (1983). Nonequilibrium solvation dynamics in solution reactions. *J. Chem. Phys.* **78**, 4174–4185
26. Bergsma, J.P., Gertner, B.J., Wilson, K.R. and Hynes, J.T. (1987). Molecular dynamics of a model S_N2 reaction in water. *J. Chem. Phys.* **86**, 1356–1376
27. Caratzoulas, S. and Schwartz, S.D. (2001). A computational method to discover the existence of promoting vibrations for chemical reactions in condensed phases. *J. Chem. Phys.* **114**, 2910–2918
28. Zavodszky, P., Kardos, J., Svingor, A. and Petsko, G. (1998). Adjustment of conformational flexibility is a key event in the thermal adaptation of protein. *Proc. Natl. Acad. Sci. USA* **95**, 7406–7411
29. Kohen, A., Cannio, R., Bartolucci, S. and Klinman, J. (1999). Enzyme dynamics and hydrogen tunneling in a thermophilic alcohol dehydrogenase. *Nature* **399**, 496–499
30. Antoniou, D. and Schwartz, S.D. (2001). Internal enzyme motions as a source of catalytic activity: rate promoting vibrations and hydrogen tunneling. *J. Phys. Chem. B* **105**, 5553–5558

31. Caratzoulas, S., Mincer, J.S. and Schwartz, S.D. (2002). Identification of a protein promoting vibration in the reaction catalyzed by horse liver alcohol dehydrogenase. *J. Am. Chem. Soc.* **124**, 3270–3276
32. Luo, J., Kahn, K. and Bruice, T.C. (1999). The linear dependence of $\log(k_{cat}/k_m)$ for reduction of NAD^+ by $PhCH_2OH$ on the distance between reactants when catalyzed by horse liver alcohol dehydrogenase and 203 single point mutants. *Bioorg. Chem.* **27**, 289–296
33. Cui, Q. and Karplus, M. (2002). Promoting modes and demoting modes in enzyme-catalyzed proton transfer reactions: a study of models and realistic systems. *J. Phys. Chem. B* **106**, 7927–7947
34. Basner, J.E. and Schwartz, S.D. (2004). Donor–acceptor distance and protein promoting vibration coupling to hydride transfer: a possible mechanism for kinetic control in isozymes of human lactate dehydrogenase. *J. Phys. Chem. B* **108**, 444–451
35. Núñez, S., Antoniou, D., Schramm, V.L. and Schwartz, S.D. (2004). Promoting vibrations in human PNP: a molecular dynamics and hybrid quantum mechanical/molecular mechanical study. *J. Am. Chem. Soc.* **126**, 15720–15729
36. Lewandowicz, A. and Schramm, V.L. (2004). Transition state analysis for human and plasmodium falciparum purine nucleoside phosphorylases. *Biochemistry* **43**, 1458–1468
37. Schramm, V.L. (2003). Enzymatic transition state poise and transition state analogues. *Acc. Chem. Res.* **36**, 588–596
38. Fedorov, A., Shi, W., Kicska, G., Fedorov, E., Tyler, P.C., Furneaux, R.H., Hanson, J.C., Gainsford, G.J., Larese, J.Z., Schramm, V.L. and Almo, S.C. (2001). Transition state structure of PNP and principles of atomic motion in enzymatic catalysis. *Biochemistry* **40**, 853–860
39. Mincer, J.S., Núñez, S. and Schwartz, S.D. (2004). Coupling protein dynamics to reaction center electron density in enzymes: an electronic protein promoting vibration in human purine nucleoside phosphorylase. *J. Theor. Comp. Chem.* **3**, 501–509
40. Dellago, C., Bolhuis, P., Csajka, F. and Chandler, D. (1998). Transition path sampling and the calculation of rate constants. *J. Chem. Phys.* **108**, 1964–1977
41. Dellago, C. and Chandler, D. (2003). Bridging the time scale gap with transition path sampling. In: Nielaba, P., Mareschal, M. and Ciccotti, G. (eds), *Bridging the Time Scales: Molecular Simulations for the Next Decade* (*Vol. 605 of Lecture Notes in Physics*). Springer Verlag, New York
42. Basner, J.E. and Schwartz, S.D. (2005). How enzyme dynamics helps catalyze a reaction, in atomic detail: a transition path sampling study, J. *Am. Chem. Soc.* **127**, 13822–13831
43. Radhakrishnan, R. and Schlick, T. (2004). Orchestration of cooperative events in DNA synthesis and repair mechanism unraveled by transition path sampling of DNA polymerase β's closing. *Proc. Natl. Acad. Sci. USA* **101**, 5970–5975
44. Amadei, A., Linssen, A.B.M. and Berendsen, H.J.C. (1993). Essential dynamics of proteins. *Proteins* **17**, 412–425
45. de Groot, B.L., Amadei, A., Scheek, R.M., van Nuland, N.A.J. and Berendsen, H.J.C. (1996). An extended sampling of the configurational space of HPr from E. coli. *Proteins* **26**, 314–322
46. Núñez, S., Wing, C., Antoniou, D., Schramm, V.L. and Schwartz, S.D. (2006). Insight into catalytically relevant correlated motions in human purine nucleoside phosphorylase, J. *Phys. Chem. A* **110**, 463–472
47. Erion, M.D., Takabayashi, K., Smith, H., Kessi, J., Wagner, S., Honger, S., Shames, S. and Ealick, S.E. (1997). Purine nucleoside phosphorylase. 1. Structure-function studies. *Biochemistry* **36**, 11725–11734
48. Wales, D. (ed.), (2003). *Energy Landscapes: Applications to Clusters, Biomolecules and Glasses*. Cambridge University Press, Cambridge, UK

49. Osborne, M., Schnell, J., Benkovic, S., Dyson, H. and Wright, P. (2001). Backbone dynamics in dihydrofolate reductase complexes: role of loop flexibility in the catalytic mechanism. *Biochemistry* **40**, 9846–9859
50. Sawaya, M. and Kraut, J. (1997). Loop and subdomain movements in the mechanism of *E. coli* dihydrofolate reductase: crystallographic evidence. *Biochemistry* **36**, 586–603
51. Rajagopalan, P., Lutz, S. and Benkovic, S. (2002). Coupling interactions of distal residues enhance dihydrofolate reductase catalysis: mutational effects on hydride ransfer rates. *Biochemistry* **41**, 12618–12628
52. Radkiewicz, J. and Brooks, C.L. (2000). Protein dynamics in enzymatic catalysis: exploration of dihydrofolate reductase. *J. Am. Chem. Soc.* **122**, 225–231
53. Garcia-Viloca, M., Truhlar, D. and Gao, J. (2003). Reaction-path energetics and kinetics of the hydride transfer reaction catalyzed by dihydrofolate reductase. *Biochemistry* **42**, 13558–13575
54. Hammes-Schiffer, S. (2004). Quantum-classical simulation methods for hydrogen transfer in enzymes: a case study of dihydrofolate reductase. *Curr. Opin. Struct. Biol.* **14**, 192–201
55. Thorpe, I. and Brooks, C. (2004). The coupling of structural fluctuations to hydride transfer in dihydrofolate reductase. *Proteins: Struct. Funct. Bioinf.* **57**, 444–457
56. Berry, R.S. and Kunz, R. (1995). Topography and dynamics of multidimensional interatomic potential surfaces. *Phys. Rev. Lett.* **20**, 3951–3954
57. Becker, O. and Karplus, M. (1997). The topology of multidimensional potential energy surfaces: theory and application to peptide structure and kinetics. *J. Chem. Phys.* **106**, 1495–1517
58. Becker, O. (1997). Geometrical versus topological clustering: insight into conformation mapping. *Proteins: Struct. Funct. Genet.* **27**, 213–226
59. Frauenfelder, H., Sligar, S. and Wolynes, P. (1991). The energy landscapes and motions of proteins. *Science* **254**, 1598–1603
60. Wolynes, P. (2005). Energy landscapes and solved protein-folding problems. *Phil. Trans. Roy. Soc. Lond. A* **363**, 453–464
61. Despa, F., Fernandez, A., Berry, R.S., Levy, Y. and Jortner, J. (2003). Interbasin motion approach to dynamics of conformationally constrained peptides. *J. Chem. Phys.* **118**, 5673–5682
62. Fichthorn, K. and Weinberg, W. (1991). Theoretical foundations of kinetic Monte Carlo simulations. *J. Chem. Phys.* **95**, 1090–1096
63. Henkelman, G., Johannesson, G. and Jonsson, H. (2000). Methods for finding saddle points and minimum energy paths. In: Schwartz, S.D. (ed.), *Theoretical Methods in Condensed Phase Chemistry*. Kluwer Academic Publishers, Dordrecht, The Netherlands
64. Evans, D. and Wales, D. (2003). The free energy landscape and dynamics of metenkephalin. *J. Chem. Phys.* **119**, 9947–9955
65. Weinan, E., Ren, W. and Vanden-Eijnden, E. (2005). Finite-temperature string method for the study of rare events. *J. Phys. Chem. B* **109**, 6688–6693

Kinetic and mechanistic studies of the reactivity of Zn–OH_n ($n = 1$ or 2) species in small molecule analogs of zinc-containing metalloenzymes

Lisa M. Berreau

Department of Chemistry and Biochemistry, Utah State University, Logan, UT, USA

Abstract

Reactive Zn–OH_n (n = 1 or 2) species are proposed in the catalytic cycles of several zinc-containing enzymes. In order to gauge the chemical factors that influence the formation and reactivity of Zn–OH_n species, synthetic model complexes have been prepared and systematically examined for biologically relevant stoichiometric and catalytic reactivity. Systems that promote the hydration of CO_2, the activation and oxidation of alcohols, and amide and phosphate ester cleavage reactions are discussed.

1 Introduction

Metalloenzymes containing a Zn–OH_n ($n = 1$ or 2) moiety catalyze a variety of chemical reactions.[1] These include CO_2 hydration, alcohol oxidation using a redox

ADVANCES IN PHYSICAL ORGANIC CHEMISTRY
VOLUME 41 ISSN 0065-3160 DOI: 10.1016/S0065-3160(06)41002-9

active NAD^+/NADH cofactor, and the hydrolysis of amide and phosphate ester groups. One approach toward elucidating detailed chemical information regarding the role of Zn–OH_n species in enzyme-catalyzed reactions involves the preparation and studies of the reactivity of small molecule analog complexes.[2] Over the past few decades, this synthetic analog approach has led to the development of a multitude of reactive model systems for zinc enzymes.[3–7] The primary purpose of this contribution is to provide a detailed description of reactive synthetic systems involving a Zn–OH_n moiety. In some cases, the stoichiometric and/or catalytic reactivity of these model systems will be compared/contrasted with reaction pathways proposed for zinc enzymes. Overall, this contribution is not meant to be exhaustive in terms of presenting all reported synthetic model systems for zinc enzymes. Instead, it is focused on a detailed presentation of kinetic and mechanistic studies of reactive complexes and builds on previous reviews that also focused primarily on reactivity.[8–14] Excellent reviews are also available that place a stronger emphasis on the structural aspects of model systems for zinc centers in metalloenzymes.[3–5]

PROPERTIES OF DIVALENT ZINC AND ZN–OH_n SPECIES

Divalent zinc has a $3d^{10}$ electron configuration and is redox inactive and diamagnetic. As a consequence of its filled shell electronic structure, ligand field stabilization effects do not influence the coordination properties of Zn(II). Instead, the coordination number of a Zn(II) center and the geometric arrangement of its ligands in a coordination complex are primarily determined by the steric and electronic properties of the ligands. An overall coordination number of four and a distorted tetrahedral geometry are most common for Zn(II) in biological systems, albeit Zn(II) centers having a coordination number of 5 are also prevalent.[5] In terms of hard–soft acid–base properties, Zn(II) is an intermediate metal ion which forms complexes with both hard (oxygen, nitrogen) and soft (sulfur) donor ligands.[1,15] Zn(II) undergoes rapid ligand exchange for monodentate ligands such as water (k_{ex} (H_2O) $= 2 \times 10^7\,s^{-1}$), which enables this metal ion to facilitate catalytic reactions. This rate of water exchange is slower than that of alkali metal ions (k_{ex} (H_2O) $\sim 10^8$–$10^9\,s^{-1}$), but faster than most other divalent $3d$ metal ions (Fe(II): $4 \times 10^6\,s^{-1}$, Co(II): $3 \times 10^6\,s^{-1}$, Ni(II), $4 \times 10^4\,s^{-1}$, Cu(II) $1 \times 10^9\,s^{-1}$).[1] In terms of ligand reactivity, it is important to note that Zn(II)–OH species exhibit nucleophilic behavior.

Zinc aqua (Zn–OH_2) species are prevalent in biological systems. When coordinated to a Zn(II) center, a water molecule can have a pK_a value that varies from ~6 to 11, with $[Zn(OH_2)_6]^{2+}$ having a p$K_a = 9.0$.[5] The position of a specific Zn–OH_2 unit in this range depends on the primary and secondary ligand coordination environment of the zinc center. A more Lewis acid Zn(II) center, and hence a lower Zn–OH_2 pK_a value, is produced when the total number of primary ligands is low (e.g. 4) and these ligands are neutral donors. For example, the Zn–OH_2 moiety in $[(THB)Zn(OH_2)]^{2+}$ (Fig. 1a) exhibits a pK_a value of 6.2.[16] This indicates that a tetrahedral $(N_{His})_3Zn(II)$–OH_2 moiety, as is found in active site of carbonic anhydrase (CA), could have a pK_a at or below physiological pH for the zinc-bound aqua

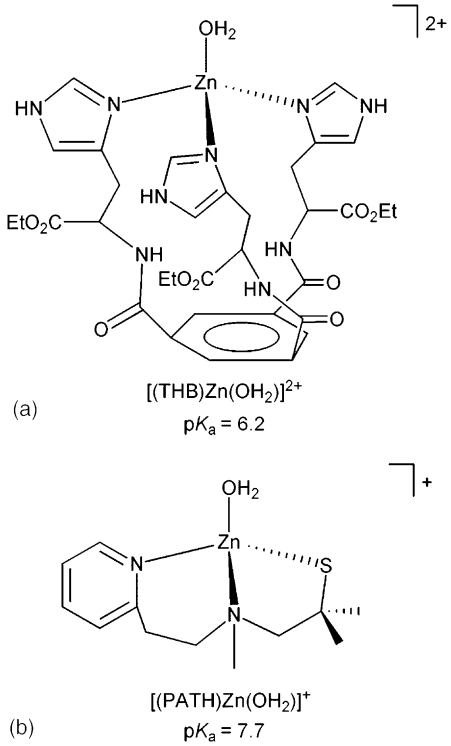

Fig. 1 Examples of four-coordinate Zn(II)–OH_2 complexes for which pK_a values have been determined. Comprehensive listings of LZn–OH_2 pK_a values for synthetic complexes have been recently compiled.[5]

ligand. Substitution of a neutral donor with an anionic ligand in the primary coordination sphere of the Zn(II) reduces the Lewis acidity of the zinc center and thus raises the pK_a of a Zn(II)–OH_2 moiety. For example, a tetrahedral $[(N_2S)Zn(OH_2)]^+$ species ($[(PATH)Zn(OH_2)]^+$, Fig. 1b) akin to the active site zinc center in peptide deformylase exhibits a pK_a value of 7.7.[17]

In terms of secondary effects, recent studies of zinc complexes supported by tripodal, tetradentate ligands indicate that the presence of intramolecular hydrogen-bonding interactions involving the oxygen atom of a zinc-bound water molecule lowers the pK_a of that water molecule.[18–20] As shown in Fig. 2, zinc complexes having a single internal hydrogen-bond donor exhibit a Zn–OH_2 pK_a value that is ~0.7–0.9 pK_a units above analogs having two internal hydrogen-bond donor groups.

ROLES FOR ZN(II) IN CATALYSIS

As zinc-containing enzymes do not exhibit spectroscopic features, such as *d–d* electronic transitions or an electron spin resonance (EPR) signal, which can be used to

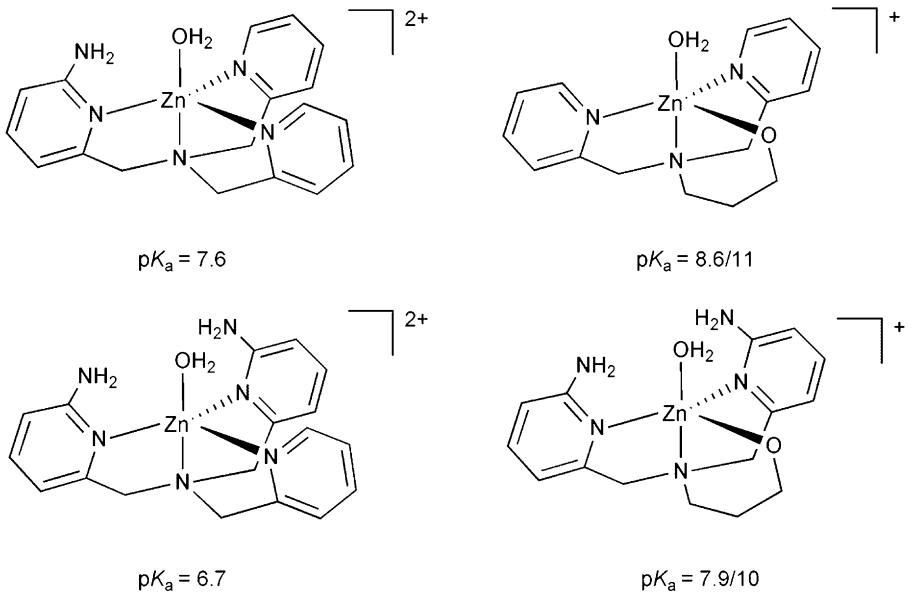

Fig. 2 Cationic portions of N_4- and N_3O-ligated Zn–OH_2 complexes having variable numbers of internal hydrogen-bond donors. The two pK_a values shown for the N_3O-ligated complexes correspond to ionization of the Zn–OH_2 and Zn–OR groups, albeit the individual values have not been assigned.

detect substrate-, intermediate-, product- or inhibitor-bound forms of the enzyme, structure–function relationships and proposed catalytic mechanisms for zinc-containing enzymes have been developed and evaluated primarily on the basis of the combined results of X-ray crystallographic, kinetic (using native and altered substrates), site-directed mutagenesis, and metal-ion substitution studies.[21,22] From these studies, it is apparent that catalytic zinc sites in metalloenzymes typically contain at least one water-occupied coordination position, in addition to three or four Zn(II)-coordinated amino acid ligands.[23] The zinc-bound water molecule can undergo one of three types of reactions within an enzyme active site. The Zn–OH_2 can (1) undergo ionization to produce a zinc hydroxide species, (2) be polarized via interaction with a catalytic base to produce a reactive nucleophile, or (3) be displaced by a substrate.[24,25] Other roles for an active site catalytic Zn(II) ion in a metalloenzyme active site can include polarization of a substrate via coordination, and/or stabilization of negative charge build-up in a transition state.

GENERAL NOTE

For the model systems described herein, when not specifically indicated, the reader should assume that the solvent is water.

2 CO_2 hydration

Carbonic anhydrases (CAs) catalyze the reversible hydration of CO_2 to form bicarbonate (Fig. 3, bottom). Four classes of CAs (α, β, γ, δ) have been identified.[26] In α-CAs, a mononuclear active site zinc center having distorted tetrahedral ligation from three histidine nitrogen donors and one water/hydroxide ligand, $(N_{His})_3Zn–OH_n$ ($n = 1$ or 2), is proposed to provide the nucleophile for CO_2 hydration.[27,28] Additionally, within the active site there is a threonine residue (Thr-199) that forms a hydrogen-bonding interaction with the Zn–OH_n moiety (Fig. 3). This threonine residue in turn forms a hydrogen bond with a glutamate residue. The secondary interaction between the Zn–OH_n moiety and Thr-199 is suggested to influence the pK_a of the Zn–OH_2 moiety, and orient the Zn–OH for nucleophilic attack on CO_2.[28,29] Notably, in a structurally characterized mutant of human CA-II (Thr-200 → His), a bound bicarbonate anion forms a hydrogen-bonding interaction involving Thr-199.[30,31] Overall, these results, combined with X-ray crystallographic studies of Co(II)-substituted human CA-II,[32] indicate that secondary hydrogen-bonding interactions are important toward influencing the chemistry of zinc-bound anions, including bicarbonate, in CAs.

A pK_a value of ~7 has been assigned to the active site zinc-bound water molecule in human CA-II.[28,33] Above pH = 7, the hydration of CO_2 is the dominant reaction, whereas below pH = 7, dehydration of CO_2 occurs. A proposed mechanism for CO_2 hydration catalyzed by a α-type CA is shown in Scheme 1. Following deprotonation of the zinc-bound water molecule, the Zn–OH acts as a nucleophile toward CO_2 to

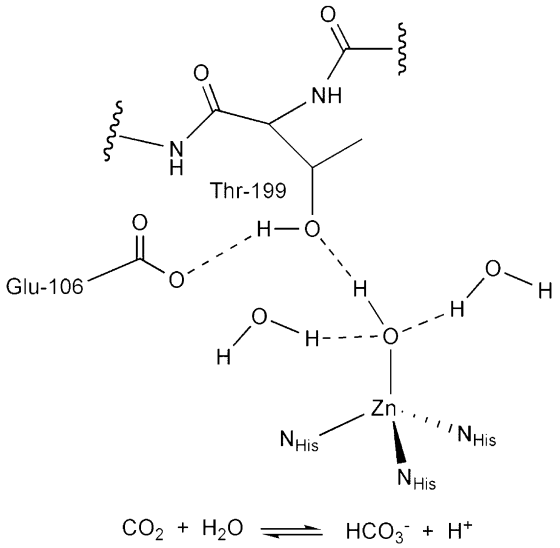

Fig. 3 (top) Active site features of a typical mammalian α-CA and (bottom) reaction catalyzed by CAs.

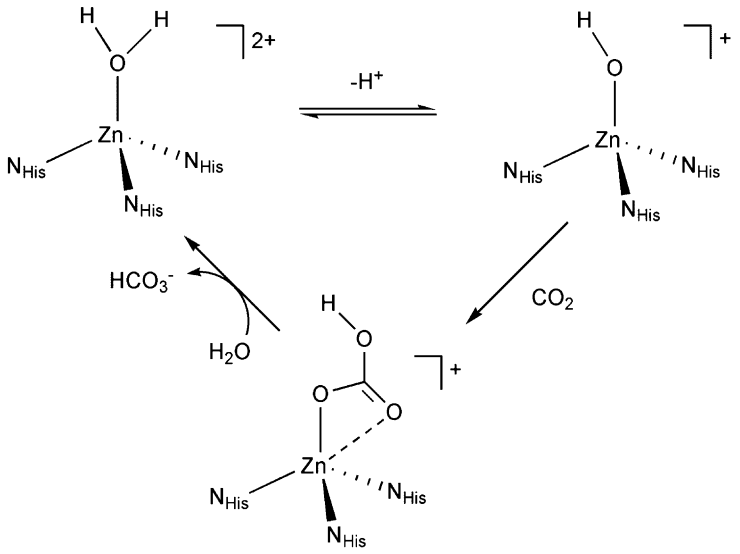

Scheme 1 Proposed catalytic mechanism of a α-type CA.

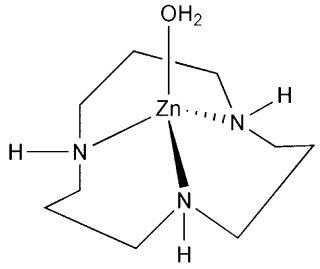

Fig. 4 [([12]aneN$_3$)Zn(OH$_2$)]$^{2+}$.

yield a zinc-bound bicarbonate anion. Displacement of the bicarbonate anion by water results in regeneration of the zinc–aqua species.[26–28,34,35]

Relatively few catalytically active model complexes for CAs have been reported. Kimura and coworkers reported a catalytically active model complex, [([12]aneN$_3$)Zn(OH$_2$)](ClO$_4$)$_2$ (Fig. 4), for α-type CAs that has been extensively examined via kinetic and mechanistic investigations.[36] This complex exhibits a p$K_a = 7.30 \pm 0.02$ (25 °C, $I = 0.1$ (NaClO$_4$)) for the zinc-bound water molecule, a value that is very similar to that found for the Zn–OH$_2$ unit in CA. Upon deprotonation, a trinuclear [([12]aneN$_3$Zn)$_3$(μ-OH)$_3$](ClO$_4$)$_3 \cdot$ HClO$_4$ species is formed, which was isolated and

crystallographically characterized. In aqueous solution, pH titration experiments indicated that $[([12]aneN_3Zn)_3(\mu\text{-}OH)_3](ClO_4)_3 \cdot HClO_4$ breaks down into two $[([12]aneN_3)Zn(OH)]^+$ cations, one $[([12]aneN_3)Zn–OH(H_2O)]^+$ cation, and four perchlorate anions.[37] Examination of the observed catalytic rate of CO_2 hydration ($(k^h_{cat})_{obs}$) versus pH (6.1–9.0) catalyzed by $[([12]aneN_3)Zn(OH)]^+$ yielded a sigmoidal-shaped curve characteristic of a kinetic process controlled by an acid–base equilibrium with a kinetic $pK_a = 7.4$. This value is similar to that found for $[([12]aneN_3)Zn(OH_2)](ClO_4)_2$ via potentiometric titration, thus indicating that the Zn–OH form of the complex is the reactive species involved in the catalytic CO_2 hydration reaction. From this data, a mechanism for the model system was proposed (Scheme 2).

Examination of the rate of bicarbonate dehydration reactivity of $[([12]aneN_3)Zn(OH_2)](ClO_4)_2$ as a function of zinc complex concentration and pH revealed that this reaction is only slightly catalyzed by the aqua ($Zn–OH_2$) form of the complex. A proposed mechanism for bicarbonate dehydration is shown in Scheme 3. Once again, the kinetically determined pK_a value matched well with that determined for $[([12]aneN_3)Zn(OH_2)](ClO_4)_2$, indicating the validity of the proposed mechanism.

Overall, $[([12]aneN_3)Zn(OH_2)](ClO_4)_2$ exhibits pH-dependent catalytic behavior for the hydration of CO_2 and dehydration of HCO_3^-. The rate-determining step of the CO_2 hydration reaction is the uptake of CO_2 by the zinc hydroxide complex. The rate-determining step in bicarbonate dehydration is substitution of the labile zinc-bound water molecule by the bicarbonate anion. The overall catalytic mechanism for both reactions is shown in Scheme 4. In considering this mechanism, it is

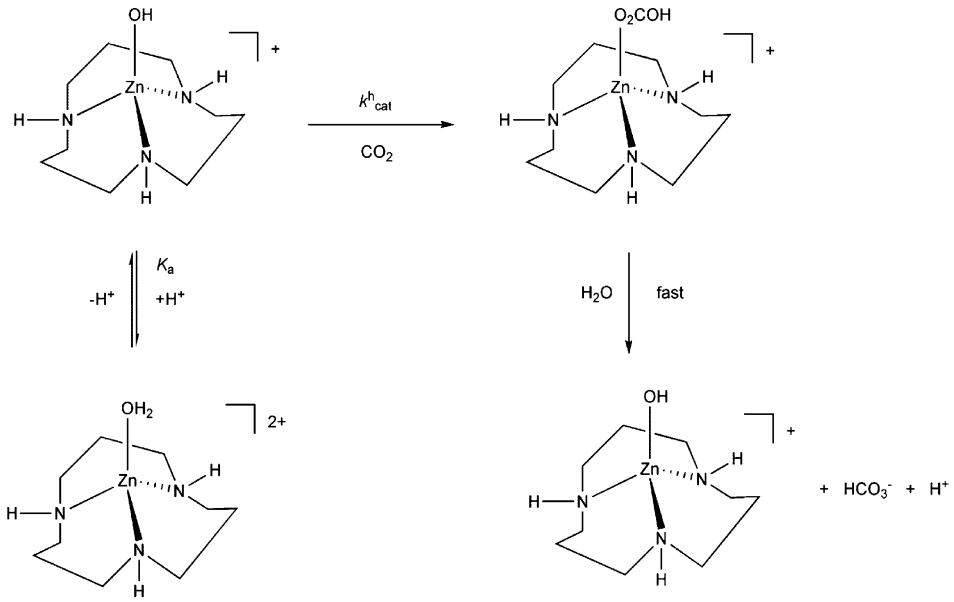

Scheme 2 Suggested mechanism for CO_2 hydration catalyzed by $[([12]aneN_3)Zn(OH)]^+$.

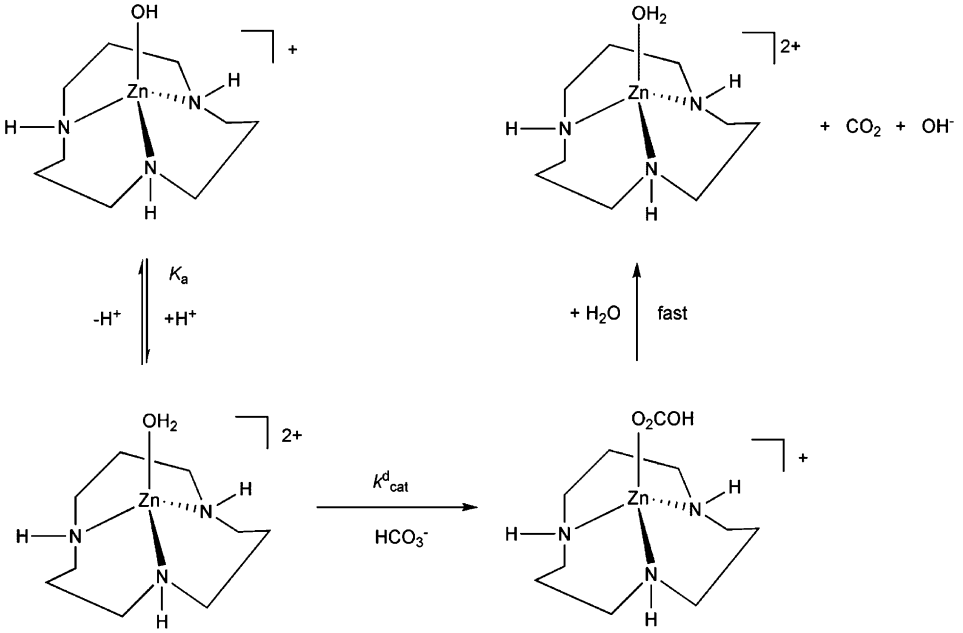

Scheme 3 Proposed mechanism for HCO_3^- dehydration catalyzed by $[([12]aneN_3)Zn(OH_2)]^{2+}$.

important to note the proton transfer processes. For example, ionization of $[([12]aneN_3)Zn(OH_2)](ClO_4)_2$ to produce the reactive zinc hydroxide species requires loss of a proton. A proton transfer process is also involved in the bicarbonate release reactivity of $[([12]aneN_3)Zn(OCO_2H)]^+$. This being the case, studies of the effect of changes in buffer type for the uncatalyzed and catalyzed hydration of CO_2 were performed. For buffers having a variety of different functional residues, no significant affect was found on the rate of either the uncatalyzed or catalyzed processes. This indicates that proton transfer is rapid and not involved in the rate-determining step of CO_2 hydration.

Similar thermodynamic and kinetic studies were performed using $[([12]aneN_4)Zn(OH_2)]^{2+}$ ([12]aneN$_4$ = 1,4,7,10-tetraazacyclododecane, cyclen, Fig. 5).[38] This complex has a thermodynamic $pK_a = 7.9 \pm 0.2$ for the zinc-bound water molecule. The hydroxide derivative of this complex, $[([12]aneN_4)Zn(OH)]^+$ ($k^h_{cat} = 3300 \pm 100\,s^{-1}$), is over five times more reactive than $[([12]aneN_3)Zn(OH)]^+$ ($k^h_{cat} = 654 \pm 57\,s^{-1}$) for the hydration of CO_2. The aqua derivative $[([12]aneN_4)Zn(OH_2)](ClO_4)_2$ ($k^d_{cat} = 51 \pm 8\,M^{-1}\,s^{-1}$) is 11 times more reactive than $[([12]aneN_3)Zn(OH_2)](ClO_4)_2$ ($k^d_{cat} = 4.7 \pm 0.6\,M^{-1}\,s^{-1}$ at 25 °C) for the dehydration of bicarbonate. While still well below the reported k^h_{cat} values for CO_2 hydration ($\sim 10^7$–$10^8\,M^{-1}\,s^{-1}$, assigned to the proton transfer step) and dehydration of bicarbonate ($k^d_{cat} \sim 10^7\,M^{-1}\,s^{-1}$, assigned to proton transfer and simultaneous release of CO_2) for α-type CAs, these complexes exhibit the highest reactivity reported to date in a model system.[33,39]

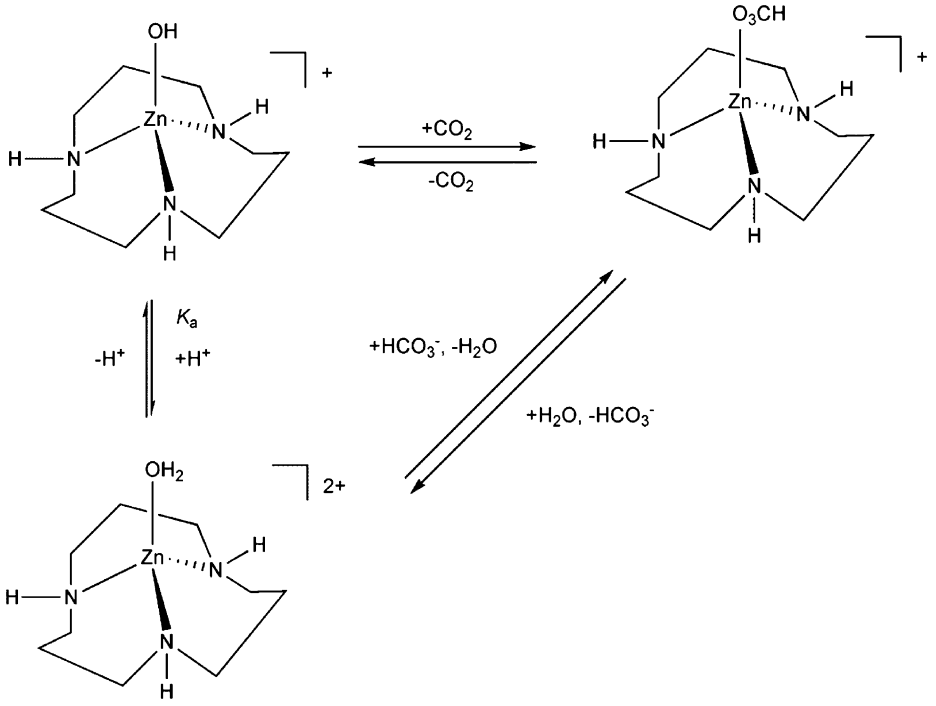

Scheme 4 Proposed mechanism for catalytic reactivity.

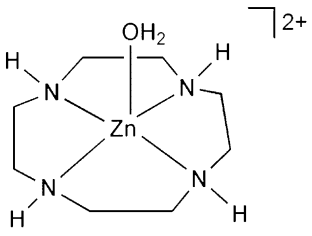

$[([12]aneN_4)Zn(OH_2)]^{2+}$

$pK_a = 7.9$

Fig. 5 $[([12]aneN_4)Zn(OH_2)]^{2+}$.

Other catalytically active species for CO_2 hydration include $[(CR)Zn–OH]^+$ ($CR = Me_2pyo[14]trieneN_4$, $k_{cat}^h = 225 \pm 23\ M^{-1}\ s^{-1}$, Fig. 6a), which exhibits a pK_a value of 8.69 at 25 °C.[40] Zinc complexes supported by tris(imidazole)phosphine-type (Fig. 6b–d) or tris(imidazole)phosphineoxide-type ligands also exhibit catalytic CO_2 hydration reactivity.[41–44] All of these complexes exhibit maximum rate constants for CO_2 hydration below $2500\ M^{-1}\ s^{-1}$ in the pH = 6–7 range. Above or below this pH

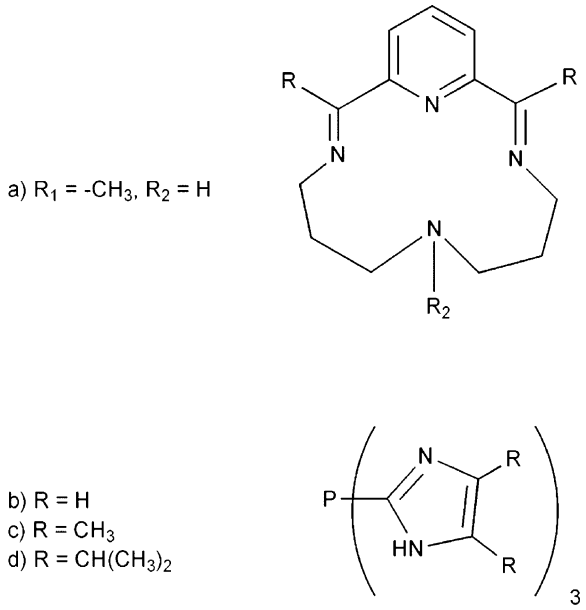

Fig. 6 Supporting chelate ligands for which catalytic CO_2 hydration reactivity has been reported for zinc derivatives.

range, the reactions are complicated by ligand protonation (low pH) or loss of Zn(II) from the chelate ligand (high pH).

The high catalytic activity of $[([12]aneN_4)Zn(OH_n)](ClO_4)_n$ ($n = 1$ or 2) derivatives in CO_2 hydration and dehydration, relative to other reported model systems, has been attributed, in part, to high stability constants for zinc binding to the supporting chelate ligand. Enhanced stability imposed by the chelate structure should make the coordinated water molecule more labile for displacement by HCO_3^-, and the zinc-bound hydroxide more nucleophilic toward CO_2.

A factor that can influence CO_2 hydration/dehydration reactivity is the overall coordination number of the zinc center and the coordination mode of a bicarbonate ligand (Fig. 7). It is reasonable to suggest that a unidentate coordinated HCO_3^- will be easier to displace, which could influence the rate of the overall hydration reaction. Data discussed below in terms of single turnover experiments supports the notion that bidentate bicarbonate coordination inhibits catalytic CO_2 hydration. Similarly, bidentate coordination of HCO_3^- could be expected to slow the dehydration reaction. Notably, X-ray crystallographic studies of bicarbonate-bound forms of a mutant CA-II, and a Co(II)-substituted form of the enzyme, have revealed both monodentate and bidentate coordination modes for the bicarbonate anion.[28,32,45]

A limitation of the above-mentioned catalytically active model systems for α-type CAs is a lack of structural characterization for the reactive species. In particular, it is of interest to independently examine, if possible, the structural and reactivity features of discrete mononuclear, tetrahedral Zn–OH, Zn–OH_2, and Zn–O_2COH

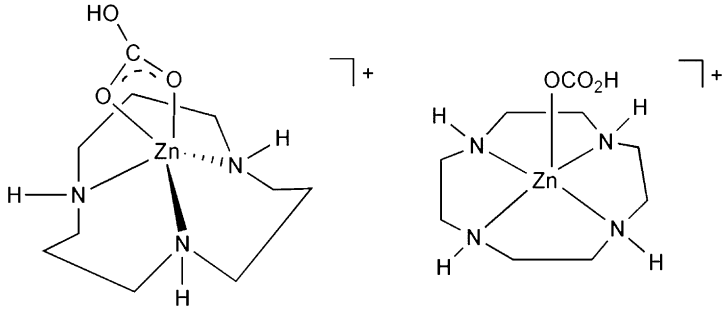

Fig. 7 Possible structures of zinc bicarbonate species supported by the [12]aneN_3 and [12]aneN_4 ligands.

complexes. In this regard, the preparation and structural characterization of mononuclear Zn–OH complexes supported by tris(imidazolyl)phosphine ($Pim^{Pri,But}$)[46] and tris(pyrazolyl)borate ($Tp^{R,R'}$)[47–49] ligands, as well as a Zn–OH_2 complex supported by the $Tp^{But,Me}$ ligand,[50] have been reported (Fig. 8).[3–5] The hydroxide complexes exhibit a Zn–O(H) bond distance (~1.85 Å) that is considerably shorter than the Zn–OH_2 (1.94 Å) distance in the zinc aqua complex {[$Tp^{But,Me}$]Zn–OH_2}{HO–B(C_6F_5)$_3$}. Of particular note in the synthetic Zn–OH_2 complex is the presence of a hydrogen-bonding interaction between the zinc-bound water molecule and the anion in the solid state. This interaction mimics that involving Thr-199 in the active site of human CA (Fig. 3).

The isolation and characterization of [$Tp^{But,Me}$]Zn–OH and {[$Tp^{But,Me}$]Zn–OH_2}{HO–B(C_6F_5)$_3$} enabled the first direct comparison of the CO_2 reactivity of tetrahedral Zn–OH and Zn–OH_2 species. Notably, while the hydroxide complex reacts with CO_2 reversibly to produce a spectroscopically identifiable [$Tp^{But,Me}$]Zn–O_2COH species,[51] the Zn–OH_2 complex is unreactive toward CO_2.[52] This comparison provides conclusive evidence to support the notion that a Zn–OH moiety is the reactive species both in α-type CA enzymes and in the catalytically active model systems described above.

The zinc carbonate complex [$Tp^{But,Me}$]Zn–O_2COH could not be isolated due to a condensation reaction with [$Tp^{But,Me}$]Zn–OH, which results in the formation of a bridging carbonate complex, {[$Tp^{But,Me}$]Zn}$_2$(μ-η^1:η^1-CO_3) (Fig. 9). However, this carbonate complex is reactive toward water to regenerate [$Tp^{But,Me}$]Zn–OH and CO_2. In this regard, in the presence of $H_2^{17}O$, [$Tp^{But,Me}$]Zn–OH catalyzes oxygen atom transfer between CO_2 and the ^{17}O-labeled water, indicating CA-type reactivity. While {[$Tp^{But,Me}$]Zn}$_2$(μ-η^1:η^1-CO_3) is reactive toward water, the zinc carbonate complex of Tp^{iPr2}, {[Tp^{iPr2}]Zn}$_2$(μ-η^1:η^2-CO_3) (Fig. 9, bottom), is unreactive. This difference is attributed to the differing coordination modes of the carbonate ligands in these complexes. Specifically, the bidentate coordination found for the carbonate ligand in {[Tp^{iPr2}]Zn}$_2$(μ-η^1:η^2-CO_3) is proposed to inhibit displacement of the carbonate ligand by water.

In regard to the reactivity of metal hydroxide complexes with CO_2, a variety of binuclear metal hydroxide complexes, supported by hydrotris(pyrazolyl)borate

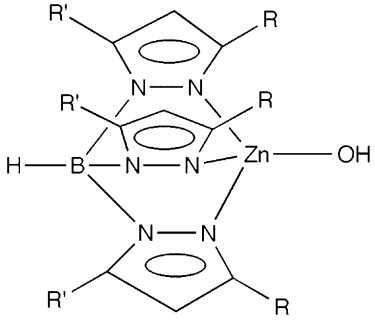

$[Tp^{But,Me}]Zn\text{-}OH$
$[Tp^{Cum,Me}]Zn\text{-}OH$

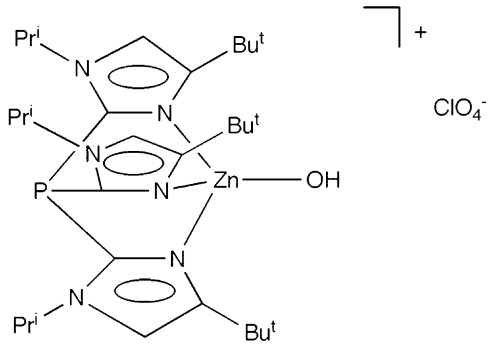

$[Pim^{But,Pri}]Zn\text{-}OH$

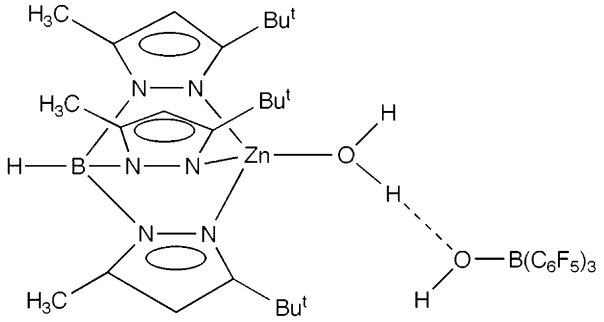

$\{[Tp^{But,Me}]Zn\text{-}OH_2\}\{HOB(C_6F_5)_3\}$

Fig. 8 Structurally characterized mononuclear tetrahedral zinc hydroxide and aqua complexes.

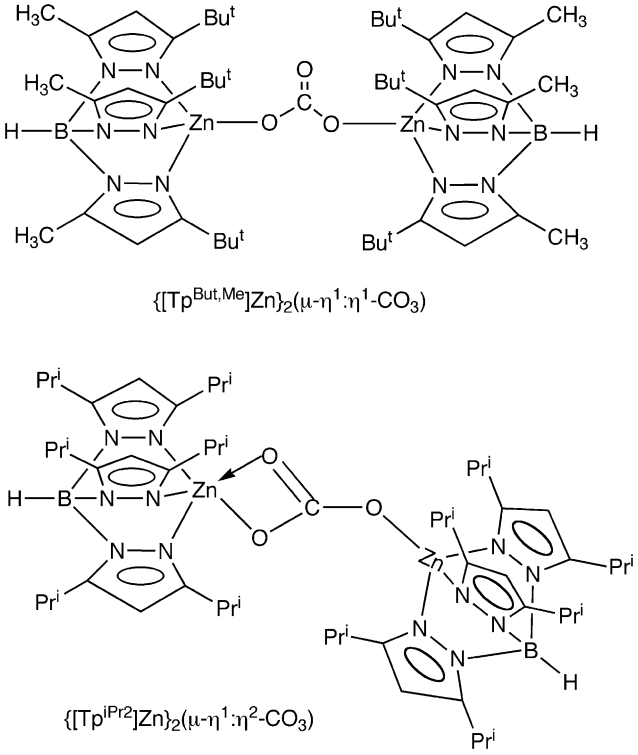

Fig. 9 Drawings of bridging bicarbonate complexes.

ligands, have been demonstrated to undergo a stoichiometric reaction with CO_2 to yield bridging carbonate complexes.[53]

An interesting, relatively unexplored area to date in terms of synthetic systems concerns the impact of secondary interactions (e.g. hydrogen bonding or hydrophobic effects) on catalytic CO_2 hydration and dehydration reactivity. As noted above, secondary hydrogen bonding likely influences the orientation and reactivity of the zinc-bound hydroxide nucleophile, as well as the coordination properties of the zinc-bound bicarbonate anion, in α-type CAs. To begin to investigate how hydrogen bonding can influence the chemistry of a Zn–OH species relevant to CAs, the CO_2 reactivity of a mononuclear zinc hydroxide complex supported by a tripodal tetradentate chelate ligand containing three internal hydrogen-bond donors, [(tnpa)Zn–OH]ClO_4 (tnpa = tris((neopentylamino)methyl)amine, Fig. 10), has been investigated.[54] In methanol solution, this complex reacts with CO_2 to produce a mononuclear zinc bicarbonate species, [(tnpa)Zn–O_2COH]ClO_4, that has been characterized by ^{1}H and ^{13}C NMR, and electrospray ionization mass spectrometry. While the X-ray crystal structure of [(tnpa)Zn–OH]ClO_4 has been reported, and moderate intramolecular hydrogen-bonding interactions involving the zinc-bound hydroxide anion were identified,[55] the solid-state structure of the bicarbonate

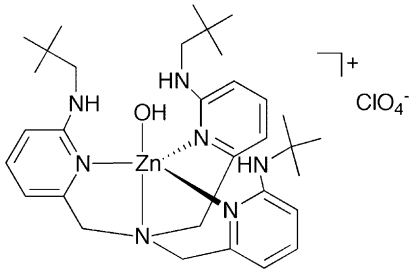

Fig. 10 [(tnpa)Zn–OH]ClO_4.

complex has not been reported. Notably, hydrogen-bonding interactions may also play a role in the CO_2 binding properties of a recently reported mononuclear zinc hydroxide complex supported by the tris(hydroxy-2-benzimidazolylmethyl)amine ligand.[56]

3 Alcohol oxidation

Zinc-containing alcohol dehydrogenase enzymes catalyze the oxidation of alcohols, or the reduction of aldehydes or ketones, using NAD^+/NADH as a required co-factor. The active site zinc center in horse liver alcohol dehydrogenase is tetrahedral and is ligated by one histidine imidazole nitrogen, two cysteine thiolates, and a water molecule.[57] A proposed catalytic cycle (Scheme 5) involves displacement of the zinc-bound water molecule by a primary or secondary alcohol substrate, followed by deprotonation of the alcohol to produce a zinc alkoxide species, which is suggested to be the active species for hydride transfer to NAD^+.[58] This hydride transfer reaction results in the formation of a zinc-bound aldehyde or ketone and NADH. Following displacement of the carbonyl compound by water, NADH is released. In this mechanism, the mononuclear distorted tetrahedral Zn(II) center is proposed to lower the pK_a of the alcohol substrate via coordination, and to stabilize the zinc-bound alkoxide species. Importantly, a nearby serine residue (Ser-48) is suggested to assist in stabilization of the zinc alkoxide via formation of a strong hydrogen-bonding interaction involving the zinc-bound oxygen atom.[58,59] From a chemical perspective, the presence of this hydrogen-bonding interaction is not surprising, as the alkoxide-bound oxygen can be expected to be a site of high electron density. This is due to the presence of filled *d*-orbitals for the Zn(II) center which prevents π-donation of electron density from the alkoxide oxygen, thus yielding a strongly polarized Zn–OR bond.[60]

Alternative mechanisms for liver alcohol dehydrogenase have also been proposed. For example, on the basis of a recent atomic resolution (1 Å) X-ray structure of horse liver alcohol dehydrogenase in complex with NADH, a proposal was put forth wherein the zinc center has a coordination number of five, with a zinc-bound water molecule being involved in protonation/deprotonation of the zinc-coordinated

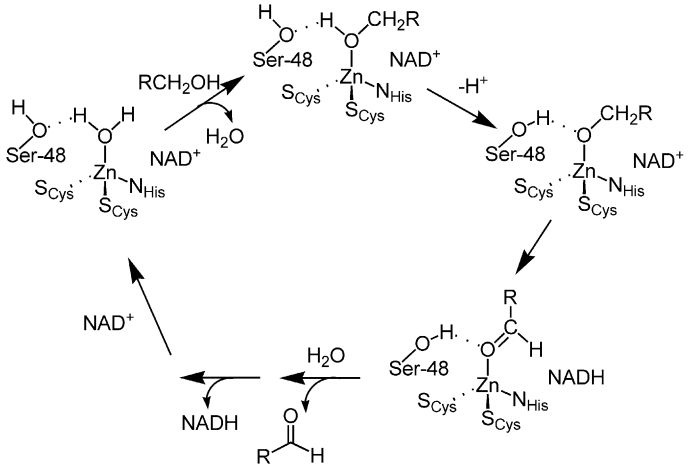

Scheme 5 Proposed catalytic cycle of horse liver alcohol dehydrogenase.

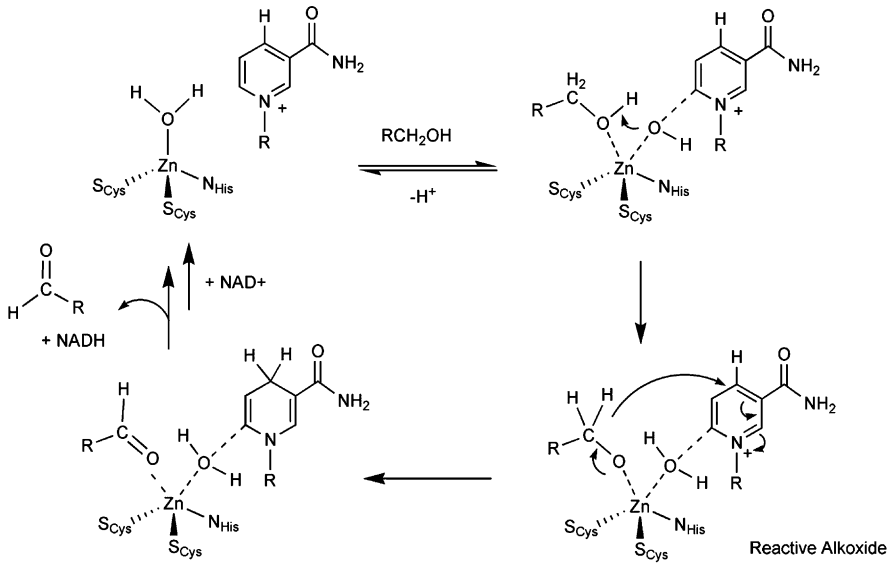

Scheme 6 Proposed mechanism for liver alcohol dehydrogenase involving a five-coordinate zinc center.

alcohol substrate (Scheme 6). Similar to the mechanism outlined in Scheme 5, a zinc alkoxide species, albeit having a coordination number of five for the metal center, is proposed as the reactive species for hydride transfer.[61] Notably, EPR spectroscopic characterization of Co(II)-substituted liver alcohol dehydrogenase, as well as time-resolved X-ray absorption spectroscopic studies of a bacterial alcohol

dehydrogenase from *Thermoanaerobacter brockii*, are consistent with the presence of a five-coordinate metal center in the presence of alcohol.[62,63]

Catalytically active model systems relevant to liver alcohol dehydrogenase are rare. In one reported system, hydride transfer between isopropanol and *p*-nitrobenzaldehyde is catalyzed by a zinc complex supported by the [12]aneN_3 ligand.[64] Specifically, heating of an isopropyl alcohol solution of *p*-nitrobenzaldehyde, containing a catalytic amount of $[([12]aneN_3)Zn(OH)]^+$ for 24 h at reflux results in the formation of $\geqslant 78$ turnovers of *p*-nitrobenzylalcohol. The source of the hydride equivalent was shown to be the methine hydrogen of $(CH_3)_2CHOH$ via labeling with deuterium ($(CH_3)_2CDOH$), which yielded monodeuterated *p*-nitrobenzylalcohol labeled at the benzylic position. This reaction is proposed to proceed via initial formation of a zinc alkoxide species, $[([12]aneN_3)Zn(OCH(CH_3)_3)]^+$ (Scheme 7). Coordination of the aldehyde to the four-coordinate zinc alkoxide species then permits hydride transfer and product formation. For this reaction to proceed, formation of the zinc alkoxide must be thermodynamically favored, and the Zn–OR bond kinetically labile.

Because *p*-nitrobenzaldehyde is a rather poor model for NAD^+, the catalytic hydride transfer reactivity of $[([12]aneN_3)Zn(OH)]^+$ in isopropanol solution was

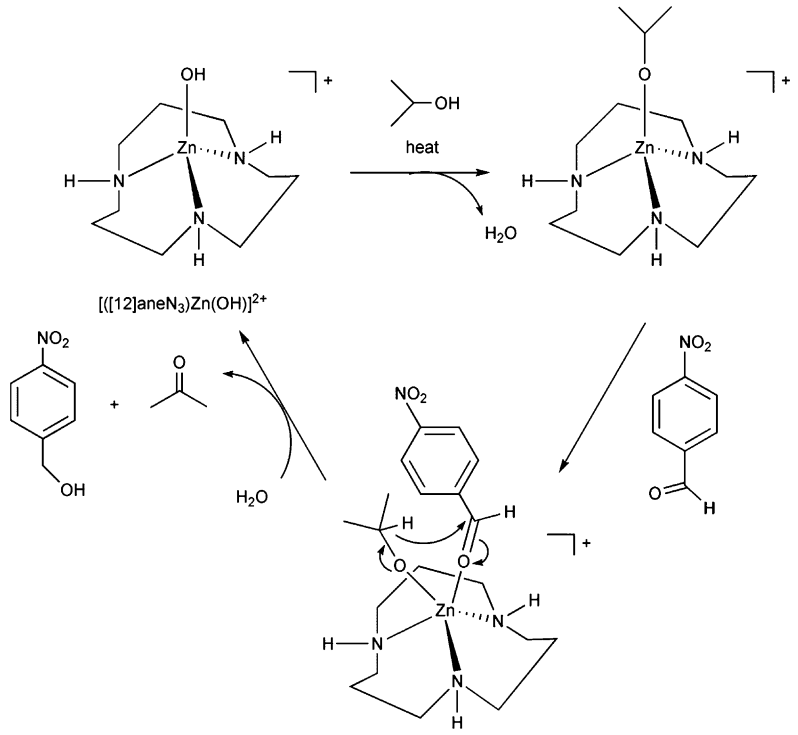

Scheme 7 Proposed mechanism for hydride transfer catalyzed by a macrocyclic zinc complex.

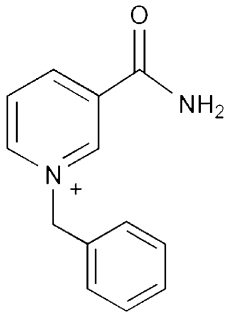

Fig. 11 *N*-benzylnicotinamide cation.

also examined using the NAD^+ mimic *N*-benzylnicotinamide chloride (Fig. 11). Though produced in low yield (17% after 24 h at reflux), formation of the 1,4-hydride transfer product is favored over the 1,6-product (~7.5:1).[64] The low overall yield of the reaction is presumably due to electrostatic repulsion between $[([12]aneN_3)Zn(OH)]^+$ and the *N*-benzylnicotinamide cation.

To examine structure/reactivity relationships for species relevant to those proposed in the catalytic cycle of liver alcohol dehydrogenase, several laboratories targeted mononuclear nitrogen/sulfur-ligated zinc alcohol and alkoxide complexes for synthesis, characterization, and reactivity studies. Preparation of these complexes required the development of new chelate ligands. For example, Parkin and Vahrenkamp employed thioimidazole derivatives to prepare new S_3- and N_2S-donor chelate ligands that enabled the isolation of rare pseudo-tetrahedral zinc alcohol complexes (Fig. 12).[65,66] These complexes exhibit Zn–O(alcohol) bond distances (1.970(3) and 1.993(3) Å) that are similar to that found in a pentafluorobenzylalcohol-bound structure of liver alcohol dehydrogenase (2.0 Å).[67] Also, both complexes exhibit a hydrogen-bonding interaction between the zinc-coordinated alcohol and another molecule of alcohol in the crystalline lattice. These secondary interactions are characterized by O···O heteroatom distances of ~2.58 Å, which is similar to the distance involving a zinc-bound alcohol and Ser-48 (2.6 Å) in an X-ray structure of liver alcohol dehydrogenase.[67]

Deprotonation of the zinc alcohol complexes shown in Fig. 12 to produce zinc alkoxide species has not been reported. Instead, mononuclear, tetrahedral zinc alkoxide complexes, supported by hydrotris(pyrazolyl)borate ligands, ($[Tp^{But,Me}$ or $Tp^{Ph,Me}$, Scheme 8), have been generated via treatment of zinc hydride precursor complexes with aliphatic alcohols.[68–70] A zinc ethoxide complex, $[Tp^{But,Me}]Zn–OEt$, was also prepared via decarboxylation of the ethyl carbonate complex, $[Tp^{But,Me}]Zn–OC(O)OEt$.[49] X-ray crystallographic studies of $[Tp^{Ph,Me}]Zn–OCH_3$ and $[Tp^{But,Me}]Zn–OEt$ revealed Zn–O bond lengths of 1.874(2) and 1.826(2) Å, respectively.[68,71] These bond distances are $\leqslant$0.1 Å shorter than found for the alcohol complexes shown in Fig. 12.

The alkoxide complexes are very water sensitive, forming equilibrium mixtures with the corresponding zinc hydroxide complex (Scheme 8) that lie far toward

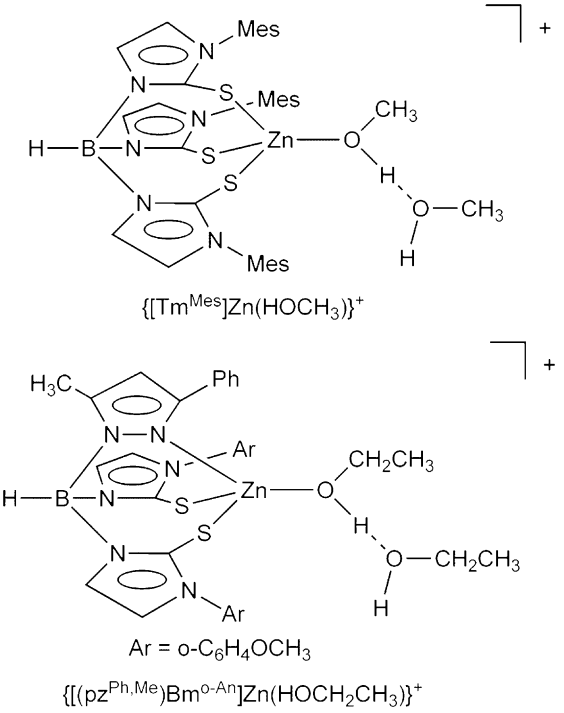

Fig. 12 Mononuclear tetrahedral zinc alcohol complexes.

the hydroxide derivative.[68,69] This indicates that in a hydrophobic secondary microenvironment, zinc alkoxide species are unstable with respect to hydrolysis. Examination of the equilibrium parameters for the methanolysis of $[Tp^{But,Me}]Zn–OH$ as a function of temperature yielded $\Delta H_{Me} = 1.2(1)\,kcal\,mol^{-1}$ and $\Delta S_{Me} = -9(1)\,eu$.[69]

Mononuclear zinc aryloxide complexes supported by hydrotris(pyrazolyl)borate ligands have enhanced stability with respect to hydrolysis (Scheme 8) as compared to the alkoxide derivatives, and can in some cases be prepared directly from the reaction of the corresponding zinc hydroxide or methoxide complex with the appropriate phenol.[69,72,73] Overall, the hydrolytic stability of each zinc aryloxide complex depends on the electronic properties of the parent phenol, with zinc aryloxide complex formation being favored for phenols having an electron-withdrawing substituent in the para position. This is evident by comparison of the equilibrium constants for the reaction of $[Tp^{But,Me}]Zn–OH$ with 4-nitrophenol ($K = 3.5(8) \times 10^3$) and *p*-methoxyphenol ($K = 4.2(9)$) at 300 K. Construction of a Hammett plot for equilibria involving a variety of substituted phenols yielded a log K versus σ plot with good linear correlation and a ρ value of 2.8.[69] DFT calculations indicate that the trend in the Hammett plot is due to the electron-withdrawing substituent enhancing the Zn–OAr bond dissociation energy to a greater extent than the H–OAr bond dissociation energy of the parent phenol. This can be rationalized by the fact

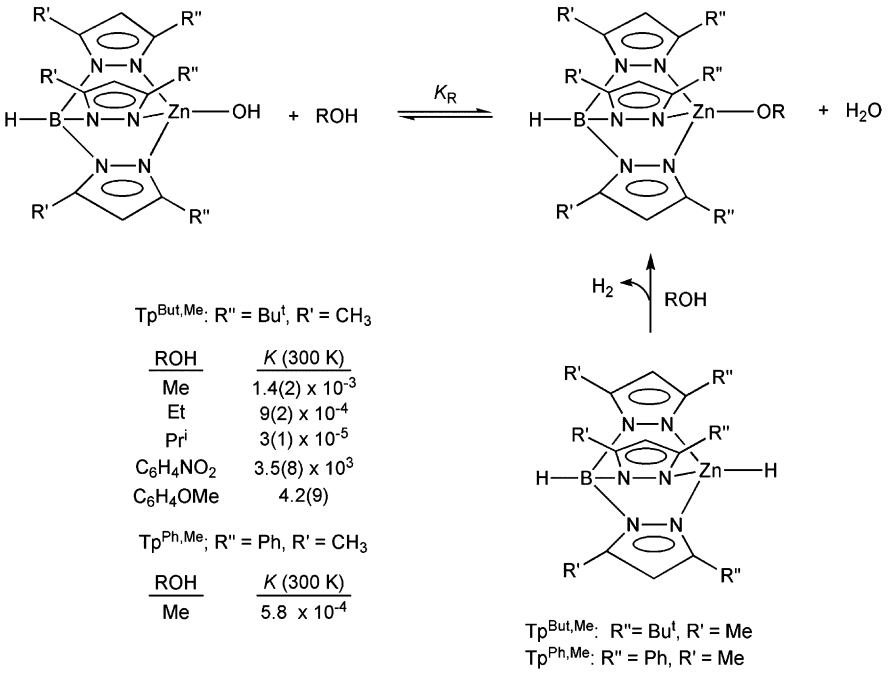

Scheme 8 Equilibrium formation of tetrahedral zinc-alkoxide and aryloxide complexes. The alkoxide complexes can be independently prepared via treatment of a zinc hydride precursor complex with the appropriate alcohol. Experimental methods for the determination of K_R (300 K) are given in reference 69.

that the more polar Zn–OAr bond would be influenced to a greater extent by an electron-withdrawing substituent than would the H–OAr bond. In the zinc complex the electron withdrawing substituent will help stabilize the enhanced anionic character at the aryloxide oxygen atom.

Similar to the hydrotris(pyrazolyl)borate zinc aryloxide complexes described above, mononuclear zinc complexes having an arylmethoxide ($-OCH_2C_6H_4-p-NO_2$, $-OCH_2C_6F_5$, $-OCH_2C_6F_5$) or alkylated methoxide ($-OCH_2CF_3$ (Scheme 9), $-OCH_2CCl_3$) group with electronegative substituents can be isolated directly from the reaction of a zinc hydroxide complex with the parent alcohol.[70,72]

In a model reaction for liver alcohol dehydrogenase, the zinc ethoxide complex $[Tp^{But,Me}]$Zn–OEt reacts stoichiometrically with *p*-nitrobenzaldehyde in benzene to produce $[Tp^{But,Me}]Zn–OCH_2C_6H_4NO_2$ and acetaldehyde (Scheme 10).[68] For a series of similar reactions involving the zinc isopropoxide complex $[Tp^{Ph,Me}]Zn–OCH(CH_3)_2$ and various aromatic aldehydes in toluene (Scheme 10), the zinc-containing products of the reaction, $[Tp^{Ph,Me}]Zn–OCH_2Ar$, were isolated in 60–70% yield, while the acetone produced was identified using ^1H NMR.[70]

Reaction of the hydrotris(pyrazolyl)borate zinc alkoxide complex $[Tp^{Cum,Me}]$Zn–OiPr with the NAD^+ mimic *N*-benzylnicotinamide chloride in isopropanol yielded a

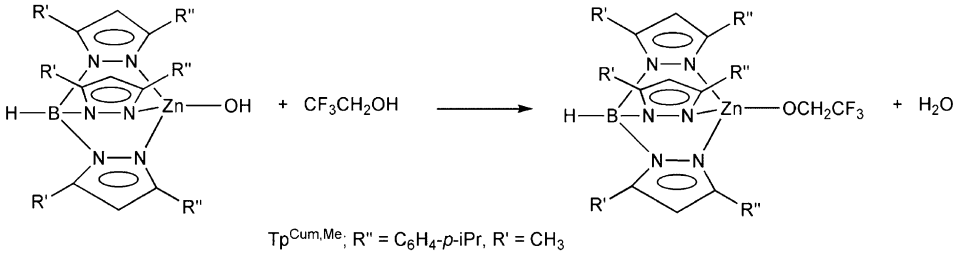

Scheme 9 Reaction of a zinc hydroxide complex with trifluoroethanol.

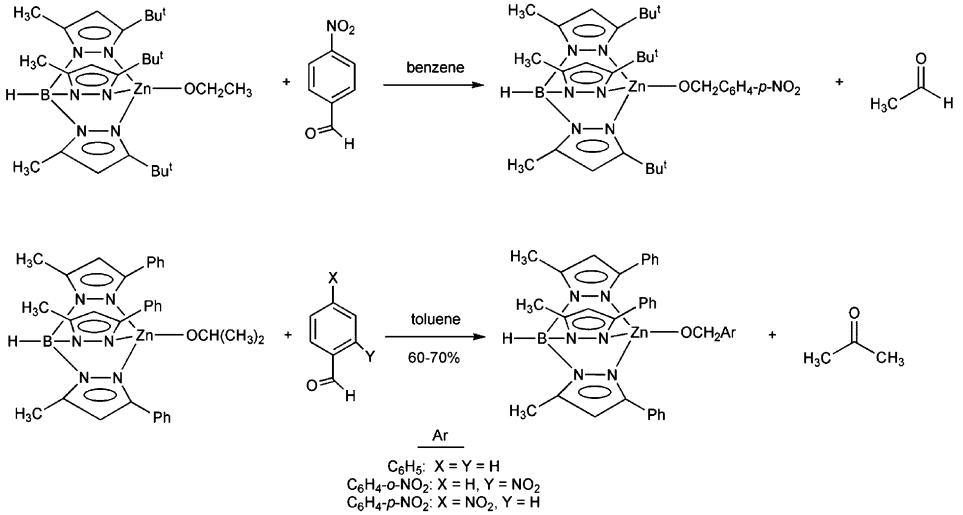

Scheme 10 Hydride transfer reactivity of zinc alkoxide complexes.

variety of products in low yields.[74] These include acetone (10–20%), as well as the zinc chloride complex [Tp^{Cum,Me}]Zn–Cl, reduced *N*-benzylnicotinamide (14%), and the radical coupling product $(BNA)_2$ (1%).

Overall, studies of hydrotris(pyrazolyl)borate-ligated zinc complexes have provided valuable insight into the chemical factors governing the formation, structural properties, and hydrolytic reactivity of tetrahedral zinc alkoxide complexes. However, the low hydride transfer reactivity of these alkoxide complexes indicates that additional factors, including perhaps secondary hydrogen-bonding interactions involving the protein, likely influence catalytic activity in alcohol dehydrogenases. To gauge the influence of hydrogen bonding on the chemistry of zinc alkoxide and hydroxide species, a new ligand (ebnpa, *N*-2-(ethylthio)ethyl-*N,N*-bis(6-neopentylamino-2-pyridylmethyl)amine, Scheme 11) was developed which combined a nitrogen/sulfur donor environment with internal hydrogen-bond donors.[75] Treatment of

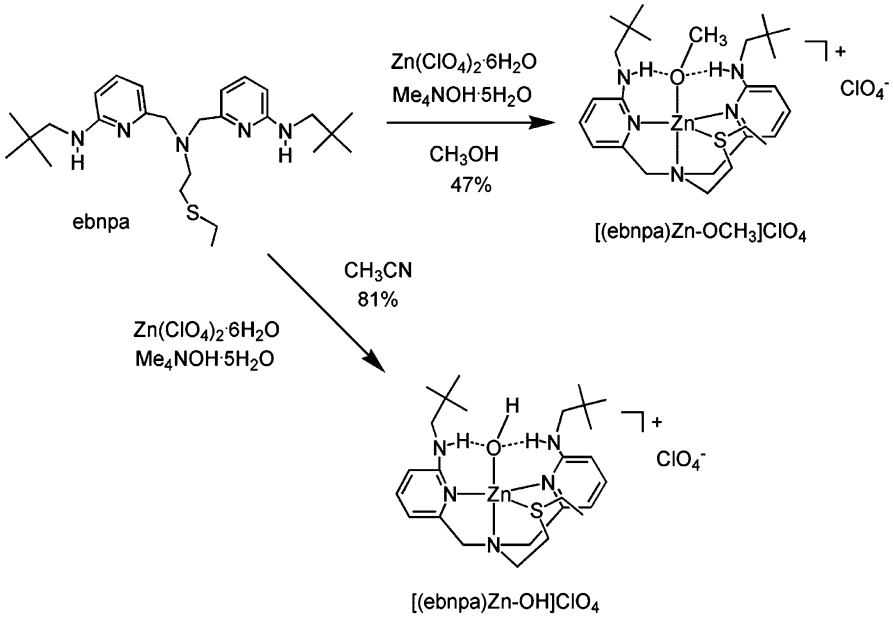

Scheme 11 Preparative routes for [(ebnpa)Zn–OCH_3]ClO_4 and [(ebnpa)Zn–OH]ClO_4.

the ebnpa ligand with equimolar amounts of $Zn(ClO_4)_2 \cdot 6H_2O$ and $Me_4NOH \cdot 6H_2O$ in methanol yielded [(ebnpa)Zn–OCH_3]ClO_4, a mononuclear N_3S-ligated zinc methoxide complex (Scheme 11). Importantly, this reaction demonstrates that use of a chelate ligand containing two internal hydrogen-bond donors enables the isolation of a zinc methoxide complex directly from methanol solution. In this regard, two mononuclear zinc methoxide complexes, $[Tp^{Ph,Me}]Zn–OCH_3$ and $[(L1)Zn(OCH_3)] \cdot [(L1)Zn(OH)] \cdot (BPh_4)_2$ (L1 = *cis*,*cis*-1,3,5-tris[(*E*,*E*)-3-(2-furyl) acrylideneamino]cyclohexane) have been found to co-crystallize with the corresponding zinc hydroxide complexes from methanol solution.[71,76] In the case of the ebnpa-ligated system, the zinc hydroxide complex [(ebnpa)Zn–OH]ClO_4 can be cleanly produced using acetonitrile as the solvent (Scheme 11).

The ebnpa-ligated zinc methoxide and hydroxide complexes exhibit nearly identical metal coordination environments, with both having a distorted trigonal bipyramidal geometry for the Zn(II) center and very similar zinc–ligand bond distances. The only notable difference involves the Zn–S distance ([(ebnpa)Zn–OCH_3]ClO_4: 2.490(3) Å; [(ebnpa)Zn–OH]ClO_4: 2.533(1) Å). For both complexes, the zinc-bound anion is involved in two moderate hydrogen-bonding interactions, each characterized by an N···O(anion) distance of 2.73–2.77 Å.

Treatment of [(ebnpa)Zn–OH]ClO_4 with methanol in acetonitrile results in the formation of an equilibrium mixture involving [(ebnpa)Zn–OCH_3]ClO_4 and water (Scheme 12). The equilibrium constant for this reaction at 304(1) K is 0.30(8). Variable temperature studies of this equilibrium yielded $\Delta H_{Me} = -0.9(1)$ kcal mol^{-1}

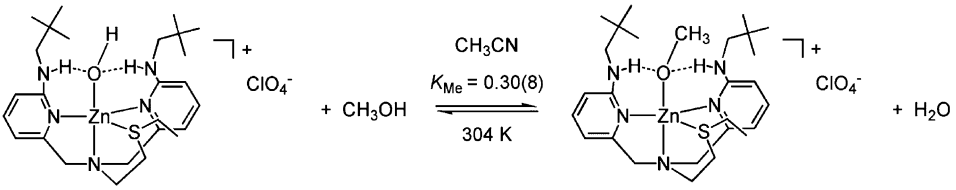

Scheme 12 Methanolysis equilibrium of ebnpa-ligated zinc hydroxide complex in acetonitrile solution.

and $\Delta S_{Me} = -5(1)$ eu. These values are notably different from those obtained for the equilibrium mixture involving $[Tp^{But,Me}]Zn–OH$ and $[Tp^{But,Me}]Zn–OCH_3$ (K_{Me} (300 K) $1.4(2) \times 10^{-3}$; $\Delta H_{Me} = 1.2(1)$ kcal mol^{-1} and $\Delta S_{Me} = -9(1)$eu; Scheme 8). These combined results indicate that the nature of the supporting chelate ligand dramatically influences the stability of zinc alkoxide species with respect to hydrolysis. While it is tempting to attribute the enhanced hydrolytic stability of $[(ebnpa)Zn–OCH_3]ClO_4$ to the presence of internal hydrogen-bond donors, additional structural features of this complex may also be important. For example, the alkoxide methyl carbon and the thioether ethyl substituent both limit water access to the alkoxide oxygen in $[(ebnpa)Zn–OCH_3]ClO_4$. Thus, steric factors may also influence the water reactivity of this complex.

4 Amide hydrolysis

REACTIONS INVOLVING MONONUCLEAR ZINC COMPLEXES

Zinc enzymes catalyze the hydrolysis of amide bonds using a variety of active site structural motifs.[77] An extensively studied enzyme of this class is carboxypeptidase A, which contains a mononuclear zinc center (Fig. 13) within the enzyme active site and catalyzes the hydrolysis of a *C*-terminal amino acid.[78,79] The mechanism of amide cleavage in carboxypeptidase A has been studied extensively.[77,78] In one proposed mechanistic pathway for this enzyme (Scheme 13), termed the ''zinc hydroxide mechanism'', the zinc center activates a water molecule for deprotonation and also assists in polarization of the substrate carbonyl moiety, thus making it more susceptible to nucleophilic attack. The zinc center also provides transition state stabilization through charge neutralization.

A structurally similar active site to that of carboxypeptidase A is found for the endopeptidase thermolysin.[77] While several crystallographic and biochemical studies favor a zinc hydroxide mechanism for thermolysin (involving Glu-143 as a general base),[80] in an alternative proposed mechanism for this enzyme, the zinc center is proposed to activate the substrate for nucleophilic attack by a non-coordinated water molecule (Scheme 14).[81,82]

In both of these mechanisms additional active site residues are indicated to play key roles in the amide cleavage process. For example, in the zinc hydroxide

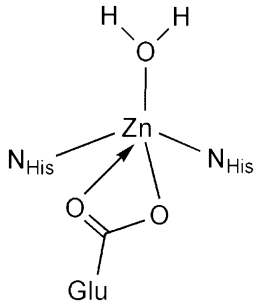

Fig. 13 Structural features of the active site zinc center in carboxypeptidase A.

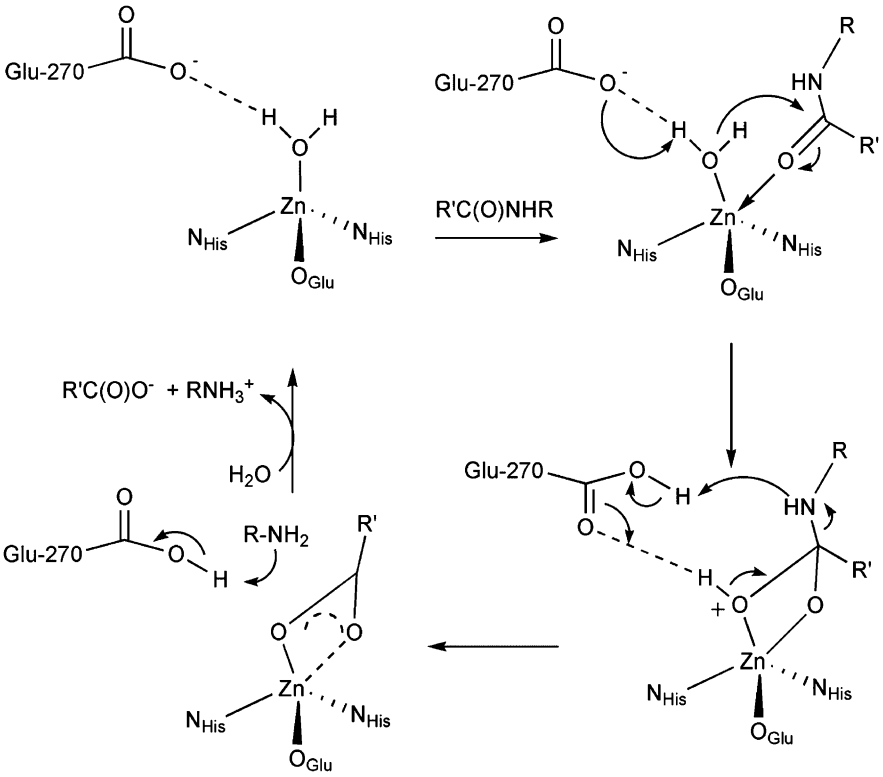

Scheme 13 Proposed mechanism for amide hydrolysis in carboxypeptidase A involving a zinc-bound hydroxide as the nucleophile.

mechanism proposed for carboxypeptidase A, positively charged residues (Arg-127 and Arg-145) provide electrostatic stabilization of the substrate. In addition, as shown in Scheme 13, Glu-270 acts as a general base to first deprotonate the zinc-bound water molecule and then protonate the amino moiety of the leaving group. In

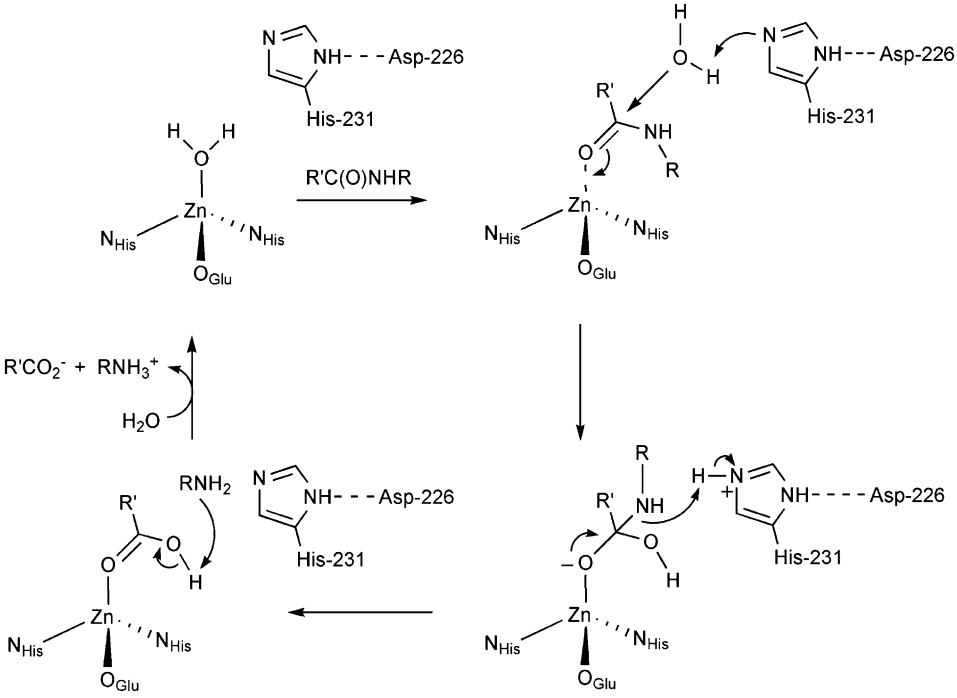

Scheme 14 Mechanism proposed for peptide hydrolysis catalyzed by thermolysin.

the mechanism proposed for thermolysin, an active site histidine residue (His-231 in thermolysin) acts as a general base to deprotonate an active site water molecule and then protonate the amine group.

There are several additional examples of zinc enzymes that contain an active site mononuclear zinc center and catalyze the hydrolysis of peptides bonds. These include carboxypeptidase B[83] and neutral protease[84] both of which contain a $[(N_{His})_2(O_{Glu/Asp})Zn–OH_2]$ coordination motif within the enzyme active site. Zinc peptidases that contain a $[(N_{His})_3Zn–OH_2]$ active site metal center include matrix metalloproteinases[85,86] and other members of the metzincins superfamily.[77,85]

Early model studies for amide-hydrolyzing metalloenzymes centered on studies of stoichiometric amide hydrolysis reactions involving exchange inert Co(III) complexes in aqueous solution.[87] These studies provided evidence that amide hydrolysis can proceed via activation of the amide carbonyl by the Co(III) center and attack by an external OH^-, or via an intramolecular pathway wherein a Co(III)–OH_n moiety ($n = 1$ or 2) attacks a chelated, but non-coordinated amide carbonyl (Fig. 14). Co(III) complexes having either amide substrate or water/hydroxide coordination exhibit significant rate enhancement for amide hydrolysis.[88,89] However, a comparative investigation of the stoichiometric formylmorpholine hydrolysis reactivity of a Co(III) complex of the 1,4,7,11-tetraazacclododecane (cyclen) ligand (Fig. 14, center column)

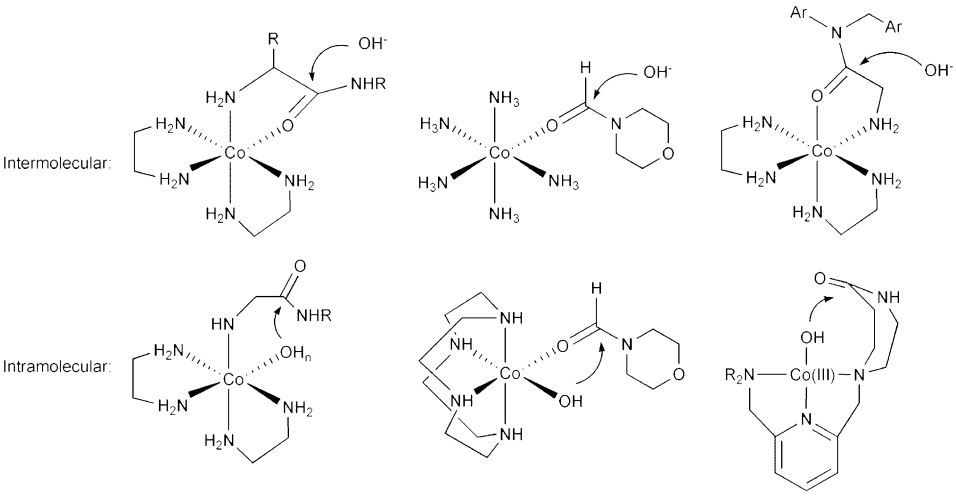

Fig. 14 Cobalt(III) complexes that exhibit inter- or intramolecular amide cleavage reactivity.

versus that of $[(NH_3)_5Co(OH_2)]^{3+}$ revealed that the greatest rate acceleration occurs when both amide substrate and hydroxide nucleophile are coordinated to the metal center simultaneously in a *cis* orientation.[90]

Sayre proposed five possible mechanisms for metal-mediated amide hydrolysis (Fig. 15).[91,92] In these proposed pathways, the metal center can be involved in electrophilic carbonyl activation (A), metal hydroxide nucleophile activation (B), and a combined mechanism involving both of these processes (C). Amide hydrolysis may also involve a metal-bound hydroxide or water molecule acting as a general base or general acid (Fig. 15d and e).

A limited number of mechanistic studies of stoichiometric amide hydrolysis reactions promoted by Zn(II) complexes have been reported. Groves and Chambers reported studies of the zinc-mediated hydrolysis of an internal amide substrate wherein amide carbonyl coordination to the zinc center is not possible (Scheme 15).[93] Examination of the rate of this reaction as a function of pH (6.5–10.5) yielded a kinetic $pK_a = 9.16$. First-order rate constants at 70 °C ($\mu = 0.5$ ($NaClO_4$)) for the Zn–OH_2 and Zn–OH-mediated amide hydrolysis reactions differed by a factor of ~100 when the data was fit to Equation (1) for the proposed mechanism shown in Scheme 16. The activation parameters determined for this reaction ($\Delta H^{\ddagger} = 22(1)\,\text{kcal mol}^{-1}$ and $\Delta S^{\ddagger} = -18(3)\,\text{eu}$) are consistent with an intramolecular hydrolysis process wherein a zinc-bound hydroxide acts as an intramolecular nucleophile to attack the amide carbonyl in the rate-determining step.

A mononuclear zinc hydroxide complex supported by a hydrophobic hydrotris(pyrazolyl)borate ligand mediates the stoichiometric hydrolysis of an activated amide.[94] As shown in Scheme 17, treatment of [($Tp^{Cum,Me}$)Zn–OH] with

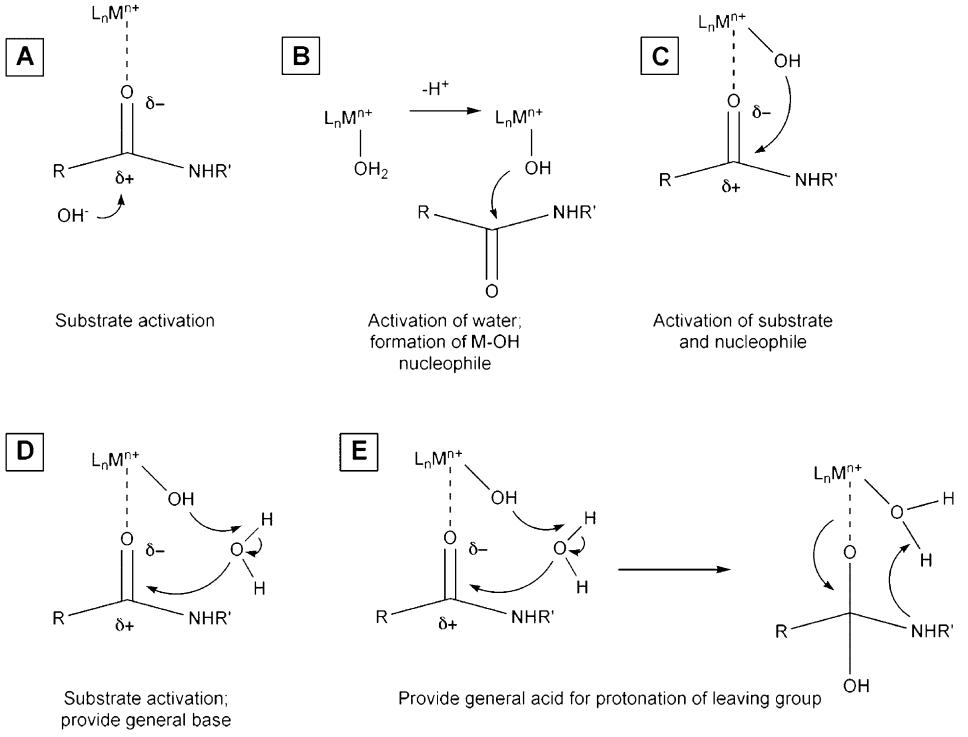

Fig. 15 Role of metal center in proposed mechanistic pathways for amide cleavage.

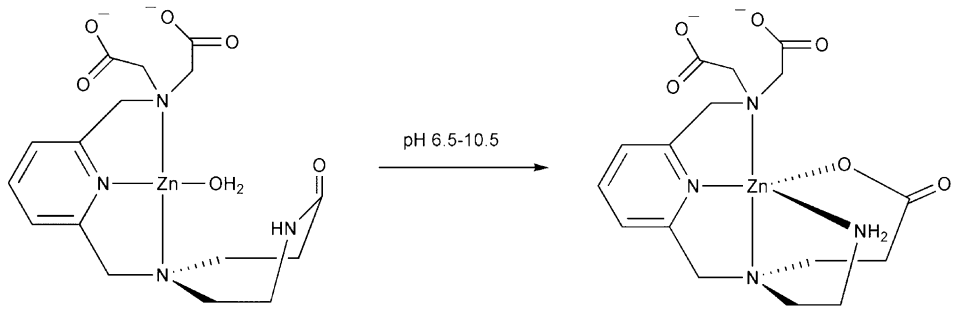

Scheme 15 Role of metal center in proposed mechanistic pathways for amide cleavage. Adapted from reference 92.

trifluoroacetamide results in the formation of a new zinc carboxylate complex.[95] The geometrical changes that occur at the zinc center during this and related hydrolysis reactions (e.g. phosphate and carboxy ester hydrolysis) have been elucidated using a Bürgi–Dunitz structural correlation method.[96] Specifically, analysis of a series of

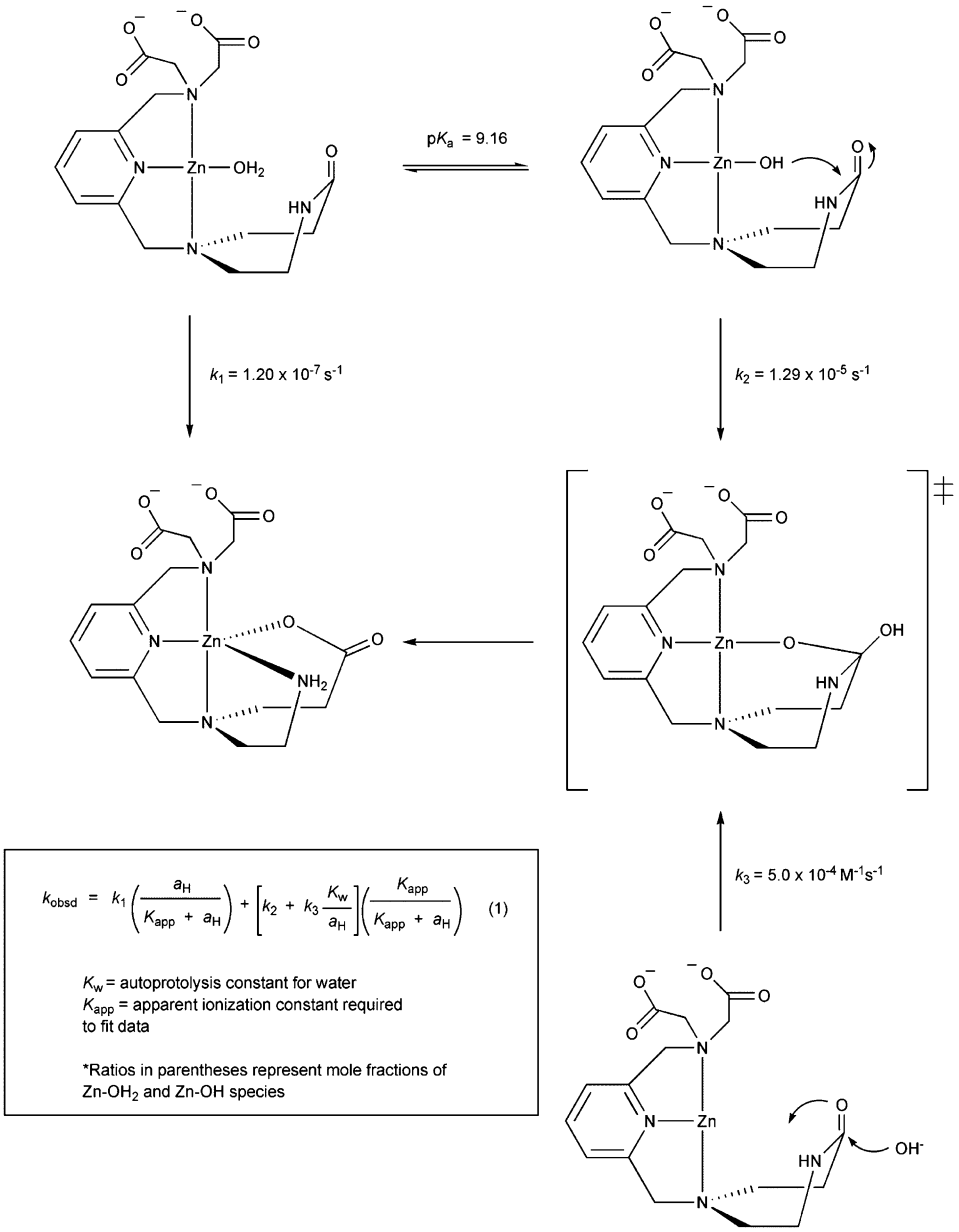

Scheme 16 Proposed mechanism and rate law for the zinc-mediated amide hydrolysis reaction.

four- and five-coordinate structures of $Tp^{R,R'}$-ligated zinc complexes suggests that the first step in substrate hydrolysis involves approach of the substrate oxygen atom to the mononuclear Zn–OH center along a three-fold axis of an incipient trigonal bipyramidal zinc structure (Scheme 18). Berry pseudorotation, which proceeds via

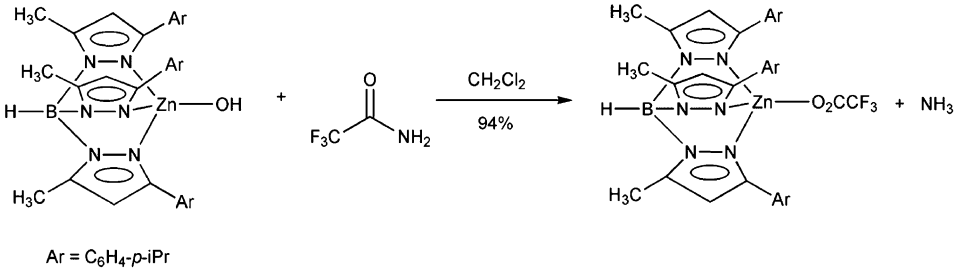

Scheme 17 Activated amide hydrolysis reactivity of [($Tp^{Cum,Me}$)Zn–OH].

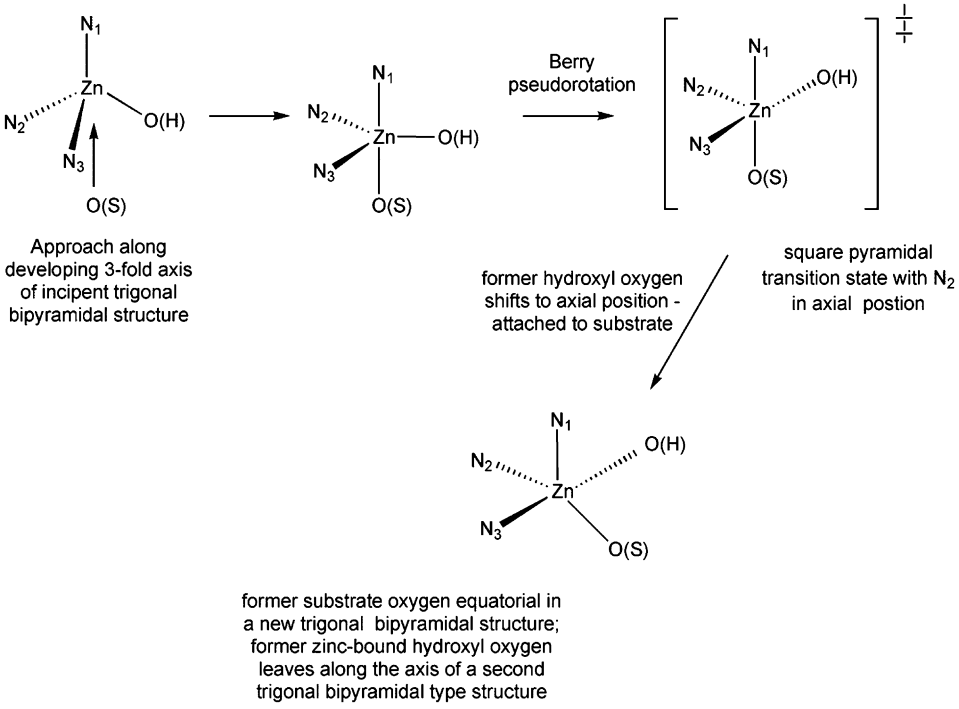

Scheme 18 Proposed geometrical changes that occur at the zinc center during a Zn–OH-promoted substrate hydrolysis reaction. This proposed pathway is based on a Bürgi–Dunitz-type structural correlation for $Tp^{R,R'}$-ligated zinc complexes.

a square pyramidal transition state, results in the substrate oxygen occupying an equatorial position and the former hydroxyl oxygen atom, which is now attached to the substrate, being placed in an axial position. If operative for the zinc centers in enzymes such as CA and carboxypeptidase A, this type of transformation indicates that product release should occur from an axial position of a five-coordinate trigonal bipyramidal-type structure.

CARBOXY ESTER HYDROLYSIS REACTIVITY OF MONONUCLEAR ZINC COMPLEXES

Carboxy esters are more easily hydrolyzed than amides and several studies of carboxy ester hydrolysis mediated by discrete mononuclear zinc complexes have been reported. These reactions are relevant to the esterase activity exhibited by some zinc hydrolases (e.g. CA[97] catalyzes the hydrolysis of 4-nitrophenyl acetate) and in some cases are also used as model reactions for amide hydrolysis.[17,36,96,98–101] For example, the mononuclear zinc hydroxide complex [([12]aneN$_3$)Zn(OH)]ClO$_4$ catalyzes the hydrolysis of methyl acetate in neutral water at 25(1)°C with a turnover time of approximately 60 min at [$CH_3C(O)OCH_3$] = 1 M and pH = 8. Development of a rate-pH profile for this reaction yielded a sigmoidal plot with a kinetic pK_a of 7.3. This value is identical to the pK_a value for [([12]aneN$_3$)Zn(OH_2)](ClO$_4$)$_2$ (Fig. 4) determined by potentiometric titration (7.30 ± 0.02) thus indicating that the zinc hydroxide form of the complex attacks the ester carbonyl in the rate-determining step of the reaction.[36]

Similar results were found for the hydrolysis of 4-nitrophenyl acetate catalyzed by [([12]aneN$_3$)Zn(OH)]ClO$_4$. The second-order rate constant for this reaction is $(3.6 \pm 0.3) \times 10^{-2}\,M^{-1}\,s^{-1}$ at 25 °C, pH = 8.2, and I = 0.10 ($NaClO_4$).[36,98] From the temperature dependence of the rate constant, an Arrhenius plot was constructed, which revealed an activation energy of $49 \pm 2\,kJ\,mol^{-1}$ for this carboxy ester hydrolysis reaction.[98] Using the zinc cyclen complex [([12]aneN$_4$)Zn(OH)]ClO$_4$, the second-order rate constant is $(1.0 \pm 0.1) \times 10^{-1}\,M^{-1}\,s^{-1}$ at 25 °C and the activation energy for the reaction is $45 \pm 2\,kJ\,mol^{-1}$.[99] The similarity of the activation energies for the [([12]aneN$_3$)Zn(OH)]ClO$_4$ and [([12]aneN$_4$)Zn(OH)]ClO$_4$ catalyzed reactions to that of the aqueous OH^--catalyzed reaction ($43 \pm 2\,kJ\,mol^{-1}$) suggests that all of these 4-nitrophenyl acetate hydrolysis reactions proceed via rate-determining attack of hydroxide (either free or zinc bound) on the ester carbonyl carbon atom (Fig. 16).[99]

Notably, addition of a methyl group to the cyclen ring (Fig. 17) results in a considerably slower reaction ($k'' = 4.7(1) \times 10^{-2}\,M^{-1}\,s^{-1}$ at 25 °C).[102] This has been attributed to steric hindrance imposed by the methyl group, which is suggested to lower the nucleophilicity of the Zn–OH moiety toward the ester substrate.

The mononuclear zinc hydroxide complex [($Tp^{Cum,Me}$)Zn–OH] promotes the stoichiometric hydrolysis of activated esters such as 4-nitrophenylacetate, triflouroacetate, and trifluorolactone (Scheme 19). Following the hydrolysis of 4-nitrophenyl acetate, the liberated product 4-nitrophenol rapidly reacts with [($Tp^{Cum,Me}$)Zn–OH] to yield [($Tp^{Cum,Me}$)Zn–O–C_6H_4–*p*-NO_2].[95,96] By monitoring the formation of [($Tp^{Cum,Me}$)Zn–O–C_6H_4–*p*-NO_2] using UV–visible spectroscopy, the second-order rate constant for the 4-nitrophenylacetate hydrolysis reaction at 25 °C was found to be $3.5 \times C\ 10^{-3}\,M^{-1}\,s^{-1}$. This rate is considerably slower than that found for the hydrolysis of 4-nitrophenylacetate by [([12]aneN$_3$)Zn(OH)]ClO$_4$ and [([12]aneN$_4$)Zn(OH)]ClO$_4$ ($(3.6 \pm 0.3) \times 10^{-2}\,M^{-1}\,s^{-1}$ and $(1.0 \pm 0.1) \times 10^{-1}\,M^{-1}\,s^{-1}$, respectively) in aqueous solution,[36,99] or by aqueous base ($9.5\,M^{-1}\,s^{-1}$ at 25 °C).[103] The slower rate of the [($Tp^{Cum,Me}$)Zn–OH]-promoted reaction is attributed to the chloroform solvent employed in the kinetic studies, which is less polar than water. Variable temperature kinetic studies of the [($Tp^{Cum,Me}$)Zn–OH]-promoted reaction, and

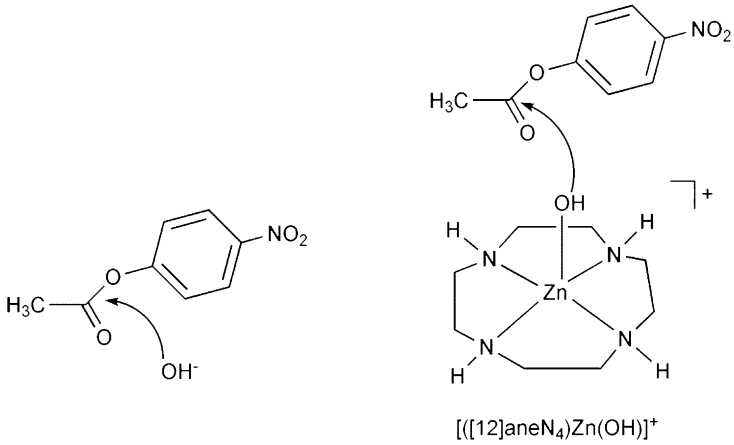

Fig. 16 Proposed pathways of 4-nitrophenyl acetate hydrolysis catalyzed by aqueous hydroxide ion and $[([12]aneN_4)Zn(OH)]^+$.

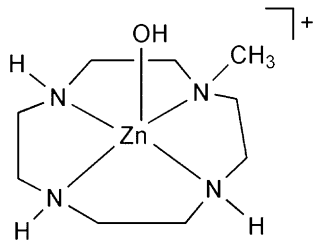

Fig. 17 $[(CH_3cyclen)Zn–OH]^+$.

construction of an Arrhenius plot, yielded an activation energy of 64.3 kJ mol^{-1}. The activation enthalpy ($\Delta H^{\ddagger} = 61.8$ kJ mol^{-1}) and entropy ($\Delta S^{\ddagger} = -85.6$ J mol K^{-1}) for this reaction were determined from a plot of $\ln(k''/T)$ versus $1/T$. Notably, these values are similar to those found for the hydrolysis of 4-nitrophenylacetate catalyzed by the N_2S(thiolate)-ligated zinc hydroxide complex [(PATH)Zn–OH] (Scheme 20; $E_a = 54.8$ kJ mol^{-1}; $\Delta H^{\ddagger} = 52.4$ kJ mol^{-1}; $\Delta S^{\ddagger} = -90.0$ J mol K^{-1}).[17] The activation parameters for the [(PATH)Zn–OH]-catalyzed reaction have been interpreted as corresponding to rate-determining attack of the zinc hydroxide moiety on the 4-nitrophenylacetate carbonyl carbon, as has been discussed for $[([12]aneN_4)Zn(OH)]^+$ (Fig. 16).

Presented in Table 1 is a summary of the second-order rate constants for the hydrolysis of 4-nitrophenyl acetate promoted by various zinc complexes in aqueous solution. A conclusion that may be drawn from this data is that change in the nature of the supporting chelate ligand dramatically influences the second-order rate constant for the carboxy ester hydrolysis reaction. Notably, the slowest rate is found for the four-coordinate zinc hydroxide species $[([12]aneN_3)Zn(OH)]^+$ which has three

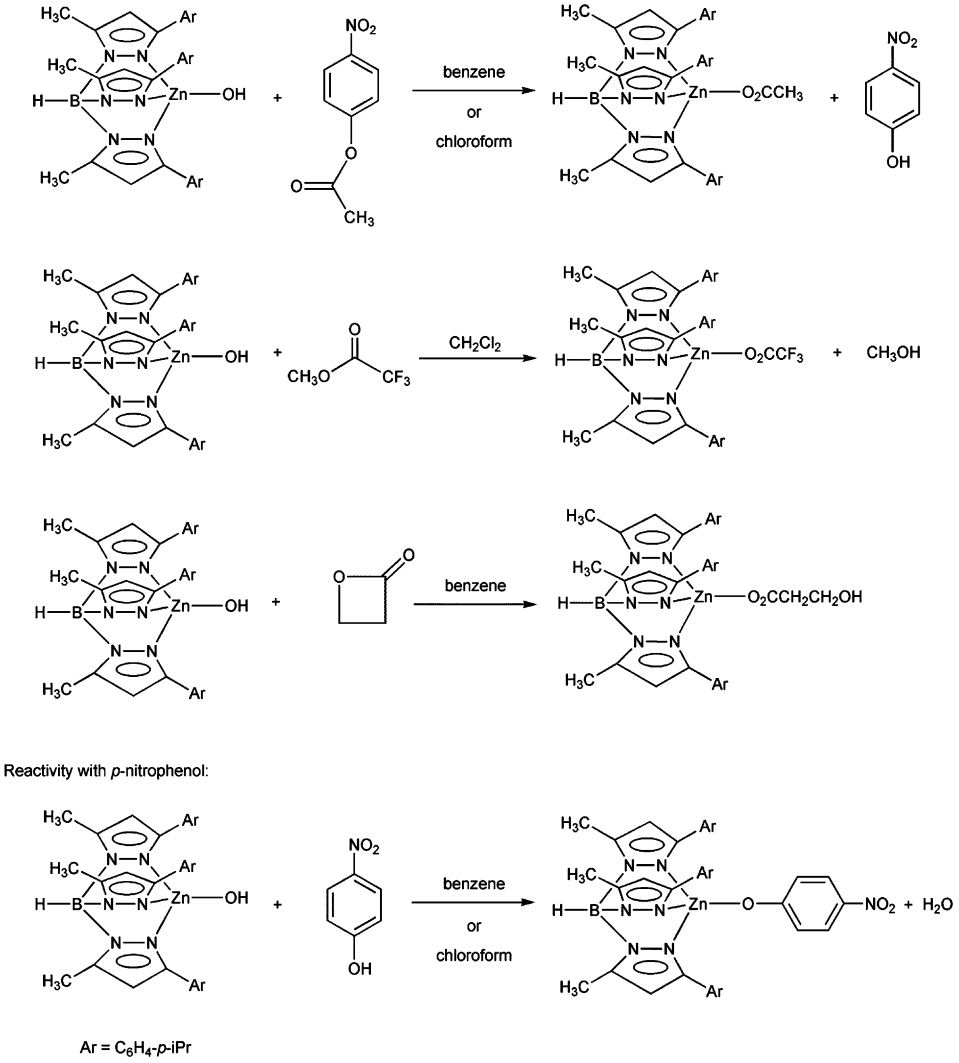

Scheme 19 Ester hydrolysis reactivity of [($Tp^{Cum,Me}$)Zn–OH].

neutral nitrogen donors, in addition to the hydroxide anion, as ligands to the zinc center. This complex also exhibits the lowest pK_a for the zinc-bound water molecule. For complexes having one additional neutral nitrogen donor (e.g. [([12]aneN_4)Zn(OH)]$^+$ and [(CH_3cyclen)Zn–OH]$^+$), the zinc center has enhanced electron density, which in turn raises the Zn–OH_2 pK_a value, and enhances the nucleophilicity of the Zn–OH moiety and the rate of carboxyester hydrolysis. As noted above, the rate of carboxyester hydrolysis mediated by [(CH_3cyclen)Zn–OH]$^+$ (Fig. 17) is influenced by steric hindrance from the methyl substituent. In [(PATH)Zn–OH], the

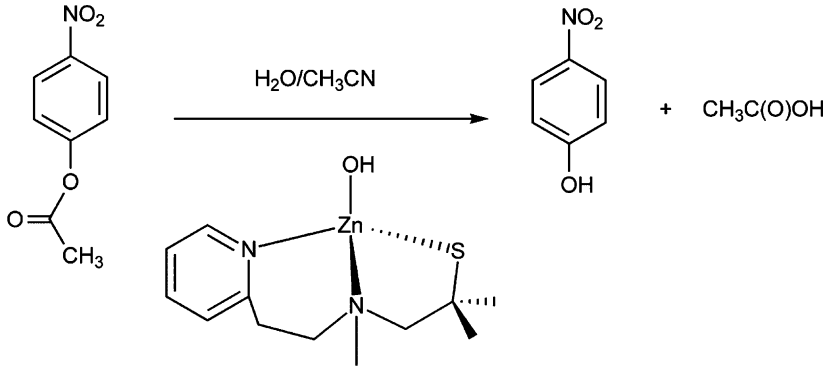

Scheme 20 4-Nitrophenyl acetate hydrolysis catalyzed by [(PATH)Zn–OH].

Table 1 Comparison of pK_a values of zinc complexes and second-order rate constants k'' ($M^{-1}\,s^{-1}$) for the hydrolysis of 4-nitrophenyl acetate at 25 °C with that of human CA-II. Adapted from reference 17.

	pK_a	k'' ($M^{-1}\,s^{-1}$)	Reference
OH^-	15.7	9.5	103
$[([12]aneN_3)Zn(OH)]^+$	7.3	0.036 ± 0.003[a]	98
$[([12]aneN_4)Zn(OH)]^+$	7.9	0.1 ± 0.01[a]	99
$[(CH_3cyclen)Zn–OH]^+$	7.68	0.047 ± 0.001[a]	102
[(PATH)Zn–OH]	8.05(5)	0.089 ± 0.003[b]	17
$[([15]aneN_3O_2)Zn–OH]^+$	8.8	0.6 ± 0.06[c]	104,105
$[(L2)Zn–OH]^+$	8.74	0.934[d]	107
Human carbonic Anhydrase II	6.8(1)	2500 ± 200[e]	108

[a] 20 mM CHES (pH = 9.3), $I = 0.10$ ($NaNO_3$), 10% (v/v) CH_3CN.
[b] H_2O/CH_3CN (90:10 v/v), $I = 0.10$ M ($NaClO_4$).
[c] $I = 0.15$ M NaCl.
[d] H_2O/CH_3CN (90:10 v/v), $I = 0.10$ M (KNO_3).
[e] k_{cat}/K_M.

four-coordinate zinc center has two neutral nitrogen donors, an alkyl thiolate, and the hydroxide anion as ligands. This complex has a pK_a value of 8.05(5) for the zinc-bound water molecule. The presence of the anionic thiolate donor enhances the electron density at the zinc center, which in turn enhances the rate of the 4-nitrophenyl acetate hydrolysis reaction relative to that found for $[([12]aneN_3)Zn(OH)]^+$. Interestingly, the pK_a values and second-order rate constants for $[([12]aneN_4)Zn(OH)]^+$ and [(PATH)Zn–OH] are similar, indicating that the Lewis acidity of the zinc centers in these two complexes are similar. In other words, the four neutral nitrogen donor ligands in $[([12]aneN_4)Zn(OH)]^+$ provide a similar amount of electron density to the zinc center as do two neutral nitrogen donors and an alkyl thiolate in [(PATH)Zn–OH].

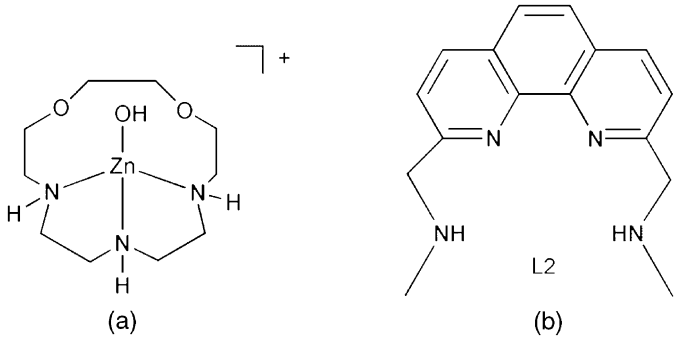

Fig. 18 (a) $[([15]aneN_3O_2)Zn(OH)]^+$ and (b) L2 ligand.

In $[([15]aneN_3O_2)Zn(OH)]^+$ (Fig. 18a), the mononuclear zinc center is ligated by three neutral nitrogen donors.[104,105] However, the pK_a for the zinc-bound water molecule (8.8) in the corresponding aqua complex is considerably higher than that found for $[([12]aneN_3)Zn(OH_2)]^{2+}$ (7.3).[98] This was suggested to be due to hydrogen bonding between the hydrogen atoms of the zinc-bound water molecule and the oxygen atoms of the macrocycle.[104,106] Despite the reduced acidity of the $[([15]aneN_3O_2)Zn(OH)]^+$ cation, it exhibits enhanced nucleophilicity toward 4-nitrophenyl acetate, with $k'' = 0.6 \pm 0.06\ M^{-1}\ s^{-1}$. This enhanced reactivity may be due to a more exposed Zn–OH moiety, as the ethylenic chains in $[([15]aneN_3O_2)Zn(OH)]^+$ may produce a subtly different coordination environment than the propylenic chains found in $[([12]aneN_3)Zn(OH)]^+$.

A zinc(II) hydroxo complex supported by a secondary amine-appended phenanthroline ligand (L2, Fig. 18b) has been reported to catalyze the hydrolysis of 4-nitrophenyl acetate with a second-order rate constant of $0.934\ M^{-1}\ s^{-1}$.[107] A mechanism involving attack of a terminal zinc hydroxide moiety on the 4-nitrophenyl acetate substrate has been proposed.

The catalytic activity of the zinc complexes given in Table 1 for 4-nitrophenylacetate hydrolysis is well below that found for free OH^- or for the zinc center for human CA-II.[108] In the case of OH^-, this is consistent with the proposed mechanism for 4-nitrophenyl acetate hydrolysis shown in Fig. 16 wherein the rate-determining step is attack on the substrate carbonyl. In this reaction, the best nucleophile will be free OH^-. In metalloenzymes such as CA, the presence of the zinc center insures that a hydroxide nucleophile can be generated at relatively low concentrations of free OH^-.

Outside the scope of coverage of this contribution are Zn(II)-promoted carboxyester hydrolysis reactions involving multinuclear zinc complexes or systems wherein the first step involves transesterification.[98,100–102,105,109–114]

β-LACTAM HYDROLYSIS

Metallo-β-lactamases catalyze the hydrolytic ring opening of a β-lactam ring in antibiotics containing this structural unit (e.g. penicillins, cephalosporins, carbapenems),

thus making the antibiotic inactive (Fig. 19).[115–118] These enzymes are gaining increasing attention in the clinical sector due to their ability to hydrolyze all β-lactam derivatives, and because there are currently no clinically useful inhibitors for metallo-β-lactamases.[119]

All metallo-β-lactamases require Zn(II) for catalytic activity.[117,118,120] The active site ligands for the zinc centers include histidine, aspartate, and cysteine amino acid ligands, and a bridging hydroxide/water moiety (Fig. 20).[121–123] For the majority of metallo-β-lactamases, maximal activity is obtained when both Zn(II) binding sites are fully occupied. However, the physiologically active form may contain only a single zinc ion in the tetrahedral $(N_{His})_3Zn_1$ binding site.[124] When two zinc centers are present, the Zn···Zn distance is approximately 3.5 Å and both metal centers are involved in coordination of a water/hydroxo moiety. The role of the second zinc center in several metallo-β-lactamases (Zn_2, Fig. 20) is still under investigation.

Distinct mechanisms may be operative for the bimetallic versus the monometallic forms of these enzymes.[125–128] Generally, mechanistic pathways have been proposed wherein the β-lactam carbonyl is polarized via interaction with a zinc center. Following nucleophilic attack by a zinc-bound hydroxide and formation of a tetrahedral intermediate, cleavage of the C–N bond occurs. Protonation of the β-lactam nitrogen atom then occurs, along with dissociation of the carboxylate moiety from the zinc center resulting in the release of the ring-opened product.

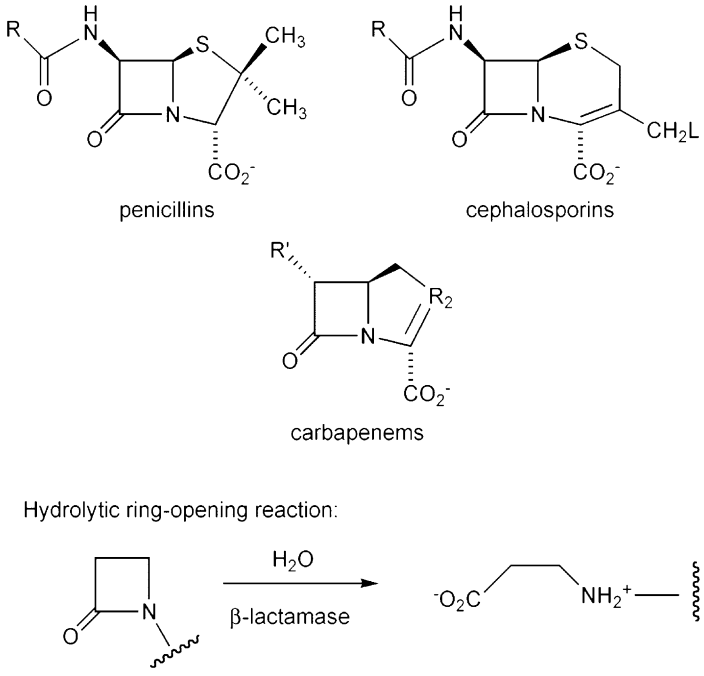

Fig. 19 (top) Types of β-lactam antibiotics and (bottom) hydrolytic ring opening catalyzed by β-lactamase enzymes.

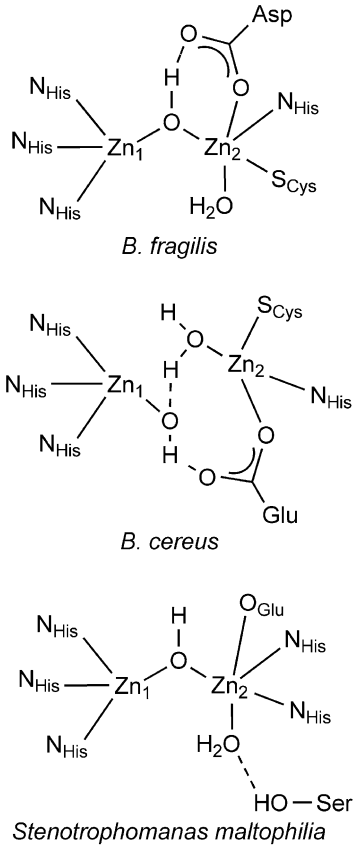

Fig. 20 Structural features of the active site zinc centers in metallo-β-lactamases.

Model studies for metallo-β-lactamases have been performed using mononuclear zinc hydroxide complexes.[99,129,130] The breadth of β-lactam hydrolysis reactivity of hydrotris(pyrazolyl)borate-ligated mononuclear zinc hydroxide complexes has been explored.[129] Treatment of the mononuclear zinc hydroxide complex [($Tp^{Ph,Me}$)Zn–OH] with simple β-lactams (β-propiolactam, 4-phenyl-β-propiolactam, Scheme 21) does not result in ring opening, but instead results in the formation of β-lactamide complexes and water. Treatment of [($Tp^{Ph,Me}$)Zn–OH] with *N*-alkyl or -aryl β-lactam derivatives instead results in no reaction (Scheme 21). Use of natural derivatives of penicillin and cephalosporin (Scheme 22) did not yield β-lactam hydrolysis, but instead coordination of the carboxylate moiety of the antibiotic derivatives to the mononuclear Zn(II) center and release of water.

Notably, only for β-lactams containing a *N*-nitrophenyl or *N*-acyl group (Scheme 23) was ring-opening lactam hydrolysis identified, albeit under rather forcing conditions (boiling toluene solution).[129] In the case of a β-lactam containing a *N*-fluoroacetyl substituent, reaction is found at the exocyclic acetyl functionality. The reactions of

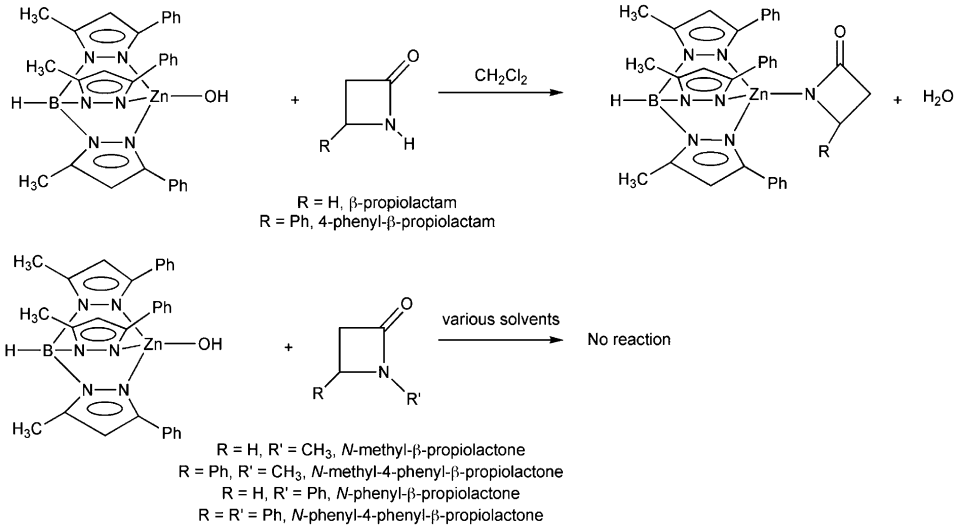

Scheme 21 Reactivity of [(Tp^{Ph,Me})Zn–OH] with unactivated β-lactams.

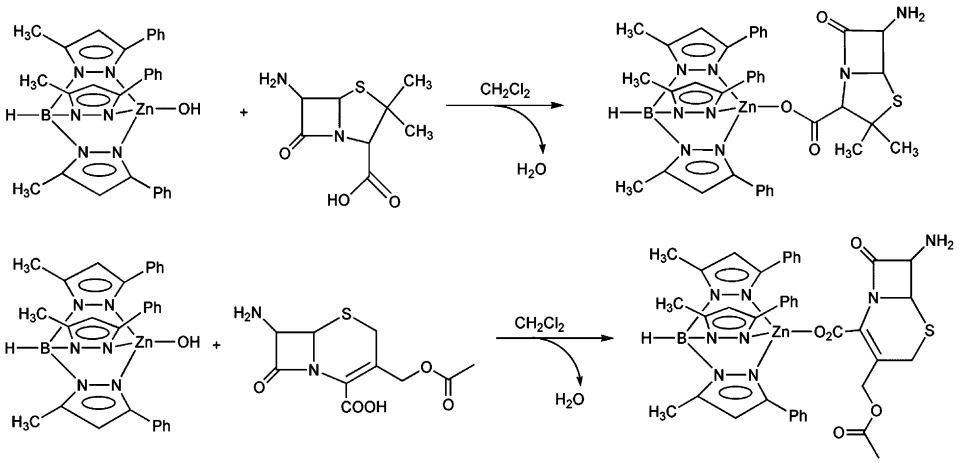

Scheme 22 Reactivity of [(Tp^{Ph,Me})Zn–OH] with derivatives of penicillin and cephalosporin.

[(Tp^{Ph,Me})Zn–OH] and [(Tp^{Cum,Me})Zn–OH] with the *N*-2,4-dinitrophenyl-appended β-lactam substrate were monitored by ^{1}H NMR under pseudo first-order conditions in $CDCl_3$. The second-order rate constants for these reactions were determined to be $0.57\,M^{-1}\,s^{-1}$ (Tp^{Ph,Me}) and $0.13\,M^{-1}\,s^{-1}$ (Tp^{Cum,Me}) at 40 °C. The slower rate for the reaction involving [(Tp^{Cum,Me})Zn–OH] is consistent with the enhanced steric hindrance and hydrophobicity of the Tp^{Cum,Me} ligand relative to Tp^{Ph,Me}.

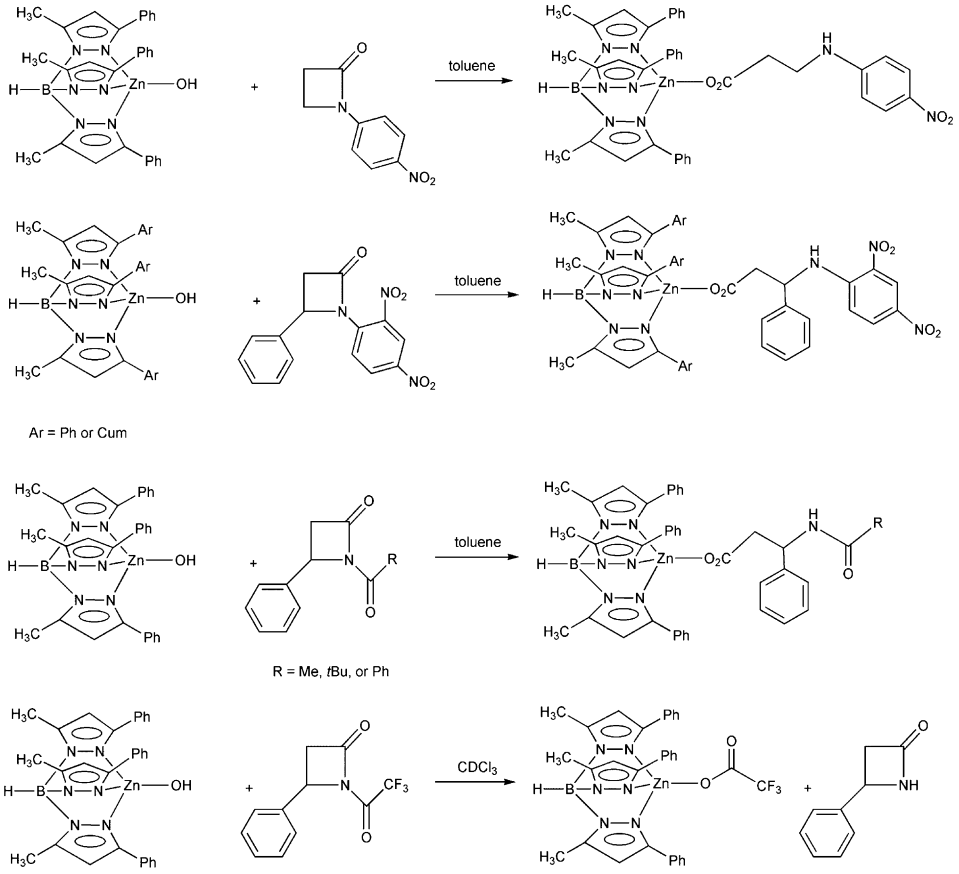

Scheme 23 Reactivity of [($Tp^{Ar,Me}$)Zn–OH] (Ar = Ph or Cum) with activated β-lactams.

Treatment of $[([12]aneN_4)Zn(OH)]^+$ with penicillin G (benzylpenicillin) at 25 °C ($pD = 9$) results in the formation of both the hydrolysis product, (5*R*)-benzylpenicilloate (Scheme 24) and an epimer of this product (5*S*-benzylpenicilloate).[99] Notably, no spectroscopic evidence was found during the course of this reaction for interaction between $[([12]aneN_4)Zn(OH)]^+$ and the β-lactam nitrogen of penicillin G. Measurement of the rate of reaction as a function of pH (6.6–9.6) yielded a sigmoidal curve and an inflection at pH = 7.9. This value is identical to the thermodynamic pK_a measured for $[([12]aneN_4)Zn(OH_2)]^{2+}$ via potentiometric titration, thus indicating that the zinc hydroxide species $[([12]aneN_4)Zn(OH)]^+$ is the reactive species for penicillin G hydrolysis. The second-order rate constant for this hydrolysis reaction is $(4.1 \pm 0.1) \times 10^{-2}\,M^{-1}\,s^{-1}$ at 25 °C and $I = 0.10$ ($NaNO_3$).[99] Variable temperature kinetic measurements in the range of 15−35 °C and construction of an Arrhenius plot yielded an activation energy for lactam hydrolysis of

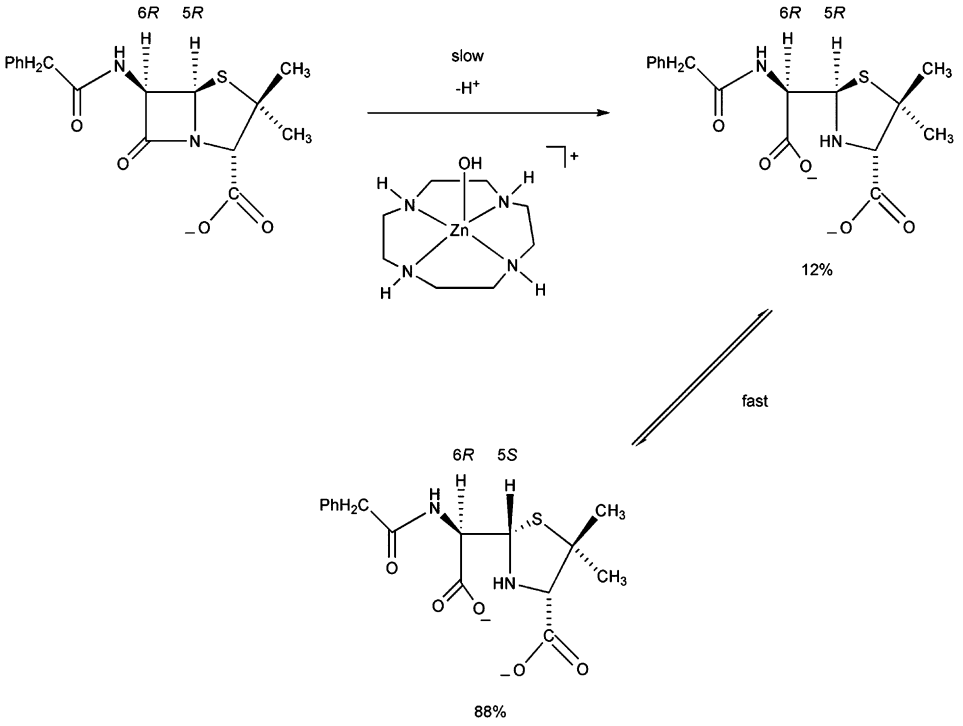

Scheme 24 Reaction of $[([12]aneN_4)Zn–OH]^+$ with penicillin G.

$49 \pm 2\,kJ\,mol^{-1}$. In a companion study, the aqueous OH^--catalyzed penicillin G hydrolysis reaction was found to have an activation energy of $61 \pm 2\,kJ\,mol^{-1}$. Interestingly, comparison of these two activation energies indicates that the zinc complex lowers the activation barrier for penicillin G hydrolysis by $\sim 12\,kJ\,mol^{-1}$. This is likely due to stabilization of the anionic tetrahedral intermediate by the divalent metal center.[99]

Mechanistic studies of the reaction catalyzed by the metallo-β-lactamase from *Bacteroides fragilis* have been performed using nitrocefin (Scheme 25) as a substrate.[127,131,132] Several theoretical studies pertinent to possible steps in the mechanistic pathway have also been reported.[133–139] Issues stemming from these studies that remain unresolved include whether the nucleophilic hydroxide is bridging or terminal, and the chemical nature of an intermediate that is detected during the hydrolysis of nitrocefin.

Mechanistic studies of nitrocefin hydrolysis catalyzed by $[Zn_2(BPAN)(\mu\text{-}OH)(\mu\text{-}O_2PPh_2)](ClO_4)_2$ (Fig. 21) have provided insight into a reaction pathway of β-lactam hydrolysis involving a binuclear zinc motif.[140] Treatment of $[Zn_2(BPAN)(\mu\text{-}OH)(\mu\text{-}O_2PPh_2)](ClO_4)_2$, which retains a binuclear cationic structure in water, with nitrocefin in a 9:1 mixture of 0.50 M HEPES buffer (in H_2O) and dimethyl sulphoxide (DMSO) results in characteristic spectroscopic changes consistent with the

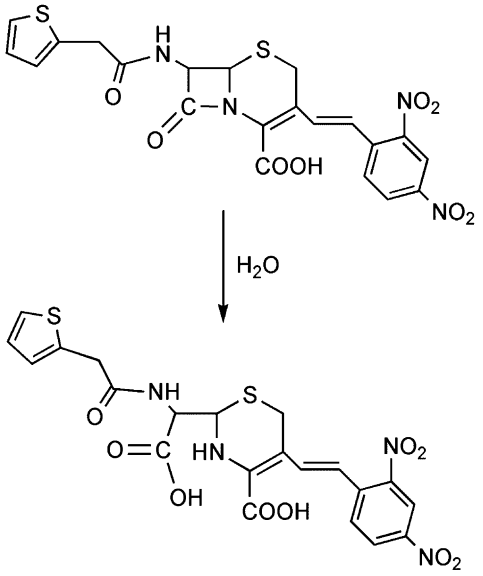

Scheme 25 Structure of nitrocefin and its hydrolysis product.

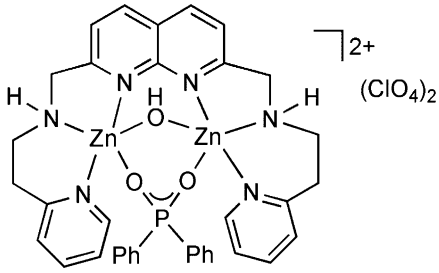

Fig. 21 $[Zn_2(BPAN)(\mu\text{-}OH)(\mu\text{-}O_2PPh_2)](ClO_4)_2$.

hydrolytic ring opening of the lactam ring. Specifically, an absorption feature that is present for nitrocefin at 390 nm ($\varepsilon = 21{,}000\,M^{-1}\,cm^{-1}$) shifts to 486 nm ($\varepsilon = 10{,}000\,M^{-1}\,cm^{-1}$) in the ring-opened product. This reaction proceeds with a rate enhancement of 2.8×10^3 relative to the uncatalyzed hydrolysis of the lactam. The rate of the reaction depends on the concentration of substrate, and increases with the presence of increasing amounts of $[Zn_2(BPAN)(\mu\text{-}OH)(\mu\text{-}O_2PPh_2)](ClO_4)_2$, but not in a linear fashion. Overall, saturation kinetic behavior is observed and was fit by invoking a proposed mechanism wherein substrate coordination to the bizinc cation precedes lactam hydrolysis. Using this mechanism, the experimental data was fit to Equation (2) (Scheme 26), which yielded $K = (1.1 \pm 0.2) \times 10^3\,M^{-1}$ and $k_2 = (3.2 \pm 1.0) \times 10^{-3}\,min^{-1}$.

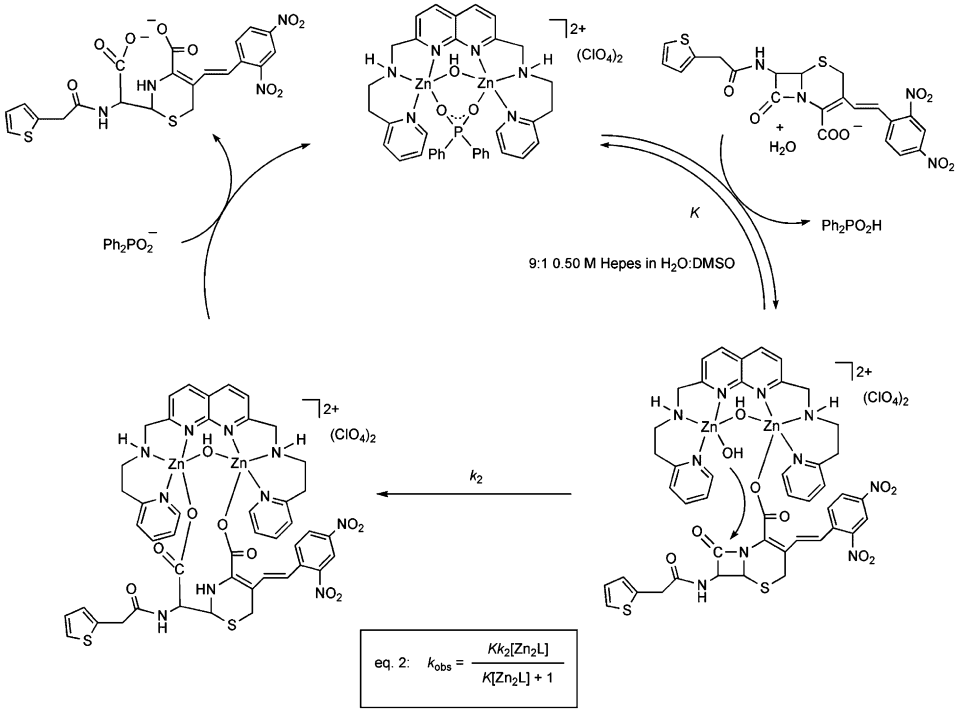

Scheme 26 Proposed mechanism for nitrocefin hydrolysis catalyzed by $[Zn_2(BPAN)(\mu\text{-}OH)(\mu\text{-}O_2PPh_2)](ClO_4)_2$.

The involvement of a terminal zinc hydroxide moiety in the hydrolysis of nitrocefin (Scheme 26), and not the bridging hydroxide ligand present in $[Zn_2(BPAN)(\mu\text{-}OH)(\mu\text{-}O_2PPh_2)](ClO_4)_2$, was determined on the basis of pH-rate studies. The rate of hydrolysis of nitrocefin catalyzed by $[Zn_2(BPAN)(\mu\text{-}OH)(\mu\text{-}O_2PPh_2)](ClO_4)_2$ increases as the pH increases, suggesting the involvement of a zinc hydroxide species. However, considering the possible involvement of either a zinc aqua or zinc hydroxide moiety as the reactive species for the lactam hydrolysis reaction, the experimental pH-rate data were fit to Equation (3) (Scheme 27). This yielded rate constants for hydrolysis by the $LZn_2\text{–}OH_2$ ($7.5 \times 10^{-4}\,min^{-1}$) and $LZn_2\text{–}OH$ ($3.4 \times 10^{-2}\,min^{-1}$) species, and a kinetic pK_a value of 8.7 ± 0.2. Notably, this pK_a value is identical to that measured for a terminal $LZn_2\text{–}OH_2$ moiety on the $[Zn_2(BPAN)(H_2O)(\mu\text{-}OH)(\mu\text{-}O_2PPh_2)](ClO_4)_2$ complex framework.[141] Overall, these results indicate that: (1) a zinc hydroxide species is significantly more reactive than a zinc aqua moiety for nitrocefin hydrolysis and (2) the reactive $LZn_2\text{–}OH$ species in this system is derived from a terminal $LZn_2\text{–}OH_2$ moiety, and the bridging hydroxide ligand is not involved in nitrocefin hydrolysis.

Further evidence for the proposed mechanistic pathway shown in Scheme 26 was derived from independent ^{13}C NMR and infrared spectroscopic studies of the

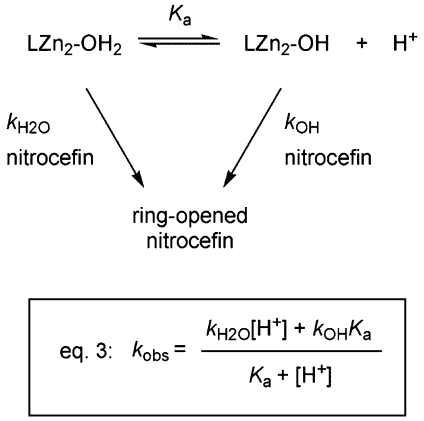

Scheme 27 Proposed mechanism and rate law for pH-dependence of nitrocefin hydrolysis.

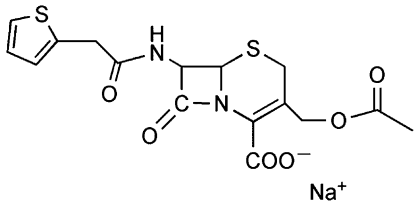

Fig. 22 Sodium salt of cephalothin.

β-lactam binding properties of $[Zn_2(BPAN)(\mu\text{-}OH)(\mu\text{-}O_2PPh_2)](ClO_4)_2$ in pure DMSO.[140] These studies revealed evidence for the interaction of the carboxylate moiety of cephalothin (Fig. 22), a nitrocefin analog, with the binuclear zinc center. Specifically, the carboxylate carbonyl carbon signal is shifted downfield in the presence of this zinc complex, which is indicative of metal coordination.[142] In addition, the presence of a ν_{COO} band at $1626\,cm^{-1}$ is consistent with monodentate coordination of the cephalothin carboxylate to Zn(II).[143–145] The amide carbonyl oxygen atom of the β-lactam ring does not interact with a zinc center, as evidenced by the fact that no significant shift in the $\nu_{C=O}$ vibration of the lactam was identified. This coordination motif, in which only the carboxylate moiety of cephalothin interacts with a zinc center, contrasts with studies of divalent metal ion-promoted hydrolysis of penicillin G, wherein bidentate coordination of the lactam to the metal center occurs via the carboxylate and the nitrogen β-lactam atom.[146] Other coordination motifs have also been proposed in reactive systems involving metal ions, including Cu(II)-coordination of the non-lactam deprotonated amide nitrogen.[147]

Additional kinetic studies performed under conditions wherein less water was present (1:9 DMSO: acetone containing 0.28 M H_2O) yielded $K = (8.9 \pm 0.3) \times 10^3\,M^{-1}$. The difference between the equilibrium binding constant K for the nitrocefin hydrolysis reaction catalyzed by $[Zn_2(BPAN)(\mu\text{-}OH)(\mu\text{-}O_2PPh_2)](ClO_4)_2$ under

these conditions, versus the same reaction performed in aqueous buffer solution ($K = (1.1 \pm 0.2) \times 10^3\,M^{-1}$), indicates that water competes with the nitrocefin substrate for coordination to the binuclear zinc complex. However, the presence of varying amounts of water does not significantly impact k_2 ($(3.2 \pm 1.0) \times 10^{-3}\,min^{-1}$ in 9:1 0.50 M HEPES (in H_2O): DMSO versus $k_2 = (6.6 \pm 1.6) \times 10^{-3}\,min^{-1}$ in 1:9 DMSO containing 0.28 M H_2O), which is consistent with a mechanism involving intramolecular attack of a Zn–OH nucleophile on a coordinated nitrocefin molecule.

Variable temperature kinetic studies of the nitrocefin hydrolysis reaction catalyzed by $[Zn_2(BPAN)(\mu\text{-}OH)(\mu\text{-}O_2PPh_2)](ClO_4)_2$ in aqueous solution (9:1 0.50 M HEPES buffer (in H_2O):DMSO) yielded $\Delta H^{\ddagger} = 62.7 \pm 3.2\,kJ\,M^{-1}$ and $\Delta S^{\ddagger} = -130 \pm 10\,J\,M^{-1}\,K^{-1}$.[140] In the absence of water (1:9 DMSO:acetone), studies of the same reaction yielded activation parameters of $\Delta H^{\ddagger} = 96.1 \pm 5.2\,kJ\,M^{-1}$ and $\Delta S^{\ddagger} = -22.4 \pm 12\,J\,M^{-1}\,K^{-1}$. The dramatic difference between these two sets of parameters suggests that diverse mechanisms are operative depending on the nature of the solvent. In water, a catalytic reaction involving intramolecular attack of a terminal LZn_2–OH moiety on a monodentate-coordinated nitrocefin substrate seems plausible (Scheme 26). However, in non-aqueous solution (1:9 DMSO:acetone), where a water molecule is not available for formation of the terminal LZn_2–OH moiety, the bridging hydroxide may shift to a terminal position prior to attack on the β-lactam, or may act as the nucleophile from the bridging position. In both of these scenarios, significant reorganization of the cation is required, which is consistent with the slower reaction (k_{obs} (DMSO:acetone) $= 2.0 \times 10^{-3}\,min^{-1}$; k_{obs} (H_2O:DMSO) $= 3.4 \times 10^{-2}\,min^{-1}$) and higher activation enthalpy for the β-lactam hydrolysis reaction. Additional factors that could influence the non-aqueous reaction include the alignment of the coordinated substrate and the hydroxide moiety, and/or the nucleophilicity of a bridging hydroxide, which would be reduced due to its interactions with two metal centers.

To gain further insight into the nature of the zinc hydroxide moiety operative for β-lactam hydrolysis in metallo-β-lactamases, studies of bizinc complexes of differing supporting chelate ligand structure were undertaken.[148] Dissolving of the bizinc complex $[Zn_2L3(\mu\text{-}NO_3)(NO_3)_2]$ in water results in the formation of $[Zn_2L3(\mu\text{-}OH)(NO_3)_2]$ (Fig. 23), which was characterized by X-ray crystallography. In this complex, the bridging hydroxide moiety and terminal bidentate nitrate ligands occupy adjacent *cis* coordination positions. Potentiometric pH titrations performed in aqueous solution yielded a pK_a value of 7.40 ± 0.10 for the bridging water ligand in $[Zn_2L3(\mu\text{-}OH_2)(NO_3)_n(sol)_{2-n}]^{(2-n)+}$.

Treatment of $[Zn_2L3(\mu\text{-}NO_3)(NO_3)_2]$ with nitrocefin in 1:9 DMSO:H_2O at pH = 7.5 results in hydrolysis of the β-lactam with $k_{obs} = 6.0 \pm 1.0\,min^{-1}$ at 313 K. This reaction is first order in nitrocefin. Similar to the reactivity displayed by $[Zn_2(BPAN)(\mu\text{-}OH)(\mu\text{-}O_2PPh_2)](ClO_4)_2$, the rate of nitrocefin hydrolysis increases with increasing concentration of $[Zn_2L3(\mu\text{-}NO_3)(NO_3)_2]$, but not in a linear fashion. The k_{obs} versus $[Zn_2L3(\mu\text{-}NO_3)(NO_3)_2]$ data for this reaction is best fit using an approach akin to that outlined in Scheme 26, which yielded $K = 107 \pm 20\,M^{-1}$. A kinetic pK_a value of 7.5 ± 0.2 was determined as outlined in Scheme 27. The nearly identical pK_a value to that measured via potentiometric titration for $[Zn_2L3(\mu\text{-}OH_2)(NO_3)_n(sol)_{2-n}]^{(2-n)+}$

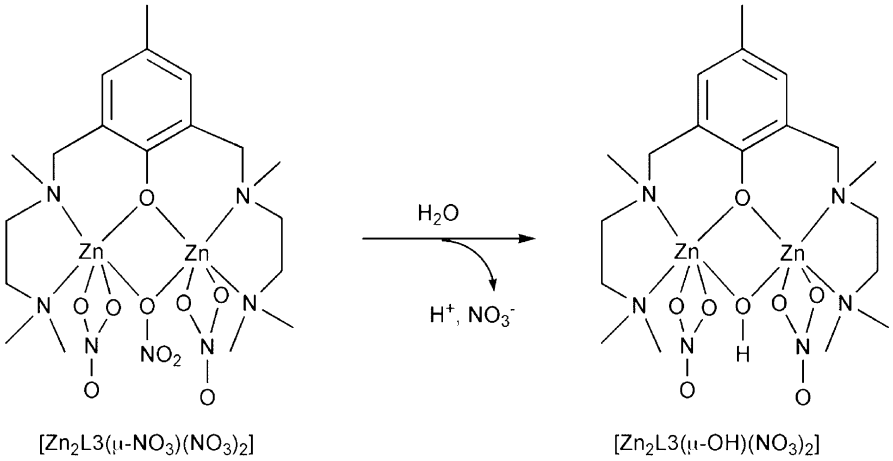

Fig. 23 Formation of $[Zn_2L_3(\mu\text{-OH})\ (NO_3)_2]$ in water.

(7.40 ± 0.10) indicates that the bridging hydroxide moiety in $[Zn_2L3(\mu\text{-OH})(NO_3)_2]$ is the nucleophile responsible for nitrocefin hydrolysis in 1:9 DMSO:H_2O solution. The poor nucleophilic character of this bridging hydroxide is indicated by the fact that the rate constant derived for nitrocefin hydrolysis by the aqua complex $[Zn_2L3\text{-}(\mu\text{-}OH_2)(NO_3)_n(sol)_{2-n}]^{(2-n)+}$ ($k_{obs} = 1.0 \times 10^{-3}\,m^{-1}$) is only 10 times less reactive than $[Zn_2L3(\mu\text{-OH})(NO_3)_2]$ ($k_{obs} = 1.0 \times 10^{-2}\,min^{-1}$).

Evidence for cephalothin (Fig. 22) or penicillin G (benzylpenicillin, Scheme 24) coordination to $[Zn_2L3(\mu\text{-}NO_3)(NO_3)_2]$ in DMSO and water solution, prior to hydrolysis, was obtained using ^{13}C NMR and infrared spectral data. Specifically, a downfield shift of the carboxylate carbon resonance, coupled with a blue shift of the $\nu_{as}(COO)$ vibration, provided evidence for monodentate coordination of the carboxylate group of the antibiotic to Zn(II) in both aqueous and organic solution. In the latter environment (1:9 DMSO:acetone) containing only a small amount of water (0.112 M), the substrate binds more tightly, with $K = (3.1 \pm 0.5) \times 10^4\,M^{-1}$.

Variable temperature kinetic studies for the hydrolysis of nitrocefin catalyzed by $[Zn_2L3(\mu\text{-OH})(NO_3)_2]$ in acetone:DMSO yielded $\Delta H^{\ddagger} = 88.4 \pm 5.3\,kJ\,M^{-1}$ and $\Delta S^{\ddagger} = -45.3 \pm 16.0\,J\,M^{-1}K^{-1}$. These values are similar to those found for nitrocefin hydrolysis catalyzed by $[Zn_2(BPAN)(\mu\text{-OH})(\mu\text{-}O_2PPh_2)](ClO_4)_2$ in 1:9 DMSO:acetone ($\Delta H^{\ddagger} = 96.1 \pm 5.2\,kJ\,M^{-1}$ and $\Delta S^{\ddagger} = -22.4 \pm 12\,J\,M^{-1}K^{-1}$) and are consistent with intramolecular attack by the bridging hydroxide on the coordinated β-lactam substrate in the rate-determining step.[140]

Comparison of the rate the hydrolysis of nitrocefin catalyzed by $[Zn_2L3(\mu\text{-OH})\text{-}(NO_3)_2]$ versus $[Zn_2L3(\mu\text{-OD})(NO_3)_2]$ gave an inverse solvent isotope effect (k_H/k_D) of 0.204.[148] Taking into consideration that free OD^- is a better nucleophile than free OH^-,[149] it was concluded that Zn–OD will be more reactive than Zn–OH and that the finding of an inverse solvent isotope effect in this reaction is consistent with rate-limiting nucleophilic attack and subsequent rapid protonation of the leaving group.

An intermediate has been spectroscopically identified in the reaction of [Zn_2L3-(μ-OH)$(NO_3)_2$] with a 10-fold excess of nitrocefin in wet DMSO.[148,150] This intermediate is relevant to an intermediate detected by stopped-flow experiments in the hydrolysis of nitrocefin catalyzed by the metallo-β-lactamase from *Bacteroides fragilis*.[127,132] UV–visible spectroscopic results and kinetic data suggest that this intermediate is anionic and has a deprotonated nitrogen atom resulting from ring opening of the lactam. The fact that this intermediate can be observed in the enzyme system suggests that protonation of the leaving group is rate determining in the enzymatic β-lactam hydrolysis reaction.[132] In the model system, the intermediate exhibits an absorption maximum at 640 nm ($\varepsilon \sim 38{,}900\ M^{-1}\,cm^{-1}$), whereas the enzyme intermediate shows an absorption at 665 nm ($\varepsilon \sim 30{,}000\ M^{-1}\,cm^{-1}$). The similarity of these two features suggests that structurally similar species are being produced. Addition of acid to the intermediate generated from [Zn_2L3(μ-OH)-$(NO_3)_2$] results in immediate spectroscopic changes consistent with the formation of the final nitrocefin hydrolysis product. This reaction is reversible, as addition of base results in the regeneration of the 640 nm feature. ^{13}C NMR and infrared measurements were used to further characterize this intermediate, and a structure was proposed on the basis of these spectroscopic studies (Fig. 24).

Using pyridinium triflate, the deprotonated amide intermediate was estimated to have $pK_a = 4.20$. This low value is consistent with Zn(II) ion stabilization of the deprotonated amide. The formation of this deprotonated amide intermediate occurs in wet DMSO with a microscopic rate constant that corresponds to the intramolecular hydrolysis of coordinated nitrocefin catalyzed by [Zn_2L3(μ-OH)$(NO_3)_2$]. Activation parameters for this reaction ($\Delta H^{\ddagger} = 77.6 \pm 8.0\ kJ\,M^{-1}$ and $\Delta S^{\ddagger} = -62.7 \pm 20.0\ J\,M^{-1}\,K^{-1}$) are within error of those found for the same reaction in acetone:DMSO

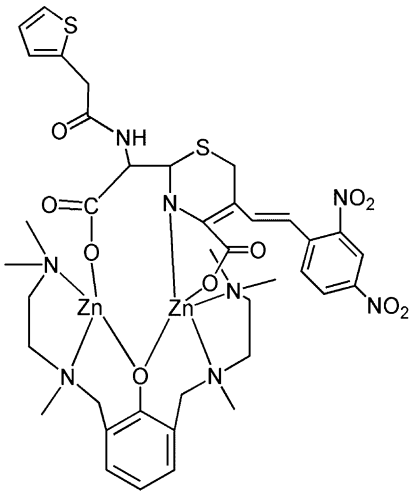

Fig. 24 Proposed structure of spectroscopically observable deprotonated intermediate in the hydrolysis of nitrocefin catalyzed by [Zn_2L3(μ-OH)$(NO_3)_2$].

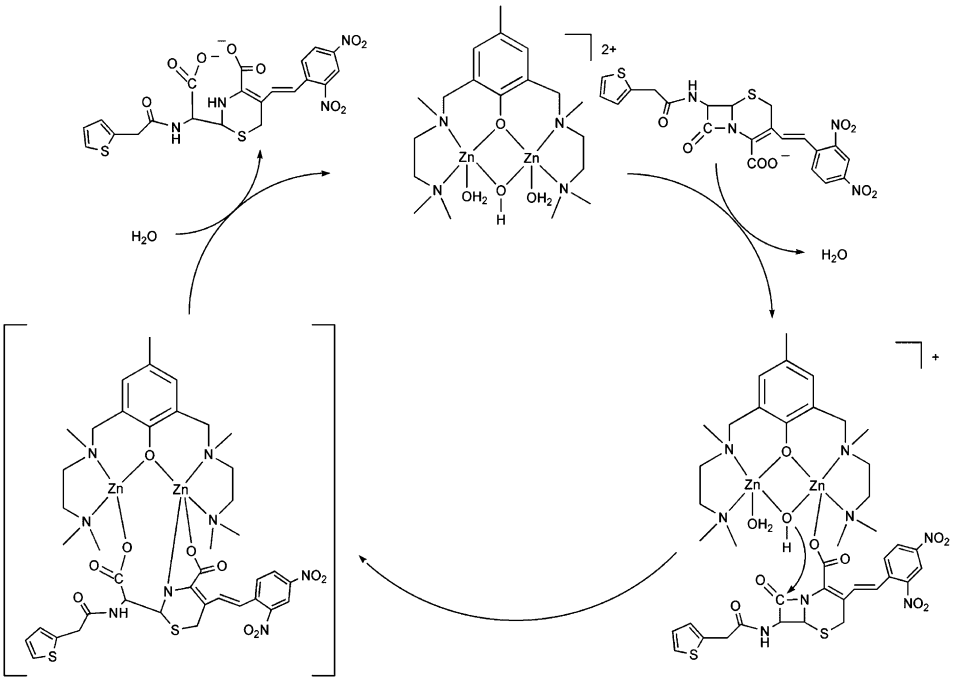

Scheme 28 Proposed mechanism for nitrocefin hydrolysis catalyzed by [Zn_2L3(μ-OH)$(NO_3)_2$] in wet DMSO. The coordinated NO_3^- ligands in the complex are replaced by water under these conditions.

($\Delta H^{\ddagger} = 88.4 \pm 5.3\ \mathrm{kJ\,M^{-1}}$ and $\Delta S^{\ddagger} = -45.3 \pm 16.0\ \mathrm{J\,M^{-1}\,K^{-1}}$). Thus, the intermediate is formed as the product of the rate-determining step as shown in Scheme 28. Overall, this mechanism has similarity to that proposed for nitrocefin hydrolysis catalyzed by the metallo-β-lactamase from *Bacteroides fragilis*.[127,131]

The nitrocefin hydrolysis reactivity of mononuclear zinc complexes has also been studied for comparison to the results obtained from the binuclear systems.[140,148] Treatment of [(bpta)Zn]$(X)_2$ (X = NO_3 or OTf, Fig. 25) with nitrocefin in aqueous solution results in hydrolysis of the β-lactam ring. The pH-dependence of the rate of the [(bpta)Zn(H_2O)]$(NO_3)_2$-catalyzed reaction yielded a kinetic $pK_a = 7.84 \pm 0.2$. This low value is consistent with the involvement of a mononuclear Zn–OH moiety as the nucleophile in the β-lactam hydrolysis reaction. At low concentration, this reaction is first-order in [(bpta)Zn–OH]NO_3, but at higher concentrations a leveling-off of the rate occurs, indicative of saturation behavior and nitrocefin coordination to the zinc complex. Fitting of the data to Equation (2) (Scheme 26) yielded the binding constant $K = 1140 \pm 106\ \mathrm{M^{-1}}$ at $[H_2O] = 13.9$ M and pH = 7.50. Increasing of the water concentration to 27.8 M resulted in a lower binding constant ($K = 425 \pm 90\ \mathrm{M^{-1}}$). This indicates that water competes with nitrocefin for coordination to the mononuclear zinc complex. At both water concentrations, the nitrocefin binding constant for [(bpta)Zn(H_2O)]$(NO_3)_2$ is notably higher than that found

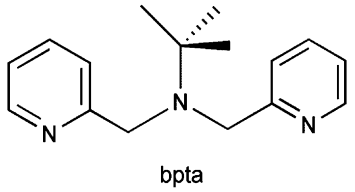

Fig. 25 Structure of the bpta ligand.

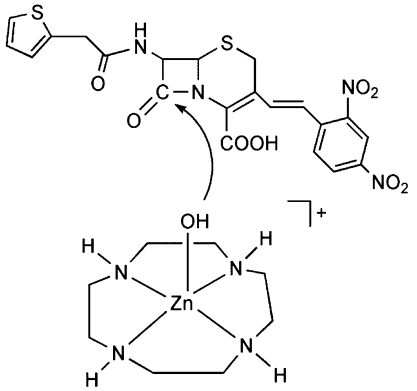

Fig. 26 Bimolecular reaction of $[([12]aneN_4)Zn(OH)]NO_3$ with nitrocefin.

for nitrocefin coordination to $[Zn_2L3(\mu\text{-}OH)(NO_3)_2]$ ($K = 107 \pm 20\,M^{-1}$). This is likely a consequence of the weaker Lewis acidity of the zinc centers in $[Zn_2L3(\mu\text{-}OH)(NO_3)_2]$ due to the presence of the anionic phenolate donor (Fig. 23) in the supporting chelate ligand.

Hydrolysis of nitrocefin catalyzed by $[([12]aneN_4)Zn(H_2O)](NO_3)_2$ (Fig. 5)[99] proceeds via a pathway that does not involve substrate coordination to the zinc center. Specifically, as the zinc center in the hydroxide species $[([12]aneN_4)Zn(OH)]NO_3$ is coordinatively saturated, the reaction proceeds via a bimolecular pathway (Fig. 26).

An important conclusion from these comparative studies is that mononuclear Zn(II) complexes can be as efficient for nitrocefin hydrolysis as binuclear systems, thus providing evidence that the second zinc center (Zn_2) in metallo-β-lactamases is not required for nucleophile activation or catalytic activity.

Studies of the hydrolysis of penicillin G promoted by a series of binuclear Zn(II) complexes (Fig. 27) have been reported.[151] These complexes, which are supported by pyrazolate-containing chelate ligands, have varying Zn···Zn distances.[152–154] In the complexes having a shorter Zn···Zn distance (**1** and **3**), a single bridging hydroxide is present. However in complexes of this series having a longer Zn···Zn distance (**2** and **4**), a terminal hydroxide ligand participates in a strong hydrogen-bonding interaction with a water molecule that is coordinated to the other zinc center. This secondary interaction produces a lower pK_a value for the aqua analogs of **2** and **4**

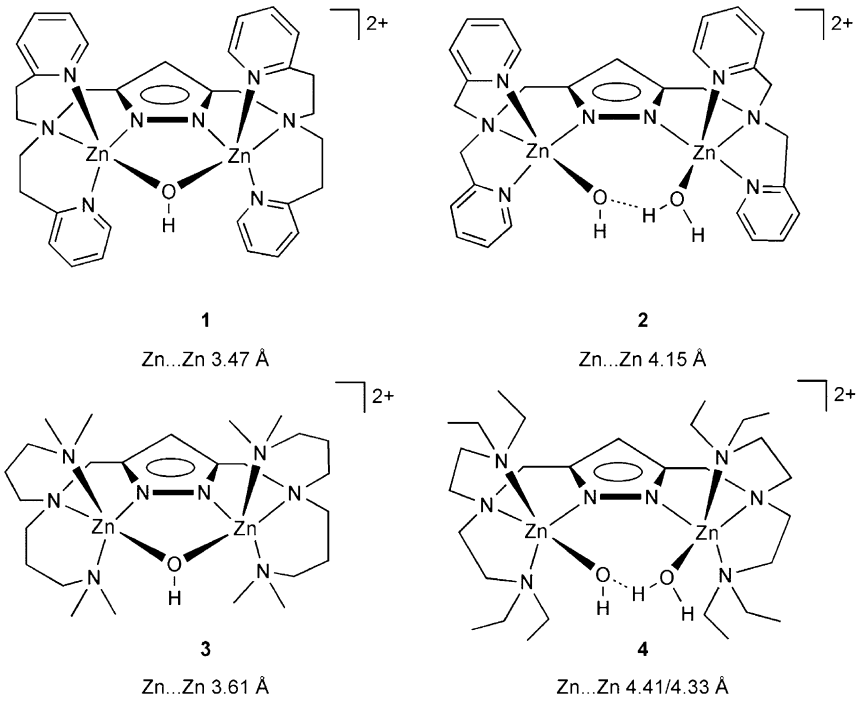

Fig. 27 Cationic portions of pyrazolate-bridged binuclear zinc hydroxide complexes.

(7.60 and 7.57, respectively) versus the pK_a value found for the aqua analog of **1** (7.96).[153–155]

Treatment of **1–3** with excess penicillin G (benzylpenicillin) in DMSO:H_2O (9:1) results in hydrolytic ring opening of the lactam. The rate of this reaction differs depending on the structural features of the zinc complex, with the reaction rate increasing in the order **2** < **1** < **3**. Complex **4** is unreactive toward penicillin G. For **3**, approximately three equivalents of the substrate are hydrolyzed in 20 min at ambient temperature. Complexes **1** and **3** show significantly enhanced reactivity relevant to $Zn(NO_3)_2 \cdot H_2O$ and $Zn(ClO_4)_2 \cdot 6H_2O$, whereas **2** and **4** show reduced reactivity. Thus, the binuclear zinc complexes produce either enhanced or diminished β-lactam hydrolysis activity depending on the structure of the cation.

X-ray crystallographic studies of the reaction products generated via admixture of the supporting chelate ligands found in **3** and **4** with $Zn(ClO_4)_2 \cdot 6H_2O$, base, and the simple β-lactam oxazetidinylacetate (oaa) provide insight into how substrate coordination may influence the structural features of the binuclear zinc complex. As shown in Fig. 28a, the binuclear zinc–oaa complex supported by the chelate ligand found in **3** contains the β-lactam coordinated in an anisobidentate fashion (Zn(1)–O(1) 2.006(3) Å, Zn(1)–O(2) 2.358(4) Å).[156] At each zinc center, one of the dimethylamino donor atoms is not coordinated, and the zinc center exhibits a

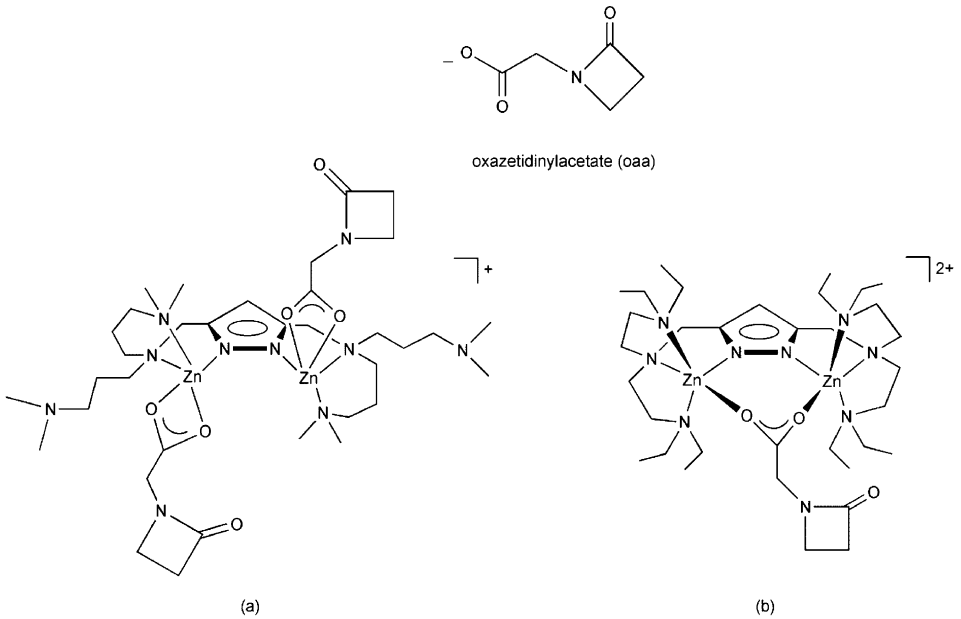

Fig. 28 Structural features of oxazetidinylacetate adducts.

distorted square pyramidal geometry.[157] The Zn···Zn distance in this complex is 4.328(1) Å. The dissociation of the amine donor in this structure may result from low stability for the six-membered chelate ring.[158,159] Using the chelate ligand found in **4** in the same type of reaction, an adduct of oaa is formed wherein the carboxylate moiety bridges the two zinc centers (Fig. 28b). In this complex, each zinc center exhibits a distorted trigonal bipyramidal geometry ($\tau = 0.86/0.79$).[157] Notably, in both of these complexes, the β-lactam carbonyl does not interact with a Zn(II) center.

The differing chelate ligand coordination properties exhibited by the β-lactam adduct complexes shown in Fig. 28 may provide evidence of why complexes **1** and **3** (Fig. 27) exhibit enhanced reactivity relative to **2** for β-lactam hydrolysis involving penicillin G, and why **4** is unreactive. In **1** and **3**, the presence of unstable six-membered chelate rings may enable dissociation of multiple N-donors, thus providing coordination sites for penicillin G coordination, including perhaps β-lactam carbonyl coordination, as well as possible binding sites for water and the formation of a Zn–OH nucleophile. ^{1}H NMR studies of equimolar mixtures of **1** (Fig. 27) and penicillin G in d_6-acetone/D_2O (8:1) at 300 K at early reaction times revealed resonances at chemical shifts intermediate between those of the free ligand and **1**, suggesting that a dynamic process may be occurring in solution wherein N-donors dissociate from the Zn(II) centers in the presence of penicillin G. When the same type of ^{1}H NMR experiment was performed using **2** and penicillin G, only minor signal broadening was observed, indicating that the zinc complex likely retains

coordination of all ligand appendages in solution. Overall, these combined studies provide evidence that the low reactivity of **2** and **4** may be due to the fact that once substrate binds to the binuclear zinc center, in a similar motif to that shown in Fig. 28b, there may not be any available Zn(II) coordination sites for β-lactam carbonyl and/or water activation.

For the structures shown Schemes 26 and 28, and in Fig. 28, coordination of the β-lactam substrate to a binuclear zinc center involves the carboxylate moiety and not the β-lactam amide carbonyl oxygen. Evidence for carboxylate coordination, and against β-lactam amide oxygen coordination in these complexes, was obtained via ^{13}C NMR and infrared spectroscopic studies, and/or by X-ray crystallography. It is worth noting that recent structural investigations of β-lactam adduct compounds have revealed that Zn(II) coordination of a β-lactam carbonyl oxygen can occur under specific conditions.[151,160] As shown in Fig. 29a, a binuclear zinc complex having bridging oxazetidinylacetate ligands has been isolated using a supporting chelate ligand having only three nitrogen donors to each zinc center.[151] Notably, the Zn–O(amide) distance in this compound (2.005(2) Å) is shorter than both Zn–O(carboxylate) distances (2.093(3) and 2.060(2) Å). Consistent with this strong interaction is the fact that the amide C–O bond in this complex is longer (1.242(4) Å) than in complexes wherein the amide oxygen does not interact with the Zn(II) center (e.g. complexes shown in Fig. 28 which exhibit C–O distances of 1.210(6) and 1.218(4) Å, respectively). The amide C–N bond is also shorter in the complexes shown in Fig. 29 than in complexes wherein the amide oxygen does not interact with the Zn(II) ion. These combined structural parameters indicate that the β-lactam amide moiety is significantly polarized upon coordination to Zn(II) center. However, these complexes are not reactive toward hydrolysis, presumably because of the anionic nature of the *N*-deprotonated β-lactam.

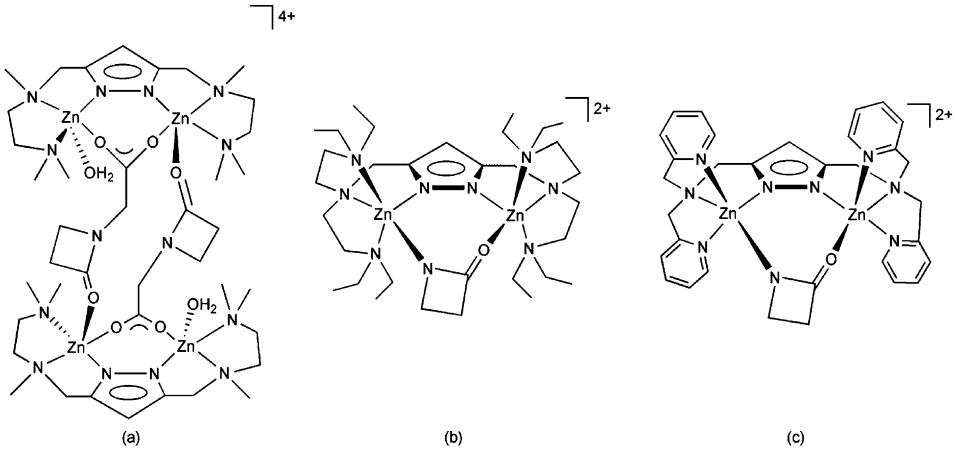

Fig. 29 Structurally characterized binuclear zinc β-lactam complexes having β-lactam carbonyl coordination.

PEPTIDE HYDROLYSIS

Metalloaminopeptidases use an active site motif containing one or two metal ions to cleave the *N*-terminal residue of a polypeptide chain.[161] The catalytic mechanism of the aminopeptidase from *Aeromonas proteolytica* (ApAP) has been outlined in great detail.[162] The active site co-catalytic zinc centers in ApAP are ligated by a mixture of carboxylate and histidine donors, with bridging hydroxide and aspartate ligands (Fig. 30). In a proposed catalytic mechanism for this enzyme, the amide carbonyl moiety of the substrate is proposed to initially bind to Zn_1 (Scheme 29). Upon substrate binding, the bridging hydroxide moiety becomes terminal on Zn_1. This process may be assisted by the formation of an interaction between the *N*-terminal amino group and Zn_2, as well as by the formation of a new hydrogen bond between this amino group and the carbonyl oxygen of a Zn_2-bound carboxylate ligand. Attack of the Zn_1–OH moiety on the activated amide carbonyl carbon yields a tetrahedral intermediate that decomposes upon protonation of the leaving group. This C–N bond-breaking is proposed as the rate-limiting step.[163]

A few model systems have been reported which mediate the hydrolysis of peptide substrates.[164–168] For example, treatment of a macrocyclic bizinc complex of the OBISDIEN (1,4,7,14,16,19-hexaaza-10,22-dioxcyclotetracosane) ligand (Scheme 30) with glycylglycine (Gly–Gly) at varying p*D* values in D_2O results in hydrolysis to produce two equivalents of glycine.[164] At 343 K, and p*D* values of 8.37 and 8.72, values for the hydrolysis rate constant (k_H) of $2.6(2) \times 10^{-7}\,s^{-1}$ and $3.5(2) \times 10^{-7}\,s^{-1}$, respectively, were obtained. Coupled with speciation studies performed as a function of pH, it was determined that three zinc hydroxide species, $[LZn_2(OH)Gly–Gly]^{2+}$, $[LZn_2(OH)_2Gly–Gly]^{+}$, and $[LZn_2(OH)_3Gly–Gly]$ (L = OBISDIEN) have similar rate constants ($k_H \sim 5 \times 10^{-7}\,s^{-1}$) for the hydrolysis reaction. These hydroxide derivatives are approximately five times more active than a similar complex having no hydroxide component (e.g. $[LZn_2(Gly–Gly)]^{3+}$, $k_H = 1.0(2) \times 10^{-7}\,s^{-1}$). A proposed mechanism for glycylglycine hydrolysis promoted by the bishydroxo complex is shown in Scheme 30.

The binuclear zinc complex $[(LH^{+})_2Zn_2(Gly–Gly)_2](ClO_4)_4$ (Fig. 31, L = 1-methyl-4-(6-amino-2-pyridylmethyl)-piperazine) was characterized by X-ray crystallography.[168] In this structure, a water molecule is positioned close (O(water)···C(carbonyl) 3.050 Å)

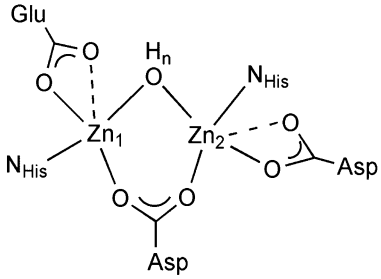

Fig. 30 Active site co-catalytic zinc centers in ApAP.

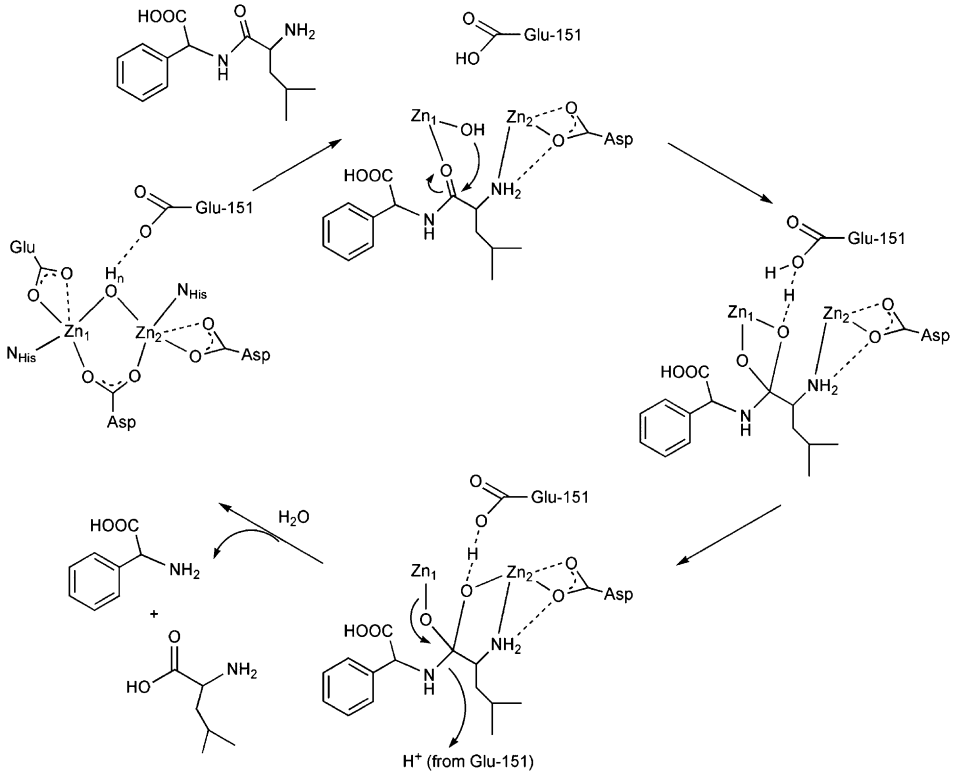

Scheme 29 Selected transformations in the proposed mechanistic pathway for peptide hydrolysis by ApAP. The zinc-coordinated amino acid ligands are shown only on the resting state structure (left) for clarity.

to the amide carbonyl carbon of Gly–Gly, the oxygen atom of which is coordinated to the zinc center. At 70 °C and pH = 7.0(1) (50 mM HEPES) the coordinated Gly–Gly in $[(LH^+)_2Zn_2(Gly–Gly)_2](ClO_4)_4$ undergoes hydrolysis over the course of days (~28% Gly–Gly hydrolysis after 5 days). The structural and reactivity properties of this complex have relevance to the monozinc peptidase aminopeptidase A.[169]

Binuclear zinc complexes have been shown to mediate the hydrolysis of the activated peptide model substrate L-leucine–*p*-nitroanilide (LNA, Fig. 32) with the reactions being followed spectroscopically by the formation of *p*-nitroaniline (λ_{max}~400 nm).[165–167] This model substrate has also been used in studies of ApAP.[170] The hydrolysis of LNA mediated by the zinc complex $[(bomp^-)]Zn_2(CH_3CO_2)_2]BPh_4$ (Fig. 33a; H(bomp): 2,6-bis[bis(2-methoxyethyl)aminomethyl]-4-methylphenol) in water/DMF (6:4) occurs via a reaction that is first-order in complex and substrate, with a second-order rate constant $k = 2.3(1) \times 10^{-3}\,M^{-1}\,s^{-1}$ at 25 °C. At best, a yield of ~65% for a single turnover reaction was obtained, indicating that

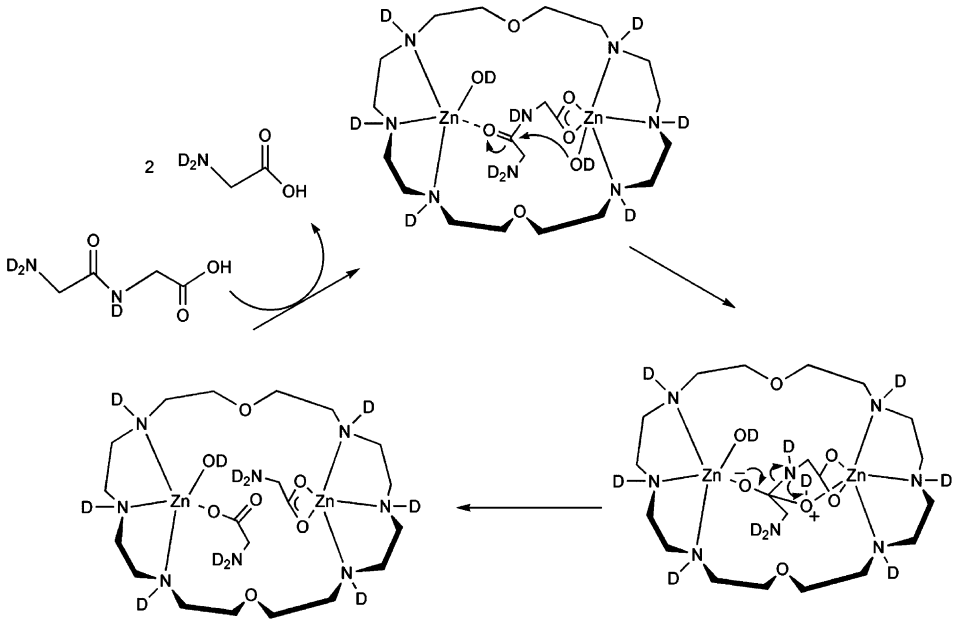

Scheme 30 Proposed mechanism for Gly–Gly hydrolysis promoted by a bizinc complex of the OBISDIEN chelate ligand.

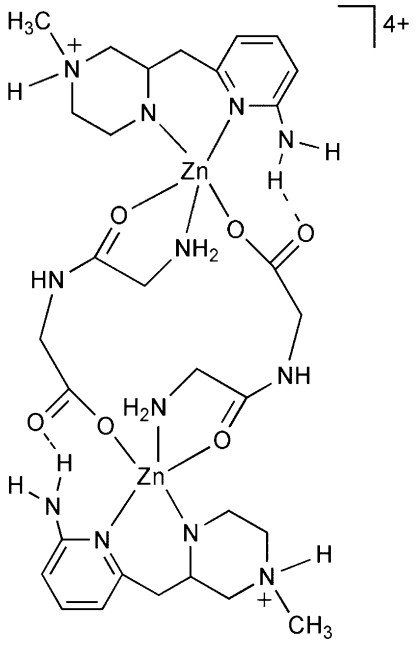

Fig. 31 Cationic portion of $[(LH^+)_2Zn_2(Gly–Gly)_2](ClO_4)_4$.

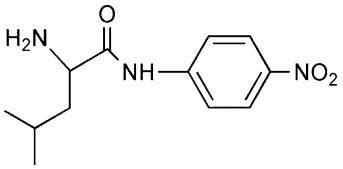

Fig. 32 L-leucine–*p*-nitroanilide (LNA).

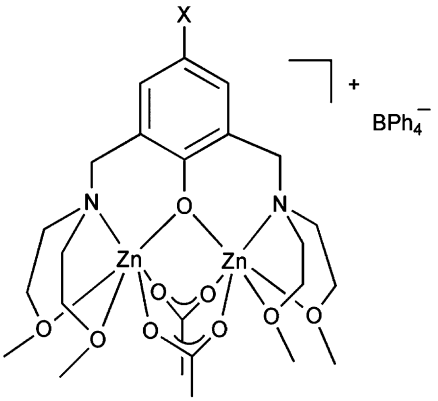

(a) X = -CH_3 ($bomp^-$)
(b) X = -NO_2 ($bonp^-$)
(c) X = -Cl ($bocp^-$)

Fig. 33 Binuclear zinc complexes that mediate the hydrolysis of *N*-*p*-nitrophenyl- L-leucine in water-containing solutions.

the zinc complex becomes inactive following substrate hydrolysis. The actual active zinc complex for the amide hydrolysis reaction in this system is not known.

Analogs of the $bomp^-$ ligand, $bonp^-$ (H(bonp): 2,6-bis[bis(2-methoxyethyl) aminomethyl]-4-nitrophenol) and $bocp^-$ (H(bocp): 2,6-bis[bis(2-methoxyethyl) aminomethyl]-4-chlorophenol) have been used to assemble zinc complexes for comparative model aminopeptidase reactivity studies.[166] Using the method of initial rates, the second-order rate constants for the hydrolysis of LNA promoted by $[(bonp^-)]Zn_2(CH_3CO_2)_2]BPh_4$ and $[(bocp^-)]Zn_2(CH_3CO_2)_2]BPh_4$ (Fig. 33b and c) at 25 °C in DMF:tricine buffer were found to be $5.9(5) \times 10^{-1}\,M^{-1}\,s^{-1}$ and $2.7(1) \times 10^{-2}\,M^{-1}\,s^{-1}$, respectively. Comparison of these rate constants to that obtained for the hydrolysis of the same substrate promoted by $[(bomp^-)]Zn_2(CH_3CO_2)_2]BPh_4$ ($2.3(1) \times 10^{-3}\,M^{-1}\,s^{-1}$) under identical conditions reveals that the inclusion of an electron withdrawing substituent on the phenolate ring increases the rate of the LNA hydrolysis reaction. Studies of the rate of this reaction as a function of pH for the $[(bomp^-)]Zn_2(CH_3CO_2)_2]BPh_4$- and $[(bocp^-)]Zn_2(CH_3CO_2)_2]$

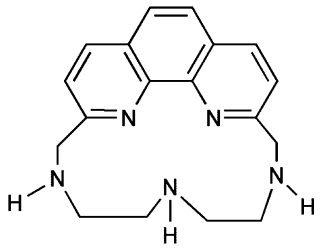

L4

Fig. 34 Phenanthroline-containing polyamine macrocyclic ligand.

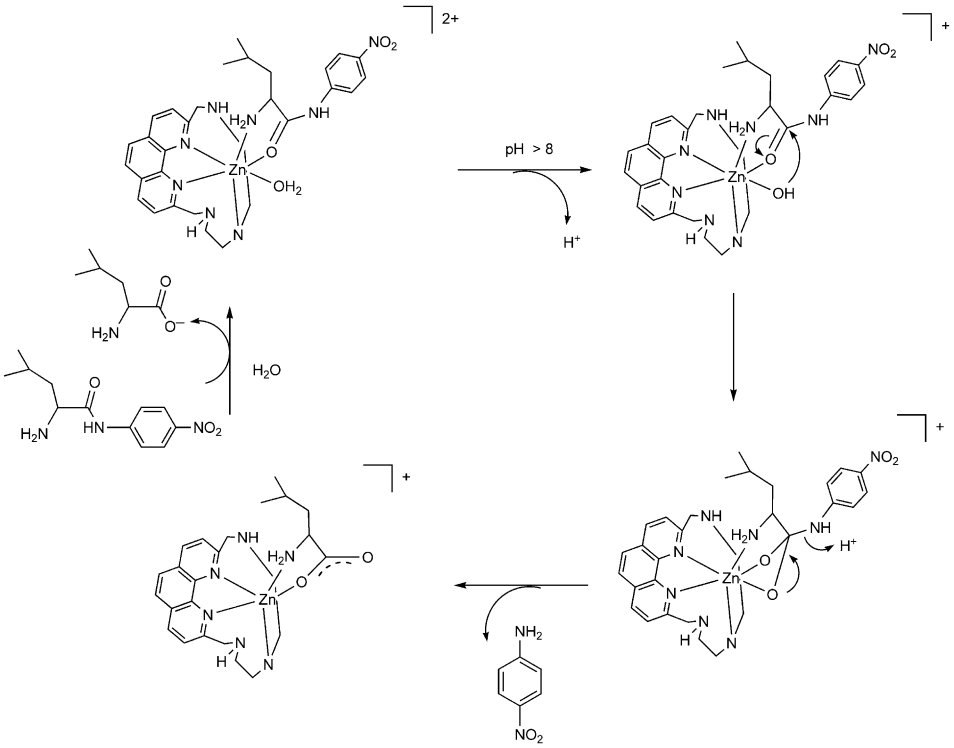

Scheme 31 Proposed mechanism for LNA hydrolysis mediated by a zinc complex of a phenanthroline-containing polyamine ligand.

BPh_4-promoted reactions yielded kinetic pK_a values of 9.4 and 9.1, respectively. Both values are suggested to correspond to the deprotonation of a $Zn–OH_2$ moiety to produce a reactive zinc hydroxide species.

A zinc complex of a phenanthroline-containing macrocycle (L4, Fig. 34) binds LNA with a log K value of 5.55 (308 K) to form $[(L4)Zn(LNA)]^{2+}$, as determined by

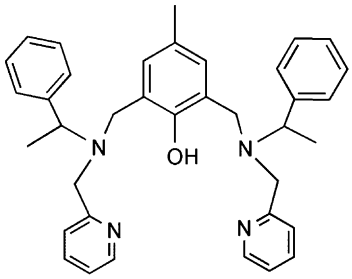

Fig. 35 H(bppmp) ligand.

potentiometric titration and ^{1}H NMR studies.[167] This complex undergoes a monodeprotonation at pH > 8, a reaction that results in either the formation of a zinc hydroxide species ($[(L4)Zn(LNA)(OH)]^+$) or a complex having a deprotonated LNA^- ligand ($[(L4)Zn(LNA^-)]^+$). This deprotonated complex is active for LNA hydrolysis to produce L-leucine and *p*-nitroaniline. When corrected for the amount of deprotonated complex in solution, this reaction proceeds with a pseudo first-order rate constant of $3.0 \times 10^{-6}\,s^{-1}$. An intramolecular mechanism is proposed for this reaction wherein a zinc-bound hydroxide attacks the coordinate LNA ligand (Scheme 31).

Zinc complexes of optically resolved forms of the dinucleating ligand H(bppmp) (2,6-bis[{(*R*/*S*)-1-phenylethyl-2-pyridylmethyl}aminomethyl]-4-methylphenol, Fig. 35) exhibit differing second-order rate constants (*R*: $3.3(7) \times 10^{-2}\,M^{-1}\,s^{-1}$; *S*: $7.6(5) \times 10^{-2}\,M^{-1}\,s^{-1}$) for the hydrolysis of LNA in DMF:H_2O (2:3) at pH = 8.0.[171] The enhanced reactivity of [(*S*-bppmpZn$_2$)(MeCO$_2$)$_2$]BPh$_4$ versus that of [(*R*-bppmpZn$_2$)(MeCO$_2$)$_2$]BPh$_4$ is attributed to better recognition of the LNA substrate by the former complex.

Outside the scope of coverage of this work are synthetic systems involving the catalytic or stoichiometric alcoholysis of esters or amides promoted by zinc ions or complexes.[172–177]

5 Phosphate ester hydrolysis

PHOSPHATE MONOESTER HYDROLYSIS

Alkaline phosphatase is one of a number of zinc-containing enzymes and nucleases that catalyze in the hydrolysis of a phosphate ester linkage.[178–186] The catalytic mechanism of *Escherichia coli* alkaline phosphatase has been extensively investigated and involves initial coordination of the phosphate monoester substrate (e.g. 4-nitrophenyl phosphate) in a bridging position between two active site zinc centers (Scheme 32).[187] A deprotonated active site serine residue then acts as a nucleophile to attack the phosphoryl group which results in cleavage of the P–O bond to the 4-nitrophenolate leaving group. In this reaction, a phosphorylserine group is formed

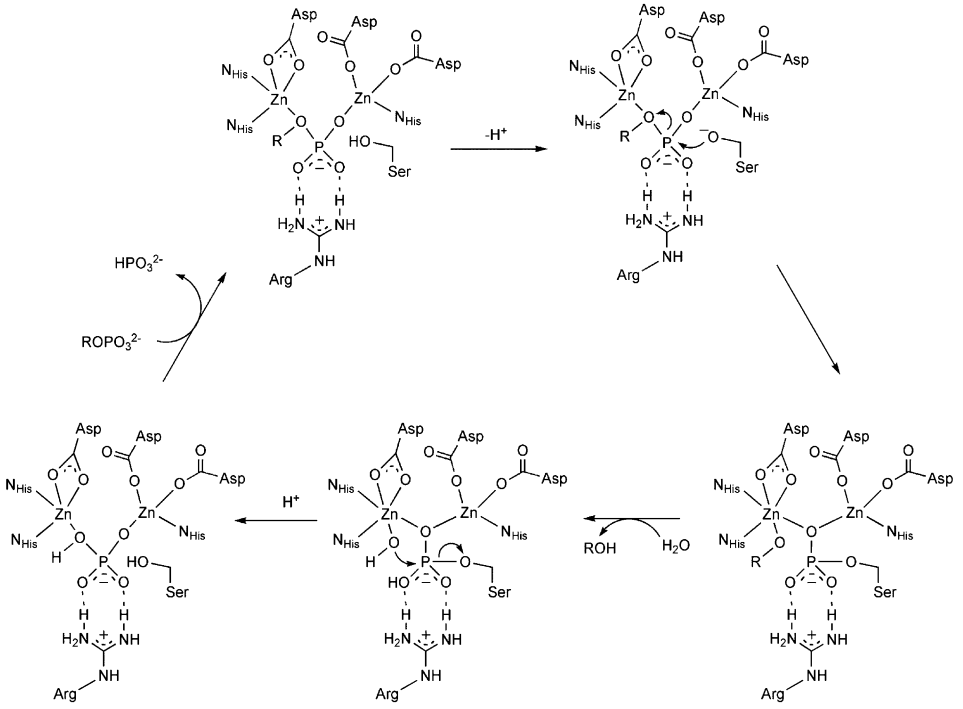

Scheme 32 Phosphate monoester hydrolysis catalyzed by alkaline phosphatase.

that remains coordinated to the binuclear zinc center. In addition, one of the two zinc ions provides stabilization for the anionic 4-nitrophenolate leaving group. Hydrolysis of the phosphorylserine group occurs via attack of a Zn–OH moiety to yield HPO_4^{2-}, which is subsequently released from the active site. As shown in Scheme 32, hydrogen-bonding interactions involving an arginine residue (Arg-166 in *E. coli*) are important throughout the catalytic cycle.

Phosphate ester hydrolysis can occur via three possible limiting mechanisms.[187] A dissociative mechanistic pathway involves an S_N1-type reaction in which a stable metaphosphate ion (PO_3^-) is formed, which then undergoes reaction with a hydroxide nucleophile to yield the final products. In an associative pathway, a stable five-coordinate phosphorane intermediate forms prior to departure of the leaving group. In a concerted pathway for phosphate ester hydrolysis, nucleophilic attack and P–O(H) bond formation occur simultaneously with P–O(R) bond cleavage involving the leaving group.

As with amide hydrolysis reactions, extensive mechanistic studies of metal-mediated phosphate monoester hydrolysis reactions have been performed using exchange inert mononuclear Co(III) complexes.[9,188–202] To date, only a few zinc complexes that promote phosphate monoester hydrolysis have been reported. A binuclear zinc complex supported by a macrocyclic cryptate ligand (Fig. 36)

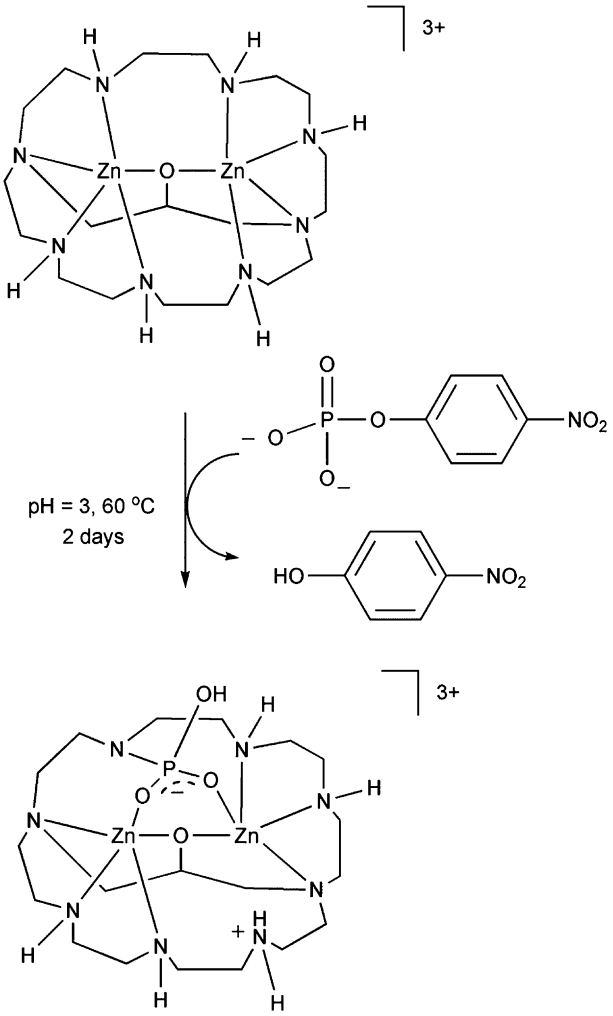

Fig. 36 Phosphate monoester hydrolysis promoted by a bizinc cryptand complex.

promotes the cleavage of 4-nitrophenyl phosphate dianion in aqueous solutions via attack of an internal amine nucleophile.[14,203] This complex contains two zinc ions separated by a distance of 3.24 Å and bridged by an alkoxide anion. Each zinc center exhibits a distorted trigonal bipyramidal geometry, with secondary and tertiary amine nitrogen donors in the axial positions. The product of the 4-nitrophenyl phosphate hydrolysis reaction is a phosophoramide derivative (Fig. 36). Kinetic studies of this reaction yielded a maximum second-order rate constant for 4-nitrophenyl phosphate hydrolysis of $(1.52 \pm 0.05) \times 10^{-3}\,M^{-1}\,s^{-1}$ at pH = 5.9 and 35 °C. Rate studies as a function of pH yielded a bell-shaped curve with $pK_1 = 5.2$ and $pK_2 = 6.3$. These values correspond to protonation constants for the substrate

($NPP^{2-} + H^+ = HNPP^-$; NPP^{2-} = 4-nitrophenyl phosphate dianion) and supporting chelate ligand ($NH + H^+ = NH_2^+$, NH = donor of macrocycle).

Treatment of bizinc complexes of a series of aryl-bridged ligands (Fig. 37a–d) with 4-nitrophenyl phosphate in DMSO and buffered water (tris (pH 8.36) or HEPES (pH 8.13)) at 55 °C results in phosphate ester hydrolysis with pseudo first-order rate constants as shown in Fig. 37.[204] Mononuclear analogs (Fig. 37e and f) also exhibit phosphate monoester hydrolysis reactivity, albeit significantly lower than that of the binuclear systems. Studies of the rate of 4-nitrophenyl phosphate hydrolysis versus pH for the reaction promoted by the binuclear zinc complex ligated by *S*,*S*′-bis (10-(1,4,7-triazacyclododecyl))-1′,3′-dithiobenzene (Fig. 37a) yielded a kinetic pK_a of 7.8. This value was attributed to deprotonation of a bridging H_2O ligand between the zinc ions. A mechanistic pathway involving attack of the bridging hydroxide on a coordinated phosphate monoester dianion has been proposed for this system.

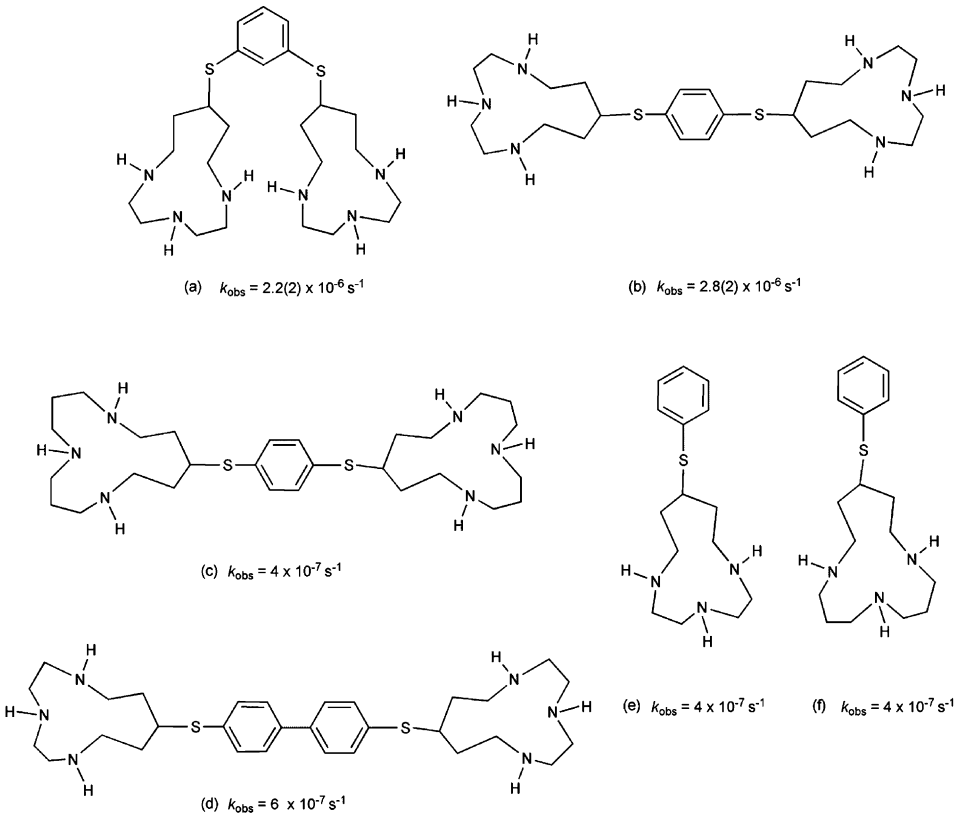

Fig. 37 Aryl-bridged ligands and pseudo first-order rate constants for the hydrolysis of 4-nitrophenyl-phophate promoted by the zinc complex of each ligand. Pseudo first-order rate constants were determined using 227 mM (dimer) or 454 mM (monomer) solutions.

The mononuclear four-coordinate zinc hydroxide complex [(Tp^{iPr2})Zn–OH] does not promote the hydrolysis of 4-nitrophenylphosphate in Et_2O solution.[205] Instead, the phosphate ester is deprotonated to give a binuclear μ-phosphate complex, [($Tp^{iPr2}Zn)_2$(μ-O_2P(O–C_6H_4–*p*-NO_2)].

Outside the scope of coverage of this contribution are Zn(II)-promoted reactions involving ATP hydrolysis.[203]

PHOSPHATE DIESTER AND TRIESTER HYDROLYSIS

Hydrolysis reactions involving phosphate diester and triester substrates, particularly bis(4-nitrophenyl) phosphate and tris(4-nitrophenyl) phosphate, have often been examined as model reactions phosphate ester cleaving enzymes. The hydrolysis of phosphotriesters is also relevant to the chemistry of phosphotriesterases, zinc-containing enzymes found in soil bacteria.[206,207] The active site of the phosphotriesterase from *Pseudomonas diminuta* contains two zinc centers ligated by a mixture of oxygen and nitrogen donors (Fig. 38).[208,209] A proposed mechanism for this enzyme involves attack of the bridging hydroxide on the coordinated phosphotriester substrate.[210]

Similar to studies of phosphate monoester hydrolysis reactions, extensive kinetic and mechanistic investigations involving exchange inert Co(III) compounds have yielded insight into the pathways of these reactions.[9,192,194,197,198,200,211–220]

Several synthetic mononuclear zinc complexes have been shown to exhibit stoichiometric or catalytic hydrolysis reactivity involving phosphate di- and/or triester substrates. For example, a mononuclear zinc complex supported by the

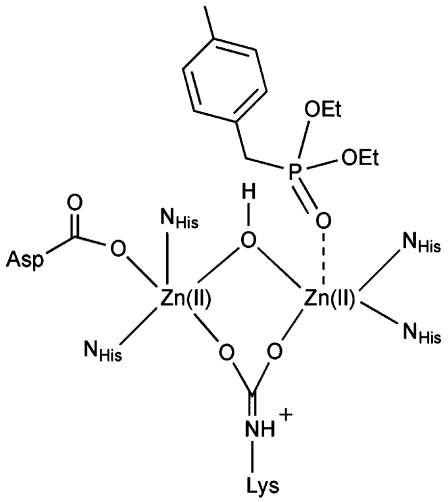

Fig. 38Structure of active site binuclear zinc cluster in the phosphotriesterase from *P. diminuta* in the presence of the competitive inhibitor diethyl-4-methylbenzyl phosphonate.

Me_2pyo[14]trieneN_4 (CR) ligand (Fig. 6a) catalyzes the hydrolysis of the triester diphenyl 4-nitrophenyl phosphate in aqueous acetonitrile solution.[221] This reaction is first-order in zinc complex and phosphate ester. On the basis of pH-rate studies, which revealed a kinetic pK_a value of 8.7,[40] the active zinc complex is proposed to be $[(CR)Zn–OH]^+$. A hybrid mechanism in which the zinc center of $[(CR)Zn–OH]^+$ serves to provide the hydroxide nucleophile, and also electrophilically activates the phosphoryl P–O bond, is favored for this system. This type of bifunctional mechanism was proposed based on the fact that the second-order rate constant for the $[(CR)Zn–OH]^+$-catalyzed reaction (2.8×10^{-1} $M^{-1}s^{-1}$) is an order of magnitude larger than that of free hydroxide ion-catalyzed hydrolysis ($2.8 \times 10^{-2}\,M^{-1}s^{-1}$). As OH^- is a better nucleophile than the zinc-coordinated hydroxide, Lewis acid activation of the substrate is also operative in this system.

Attachment of a cyclodextrin unit to an N–CH_3 form of the CR macrocycle (Fig. 39) yielded a zinc complex with only modestly improved effectiveness ($k_2 = 21.7 \times$ $10^{-2}\,M^{-1}s^{-1}$) over the mononuclear system ($k_2 = (3.80 \pm 0.05) \times 10^{-2}\,M^{-1}s^{-1}$) for the hydrolysis of diphenyl 4-nitrophenyl phosphate under identical conditions.[109] This enhancement is proposed to be due to binding of 4-nitrophenolate moiety in the cyclodextrin cavity.

Bifunctional analogs of the $[(CR)Zn]^{2+}$ (Fig. 6a) structure in which an auxiliary catalytic imidazole or thiophenol group has been incorporated (Fig. 40) exhibit enhanced reactivity for the intramolecular transesterification reaction of 2-hydroxypropyl 4-nitrophenyl phosphate (HPNP) relative to the parent complex.[222]

Zinc complexes of the cyclen ([12]aneN_4 = 1,4,7,10-tetraazacyclododecane) ligand have been extensively studied in terms of phosphate ester hydrolysis reactivity. For example, a proposed binuclear Zn(II) hydroxide complex of cyclen was reported to enhance the rate of hydrolysis of ethyl(2,4-dinitrophenyl)-methylphosphonate and diethyl(2,4-dinitrophenyl) phosphate.[223,224] It should be noted that the nuclearity of the zinc–cyclen complex in solution was not conclusively identified in this work.

The mononuclear zinc complexes $[([12]aneN_3)Zn(OH_2)](ClO_4)_2$ (Fig. 4) and $[([12]aneN_4)Zn(OH_2)](ClO_4)_2$ (Fig. 5) promote the hydrolysis of the triester tris(4-nitrophenyl) phosphate and the diester bis(4-nitrophenyl) phosphate.[225] For these

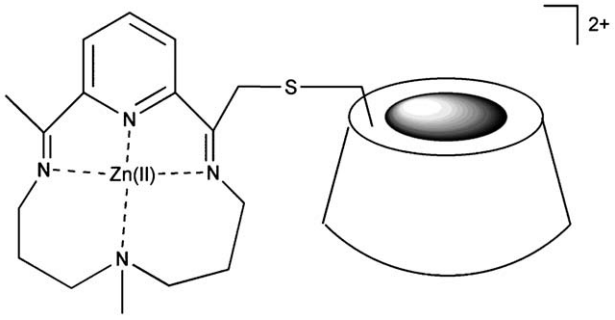

Fig. 39 Cationic portion β-cyclodextrin-appended zinc complex.

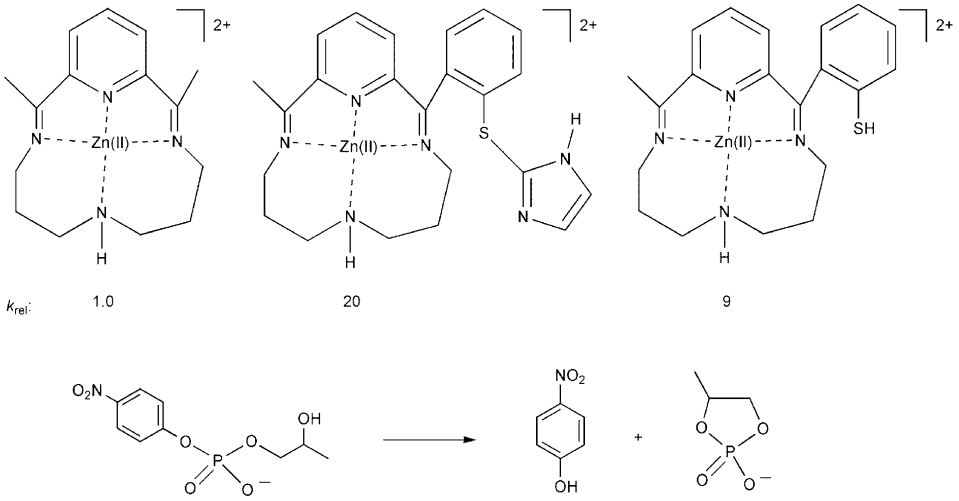

Fig. 40 (top) Cationic portion of bifunctional zinc complexes and relative second-order rate constant values and (bottom) intramolecular transesterification reaction of 2-hydroxypropyl 4-nitrophenyl phosphate (HPNP).

reactions, pH-rate profiles indicate that the active species are the zinc hydroxide derivatives [([12]aneN_3)Zn(OH)]ClO_4 and [([12]aneN_4)Zn(OH)]ClO_4. For the phosphate triester hydrolysis reactions, the second-order rate constants at 25 °C and $I = 0.20$ for free OH^-, [([12]aneN_3)Zn(OH)]ClO_4, and [([12]aneN_4)Zn(OH)]ClO_4 are 10.7 ± 0.2, 7.0 ± 0.2, and $3.7 \pm 0.2\ M^{-1}\,s^{-1}$, respectively. Thus, free OH^- ion is the most reactive species for the hydrolysis of tris(4-nitrophenyl) phosphate. However, for the hydrolysis of bis(4-nitrophenyl) phosphate, [([12]aneN_3)Zn(OH)]ClO_4 ($k = (8.5 \pm 0.2) \times 10^{-5}\ M^{-1}\,s^{-1}$) is approximately four times more reactive than [([12]aneN_4)Zn(OH)]ClO_4 ($k = (2.1 \pm 0.2) \times 10^{-5}\ M^{-1}\,s^{-1}$) and free OH^- ($k = (2.4 \pm 0.1) \times 10^{-5}\ M^{-1}\,s^{-1}$) at 35 °C and $I = 0.20$ (Na^+). The differing hydrolytic reactivity of [([12]aneN_3)Zn(OH)]ClO_4 (relative to free OH^-) for activated phosphate triester versus diester hydrolysis has been explained in terms of differing mechanistic pathways. Specifically, in the triester hydrolysis reaction, the Zn(II) center of [([12]aneN_3)Zn(OH)]ClO_4 is primarily proposed to provide the nucleophile, with little or no interaction with the P = O group of the substrate (Fig. 41). However, in the phosphate diester hydrolysis reaction, a hybrid-type mechanism is proposed wherein the zinc center is suggested to provide the hydroxide nucleophile as well as electrophilic activation of the P = O moiety of the monoanionic diester substrate.

Insight into the role of the serine nucleophile in the catalytic cycle of alkaline phosphatase was gained through studies of the bis(4-nitrophenyl) phosphate reactivity of a mononuclear Zn(II) complex supported by the (*S*)-1-(2-hydroxy-2-phenylethyl)- 1,4,7,10-tetrazacyclodecane ligand (Scheme 33).[226] In aqueous solution, this complex exhibits a pK_a value for the zinc-bound alkoxide moiety of 7.30 ± 0.02.

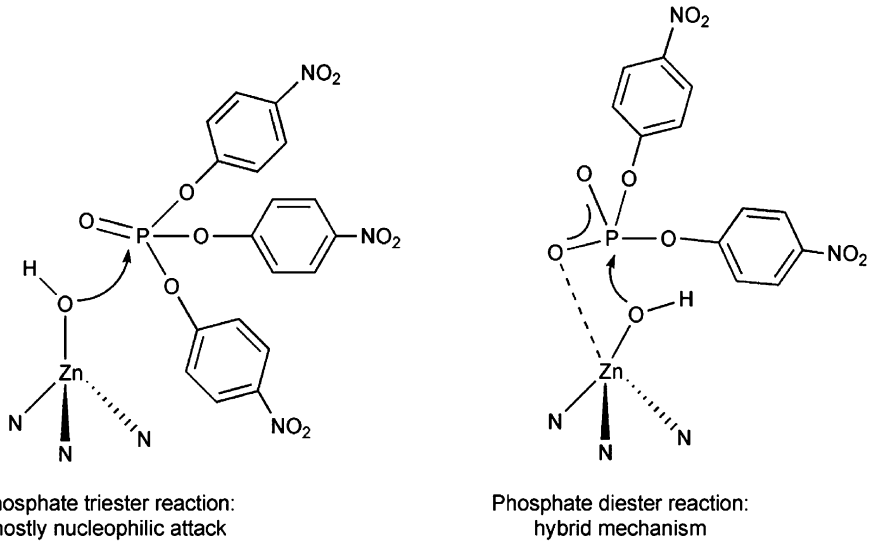

Fig. 41 Proposed mechanisms for phosphate triester and diester hydrolysis promoted by [([12]aneN$_3$)Zn(OH)]ClO$_4$.

A phosphoryl transfer reaction from bis(4-nitrophenyl) phosphate to the zinc-bound alkoxide moiety is promoted by this complex in aqueous solution (pH = 6.0–10.3) at 35°C and $I = 0.10$ M ($NaNO_3$). A pH-rate profile for this reaction yielded a sigmoidal curve and a kinetic pK_a value of 7.4. As this value corresponds to that measured for the Zn–OR moiety by potentiometric titration, the zinc-bound alkoxide was confirmed as the reactive nucleophile for phosphoryl transfer. The rate of this reaction is 125 times greater than for the bis(4-nitrophenyl) phosphate hydrolysis reaction promoted by [([12]aneN$_4$)Zn(OH)]ClO$_4$.[225] Following phosphoryl transfer to the alkoxide moiety, a second reaction occurs wherein the pendant phosphorylated alcohol undergoes hydrolysis to yield a coordinated phosphate monoester product. This intramolecular reaction involves water activation by the mononuclear zinc center to produce a reactive Zn–OH nucleophile (Scheme 33). The final product is unreactive toward further hydrolysis. Similar studies were performed using a zinc complex of a N_2O (alkoxide) ligand. These studies revealed a 10^4 rate enhancement for the hydrolysis of the phosphotriester diethyl(4-nitrophenyl) phosphate.[227] Involvement of a zinc-bound alkoxide nucleophile to form a phosphorylated ligand intermediate was proposed for this reaction.

Kinetic studies of reactions of three tris(pyrazolyl)borate-ligated zinc hydroxide complexes ([(Tp^{R,Me})Zn–OH], Fig. 42, top) with triorganophosphate ester substrates in chloroform provided evidence for a concerted or hybrid-type mechanism.[96] The reactions under study in this case are stoichiometric (Fig. 42, bottom) and involve generation of 4-nitrophenol (R‴ = OC$_6$H$_4$–*p*-NO$_2$). Notably, this acidic phenol rapidly undergoes reaction with the starting [(Tp^{R,Me})Zn–OH] complex to yield [(Tp^{R,Me})Zn–OC$_6$H$_4$–*p*-NO$_2$] derivatives. This second reaction is at least

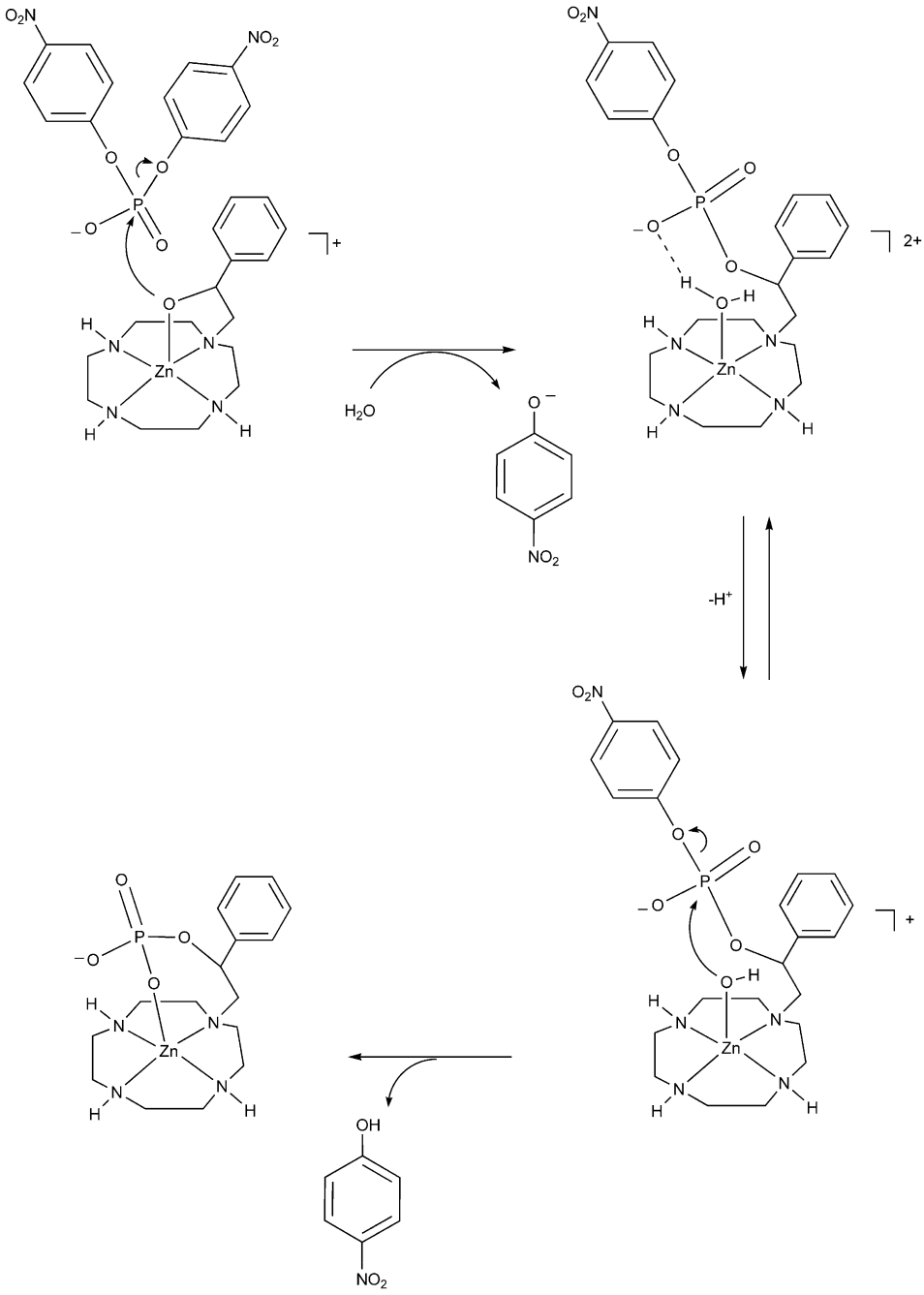

Scheme 33 Proposed reaction pathway for phosphate ester hydrolysis involving an internal alkoxide nucleophile.

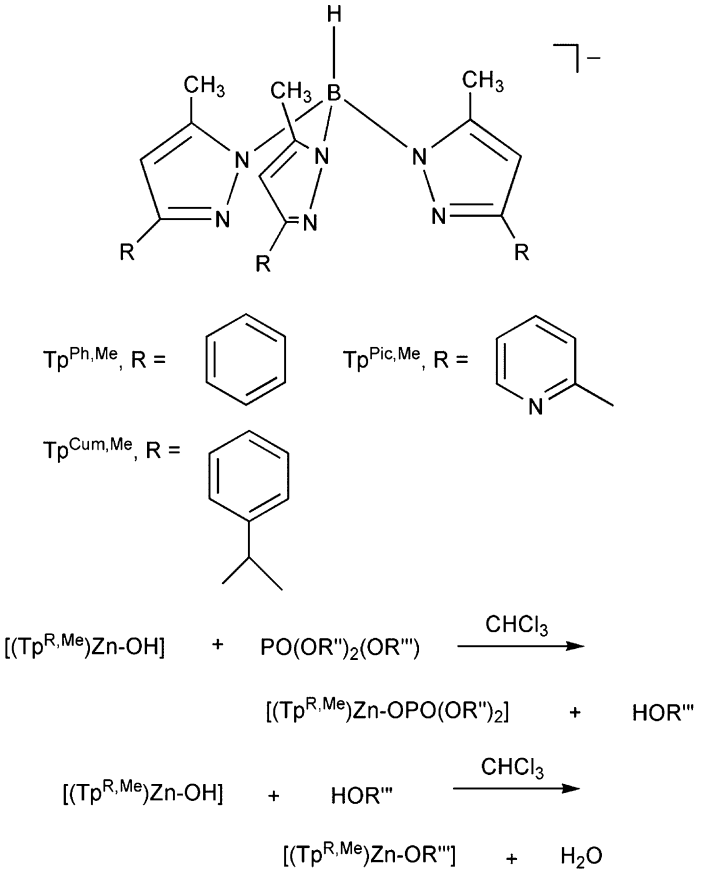

Fig. 42 Phosphate triester hydrolysis reactivity of [(Tp^{R,Me})Zn–OH] compounds.

two orders of magnitude faster than the initial phosphate triester hydrolysis reaction and is thus not a problem in kinetic studies. The phosphate triester cleavage reactions are first-order both in the zinc complex and phosphate ester. Determination of the second-order rate constant for reaction of each zinc complex with the phosphate triester substrate as a function of temperature in the range of 17.5–47.5 °C enabled the construction of Arrhenius and Eyring plots. Activation energies were determined and ranged from 46 to 69 kJ mol^{-1}. The activation entropies ranged from −54 to −126 J mol K^{-1} and were suggested to indicate a degree of ordering in the transition state. A hybrid-type mechanism was proposed in which a four-centered arrangement is present in the activated complex. These reactions are proposed to follow a trajectory (Scheme 18) as outlined previously for amide hydrolysis. It should be noted that a similar phosphate ester hydrolysis reaction had been previously reported involving [(Tp^{iPr2})Zn–OH], albeit kinetic studies were not performed.[205]

Kinetic studies of the reaction of a mononuclear N_2S(thiolate)-ligated zinc hydroxide complex (PATH)Zn–OH with tris(4-nitrophenyl) phosphate in 33% ethanol–water and $I = 0.10$ ($NaNO_3$) also point to a hybrid-type mechanism (Fig. 43).[228] Overall, this reaction is second order and a pH-rate profile indicates that the zinc hydroxide species (PATH)Zn–OH is involved in the reaction. The maximum rate constant for this reaction ($16.1(7)\,M^{-1}\,s^{-1}$) is higher than that reported for free hydroxide ion ($10.7 \pm 0.2\,M^{-1}\,s^{-1}$).[225] This implies that a simple mechanism involving nucleophilic attack is not operative, as free OH^- is a better nucleophile. Studies of the temperature dependence of the second-order rate constants for this reaction yielded activation parameters of $\Delta H^{\ddagger} = 36.9(1)\,kJ\,mol^{-1}$ and $\Delta S^{\ddagger} = -106.7(4)\,J\,mol\,K^{-1}$. The negative entropy is consistent with considerable order in the transition state and a hybrid-type mechanism (Fig. 43, bottom).

The reactivity of zinc complexes supported by a variety of tridentate amine donor ligands (Fig. 44) with diphenyl 4-nitrophenyl phosphate in 20% (v/v) acetonitrile–water, and with 2,4-dinitrophenyl diethyl phosphate in 1% (v/v) in methanol–water, has been investigated.[229,230] For the former reaction, the second-order rate constant for the hydrolysis of 2,4-dinitrophenyl diethyl phosphate correlates linearly with the $-\Delta H$ value for the formation of the $[(ligand)Zn(OH_2)]^{2+}$ complex from free chelate ligand and aqueous zinc ion. This indicates that in this series of complexes, faster hydrolysis of 2,4-dinitrophenyl diethyl phosphate corresponds to weaker chelate

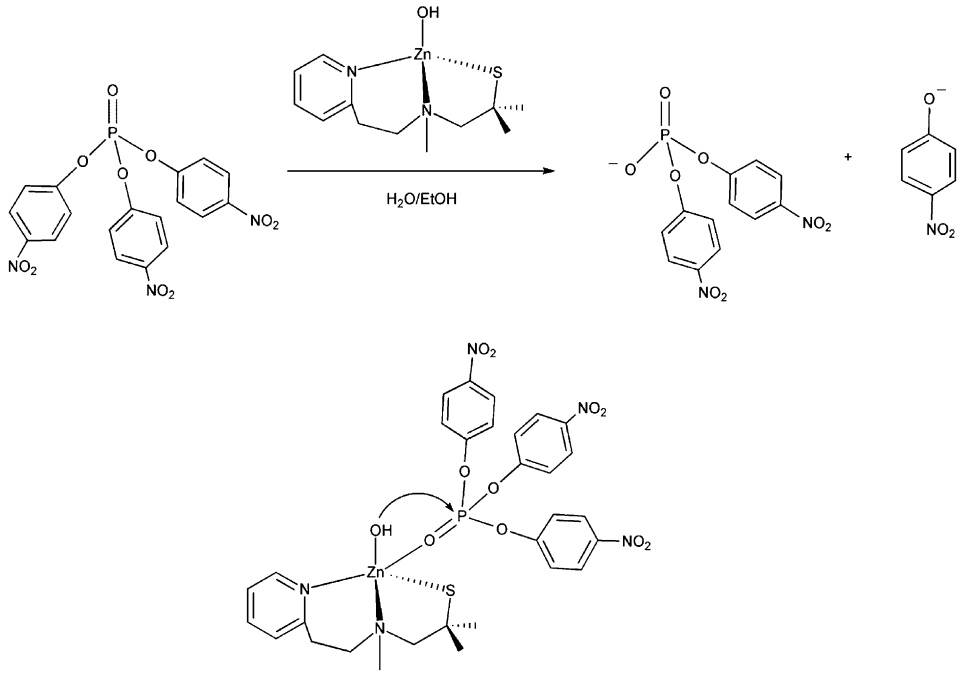

Fig. 43 (top) Tris(4-nitrophenyl) phosphate reaction involving (PATH)Zn–OH and (b) proposed reactive species in a hybrid-type mechanistic pathway.

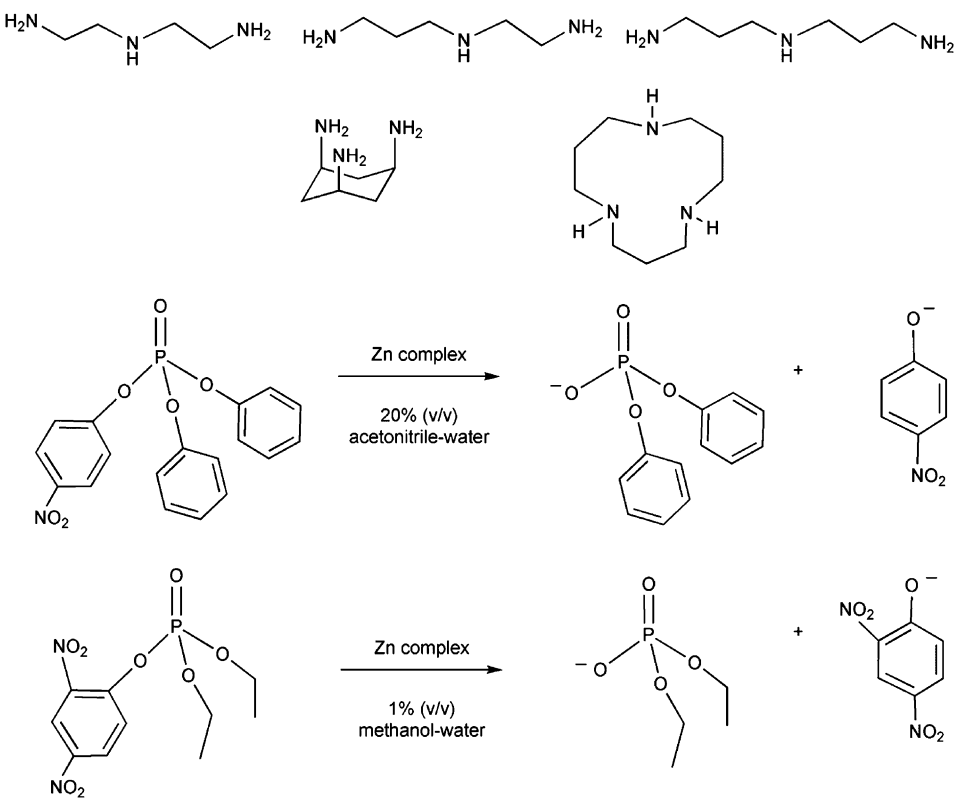

Fig. 44 (top) Tridentate amine donor ligands and (bottom) phosphate triester hydrolysis reactions promoted by zinc complexes of these ligands.

ligand binding to the zinc center. This weaker coordination in turn correlates with a more Lewis acidic zinc ion, and a lower pK_a value for the zinc-bound water molecule. Similar results have been obtained for the hydrolysis reaction of 2,4-dinitrophenyl diethyl phosphate.[230] These reactions are proposed to take place via a mechanism wherein a zinc-coordinated hydroxide ion attacks the coordinated phosphate triester.

In a separate study, zinc complexes of a variety of macrocyclic and linear polyamines (Fig. 45) have been probed for transesterification reactivity involving 2-hydroxypropyl 4-nitrophenyl phosphate (HPNP, Fig. 40, bottom) and for hydrolysis reactivity involving the phosphate diester bis(4-nitrophenyl) phosphate.[231] As outlined below, for the ligands shown in Fig. 45, tridentate donors that coordinate to the zinc center in a facial or tripodal coordination mode produce the most reactive complexes. This is because the lower coordination number of these ligands (relative to tetradentate donor analogs) allows for coordination positions to be available for interactions between the zinc center and the phosphate ester. Examination of the pH-dependence of the HPNP-transesterification reaction involving Zn(II) complexes of L5–L7 and L9–L12 revealed a sigmoidal curves

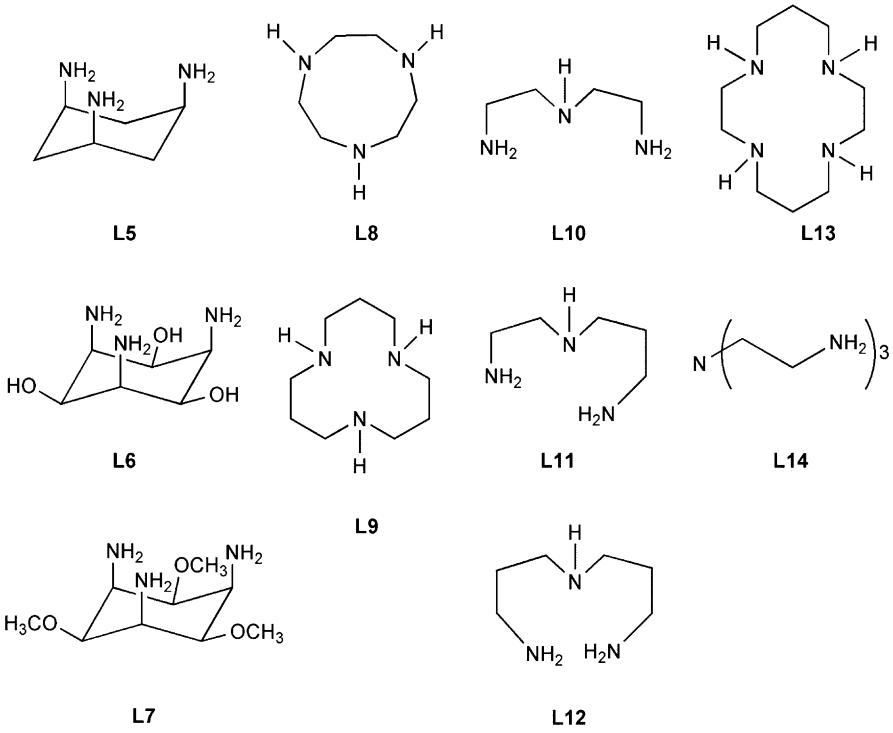

Fig. 45 Macrocyclic and linear polyamine ligands.

and kinetic pK_a values that are similar to the pK_a values determined by potentiometric titration for a zinc-coordinated water molecule. Working at a pH high enough to ensure full deprotonation of the Zn–OH_2 moiety in each complex, variable concentration studies indicated a first-order dependence on zinc complex concentration and overall second-order reactions for HPNP transesterification. Analysis of the range of second-order rate constants obtained for zinc complexes of ligands L5–L9 in a Brønsted plot (log K versus pK_a (kinetic)) at 25 °C yielded a linear correlation and β_{nuc} value of 0.75. Interpretation of this value is discussed below in comparison to that obtained in reactions involving the hydrolysis of bis-4-nitrophenylphosphate. A solvent deuterium isotope effect value ($^{D}k = 1.43$) was determined for the transesterification reaction involving the L6-ligated zinc complex at pH = 10.5. This ^{D}k value is consistent with nucleophilic attack involving the Zn–OR species of the coordinated substrate (Fig. 46) and not general base catalysis.

For the hydrolysis of bis-4-nitrophenylphosphate hydrolysis promoted by zinc complexes of L5–L14, kinetic studies were carried out at pH = 11 to ensure full deprotonation of the Zn–OH_2 moiety of the complexes. Rate constants obtained at 25 °C were used in the preparation of a Brønsted plot. In this plot, reactivity differences as a function of the type of chelate ligand present are clearly evident. Zinc complexes supported by L5–L7 and L9 exhibit the highest reactivity and the

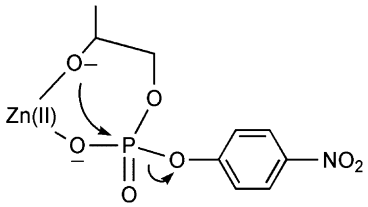

Fig. 46 Proposed intramolecular nucleophilic attack in the transesterification of HPNP.

rate constants for these reactions exhibit a linear correlation in the Brønsted plot ($\beta_{nuc} = 0.20$). The complexes of L13 and L14 exhibit the lowest bis-4-nitrophenylphosphate hydrolysis reactivity, whereas the complexes supported by a tridentate linear ligand (L10–L12, Fig. 45) exhibit intermediate efficiency, albeit with no linear correlation in the log K versus pK_a plot.

The β_{nuc} values obtained for the reactions involving zinc complexes of L5–L9 (HPNP transesterification) and L5–L7 and L9 (bis-4-nitrophenylphosphate (diester) hydrolysis) are an indication of two opposing effects of the zinc center, specifically the involvement of the metal center in substrate activation, and the loss of efficiency of the nucleophile due to zinc coordination. These β_{nuc} values differ notably from the value ($\beta_{nuc} = -0.15$) determined for phosphate triester hydrolysis promoted by zinc complexes of the ligands shown in Fig. 44.[230] This difference has been interpreted to indicate that for HPNP transesterification and BNP hydrolysis, the efficiency of the zinc-bound nucleophile is more important in determining intrinsic complex reactivity than is substrate activation, whereas for the hydrolysis of phosphate triesters, activation of the substrate is more important. This difference is attributed to the fact that for HPNP and BNP reactivity, negative charge build-up during the reaction is localized on an oxygen atom that is not directly bound to the zinc center. However, for phosphate triester hydrolysis, anionic charge build-up occurs on the zinc-bound oxygen atom and is stabilized by the metal center. Therefore, for the HPNP and BNP reactions, the zinc center is less able to stabilize the increasing negative charge on the substrate and the reactivity of the zinc-bound nucleophile instead plays a major role.

Mononuclear zinc hydroxide complexes supported by tripodal tetradentate ligands, some of which contain hydrophobic bulky appendages (tris(2-aminoethyl) amine (L15), *N*,*N*′,*N*″-tris(2-benzylaminoethyl)amine (L16), and *N*,*N*′,*N*″-tris(imbenzyl-L-histidylethylaminoethyl)amine (L17) ligands (Fig. 47)), have been identified via pH-rate profile studies as the reactive species involved in hydrolysis reactions of bis-4-(nitrophenyl) phosphate and tris(4-nitrophenyl) phosphate in 33% methanol/water.[232] The Zn(II) hydroxide complex of L17 exhibits higher efficiency in both phosphate diester and triester hydrolysis reactions than the zinc complexes of the other two tripodal tetradentate ligands. This is despite a lower pK_a (7.43) value for the $[(L17)Zn(OH_2)]^{2+}$ species ($[(L15)Zn(OH_2)]^{2+}$: 10.72; $[(L16)Zn\ (OH_2)]^{2+}$: 9.61) suggesting that the phosphate ester cleavage reactivity of the zinc complex of L17 is not determined solely by the nucleophilicity of the Zn–OH moiety. Some properties of the L17 ligand that may come into play in influencing the reaction pathway for

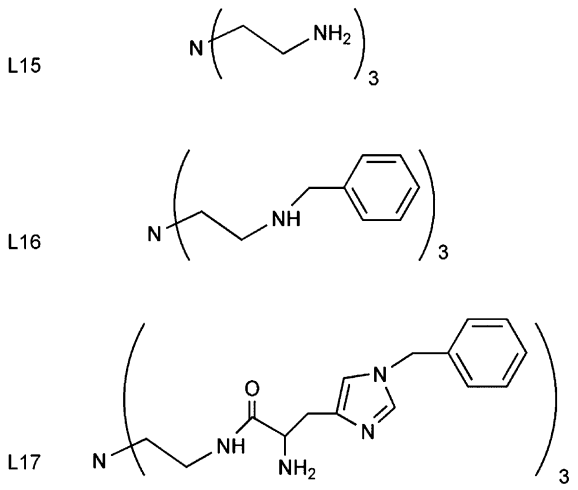

Fig. 47 Tripodal tetradentate ligands.

phosphate ester hydrolysis include the more labile nature of the imidazole donors, the nature of the chelate ring size formed in zinc complexes, and an overall increased flexibility within the chelate ligand structure.

Mononuclear zinc complexes of *N*,*N*′,*N*″′-tris(3-aminopropyl)amine ligands having either hydrogen atoms or methyl groups as the substituents on the coordinating nitrogen atoms exhibit slight catalytic activity for the hydrolysis of the phosphotriester 2,4-dinitrophenyl diethyl phosphate.[233] A zinc hydroxide complex is proposed as the reactive species that promotes phosphotriester hydrolysis.

Binuclear zinc complexes wherein each metal center is supported by a tripodal tetradentate ligand environment involving a bridging phenolate donor are reactive toward tris(4-nitrophenyl) phosphate and bis(4-nitrophenyl) phosphate in ethanol/water.[234] The pH-rate profile studies of these reactions are consistent with a mechanism that involves the formation of a reactive mononuclear zinc hydroxide species via cleavage of the binuclear solid-state structure. This mononuclear Zn–OH species is proposed to act as the nucleophile toward the phosphate ester substrate.

Chelate tetradentate tripodal ligands having internal hydrogen-bond donors (L18–L20, Fig. 48) produce zinc complexes with enhanced phosphate diester transesterification and hydrolysis reactivity relative to analogs that lack secondary hydrogen-bonding interactions.[20] Comparison of the bis(4-nitrophenyl) phosphate reactivity of zinc complexes of a series of N_3O-donor ligands (Fig. 48) revealed that zinc complexes of the L18 and L19 ligands produced transesterification products (4-nitrophenol and the *O*-phosphorylated chelate ligand) whereas the L20 ligand produced only phosphate ester hydrolysis products. For the transesterification reaction of the L19-ligated zinc complex, the second-order rate constant is $9.7 \times 10^{-2}\,M^{-1}\,s^{-1}$ at pH = 7.0 and 25 °C. This rate is approximately six orders of magnitude faster than the spontaneous hydrolysis of bis(4-nitrophenyl) phosphate

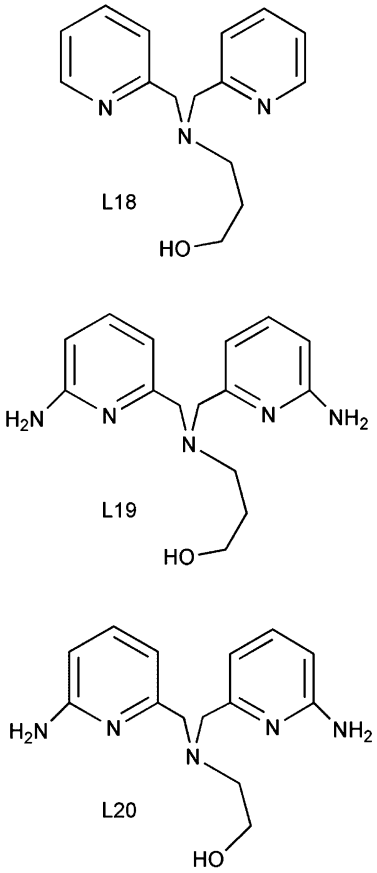

Fig. 48 Tripodal tetradentate ligands having internal hydrogen-bond donor amine substituents.

under identical conditions. The rate enhancement is attributed to the enhanced nucleophilicity of an alkoxide (versus hydroxide) and the presence of secondary hydrogen-bonding interactions. In addition to the zinc center, the hydrogen bonds can provide additional Lewis acid activation for the phosphate diester substrate, and may assist in the stabilization of a dianionic intermediate. Additional evidence of the influence of secondary hydrogen-bonding interactions was derived from comparison of the bis(4-nitrophenyl) phosphate transesterification reactivity of the zinc complexes of L18 and L19, which revealed a 230-fold reactivity increase for the latter complex. For the hydrolysis reaction involving the L20-ligated zinc complex, the rate acceleration is $\sim 10^5$ over that of the uncatalyzed reaction.

Comparative studies of the HPNP-transesterification reactivity (Fig. 40, bottom) of $[(tapa)Zn(H_2O)]^{2+}$ and $[(tpa)Zn(H_2O)]^{2+}$ (Fig. 49) revealed that the rate of cyclization of the substrate is accelerated by a factor of 3×10^6-fold for the former

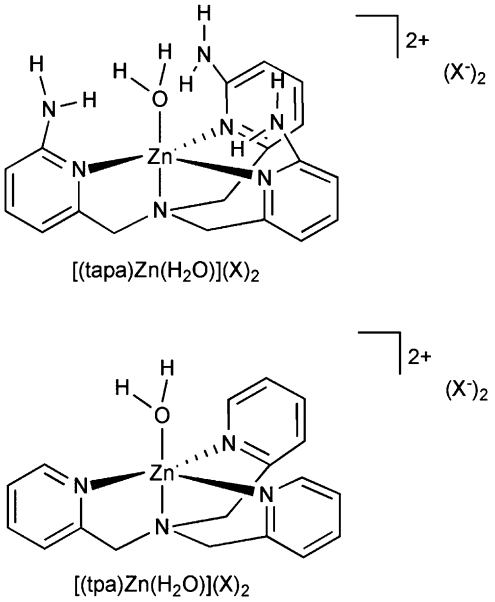

Fig. 49 Structural drawings of $[(tapa)Zn(H_2O)]^{2+}$ and $[(tapa)Zn(H_2O)]^{2+}$.

complex and 4×10^3-fold for the latter complex over the uncatalyzed reaction.[235] The difference between these rate enhancements is attributed to enhanced stabilization of a dianionic intermediate in HPNP hydrolysis via secondary hydrogen-bonding interactions.

Several multinuclear zinc complexes that exhibit phosphate diester and triester reactivity have been reported. A binuclear analog of $[(CR)Zn]^{2+}$ (Fig. 6a) in which two $[(CR)Zn]^{2+}$ units are linked by an aromatic spacer was found to be ~4.4 times more effective in terms of the hydrolysis of diphenyl 4-nitrophenyl phosphate in CH_3CN:H_2O at 25 °C than its mononuclear analog.[204]

The phosphate diester hydrolysis (using bis(4-nitrophenyl) phosphate) and transesterification (using 2-hydroxypropyl 4-nitrophenyl phosphate) reactivity of the family of binuclear zinc complexes shown in Fig. 37 was examined in studies directed at elucidating how the nature of the ligand bridge influences reactivity.[204] The complex supported by a ligand having a biphenyl linker (Fig. 37d) exhibited the highest reactivity for both substrates. A proposed pathway for the reaction involving bis(4-nitrophenyl) phosphate is shown in Fig. 50. In this reaction, substrate activation is proposed to occur at one zinc center, whereas the nucleophile is generated at the other zinc center. Consistent with this proposed pathway is the identification of a pK_a value of 8 in the pH-rate profile of the reaction. This value is consistent with deprotonation of a terminal Zn–OH_2 moiety.

Mono- and binuclear Zn(II) nitrate complexes of the bis(1-methylimidazol-2-ylmethyl)ethylamine and *N*,*N*,*N*′,*N*′-tetrakis(1-methylimidazol-2-ylmethyl)pentane-1,5-diamine ligands (Fig. 51) catalyze the hydrolysis of tris-4-nitrophenyl phosphate

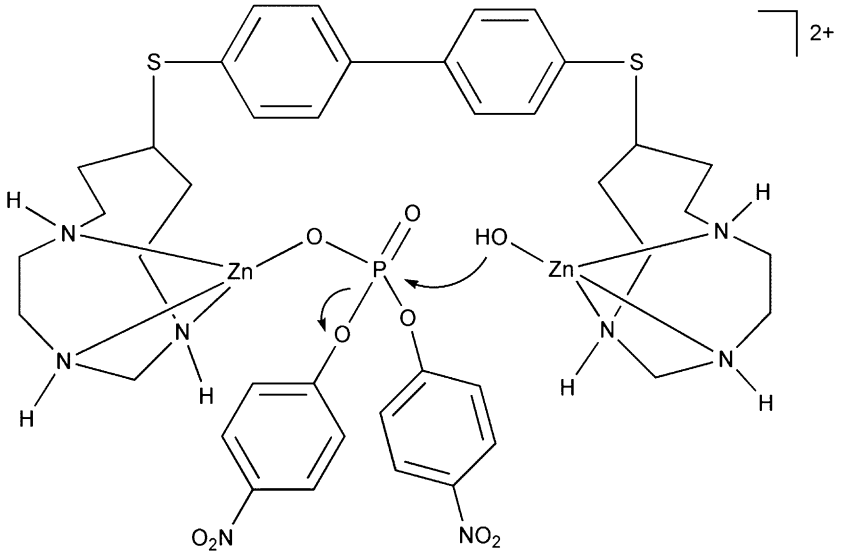

Fig. 50 Proposed reaction pathway for the hydrolysis of bis(4-nitrophenyl) phosphate promoted by a biphenyl-bridged complex.

to produce bis(4-nitrophenyl) phosphate in 33% ethanol–water solution.[236] No further reaction with the phosphate diester product occurs in this system. Acidic (e.g. aqua) and basic (e.g. hydroxo) forms of both complexes catalyze the hydrolysis of the phosphate triester, with the activity increasing for both types of complexes with increasing pH, which is consistent with the formation of a reactive zinc hydroxide species that may be acting as a nucleophile or general base. The mononuclear complex exhibits higher reactivity, which is consistent with the higher pK_a value (8.16), and formation of a terminal Zn–OH moiety in this complex, whereas a bridging $Zn_2(\mu\text{-OH})$ ($pK_a = 6.99$) is formed in the binuclear derivative. No evidence was found for pre-equilibrium formation of a substrate adduct in these reactions.

Zinc complexes of macrocyclic N- and N/O-donor ligands (L21–L24, Fig. 52) promote the hydrolysis of bis(4-nitrophenyl) phosphate to produce 4-nitrophenyl phosphate and 4-nitrophenol via varying mechanistic pathways.[105,237–241] For example, comparison of the bis(4-nitrophenyl) phosphate reactivity of mono- and binuclear zinc monohydroxo complexes of the L21 ligand revealed that the mononuclear zinc hydroxide complex is more effective at hydrolyzing the phosphate diester substrate than the binuclear monohydroxo complex.[237] Important differences between the reactions involving the mono- versus binuclear complexes include the nature of the nucleophile (terminal Zn–OH versus bridging Zn–OH) and possible differences in recognition of the substrate by the metal complex. In the monozinc complex (Fig. 53), a better nucleophile is present (terminal Zn–OH), but the substrate can interact with only a single Zn(II) center. In the bizinc complex, a poorer

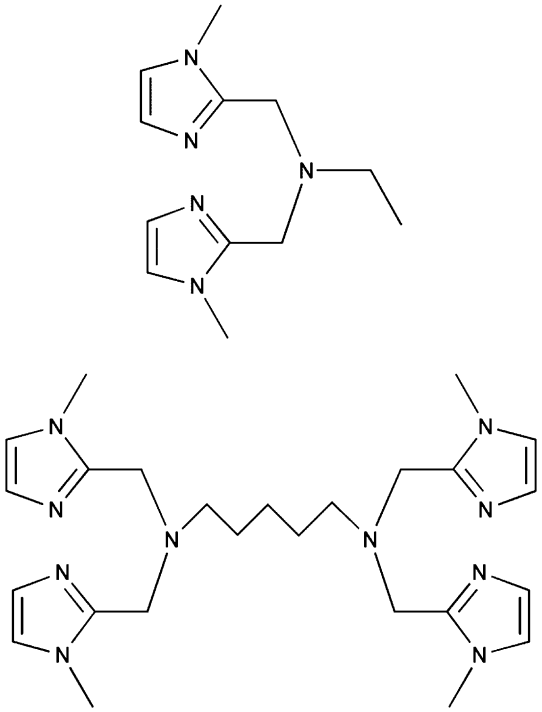

Fig. 51 Bis(1-methylimidazol-2-ylmethyl)ethylamine; (top) and *N*,*N*,*N*′,*N*′-tetrakis(1-methylimidazol-2-ylmethyl)pentane-1,5-diamine (bottom) ligands.

nucleophile (bridging Zn–OH) is present but better Lewis activation of the substrate is likely achieved as the phosphate diester can bridge the two zinc centers.

The rate of hydrolysis of bis(4-nitrophenyl) phosphate is approximately 10-fold higher for a binuclear $Zn_2(OH)_2$ complex of the L22 ligand (Fig. 52) versus a mononuclear zinc hydroxide complex of the L23 ligand at 308 K.[105] In this system, a monohydroxide binuclear zinc complex ($Zn_2(\mu$-OH)) does not promote phosphate diester hydrolysis. The 10-fold rate enhancement found for the reaction involving the binuclear $Zn_2(OH)_2$ complex was explained via cooperative interaction between the zinc centers. As shown in Fig. 54, the reaction is proposed to take place via attack of a terminal Zn–OH moiety on a phosphate diester substrate that is interacting with both zinc centers. This suggests a cooperative role for the two zinc centers in the phosphate diester hydrolysis reaction.

Inclusion of an alcohol appendage in the L24 ligand framework (Fig. 52) results in a reaction pathway for bis(4-nitrophenyl) phosphate hydrolysis that involves initial nucleophilic attack of a zinc-bound alkoxide moiety on the substrate to give a phosphorylated intermediate (Scheme 34).[239] This intermediate, similar to the phosphorylated serine intermediate proposed in the catalytic cycle of alkaline phosphatase, is subsequently attacked by a Zn–OH moiety to yield 4-nitrophenyl

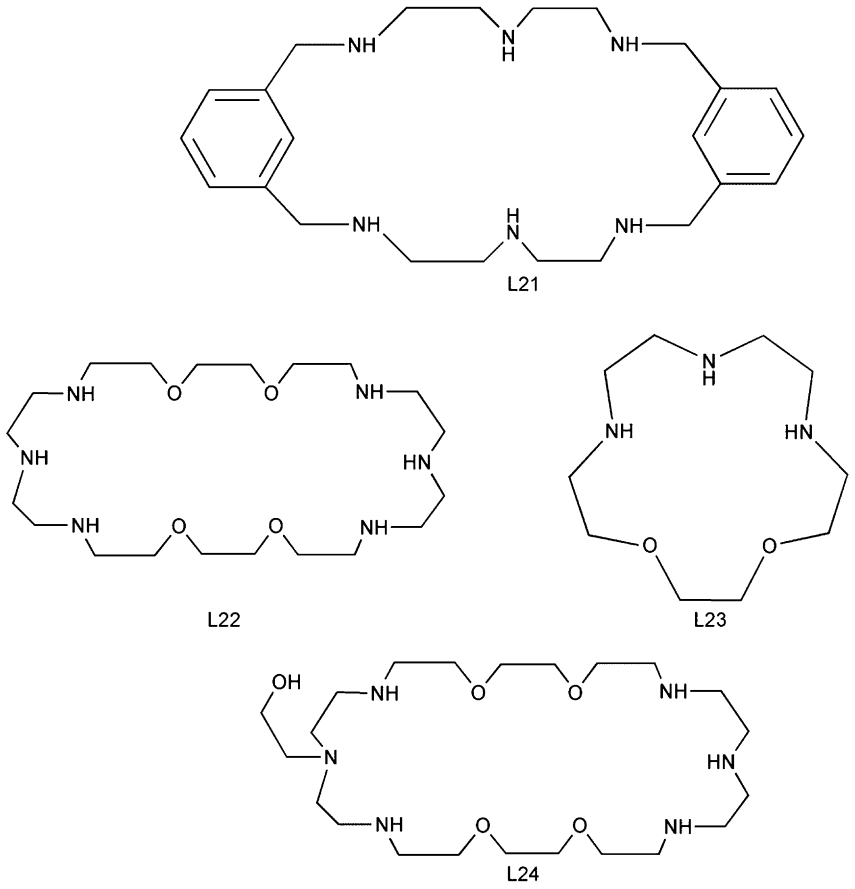

Fig. 52 Macrocyclic N- and N/O-donor ligands.

phosphate as the final product. Evidence for the initial formation of a new phosphoryl species in the L24-ligated system comes from ^{31}P NMR where a new resonance appears at 7.3 ppm in aqueous solution as the signal for bis(4-nitrophenyl) phosphate at −8.2 ppm decays. The final phosphate-appended product is subsequently detected by the appearance of a resonance at 7.8 ppm ($J_{H-P} = 11.2$ ppm).

Introduction of a phenanthroline moiety into a chelating macrocyclic ligand (L25, Fig. 55) yields a $[LZn_2(OH)_2]^{2+}$ complex with enhanced bis(4-nitrophenyl) phosphate ester hydrolysis reactivity in aqueous solution relative to $[LZn_2(OH)_2]^{2+}$ complexes of structurally similar ligands (L26 and L27, Fig. 55).[238] The second-order rate constants for these reactions are $62 \times 10^{-5}\,M^{-1}\,s^{-1}$ (L25), $8 \times 10^{-5}\,M^{-1}\,s^{-1}$ (L26), and $4 \times 10^{-5}\,M^{-1}\,s^{-1}$ (L27), respectively. A hybrid-type mechanism akin to that shown in Fig. 54 is proposed wherein the phosphate diester substrate binds to both zinc centers of the $[LZn_2(OH)_2]^{2+}$ complex followed by intramolecular attack of a terminal Zn–OH moiety. The enhanced reactivity of $[L25Zn_2(OH)_2]^{2+}$ is

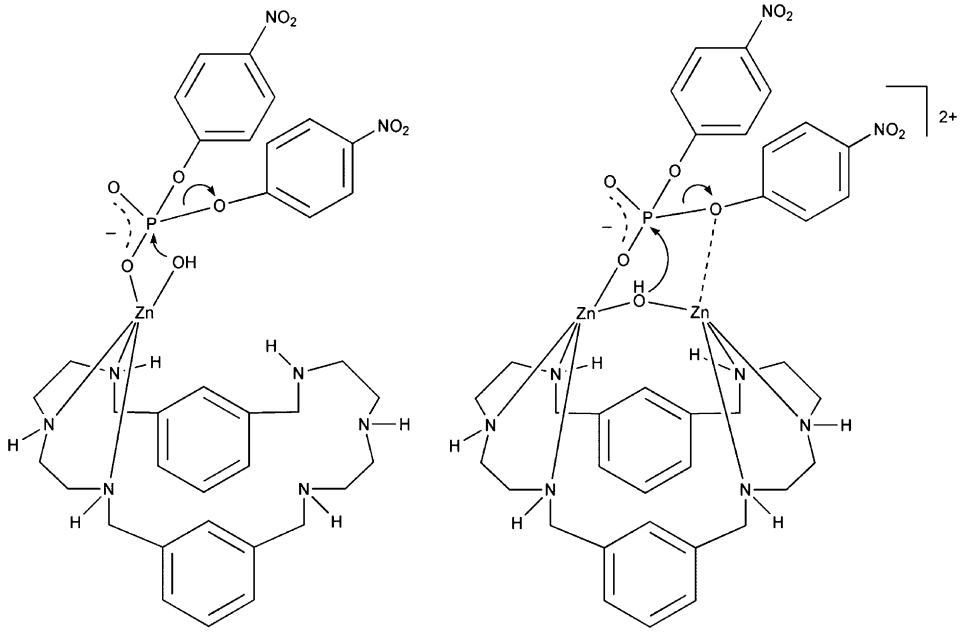

Fig. 53 Proposed mechanistic pathways for bis(4-nitrophenyl) phosphate hydrolysis reactivity of mono- and bizinc complexes of the L21 ligand.

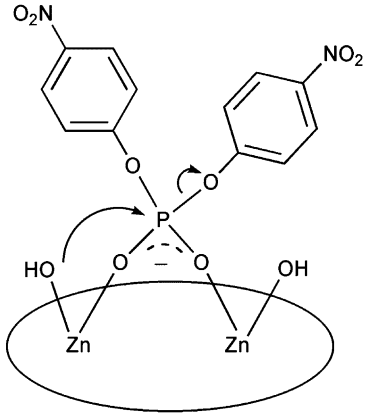

Fig. 54 Proposed reaction pathway of bis(4-nitrophenyl) phosphate hydrolysis promoted by a binuclear zinc complex of the L22 macrocyclic ligand.

attributed to the presence of the phenanthroline moiety, which may promote coordination of bis(4-nitrophenyl) phosphate via π-stacking and hydrophobic interactions with the aromatic rings of the substrate, and cooperative effects between the zinc centers.

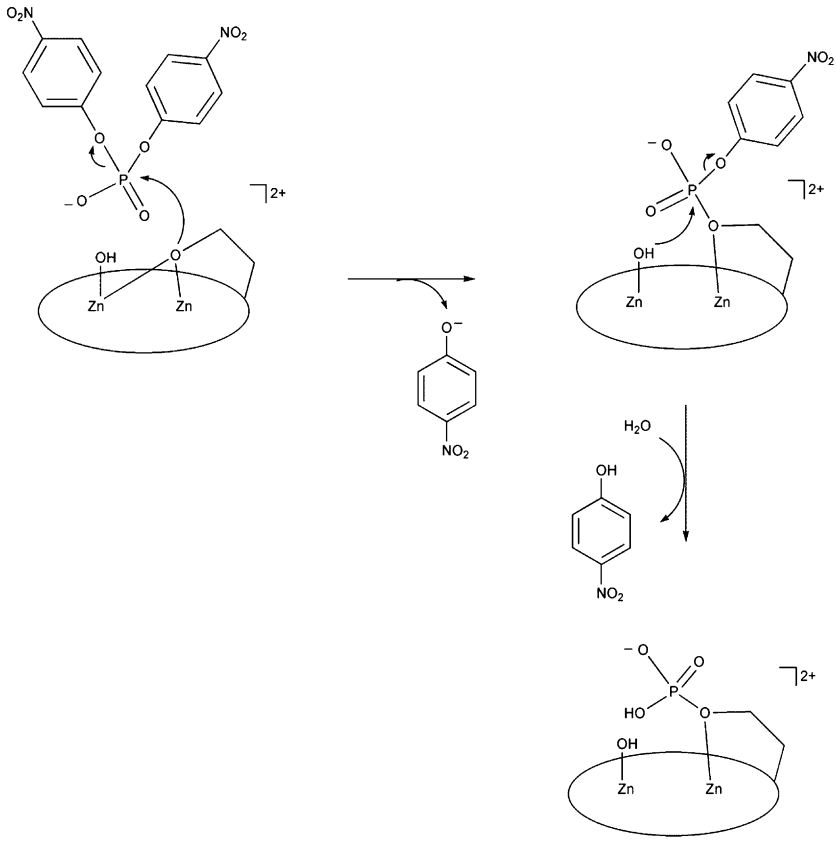

Scheme 34 Proposed reaction pathway for bis(4-nitrophenyl)phosphate hydrolysis promoted by a bizinc complex of the L24 macrocyclic ligand.

Dipyridine-containing macrocyclic ligands (L28–L30, Fig. 56) have also been used to prepare zinc complexes for phosphate diester cleavage reactivity studies.[240] Active complexes of these ligands for the hydrolysis of bis(4-nitrophenyl) phosphate have in common the presence of one or more Zn–OH units. A zinc hydroxide complex of L28, $[L28Zn(OH)]^{+}$ exhibits a second-order rate constant ($(1.1 \pm 0.06) \times 10^{-4}\,M^{-1}\,s^{-1}$) that is considerably lower than bizinc complexes of the L29 and L30 ligands ($[L29Zn_2(OH)_2]^{2+}$: $(9.6 \pm 0.3) \times 10^{-4}\,M^{-1}\,s^{-1}$; $[L30Zn_2(OH)]^{3+}$: $(19.3 \pm 1.0) \times 10^{-4}\,M^{-1}\,s^{-1}$). This indicates a cooperative role for the zinc centers in the latter two complexes. For the reaction promoted by $[L29Zn_2(OH)_2]^{2+}$, a mechanistic pathway similar to that shown in Fig. 54 is proposed. This is consistent with the availability of multiple open coordination positions at each zinc center in complexes of the L29 ligand, which provides only three nitrogen donors per zinc center. For the zinc complex of the L30 ligand, the active species is proposed to have monodentate coordination of the substrate at one zinc center, and a terminal zinc hydroxide at the

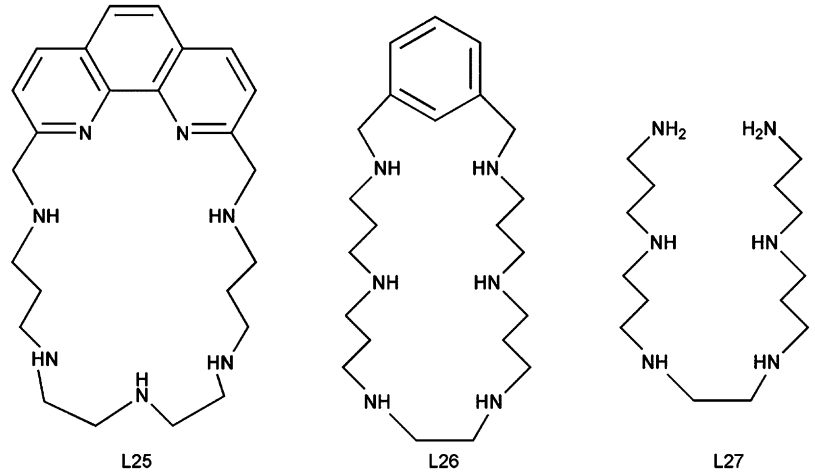

Fig. 55 L25–L27 ligands.

other zinc center (Fig. 57). As the L30 ligand provides five nitrogen donors per zinc center, this would give each an overall coordination number of six. Hydrophobic and π-stacking interactions involving the pyridyl macrocycles are suggested to enhance substrate coordination to $[L29Zn_2(OH)_2]^{2+}$ and $[L30Zn_2(OH)]^{3+}$ in a similar fashion to that proposed for the phenanthroline containing macrocyclic ligand discussed above.[238]

A binuclear zinc complex of the macrocyclic phenolate-containing ligand BDBPH (Fig. 58) contains zinc centers that are each ligated by three amine donors and bridged by two phenolate oxygen atoms.[242] In a solid-state structure, each zinc center also coordinates a methanol molecule to give an overall distorted octahedral geometry and a Zn–Zn distance of 3.146 Å. In 75% ethanol–water solution, a terminal Zn–OH moiety can be generated at a pH above 9.90. The rate of hydrolysis of tris(4-nitrophenyl) phosphate promoted by this binuclear zinc complex increased in the pH range 9.0–10.5. This reaction is proposed to take place via attack of a terminal Zn–OH moiety on the coordinated tris(4-nitrophenyl) phosphate substrate (Fig. 58). Stabilization of the anionic bis(4-nitrophenyl) phosphate product is suggested to occur by coordination to the binuclear zinc complex.

A similar mechanistic pathway to that shown in the lower portion of Fig. 58 is proposed for tris(4-nitrophenyl) phosophate hydrolysis promoted by binuclear zinc complexes of phenol-based ligands, albeit no kinetic or mechanistic studies were reported for these reactions.[243]

A zinc complex of the BPAN (2,7-bis[2-(2-pyridylethyl)aminomethyl]-1,8-naphthyridine ligand, $[(BPAN)Zn_2(\mu\text{-}OH)(\mu\text{-}Ph_2PO_2)](ClO_4)_2$, Fig. 27) catalyzes the transesterification of the RNA model substrate HPNP (2-hydroxypropyl 4-nitrophenyl phosphate (Fig. 40, bottom) in aqueous buffered solution (HEPES) containing 1% CH_3CN.[141] The rate of this reaction was found to be ~7 times fast than the reaction catalyzed by a mononuclear Zn(II) complex of bpta (Fig. 25). A pH-rate

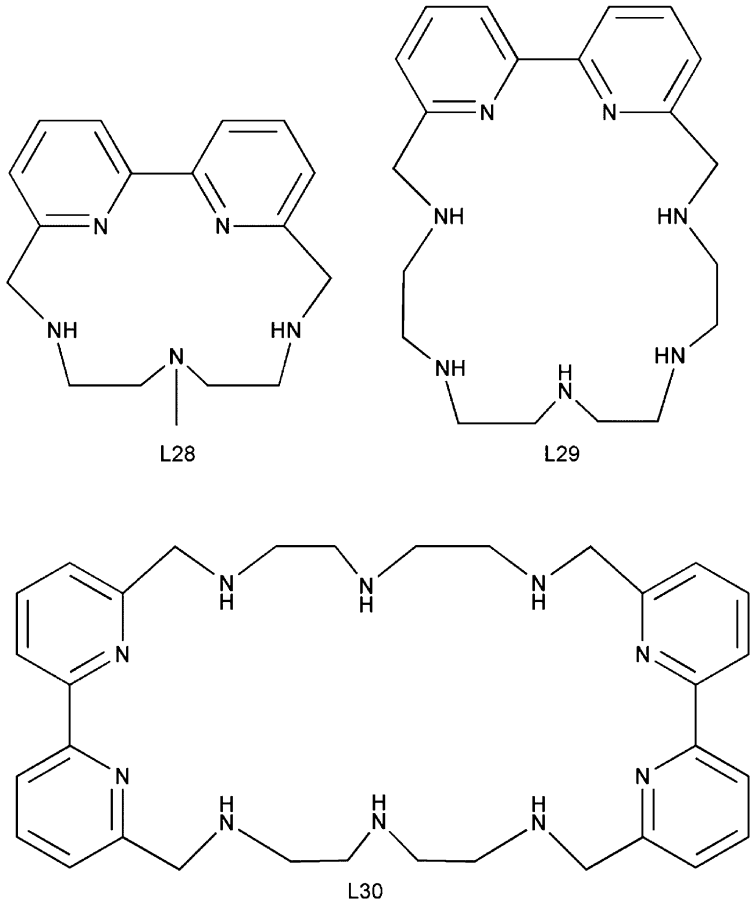

Fig. 56 L28–L30 ligands.

profile for the reaction involving $[(BPAN)Zn_2(\mu\text{-}OH)(\mu\text{-}Ph_2PO_2)](ClO_4)_2$ revealed an inflection point at pH = 6.97. This value matches a pK_a value determined by potentiometric titration and is assigned to the deprotonation of the bridging water ligand in $([BPAN)Zn_2(\mu\text{-}OH_2)(\mu\text{-}Ph_2PO_2)](ClO_4)_3$. These combined results indicate that the bridging hydroxide moiety in $([BPAN)Zn_2(\mu\text{-}OH)(\mu\text{-}Ph_2PO_2)](ClO_4)_2$ is the base involved in catalyzing the intramolecular transesterification reaction. Further studies indicated that the bridging hydroxide moiety serves as a general base in the HPNP-transesterification reaction.

The $[(BPAN)Zn_2(\mu\text{-}OH)(\mu\text{-}Ph_2PO_2)](ClO_4)_2$ complex also promotes the hydrolysis of bis(4-nitrophenyl) phosphate.[140] This reaction proceeds via initial coordination of the substrate to the binuclear zinc complex ($K = 86 \pm 32\,M^{-1}$). Studies of the effect of pH on this reaction revealed a kinetic pK_a of 7.06 ± 0.05, which is consistent with deprotonation of a bridging water molecule. Thus, a bridging hydroxide is the

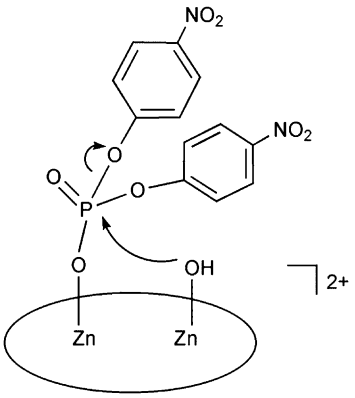

Fig. 57 Proposed reactive species in the hydrolysis of bis(4-nitrophenyl) phosphate promoted by $[L30Zn_2(OH)]^{3+}$.

reactive species, which could either act as a nucleophile or as a general base. These two possibilities were distinguished by reducing the amount of water present in the reaction mixture, with acetonitrile being used as the cosolvent. This produced a slowing of the rate of phosphate diester hydrolysis indicating that a general base-type mechanism is operative (Scheme 35). Notably, $[(BPAN)Zn_2(\mu\text{-}OH)(\mu\text{-}Ph_2PO_2)](ClO_4)_2$ is only 1.8 times more reactive toward bis(4-nitrophenyl) phosphate than a mononuclear zinc complex of the bpta ligand (Fig. 25).

HPNP transesterification (Fig. 40, bottom) is catalyzed by mono- and bizinc complexes of the *cis*-2,4,6-traminocyclohexane-1,3,5-triol-contaning ligands (L6, L31, and L32) shown in Fig. 59.[244] For the zinc complexes of L31 and L32, bell-shaped pH-rate profiles were obtained for the HPNP-transesterification reaction, indicating deprotonation of two acidic functionalities. The first deprotonation leads to the formation of the reactive species, whereas the second deprotonation results in loss of activity. The mononuclear zinc complex of the L6 ligand exhibits a sigmoidal pH-rate profile, indicating a single deprotonation that leads to reactivity. Overall, the mononuclear zinc complex of L6 is intrinsically more reactive than the bizinc complexes of L31 and L32, as evidenced by comparison of their respective limiting rate constants (k_{lim}; $[L6Zn]^{2+}$, $9.7 \times 10^{-3}\,s^{-1}$; $[L31Zn_2]^{4+}$, $1.5 \times 10^{-3}\,s^{-1}$; $[L32Zn_2]^{4+}$, $2.6 \times 10^{-3}\,s^{-1}$). However, the bizinc complexes have a higher affinity for the substrate (K_b: $[L6Zn]^{2+}$, $33\,M^{-1}$; $[L31Zn_2]^{4+}$, $107\,M^{-1}$; $[L32Zn_2]^{4+}$, $67\,M^{-1}$). The mechanism for HPNP transesterification catalyzed by the mononuclear $[L6Zn]^{2+}$ complex is suggested to involve simultaneous zinc coordination of the substrate alcohol and phosphate ester groups (Fig. 46). Reactions involving $[L31Zn_2]^{4+}$ and $[L32Zn_2]^{4+}$ may proceed either via the involvement of a zinc-bound hydroxide acting as a base (Fig. 60, left) or via multiple site activation of the substrate and intramolecular attack of a zinc-bound alkoxide moiety (Fig. 60, right). The bell-shaped pH-rate profile for the bizinc systems is attributed to the sequential deprotonation of two zinc-bound water molecules. The first deprotonation reaction

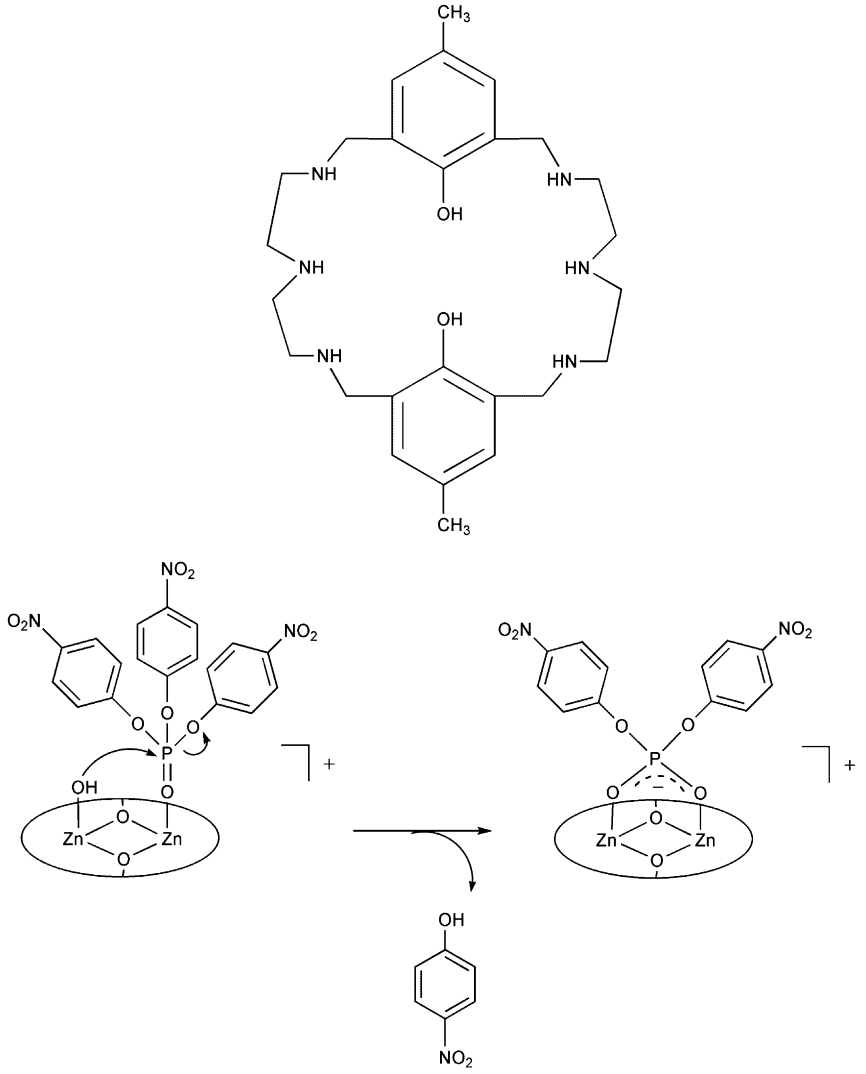

Fig. 58 (top) BDBPH ligand and (bottom) proposed mechanism for tris(4-nitrophenyl) phosphate hydrolysis.

would yield a Zn–OH species that is active for HPNP transesterification, whereas the second deprotonation would yield a $Zn_2(OH)_2$ species that may interact with the substrate more weakly, perhaps due to blocking of coordination positions as a consequence of bridging hydroxide formation.

Binuclear zinc complexes of pyrazolate-based chelate ligands (Fig. 61) exhibit differing bis(4-nitrophenyl) phosphate hydrolysis reactivity depending on the nature of the supporting chelate ligand.[153] Plots of the pseudo first-order rate constant

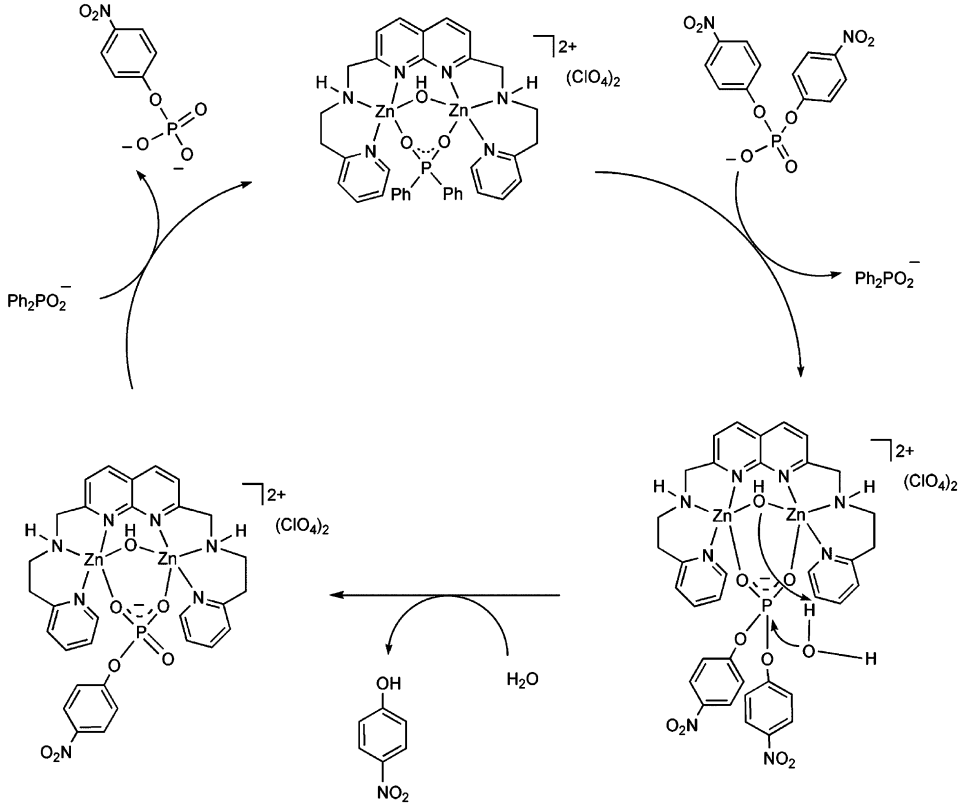

Scheme 35 Proposed mechanism for bis(4-nitrophenyl) phosphate hydrolysis promoted by $[(BPAN)Zn_2(\mu\text{-}OH)(\mu\text{-}Ph_2PO_2)](ClO_4)_2$.

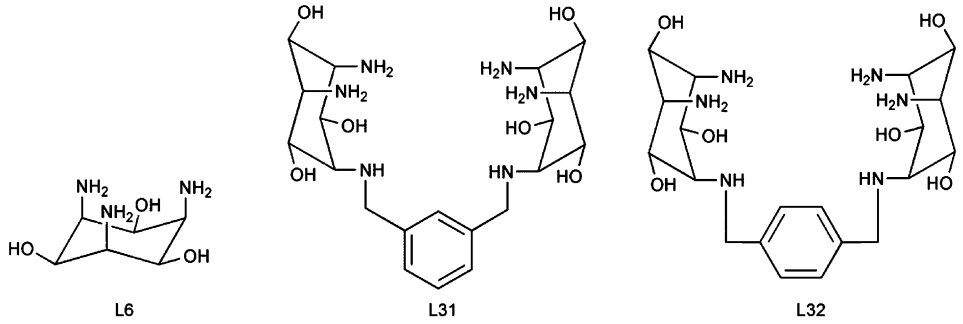

Fig. 59 The cis-2,4,6-traminocyclohexane-1,3,5-triol-containing ligands.

versus pH for phosphate diester hydrolysis promoted by **5** and **6** yielded kinetic pK_a values consistent with the presence of a reactive zinc hydroxide species. Overall, the reactions are second order and exhibit saturation-type behavior, with **5** ($k = (3.3 \pm 0.3) \times 10^{-5}\,M^{-1}\,s^{-1}$) exhibiting significantly lower reactivity than **6**

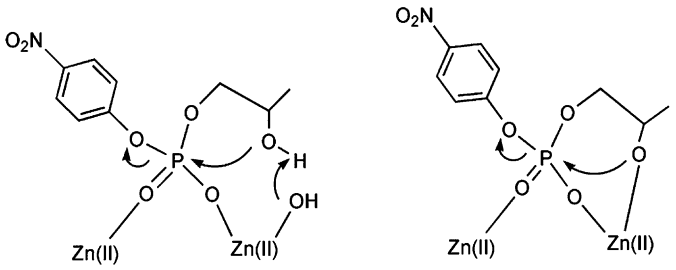

Fig. 60 Possible mechanistic pathways for HPNP transesterification catalyzed by bizinc complexes of the L31 and L32 ligands.

($(1.1 \pm 0.1) \times 10^{-3}\,M^{-1}\,s^{-1}$) at pH = 8.2, presumably because the hydroxide anion is held more tightly in **5**, which diminishes its nucleophilicity. The proposed mechanism for bis(4-nitrophenyl) phosphate hydrolysis in these systems involves initial equilibrium formation of a zinc complex-substrate adduct followed by phosphate ester hydrolysis. Using this model, substrate binding constants of $K = 24 \pm 3\,M^{-1}$ (**4**) and $18 \pm 1\,M^{-1}$ (**6**) have been determined. These values indicate that the initial substrate coordination is weak, as has been reported for other binuclear zinc complexes.[140,141]

Interestingly, the binuclear zinc O_2H_3-bridged species **4** is unreactive toward bis(4-nitrophenyl) phosphate at pH > 7.5. This is attributed to bidentate coordination of the substrate to the binuclear zinc complex with complete displacement of the O_2H_3 unit. The zinc centers in the resulting structure each have a coordination number of five, and there is likely not room for coordination and activation of a water molecule. Comparison of the ligand structures in **4** and **6** indicates that while substrate coordination also occurs in **6**, the lower overall coordination number of the supporting chelate ligand enables a coordination position to be available on each zinc center for formation of a Zn–OH_2/Zn–OH moiety. In addition, as **6** exhibits enhanced phosphate diester reactivity relative to $Zn(ClO_4)_2$, cooperativity between proximal zinc centers occurs.

Comparison of the bis(4-nitrophenyl) phosphate hydrolysis reactivity of **1** and **2** (Fig. 27) in DMSO:buffered water (1:1) at 50 °C revealed that the complex having the greater Zn···Zn separation is more reactive (**1**: $k = (1.6 \pm 0.1) \times 10^{-4}\,M^{-1}\,s^{-1}$; **2**: $(4.6 \pm 0.1) \times 10^{-4}\,M^{-1}\,s^{-1}$).[154] pH-rate studies are consistent with the involvement of a Zn–OH moiety in these hydrolytic reactions. Saturation-type behavior is observed in terms of substrate concentration for both reactions. Substrate binding constants were determined (**1**: $k = 19.6 \pm 2.1\,M^{-1}$; **2**: $17.9 \pm 1.3\,M^{-1}$) and found to be nearly identical. Notably, k_{cat} values for **1** ($(4.9 \pm 0.4) \times 10^{-6}\,s^{-1}$) and **2** ($(2.3 \pm 0.1) \times 10^{-5}\,s^{-1}$) differ by a factor of approximately 5. Thus, the enhanced hydrolytic efficiency of **2** for the hydrolysis of bis(4-nitrophenyl) phosphate is not due to differing substrate affinities for the complexes, but instead to intrinsically higher reactivity for the system having the larger Zn···Zn separation.

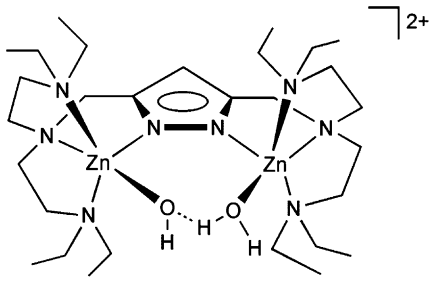

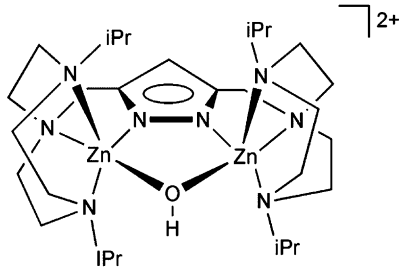

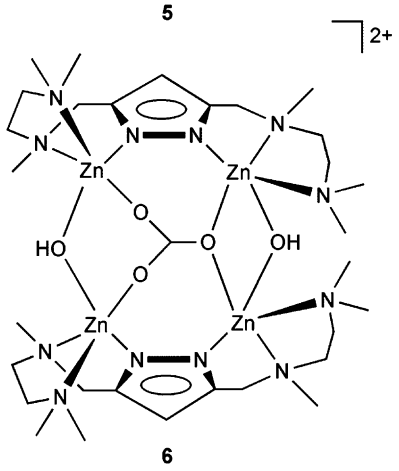

Fig. 61 Binuclear zinc complex of pyrazolate-based chelate ligands.

The 2-hydroxypropyl 4-nitrophenyl phosphate (HPNP) transesterification reactivity (Fig. 40, bottom) of binuclear zinc complexes of the dianionic ICIMP and trianionic BCIMP ligands (Fig. 62) have been compared.[245] Notably, both of these ligands contain imidazole and carboxylate donors akin to protein-derived residues that are found as ligands to the zinc centers in phosphate-ester-hydrolyzing enzymes such as phosphotriesterase. The initial rate for HPNP transesterification promoted by $[(ICIMP)Zn_2(Ph_2Ac)]ClO_4$ in 50% acetonitrile–water solution (tris buffer) was determined to be five times faster than the reaction promoted by $[(BCIMP)Zn_2(Ph_2Ac)]$.

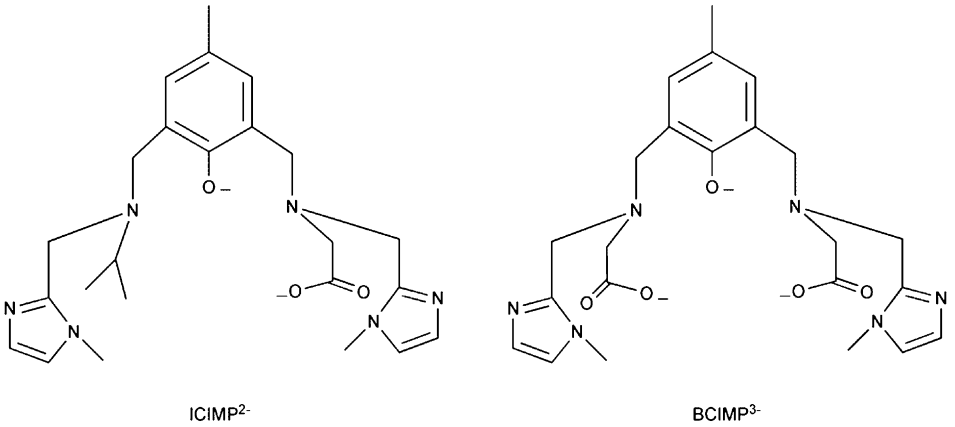

Fig. 62 Dianionic ICIMP and trianionic BCIMP ligands.

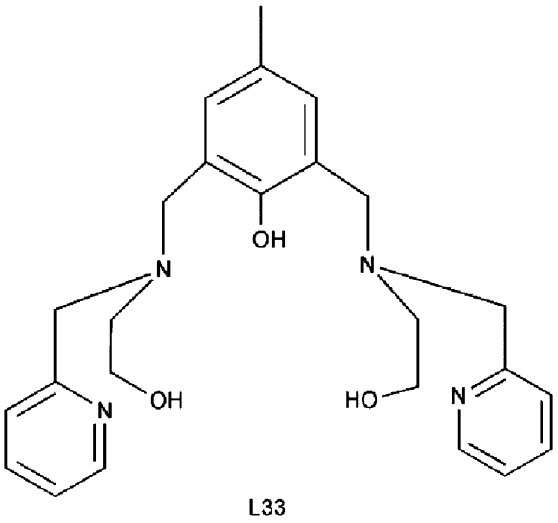

Fig. 63 L33 ligand.

The difference in reactivity for these two complexes is attributed to the availability of an open coordination position in the ICIMP-ligated complex.

A binuclear zinc complex of the 2,6-bis{[(2-pyridylmethyl)(2-hydroxyethyl) amino]methyl}-4-methylphenol ligand (L33, Fig. 63) catalyzes the hydrolysis of bis(4-nitrophenyl) phosphate in aqueous buffer solution to yield 4-nitrophenol and 4-nitrophenyl phosphate.[246] Analysis of the pH-rate profile revealed a sigmoidal-shaped curve with a $pK_a = 7.13$. This value is similar to a deprotonation event characterized by potentiometric titration and has been assigned to deprotonation of

a ligand alcohol appendage. Additional kinetic and mechanistic studies in DMSO solution indicate that a similar reaction takes place under these conditions, thus providing further evidence that the reactive nucleophile is a zinc alkoxide species. A proposed mechanism for bis(4-nitrophenyl) phosphate hydrolysis catalyzed by this binuclear complex involves initial weak coordination ($K_b = 16.26\,M^{-1}$) of the phosphate diester substrate followed by intramolecular attack of the alkoxide moiety. Cleavage of the P–O bond of the leaving group (4-nitrophenolate) followed by displacement of the phosphate monoester product (4-nitrophenyl phosphate) is proposed to complete the catalytic cycle (Scheme 36).

Binuclear zinc hydroxide complexes of the neutral L34 and L35 (Fig. 64) ligands promote phosphate ester hydrolysis.[247] For L34, dihydroxo ($[(L34)Zn_2(OH)_2]^{2+}$) and trihydroxo ($[(L34)Zn_2(OH)_3]^{+}$) species show similar second-order rate constants ($\sim 6 \times 10^{-5}\,M^{-1}\,s^{-1}$). This level of reactivity is similar to that encountered for mononuclear zinc complexes and suggests that the zinc centers act independently in the phosphate ester hydrolysis reaction. This is consistent with the large distance between the zinc centers imparted by the chelate ligand in these complexes. For the L35 ligand, the trihydroxo derivative complex exhibits a second-order rate constant of $4.2 \times 10^{-3}\,M^{-1}\,s^{-1}$. The enhanced reactivity of $[(L35)Zn_2(OH)_3]^{+}$ is suggested to result from an optimal Zn···Zn distance which enables bridging coordination of the bis(4-nitrophenyl) phosphate substrate in a complex that also contains a nucleophilic terminal Zn–OH moiety.

Catalytic HPNP-tranesterification reactivity (Fig. 40, bottom has been reported for zinc complexes assembled using calix[4]arene ligands (Fig. 65).[172,248–251] Complex **9** induces a 23,000-fold rate enhancement over the uncatalyzed intramolecular cyclization reaction of HPNP.[248] Kinetic and mechanistic studies indicate strong binding of the HPNP substrate to the complex ($K = 5.5 \times 10^{-4}\,M^{-1}$) and a k_{cat} value of $7.7 \times 10^{-4}\,s^{-1}$ at pH = 7.0 in acetonitrile/20 mM HEPES (1:1) at 25 °C. As **9** is 50 times more active for HPNP transesterification than **8**, which contains only one zinc center, cooperativity between metal centers occurs in the former complex. Notably, the monozinc calix[4]arene complex **8** is 6 times more reactive than **7**. This result provides evidence that the hydrophobic calix[4]arene moiety plays an important role in the reaction.

Incorporation of internal dimethylamino groups on the calix[4]arene structure yielded **10**, which exhibits a substrate binding affinity that is 30-fold reduced ($K = 0.19 \times 10^{-4}\,M^{-1}$) and a rate constant that is reduced by a factor of 2 ($k_{cat} = 3.6 \times 10^{-4}\,s^{-1}$).[250] In addition, the pH optimum for **9** (pH = 7.5) is considerably higher than that found for **10** (pH = 6.8) These differences suggest that a different catalytic mechanism may be operative in the transesterification of HPNP catalyzed by **9** and **10**. For **9**, the reaction pathway is proposed to involve activation of the HPNP substrate by one zinc center, whereas the second zinc center may coordinate the hydroxyl appendage of the substrate, thus lowering its pK_a value, or may provide a Zn–OH group to deprotonate the substrate (Fig. 66, top). For the reaction involving **10**, double Lewis activation of the substrate is proposed, with an internal dimethyl amino group serving as the base for deprotonation of the substrate (Fig. 66, bottom).

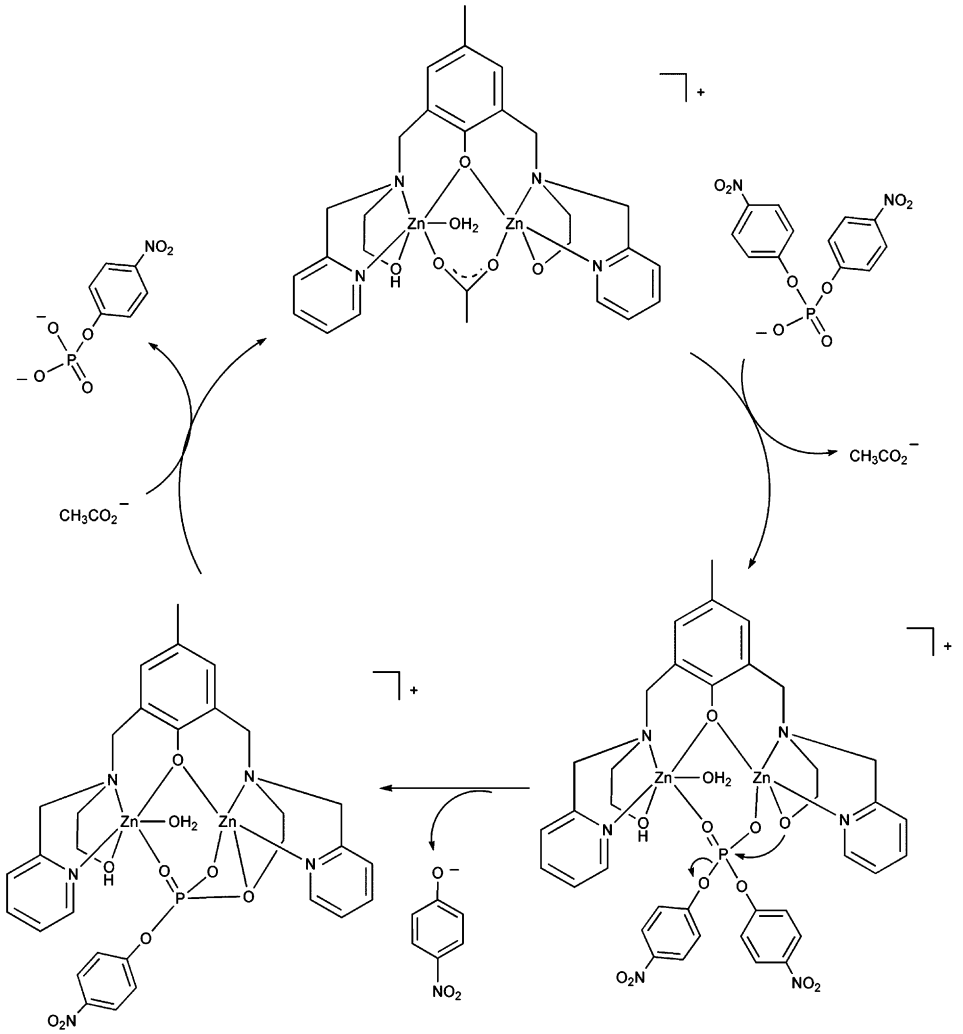

Scheme 36 Proposed mechanism for the hydrolysis of bis(4-nitrophenyl)phosphate catalyzed by a binuclear zinc complex of the L33 ligand.

Flexibility is important in term of the HPNP reactivity of the calix[4]arene complexes, as evidenced by the fact that the constrained analog **11** (Fig. 65) exhibits both a lower substrate affinity ($K = 0.70 \times 10^{-4}\,M^{-1}$) and catalytic rate ($k_{cat} = 0.95 \times 10^{-4}\,s^{-1}$) than **9**.[249]

Positioning of the zinc centers on the calix[4]arene framework also influences HPNP-tranesterification reactivity.[172] Specifically, the 1,2-vicinal complex **12** is a significantly less effective catalyst for HPNP transesterification than **9**.

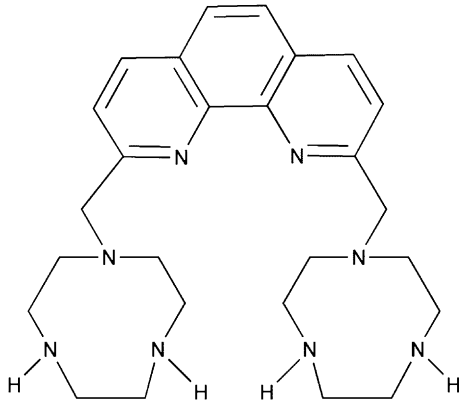

L34

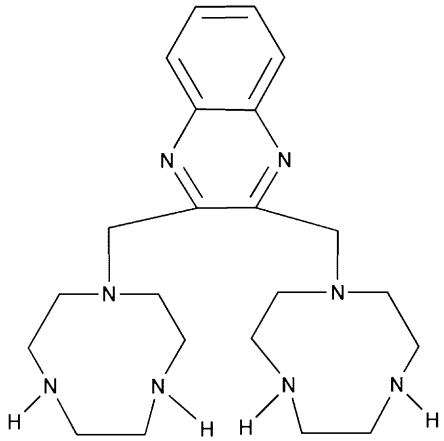

L35

Fig. 64 L34 and L35 ligands.

A calix[4]arene derivative having three appended zinc centers (Fig. 67) exhibits decreased substrate binding ($K = 0.70 \times 10^{-4}\,M^{-1}$) relative to **9** (Fig. 65), but an increased catalytic rate ($k_{cat} = 24 \times 10^{-4}\,s^{-1}$) for the transesterification of HPNP.[249] The mechanism of this reaction is proposed to involve substrate activation by two zinc centers, with the third providing a Zn–OH moiety to deprotonate the substrate (Fig. 67).

Binuclear zinc hydroxide complexes of the Htdmbpo and Hbdmbbppo ligands (Fig. 68) promote the transesterification of HPNP (Fig. 40, bottom).[252] Binding constants and catalytic rate constants were determined for the respective complexes. The Htdmpo-ligated zinc complex exhibits a slighter higher rate constant ($1.10 \times 10^{-3}\,s^{-1}$) than the Hbdmbbppo-ligated complex ($8.33 \times 10^{-4}\,s^{-1}$). However,

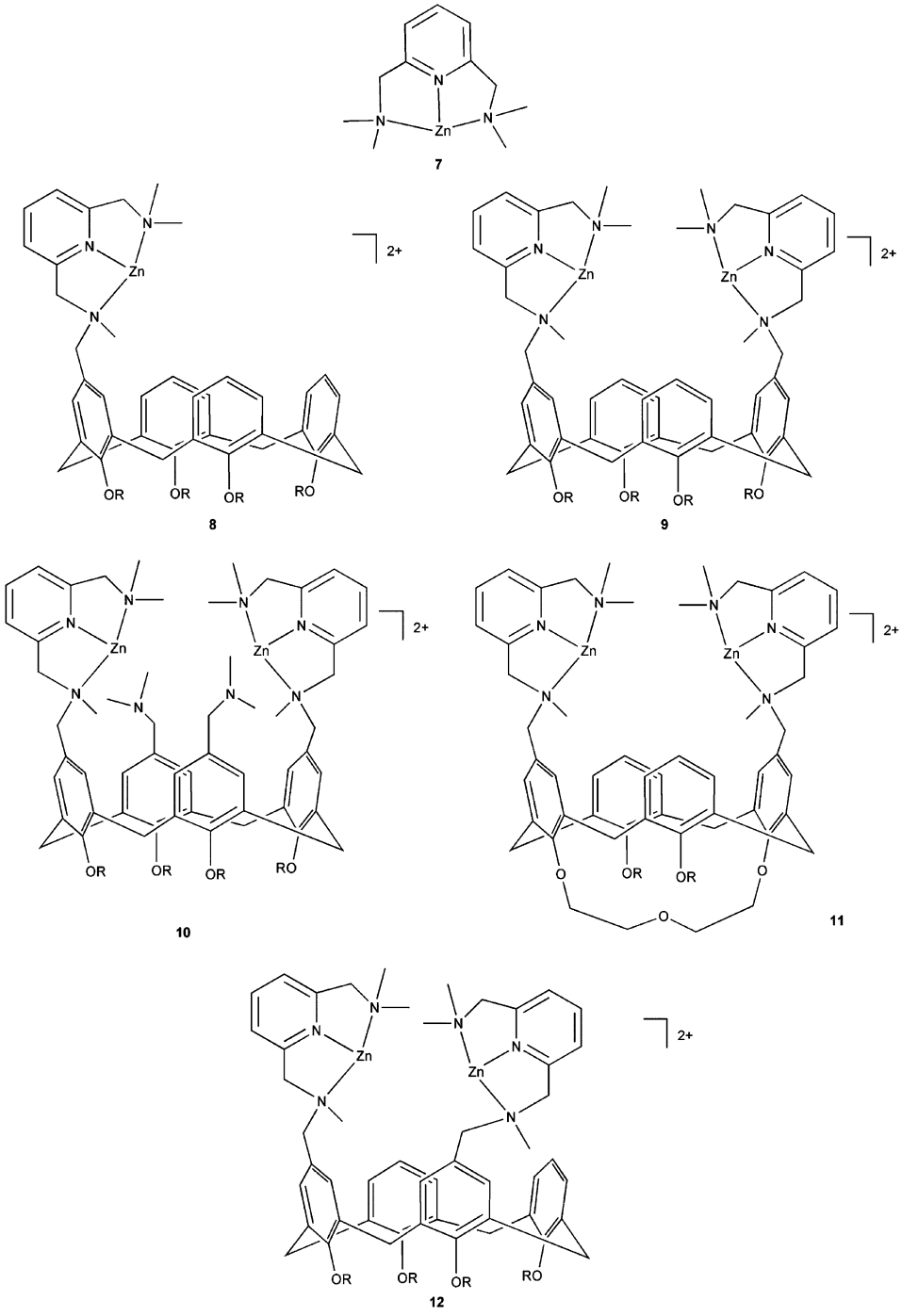

Fig. 65 Calix[4]arene complexes examined for HPNP-transesterification reactivity.

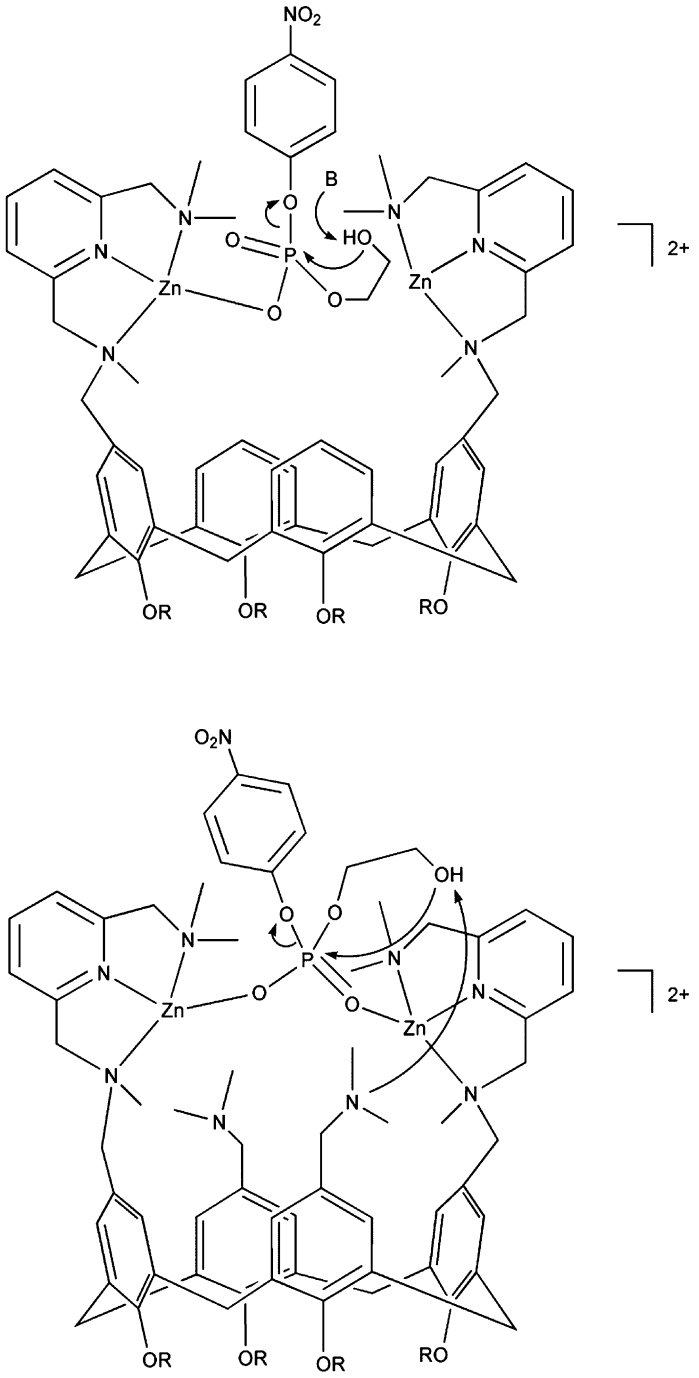

Fig. 66 Proposed mechanistic pathways for the transesterification of HPNP catalyzed by **9** (top) and **10** (bottom).

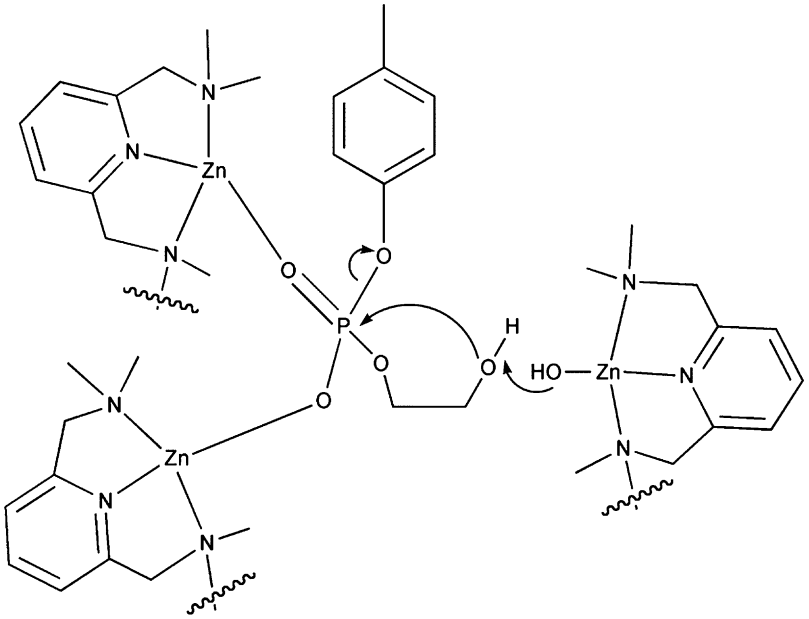

Fig. 67 Proposed mechanism for HPNP transesterification catalyzed by a trinuclear $(N_3Zn)_3$-appended calix[4]arene complex. The calix[4]arene unit is not shown for clarity.

the later complex exhibits substrate binding that is 2.5 times more effective, which results in a higher overall activity for the complex of the asymmetric Hbdmbbppo ligand. For these complexes, a mechanism for HPNP transesterification is proposed wherein the substrate binds to the binuclear zinc center in a μ-1,3-bridging fashion, with a terminal zinc hydroxide moiety serving as a general base for the deprotonation of the HPNP alcohol hydroxy group. A similar mechanism has been proposed for HPNP transesterification promoted by a binuclear zinc complex of the bimido ligand (Fig. 69, top), and a preorganized mixed imidazole/carboxylate-donor ligand (Fig. 69, bottom).[253,254]

Extensive studies of HPNP transesterification (Fig. 40, bottom) promoted by zinc complexes of 1,4,7-triazacyclononane-containing ligands ($[(L36OH)Zn]^{2+}$ and $[(L(37)O)Zn_2]^{3+}$, Fig. 70) have provided important insight into the role of the metal complex in the reaction.[255,256] As shown in Fig. 70, Zn(II) complexes of the L36OH and L37O ligands can have different protonation states for the alcohol portion of the chelate ligand. For the mononuclear complex, the alcohol remains protonated up to pH = 10.4. However, in the binuclear complex, deprotonation of the alcohol occurs below pH = 6. Ionization of a zinc-bound water molecule occurs with $pK_a = 9.2$ for the $[(L36OH)Zn]^{2+}$ and with $pK_a = 8.0$ for $[(L(37)O)Zn_2]^{3+}$. For both complexes, it is proposed that this ionization results in the formation of a terminal Zn–OH moiety, which acts to deprotonate the HPNP substrate in the transesterification reaction, perhaps through general base catalysis as is shown in Fig. 60 (left).[257,258] Enhanced reactivity for the binuclear $[(L(37)O)Zn_2]^{3+}$ complex

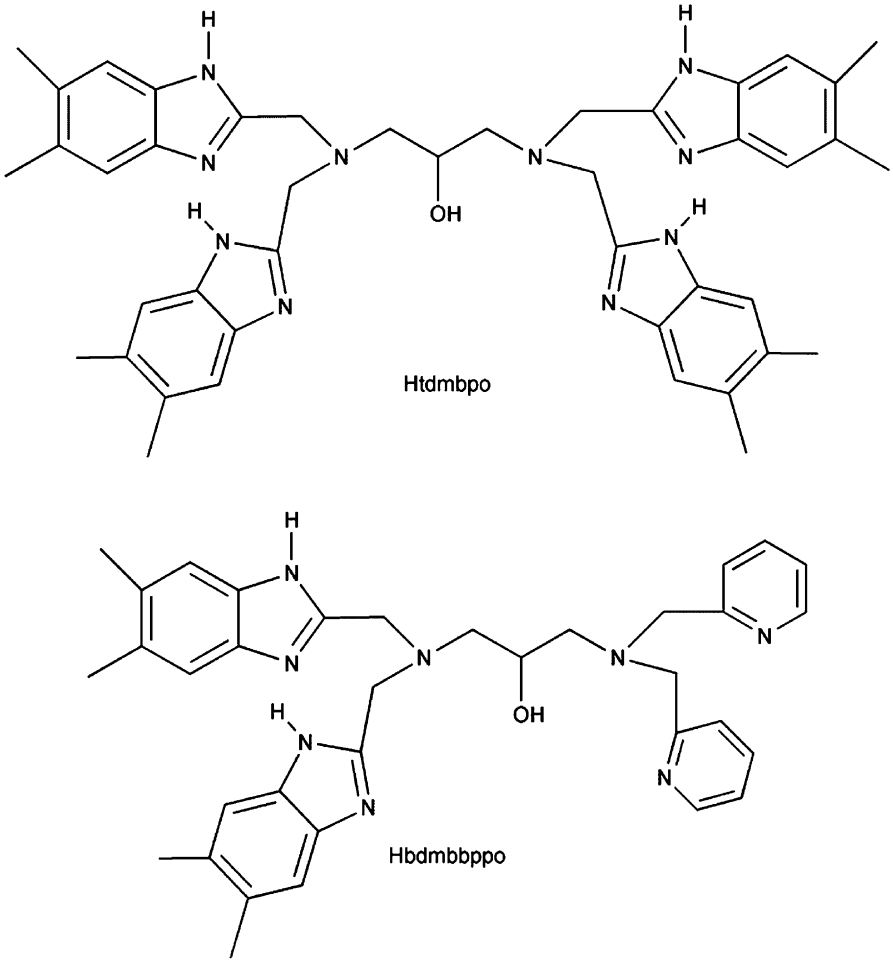

Fig. 68 Htdmbpo and Hbdmbbppo ligands.

versus the mononuclear $[(L36OH)Zn]^{2+}$ complex in this reaction is rationalized on the basis of cooperative roles for the zinc centers in $[(L(37)O)Zn_2]^{3+}$ in facilitating the loss of a proton from the Michaelis complex between the metal complex and the substrate, and in stabilizing the transition state. Notably, comparison of the second-order rate constant for HPNP transesterification by $[(L(37)O)Zn_2]^{3+}$ ($0.25\,M^{-1}\,s^{-1}$) with the first-order rate constant for the uncatalyzed reaction ($k = 3.8 \times 10^{-8}\,s^{-1}$) at pH = 7.6 indicates that the transition state of the metal-catalyzed reaction is stabilized by 9.3 kcal mol^{-1}. From inhibition studies, it was proposed that 2.4 kcal mol^{-1} of this stabilization involves the ground state Michaelis complex whereas the remaining stabilization is achieved as the transition state for HPNP transesterification is approached.

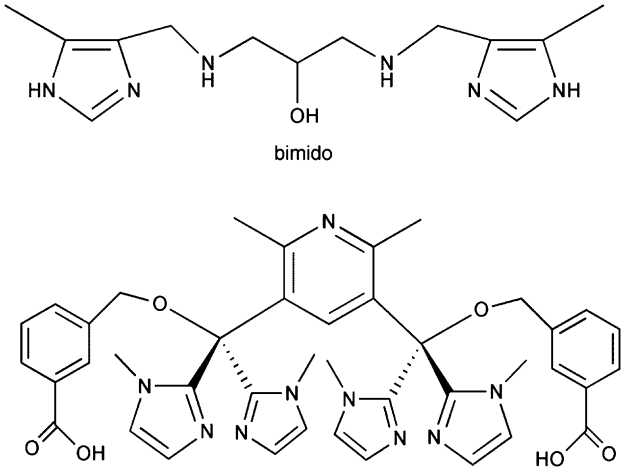

Fig. 69 (top) Structure of bimido ligand and (bottom) preorganized mixed imidazole/carboxylate-donor ligand.

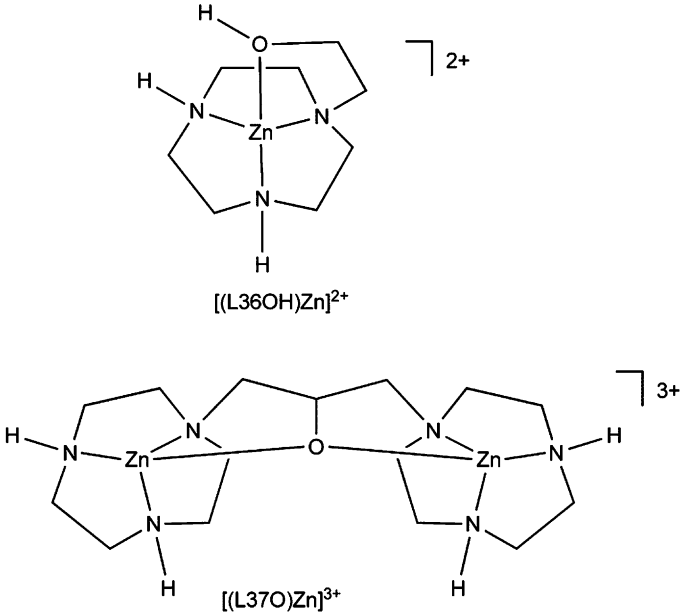

Fig. 70 $[(L36OH)Zn]^{2+}$ and $[(L37O)Zn_2]^{3+}$.

Binuclear zinc complexes of triazacyclononane-containing ligands having different bridge structures (Fig. 71) exhibit second-order rate constants for HPNP transesterification that are only 3–5 times larger than that exhibited by the mononuclear $[(L36OH)Zn]^{2+}$ complex.[256] This behavior is contrasted by that of

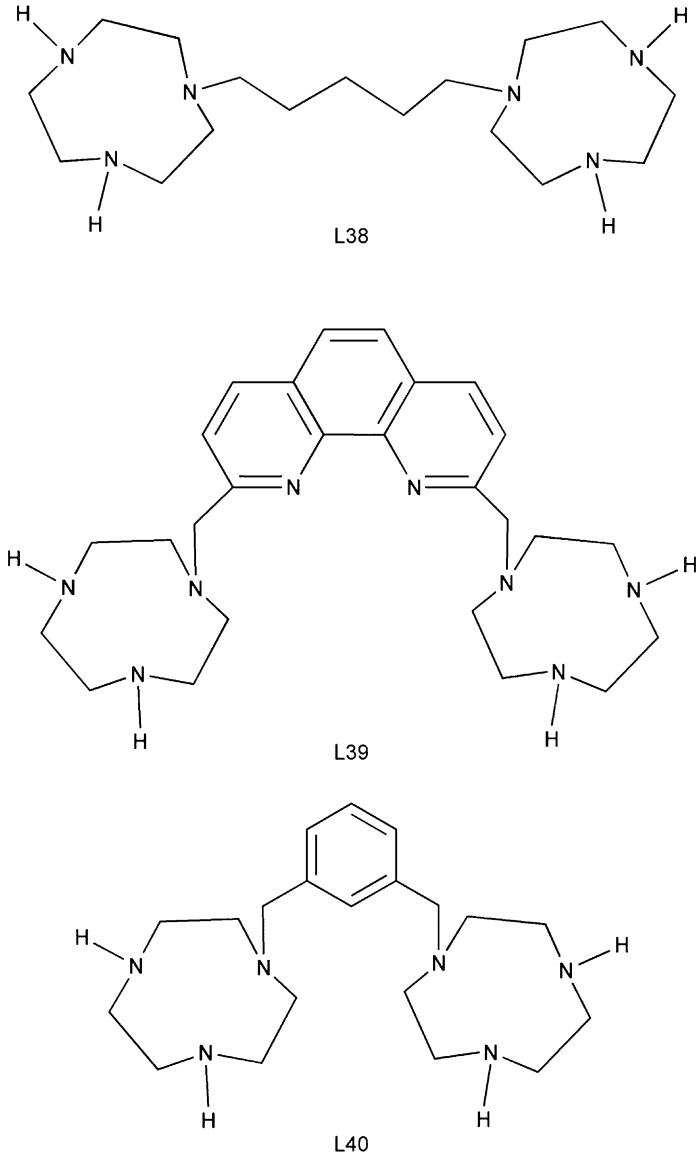

Fig. 71 L38–L40 ligands.

$[(L(37)O)Zn_2]^{3+}$, which exhibits a second-order rate constant that is 120-fold larger than that found for $[(L36OH)Zn]^{2+}$. This dramatic difference in reactivity for the binuclear complexes is attributed to cooperative interactions in $[(L(37)O)Zn_2]^{3+}$ that are not achievable using the binuclear ligands (L38–L40) shown in Fig. 71. For example, the two centers in $[(L(37)O)Zn_2]^{3+}$ may be an optimal distance to provide

electrostatic stabilization of the transition state. Overall, the catalytic power of $[(L(37)O)Zn_2]^{3+}$ (Fig. 70, bottom) is approximately half of that exhibited by enzyme catalysts, with a rate acceleration of 9.8×10^6-fold for the transesterification of HPNP. This acceleration is primarily attributed to electrostatic stabilization of the anionic transition state of the reaction by the compact cationic zinc complex.[258] On the basis of these results, it has been argued that electrostatic considerations should be a primary issue in the design of new small molecule catalysts for phosphate diester cleavage.

A few trinuclear zinc complexes have been reported that promote the cleavage of phosphate esters. For example, calix[4]arene systems having three N_3-ligated Zn(II) centers, and which promote the transesterification of HPNP, have been previously

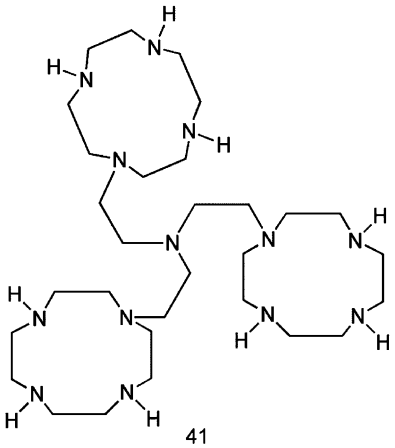

41

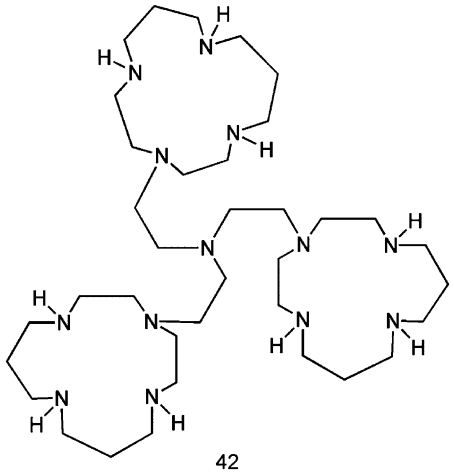

42

Fig. 72 L41 and L42 ligands.

discussed herein.[249] Trinuclear zinc complexes having N_4-donor macrocyclic donors (L41 and L42, Fig. 72) coordinated to each zinc center form mono-, di-, and trihydroxo complexes in aqueous solution. For both ligand types, only the di- and trihydroxo species ($[(L41/42)Zn_3(OH)_2]^{4+}$ and $[(L41/L42)Zn_3(OH)_3]^{3+}$) promote bis(4-nitrophenyl) phosphate hydrolysis.[259] The reactivity found for these multinuclear complexes significantly exceeds that exhibited by the mononuclear complex $[([12]and N_4)Zn(OH)]^{+}$, indicating a cooperative effect between the zinc centers in the trinuclear complexes. For these reactions, an associative mechanism is proposed wherein the bis(4-nitrophenyl) phosphate substrate initially bridges two zinc centers and subsequently undergoes nucleophilic attack from a terminal Zn–OH moiety on the third zinc center. In support of this proposal, it was noted that higher reactivity is found for the L42-ligated system, which has higher pK_a values for the formation of Zn–OH species. Notably, in these systems, similar second-order rate constants are found for the phosphate ester cleavage reactions promoted by the bis- and trihydroxo derivatives. This is likely due to a lower Lewis acidity for the zinc centers in the trihydroxo complex, which would modulate the degree to which the complex can activate the substrate toward nucleophilic attack. Therefore, despite an expected higher nucleophilicity for the Zn–OH units in the trihydroxo complex, similar overall hydrolysis reactivity to the bishydroxo complex is observed.

Outside the scope of coverage of this contribution are studies of zinc complexes having peptide-based ligands[260–262] and Zn(II)-complex-promoted reactions involving RNA or DNA hydrolysis.[261,263–288]

References

1. Lippard, S.J. and Berg, J.M. (1994). *Principles of Bioinorganic Chemistry*. University Science Books, Mill Valley, CA
2. Karlin, K.D. (1993). *Science* **261**, 701–708
3. Parkin, G. (2000). *Chem. Commun.* 1971–1985
4. Parkin, G. (2001). *Met. Ions Biol. Syst.* **38**, 411–460
5. Parkin, G. (2004). *Chem. Rev.* **104**, 699–768
6. Kimura, E., Koike, T. and Shionoya, M. (1997). *Struct. Bond.* **89**, 1–28
7. Weston, J. (2005). *Chem. Rev.* **105**, 2151–2174
8. Kimura, E. (1994). *Prog. Inorg. Chem.* **41**, 443–491
9. Chin, J. (1991). *Acc. Chem. Res.* **24**, 145–152
10. Bashkin, J.K. (1999). *Curr. Opin. Chem. Biol.* **3**, 752–758
11. Suh, J. (2003). *Acc. Chem. Res.* **36**, 562–570
12. Suh, J. (1992). *Acc. Chem. Res.* **25**, 273–279
13. Breslow, R. (1995). *Acc. Chem. Res.* **28**, 146–153
14. Kimura, E. and Kikuta, E. (2000). *J. Biol. Inorg. Chem.* **5**, 139–155
15. Martin, R.B. (2002). *Inorg. Chim. Acta* **339**, 27–33
16. Gelinsky, M., Vogler, R. and Vahrenkamp, H. (2002). *Inorg. Chem.* **41**, 2560–2564
17. diTargiani, R.C., Chang, S., Salter, M.H., Hancock, R.D. and Goldberg, D.P. (2003). *Inorg. Chem.* **42**, 5825–5836
18. Mareque-Rivas, J.C., Prabaharan, R. and de Rosales, R.T.M. (2004). *Chem. Commun.* 76–77
19. Mareque-Rivas, J.C., Prabaharan, R. and Parsons, S. (2004). *Dalton Trans.* 1648–1655

20. Livieri, M., Mancin, F., Tonellato, U. and Chin, J. (2004). *Chem. Commun*. 2862–2863
21. Vallee, B.L. and Williams, R.J.P. (1968). *Proc. Natl. Acad. Sci.* **59**, 498–505
22. Maret, W. and Vallee, B.L. (1993). *Method. Enzymol.* **226**, 52–71
23. Vallee, B.L. and Auld, D.S. (1992). *Faraday Discuss. Chem. Soc.* **93**, 47–65
24. Vallee, B.L. and Auld, D.S. (1993). *Acc. Chem. Res.* **26**, 543–551
25. Vallee, B.L. and Auld, D.S. (1990). *Biochemistry* **29**, 5647–5659
26. Tripp, B.C., Smith, K. and Ferry, J.G. (2001). *J. Biol. Chem.* **276**, 48615–48618
27. Lindskog, S. (1997). *Pharmacol. Ther.* **74**, 1–20
28. Christianson, D.W. and Cox, J.D. (1999). *Annu. Rev. Biochem.* **68**, 33–57
29. Krebs, J.F., Ippolito, J.A., Christianson, D.W. and Fierke, C.A. (1993). *J. Biol. Chem.* **268**, 27458–27466
30. Hakansson, K., Carlsson, M., Svensson, L.A. and Liljas, A. (1992). *J. Mol. Biol.* **227**, 1192–1204
31. Bertini, I., Luchinat, C., Mangani, S. and Pierattelli, R. (1995). *Comment. Inorg. Chem.* **17**, 1–15
32. Hakansson, K. and Wehnert, A. (1992). *J. Mol. Biol.* **228**, 1212–1218
33. Silverman, D.N. and Lindskog, S. (1988). *Acc. Chem. Res.* **21**, 30–36
34. Liljas, A., Hakansson, K., Jonsson, B.H. and Xue, Y. (1994). *Eur. J. Biochem.* **219**, 1–10
35. Christianson, D.W. and Fierke, C.A. (1996). *Acc. Chem. Res.* **29**, 331–339
36. Kimura, E., Shiota, T., Koike, T., Shiro, M. and Kodama, M. (1990). *J. Am. Chem. Soc.* **112**, 5805–5811
37. Zhang, X., van-Eldik, R., Koike, T. and Kimura, E. (1993). *Inorg. Chem.* **32**, 5749–5755
38. Zhang, X. and van-Eldik, R. (1995). *Inorg. Chem.* **34**, 5606–5614
39. Nakata, K., Shimomura, N., Shiina, N., Izumi, M., Ichikawa, K. and Shiro, M. (2002). *J. Inorg. Biochem.* **89**, 255–266
40. Woolley, P. (1975). *Nature* **258**, 677–682
41. Tabushi, I., Kuroda, Y. and Mochizuki, A. (1980). *J. Am. Chem. Soc.* **102**, 1152–1153
42. Huguet, J. and Brown, R.S. (1980). *J. Am. Chem. Soc.* **102**, 7571–7572
43. Brown, R.S., Curtis, N.J. and Huguet, J. (1981). *J. Am. Chem. Soc.* **103**, 6953–6959
44. Slebocka-Tilk, H., Cocho, J.L., Frakman, Z. and Brown, R.S. (1984). *J. Am. Chem. Soc.* **106**, 2421–2431
45. Xue, Y., Liljas, A., Jonsson, B.H. and Lindskog, S. (1993). *Proteins* **17**, 93–106
46. Kimblin, C., Allen, W.E. and Parkin, G. (1995). *J. Chem. Soc. Chem. Commun*. 1813–1815
47. Alsfasser, R., Trofimenko, S., Looney, A., Parkin, G. and Vahrenkamp, H. (1991). *Inorg. Chem.* **30**, 4098–4100
48. Ruf, M. and Vahrenkamp, H. (1996). *Inorg. Chem.* **35**, 6571–6578
49. Alsfasser, R., Ruf, M., Trofimenko, S. and Vahrenkamp, H. (1993). *Chem. Ber.* **126**, 703–710
50. Bergquist, C. and Parkin, G. (1999). *J. Am. Chem. Soc.* **121**, 6322–6323
51. Looney, A., Han, R., McNeill, K. and Parkin, G. (1993). *J. Am. Chem. Soc.* **115**, 4690–4697
52. Bergquist, C., Fillebeen, T., Morlok, M.M. and Parkin, G. (2003). *J. Am. Chem. Soc.* **125**, 6189–6199
53. Kitajima, N., Hikichi, S., Tanaka, M. and Moro-oka, Y. (1993). *J. Am. Chem. Soc.* **115**, 5496–5508
54. Yamaguchi, S., Tokairin, I., Wakita, Y., Funahashi, Y., Jitsukawa, K. and Masuda, H. (2003). *Chem. Lett.* **32**, 406–407
55. Jeffrey, G.A. (1997). *An Introduction to Hydrogen Bonding*. Oxford University Press, New York, NY
56. Echizen, T., Ibrahim, M.M., Nakata, K., Izumi, M., Ichikawa, K. and Shiro, M. (2004). *J. Inorg. Biochem.* **98**, 1347–1360

57. Eklund, H., Nordstrom, B., Zeppezauer, E., Soderlund, G., Ohlsson, I., Boiwe, T., Soderberg, B.O., Tapia, O., Branden, C.-I. and Akeson, A. (1976). *J. Mol. Biol.* **102**, 27–59
58. Ramaswamy, S., Park, D.-H. and Plapp, B.V. (1999). *Biochemistry* **38**, 13951–13959
59. Agarwal, P.K., Webb, S.P. and Hammes-Schiffer, S. (2000). *J. Am. Chem. Soc.* **122**, 4803–4812
60. Mayer, J.M. (1988). *Comment. Inorg. Chem.* **8**, 125–135
61. Meijers, R., Morris, R.J., Adolph, H.W., Merli, A., Lamzin, V.S. and Cedergren-Zeppezauer, E.S. (2000). *J. Biol. Chem.* **276**, 9316–9321
62. Sartorius, C., Gerber, M., Zeppezauer, M. and Dunn, M.F. (1987). *Biochemistry* **26**, 871–882
63. Kleifeld, O., Rulisek, L., Bogin, O., Frenkel, A., Havias, Z., Burstein, Y. and Sagi, I. (2004). *Biochemistry* **43**, 7151–7161
64. Kimura, E., Shionoya, M., Hoshino, A., Ikeda, T. and Yamada, Y. (1992). *J. Am. Chem. Soc.* **114**, 10134–10137
65. Kimblin, C., Bridgewater, B.M., Churchill, D.G. and Parkin, G. (1999). *Chem. Commun*. 2301–2302
66. Seebacher, J., Shu, M. and Vahrenkamp, H. (2001). *Chem. Commun*. 1026–1027
67. Ramaswamy, S., Eklund, H. and Plapp, B.V. (1994). *Biochemistry* **33**, 5230–5237
68. Bergquist, C. and Parkin, G. (1999). *Inorg. Chem.* **38**, 422–423
69. Bergquist, C., Storrie, H., Koutcher, L., Bridgewater, B.M., Friesner, R.A. and Parkin, G. (2000). *J. Am. Chem. Soc.* **122**, 12651–12658
70. Brombacher, H. and Vahrenkamp, H. (2004). *Inorg. Chem.* **43**, 6042–6049
71. Boerzel, H., Koeckert, M., Bu, W., Spingler, B. and Lippard, S. (2003). *Inorg. Chem.* **42**, 1604–1615
72. Walz, R., Weis, K., Ruf, M. and Vahrenkamp, H. (1997). *Chem. Ber.* **130**, 975–980
73. Brombacher, H. and Vahrenkamp, H. (2004). *Inorg. Chem.* **43**, 6054–6060
74. Walz, W. and Vahrenkamp, H. (2001). *Inorg. Chim. Acta* **314**, 58–62
75. Garner, D.K., Fitch, S.B., McAlexander, L.H., Bezold, L.M., Arif, A.M. and Berreau, L.M. (2002). *J. Am. Chem. Soc.* **124**, 9970–9971
76. Cronin, L. and Walton, P.H. (2003). *Chem. Commun*. 1572–1573
77. Lipscomb, W.N. and Strater, N. (1996). *Chem. Rev.* **96**, 2375–2434
78. Christianson, D.W. and Lipscomb, W.N. (1989). *Acc. Chem. Res.* **22**, 62–69
79. Mangani, S., Carloni, P. and Orioli, P. (1992). *Coord. Chem. Rev.* **120**, 309–324
80. Matthews, B.W. (1988). *Acc. Chem. Res.* **21**, 333–340
81. Mock, W.L. and Stanford, D.J. (1996). *Biochemistry* **35**, 7369–7377
82. Mock, W.L. and Aksamawati, M. (1994). *Biochem. J.* **302**, 57–68
83. Schmid, M.F. and Herriott, J.R. (1976). *J. Mol. Biol.* **103**, 175–190
84. Stark, W., Pauptit, R.A., Wilson, K.S. and Jansonius, J.N. (1992). *Eur. J. Biochem.* **207**, 781–791
85. Bode, W., Gomis-Ruth, F.X. and Stockler, W. (1993). *FEBS Lett* **331**, 134–140
86. Pelmenschikov, V. and Siegbahn, P.E.M. (2002). *Inorg. Chem.* **41**, 5659–5666
87. Sutton, P.A. and Buckingham, D.A. (1987). *Acc. Chem. Res.* **20**, 357–364
88. Schepartz, A. and Breslow, R. (1987). *J. Am. Chem. Soc.* **109**, 1814–1826
89. Groves, J.T. and Baron, L.A. (1989). *J. Am. Chem. Soc.* **111**, 5442–5448
90. Takasaki, B.K., Kim, J.H., Rubin, E. and Chin, J. (1993). *J. Am. Chem. Soc.* **115**, 1157–1159
91. Sayre, L.M. (1986). *J. Am. Chem. Soc.* **108**, 1632–1635
92. Hegg, E.L. and Burstyn, J.N. (1998). *Coord. Chem. Rev.* **173**, 133–165
93. Groves, J.T. and Chambers, R.R. (1984). *J. Am. Chem. Soc.* **106**, 630–638
94. Vahrenkamp, H. (1999). *Acc. Chem. Res.* **32**, 589–596
95. Ruf, M. and Vahrenkamp, H. (1996). *Chem. Ber.* **129**, 1025–1028

96. Rombach, M., Maurer, C., Weis, K., Keller, E. and Vahrenkamp, H. (1999). *Chem. Eur. J.* **5**, 1013–1027
97. Pocker, Y. and Stone, J.T. (1967). *Biochemistry* **6**, 668–678
98. Kimura, E., Nakamura, I., Koike, T., Shionoya, M., Kodama, Y., Ikeda, T. and Shiro, M. (1994). *J. Am. Chem. Soc.* **116**, 4764–4771
99. Koike, T., Takamura, M. and Kimura, E. (1994). *J. Am. Chem. Soc.* **116**, 8443–8449
100. Ozturk, G. and Akkaya, E.U. (2004). *Org. Lett.* **6**, 241–243
101. Wendelstorf, C., Warzeska, S., Kovari, E. and Kramer, R. (1996). *Dalton Trans*. 3087–3092
102. Koike, T., Kajitani, S., Nakamura, I., Kimura, E. and Shiro, M. (1995). *J. Am. Chem. Soc.* **117**, 1210–1219
103. Jencks, W.P. and Gilchrist, M. (1968). *J. Am. Chem. Soc.* **90**, 2622–2637
104. Bazzicalupi, C., Bencini, A., Bencini, A., Bianchi, A., Corana, F., Fusi, V., Giorgi, C., Paoli, P., Paoletti, P., Valtancoli, B. and Zanchini, C. (1996). *Inorg. Chem.* **35**, 5540–5548
105. Bazzicalupi, C., Bencini, A., Bianchi, A., Fusi, V., Giorgi, C., Paoletti, P., Valtancoli, B. and Zanchi, D. (1997). *Inorg. Chem.* **36**, 2784–2790
106. Bazzicalupi, C., Bencini, A., Bianchi, A., Fusi, V., Paoletti, P. and Valtancoli, B. (1994). *J. Chem. Soc. Dalton Trans*. 3581–3588
107. Su, X., Sun, H., Zhou, Z., Lin, H., Chen, L., Zhu, S. and Chen, Y. (2001). *Polyhedron* **20**, 91–95
108. Kiefer, L.L. and Fierke, C.A. (1994). *Biochemistry* **33**, 15233–15240
109. Breslow, R. and Singh, S. (1988). *Bioorg. Chem.* **16**, 408–417
110. Xia, J., Xu, Y., Li, S., Sun, W., Yu, K. and Tang, W. (2001). *Inorg. Chem.* **40**, 2394–2401
111. Huang, J., Li, D., Li, S., Yang, D., Sun, W. and Tang, W. (2004). *J. Inorg. Biochem.* **98**, 502–509
112. Zhu, S., Chen, W., Lin, H., Yin, X., Kou, F., Lin, M. and Chen, Y. (1997). *Polyhedron* **16**, 3285–3291
113. Molenveld, P., Engbersen, J.F.J., Kooijman, H., Spek, A.L. and Reinhoudt, D.N. (1998). *J. Am. Chem. Soc.* **120**, 6726–6737
114. Ge, Q., Guo, Y., Lin, H., Gao, D., Lin, H. and Zhu, S. (2004). *Can. J. Chem.* **82**, 409–417
115. Page, M.I. and Laws, A.P. (1998). *Chem. Commun*. 1609–1617
116. Fisher, J.F., Meroueh, S.O. and Mobashery, S. (2005). *Chem. Rev.* **105**, 395–424
117. Cricco, J.A. and Vila, A.J. (1999). *Curr. Pharm. Des.* **5**, 915–927
118. Wang, Z., Fast, W., Valentine, A.M. and Benkovic, S.J. (1999). *Curr. Opin. Chem. Biol.* **3**, 614–622
119. Walsh, T.R., Toleman, M.A., Poirel, L. and Nordmann, P. (2005). *Clin. Microbiol. Rev.* **18**, 306–325
120. Heinz, U. and Adolph, H.W. (2004). *Cell. Mol. Life Sci.* **61**, 2827–2839
121. Fabiane, S.M., Sohi, M.K., Wan, T., Payne, D.J., Bateson, J.H., Mitchell, T. and Sutton, B.J. (1998). *Biochemistry* **37**, 12404–12411
122. Concha, N.O., Rasmussen, B.A., Bush, K. and Herzberg, O. (1996). *Structure* **4**, 823–836
123. Ullah, J.H., Walsh, T.R., Taylor, I.A., Emery, D.C., Verma, C.S., Gamblin, S.J. and Spencer, J. (1998). *J. Mol. Biol.* **284**, 125–136
124. Wommer, S., Rival, S., Heinz, U., Galleni, M., Frere, J.M., Franceschini, N., Amicosante, G., Rasmussen, B., Bauer, R. and Adolph, H.W. (2002). *J. Biol. Chem.* **277**, 24142–24147
125. Cricco, J.A., Orellano, E.G., Rasia, R.M., Ceccarelli, E.A. and Vila, A.J. (1999). *Coord. Chem. Rev.* **190–192**, 519–535
126. Rasia, R.M. and Vila, A.J. (2002). *Biochemistry* **41**, 1853–1860
127. Wang, Z., Fast, W. and Benkovic, S.J. (1999). *Biochemistry* **38**, 10013–10023

128. Hernandez Valladares, M., Kiefer, M., Heinz, U., Soto, R.P., Meyer-Klaucke, W., Nolting, H.F., Zeppezauer, M., Galleni, M., Frere, J.-M., Rossolini, G.M., Amicosante, G. and Adolph, H.-W. (2000). *FEBS Lett.* **467**, 221–225
129. Gross, F. and Vahrenkamp, H. (2005). *Inorg. Chem.* **44**, 4433–4440
130. Ogawa, K., Nakata, K. and Ichikawa, K. (1998). *Chem. Lett*. 797–798
131. Wang, Z. and Benkovic, S.J. (1998). *J. Biol. Chem.* **273**, 22402–22408
132. Wang, Z., Fast, W. and Benkovic, S.J. (1998). *J. Am. Chem. Soc.* **120**, 10788–10789
133. Diaz, N., Sordo, T.L., Suarez, D., Mendez, R. and Martin-Villacorta, J. (2004). *New J. Chem.* **28**, 15–25
134. Suarez, D., Diaz, N. and Merz, K.M. (2002). *J. Comput. Chem.* **23**, 1587–1600
135. Krauss, M., Gresh, N. and Antony, J. (2003). *J. Phys. Chem. B* **107**, 1215–1229
136. Antony, J., Gresh, N., Olsen, L., Hemmingsen, L., Schofield, C.J. and Bauer, R. (2002). *J. Comput. Chem.* **23**, 1281–1296
137. Suarez, D., Brothers, E.N. and Merz, K.M. (2002). *Biochemistry* **41**, 6615–6630
138. Dal Peraro, M., Vila, A.J. and Carloni, P. (2003). *Inorg. Chem.* **42**, 4245–4247
139. Krauss, M., Gilson, H.S.R. and Gresh, N. (2001). *J. Phys. Chem. B* **105**, 8040–8049
140. Kaminskaia, N.V., He, C. and Lippard, S.J. (2000). *Inorg. Chem.* **39**, 3365–3373
141. He, C. and Lippard, S.J. (2000). *J. Am. Chem. Soc.* **122**, 184–185
142. Woon, T.C., Wickramasinghe, W.A. and Fairlie, D.P. (1993). *Inorg. Chem.* **32**, 2190–2194
143. Zevaco, T.A., Gorls, H. and Dinjus, E. (1998). *Polyhedron* **17**, 2199–2206
144. Kupka, T. (1997). *Spectrochim. Acta A* **53**, 2649–2658
145. Ferrer, E.G. and Williams, P.A.M. (1997). *Polyhedron* **16**, 3323–3325
146. Page, M.I. (1984). *Acc. Chem. Res.* **17**, 144–151
147. Hay, R.W., Basak, A.K., Pujari, M.P. and Perotti, A. (1989). *J. Chem. Soc. Dalton Trans*. 197–201
148. Kaminskaia, N.V., Spingler, B. and Lippard, S.J. (2000). *J. Am. Chem. Soc.* **122**, 6411–6422
149. Jencks, W.P. (1987). *Catalysis in Chemistry and Enzymology*. Dover Publications, Inc., New York
150. Kaminskaia, N.V., Spingler, B. and Lippard, S.J. (2001). *J. Am. Chem. Soc.* **123**, 6555–6563
151. Bauer-Siebenlist, B., Dechert, S. and Meyer, F. (2005). *Chem. Eur. J.* **11**, 5343–5352
152. Meyer, F. and Rutsch, P. (1998). *Chem. Commun*. 1037–1038
153. Bauer-Siebenlist, B., Meyer, F., Farkas, E., Vidovic, D., Cuesta-Seijo, J.A., Herbst-Irmer, R. and Pritzkow, H. (2004). *Inorg. Chem.* **43**, 4189–4202
154. Bauer-Siebenlist, B., Meyer, F., Farkas, E., Vidovic, D. and Dechert, S. (2005). *Chem. Eur. J.* **11**, 4349–4360
155. Meyer, F., Heinze, K., Nuber, B. and Zsolnai, L. (1998). *J. Chem. Soc. Dalton Trans*. 207–214
156. Kleywegt, G.J., Wiesmeijer, W.G.R., Van Driel, G.J., Driessen, W.L., Reedijk, J. and Noordik, J.H. (1985). *J. Chem. Soc. Dalton Trans*. 2177–2184
157. Addison, A.W., Rao, T.N., Reedijk, J. van Rijn, J. and Verschoor, G.C. (1984). *J. Chem. Soc. Dalton Trans*. 1349–1356
158. Ackermann, J., Meyer, F., Kaifer, E. and Pritzkow, H. (2002). *Chem. Eur. J.* **8**, 247–258
159. Meyer, F., Jacobi, A., Nuber, B., Rutsch, R. and Zsolnai, L. (1998). *Inorg. Chem.* **37**, 1213–1218
160. Meyer, F. and Pritzkow, H. (2005). *Eur. J. Inorg. Chem*. 2346–2351
161. Lowther, W.T. and Matthews, B.W. (2002). *Chem. Rev.* **102**, 4581–4608
162. Holz, R.C. (2002). *Coord. Chem. Rev.* **232**, 5–26
163. Chen, G., Edwards, T., D'souza, V.M. and Holz, R.C. (1997). *Biochemistry* **36**, 4278–4286

164. Luiz, M.T.B., Szpoganicz, B., Rizzoto, M., Basallote, M.G. and Martell, A.E. (1999). *A.E. Martell Inorg. Chim. Acta* **287**, 134–141
165. Sakiyama, H., Mochizuki, R., Sugawara, A., Sakamoto, M., Nishida, Y. and Yamasaki, M. (1999). *Dalton Trans*. 997–1000
166. Sakiyama, H., Igarashi, Y., Nakayama, Y., Hossain, M.J., Unoura, K. and Nishida, Y. (2003). *Inorg. Chim. Acta* **351**, 256–260
167. Bazzicalupi, C., Bencini, A., Berni, E., Bianchi, A., Fornasari, P., Giorgi, C. and Valtancoli, B. (2003). *Eur. J. Inorg. Chem*. 1974–1983
168. Mareque-Rivas, J.C., Salvagni, E. and Parsons, S. (2004). *Chem. Commun*. 460–461
169. Iturrioz, X., Rozenfeld, R., Michaud, A., Corvol, P. and Llorens-Cortes, C. (2001). *Biochemistry* **40**, 14440–14448
170. Stamper, C., Bennett, B., Edwards, T., Holz, R.C., Ringe, D. and Petsko, G. (2001). *Biochemistry* **40**, 7035–7046
171. Sakiyama, H., Ono, K., Suzuki, T., Tone, K., Ueno, T. and Nishida, Y. (2005). *Inorg. Chem. Commun.* **8**, 372–374
172. Cacciapaglia, R., Casnati, A., Mandolini, L., Reinhoudt, D.N., Salvio, R., Sartori, A. and Ungaro, R. (2005). *J. Org. Chem.* **70**, 624–630
173. Neverov, A.A., Montoya-Pelaez, P.J. and Brown, R.S. (2001). *J. Am. Chem. Soc.* **123**, 210–217
174. Montoya-Pelaez, P.J. and Brown, R.S. (2002). *Inorg. Chem.* **41**, 309–316
175. Szajna, E., Makowska-Grzyska, M.M., Wasden, C.W., Arif, A.M. and Berreau, L.M. (2005). *Inorg. Chem.* **44**, 7595–7605
176. Mareque-Rivas, J.C., de Rosales, R.T.M. and Parsons, S. (2003). *Dalton Trans*. 2156–2163
177. Mareque-Rivas, J.C., Salvagni, E., Prabaharan, R., de Rosales, R.T.M. and Parsons, S. (2004). *Dalton Trans*. 172–177
178. Coleman, J.E. (1992). *Annu. Rev. Biophys. Biomol. Struct.* **21**, 441–483
179. Strater, N., Lipscomb, W.N., Klabunde, T. and Krebs, B. (1996). *Angew. Chem. Int. Edit.* **35**, 2024–2055
180. Wilcox, D.E. (1996). *Chem. Rev.* **96**, 2435–2458
181. Coleman, J.E. (1998). *Curr. Opin. Chem. Biol.* **2**, 222–234
182. Holtz, K.M. and Kantrowitz, E.R. (1999). *FEBS Lett* **462**, 7–11
183. Holtz, K.M., Stec, B. and Kantrowitz, E.R. (1999). *J. Biol. Chem.* **274**, 8351–8354
184. Stec, B., Holtz, K.M. and Kantrowitz, E.R. (2000). *J. Mol. Biol.* **299**, 1303–1311
185. Jedrzejas, M.J. and Setlow, P. (2001). *Chem. Rev.* **101**, 607–618
186. O'Brien, P.J. and Herschlag, D. (2002). *Biochemistry* **41**, 3207–3225
187. Hengge, A.C. (2005). In *Advances in Physical Organic Chemistry*, Richard, J. (ed.), Vol. 40, pp. 49–107. Academic Press, New York, NY
188. Harrowfield, J.M., Jones, D.R., Lindoy, L.F. and Sargeson, A.M. (1980). *J. Am. Chem. Soc.* **102**, 7733–7741
189. Jones, D.R., Lindoy, L.F. and Sargeson, A.M. (1983). *J. Am. Chem. Soc.* **105**, 7327–7336
190. Chin, J. and Banaszczyk, M. (1989). *J. Am. Chem. Soc.* **111**, 4103–4105
191. Connolly, J.A., Banaszczyk, M., Hynes, R.C. and Chin, J. (1994). *Inorg. Chem.* **33**, 665–669
192. Rawji, G., Hediger, M. and Milburn, R.M. (1983). *Inorg. Chim. Acta* **79**, 247–248
193. Rawlings, J., Hengge, A.C. and Cleland, W.W. (1997). *J. Am. Chem. Soc.* **119**, 542–549
194. Hendry, P. and Sargeson, A.M. (1990). *Inorg. Chem.* **29**, 92–97
195. Williams, N.H., Lebuis, A.-M. and Chin, J. (1999). *J. Am. Chem. Soc.* **121**, 3341–3348
196. Williams, N.H. (2004). *Biochem. Biophys. Acta* **1697**, 279–287
197. Humphry, T., Forconi, M., Williams, N.H. and Hengge, A.C. (2004). *J. Am. Chem. Soc.* **126**, 11864–11869
198. Hettich, R. and Schneider, H. (1997). *J. Am. Chem. Soc.* **119**, 5638–5647

199. Seo, J.S., Sung, N.D., Hynes, R.C. and Chin, J. (1996). *Inorg. Chem.* **35**, 7472–7473
200. Kenley, R.A., Fleming, R.H., Laine, R.M., Tse, D.S. and Winterle, J.S. (1984). *Inorg. Chem.* **23**, 1870–1876
201. Norman, P.R. and Cornelius, R.D. (1982). *J. Am. Chem. Soc.* **104**, 2356–2361
202. Hendry, P. and Sargeson, A.M. (1990). *Prog. Inorg. Chem.* **38**, 201–258
203. Koike, T., Inoue, M., Kimura, E. and Shiro, M. (1996). *J. Am. Chem. Soc.* **118**, 3091–3099
204. Chapman, W.H. and Breslow, R. (1995). *J. Am. Chem. Soc.* **117**, 5462–5469
205. Hikichi, S., Tanaka, M., Moro-Oka, Y. and Kitajima, N. (1992). *J. Chem. Soc. Chem. Commun*. 814–815
206. Dumas, D.P., Caldwell, S.R., Wild, J.R. and Raushel, F.M. (1989). *J. Biol. Chem.* **264**, 19659–19665
207. Mulbry, W.W., Karns, J.S., Kearney, P.C., Nelson, J.O., McDaniel, C.S. and Wild, J.R. (1986). *Appl. Environ. Microbiol.* **51**, 926–930
208. Benning, M.M., Shim, H., Raushel, F.M. and Holden, H.M. (2001). *Biochemistry* **40**, 2712–2722
209. Vanhooke, J.L., Benning, M.M., Raushel, F.M. and Holden, H.M. (1996). *Biochemistry* **35**, 6020–6025
210. Aubert, S.D., Li, Y. and Raushel, F.M. (2004). *Biochemistry* **43**, 5707–5715
211. Chin, J., Banaszczyk, M., Jubian, V. and Zou, X. (1989). *J. Am. Chem. Soc.* **111**, 186–190
212 Williams, N.H., Cheung, W. and Chin, J. (1998). *J. Am. Chem. Soc.* **120**, 8079–8087
213. Williams, N.H., Takasaki, B., Wall, M. and Chin, J. (1999). *Acc. Chem. Res.* **32**, 485–493
214. Kim, J.H. and Chin, J. (1992). *J. Am. Chem. Soc.* **114**, 9792–9795
215. Chung, Y.S., Akkaya, E.U., Venkatachalam, T.K. and Czarnik, A.W. (1990). *Tetrahedron Lett.* **31**, 5413–5416
216. Chin, J. and Zou, X. (1988). *J. Am. Chem. Soc.* **110**, 223–225
217. Wahnon, D., Lebuis, A.-M. and Chin, J. (1995). *Angew. Chem. Int. Edit.* **34**, 2412–2414
218. Humphry, T., Forconi, M., Williams, N.H. and Hengge, A.C. (2002). *J. Am. Chem. Soc.* **124**, 14860–14861
219. Tafesse, F. and Milburn, R.M. (1987). *Inorg. Chim. Acta* **135**, 119–122
220. Jones, D.R., Lindoy, L.F. and Sargeson, A.M. (1984). *J. Am. Chem. Soc.* **106**, 7807–7819
221. Gellman, S.H., Petter, R. and Breslow, R. (1986). *J. Am. Chem. Soc.* **108**, 2388–2394
222. Breslow, R., Berger, D. and Huang, D.-L. (1990). *J. Am. Chem. Soc.* **112**, 3686–3687
223. Norman, P.R. (1987). *Inorg. Chim. Acta* **130**, 1–4
224. Norman, P.R., Tate, A. and Rich, P. (1988). *Inorg. Chim. Acta* **145**, 211–217
225. Koike, T. and Kimura, E. (1991). *J. Am. Chem. Soc.* **113**, 8935–8941
226. Kimura, E., Kodama, Y., Koike, T. and Shiro, M. (1995). *J. Am. Chem. Soc.* **117**, 8304–8311
227. Kady, I.O., Tan, B., Ho, Z. and Scarborough, T. (1995). *J. Chem. Soc. Chem. Commun*. 1137–1138
228. Goldberg, D.P., diTargiani, R.C., Namuswe, F., Minnihan, E.C., Chang, S., Zakharov, L.N. and Rheingold, A.L. (2005). *Inorg. Chem.* **44**, 7559–7569
229. Fujii, Y., Itoh, T., Onodera, K. and Tada, T. (1995). *Chem. Lett.* **24**, 305–306
230. Itoh, T., Fujii, Y., Tada, T., Yoshikawa, Y. and Hisada, H. (1996). *Bull. Chem. Soc. Jpn.* **69**, 1265–1274
231. Bonfa, L., Gatos, M., Mancin, F., Tecilla, P. and Tonellato, U. (2003). *Inorg. Chem.* **42**, 3943–3949
232. Ibrahim, M.M., Shimomura, N., Ichikawa, K. and Shiro, M. (2001). *Inorg. Chim. Acta* **313**, 125–136
233. Ibrahim, M.M., Ichikawa, K. and Shiro, M. (2003). *Inorg. Chim. Acta* **353**, 187–196

234. Adams, H., Bailey, N.A., Fenton, D.E. and He, Q.-Y. (1996). *J. Chem. Soc. Dalton Trans*. 2857–2865
235. Feng, G., Mareque-Rivas, J.C., de Rosales, R.T.M. and Williams, N.H. (2005). *J. Am. Chem. Soc.* **127**, 13470–13471
236. Clewley, R.G., Slebocka-Tilk, H. and Brown, R.S. (1989). *Inorg. Chim. Acta* **157**, 233–238
237. Jurek, P. and Martell, A.E. (1999). *Inorg. Chim. Acta* **287**, 47–51
238. Aguilar, J., Bencini, A., Berni, E., Bianchi, A., Garcia-Espana, E., Gil, L., Mendoza, A., Ruiz-Ramirez, L. and Soriano. C. (2004). *Eur. J. Inorg. Chem*. 4061–4071
239. Bazzicalupi, C., Bencini, A., Berni, E., Bianchi, A., Fedi, V., Fusi, V., Giorgi, C., Paoletti, P. and Valtancoli, B. (1999). *Inorg. Chem.* **38**, 4115–4122
240. Bazzicalupi, C., Bencini, A., Berni, E., Bianchi, A., Fornasari, P., Giorgi, C. and Valtancoli, B. (2004). *Inorg. Chem.* **43**, 6255–6265
241. Kong, D., Martell, A.E. and Reibenspies, J. (2002). *Inorg. Chim. Acta* **333**, 7–14
242. Kong, D. and Martell, A.E. (2002). *J. Reibenspies Inorg. Chim. Acta* **333**, 7–14
243. Abe, K.-J., Izumi, J., Ohba, M., Yohoyama, T. and Okawa, H. (2001). *Bull. Chem. Soc. Jpn.* **74**, 85–95
244. Mancin, F., Rampazzo, E., Tecilla, P. and Tonellato, U. (2004). *Eur. J. Org. Chem*. 281–288
245. Carlsson, H., Haukka, M. and Nordlander, E. (2004). *Inorg. Chem.* **43**, 5681–5687
246. Chen, J., Wang, X., Zhu, Y., Lin, J., Yang, X., Li, Y., Lu, Y. and Guo, Z. (2005). *Inorg. Chem.* **44**, 3422–3430
247. Arca, M., Bencini, A., Berni, E., Caltagirone, C., Devillanova, F.A., Isaia, F., Garau, A., Giorgi, C., Lippolis, V., Perra, A., Tei, L. and Valtancoli, B. (2003). *Inorg. Chem.* **42**, 6929–6939
248. Molenveld, P., Kapsabelis, S., Engbersen, J.F.J. and Reinhoudt, D.N. (1997). *J. Am. Chem. Soc.* **119**, 2948–2949
249. Molenveld, P., Stikvoort, W.M.G., Kooijman, H., Spek, A.L., Engbersen, J.F.J. and Reinhoudt, D.N. (1999). *J. Org. Chem.* **64**, 3896–3906
250. Molenveld, P., Engbersen, J.F.J. and Reinhoudt, D.N. (1999). *Eur. J. Org. Chem*. 3269–3275
251. Molenveld, P., Engbersen, J.F.J. and Reinhoudt, D.N. (2000). *Chem. Soc. Rev.* **29**, 75–86
252. Albedyhl, S., Schnieders, D., Jancso, A., Gajda, T. and Krebs, B. (2002). *Eur. J. Inorg. Chem*., 1400–1409
253. Gajda, T., Kramer, R. and Jancso, A. (2000). *Eur. J. Inorg. Chem*. 1635–1644
254. Worm, K., Chu, F., Matsumoto, K., Best, M.D., Lynch, V. and Anslyn, E.V. (2003). *Chem. Eur. J.* **9**, 741–747
255. Iranzo, O., Kovalevsky, A.Y., Morrow, J.R. and Richard, J.P. (2003). *J. Am. Chem. Soc.* **125**, 1988–1993
256. Iranzo, O., Elmer, T., Richard, J.P. and Morrow, J.R. (2003). *Inorg. Chem.* **42**, 7737–7746
257. Iranzo, O., Richard, J.P. and Morrow, J.R. (2004). *Inorg. Chem.* **43**, 1743–1750
258. Yang, M.Y., Iranzo, O., Richard, J.P. and Morrow, J.R. (2005). *J. Am. Chem. Soc.* **127**, 1064–1065
259. Bazzicalupi, C., Bencini, A., Berni, E., Giorgi, C., Maoggi, S. and Valtancoli, B. (2003). *Dalton Trans.* 3574–3580
260. Scarso, A., Scheffer, U., Gobel, M., Broxterman, Q.B., Kaptein, B., Formaggio, F., Toniolo, C. and Scrimin, P. (2002). *Proc. Natl. Acad. Sci.* **99**, 5144–5149
261. Ichikawa, K., Tarani, M., Uddin, M.K., Nakata, K. and Sato, S. (2002). *J. Inorg. Biochem.* **91**, 437–450
262. Yamada, K., Takahashi, Y., Yamamura, H., Araki, S., Saito, K. and Kawai, M. (2000). *Chem. Commun.* 1315–1316

263. Shelton, V.M. and Morrow, J.R. (1991). *Inorg. Chem.* **30**, 4295–4299
264. Morrow, J.R. (1996). *Met Ions Biol Syst* **33**, 561–592
265. Kovari, E. and Kramer, R. (1994). *Chem. Ber.* **127**, 2151–2157
266. Yashiro, M., Ishikubo, A. and Komiyama, M. (1995). *J. Chem. Soc. Chem. Commun.* 1793–1794
267. Yashiro, M., Ishikubo, A. and Komiyama, M. (1997). *Chem. Commun.* 83–84
268. Matsuda, S., Ishikubo, A., Kuzuya, A., Yashiro, M. and Komiyama, M. (1998). *Angew. Chem. Int. Edit.* **37**, 3284–3286
269. Kawahara, S. and Uchimaru, T. (2001). *Eur. J. Inorg. Chem.* 2437–2442
270. Ait-Haddou, H., Sumaoka, J., Wiskur, S.L., Folmer-Andersen, J.F. and Anslyn, E.V. (2002). *Angew. Chem. Int. Edit.* **41**, 4013–4016
271. Yashiro, M. and Kawahara, R. (2004). *J. Biol. Inorg. Chem.* **9**, 914–921
272. Yashiro, M., Kaneiwa, H., Onaka, K. and Komiyama, M. (2004). *Dalton Trans.* 605–610
273. Basile, L.A., Raphael, A.L. and Barton, J.K. (1987). *J. Am. Chem. Soc.* **109**, 7550–7551
274. Fitzsimons, M.P. and Barton, J.K. (1997). *J. Am. Chem. Soc.* **119**, 3379–3380
275. Sissi, C., Mancin, F., Palumbo, M., Scrimin, P., Tecilla, P. and Tonellato, U. (2000). *Nucleos. Nucleot. Nucl.* **19**, 1265–1271
276. Sissi, C., Rossi, P., Felluga, F., Formaggio, F., Palumbo, M., Tecilla, P., Toniolo, C. and Scrimin, P. (2001). *J. Am. Chem. Soc.* **123**, 3169–3170
277. Aka, F.N., Akkaya, M.S. and Akkaya, E.U. (2001). *J. Mol. Catal. A* **165**, 291–294
278. Copeland, K.D., Fitzsimons, M.P., Houser, R.P. and Barton, J.K. (2002). *Biochemistry* **41**, 343–356
279. Boseggia, E., Gatos, M., Lucatello, L., Mancin, F., Moro, S., Palumbo, M., Sissi, C., Tecilla, P., Tonellato, U. and Zagotto, G. (2004). *J. Am. Chem. Soc.* **126**, 4543–4549
280. Nomura, A. and Sugiura, Y. (2004). *J. Am. Chem. Soc.* **126**, 15374–15375
281. Morrow, J.R. and Iranzo, O. (2004). *Curr. Opin. Chem. Biol.* **8**, 192–200
282. Liu, C., Wang, M., Zhang, T. and Sun, H. (2004). *Coord. Chem. Rev.* **248**, 147–168
283. Mancin, F., Scrimin, P., Tecilla, P. and Tonellato, U. (2005). *Chem. Commun.* 2540–2548
284. Reddy, P.R., Mohan, S.K. and Rao, K.S. (2005). *Chem. Biodivers.* **2**, 672–683
285. Xiang, Q., Zhang, J., Liu, P., Xia, C., Zhou, Z., Xie, R. and Yu, X. (2005). *J. Inorg. Biochem.* **99**, 1661–1669
286. Peng, W., Liu, P., Jiang, N., Lin, H., Zhang, G., Liu, Y. and Yu, X. (2005). *Bioorg. Chem.* **33**, 374–385
287. Molenveld, P., Engbersen, J.F.J. and Reinhoudt, D.N. (1999). *Angew. Chem. Int. Ed.* **38**, 3189–3192
288. Chu, F., Smith, J., Lynch, V.M. and Anslyn, E.V. (1995). *Inorg. Chem.* **34**, 5689–5690

Mechanisms for nucleophilic aliphatic substitution at glycosides

NICOLE A. HORENSTEIN

Department of Chemistry, University of Florida, Gainesville, Florida, 32611 7200 USA

Abstract

Much of carbohydrate chemistry and biochemistry is centered on bond forming and bond breaking reactions at the anomeric carbon of glycosides. No single mechanism adequately covers the scope of these reactions, because differences in sugar substituents, stereochemistry, leaving groups, nucleophiles, and catalysts can influence the mechanistic pathway taken. The influence of solvent is only now beginning to become apparent in greater detail. Several methods exist to probe the mechanisms of these reactions; they include a variety of kinetic studies, including isotope effects, and computational methods. It has been found that typical reactions will uniquely utilize a mechanism somewhere within a continuum between A_ND_N and $D_N + A_N$ mechanisms. With knowledge of the factors that determine the mechanism, synthetic method development will be furthered and a deeper understanding of biological catalysis is likely to be gained.

ADVANCES IN PHYSICAL ORGANIC CHEMISTRY
VOLUME 41 ISSN 0065-3160 DOI: 10.1016/S0065-3160(06)41005-4

1 Scope and rationale for this review

This chapter is focused primarily on the mechanisms of non-enzymatic nucleophilic displacement reactions at the anomeric carbon of glycopyranosides. This includes solvolysis (primarily hydrolysis) reactions and reactions leading to creation of glycosides (glycosidation). Interestingly, a rich chemistry of the anomeric carbon functioning as a *nucleophile* is known, but will not be covered here.[1] Enzyme-catalyzed glycosyl transfer reactions are not the focus of this review, however excellent reviews are available that treat *N*- and *O*-glycohydrolase enzyme mechanisms.[2–4] This review is primarily focused on the literature from 2002. Interested readers are referred to the excellent reviews[5,6] by Bennet and Kitos, and Berti and Tanaka which cover work prior to 2002. Some of the key areas of coverage include the issue of the timing of steps in reactions at the anomeric carbon, the role of substituent identity and stereochemistry in reactivity and product stereochemistry at the anomeric center, lifetime of glycosyl oxocarbenium ions, computational analyses of reaction pathways and conformational analysis of oxocarbenium ions, and gas-phase studies of oxocarbenium ions. Despite some overlap with prior reviews, several highlights from the relevant literature are first presented to facilitate readers' perspectives.

There are several reasons for interest in the mechanistic chemistry of the glycosidic bond. First, carbohydrate chemistry is one of the oldest areas of inquiry in organic chemistry, yet still remains an extremely active field in synthetic, mechanistic, and biochemical studies. The driving force for this is a combination of different factors. In biology, complex carbohydrates play a critical role in cellular recognition events and disease states.[7,8] Mechanistic studies can impact many aspects of biological science by providing a solid basis for understanding factors important in the biosynthesis of glycans. The richness and diversity of carbohydrate structures begins at the level of the many variations in the monosaccharide building blocks. This is further expanded by the many regioisomers and stereoisomers that can be obtained when oligosaccharides and higher polymers are assembled by creation of the glycosidic linkage between monosaccharides. As will become apparent in later sections, the fundamental chemistry of the glycosidic carbon is exquisitely sensitive to the three-dimensional disposition, and identity of functional groups that surround it. Considerable work remains to characterize and understand these factors in detail. Further, synthetic chemists are pressed to assemble ever more complex saccharide structures. Mechanistic understanding of the basic process of glycoside hydrolysis and formation is likely to facilitate further synthetic method development[9] and continue to provide insights into enzyme catalytic mechanisms. Finally, as a purely

intellectual pursuit, the mechanisms of nucleophilic displacements at glycosidic carbon turn out to be rather interesting, because no single mechanism exists. Rather, a mechanistic continuum is operative, and the precise mechanism is a complex function of saccharide structure, leaving group properties, nucleophile properties, solvent, and the nature of catalysis. The tools of kinetic isotope effects (KIEs), computational methods, and even gas-phase chemistry are now being applied to more complex systems, often of direct synthetic relevance.

2 Introduction and general points

In the simplest sense, the reaction under discussion is the net exchange of a nucleophile for a leaving group, often an alkoxy substituent, at C-1 (the "anomeric" carbon) in a cyclic acetal or ketal as shown in Scheme 1.

An important structural distinction must be made between simple acetals and ketals versus their more complex carbohydrate homologs, the aldoses and ketoses. The rich hydroxylation patterns found in the naturally occurring saccharides can impact the mechanisms and outcome of nucleophilic displacement reactions. This review is primarily focused on nucleophilic displacements at the anomeric center of glycosides, though some reference to model acetal chemistries will be made. Aldofuranose and aldopyranose anomeric carbons have a secondary substitution pattern, one group being the ring alkoxy and the other the ring alkyl substituents. The cyclic forms of ketoses can be considered to have tertiary anomeric centers. The cleavage of a glycosidic bond only occurs significantly under acid catalysis; rates of hydrolysis are greatly diminished at neutral and alkaline pH values for alkyl aglycons,[10] though spontaneous or base-catalyzed loss of aglycon can be significant for leaving groups that are either highly stabilized or positively charged in the glycoside. Capon[11] has extensively reviewed the literature for acid-catalyzed hydrolysis and glycosylations prior to 1969, and Cordes and Bull[12] have reviewed the mechanisms for hydrolysis of acetals and related compounds.

A closer look at glycoside chemistry, utilizing analyses of product stereochemistry, trapping experiments, and KIEs reveal that much like displacement reactions at secondary aliphatic carbon, a mechanistic continuum is possible ranging from dissociative loss of the aglycon, first producing a solvent-equilibrated glycosyl oxocarbenium ion, followed by nucleophilic capture, to an associative mechanism, featuring concomitant attack of a nucleophile and loss of the aglycon.[13] The IUPAC nomenclature will be favored here, thus the two limiting processes mentioned above are referred to as ($D_N + A_N$) and ($A_N D_N$), respectively.[14] These two extremes represent an oversimplification of the nature of possible intermediates; Scheme 2 illustrates an expanded view of the possible steps that may be relevant in a glycoside

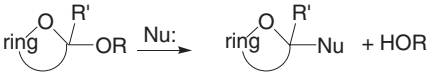

Scheme 1.

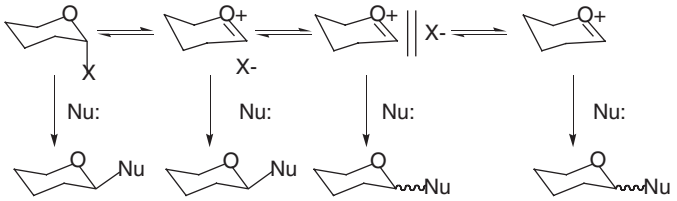

Scheme 2.

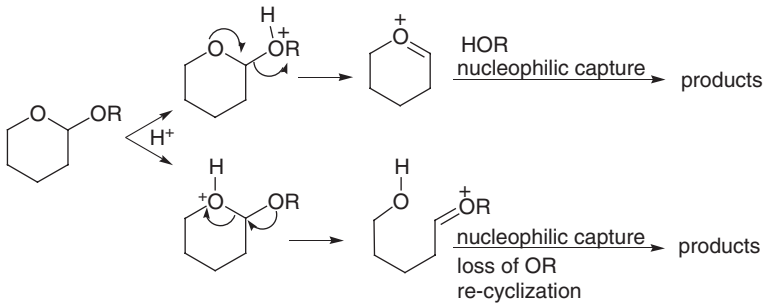

Scheme 3.

solvolysis or nucleophilic displacement reaction. Richard and coworkers have recently reviewed mechanistic considerations of ion pairing for solvolysis of non-glycoside compounds.[15]

Where the reacting sugar is finally captured in the mechanistic scheme, Scheme 2 will be determined by the nucleophilicities of the leaving group X and Nu, solvent effects, and the stability of the oxocarbenium ion. An early insight into the mechanism of substitution at the glycosidic carbon comes from the observation that few of these reactions are stereospecific; immediately arguing for mechanisms that will typically involve oxocarbenium ions. As will be discussed, oxocarbenium ion chemistry is dominant but not exclusively so, since there is good evidence to suggest that A_ND_N processes do occur.

The acid-catalyzed cleavage of a glycosidic bond can involve exocyclic cleavage of the protonated glycoside, or first involve endocyclic cleavage of the ring C–O bond, in a pathway that involves more steps to lead to the final substitution product (Scheme 3). Reactions of pyranosides have generally been considered to proceed with exocyclic C–O cleavage, however there are indications that the endocyclic pathway can be operative.[16–18]

In studies employing a pseudosymmetric deuterated acetal (Scheme 4), Anslyn and coworkers explored the preference for endocyclic versus exocyclic cleavage as a function of the starting acetal stereochemistry.[17] They found that the α-acetal with the leaving isopropoxyl group axial gave only products arising from the exocyclic pathway, while the β-configured anomer afforded products deriving from both pathways. An analysis of the effect of temperature on the product distribution for methanolysis of the β-acetal allowed calculation of $\Delta H^{\ddagger}$ and $\Delta S^{\ddagger}$ for the endo- and

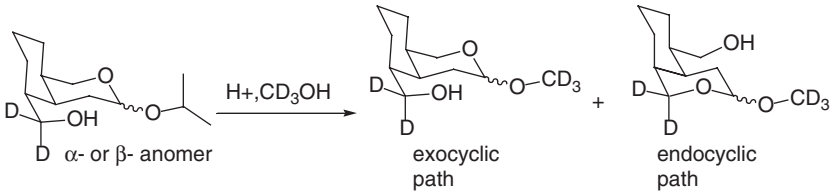

Scheme 4.

exocyclic paths. Increasing fractions of endocyclic cleavage were observed at decreasing temperatures. The enthalpy and entropy activation parameters for endocyclic cleavage were $19.2 \pm 1.4\,\text{kcal mol}^{-1}$ and -12.6 ± 6.1 e.u., while for exocyclic cleavage they were $22.8 \pm 1.1\,\text{kcal mol}^{-1}$ and 3.7 ± 3.8 e.u. While the respective enthalpic terms are quite similar there is a substantial difference in the entropic terms which accounts for the diminishing amount of exocyclic cleavage at lower temperatures. Further, the -12 e.u. observed for the endocyclic activation entropy was considered to be too negative to be solely accounted for by freezing of the exocyclic C–O bond in the transition state. Thus the large negative value was used to propose that nucleophilic participation (by solvent) is a larger component of the endocyclic pathway than found for the exocyclic pathway. These conclusions need to be considered cautiously since the differences in entropy of activation could reflect differences in solvation without requiring nucleophilic participation per se. For example, in the endocyclic model, liberation of the endocyclic oxygen could in principle involve a different change in solvent structure than for liberation of the exocyclic aglycon oxygen. The modest enthalpic advantage to the endocyclic route was rationalized on the basis of the endocyclic bond being weakened due to partial $n \rightarrow \sigma^*$ donation from the exocyclic O to the anomeric carbon. There are few confirmed reports of endocyclic cleavage of pyranosides, and it is generally assumed that the exocyclic pathway is operative. What is certain from these model studies is that an endocyclic pathway may be competitive with exocyclic pathways under the appropriate conditions, including a β-aglycon leaving group, and lower temperatures. This point is worth keeping in mind.

3 Key experimental methods

Two invaluable methodologies that can probe the structure of transition states and the lifetimes of short-lived glycosyl oxocarbenium ion intermediates are KIEs and competitive trapping methods. This section presents a brief overview and discussion of these methods; readers are referred to excellent reviews for more in depth commentary.[6,15] Sugars are extremely well suited to KIE studies because all of the atoms at and around the glycosidic bond can be isotopically labeled to report on changes in bonding that occur in proceeding from the ground to transition states. Scheme 5 illustrates the positions about a glycoside that can be labeled and are particularly useful.

The α-^{2}H (or ^{3}H) secondary KIE has seen extensive application in glycoside cleavage reactions. To a lesser degree, secondary β-^{2}H (or ^{3}H) and primary ^{13}C (or

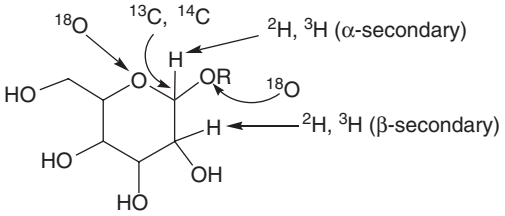

Scheme 5.

^{14}C) isotope effects have also been employed. The α-effect arises when the force constants at the anomeric carbon differ in the rate-limiting transition state from the ground state. This KIE has been taken to provide a measure of the degree of rehybridization from sp_3 towards sp_2 at the transition state. Often, a sizeable isotope effect at H-1 has been used to suggest that the mechanism of the hydrolysis is a dissociative one, with the implication that an oxocarbenium ion intermediate is formed subsequent to the transition state reported on by the KIE. This may be in error however, because even in a concerted bimolecular process, the hybridization at the anomeric carbon is changing and therefore this alternate mechanism is not ruled out by the observation of an α-deuterium KIE. Probably for synthetic reasons, the β-deuterium and primary carbon effects have been employed less often. This is unfortunate, because they provide a clearer picture of the reaction mechanism. The origin of the β-KIE is primarily due to hyperconjugation between the β-hydron and the partially vacant orbital at C1. The isotope effect is sensitive to charge development at the anomeric carbon, and provides a more reliable estimate of charge than the α-effect can. The primary carbon isotope effect is complementary to the β-deuterium KIE. The origin of the KIE at carbon is related to the net loss of vibrational energy between ground state and transition state, along with a contribution to reaction coordinate motion. Concerted bimolecular displacements produce large KIEs ($^{13/12}k > 1.03$; $^{14/12}/k > 1.06$) while dissociative reactions that feature oxocarbenium ion-like transition states without nucleophilic participation have KIEs that are below 1.03 or 1.06, respectively, for ^{13}C or ^{14}C isotopes.

Thus, a pattern of a large β-deuterium KIE and a small carbon KIE are indica tive of a dissociative transition state, while small β-deuterium isotope effects and a large carbon isotope effect provide the signature of an associative transition state involving both a leaving group and a nucleophile. Observation of the latter pattern then necessarily rules out an oxocarbenium ion intermediate, and strongly points towards an A_ND_N mechanism. On the other hand, KIEs that identify a dissociative transition state cannot rule out the case of a very weakly associated nucleophile, and cannot report on post-rate-determining events. Ring ^{18}O KIEs can report on bonding changes between the anomeric carbon and the ring oxygen (i.e. C1–O5 in a pyranose). In a mechanism involving oxocarbenium ion-like transition states, the participation of non-bonding electrons of the ring oxygen causes a net tightening of force constants around this atom, with an associated inverse KIE with values between 0.98 and 1.00. It is interesting to consider how

possible changes in solvation at O-5 between the ground and transition states might perturb the O-18 KIE.

For substitution mechanisms that involve formation of a discrete oxocarbenium ion intermediate, it is possible to trap the intermediate with nucleophiles that result in configurationally stable products. A stereochemical analysis leads to information about the concertedness of the reaction, and quantification of the ratio of products arising from the solvolytic capture to products arising from capture by added nucleophile can provide an estimate of the lifetime for the oxocarbenium ion. In the absence of other nucleophilic species, the solvolytic capture by water is not a useful stereochemical probe because the products often mutarotate at a rate that is far too great to allow identification of the initially formed product's stereochemistry. If stable product mixtures are obtained that reflect both retention and inversion with respect to the original glycosidic stereochemistry, this indicates that the reacting glycon has progressed to solvent-separated and/or -equilibrated oxocarbenium ions. If inversion is observed, this could indicate either an A_ND_N mechanism or reaction with nucleophile from an intimate ion pair. Depending on the relative values of the rate constants, multiple reaction modes could operate simultaneously. Trapping with powerful nucleophiles such as azide affords the possibility of "clocking" the lifetime of reactive oxocarbenium ion species. The rate diffusion controlled rate constant for capture of a carbenium ion by a strong negatively charged nucleophile is approximately $5 \times 10^9\,M^{-1}\,s^{-1}$.[15] In a competitive trapping experiment, in which the same oxocarbenium ion species can be captured by azide or solvent (typically water), product ratios for azide versus solvent trapped product yields the ratio of rate constants. The known rate constant for the azide reaction allows determination of the rate constant for the water reaction, and its reciprocal represents the lifetime of the cation. Note that highly stabilized carbenium ions may have an intrinsic barrier to capture by azide, and for such species the assumption of diffusion controlled capture will not be valid.[19] Sugar-derived oxocarbenium ions are on the order of stability of the *t*-butyl cation, and are sufficiently reactive to lend themselves to this methodology.

4 Studies of glucosides

SOLVOLYSIS AND TRAPPING EXPERIMENTS

A little over 30 years ago it was commonly thought that acid-catalyzed aldopyranoside substitutions at the anomeric carbon proceeded by dissociative mechanisms that involved oxocarbenium ion intermediates (formerly referred to as oxycarbonium ions).[11,12] However, evidence was available that suggested this generality might not be valid. Vernon and coworkers showed that methanolysis of phenyl glucopyranosides proceeds with considerable inversion of configuration, suggesting that the oxocarbenium ion species was not solvent equilibrated.[20] Interestingly, that same study presented an early use of ^{18}O leaving group KIEs, and used these data to argue in favor of a dissociative mechanism involving exocyclic glycosidic bond

cleavage. A quantitative sense of the degree of stability of oxocarbenium ion species was lacking however. In mixtures of ethanol/trifluoroethanol, solvolysis of glucopyranosides yielded product distributions that were sensitive to both leaving group and the starting anomeric configuration.[21] This result is inconsistent with a mechanism involving a solvent-equilibrated oxocarbenium ion. Interestingly, the proportion of ethyl glycoside to trifluoroethyl glycoside did not correlate with retention or inversion pathways – surprising, given the greater nucleophilicity of ethanol. This led to the conclusion that the transition state involved the solvent's facilitation of leaving group departure.[21]

In 1986, Bennet and Sinnott reported a comparison of salt effects for solvolysis of aldopyranosides versus methoxymethyl acetals in water, as part of a larger study that featured KIEs for glucoside hydrolysis.[22] It was found that dinitrophenyl (DNP) glucoside hydrolysis was nearly insensitive to addition of a variety of salts having a wide range of nucleophilicities and basicities, while the methoxymethyl acetals were clearly sensitive to the nucleophilicity of the added salt. The results led to the conclusion that the glucopyranosides did not involve a nucleophilic component at the transition state, possibly explained by the stricter steric requirements for attack at the more hindered secondary anomeric carbon of an aldopyranosyl ring as compared to the primary carbon of a methoxymethyl compound. Though not proof, the results suggested that an oxocarbenium ion intermediate with a very short lifetime was formed.

In 1989, Amyes and Jencks reported a study of azide common ion inhibition for solvolysis of a series of α-azido ethers (Fig. 1).[23] The rate constants k_{HOH} for addition of water to the oxocarbenium ions were determined with an assumed diffusion controlled second-order rate constant k_{az} of $5.0 \times 10^9\ M^{-1}\ s^{-1}$ for attack on the oxocarbenium ion by azide and the observed rate suppression by varying concentrations of added azide, as determined from Equation (1). With k_{HOH} in hand, the lifetime of the oxocarbenium ion was taken as k_{HOH}^{-1}

$$k_{obs} = k_{solv}k_{HOH}/k\left(k_{HOH} + k_{az}[N_3^-]\right) \tag{1}$$

From the estimated lifetimes for the series (Fig. 1), it was possible to propose a series of substituent effects on oxocarbenium ion lifetime, which were then used to

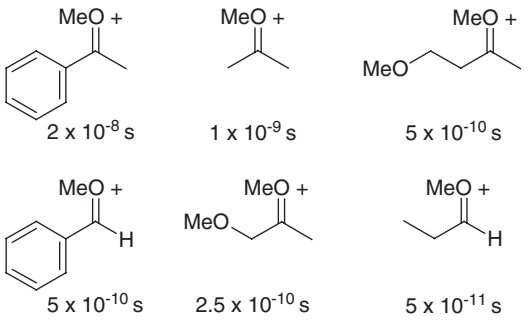

Fig. 1 Oxocarbenium ion lifetimes in aqueous solution. Adapted from Ref. [23].

estimate that the lifetime of a glycopyranosyl oxocarbenium was on the order of 10^{-12} s. Estimates of the equilibrium constants for formation of the oxocarbenium ion from the azido ether were also reported in this study. They were obtained by dividing the observed first-order rate constant for solvolysis by the apparent first-order rate constant for capture of the oxocarbenium ion by azide at a given concentration. The results are interesting and show that substituents have a greater effect on K_{eq} for oxocarbenium ion formation than for the rate at which water captures the oxocarbenium ion. A comparison pertinent to sugar chemistry is between the acetone *O*-methyl and the β-methoxy acetone *O*-methyl oxocarbenium ions which serve as models for the glucosyl and 2-deoxyglucosyl oxocarbenium ions, respectively. The observed rate constants for capture of these two species by water is differed by a factor of 4, but the ratio of the equilibrium constants for formation of these species is approximately 600. Thus, 2-deoxysugar oxocarbenium ions have a significantly greater intrinsic stability than their 2-hydroxy counterparts, but their reactivity is very much the same. This provides an indication that the transition states for their capture is early.

It has been shown that changes of leaving group and nucleophile can affect the nature of the substitution reaction in a profound way. The α-anomer of glucopyranosyl fluoride was examined in its reaction with a charged and uncharged nucleophiles in water.[24] Reactions were first order in concentration for anionic nucleophiles, but the rate was independent of concentration of uncharged (amine) nucleophiles. The Swain–Scott plot (Fig. 2) of the second-order rate constants for a given anionic nucleophile versus its *n* value had a modest slope of 0.18, indicating a weakly nucleophilic transition state. The stereochemical course of the reaction was complete inversion for azide as the nucleophile, consistent with a mechanism

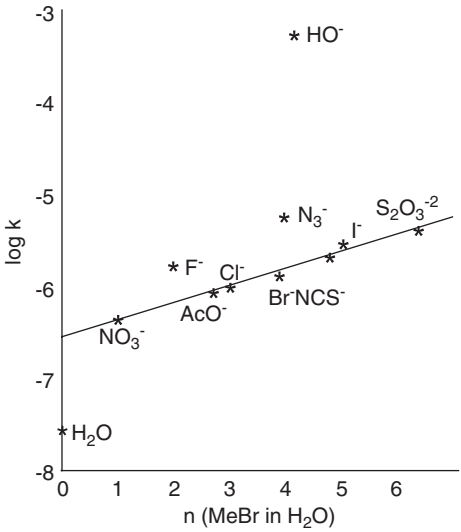

Fig. 2 Swain–Scott plot for reactions of nucleophiles with α-D-glucopyranosyl fluoride in water. Adapted from Ref. [24].

involving a concerted bimolecular substitution at the anomeric carbon. By product analysis, all of the β-azido glucoside observed could be accounted for by the observed second-order rate constant for the azide reaction. This excludes any significant contribution to the reaction from azide trapping of solvent-separated or -equilibrated oxocarbenium ion species. On the other hand, a modest rate dependence on [nuc^-] could be rationalized on the basis of a stepwise preassociation mechanism in which a tight ion pair reacts with the nucleophile. However, the Swain–Scott plot is linear over the region of nucleophiles stronger and weaker than fluoride. In the stepwise mechanism, there would be a break in the plot corresponding to a change in rate-determining step with nucleophiles better than the leaving group fluoride. This can be rationalized by the idea that loss of fluoride is slower than attack by a better nucleophile, but with weaker nucleophiles, fluoride loss is faster, leading to a non-linear free energy relationship. The results with the fluoro leaving group lead to another key aspect of nucleophilic substitution at the anomeric center, namely that the nature of the leaving group can determine whether or not an intermediate can exist. In this case, the fluoride leaving group is an effective nucleophile for the return reaction from the ion pair, so in the presence of fluoride, the ion does not exist in an experimentally detectable way. Leaving groups such as alkoxy are protonated at the transition state in acid-catalyzed hydrolysis and are much less effective nucleophiles from the ion pair, being uncharged. They are able to diffuse away more rapidly than recapture the oxocarbenium ion, allowing this species to exist as a discrete intermediate.

KIE STUDIES

The acid-catalyzed hydrolysis of α- and β-methyl glucopyranosides has been studied with multiple KIEs.[22,25] Scheme 6 presents a composite representation of the isotopically substituted positions used in the studies. Table 1 presents selected KIE results.

Several observations bear mention from this study. First, both anomers hydrolyze via transition states that have substantial oxocarbenium ion character (significant β-^{2}H effects) are lacking in nucleophilic participation (small ^{13}C KIEs), and are late with respect to loss of the methyl alcohol aglycon (significant leaving group, ^{18}O KIE). These results are consistent with a $D_N{}^*A_N$ or $D_N + A_N$ pathway. Closer inspection of the data reveals significant differences in the β-D KIEs and ring ^{18}O KIEs for each anomer. This led to the conclusion that there are differences in the

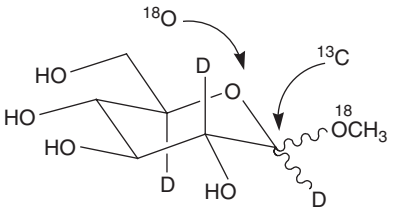

Scheme 6.

Table 1 Selected KIE results[22,25]

Isotope label	α-methyl glucoside KIE	β-methyl glucoside KIE
α-D	1.137	1.089
β-D	1.073	1.045
^{18}O-methoxyl	1.026	1.024
^{18}O-ring	0.996	0.991
^{13}C-anomeric	1.007	1.011

transition state conformation of each sugar. Namely, the α-anomer proceeds via a flattened $^{1}S_{3}$ skew boat transition state, while the β-anomer resembled a flattened $^{4}C_{1}$ chair at the transition state. The lack of any observed nucleophilic character (small primary ^{13}C KIEs) in these transition states supports the idea that subsequent oxocarbenium ion intermediates are formed as discussed above.

Following Banait and Jencks[24] work on azide trapping of fluorosugars, Sinnotts group measured the KIEs for this and related nucleophilic displacements of fluoroglucosides.[26] Perhaps the most important KIE was the primary ^{13}C KIE at the anomeric carbon. Hydrolysis of α-fluoroglucopyranoside resulted in large ^{13}C KIEs of 1.032, indicative of a transition state having bimolecular character and significant nucleophilic participation. The β-^{2}H KIE was still substantial at 1.067, indicating that the transition state had oxocarbenium ion character. In accord with the β-^{2}H KIE, the ^{18}O KIE for the ring oxygen atom was strongly inverse at 0.984 indicating that the ring oxygen was in a tighter environment at the transition state compared to the ground state. In terms of structure this corresponds to the endocyclic O-anomeric C bond as having partial double bond character, or being ''oxocarbenium ion like''. Taken together, the KIEs point to a transition state that is exploded with regard to bond order to the departing fluoride and incoming water, but still involves bonding between each of these groups and the anomeric carbon. The KIE data also point to another subtlety in the reactivity of glucose towards nucleophilic substitution. The β-D-fluoroglucopyranoside hydrolysis reactions show a smaller ^{13}C KIE (1.017) indicating less nucleophilic participation in this transition state. In the presence of azide, the ^{13}C KIE for substitution of α-D-glucopyranosyl fluoride rises dramatically to 1.085. This KIE is the signature for a concerted bimolecular displacement, and demonstrates that in the presence of a suitable nucleophile, and a nucleophilic leaving group, the oxocarbenium ion pathway is not followed.

5 Studies of deoxyglucosides

MECHANISMS

The solvolysis of 2-deoxyglucopyranosides has been studied extensively by the Bennet laboratory with emphasis on the progression through the dissociative mechanistic continuum and characterization of the lifetime of the 2-deoxyglucosyl oxocarbenium ion.

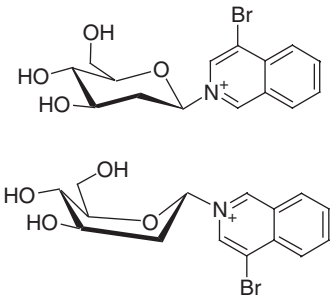

Scheme 7.

Solvolysis of both α- and β-2-deoxyglucopyranosyl-isoquinolinium salts allowed generation of oxocarbenium ions with a poorly nucleophilic leaving group (Scheme 7). It was observed that solvolysis of the β-anomer in the presence of the series of nucleophilic monoanions AcO^-, Cl^-, Br^-, and N_3^- gave a Swain–Scott parameter of 0.03 ± 0.05. Similarly, solvolysis of the α-compound in the presence of the same series of salts afforded a Swain–Scott parameter of 0.03 ± 0.10. The results indicate little or no sensitivity to anion nucleophilicity and therefore point to a mechanism that does not involve an A_ND_N transition state.[27,28]

Later work concluded that while the 2-deoxyglucosyl isoquinolinium compounds do not react by an A_ND_N mechanism, neither do they solvolyze via a free oxocarbenium ion.[29] The key result was the observation that in aqueous/alcohol mixtures, solvolysis of 2-deoxyglucopyranosyl-isoquinolinium anomers affords diastereomeric product mixtures whose composition depended on the starting anomeric configuration of the glycoside. This ruled out a solvent-equilibrated oxocarbenium ion intermediate for the solvolysis of the diastereomeric glycosides. This narrows the focus of the mechanistic framework for the formation of substitution products at the stage of an ion–molecule pair and a solvent-separated ion–molecule pair. In methanol/water and ethanol/water systems the α-anomer showed a modest preference for formation of inverted products, while the β-anomer showed a strong preference for inversion. The observation of some retained product in all cases demonstrates that the reaction manifold must include the solvent-separated ion–molecule complexes. Interestingly, in trifluoroethanol/water mixtures, the α-anomer afforded the retention products as the major component, and following this same trend, the β-anomer showed reduced preference for inversion. The model invoked to explain this pattern (Scheme 8) involves general base catalysis from isoquinoline in the solvent-separated ion–molecule complex, providing a bias towards retention.

LIFETIMES OF OXOCARBENIUM IONS

Solvolysis of 2-deoxyisoquinolinium salts in the presence of azide does not show A_ND_N kinetic behavior, and the 2-deoxyglucosyl oxocarbenium ion is not solvent

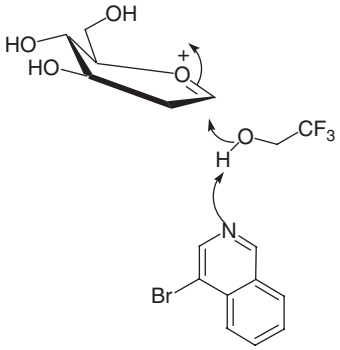

Scheme 8.

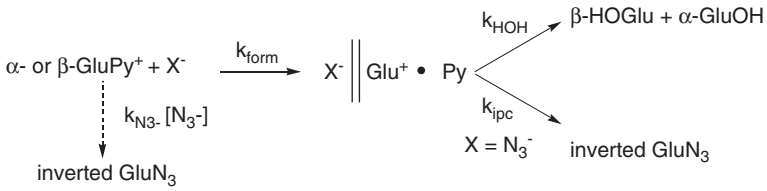

Scheme 9.

equilibrated. Its reactions will occur from solvent-separated ion or ion–molecule pairs in the $D_N{}^*A_N$ mechanism.[29] In the presence of the good nucleophile azide, competitive trapping of the oxocarbenium ion yields a mixture of 2-deoxyglucose and inverted 1-azido 2-deoxyglucoside. That the inverted azido product predominated indicates that the collapse of the solvent-separated ion pair of azide and oxocarbenium ion to intimate ion pair is faster than reorganization of the solvent-separated ion pair to place azide on the other face of the oxocarbenium ion (Scheme 9). The net rate constant of diffusion of a leaving group from the oxocarbenium ion and solvent reorganization, k_{form}, can be estimated to be on the order of 1×10^{-11} s, as described.[15] Thus, the 2-deoxyglucosyl oxocarbenium ion is very much on the border of having a real lifetime, but can be detected.

As a result of these studies, and the approximately 4-fold greater stability attributed to 2-deoxyglycosyl oxocarbenium ions over their 2-hydroxy counterparts, Zhu and Bennet estimated that the lifetime for the 2-deoxyglucosyl oxocarbenium ion is on the order of 2×10^{-11} s, and $\sim 10^{-12}$ s for the glucosyl oxocarbenium ion in water, consistent with prior results.[29]

6 Studies of *N*-acetyl neuraminic acids

N-acetyl neuraminic acid (NeuAc) is a saccharide of unusual structure compared to glucose, fructose, and other common monosaccharides (Scheme 10). The sugar is

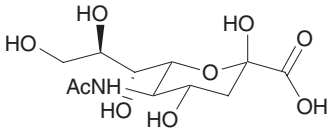

Scheme 10.

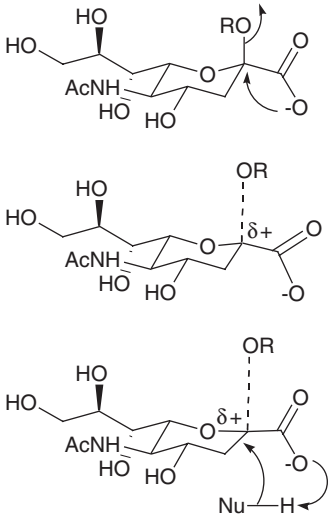

Scheme 11.

formally a 2-deoxyketose, and additionally has a carboxylic acid residue attached to the anomeric center. The carboxyl group is highly acidic with a pK_a of approximately 2.7 for *O*-glycosides and 0.36–0.74 for cationic *N*-glycosides.[30–32] Within the context of nucleophilic substitution at the anomeric carbon, the chemistry is potentially richer than for glucose and other aldoses. As discussed earlier for 2-deoxyglucose, the absence of a hydroxyl substituent adjacent to the anomeric carbon is stabilizing for oxocarbenium ion-like transition states and for the intermediates which could be subsequently formed. NeuAc is not a typical ketose; the anomeric center is substituted with an electron-rich and potentially nucleophilic carboxylate group. One could consider the potential of this group to participate in displacement reactions at the anomeric center, or functioning to stabilize an oxocarbenium ion intermediate, and/or acting as an intramolecular general base to facilitate capture of the oxocarbenium ions by nucleophiles as indicated in Scheme 11.

KIE STUDIES

β-dideuterium, primary ^{14}C, and primary ^{13}C KIEs have been measured for NeuAc glycoside hydrolysis containing α-*p*-nitrophenyl, β-cytidine monophosphate, and

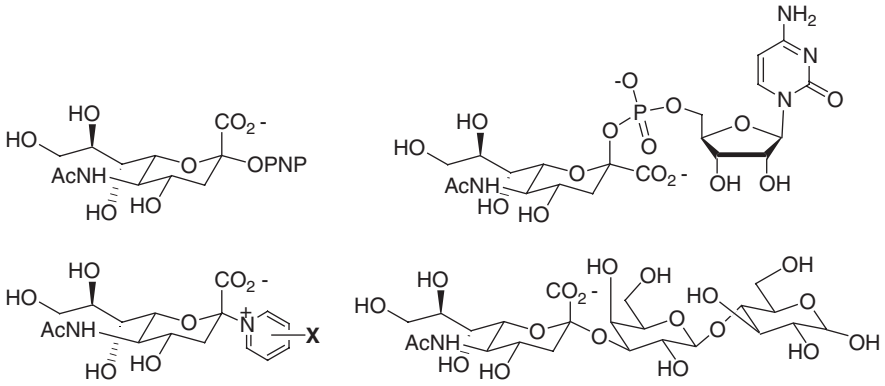

Scheme 12.

α-lactosyl glycosides (Scheme 12). Note that the structure of NeuAc precludes measurement of α-secondary hydrogen isotope effects. A primary ^{14}C KIE of 1.030 was observed for solvolysis of CMP–NeuAc at pH 5.0.[31] As discussed earlier, a carbon KIE of this low is indicative of a transition state lacking significant nucleophilic assistance. Acid-catalyzed solvolysis of NeuAc α (2→3) lactose afforded a ^{13}C KIE of 1.016, which compares well to the ^{14}C for solvolysis of CMP–NeuAc.[33] Again, the results indicated that the transition state involved insignificant nucleophilic participation. From the limited results available, the degree of nucleophilic participation is the same for solvolysis of NeuAc glycosides whether the starting configuration is α or β, and with leaving groups of low and high reactivity. Though the C2 anomeric carbon of NeuAc has three non-hydrogen substituents and is somewhat hindered, it is interesting that "A_ND_N-like" chemistry has been identified for NeuAc in the case of the *trans*-sialidase enzyme. *Trans*-sialidase-catalyzed substitution of NeuAc α (2→3) lactose affords large (1.03) primary ^{13}C KIEs, which led to the conclusion that a covalent intermediate was formed on the enzyme.[33] This was confirmed by isolation of radioactive enzyme substrate adducts in quench experiments[34] and subsequent kinetic and structural studies with fluoro NeuAc substrate analogs.[35,36] One interesting lesson in all of this is that while solution studies of NeuAc solvolysis mechanisms have thus far shown no indication of a propensity towards A_ND_N chemistry, an enzyme can utilize this pathway, despite the bulky environment at the anomeric center. Finally, with regard to carbon isotope effects, KIEs have not been measured for α-aryl or pyridinium glycosides of Neuac. This is of some importance, because as will be discussed below, there are conflicting opinions regarding the likelihood of nucleophilic participation of the carboxylate group.

β-deuterium isotope effects point to varying degrees of oxocarbenium ion development in the transition state, depending on the leaving group. Solvolysis of CMP–NeuAc[31] at pHs 4.0, 5.0, and 6.0 proceeded with observed β-dideuterium KIEs of 1.25 ± 0.02, 1.276 ± 0.008, and 1.354 ± 0.008. Some elimination to 2,3-dehydro NeuAc[37] accompanied solvolysis at pH 5.0 and 6.0 (but not at pH 4.0) so it was necessary to account for the contribution that β-elimination makes to the

observed isotope effect.[31] Studies of the effect of buffer concentration on elimination argued against buffer functioning as a general base in the elimination reaction. Further, production of 2,3-dehydro NeuAc from CMP–NeuAc is nearly pH independent between pH 8.0 and 10.0.[37] Solution of simultaneous equations for the KIE data at pH 5.0 and 6.0 with 0.02 and 0.095 mol fractions for elimination, respectively, yielded values of 5.1 and 1.26 for the primary and secondary KIEs. Solvolysis of CMP–NeuAc at pH 4.0 proceeds without detectable β-elimination, and affords a β-^{2}H KIE of 1.25 ± 0.02, in excellent agreement with the estimated value above. The large value observed for the dideuterium KIE is significant, because it indicates that the transition state is late with respect to loss of the leaving group and the anomeric carbon bears considerable positive charge. The β-deuterium isotope effects are lower for alkyl or aryl NeuAc glycosides; note however that these substrates (Scheme 12) have the α-configuration, whereas CMP–NeuAc is a β-glycoside. Sinnott and coworkers[30] reported a series of β-^{2}H isotope effects for solvolysis of α-*p*-nitrophenyl NeuAc. At pH 1.00, the carboxyl group of α-*p*-nitrophenyl NeuAc (pK_a 2.69) is largely protonated, and the observed β-dideuterium KIE was 1.10. Interestingly, the isotope effect drops as the carboxyl group ionizes. At pH 2.69 the observed KIE was 1.08, and at pH 6.67 it was 1.07. The interpretation of these data involved a late transition state with respect to departure of *p*-nitrophenolate, but involved nucleophilic participation once the carboxyl group was ionized. Solvolysis of NeuAc-α(2→3) lactose at pH 1.0, 37 °C, afforded a β-deuterium KIE of 1.11,[33] virtually identical to the value measured for the *p*-nitrophenyl NeuAc glycoside.[30] At this pH the leaving groups could be considered to be of approximately equal reactivity (as protonated oxonium ions) and so the similarity of the two isotope effects argues for similar transition states. Taken with the primary ^{13}C data, the results indicate that the transition state at low pH does not involve nucleophilic participation. Once again, primary carbon isotope effects for *p*-nitrophenyl substituted NeuAc were not measured at any pH, but would be of considerable interest to further probe for nucleophilic character in the transition state. The axial β-CMP is approximately 10 times more reactive as a leaving group than an equatorial α-*p*-nitrophenyl, and it is conceivable that even poorer leaving groups could require nucleophilic assistance.

One question for both solution and enzymatic reactions of the natural NeuAc donor, CMP–NeuAc, is if acid catalysis is operative, whether it is general or specific, and the site at which the proton is delivered. Studies of pH versus rate for solvolysis of CMP–NeuAc were consistent with a mechanism for solvolysis at pH 5.0 that featured specific acid catalysis of the dianion. At the time of the original studies,[31] it was suggested that the departing CMP could be either at the former glycosidic oxygen, or one of the more basic non-bridging phosphoryl oxygens. Subsequently it was suggested[38] that the bridging glycosidic oxygen was the likely protonation site on the basis of inverse solvent deuterium isotope effects. As pointed out by Bennet, microscopic reversibility would argue in favor of protonation occurring at the non-bridging position, which would allow a negatively charged phosphate oxygen to attack the oxocarbenium ion, rather than a much less nucleophilic protonated oxygen.[5] A productive approach to this question involved ^{18}O leaving group isotope effects[39] (Scheme 13).

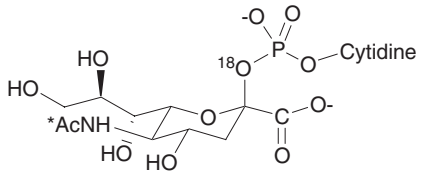

Scheme 13.

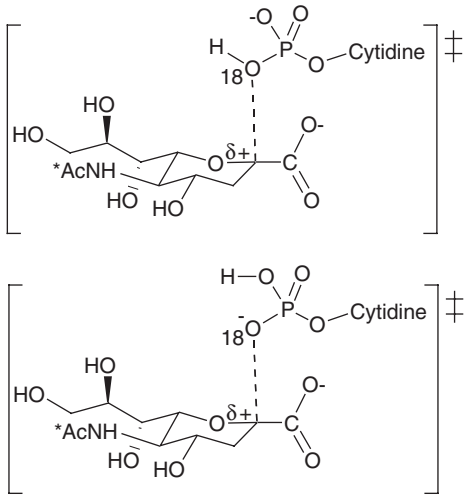

Scheme 14.

Solvolysis of [2-^{18}O] CMP NeuAc at pH 5.0 in acetate buffer afforded a KIE of 1.003 ± 0.005. The ab initio modeling (6-31G* basis set) of the KIE predicted an isotope effect of 1.023 for protonation at the bridging position, while protonation at the non-bridge position gave a predicted KIE of 1.017. Thus, the data is best fit by the non-bridge protonation model (Scheme 14).

TRAPPING STUDIES AND OXOCARBENIUM ION LIFETIMES

If solvolysis of CMP–NeuAc required nucleophilic participation of the carboxylate, this would proceed via a transient α-lactone, and in a second step give net retention to afford the β-anomer. A direct displacement of CMP by solvent without carboxylate participation would yield the α-anomer, while a transition state that resulted in formation of a sialyl oxocarbenium ion would proceed with results ranging from inversion to racemization depending on whether the oxocarbenium ion lived long enough to equilibrate with solvent. Solvolysis of CMP–NeuAc in methanol/water mixtures at pH 5.0, resulted in ~1:1 ratios of α- and β-methyl glycosides of NeuAc as determined by ^{1}H-NMR.[31] The α/β-methyl glycoside ratio was invariant when the mol fraction of methanol was increased by over 50%, which shows

that there is no methanol concentration dependence over this range. The results are consistent with near or complete solvent equilibration of the sialyl cation; preassociation pathways would be expected to be sensitive to the methanol mol fraction. The selectivity for water versus methanol attack was approximately 1.3. The selectivity for methanol attack in water/methanol is rather low at 1.3:1; high ratios favoring methanol trapping are associated with stable cations, low ratios are typically associated with highly reactive, short-lived carbenium ion pairs. For a series of cumyl cations, the corresponding methanol/trifluoroethanol trapping ratios revealed a limiting minimum ratio of 2 for cations with a lifetime shorter than 10^{-10} s.[40] Such cations were described as ion pairs which reacted with solvent before diffusion of the leaving group could occur. Alternative factors which could favor a low methanol/water trapping ratio might include steric effects disfavoring methanol attack at a bulky tertiary center, or a localized polarity effect which could favor water for solvation of a charge-separated transition state or tight ion pair.

Solvolysis of CMP–NeuAc in 1.8 M acetate buffer at pH 5.0 containing 0.9 M azide results in the formation of both anomers of 2-deoxy-2-azido NeuAc in addition to NeuAc as determined by ^{1}H-NMR product analysis.[38] The relative percentages of α- and β-NeuAc and α- and β-N_3–NeuAc were 5, 68, 25, and 2, respectively. A modest rate dependence on [azide] was observed with an apparent bimolecular rate constant of $(2.1 \pm 0.3) \times 10^{-3}\,M^{-1}\,min^{-1}$ which could only account for half of the α-azido-NeuAc formed. Comparison of rate, product ratio, and stereochemical data indicate that concurrent pathways for formation of N_3–NeuAc are operative, with 17% of product forming from reaction of azide and the tight ion pair, 12% via the solvent-separated ion pair, and 6% from the free NeuAc oxocarbenium ion. From the corrected product ratio data, the lifetime of the oxocarbenium ion was estimated to be $\geq 3 \times 10^{-11}$ s. Taken in conjunction with the data for trapping in methanol, the neuraminyl oxocarbenium ion is probably able to equilibrate with solvent in the absence of a strong nucleophile-like azide, but in its presence only a fraction is able to proceed past the ion pair stage.

Bennet and coworkers studied the spontaneous hydrolysis of a series of pyridinium glycosides of NeuAc[32] (Scheme 15, **1**). These compounds simplify the acid–base considerations for the hydrolytic mechanism by fixing a positive charge on the reactant-state leaving group, leaving only the anomeric carboxyl group as a consideration. Study of the observed rate versus pH led to a rate law for solvolysis that had two rate constants corresponding to spontaneous hydrolysis of the zwitterions (carboxylate) and spontaneous hydrolysis of the cation (carboxyl protonated).

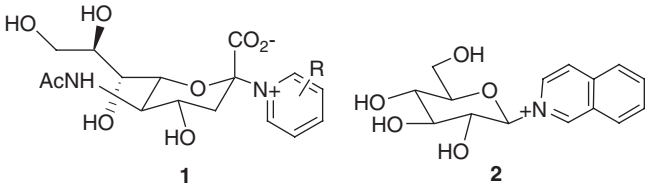

1 **2**

Scheme 15.

For the series of pyridinium substrates, the rate constant for hydrolysis of the zwitterions was only about 3 times greater than for the protonated form. The relative nucleophilicity of the acetic acid/acetate pair spans a considerably greater range, so this was taken as an indication that the ionized carboxyl would show a greater rate difference from the protonated form if it was functioning as a nucleophile. The comparison with acetate may have its shortcomings – acetate does not have the ring strain penalty associates with α-lactone formation, so in the case of a hypothetical α-lactone-like transition state, the enhanced nucleophilicity of a carboxylate group might be tempered by the ring strain. The β_{lg} values for the two processes were identical at −1.22, indicating a similar and late transition state structure with respect to the leaving group, whether or not the carboxylic group was protonated or not. The reported activation parameters $\Delta H^{\ddagger} = 112\,\mathrm{kJ\,mol^{-1}}$ and $\Delta S^{\ddagger} = 28\,\mathrm{J\,mol^{-1}\,K^{-1}}$ for the unsubstituted pyridinium glycoside was considered most consistent with a transition state not involving nucleophilic participation of the carboxyl group. However, the $\Delta S^{\ddagger} = +48\,\mathrm{J\,mol^{-1}\,K^{-1}}$ for pH independent solvolysis of α-PNP NeuAc was considered[30] to be circumstantially supportive of a nucleophilic role for the carboxylate. The large positive $\Delta S^{\ddagger}$ term was rationalized on the basis of liberation of water solvating the carboxylate at the nucleophilic transition state.[30] These two reports are difficult to reconcile on their own, but as discussed earlier, the issue of carboxylate nucleophilicity might be further addressed by application of carbon KIEs at the anomeric center. Also, data obtained for product analyses of solvolyses of pyridinium *N*-glycosides of NeuAc (discussed below) argue against nucleophilic carboxylate participation as the *sole* reaction manifold.

Armed with earlier correlations of reactivity and oxocarbenium ion lifetimes, Bennet and coworkers[32] used the 2-deoxyisoquinolinium salt **2** (Scheme 15) as a model to make a correlation between its reactivity and known cation lifetime and the neuraminyl pyridinium ion's reactivity to estimate the lifetime of the neuraminyl oxocarbenium ion to be 3×10^{-11} s, in agreement with studies utilizing the azide trapping method.[38]

In 2004, Knoll and Bennet[41] reported a study of the aqueous methanolysis of the α-3,4-dihydro-2H-pyrano[3,2-c]pyridinium *N*-glycoside of NeuAc **3** (Scheme 16). This study was aimed at addressing the possibility that the NeuAc carboxylate group plays a nucleophilic role in the overall displacement process at the anomeric center. One would predict that overall retention stereochemistry would be observed in a two-step displacement process involving initial intramolecular attack by the carboxylate group, followed by backside attack from solvent (Scheme 17). Solvolysis of

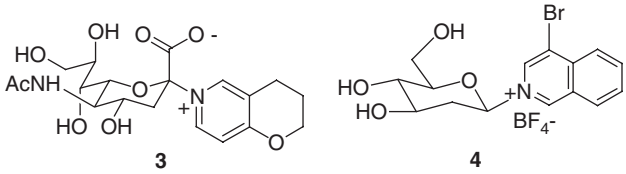

Scheme 16.

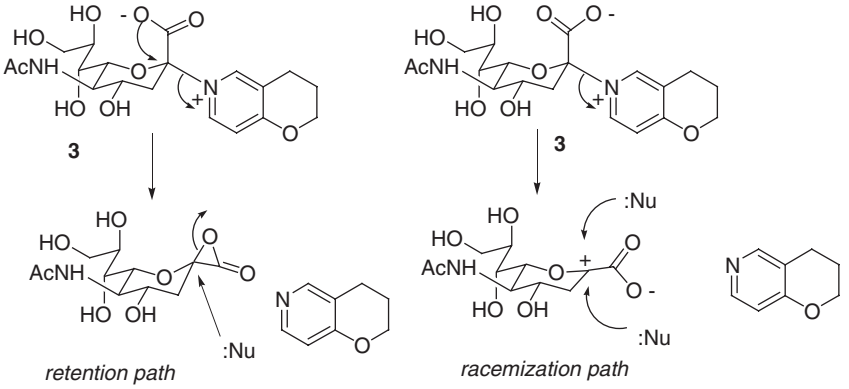

Scheme 17.

3 in either 100% or 50% aqueous MeOH afforded β-methyl glycoside (in 50% MeOH over 50% of the product was the hemiketal product). This result is consistent with a mechanistic model not involving the carboxylate as a nucleophile, at least when presented with the presence of a methanol nucleophile. In that same work, a study of the effect of solvent polarity on k_{obs} was reported. Variation of the %MeOH content between 0% and 100% resulted in only a 10-fold increase in k_{obs} for the 100% MeOH runs. This relative insensitivity to solvent polarity change was considered a good indication that an intramolecular carboxylate pathway was not operative, since such a pathway would have a much lesser charge distribution at the transition state and should have been more sensitive to the decreasing polarity of the reaction mixture than was observed. In comparison, the authors compared the data for **3** to that previously reported for **4**, a 2′-deoxy-3-bromiisoquinolinium glucosyl salt. This compound, which cannot experience nucleophilic participation by a carboxylate would have been expected to be *less sensitive to solvent polarity than the hypothetical nucleophilic carboxylate reactions of* **3**, however it was found to be slightly more sensitive to solvent polarity.

As a final point in these experiments, it was noted that the selectivity ratio for formation of methyl glycoside via MeOH attack versus hemiketal via water attack (k_{MeOH}/k_{H_2O}) was about 1.6 whereas the ratio for solvolysis of CMP–NeuAc was about 1.3.[31] Higher ratios reflect methanol's greater selectivity for stabilized carbenium ion species, and the relatively low values seen for either **3** or CMP–NeuAc provide an indication that the oxocarbenium ion species derived from either substrate are of limited lifetime (i.e. stability). One must be careful when comparing data from differing leaving groups of different glycosidic bond stereochemistry, as discussed below.

In 2005, Dookhun and Bennet reported a study of the stability of β-aryl *N*-acetylneuraminides (**5**, Scheme 18).[42] Note that the natural glycosyltransfer substrate, CMP–NeuAc and the compounds in this study were of the β-configuration, whereas prior studies of solvolysis of NeuAc aryl glycosides had been conducted on the α-glycosides **6**. Bennet concluded that the β-aryl glycosides are

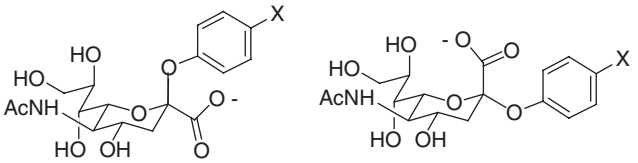

Scheme 18.

approximately 10-fold more stable than expected, and attributed their increased stability relative to the α-glycosides as deriving from ground-state steric strain present in the α-compounds, and absent in the β-compounds. The α-compounds place the carboxylate group in the axial position, a position considered to be less favored thermodynamically. The spontaneous hydrolysis of the α-compound is 100 times faster than that of the β-compound. As had been proposed for the solvolysis of the natural CMP–NeuAc, it was also suggested that the β-aryl glycosides showed no evidence for intramolecular participation of the carboxylate group. The evidence constituting this conclusion included the observation that during aqueous alcoholysis, products of both inversion and retention were observed. Another piece of supporting evidence was presented in that the β_{lg} values for either anomer of PNP–NeuAc were quite similar, yet their reactivities differ 100-fold. Given this, it would seem unlikely that carboxylate assistance was operative. Another piece of supporting information was found in the experimentally estimated activation entropies, which were approximately $+60$ and $+30$ e.u. for the β- and α-anomers of PNP–NeuAc, respectively. Such strongly positive values are consistent with transition states that are dissociative, without an intramolecular nucleophilic component, with any effect of transition state desolvation not withstanding. The smaller activation entropy for the α-anomer was attributed to a ground-state effect, whereby in the ground state, the less well-solvated α-anomer and the better solvated β-anomer, reach similarly dissociative and similarly solvated transition states.

7 Substituent effects on glycoside reactivity

POSITION ON THE RING

The hydroxylation pattern of a saccharide affects its chemical reactivity and behavior. Deoxy aldopyranosides lacking the hydroxyl group at the 2′-position are more reactive towards hydrolysis by approximately three orders of magnitude[11] and form oxocarbenium ion intermediates that are estimated to be 4-fold more stable than their 2-hydroxy counterparts. Withers and coworkers reported on the kinetics for the pH independent hydrolysis of a series of substituted β-2,4-DNP glycopyranosides.[43] The glycon series consisted of the ''native'' saccharides glucose, galactose, allose, and mannose and their deoxy- and fluoro-substitutions at the 2,3,4, and 6 positions. Based on measured solvolytic rate constants, Hammett plots were

constructed that revealed the rate constant correlated well with σ_I. Further, the sensitivity to the substituent was greatest for the 2-position and least for the 6-position, in general agreement with a model that involves the substituent interacting with the reaction center via field effects. When the observed rate constants were compared with the relative rates calculated by a Kirkwood–Westheimer analysis, excellent correlations were obtained. This indicates that the oxocarbenium ion-like transition state stability is under the strong influence of field effects from the substituents. Another aspect of reactivity is the impact of glycosyl substituents on conformation and the ensuing stereocontrol for product formation (Fig. 3).

SUBSTITUENT STEREOCHEMISTRY

While it has been known[44] that equatorial substituents on the glycon afford slower hydrolysis rates than axial ones, the source of this phenomenon was originally attributed by Edward to steric interactions.[45] Recent studies suggest that substituent effects can often be largely attributed to electronic factors. Experimental and computational studies[46] of the acetolysis of gluco- and galacto-2,3,6 tri-*O*-methyl pyranosides supported this idea (Scheme 19). The 4-substituent was either methoxy, acetoxy, or acetamido, and showed that whereas the glucoside was only modestly sensitive to variation of the 4-substituent (ca. 3-fold rate variation) the galactosides having the 4-substituent axial showed ca. 50-fold variation in k_{obs}. Methoxy provided the fastest rates and the acetamido substituted compound was the slowest. Interestingly, ab initio analysis of a model (*trans*-4-acetamido-1-methoxy pyran) for the 4-axial acetamido oxocarbenium ion showed that the nitrogen was pyrimidalized, with its lone pair directed towards the positive charge. The ground-state methyl pyranoside did not show this effect.

In 2002, Kirby and coworkers[47] compared hydrolytic rate constants for methyl homologs of tetrahydropyrans and found a range of rate constants differing by a factor of approximately 4; whereas acyclic analogs hydrolyzed faster, as indicated in Scheme 20 which presents structures and values for k_{obs}. The data were compared to the observation that the *hydroxylated* THP ring (i.e. glycopyranosides) can lead to rate reductions of a million-fold relative to the parent THP acetal. After the counterbalancing electron-releasing effects of the methyl substituted THP acetals were taken into consideration, it was estimated that the steric or torsional effects of equatorial substituents in glycopyranosides is only worth two orders of magnitude for the rate reduction, the balance primarily deriving from electronic factors of the hydroxyl substituents.

Bols and coworkers reported linear free energy relationships for the hydrolysis of glycopyranosides.[48] Axial and equatorial substituent effects, determined from amine basicity of similarly configured compounds, were employed.[49] The two reactions studied were the spontaneous hydrolysis of 2,4-DNP glycosides, and the specific acid-catalyzed hydrolysis of methyl glycosides (Scheme 21).

Axial groups are less retarding than equatorial ones at the same position. Outstanding correlations of $-\log k_{obs}$ and substituent effect were observed, with near

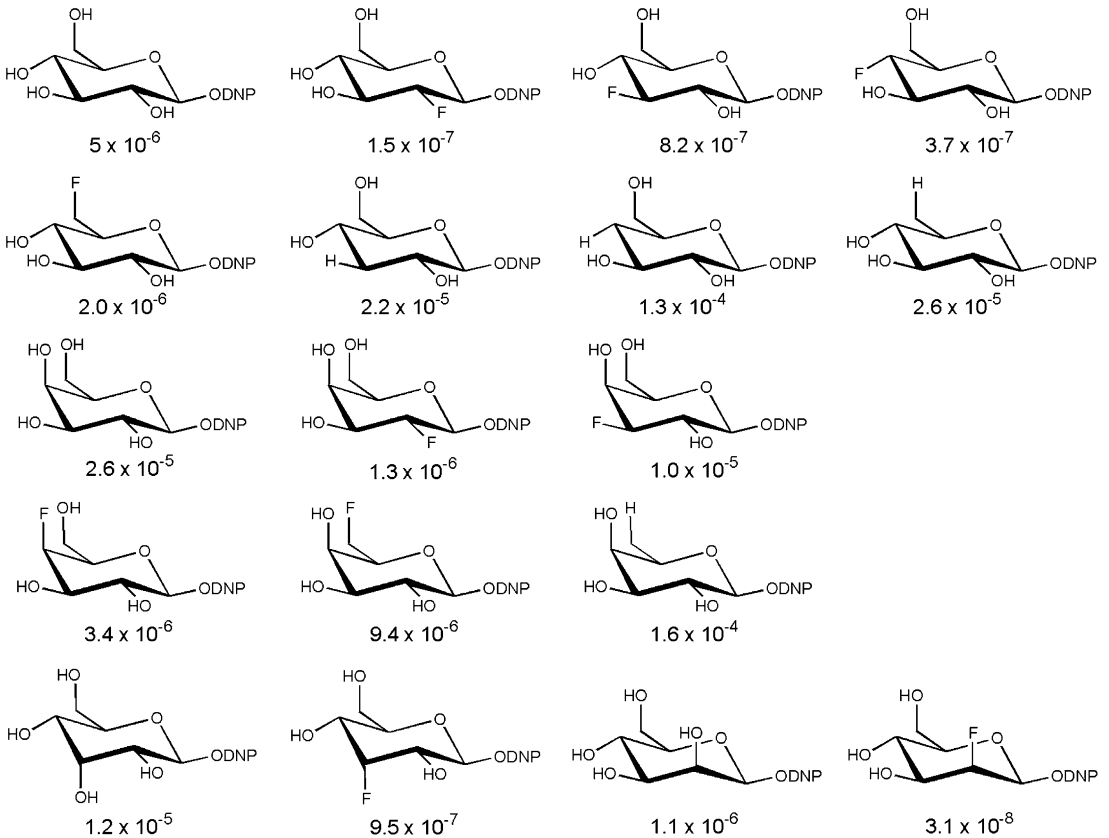

Fig. 3 Series of DNP glycosides used to determine substituent effects. Numbers under each structure represent k_{obs} for hydrolysis; units are s^{-1}. Adapted from Ref. [43].

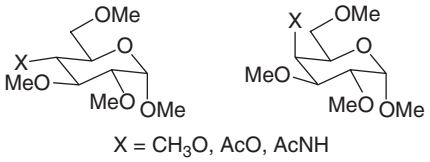

Scheme 19.

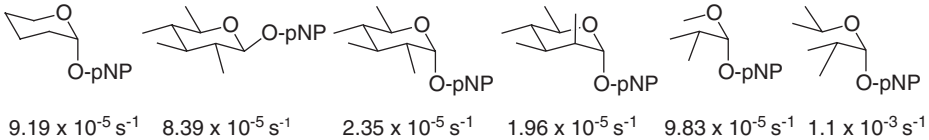

Scheme 20.

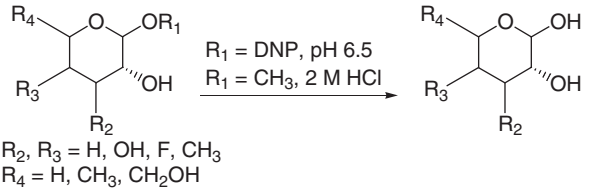

Scheme 21.

unity slopes. The analysis led to the conclusion that electronic effects of substituents are a primary factor in influencing hydrolytic rate. In a subsequent study[50] it was shown that in the series presented in Scheme 22, bulkier groups in the axial position are not predictive for increased rates over compounds placing similar substituents in the equatorial one. Of course, some care must be placed in the above analyses, since the assumption that the chemistry is occurring from $^4C_1$ conformations is subject to interpretation given that the transition states must feature flattened pyranoside rings.

That axially placed, electron-withdrawing groups have a higher reactivity led to the proposal that in general, glycosides able to place a hydroxyl substituent axially would hydrolyze faster than those that could not. As a test, conformationally locked anhydrosugar glycosides in the $^1C_4$ conformation were synthesized and the kinetics for hydrolysis determined and compared to data for the $^4C_1$ methyl pyranosides[44,51] (Scheme 23). For example, a 248-fold acceleration for hydrolysis of anhydro **8** versus monocyclic **7** was observed. The mechanistic interpretation was that axially disposed hydroxyl groups in **8** were not destabilizing compared to the all-equatorial hydroxyl groups in methyl glucoside **7**. An alternate explanation was that relief of ring strain contributes to the reactivity of the anhydro sugar. It is noteworthy that the methyl galactoside **9** and its anhydro derivative **10** (which exists in the boat conformation) have similar rate constants for hydrolysis, suggesting that simple relief of strain does not account for the dramatic rate difference between **7** and **8**. An added complexity

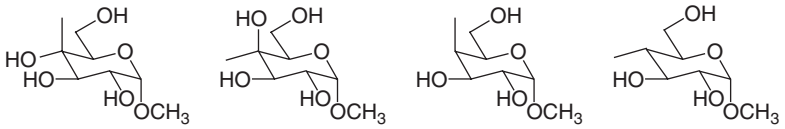

Scheme 22.

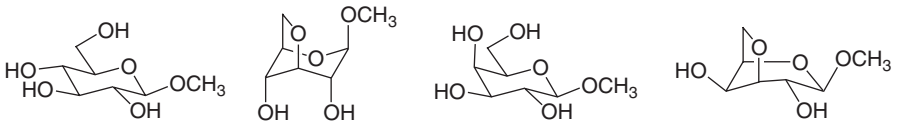

Scheme 23.

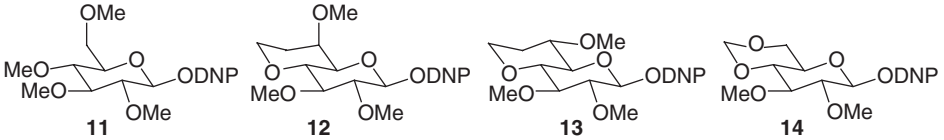

Scheme 24.

arises when one considers that hydrolysis of **8** does not lead to the anhydroglucose, but instead affords the bicyclic furanose which indicates endocyclic cleavage. As a result, it is difficult to directly apply the data to address the role that axial hydroxyls may play in the exocyclic cleavage of pyranosides. Perhaps computational analyses can be used to shed light on the basis for reactivity in the anhydro series with axially disposed hydroxyl groups.

In addition to considering the impact of the stereochemistry of ring substituents on glycoside reactivity, one may consider the conformational itinerary available to the hydroxymethyl group. In a recent investigation, Bols and coworkers reported a study of the spontaneous rate of hydrolysis of DNP glycosides of glucose and analogs as presented in Scheme 24.[52] Clearly, the data support the idea that the tg conformation is the least reactive, with compound **14** being some 14 times less reactive than monocyclic **11** with the hydroxymethyl group free. One can rationalize the data based on the dipole for the C6–O6 bond either stabilizing or destabilizing an oxocarbenium ion-like transition state depending upon its conformation. As a practical matter, "disarmed" glycosyl donors[53,54] bearing a 4,6-acetal-protecting group can be considered to be both electronically, and torsionally disarmed, since neither **12** or **13** (Scheme 24) recover full reactivity relative to the unrestrained **11**.

8 Pyranosyl oxocarbenium ion conformations and reactivity

Oxocarbenium ions are typically key intermediates of nucleophilic substitution at glycosidic carbon. A better understanding of the subtle interplay of steric and electronic factors that dictate final product diastereoselectivity requires an in-depth understanding of how substituents on a pyranosyl ring influence conformation and reactivity. The design of synthetic methods that are highly diastereoselective for glycoside conformation is one area in which new developments may be furthered through understanding of oxocarbenium ion conformations. A pyranosyl oxocarbenium ion ring is flattened, and commonly resides in a half-chair conformation. Molecular mechanics[55] and ab initio calculations[46] revealed that whereas alkyl substituents at the 3 or 4 position are modestly favored in the pseudoequatorial position, the hydroxyl group is strongly favored when in the pseudoaxial position (Scheme 25). The rationale for this stems from the idea that electrostatic interaction between non-bonding electron on the hydroxyl and the positively charged atoms of the oxocarbenium ion is facilitated when axial, simply because the charged sites are closer in this conformation. The second point concerns the trajectory for nucleophilic attack. The two faces of the oxocarbenium ion are diastereomeric, and axial attack on one face leads to a twist boat-like transition state, whereas attack on the other face gives a sterically favored chair-like transition state. As shown in Scheme 26, the attack on a half-chair with its 4-substituent in the pseudoequatorial

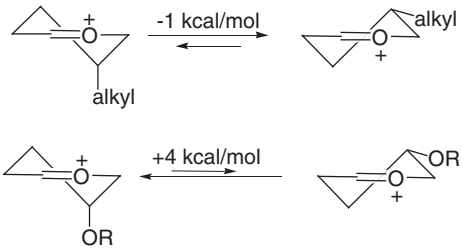

Scheme 25.

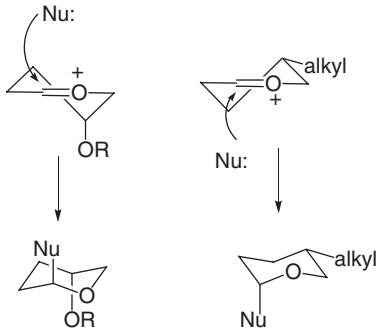

Scheme 26.

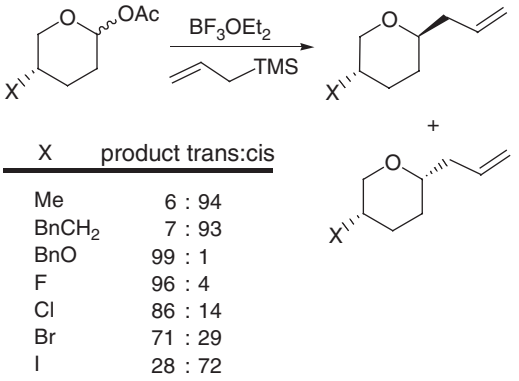

X	product trans:cis
Me	6 : 94
$BnCH_2$	7 : 93
BnO	99 : 1
F	96 : 4
Cl	86 : 14
Br	71 : 29
I	28 : 72

Scheme 27.

position provides products with 1,4-*cis* stereochemistry, whereas attack on a half-chair with its substituent in the pseudoequatorial position gives products with 1,4-*trans*-stereochemistry.

With these considerations in mind, Woerpel and coworkers[56] reported a study of the substituent effects for nucleophilic addition to tetrahydropyranyl oxocarbenium ions, substituted at the 2,3, or 4 positions with alkyl, hydroxyl, alkoxy, and halogen substituents. The starting THP acetates were used as an anomeric mixture in these experiments. Scheme 27 presents selected data for the 4-substituted THP acetate reactions. A dramatic reversal of selectivity from *cis* to *trans* is realized in changing X from alkyl to heteroatom. The halogen series is interesting because it presents good experimental evidence against the idea that polar 4-substituents can promote *trans*-selectivity via anchimeric assistance. If this was the dominant mode, one would have anticipated that the larger halogens would have been more effective at promoting *trans*-selectivity. The results are consistent with an axially disposed substituent providing through space electronic stabilization of an oxocarbenium ion intermediate. One assumption implicit in these experiments is that the anomeric mixture of acetates proceeds to the same solvent-equilibrated oxocarbenium ion. While not demonstrated here, work on similar systems (mentioned below) argues that this is indeed the case. One nice feature of the studies with X at the 4-position is that it is too remote from the oxocarbenium ion carbon to influence the transition state trajectory of the nucleophile. In the case of the 2- and 3-substituted compounds studied, this is not the case. Superposition of the aforementioned electronic effects and transition state steric interactions seems to be operative.

An interesting study that provided compelling evidence for axial electronegative groups being stabilizing to oxocarbenium ions utilized NMR, crystallographic, and computational studies of dioxocarbenium ions that derived from 4-substituted 1-ethoxy THP.[57] Unlike oxocarbenium ions derived from sugars or tetrahydropyrans, these compounds are sufficiently stable to isolate and characterize spectroscopically. The dioxocarbenium ion $SbCl_6$ salts were crystallized and unambiguously shown to place the benzyloxygroup of **15** and the methyl group of **16** in the pseudoaxial and

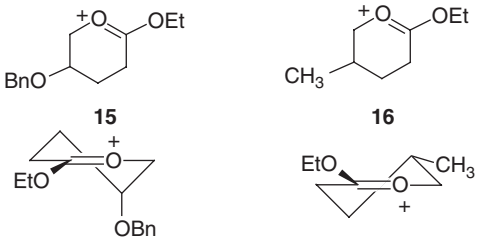

Scheme 28.

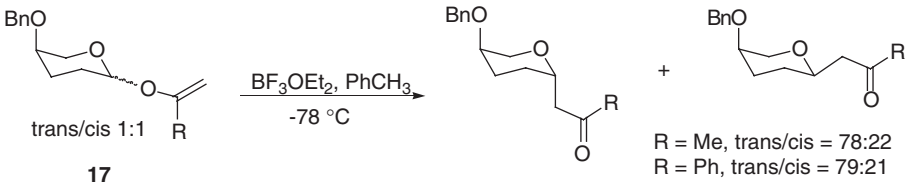

Scheme 29.

pseudoequatorial positions, respectively (Scheme 28). In the solution phase, the same conformation for **15** was determined from ^{1}H-NMR on the basis of coupling constants to the methine hydrogen at C-4. Similarly, **16** displayed a spectrum with two large diaxial coupling constants (11.2, 14.1 Hz) as part of the splitting of H-4, consistent with it being pseudoaxial, and the methyl group pseudoequatorial.

Calculations (MP2/6-31G*) allowed an estimate of the relative preference for **15** and **16** to place the alkoxy and methyl groups pseudoaxially and pseudoequatorially, respectively. Compound **15** placed the benzyloxy group pseudoaxial, with a 5.3 kcal mol^{-1} preference, whereas **16** resided in a conformation placing the methyl pseudoequatorial with a modest 1.0 kcal mol^{-1} preference.

In a study aimed at probing the reactivity of pyranosyl oxocarbenium ions, Shenoy and Woerpel reported on the diastereoselectivity associated with the intramolecular O to C rearrangement of 4-alkoxy 1-vinyl ethers **17** (Scheme 29).[58]

The authors were interested in using this system to establish the importance of tight ion pair intermediates in dictating product stereochemistry. The observation that either configuration of starting enol ether acetal afforded essentially the same "anomeric" ratio of C-alkylated product led to the conclusion that tight ion pairing was not operative in this system. As a further check, a crossover experiment (Scheme 30) was performed with molecules **18** and **19**.

The results provide excellent evidence that an oxocarbenium ion is generated, and that this and the generated Lewis acid–enolate complexes are able to equilibrate. Hence, in this system, ion pairing is not a factor in determining facial selectivity for capture of the oxocarbenium ion. One important factor is the nature of the leaving group in this system. As the BF_3 complex, its nucleophilicity is likely tempered and this would promote progress to the equilibrated oxocarbenium ion. Most

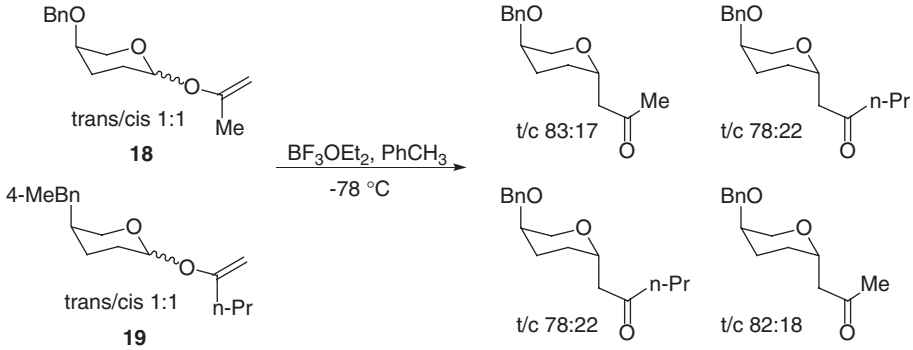

Scheme 30.

importantly, the roughly 4:1 diastereoselectvity observed in this system may be attributed to the propensity of the oxocarbenium ions to react from the half-chair conformation that places the 4-alkoxy group axially, and that it serves as a determinant of facial selectivity for capture of the oxocarbenium ion.

It is clear from the substituent effect studies conducted over the last few years that the identity and stereochemistry of pyran substituents can dramatically influence both the rate for creation of the oxocarbenium ion, the subsequent conformation of the oxocarbenium ion, and the stereoselectivity for product formation. As the system becomes more substituted (e.g. compare galactose to 4-hydroxy THP) the interplay of the different substituents becomes exceptionally complex. Further, in cases where specific solvation/desolvation events and hydrogen bonding may occur, a higher level of complexity arises. Sorting through these effects is incredibly difficult, and two areas which hold considerable promise in helping to do this are computational methods and gas-phase chemistry. Computational methods are becoming sufficiently inexpensive such that synthetically realistic molecules may be employed, rather than simple models. Methodologies including ab initio techniques, hybrid QM/MM models, and dynamics are all finding application in the area of mechanistic carbohydrate chemistry. Gas-phase chemistry affords the opportunity to do two things that can not be done in solution: (1) remove solvation effects and (2) allow for detection and kinetic studies on unstable intermediates (i.e. oxocarbenium ions). The following sections present some of the most recent studies that have helped shed light on aspects of glycosyl bond chemistry that would be difficult to do otherwise.

9 Computational analyses of oxocarbenium ion reactions

FISCHER GLYCOSYLATION

An interesting semi-empirical study[59] (PM3/COSMO) explored the mechanistic manifolds open to the Fisher glycosylation of **20** in HCl/methanol to provide **21**

(Scheme 31). It was concluded that the reaction proceeded by exocyclic loss of the anomeric hydroxyl, followed by oxocarbenium ion capture by methanol, as opposed to a mechanism involving endocyclic ring opening. This was in agreement with experimental work in which only furanosides were reported as products.[60] Surprisingly the key energetic barrier that excluded the ring-opening pathway did not involve C–O bond formation or breakdown, but instead involved a proton transfer step from the acyclic intermediate exchanging the position of the proton in the hemiacetal from the methoxyl group to the hydroxyl group, as in 22 → 23. It seems possible that other factors such as strain and conformational biasing against pyranoside formation could also have been influential in determining the experimentally observed lack of pyranosides.

MOLECULAR DYNAMICS

Stubbs and Marx reported Car–Parrinello ab initio molecular dynamics studies for the specific-acid-catalyzed glycosidic bond formation between α-D-glucopyranose and methanol (which corresponds to the cleavage reaction by microscopic reversibility)[61,62] (Scheme 32). In this work, particular attention was paid to the role of the aqueous solvent, and as a computational study is particularly noteworthy for explicit consideration of solvent molecules. The dynamics simulations required constraints on the reaction coordinate (the methanol oxygen/oxocarbenium ion carbon distance) to ensure driving it along a productive pathway over the short time-course of the dynamics simulation, over a time period of approximately 15 ps.

The reaction between α-D-glucopyranose and methanol was shown to proceed by a $D_N{}^*A_N$ mechanism as outlined in Scheme 32. The initial dissociation step included

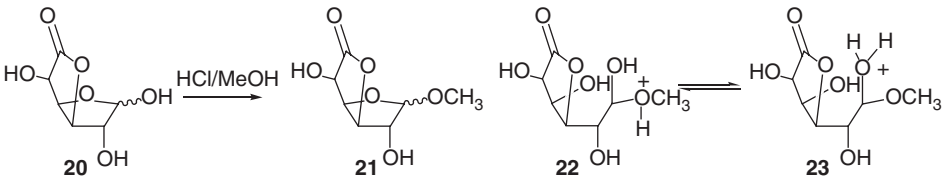

Scheme 31.

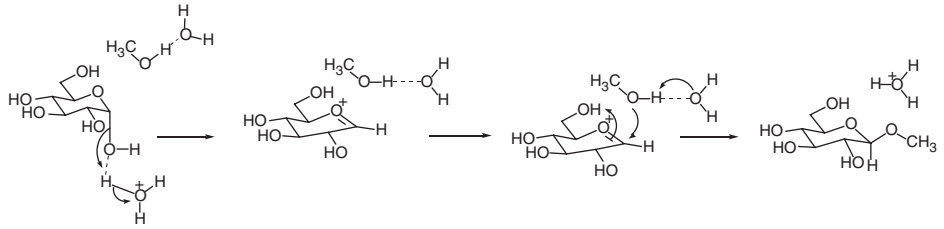

Scheme 32.

the concerted protonation of the O_1 hydroxyl leaving group, and formation of double bond character between the ring oxygen and former anomeric carbon. This step resulted in formation of a very short-lived oxocarbenium ion. In the second step, the glycosidic bond is formed between methanol and C_1 of the oxocarbenium ion ring, with associated loss of double bond character between C_1 and O_5, and proton transfer from the methanol-derived glycosidic oxygen. The authors concluded that the oxocarbenium ion was not solvent equilibrated, in agreement with experimental estimates[23,24,27,28] that the lifetime of the glucosyl oxocarbenium ion is also on the ps time scale. When the latent nucleophile methanol was *not* constrained to be proximate to the nascent oxocarbenium ion, protonations of the leaving group hydroxyl were found to be unproductive. In other words, only runs featuring intimate association of methanol led to productive dissociation of the protonated hydroxyl that then resulted in oxocarbenium ion formation. This is consistent with the idea that the oxocarbenium ion is too unstable and short lived to exist without participation of solvent. Another intriguing result of the dynamics study involved the observation of the transient desolvation of the pyranose ring oxygen over the existence of the oxocarbenium ion intermediate. This makes some sense, given that hydrogen bonding to the oxygen would render it a poorer electron donor to the electron deficient oxocarbenium ion carbon. It was also pointed out that one strength of the calculations was that only with solvation included would this feature be observed, raising a possible caveat for calculations on glycosyltransfer systems that fail to include solvation effects in an explicit manner. The predicted desolvation of the ring oxygen also raises the question as to what impact this could have on ^{18}O KIEs; it would be interesting to model these isotope effects in the presence and absence of solvation to see if they might be of some value in detecting solvation changes at the ring oxygen.

NEURAMINIC ACID TRANSITION STATES

Another area where computational studies have provided interesting insights is with regard to the oxocarbenium ion derived from NeuAc. As mentioned earlier, this sugar possess a carboxylate group that has been the subject of scrutiny with regards to its impact on glycoside breaking or formation. Intuitively, an oxocarbenium ion with an α-carboxylate might be predicted to be an especially stable one, due to the very proximate electrostatic interaction. Models for the 2-deoxyglucosyl oxocarbenium ion and the neuraminyl oxocarbenium ion were compared at the RHF/6-31G** level with regards to stable complex formation with water and the subsequent transition state barrier for capture of the oxocarbenium ion by the proximate water molecules.[63] The microsolvated structures are shown in Scheme 33. The two ion–molecule complexes **24** and **25** have distances of 2.39 and 2.57 Å between the nucleophilic water oxygen and the oxocarbenium ion carbon. The closer distance for **24** may be a reflection of the lack of carboxylate stabilization, i.e. greater ion–dipole interaction is required to stabilize complex **24**.

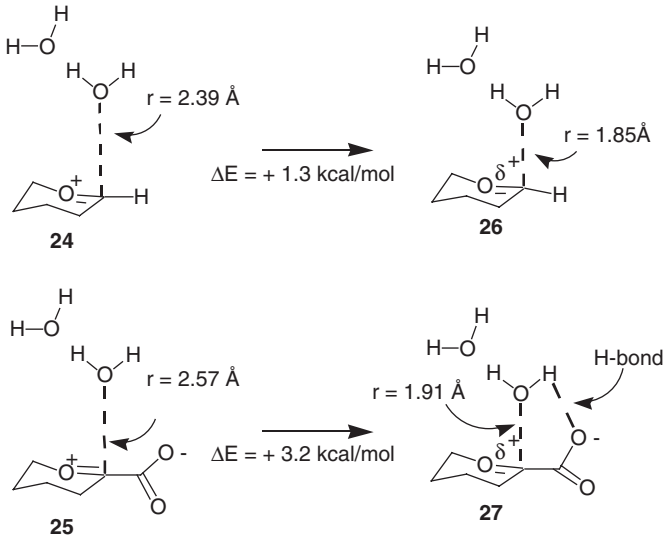

Scheme 33.

The barrier for capture of the 2-deoxyglucosyl oxocarbenium ion (**24**→**26**) is 1.3 kcal mol^{-1} while for the neuraminyl ion (**25**→**27**) the barrier is 3.2 kcal mol^{-1} both of these values were corrected for zero-point energy. These results agree with experiments that indicated the NeuAc oxocarbenium ion is marginally more stable than the 2-deoxyglucosyl oxocarbenium ion.

The ab initio calculated transition structure **27** (Scheme 33) features a strong hydrogen bond between the incoming nucleophile and the α-carboxylate group. Given that positive charge is passed into the attacking nucleophile as it bonds with the oxocarbenium ion, an estimate was made of the amount of stabilization a hydrogen bond might provide.[63] If the carboxylate stabilizes the transition state for nucleophilic attack on the oxocarbenium ion, this would shorten the "intrinsic" lifetime of the oxocarbenium ion. In single point calculations that either rotated the water cluster away from the carboxylate, or when the carboxylate was rotated to remove the hydrogen bond, an estimate for the hydrogen bond strength of ~8 kcal mol^{-1} was obtained. The lack of a fully solvated model argues however that this estimate is likely to be too high. Even with lower values attributed to the energetics of this hydrogen bond, the calculations supported the idea that the barrier for capture of the NeuAc oxocarbenium ion is lowered via the hydrogen bond. In any case, it is hard to rationalize why an α-carboxylate would not *intrinsically* stabilize the oxocarbenium ion – the only question, and it remains open, is to what extent? This provides a hypothesis to explain why the oxocarbenium ion derived from NeuAc is not significantly more long lived than the glucosyl oxocarbenium ion: the ability of the carboxylate to interact with attacking water in the transition state provides a considerable amount of catalysis via the hydrogen bond, which may proceed to bona fide general base catalysis as the glycosidic bond is formed. The

issues of base catalysis for nucleophilic capture of oxocarbenium ions of varying stability has been discussed by Richard and Jencks.[64]

α-LACTONES

The neuraminic acids have a carboxylate group immediately adjacent to the anomeric center begs the question as to if and how it might participate in displacement reactions. As presented in earlier sections, there is no overwhelming experimental evidence to indicate α-lactone intermediates are the *major* pathway for NeuAc glycoside hydrolysis, yet neither has the data ruled out if it might be a component of an overall reaction's manifolds. The α-lactone compounds are indeed known[65] but are too unstable to exist in nucleophilic media at room temperature. Hence, computational techniques are well suited to examine carboxylate function in neuraminic acid glycosyltransfer reactions. Williams has addressed the energetic issues surrounding intramolecular participation of the carboxyl group by computational methods, utilizing AIM analysis, with and without inclusion of solvent effects (ICPM models).[66] High-level computations on hydroxyoxiranone **28a** (Scheme 34) indicated that it is better represented electronically by **28b** and **28c**, whereas its geometry is α-lactone like in terms of it still maintaining an acute angle with respect to the lactone oxygen–lactone carbonyl carbon and α-carbon.

The nature of bonding in this system shows sensitivity to solvation. With the ICPM model and a dielectric of 78, the zwitterionic character of **34** increased over the gas phase. While one may criticize the non-explicit nature of the solvation model used in these calculations, subsequent work[67] on related oxiranone supported this conclusion with calculations employing QM/MM techniques that explicitly account for water (DFT/TIP3). In a recent study[68] that utilized time resolved IR spectroscopy and DFT calculations, it was reported that α-lactones are sensitive to medium polarity, with more polar media favoring zwitterionic forms. Further, electron-withdrawing substituents on the α-carbon favor the cyclic structure, but electron release favors the zwitterionic form. Hence, experimental and computational studies of model α-lactones provide the strong sense that an α-lactone intermediate during NeuAc glycoside bond changes would be disfavored by polar aqueous environments and the electron-releasing NeuAc ring oxygen. Just as a number of experimental studies of NeuAc glycosyl transfer have suggested the possibility of α-lactone intermediacy, but never found strong experimental support, the model work in this field also is not strongly supportive of the α-lactone hypothesis for the solvolysis of NeuAc glycosides.

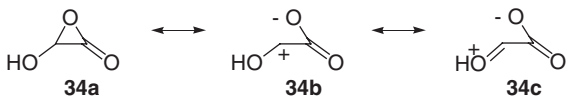

Scheme 34.

10 Mechanistic studies of ''synthetic'' reactions and glycon donors

Mechanistic study of the hydrolysis reactions of unsubstituted sugars reveals considerable complexity in the mechanisms of these reactions. Studies aimed at the very practical and important problem of understanding glycosylation mechanisms with synthetic glycon donors bearing their requisite protecting groups face a considerably more difficult challenge due to the additional perturbations that the protecting groups can cause via steric, conformational, and electronic factors. Experimentally, the nature of glycon-protecting group can exert a profound outcome on the glycosylation reaction via conformational and electronic factors.[53,54] Another point is that modern synthetic methods[9] often utilize ''latent'' leaving groups that typically require activation; the mechanisms of the reactions need not resemble those of acid-catalyzed glycoside hydrolysis (or Fischer glycosylation). Relatively inexpensive and accurate computational methods are now available to address these issues, and these approaches may ultimately provide information of predictive utility to optimize stereo- and regio-selective syntheses.

Crich and Chandrasekera recently reported a KIE study of 4,6-*O*-benzylidine, 2,3-benzyl mannosyl triflate in its reaction with a saccharide donor as shown in Scheme 35.[69] The competitive method was used, and relied on ^{1}H-NMR integrals of the ratios for the remote *O*-benzylidine acetal hydrogen versus the anomeric hydrogen. After correcting the KIE to 25 °C, the average for three independent runs was 1.12. This value was taken as evidence for a transition state that was highly dissociative, however the discrimination between a mechanism involving nucleophilic association and one involving a tight ion pair was not possible. This system would be well suited for application of primary ^{13}C KIEs, which would help discriminate between these two mechanistic possibilities.

Whitfield and coworkers,[70,71] discussed interesting computational studies of the anomeric selectivity for glycosylation pathways of galactosyl, glucosyl, and mannosyl compounds, differing in the flexibility of the pyran ring as controlled by the presence or absence of cyclic acetal-protecting groups (Scheme 36). Of particular note is that the work was centered on saccharide compounds that could be employed in synthetic work. The methodology employed was DFT with a continuum dielectric model. The key outcome of this work was the suggestion that differing product anomeric selectivity as a function of the nature of the sugar and protecting groups is largely derived from conformational effects on the oxocarbenium ion intermediates and hydrogen bonding interactions between the incipient nucleophile and substituents

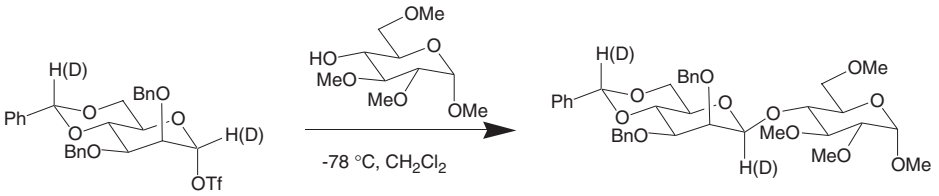

Scheme 35.

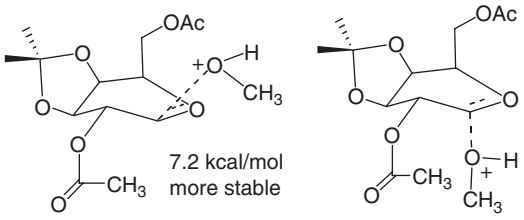

Scheme 36.

on the oxocarbenium ion. It was suggested that a rigid ring will limit the accessible conformations for the oxocarbenium ion, and in conjunction with the presence of a hydrogen bonding interaction with nucleophile could render one face of the oxocarbenium ion more accessible than the other.

For example, in the case of the 2,3-isopropylidene galactose addition reaction, attack on the β-face is favored by 7.2 kcal mol^{-1} largely driven by hydrogen bonding between the acetate at O-6 and the incoming methanol. As pointed out, it is likely that the importance of hydrogen bonding is overestimated, since the α-attack mode would still involve hydrogen bonding to solvent, despite the lack of the intramolecular hydrogen bond found for β-attack. In 2005 this line of inquiry was extended and developed into the "two-conformer hypothesis".[72] This essentially states that glycosyl oxocarbenium ions exist in two (or more) related energy conformations. Analysis of the conformational itinerary available to tetramethyl glucosyl and mannosyl oxocarbenium ions, and their ion–dipole complexes with methanol were carried out with DFT methods. In short, ion–dipole complexes of the oxocarbenium ion and nucleophile that will capture it can exist in a total of at least four species (when both α- and β-complexes are considered). The energetics of which face is most favorably added to are dominated by hydrogen bonding interactions between the nucleophile and sugar substituents, and whether attack from the α- or β-face forces the transition state to go through chair-like or boat-like structures. $^{4}H_{3}$ conformations for both gluco- and manno-oxocarbenium ions were identified as the low-energy minimum. However, close in energy were the ^{3}E for the mannosyl ion ($+1.9$ kJ mol^{-1}) and $^{5}S_{1}$ for the glucosyl ion ($+4.7$ kJ mol^{-1}). While these studies do not explicitly account for solvation, they illustrate the importance of conformational analysis in coming to understand oxocarbenium ion capture.

11 Experimental gas-phase studies

The study of glycoside formation and breaking in the gas phase is not as esoteric as it might appear. The very short lifetimes of glycosyl oxocarbenium ions in solution require that their study be via indirect competitive kinetic experiments. Knowledge of the barrier for capture of these species, whether as free oxocarbenium ions or as ion–molecule pairs, is difficult to obtain by direct methods. On the other

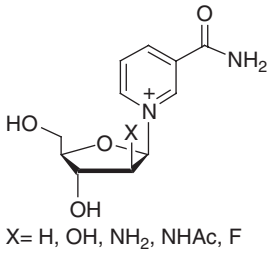

Scheme 37.

hand, gas-phase studies, such as those conducted in a mass spectrometer would in principle allow direct observation and experimentation with these species.

In 1994, Oppenheimer and coworkers[73] reported a study of the gas-phase generation of arabinosyl oxocarbenium ions via use of tandem positive-ion liquid secondary ion mass spectrometry (LSIMS) (Scheme 37). Plots of log ([oxocarbenium ion]/([M^+] + [oxocarbenium ion])) versus σ_F values for the 2′-substituents X showed excellent correlation with $\rho_F = -0.75$. In solution, the rate constants for solvolysis of the same series afford a ρ_I of –6.7. While the basis for this difference in ρ is not clear, it is reasonable to propose that the reaction in the gas phase is similar in nature to the solution reaction. With ion trap or FTICR instrumentation, studies such as these might be extended to following the fate of the oxocarbenium ion as it reacted with nucleophiles introduced into the mass spectrometer.

Denekamp and Sandlers reported electrospray ionization Fourier transform ion cyclotron resonance mass spectrometry (ESI-FTICR-MS) studies of protected gluco- and galacto-pyranosides to determine the factors that influence oxocarbenium ion generation and stability.[74,75] The protecting groups employed were acetyl, benzoyl, methyl, benzyl, and trimethylsilyl groups. Benzoyl or arylthio leaving groups at the anomeric center were used, and the ammoniated parent ion was the initial species isolated in the mass spectrometer, prior to CID. Oxocarbenium ions were observed after CID of ammoniated parent ions when the protecting groups were Bz or Ac, but not for Bn or Me groups. It was concluded that while participating and electron-withdrawing protecting groups, i.e. Bz, Ac facilitate oxocarbenium ion formation, electron-releasing alkyl groups disallow oxocarbenium ion formation. On this basis it was suggested that saccharides with alkyl protection may not proceed by the "S_N1" ($D_N + A_N$) mechanism, and possibly proceed by an "S_N2" mechanism. This conclusion could only apply to the gas phase, since alkyl-protected glycosyl donors do not show rigid adherence to inversion of configuration, as would be anticipated for an A_ND_N reaction. Further, in the gas phase the oxocarbenium ion species may indeed be generated, but more rapidly fragment rendering its detection difficult. It may well be that the neighboring group participation of the esters with the ability to extensively delocalize charge (e.g. see Scheme 38) yields a much more stabilized, and hence detectable ion. It is quite possible that the actual structure observed in the MS was the intramolecular adducts of the ester-protecting group at C2, bonding to C1. Secondly, it is clear that at least

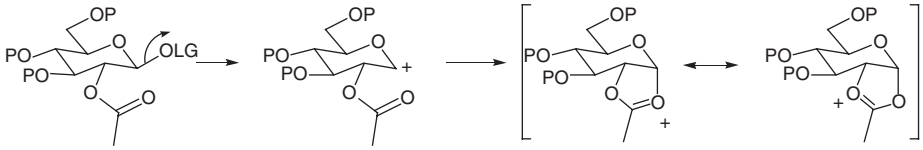

Scheme 38.

in solution, KIE studies have revealed that with good leaving groups, hydrolysis of *unsubstituted* (and hence, electron-releasing and non-participatory) glucosides typically proceeds by dissociative $D_N{*}A_N$ mechanisms.[5,25] Of course in the gas phase the lack of solvation could well change the landscape for oxocarbenium ion chemistry, lending itself towards pathways involving elimination and fragmentation. It will be interesting to see if with more labile leaving groups, and gentler fragmentation methods, it might be possible to generate and isolate glycosyl oxocarbenium ions in the FTICR when the saccharide is substituted with alkyl-protecting groups, or even without protection. Another approach which might prove informative, if necessary, is to utilize simpler analogs of glycosyl oxocarbenium ions, which may be less prone to decomposition, should this prove to be a problem with the glycosyl compounds.

Finally, considerable progress has been made with regard to gas-phase conformational analysis of monosaccharides and their hydrated complexes by comparison of their IR spectra with that predicted by ab initio calculations.[76–78] Many of the tools are therefore available to place a sugar in the gas phase, cleave the glycosidic bond, isolate the oxocarbenium ion, and then have the opportunity to study the kinetics for nucleophilic capture by *direct* kinetic techniques. Experiments such as competitive KIEs for capture of the oxocarbenium ion also seem possible. Such work may allow direct experimental determination of oxocarbenium ion lifetimes, barriers for capture, and transition state structures. Differences observed between gas-phase results and those in solution may reveal the role that solvent plays in the reaction.

12 Conclusions

A fairly detailed mechanistic understanding is available for acid-catalyzed hydrolytic reactions of glucosides, deoxyglucosides, and NeuAc. The nucleophilic displacement reaction mechanisms can range from A_ND_N to $D_N + A_N$, heavily influenced by the leaving group and nucleophile combination employed. The lifetimes of any glycosyl oxocarbenium ion characterized thus far are all sub-nanosecond. Direct experimental measurements of the barrier height for capture of the oxocarbenium species are not yet reported. Further, the role of substituents on oxocarbenium ion lifetimes are limited to either H, OH, or F at what would be C2 of an aldopyranose. Many opportunities exist to further the knowledge based on monosaccharides other than those derived from glucose or NeuAc. Reactions using modern glycosidation methods are comparatively uncharacterized; work here is likely to facilitate new synthetic

method development. Finally, the prospects for mechanistic study of the glycosidic bond in the gas phase, in conjunction with computational methods, are excellent and relatively untapped, with the offer of insights into this chemistry that would be available in no other way.

Acknowledgments

This work was supported by grants MCB-9501866, MCB0091881 from the National Science Foundation, and GM 059322 from the National Institutes of Health.

References

1. Somsak, L. (2001). *Chem. Rev.* **101**, 81–135
2. Berti, P.J. and McCann, J.A.B. (2006). *Chem. Rev.* **106**, 506–555
3. Vasella, A., Davies, G.J. and Bohm, M. (2002). *Curr. Opin. Chem. Biol.* **6**, 619–629
4. Zechel, D.L. and Withers, S.G. (2000). *Accounts Chem. Res.* **33**, 11–18
5. Bennet, A.J. and Kitos, T.E. (2002). *J. Chem. Soc. Perk. Trans.* **2**, 1207–1222
6. Berti, P.J. and Tanaka, K.S.E. (2002). *Adv. Phys. Org. Chem.* **37**, 239–314
7. Bucior, I. and Burger, M.M. (2004). *Curr. Opin. Struc. Biol.* **14**, 631–637
8. Dube, D.H. and Bertozzi, C.R. (2005). *Nat. Rev. Drug Discov.* **4**, 477–488
9. Garegg, P.J. (2004). *Adv. Carbohyd. Chem. Biochem.* **59**, 69–134
10. Wolfenden, R., Lu, X.D. and Young, G. (1998). *J. Am. Chem. Soc.* **120**, 6814–6815
11. Capon, B. (1969). *Chem. Rev.* **69**, 407–498
12. Cordes, E.H. and Bull, H.G. (1974). *Chem Rev.* **74**, 581–603
13. Winstein, S., Klinedinst, P.E. and Robinson, G.C. (1961). *J. Am. Chem. Soc.* **83**, 885–895
14. Guthrie, R.D. and Jencks, W.P. (1989). *Accounts Chem. Res.* **22** (10), 343–349
15. Richard, J.P., Amyes, T.L., Toteva, M.M. and Tsuji, Y. (2004). *Adv. Phys. Org. Chem.* **39**, 1–26
16. McPhail, D.R., Lee, J.R. and Fraser-Reid, B. (1992). *J. Am. Chem. Soc.* **114**, 1905–1906
17. Liras, J.L. and Anslyn, E.V. (1994). *J. Am. Chem. Soc.* **116**, 2645–2646;Liras, J.L., Lynch, V.M. and Anslyn, E.V. (1997). *J. Am. Chem. Soc.* **119**, 8191–8200
18. Deslongchamps, P., Li, S.G. and Dory, Y.L. (2004). *Org. Lett.* **6**, 505–508
19. Richard, J.P. (1995). *Tetrahedron* **51**, 1535–1573
20. Banks, B.E.C., Meinwald, Y., Rhind-Tutt, A.J., Sheft, I., Vernon, C.A., *J. Chem. Soc.* (1961) 3240–3246
21. Sinnott, M.L. and Jencks, W.P. (1980). *J. Am. Chem. Soc.* **102**, 2026–2032
22. Bennet, A.J. and Sinnott, M.L. (1986). *J. Am. Chem. Soc.* **108**, 7287–7294
23. Amyes, T.L. and Jencks, W.P. (1989). *J. Am. Chem. Soc.* **111**, 7888–7900
24. Banait, N.S. and Jencks, W.P. (1991). *J. Am. Chem. Soc.* **113**, 7951–7958
25. Lee, J.K., Bain, A.D. and Berti, P.J. (2004). *J. Am. Chem. Soc.* **126**, 3769–3776
26. Zhang, Y., Bommuswamy, J. and Sinnott, M.L. (1994). *J. Am. Chem. Soc.* **116**, 7557–7563
27. Huang, X., Surry, C., Hiebert, T. and Bennet, A.J. (1995). *J. Am. Chem. Soc.* **117**, 10614–10621
28. Zhu, J. and Bennet, A.J. (1998). *J. Am. Chem. Soc.* **120**, 3887–3893
29. Zhu, J. and Bennet, A.J. (2000). *J. Org. Chem.* **65**, 4423–4430
30. Ashwell, M., Guo, X. and Sinnott, M.L. (1992). *J. Am. Chem. Soc.* **114**, 10158–10166
31. Horenstein, B.A. and Bruner, M. (1996). *J. Am. Chem. Soc.* **118**, 10371–10379

32. Chou, D.T.H., Watson, J.N., Scholte, A.A., Borgford, T.J. and Bennet, A.J. (2000). *J. Am. Chem. Soc.* **122**, 8357–8364
33. Yang, J.S., Schenkman, S. and Horenstein, B.A. (2000). *Biochemistry* **39**, 5902–5910
34. Yang, J. (2001). *Doctoral Dissertation*. University of Florida, Gainesville, FL
35. Watts, A.G., Damager, I., Amaya, M.L., Buschiazzo, A., Alzari, P., Frasch, A.C. and Withers, S.G. (2003). *J. Am. Chem. Soc.* **125**, 7532–7533
36. Amaya, M.F., Watts, A.G., Damager, T., Wehenkel, A., Nguyen, T., Buschiazzo, A., Paris, G., Frasch, A.C., Withers, S.G. and Alzari, P.M. (2004). *Structure* **12**, 775–784
37. Beau, J., Schauer, R., Haverkamp, J., Kamerling, J.P., Dorland, L. and Vliegenthart, J.F.G. (1984). *Eur. J. Biochem.* **140**, 203–208
38. Horenstein, B.A. and Bruner, M. (1998). *J. Am. Chem. Soc.* **120**, 1357–1362
39. Burke, E., Bruner, M., and Horenstein, N.A. Unpublished results
40. Richard, J.P., Amyes, T.L. and Vontor, T. (1991). *J. Am. Chem. Soc.* **113**, 5871–5873
41. Knoll, T.L. and Bennet, A.J. (2004). *J. Phys. Org. Chem.* **17**, 478–482
42. Dookhun, V. and Bennet, A.J. (2005). *J. Am. Chem. Soc.* **127**, 7458–7465
43. Namchuk, M.N., McCarter, J.D., Becalski, A., Andrews, T. and Withers, S.G. (2000). *J. Am. Chem. Soc.* **122**, 1270–1277
44. Overend, W.G., Rees, C.W., Sequeira, J.S., (1962). *J. Chem. Soc*. 3429–3440
45. Edward, J.T., (1955). *Chem. Ind*. 1102–1104
46. Miljkovic, M., Yeagley, D., Deslongchamps, P. and Dory, Y.L. (1997). *J. Org. Chem.* **62**, 7597–7604
47. Dean, K.E.S., Kirby, A.J. and Komarov, I.V., (2002). *J. Chem. Soc. Perk. Trans. 2* 337–341
48. Bols, M., Liang, X. and Jensen, H.H. (2002). *J. Org. Chem.* **67**, 8970–8974
49. Jensen, H.H., Lyngbye, L., Jensen, A. and Bols, M. (2002). *Chem. Eur. J.* **8**, 1218–1226
50. Jensen, H.H. and Bols, M. (2003). *Org. Lett.* **5**, 3419–3421
51. McDonnell, C., Lopez, O., Murphy, P., Fernandez Bolanos, J.G., Hazell, R. and Bols, M. (2004). *J. Am. Chem. Soc.* **126**, 12374–12385
52. Jensen, H.H., Nordstrom, L.U. and Bols, M. (2004). *J. Am. Chem. Soc.* **126**, 9205–9213
53. Fraser-Reid, B., Wu, Z., Udodong, U.E. and Ottosson, H. (1990). *J. Org. Chem.* **55**, 6068–6070
54. Fraser-Reid, B., Wu, Z., Andrews, C.W. and Skowronski, E. (1991). *J. Am. Chem. Soc.* **113**, 1434–1435
55. Woods, R.J., Andrews, C.W. and Bowen, J.P. (1992). *J. Am. Chem. Soc.* **114**, 859–864
56. Ayala, L., Lucero, C.G., Romero, J.A.C., Tabacco, S.A. and Woerpel, K.A. (2003). *J. Am. Chem. Soc.* **125**, 15521–15528
57. Chamberland, S., Ziller, J.W. and Woerpel, K.A. (2005). *J. Am. Chem. Soc.* **127**, 5322–5323
58. Shenoy, S.R. and Woerpel, K.A. (2005). *Org. Lett.* **7**, 1157–1160
59. Nowacki, A., Blazejowski, J. and Wisniewski, A. (2003). *J. Mol. Struc.* (*Theochem*) **664–665**, 217–228
60. Phillips, D.D. (1954). *J. Am. Chem. Soc.* **76**, 3598–3599
61. Stubbs, J.M. and Marx, D. (2003). *J. Am. Chem. Soc.* **125**, 10960–10962
62. Stubbs, J.M. and Marx, D. (2005). *Chem. Eur. J.* **11**, 2651–2659
63. Horenstein, B.A., (1999). *ACS Sym. Ser.* 721, Truhlar, D. and Morokuma, K. (eds), 411–423
64. Richard, J.P. and Jencks, W.P. (1984). *J. Am. Chem. Soc.* **106**, 1396–1401
65. Adam, W., Liu, J.-C. and Rodriguez, O. (1973). *J. Org. Chem.* **38**, 2269–2270
66. Firth-Clark, S., Rodriquez, C.F. and Williams, I.H., (1997). *J. Chem. Soc. Perk. Trans. 2* 1943–1948
67. Buchanan, J.G., Charlton, M.H., Mahon, M.F., Robinson, J.J., Ruggiero, G.D. and Williams, I.H. (2002). *J. Phys. Org. Chem.* **15**, 642–646
68. Showalter, B.M. and Tosacano, J.P. (2004). *J. Phys. Org. Chem.* **17**, 743–748

69. Crich, D. and Chandrasekera, N.S. (2004). *Angew. Chem. Int. Edit.* **43**, 5386–5389
70. Nukada, T., Berces, A., Zgierski, M.Z. and Whitfield, D.M. (1998). *J. Am. Chem. Soc.* **120**, 13291–13295
71. Nukada, T., Berces, A. and Whitfield, D.M. (2002). *Carbohyd. Res.* **337**, 765–774
72. Nukada, T., Berces, A., Wang, L.J., Zgierski, M.Z. and Whitfield, D.M. (2005). *Carbohyd. Res.* **340**, 841–852
73. Buckley, N., Handlon, A.L., Maltby, D., Burlingame, A.L. and Oppenheimer, N.J. (1994). *J. Org. Chem.* **59**, 3609–3615
74. Denekamp, C. and Sandlers, Y. (2005). *J. Mass Spectrom.* **40**, 765–771
75. Denekamp, C. and Sandlers, Y. (2005). *J. Mass Spectrom.* **40**, 1055–1063
76. Talbot, F.O. and Simons, J.P. (2002). *Phys. Chem. Chem. Phys.* **4**, 3562–3565
77. Jockusch, R.A., Talbot, F.O. and Simons, J.P. (2003). *Phys. Chem. Chem. Phys.* **5**, 1502–1507
78. Simons, J.P., Jockusch, R.A., Carcabal, P., Hunig, I., Kroemer, R.T., Macleod, N.A. and Snoek, L.C. (2005). *Int. Rev. Phys. Chem.* **24** (3–4), 489–531

The interpretation and mechanistic significance of activation volumes for organometallic reactions

RUDI VAN ELDIK and COLIN D. HUBBARD

Institute for Inorganic Chemistry, University of Erlangen-Nürnberg, Erlangen, Germany

1 Introduction: basic principles and theory

An initial effort to understand the effect of hydrostatic pressure on reaction rates was presented at the beginning of the last century.[1] The argument could be developed from the thermodynamic relationship between the volume change for a reaction, ΔV, the change in Gibbs free energy (ΔG) for the reaction, and the hydrostatic pressure, P. Since:

$$\mathrm{V} = (\delta \mathrm{G}/\delta \mathrm{P})_{\mathrm{T}} \tag{1}$$

therefore:

$$\Delta \mathrm{V} = (\delta \Delta \mathrm{G}/\delta \mathrm{P})_{\mathrm{T}} \tag{2}$$

ADVANCES IN PHYSICAL ORGANIC CHEMISTRY
VOLUME 41 ISSN 0065-3160 DOI: 10.1016/S0065-3160(06)41001-7

Since:

$$\Delta G = -RT \ln K \tag{3}$$

in which K is the equilibrium constant for the reaction, R is the ideal gas constant and T is the absolute temperature:

$$(\delta \ln K/\delta P)_T = -\Delta V/RT \tag{4}$$

To generate an expression for the effect of pressure upon equilibria and extend it to reaction rates, this early work consisted of drawing an analogy with the effect of temperature on reaction rates embodied in the Arrhenius equation of the late 19th century.[2] In the more coherent understanding since the development of transition state theory (TST),[3–6] the difference between the partial molar volumes of the transition state and the reactant state is defined as the volume of activation, $\Delta V_f^{\neq}$, for the forward reaction. A corresponding term $\Delta V_r^{\neq}$ applies for the reverse reaction. Throughout this contribution $\Delta V^{\neq}$ will be used and is assumed to refer to the forward reaction unless an equilibrium is under discussion. Thus:

$$\Delta V = \Delta V_f^{\neq} - \Delta V_r^{\neq} \tag{5}$$

These parameters can be displayed as a volume profile for a reaction to complement other thermodynamic parameter profiles of free energy, enthalpy and entropy. It is also possible in certain circumstances, discussed below, to place the volume profile on an absolute scale rather than only on a relative volume scale.

Assuming for the moment that the volume parameters can be obtained from experimental practice, an important question is what do the numerical values signify, and furthermore what changes in molecular species are occurring giving rise to a volume change? In other words is there a quantitative framework of interpretation of volume parameters? It was discerned that partial molar volume changes consist primarily of two components.[7,8] The first results from volume changes of the molecular species themselves, e.g. bond breakage or bond formation (complete or partial), isomerisation or bond deformation. When intrinsic changes give rise to an increase or decrease in polarity or charge development or charge neutralisation in species the second component manifests itself in solvation changes. In the presence of a charged species surrounding solvent molecules are reduced in their molecular volume, an effect termed electrostriction. Hence an increase or decrease in polarity or charge causes a change in the extent of electrostriction. Thus:

$$\Delta V = \Delta V_{intr} + \Delta V_{solv} \tag{6}$$

and

$$\Delta V^{\neq} = \Delta V_{intr}^{\neq} + \Delta V_{solv}^{\neq} \tag{7}$$

If a volume parameter can be determined with reasonable precision, the mechanistic features of the reaction can be assessed, and set in the context of the magnitude of a given volume parameter. This is not necessarily a straightforward process and guidelines have been developed for intrinsic mechanistic features based on compilations of volume parameters assembled in the literature.[9–12] In general, except

for related series of reactions, each system must be examined and analysed based on its own characteristics and the underlying chemistry.

Historically, determination of volumes of activation was more prevalent in organic chemistry and early work also considered the possible relationship between the volume of activation and the entropy of activation.[9,13] In the past several decades growth in the incidence of reports of determination of activation volumes of inorganic reactions, particularly those of coordination compounds, has greatly increased.[12,14–16] Bioinorganic chemistry has witnessed an increase in the application of the volume of activation as a mechanistic indicator.[16] Organometallic chemistry, one important aspect of which is the use of metal complexes in activation of organic molecules to promote conversion of them into other (more useful) molecules and related catalytic cycles, has blossomed as a field of endeavour. This is evident since several journals are dedicated to reports of organometallic synthetic and reaction chemistry. Furthermore comprehensive series have appeared[17] and organometallic chemistry is frequently presented in prestigious journals since many organometallic reactions have beside their intrinsic interest significant industrial relevance and economic impact. Consequently, mechanistic studies have assumed considerable importance for understanding individual steps within overall catalytic cycles. Successful elucidation of the reaction mechanism permits modification and tuning of reaction systems to improve yields or efficiency. Of various experimental variables that may be explored, e.g. concentration, ionic strength in appropriate media, electrolyte, solvent, substituents, isotopic substitution and temperature, the variation of hydrostatic pressure leading to the volume of activation can often provide decisive mechanistic information.[18]

The purpose of this contribution is to illustrate the value and significance of volumes of activation in a wide range of organometallic chemistry reactions. This will follow an outline of basic experimental design and the methods and experimental practice in determining volumes of activation.

Upon modifying Equation (4) to be applicable to the equilibrium between the transition state and the reactant state from TST, the equation that can be applied to experimental kinetic data (rate constants, k_p at various pressures) is developed:

$$(\delta \ln k_P/\delta P)_T = -\Delta V^{\neq}/RT \tag{8}$$

The integrated form:

$$\ln k_P = \ln k_0 - (\Delta V^{\neq}/RT)P \tag{9}$$

may be used to obtain the volume of activation by plotting $\ln k_p$ versus P, where k_0 is the value of the rate constant at zero pressure. In fact the latter parameter is always very close to the value of the rate constant at atmospheric pressure. If such a plot is linear, the volume of activation is readily obtained from the slope. This is nearly always the case for pressures in the range 0–150 MPa (1 atm = 1.01325×10^5 Pa). When the volume of activation is not independent of pressure and the plot is non-linear, there are various treatments of the data that allow extraction of the volume of activation.[19–22] In addition there are reviews[23] and mathematical treatments from a thermodynamics standpoint[24] of the physicochemical effects of

pressure. The dependence of $\Delta V^{\neq}$ on pressure is characterised by the term $\Delta\beta^{\neq}$, the compressibility of activation. When required the compressibility of activation could be obtained by extending the pressure range of kinetics measurements. However, this can increase the technical specifications of apparatus, and is often not necessary. The dependence on pressure of the volume of activation arises mostly when the properties of the solvent are significantly affected by increasing pressure, giving rise to a second effect upon the pressure variation of the rate constant. This latter effect is normally small for aqueous media and is more likely to manifest itself when a reaction is conducted in an organic solvent. While the dependence on pressure of the volume of activation is of considerable interest, particularly from the point of view of the effect of pressure on solvent properties, this aspect will not be treated further here. Nevertheless the effect of pressure on solvent properties, e.g. upon the melting point (m.p.), must be considered in experimental design: the m.p. of benzene at atmospheric pressure is 5.5 °C and is about 100 °C at 500 MPa, whereas water has an m.p. of – 9 °C at 100 MPa.[25] Other factors that need to be addressed in aqueous solutions are the effect of pressure on the ion-product constant for water, thus affecting the pH scale, and the effect of pressure on the pK_a values of weak acids and pK_b values of weak bases. In addition to the effects of pressure on the compressibility and the m.p. of a solvent, the boiling point, viscosity, density, dielectric constant and conductivity are also affected by pressure and cognisance of these effects must be undertaken when relevant in design of experiments.

When the rate constant is increased by increasing pressure, $\Delta V^{\neq}$ is negative, and conversely when the rate constant is decreased by increasing pressure, $\Delta V^{\neq}$ is positive. Why are pressures up to 150 MPa typically used? It will be shown from typical values of $\Delta V^{\neq}$ that a smaller range would not normally be adequate to establish $\Delta V^{\neq}$ with sufficient precision for mechanistic diagnosis.

Obviously, if the rate law is complex so that activation parameters obtained are composites of several terms then interpretation becomes more difficult as the experimentally acquired volume of activation needs to be appropriately apportioned. However, in some cases varying the experimental conditions, concentrations for example, a complex rate law can be reduced to a simpler form with attendant lowering of interpretation difficulties.

It is clear that from the integrated form of Equation (4) the volume of reaction can be obtained if the equilibrium constant can be determined over a range of pressure. If the volume of activation is not experimentally accessible for one of the directions of the reaction, ΔV can be used to calculate its value. Under certain conditions and with suitable properties of reactants and/or products it may be possible to determine their partial molar volumes, hence allowing development of a volume profile on an absolute volume basis, as noted above. Even if ΔV can be determined either from the pressure dependence of the equilibrium constant and/or from use of Equation (5), it may be possible to confirm its value by determination of the partial molar volumes from density measurements. The conditions for conducting successful determinations of partial molar volumes are rather stringent and will be described in Section 2. The method depends on measuring the density, d, of several solutions of different concentrations of the reactant or product. The following equation is used to obtain

the apparent molar volume, ϕ at each molar concentration, c:

$$\phi = (\mathrm{MW}/d) - ((d - d_0)/d_0) \times (1000)/c \quad (10)$$

The density of the solvent is d_0 and MW is the molar mass of the solute. The values of the apparent molar volume are plotted against concentration and the partial molar volume is the value obtained by extrapolation to zero concentration.

2 Experimental

GENERAL CONSIDERATIONS

The methods, techniques, apparatus and instruments relating to determination of volumes of activation for organic, inorganic and bioinorganic reactions, in most cases, can be applied in organometallic chemistry. Several publications have covered the practical aspects of determining kinetic parameters at elevated pressures.[16,26–33] These should be consulted for complete details, and they also illustrate the history and development of methodology in high pressure chemistry kinetics practice. Determination of rate constants from kinetic data at ambient pressure has been described in several authoritative works.[6,34–40] The processing of kinetic data to obtain kinetic parameters at high hydrostatic pressures is usually essentially no different. The emphasis here will be on the techniques of high pressure practice and the apparatus and equipment that are required. A system (e.g. type of instrument and monitoring method) that is suitable for following the kinetics at ambient pressure requires adaptation or modification for use at elevated pressures. The actual application of pressure is by standard arrangements of pumps with appropriately placed high pressure rated valves: these aspects will not be emphasised here, and literature that provides both more information and further sources may be consulted. Pressure measurement is either by a Bourdon-type gauge or a pressure transducer. Since small increments or decrements of pressure cause almost negligible changes in rate, pressure measurements to an accuracy of 1–2% or less are acceptable.

There are many organometallic reactions requiring the presence of one or more gases in the reacting solution and in equilibrium with the same gases above the solution. The pressure of the gas is often subject to variation, but this is for the purpose of improving synthetic yield or for improving catalytic efficiency. The pressures involved are usually well below those of hydrostatic pressures applied in the volume parameter determination and these experiments do not result in obtaining volumes of activation. While such reactions are extremely important in the context of using metal complexes in organic transformations with gases under pressure, they will not be included here. However, reference may be made to some key sources,[41–44] particularly as some of these studies make use of very specialised instrumentation.

The design and construction of high pressure containers or cells depend on the monitoring method and whether the reaction may be classified as conventional in its time range or is a fast reaction. The division between the two is not defined and in

some cases is somewhat different from the division at ambient pressure. If the reactants are mixed at ambient pressure, monitoring of reaction progress can commence as soon as the monitoring process operates, providing the reactants have been thermally equilibrated in advance. Upon pressure application to the mixed reactants the temperature of the system increases quite rapidly. The extent depends on the magnitude of pressure and on the heat capacity of the solvent. Aqueous media are less affected by heating under compression. Nevertheless the time of restoration to the temperature of kinetics measurement means that conventional time range involves reactions having half-lives of the order of 10 min for high pressure reactions rather than a few to several seconds for ambient pressure experiments. Obviating this problem can be accomplished in some cases by the simple expedients of either studying the reaction kinetics at a much lower temperature or in the case of second-order reactions diluting the reactants.

CONVENTIONAL TIME-RANGE REACTIONS

For reactions that are slow at room temperature, one approach is to initiate reaction and confine the reaction to an autoclave. Following decompression the contents can be analysed to assess the progress of the reaction. This procedure was used to determine the first volume of activation for an inorganic reaction. Apparently only one elevated pressure was used to estimate the value.[44] In more current practice repeating the process and arresting the reaction at different time intervals could lead to a reaction profile at a given pressure. The whole procedure would then be repeated at several different pressures, and kinetic data treated according to Equation (9). Obviously such a primitive method is to be avoided, as it is very labour intensive and wasteful of reactants. It would only be satisfactory if the analysis is very rapid compared with the reaction rate or the reaction can be quenched immediately upon decompression.

An extension of this method would allow periodic aliquot sampling from a container whose contents are subjected to high pressure. Obvious conditions govern whether this method would be satisfactory. They are as follows:

(1) The reaction progress must be very slow relative to the time required for aliquot removal and time of sample analysis, or in the latter case a rapid quench can be carried out. A rapid analytical method is UV/visible spectrophotometry.
(2) Pressure restoration inside the container following each sample removal must be very rapid compared with the rate of reaction.
(3) The reaction rate must be slow so that the half-life of reaction is much longer than the time required for sample introduction into and sealing of the pressure vessel, and for thermal equilibration following heating of the sample caused by compression, as noted above.

Sample overheating can be avoided by stepwise pressure application. For this type of pressure apparatus the container must be sufficiently robust to withstand high

pressures. If the material is steel or other metal alloy an inert inner coating may be required if the sample contains metal coordinating or particularly chelating ligands with high stability constants for metal complex formation. This in turn may cause a sealing problem as the aliquot sampling method depends on successful operation of a piston, usually of Teflon with one or more "O" rings that move to compensate for the volume change upon each sample removal. A piston-cylinder apparatus has been widely used and volumes of activation determined. Most reports are of substitution reactions[45–49] and one of electron transfer of transition metal complexes.[50] The method has also been used for organometallic reactions.[51,52] A representative sample apparatus is schematically shown in Fig. 1.

A much more efficient method of obtaining kinetic parameters involves continuous monitoring of the reaction sample while it is subject to hydrostatic pressure, i.e. an *in situ* sampling method. This necessitates construction of a pressurisable sample container that can be incorporated within the observation housing of an instrument. The preferred option is to modify a commercial instrument, although this may have the drawback of requiring dedication of the instrument to the high pressure mode. Interchange between high pressure and ambient pressure modes may be a time-consuming exercise. There are two approaches that can be described for the most

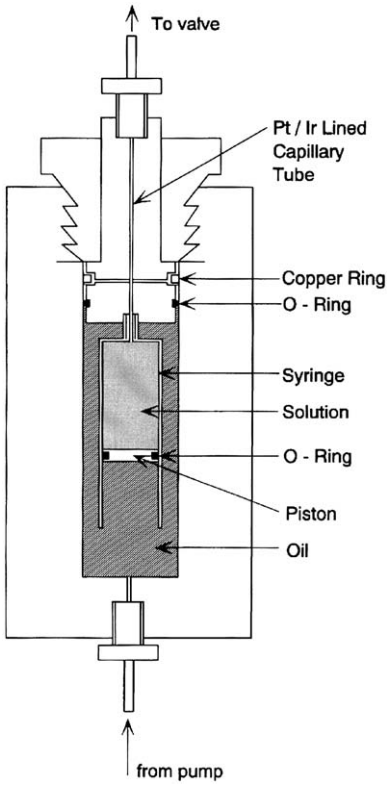

Fig. 1 An example of a piston-cylinder high pressure apparatus.

frequently applied monitoring method, UV/visible spectrophotometry. One uses a pressurisable cuvette that is aligned with the light path of a spectrophotometer, and the cuvette is held in place by a metal block, also possessing optical windows. The metal block contains thermostatted external circulating fluid and optically transparent pressurisable fluid surrounding the cuvette. The cuvette is typically of the ''pill-box'' type, designed several decades earlier.[53] The pill-box cuvette is cylindrical with two concentric cylinders that can be rotated for sealing after filling with a reacting sample. Incident and transmitted light pass through the optically flat circular end windows. The design allows for path length reduction upon compression of the contents by the surrounding compressed fluid, usually, *n*-heptane. A schematic diagram of a pill-box cell and its enclosing pressurisable container is shown in Fig. 2.

A second variant uses a metal block containing a machined out cuvette and windows that is placed in the cell compartment of a spectrophotometer. The pressure is applied directly to the reacting solution via a piston.[54] Again any reaction containing reagents sensitive to the metal of the block could not be used in this variation. In both types of UV/visible *in situ* monitoring the pressure is applied via a standard array of high pressure pumps and appropriately positioned high pressure rated valves. A direct pressure device is illustrated in Fig. 3.

The advantages are, obviously, a continuous record of the reaction, allowing instant observation of deviations from normal kinetic progress, ability to apply data fitting routines to yield kinetic parameters, and greater results throughput. In reaction systems that require anhydrous or oxygen-free conditions, filling of the pill-box can be carried out in an appropriate glove-box. For oxygen-sensitive reactions a special cell has been developed as well.[22] The second method, of applying pressure to a solution directly, has mostly been used for aqueous media and where no restrictions on exposure to air were important. It is worth noting that the piston-cylinder apparatus with aliquot sampling requires typically about 0.1 dm^3 of solution per run, the second of the *in situ* methods requires about 0.005 dm^3, and the pill-box uses a similar volume of solution as a standard 1 cm path length cuvette (ca. 0.003 dm^3). The emphasis has been on UV/visible spectrophotometry since the preponderance of reports in several areas of chemistry exploits this method. A high pressure cell capable of monitoring changes in conductivity has been constructed but not widely used.[54] In principle circular dichroism, fluorescence or infrared (IR) spectroscopies could also be used as rapid monitoring methods, providing successful interfacing with a high pressure container arrangement is extant. An updated version of a high pressure apparatus, using a pill-box, in which the detection system has been enlarged from UV/visible to the near-IR region and for special circumstances pressures up to 400 MPa may be applied, has been described.[55]

A separate section will be devoted to covering the monitoring of reaction progress at high pressure by nuclear magnetic resonance (NMR) spectroscopy. Although there have been no reports to date, in principle for sufficiently slow reactions aliquot samples from a piston-cylinder apparatus could be followed by NMR spectroscopy; however, such a procedure would not be viable because of the large solution volumes required if deuterated solvents were to be used.

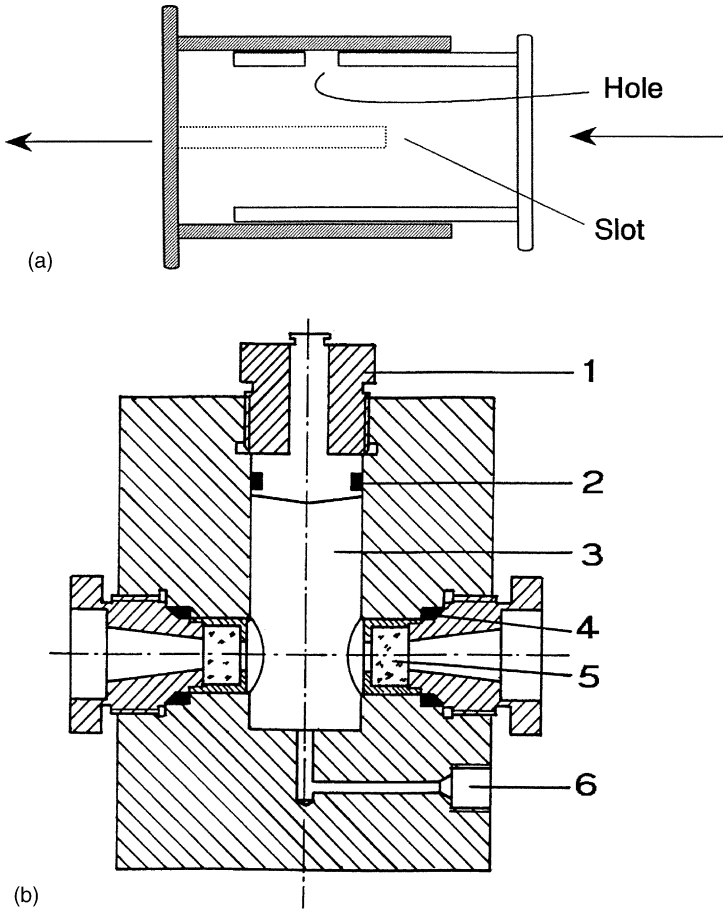

Fig. 2 (a) Schematic presentation of a ''pill-box'' optical cell for measurements on solutions at high hydrostatic pressures. The slot and hole allow the pill-box cell to be filled and extra liquid to be released on closing the cell. (b) Schematic view of a two-window high pressure cell to accommodate the pill-box optical cell for pressures up to 200 Mpa. 1: pressure plug; 2: O-ring; 3: reaction compartment; 4: Δ- and O-ring; 5: sapphire window and 6: pressure connection.

For situations when temperature or concentration lowering does not achieve the objective of increasing the reaction half-life to a level suitable for the methods described above, a special arrangement for mixing reactants quickly has been devised.[22] This device should not be included in the subsequent section on rapid reactions. By mixing quickly here, the term refers to about 5 s, whereas below, mixing times of a few milliseconds are discussed. The reactants are equilibrated thermally and under pressure, but are separated by a thin membrane. The membrane can be broken by a magnetic-field-activated mixing bar, and the mixed solution monitored. Thus the method is suitable for reaction half-lives of about 10 s and longer.

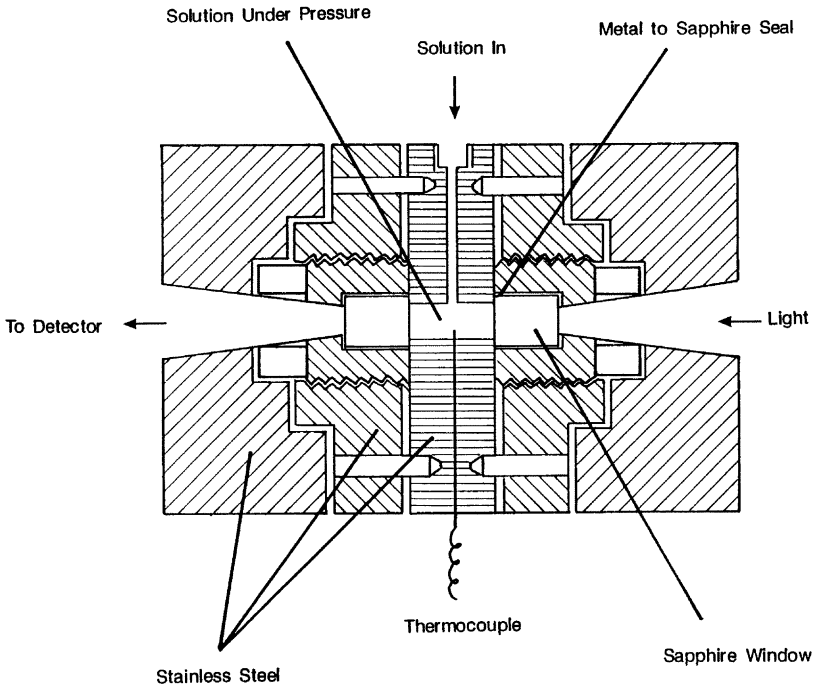

Fig. 3 High pressure cell in which pressure is applied directly to the sample solution.

It should be noted that although high pressure pumps and valves are standard and readily available, most of the high pressure containers and cells have been constructed in individual investigators' laboratories and workshops, and are not commercially available.

RAPID REACTIONS

Mixing methods

This section will be in two parts. First the methods for rapidly mixing reactants at ambient pressure, and subsequently extending this to rapid mixing at elevated pressures, will be described, while a second part will mention methods for studying fast reactions that are complete within the time that the reactant solutions can be physically mixed. Again, adaptation of the latter approach to high pressure will be noted. The methods herein are applicable to thermal reactions. A later section will present methods for reactions that are induced by radiation.

The objective of rapidly mixing reactant solutions for kinetics measurements was first reported about 80 years ago. The method required continuous flowing of solutions, and the term continuous flow was assigned to the method.[56] Reactant solutions were flowed along tubes and mixed at a Y-type junction. Whereupon

observation and measurement of an appropriate property at given distances from the Y-junction, with knowledge of the flow rate, permitted the development of a kinetic profile. The absence of very rapid detection and rapid flow rates limited the method as large volumes of reactant solutions were needed. Further development took the form of the accelerated-flow method,[57] and the stopped-flow (s.f.) method. The latter has its origin[58] in the 1930s and several investigators developed their own version. The history and development of s.f. can be followed.[59] The reactant solutions are driven manually or by mild pressure activation through a special mixer. The observation chamber is at 90° to the direction of flow in most versions. A rapidly acting receiver syringe with piston that arrests the flow of mixed solution signalled a significant improvement in time resolution.[60–62] Stopping the mixed solution flow triggers the recording of signal changes. In the usual configurations about 0.15 cm^3 of each solution per run is required. Use of an exit valve allows several replicate runs to be conducted before recharging with fresh reactant solutions is required. Commercial versions of s.f. instruments currently available are fundamentally based on some of the early versions, and now, naturally have far superior data collection and processing capability. The instrument dead-time of a few milliseconds means that reactions down to a half-life of several milliseconds can be studied. Almost all instruments use UV/visible signal changes as a means of following kinetics processes. The flow must be turbulent and solution viscosity must be in an appropriate range. The method is not suitable for mixing solutions of widely different ionic strength, or of different solvent composition. Reactions that are markedly exothermic or endothermic can, upon mixing reactants, introduce heating or cooling effects leading to complications that may not be recognised. A rapid mixing device has been coupled to a cell for monitoring reacting organometallic species via IR spectroscopy.[63] Other properties of reacting systems, e.g. changes in conductivity, circular dichroism or fluorescence, could also be used in conjunction with the s.f. mixing approach.

Adaptation of the s.f. method to kinetics studies at high pressures (hpsf) can only be viable if the reactant solutions are already under stable thermal and pressure conditions prior to mixing. This has been achieved by immersing an s.f. unit inside a pressurisable container. Another important feature of one design[64] is that by using smaller quantities of reactant solution than in ambient pressure s.f. units, more measurements can be made before decompression and recharging the unit with fresh reactant solutions are required. This has been accomplished by using the tightness of fit of the stopping and reactant pistons to arrest flow once the applied pressure from a stepping motor to the reactant solution pistons is removed, and there is no outlet valve. In this way about 30 replicate measurements may be made with one filling of the system and allows the system to be compressed to several different pressures before refilling. The windows of the s.f. unit are aligned with windows in the pressurisable vessel, and UV/visible absorbance changes are usually the means of following reaction progress. However, an instrument that monitors fluorescence signals has been constructed and employed.[65] Several hpsf units have been devised and reported following the first version described by Heremans[66] and colleagues.[64,67–74] The technical facts may be consulted. Generally the dead-time is longer than on

ambient pressure s.f. units, although the dead-time has been reduced on some later instruments.[72,74] Instruments currently in use are either that used in Erlangen or those instruments based on the design of the Merbach group and commercially available,[69,75] and the other relies on a coupling between the driving and receiving syringes to reduce the dead-time.[74,76] Figs. 4 and 5 provide schematic illustrations of hpsf instruments.

They have been most widely used to follow the kinetics of ligand substitution and electron transfer reactions of transition metal coordination compounds, although as will be described below also in several organometallic chemistry reaction kinetics studies.

Relaxation methods

When a reaction is faster than the time taken to physically mix solutions other means of following the reaction kinetics must be found. A category of methods, known as relaxation methods, originated in the 1950s.[77] A reaction system at equilibrium is subject to a rapid perturbation (in principle any property upon which the equilibrium depends can be employed to perturb the equilibrium). The subsequent relaxation to a new equilibrium position is a function of the kinetics of the forward and backward reactions, and the relaxation signal can be analysed to yield kinetic parameters.[76] Methods of perturbation of equilibrium include a temperature jump, a pressure jump, electric impulse, alternating electrical field, ultrasonic absorption, microwaves and a photochemical flash. The last method will be treated separately in a general section on radiation-induced reactions. Relaxation methods and the methods of analysis of relaxation signals have been included in several publications on fast reactions in solution.[59,78–83]

Of the relaxation methods only the temperature-jump and pressure-jump methods have been adapted for high pressure application, and of these two only the former (hptj) has been used in many systems for volume of activation determinations. Despite the flurry of activity in developing hptj,[84–88] the method has not found application in organometallic chemistry, although in principle it could be employed if the system properties and solvent were suitable.

Details of a standard pressure-jump instrument[89] and high-pressure pressure-jump cells can be obtained from appropriate literature.[90–93] The method has found very limited application and not at all in organometallic chemistry. Commercial units or modules for high pressure relaxation methods are not available.

RADIATION-INDUCED REACTIONS

Photo-induced methods

In principle reactions that are induced by a light signal could be in the conventional time range, or rapid, requiring rapid data acquisition. The latter class of reactions became a reality in the history of this research area upon the development of fast

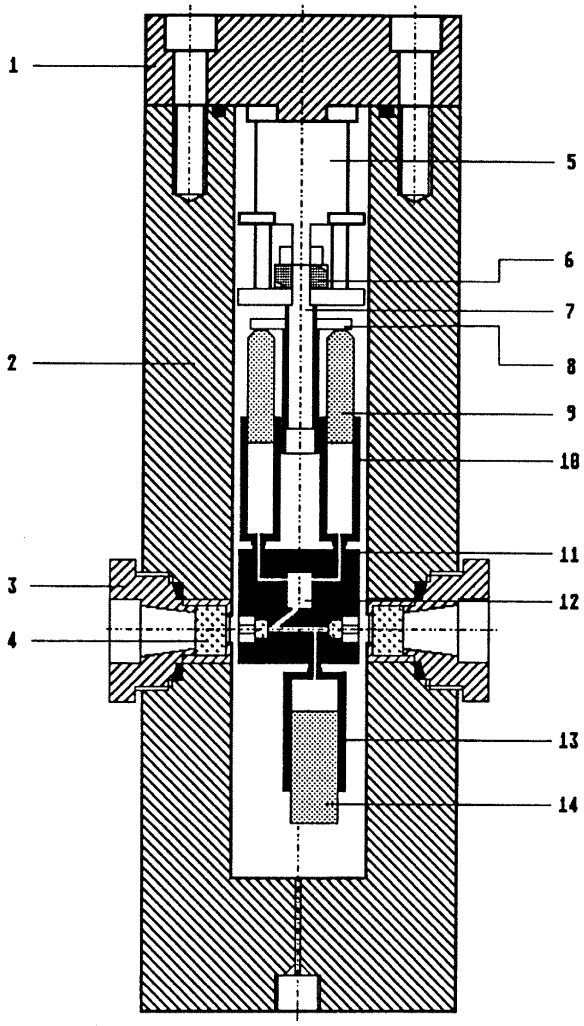

Fig. 4 Schematic presentation of a high pressure s.f. unit. 1: lid to overall unit; 2: outer vessel; 3: window holder; 4: quartz windows; 5: electric motor; 6: motor actuator; 7: s.f. unit positioning rod; 8: syringe driving plate; 9: drive syringe (inner); 10: drive syringe (outer); 11: block holding windows, mixer and syringe attachment points; 12: mixing jet; 13: stop syringe (outer) and 14: stop syringe (inner).

flash lamp technology, and flash photolysis and flash spectroscopy emerged as techniques for studying rapid kinetics of photochemically induced reactions and transient spectra of species in the micro- to millisecond range.[94] The properties of the system will determine whether the photosensitivity would lead to relaxation kinetics or non-relaxation kinetics. Subsequently the time range of measurement has been reduced by orders of magnitude enabling reactions in the nano- and picosecond

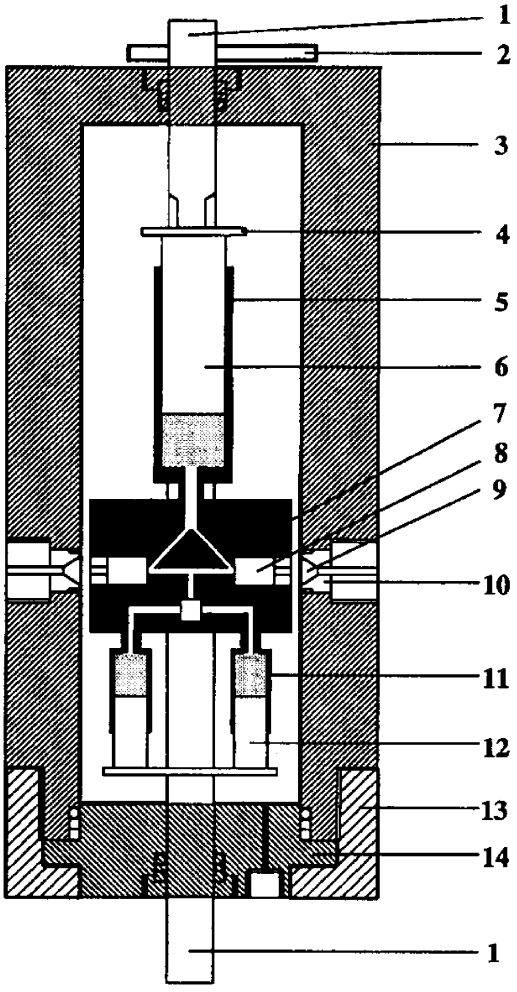

Fig. 5 Cross-sectional diagram of high pressure vessel and s.f. unit. 1: rod made of AISI 316; 2: lever to revolve rod; 3: high pressure vessel; 4: push–pull rod; 5: receiver syringe; 6: receiver-syringe piston; 7: mixer and optical cell block; 8: quartz; 9: sapphire window; 10: sapphire window holder; 11: reactant syringe; 12: reactant-syringe piston; 13: high pressure vessel lid holder and 14: high pressure vessel lid.

range to be studied. Adaptation of these and conventional time methods for high pressure studies of photochemical and photophysical processes was undertaken by several investigators.[95–100] Examples of some later applications for selected systems are available.[101–104] The pill-box cell and enclosing high pressure container can be used, with modification, for slow reactions.[105] In most cases the adaptation involves addition of at least one window in order to be able to initiate reaction and two other windows are used for the subsequent spectrophotometric monitoring of the kinetics.

The high pressure system of pumps and valves need not differ from those used for mixing of reactant solutions. Among organometallic reactions whose kinetics at elevated pressure have been studied following photochemical energy induction are reactions of metal carbonyl complexes. The most frequently used monitoring method is UV/visible spectrophotometry. Time-resolved infrared (TRIR) spectroscopy has been applied recently in studies of iron–carbonyl complexes in supercritical fluids[106] and in studies of molybdenum–carbonyl complexes[107] where moderate gas pressures were used. Although these particular studies did not result in determination of volumes of activation, it is evident that TRIR spectroscopy could be used in appropriate cases in association with high pressure kinetics.

Pulse radiolysis

In this method of inducing reaction, usually in aqueous medium, an electron beam forms radicals from the radiolysis of water in a few microseconds. Subsequent radical reactions with a variety of substrates can be monitored. Authoritative reviews that include results from high pressure kinetics studies have appeared recently.[108,109] A specially designed pill-box cell has been developed to enable certain radical reactions to be studied at high pressures. An initial difficulty to construct a cell that is sufficiently robust to withstand high pressures, but allows a required level of electron flux to enter the cell, has been overcome by design of a special window (see Fig. 6).[110]

It should be emphasised that the combination of pulse radiolysis reaction induction and high pressure kinetics capability means that the method is restricted to a very small number of investigators, and commercial units are unavailable. Changes in absorbance in the UV/visible region are used to monitor reaction kinetics. Radical reactions are very rapid and fast data acquisition capability is required. General literature on pulse radiolysis as a method is available.[111] An account of the value of high pressure kinetics in combination with pulse radiolysis in mechanistic insight provides a survey of the scope and range of reactions studied.[108]

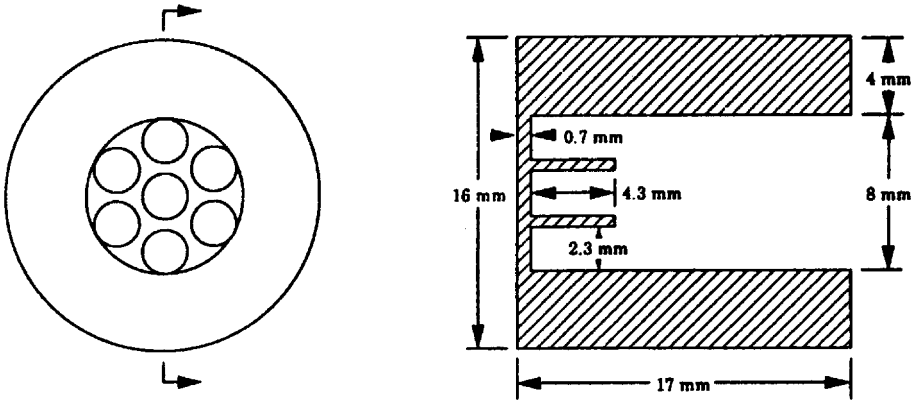

Fig. 6 Schematic diagram of the electron beam window for high pressure pulse radiolysis. The electron beam enters from the right side.

ELECTROCHEMICAL METHODS

The subject of redox reactions embraces a considerable variety of reactions. In homogeneous solution there are many spontaneous reactions, self-exchange reactions or non-symmetrical electron transfer reactions, for example. The kinetics of many of these have been studied by UV/visible spectrophotometry at both ambient and elevated pressures.[50,112] The kinetic parameters and volumes of activation for some self-exchange reactions have been obtained using ambient and high pressure NMR (HPNMR) spectroscopy, radiochemical tracer methods or s.f. circular dichroism.[113,114] Some investigators have been interested in redox reactions at electrodes in electrochemical cells. In some cases the purpose was to obtain the volume of activation for a self-exchange reaction indirectly.[114] A recent authoritative review has described in detail the methods for studying electrode reaction kinetics, including the more familiar cyclic voltammetry and alternating current polarography methods.[115] This review also outlined the relationship between homogeneous versus heterogeneous self-exchange electron transfer, and emphasised the insight obtained from pressure effects. The technology for studying electrode reaction kinetics at high pressure is specialised. A three-electrode cell constructed from Teflon or stainless steel depending on the chemical considerations is sealed inside a thermostattable steel pressure vessel, suitable for pressures up to 400–500 MPa.[116,117] The design issues and operating difficulties needing to be addressed to ensure successful measurements have been indicated. Of the three electrodes, one is the working electrode, a second is the counter electrode and the third is the reference electrode that is designed to allow ionic contact and to allow compression of the solution in the reference compartment. Overall the cell has a movable piston to allow compression of the reaction medium. As with many high pressure devices, the pressurising fluid is hexane or heptane and is separated from the oil of the hydraulic pump by a piston separator vessel. The pressure dependence of solution viscosity can be significant for organic solvents, but is conveniently negligible for aqueous solutions. How the pressure dependence of solvent viscosity, when applicable, is accounted for has been addressed. Fig. 7 is an example of a high pressure cell and apparatus for electrode kinetics that permits determination of volumes of activation for both coordination and organometallic compound couples.

Other aspects of high pressure electrochemistry kinetics can be obtained from a review by two of the leading experts.[118]

NMR SPECTROSCOPY

The presence of magnetically active nuclei of sufficient sensitivity and abundance in a reacting system provides a potentially excellent method of monitoring the kinetics of reaction.[119] Providing the reaction is sufficiently slow, measurements can commence in a reasonably short time after introduction of the sample into a spectrometer at ambient pressure. One or more signals can be employed in developing a kinetic profile. Adapting NMR probes for measurements at elevated pressures is an exercise that has occupied some investigators from the early period of electromagnet-based

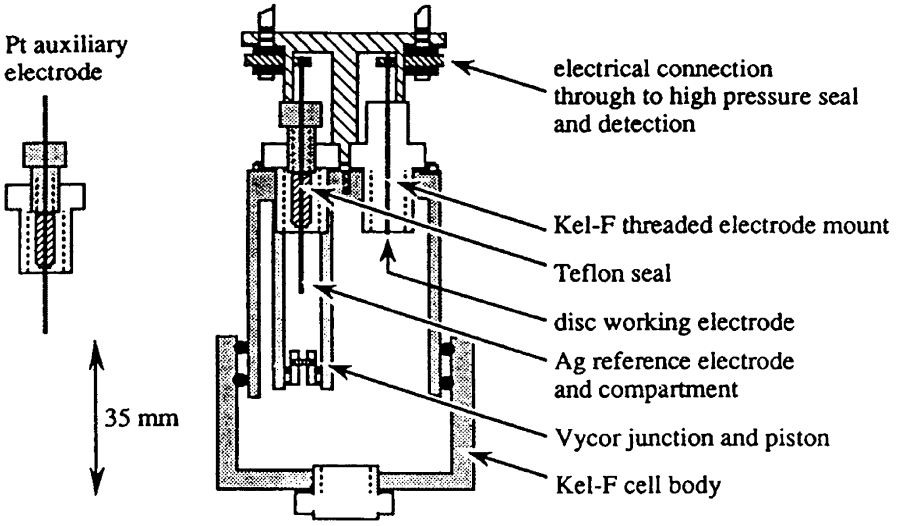

Fig. 7 High pressure electrochemical cell.

spectrometers,[120,121] to the current generation of high resolution, cryomagnet spectrometers.[32,122] The development of HPNMR spectroscopy can also be traced from relevant reports and reviews.[123–125] The adaptation is not simple as materials of the high pressure probe must not interfere with instrument operation. Since an instrument may need to be dedicated to high pressure mode, NMR spectrometers equipped for high pressure measurements are not common laboratory currency.

Pioneering studies by Connick and coworkers led to an understanding of the hydration and lability of the hydration of certain paramagnetic ions.[126] Using water enriched in ^{17}O, they were able to follow the kinetics of exchange of water between the coordination sphere of each of the aqua ions of Mn(II), Fe(II), Co(II) and Ni(II) and bulk solvent. Kinetic parameters from ^{17}O NMR spectra at various temperatures were extracted from modified Bloch equations. Determination of the water exchange rate constants was important in establishing that rates of complex formation reactions of these metal ions were controlled principally by the respective rates of water exchange. A mechanism embodying these features became known as the Eigen–Wilkins mechanism.[127,128] Results from hptj experiments on metal-complex-formation reactions yielded positive volumes of activation of magnitudes that supported the mechanism.[129–132] It also illustrated some time ago the power of high pressure kinetics experiments as strongly confirmative of mechanisms proposed on the basis of ambient pressure kinetics results. Against this background, high pressure probes for NMR (HPNMR) spectrometers that could be used at pressures up to 200 MPa were developed.[32,122] These instruments have been used extensively to obtain kinetic parameters for exchange of water and other solvents on several transition metal ions, on some main group solvento cations. More recently there has been emphasis on the lanthanides.[133] Volumes of activation were also acquired, and also in some cases where non-solvent, non-exchanging ligands are also present. In the context of solvent

exchange on solvento-organometallic compounds, the volume of information is much smaller. Nevertheless, some dramatic effects are observed and will be reported below. Examples of HPNMR probes are shown in Figs. 8 and 9. Details of the construction and materials used are beyond the scope of this article. However, the figures themselves are very illustrative and further details can be obtained.

There has been considerable activity also in developing HPNMR instruments in another and very important area of organometallic chemistry. Conversion of organic substrates into products of greater value, catalysed by organometallic compounds, and understanding the mechanism of individual steps or a whole catalytic cycle, are goals of many investigators. In many reactions the substrate in a solvent is converted and the reaction catalysed in the presence of gases at high pressure. As stated earlier there has been progress in addressing the mechanistic pathways by using HPNMR spectroscopy, using ^{13}C and ^{1}H nuclei.[41–44] An objective is to study the reactions as a function of gas pressure to optimise yield as well as elucidate mechanism. Typical pressures are at least an order of magnitude lower than is the homogeneous systems described and volumes of activation are not determined. However, the technical aspects of the instrumentation are of interest and valuable to other high pressure practitioners.

PARTIAL MOLAR VOLUMES FROM DENSITY MEASUREMENTS

Various specification densitometers are available commercially, and operate on the principle of a sound wave whose frequency depends on the density of the solution. The density of air and of the solvent must also be determined. The volume of liquid required is about 2–3 cm^3 and each measurement takes only a few minutes. The range of concentrations needed for viable measurements is usually much higher than is used in relevant kinetics experiments and therefore sample solubility, scarcity or solution stability can limit the extent of possible measurement. The need for moderately high concentrations can be seen from examination of Equation (10) since the difference in densities between each solution and the solvent is part of the calculation. In fact densities to six significant figures are usually required. Other critical factors are that the temperature must be precisely ($\pm 0.01\,^{\circ}C$, ideally) and reproducibly known since densities are very sensitive to temperature. Highly pure solutes and solvents should be used and solvent outgassing is important. Solutes in volatile or mixed solvents do not yield usable results. In addition to obtaining reaction volumes from partial molar volumes of reactants and products, the simple method of dilatometry can be applied.

MISCELLANEOUS TOPICS

Range of values and correlation of $\Delta V^{\neq}$ with $\Delta S^{\neq}$

Based on compilations of values of $\Delta V^{\neq}$ it can be seen that typical values are within the range of $\pm 30\,cm^3\,mol^{-1}$, although some organic reactions extend that range to

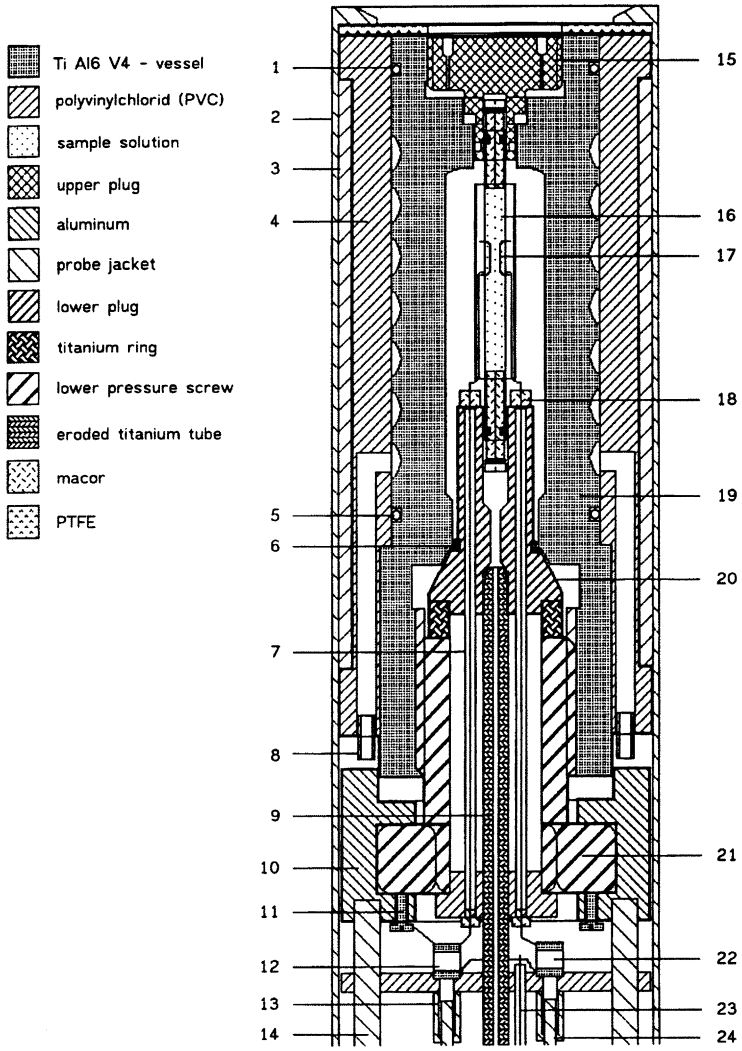

Fig. 8 Design features of a wide bore probe head for HPNMR (400 MHz) measurements. 1: O-ring; 2: probe jacket; 3: thermal insulation; 4: polyvinyl chloride; 5: O-ring; 6: O-ring; 7: semi-rigid coaxial cable; 8: connection to thermostat; 9: titanium tube; 10: lid; 11: screw; 12: capacitor; 13: capacitor holder; 14: aluminium tube; 15: upper plug; 16: sample tube; 17: saddle coil; 18: –Macor; 19: TiAl6V4 vessel; 20: lower plug; 21: lower pressure screw; 22: capacitor; 23: coaxial cable and 24: capacitor holder.

$\pm 50\,cm^3\,mol^{-1}$. Volumes of activation of $+30$ or $-30\,cm^3\,mol^{-1}$ correspond, respectively, to a rate retardation and a rate acceleration of about a factor of 3.5 at 100 MPa pressure relative to ambient pressure. For these values most methods yield precision of about $\pm 5\%$. For reactions that are less sensitive to pressure the precision is usually progressively reduced as the modulus of the volume of activation is reduced.

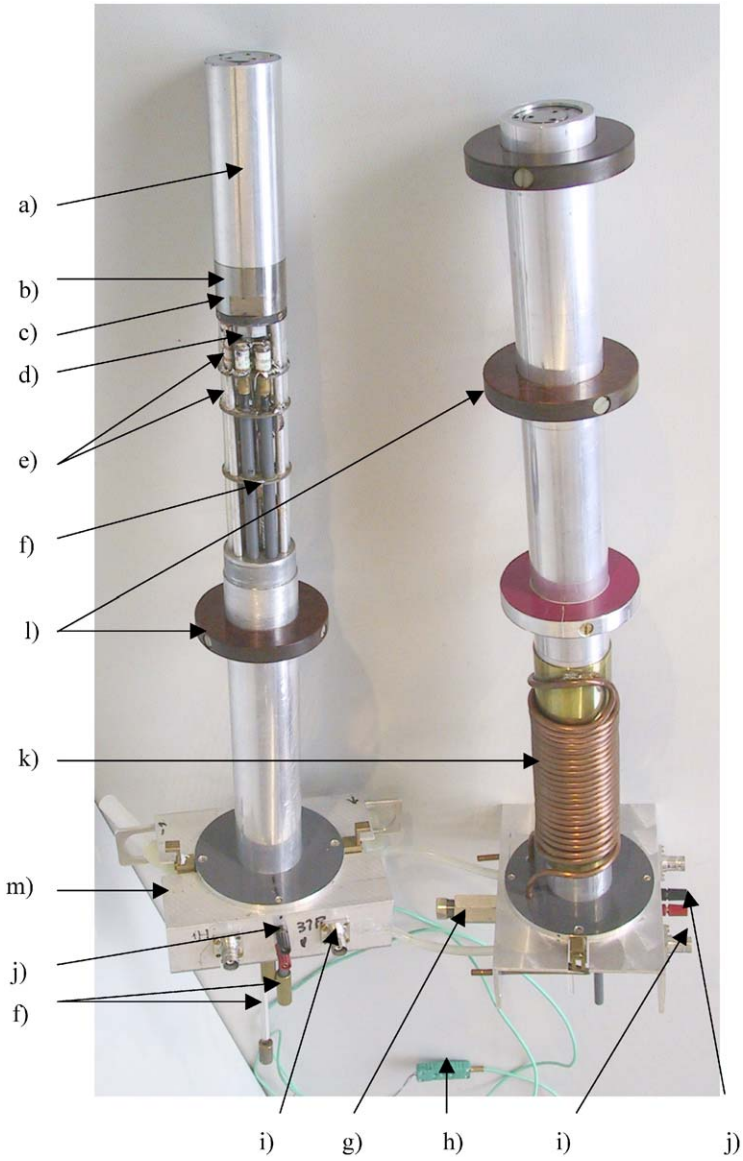

Fig. 9 Photograph of two narrowbore probeheads. a: aluminium jacket sealing the double helix used for thermostating; b: high pressure vessel; c: platform carrying the autoclave; d: capacitors; e: capacitor platforms; f: tuning rods; g: high pressure connector; h: thermocouple; i: BNC connector; j: Pt-100 connector; k: copper tubing and l: widebore adapter.

However, actual precision can depend on the reaction, the particular method of high pressure kinetics measurement and the quality of the instrument. As noted earlier, measurement of pressure at a precision or accuracy of 1–2% is acceptable, as reaction rate sensitivity to pressure would not be detectable within this range.

For many inorganic and bioinorganic reactions the volume of activation has been obtained from measurements at 25 °C. It prevails that the volume of activation is not particularly sensitive to temperature change. This is convenient in that values obtained for different reactions at different temperatures in most cases can be compared directly. Differences at various temperatures for a given reaction can be expected to be within the error of each measurement. Clearly this does not apply to any temperature, and a useful guideline could be that ± 20 °C from the standard 25 °C of measurement should yield no significant difference in the value of $\Delta V^{\neq}$. This can be seen from Equation (9).

When it is experimentally feasible, the temperature dependence of $\Delta V^{\neq}$ can be compared with the pressure dependence of the entropy of activation. The equality of these terms is defined from extending the Maxwell thermodynamic equality:

$$(\delta \mathrm{V_i}/\delta \mathrm{T})_\mathrm{P} = -(\delta \mathrm{S_i}/\delta \mathrm{P})_\mathrm{T} \tag{11}$$

to an equilibrium or a reaction, viz:

$$(\delta \Delta \mathrm{V}/\delta \mathrm{T})_\mathrm{P} = -(\delta \Delta \mathrm{S}/\delta \mathrm{P})_\mathrm{T} \tag{12}$$

$$(\delta \Delta \mathrm{V}^{\neq}/\delta \mathrm{T})_\mathrm{P} = -(\delta \Delta \mathrm{S}^{\neq}/\delta \mathrm{P})_\mathrm{T} \tag{13}$$

In some cases the experimental agreement is reasonable.

Several investigators have examined the possible correlation of these two activation parameters, particularly for series of similar reactions.[134–136] Correlations have been attempted for reactions of transition metal coordination compounds, such as ligand substitution or isomerisation, or solvent exchange,[135–137] and the issue has been addressed recently.[138] However, correlations for these parameters for organometallic reactions have not yet been developed.

Safety considerations

Typical sample capacities of solutions in most of the hydrostatic high pressure methods described are in the range of a few cubic centimetres of solution under various compression regimes. A considerably higher volume of the pressurising liquid is maintained at the same pressure. If any component of the overall system under pressure fails liquid leakage can occur and the pressure reverts to ambient immediately. Therefore, the safety aspect is similar to proper laboratory practice in treatment of solvent or solute spillage, particularly if the materials are hazardous or toxic. Since component failure is accompanied by rapid decompression normally, only a fraction of the total liquid that was under pressure will leak. In the case of a piston-cylinder apparatus, the volume of sample can be as high as 0.1 $\mathrm{dm^3}$ and therefore the potential for more liquid leakage exists. Providing the pressure is delivered by liquid under pressure, normal safe laboratory practice should be adequate providing the temperature of the system is close to ambient. However, if compressed gases are used to deliver pressure to the pressurisable liquid, then safety practice consistent with other applications of compressed gases is required. When large volumes of liquids, up to 200 $\mathrm{dm^3}$, are used in materials processing to bring

about physicochemical change, additional safety measures to protect operators from potentially large volumes of hot liquids leaking must be in place.

3 Volumes of activation for thermal organometallic reactions

In this section a summary of an accepted mechanistic classification scheme will be presented. This scheme applies to many of the organometallic reactions that will be described. Following this, reactions of interest will be grouped together according to their common reaction type, e.g. solvent exchange, ligand substitution, oxidation–reduction, small molecule reactions, photochemically initiated reactions and others. When a particular sub-field of research is currently active, mostly only relatively recent reports will be included and these may be examined for reference to earlier developments in the sub-field. In other cases when a sub-field has become dormant the latest reports generally available will be presented. It should also be emphasised that this account is not an exhaustive one of all volumes of activation determined in recent organometallic chemistry studies. Nevertheless, to our knowledge the vast majority of reports has been included.

A set of generally accepted guidelines for mechanistic diagnosis from volumes of activation has been provided. A mechanistic classification of substitution reactions of transition metal complexes used the letters, D, A and I.[139] A dissociative process with an identifiable intermediate of lower coordination number is assigned D. An associative process with an identifiable intermediate of higher coordination number is termed an A mechanism. An interchange process, labelled I, is one in which acts of bond breaking and making occur, and either took place within a pre-formed aggregate or were synchronous processes. The I mechanism could be further subclassified into I_d and I_a. The former refers to a dissociatively activated interchange mechanism that has a rate-determining transition state in which bond cleavage is more important than bond formation. Conversely, an I_a mechanism is one that has a transition state in which there is more bond formation than bond cleavage. The nomenclature has been compared with that used for organic reactions.[140] Other often unrecognised subtleties have been considered at length. This literature may be fruitfully consulted.[140] At least for solvent exchange processes, the assignment of mechanism based on $\Delta V^{\neq}$ is reasonably straightforward, providing the numerical values are not close to zero, since electrostriction effects are absent or negligible.[125,141] It has been estimated that for water exchange on an octahedral complex via a D or A mechanism, the value of $\Delta V^{\neq}$ would be about $\pm 13\,\mathrm{cm^3\,mol^{-1}}$, respectively.[142] Values for solvents other than water will clearly differ. If experimental values in water exchange reactions progress from these limits towards zero it has become a practice to assume that these values represent I mechanisms of "d" or "a" character, and that a value of zero would indicate a pure interchange process. The difficulty is that these assignments are based on arguments that take no account of other possible volume changes among the non-exchanging ligands and attendant alterations to the partial molar volume (that are not accessible). It is also noted that for all reactions, volume changes may occur in parts of molecules not involved in the

reaction itself, and these cannot be accounted for or estimated. Nevertheless, as a first approximation the literature contains many mechanistic assignments based on the volume of activation. In the following sections abbreviations used are nearly always those provided by the respective authors.

SOLVENT EXCHANGE

The kinetics and mechanism of solvent exchange from fully solvated or partially solvated metal cations have been extensively studied, mostly by NMR and HPNMR spectroscopies.[32,133] The range of solvent exchange rates encountered varies over 20 orders of magnitude. The effects of the presence of non-exchanging ligands on both rates and coordination geometry can be very pronounced.[15,32,133,143–146] Early studies were mostly on the solvento cations or aquamonohydroxy cations of the first row of transition metals. More recently, reports on solvent exchange kinetics and mechanism of second- or third-row transition metal cations, some main group solvento cations, lanthanide cations and some actinide cations have appeared.[133,143] The non-exchanging ligands invariably have been coordinating ligands. One reason for these studies, beside their intrinsic interest, is that they assist in understanding metal-complex-formation reactions in which one or more solvent molecules is/are replaced by a coordinating or chelating ligand. In the case of some lanthanide ions the development of appropriately functioning magnetic imaging reagents for medicinal purposes, composed of solvento complexes of lanthanides, drives the studies forward. Theoretical studies conducted on several of these solvent exchange reactions have usually shown accord with the mechanisms based on experimental activation parameters including the volume of activation.[147–153]

Dramatic changes in the kinetic lability of solvent exchange have been observed when some of the coordinated solvent molecules are replaced by an organic moiety. For example, hexa-aqua ruthenium(II) has a water exchange rate constant of $1.8 \times 10^{-2}\,s^{-1}$ at 298 K,[154] while water exchange on $Ru(\eta^5\text{-}C_6H_6)(H_2O)_3^{2+}$ is characterised by a rate constant of $11.5\,s^{-1}$ at the same temperature.[155] Clearly the water exchange mechanism for the arene-aqua ions is characterised by a strong *trans*-labilising effect of the aromatic ligand on coordinated water. The thermal activation parameters, $\Delta H^{\neq}$ of 88 and 76 kJ mol^{-1} and $\Delta S^{\neq}$ values of +16 and +30 J mol^{-1} K^{-1} for the hexa-aqua and aqua-arene complexes, respectively, would imply that the change in free energy of activation is a consequence of both parameters. However, the magnitude of error on the entropy of activation values is such that the two values are not statistically different. The volumes of activation, –0.4 and +1.5 cm^3 mol^{-1} for the hexa-aqua and the arene-aqua complex, respectively, indicate an interchange mechanism with approximately equal contributions of bond breaking and bond making for the former species. The latter value indicates an interchange mechanism in which bond breaking is slightly ahead of bond making, according to the authors. However, these findings can hardly be definitive given the small difference and errors associated with both values. Interestingly the osmium(II) analogue, $Os(\eta^5\text{-}C_6H_6)(H_2O)_3^{2+}$, has the same solvent exchange rate constant as the corresponding ruthenium

compound,[155] and is characterised by a 10 kJ mol^{-1} smaller enthalpy of activation, an essentially zero entropy of activation and a modest, +2.9 cm^3 mol^{-1}, volume of activation. The latter parameter suggests a slightly more dissociative interchange mechanism than for the ruthenium water exchange. The lack of proof for the existence of a hexa-aqua osmium(II) species, has been noted[156,157] and therefore a comparison that could be made in the ruthenium case cannot be made for the activation parameters for the osmium species.

Even more dramatic rate enhancements occur for acetonitrile exchange on solvento-, arene-solvento- and cyclopentadienyl-solvento-ruthenium(II) complex species. The substitution lability of CH_3CN increases along the series $Ru(CH_3CN)_6^{2+}$, $Ru(\eta^6\text{-}C_6H_6)(CH_3CN)_3^{2+}$, $Ru(\eta^5\text{-}C_5H_5)(CH_3CN)_3^{+}$ by five orders of magnitude for each step. The kinetics were monitored by ^{1}H NMR spectroscopy.[158] The increase correlates with a corresponding stepwise lengthening of the Ru–N distance by 0.03 Å, and indicates the significant progressive *trans*-labilisation enhancement. Enthalpy of activation decrements were, respectively, 28 and 16 kJ mol^{-1}. The values of $\Delta V^{\neq}$ provide clear evidence for mechanistic change. For the solvento cation the value was +0.4 cm^3 mol^{-1}, whereas the values were +2.4 and +11.1 cm^3 mol^{-1} for the arene and cyclopentadienyl species respectively, interpreted as interchange, interchange dissociative and dissociative, respectively. From the findings for both solvents it may be speculated that $Ru(\eta^5\text{-}C_5H_5)(H_2O)_3^{+}$ should exchange water ligands very rapidly.

A comprehensive preparative, structural and kinetics study (of water exchange and substitution) of several π-arene complexes of cobalt, rhodium, iridium and ruthenium has been undertaken.[159] As noted earlier, π-arene molecules upon substituting water molecules in $[M(H_2O)_6]$ (charges omitted) to yield $[LM(H_2O)_3]$, L = η^6-benzene or η^5-pentamethylcyclopentadienyl ion (Cp*), M = Co, Rh, Ir, Ru, increase the lability of the three residual water molecules drastically. The effect is most pronounced for anionic ligands. The labilisation effect is neutralised by two orders of magnitude when two of the surviving water molecules are replaced by 2,2'-bipyridine (bpy). There is a strong effect of the variation of metal ion with the lability of coordinated water in $[Cp^*M(bpy)(H_2O)]^{2+}$ following the order Co << Rh > Ir. Thermal activation parameters and a series of kinetics results on formation reactions by s.f. spectrophotometry provided evidence that could be interpreted to show that water exchange on $[Cp^*M(bpy)(H_2O)]^{2+}$ proceeds by a dissociative interchange mechanism. The rates of water exchange in $[Cp^*M(H_2O)_3]^{2+}$ (M = Rh, Ir) were followed at ambient and elevated pressures, by ^{17}O NMR spectroscopy, yielding respectively activation volumes of +0.6 and +2.4 cm^3 mol^{-1}. These values are indicative of an interchange mode of mechanism with a modest dissociative character.

Attention has been drawn to the connection between mechanisms of solvent exchange for arene–osmium compounds cited earlier and on dihydrogen–amine complexes of osmium, *trans*-$[Os(en)_2(\eta^2\text{-}H_2)S]^{2+}$, S = H_2O, CH_3CN.[160] The values of the volumes of activation for solvent exchange from ^{17}O NMR (H_2O exchange) or ^{1}H NMR (CH_3CN) spectroscopy were –1.5 and –0.5 cm^3 mol^{-1}, respectively. At face value parameters of this magnitude would be indicative of an I mechanism. However, it was argued from results of complex-formation reactions, and a previously cited argument, that the volumes of activation were also influenced by a contraction

of bonds of the metal to the non-reactive ligands. Thus solvent exchange on these osmium–dihydrogen complexes was dissociative interchange, I_d or dissociative, D. Therefore, it is a similar mechanistic situation to the I_d mechanism for water exchange on the osmium organometallic complexes.

It has been pointed out that ruthenium(II) possesses properties that allow it to be a focus of studies of organometallic chemistry of Ru(II) in water.[161] In addition some Ru(II) aqua complexes are key intermediates in processes connected with antitumour activity of Ru(II) and Ru(III) compounds.[162] These facts formed part of the interest behind studies aimed at understanding factors that govern the reactivity of ligands in the first coordination sphere of the Ru(II) centre.[163] Specifically the effect of L (L = H_2O, CH_3CN, $(CH_3)_2SO$, $H_2C=CH_2$, CO, $F_2C=CH_2$, N_2) on the rates of bound water at the axial (*trans*) and equatorial (*cis*) positions and on the redox potentials of $[Ru(H_2O)_5L)]^{2+}$ has been examined. Compared with square planar complexes *cis* and *trans* effects on reactivities are less well understood in complexes of octahedral geometry. The kinetics of water exchange were monitored by ^{17}O NMR spectroscopy, and in the case of the ethene compound as a function of pressure. The kinetics results set the order of L for both *cis* and *trans* effects, and a correlation between lability and calculated $Ru–H_2O_{ax}$ bond energies was indicated. Density functional theory was used to calculate properties of the ruthenium species. Rate constants for mono-complex formation between the ruthenium aqua ion and different ligands were very similar and an interchange I_d mechanism was assigned even though $\Delta V^{\neq}$ for water exchange on hexa-aqua Ru(II) was close to zero (vide supra). The $\Delta V^{\neq}$ values for water exchange on the axial and equatorial positions of the ethene complexes are $+6.5$ and $+6.1\,cm^3\,mol^{-1}$, respectively, and reflect the strong dissociative character of the mechanism. Large positive values of the entropy of activation supported this conclusion.

It was recognised that most of the earlier work on solvent exchange on organometallic–solvento–complexes featured second- (4d) or third-row (5d) transition metals. An extension to the first row was sought for the Group VII carbonyl aqua ions $[(CO)_3M(H_2O)_3]^+$, M = Tc, Re.[164] There was a degree of uncertainty about the authenticity of the species when M = Mn, but a spectroscopic characterisation has confirmed the species as *fac*-$[(CO)_3Mn(H_2O)_3]^+$.[164] The aqueous solution characteristics of this species strongly depend on the solution pH and the formation of polynuclear metal species is prevalent but not identical for the rhenium and manganese analogues. Species interconversion rates are also different. The 1+ oxidation state for these species is considered to arise from CO groups stabilising the t_{2g} orbitals by back bonding, effecting a low-spin configuration and by shifting the oxidation potential $M^{2+/+}$ to a more positive value, thus stabilising the monovalent species. Under appropriate solution conditions, the water exchange process on $[(CO)_3Mn(H_2O)_3]^+$ can be monitored by ^{17}O NMR spectroscopy. The interpretation of signal intensity changes indicated that carbonyl oxygen exchange occurs as shown below:

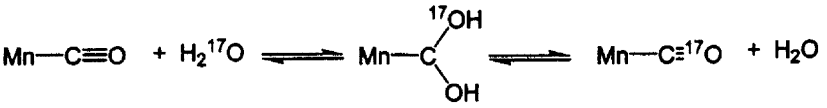

(14)

This type of exchange was not observed for the corresponding rhenium compound. Fitting procedures from studying the water exchange rate at different temperatures yielded k_{ex} at 298 K of $19\,s^{-1}$, and $\Delta H^{\neq} = 68\,kJ\,mol^{-1}$ and $\Delta S^{\neq} = 8\,J\,mol^{-1}\,K^{-1}$. The exchange rate constant shows that water exchanges almost four orders of magnitude faster than on the corresponding rhenium compound. A preliminary value for water exchange on the Tc compound is sufficient to show that the exchange rate decreases in the order Mn > Tc > Re. This was suggested to be consistent with the order of water exchange on $Co^{3+}/Rh^{3+}/Ir^{3+}$ aqua ions. However, the strong labilising effect of Cp*, more prominent for the heavier metals, reverses this lability order of water exchange on $[Cp^*M(bpy)(H_2O)]^{2+}$, M = Co, Rh, Ir.[159] The activation volume for water exchange on $[(CO)_3Mn(H_2O)_3]^+$ is $-4.5\,cm^3\,mol^{-1}$, indicative of an associative activation mode (I_a or A). On the basis of a volume of activation determination the water exchange mechanism on the rhenium cation is interpreted as I_d, a contrasting finding, and an unexpected trend. At present the substitution of water by another ligand on $[(CO)_3Mn(H_2O)_3]^+$ has yet to be investigated and therefore cannot be compared with the situation pertaining to the rhenium analogue, where the substitution mechanism appears to undergo a changeover from I_d with a hard donor, to I_a for a soft donor.[165]

LIGAND SUBSTITUTION

In this section the coverage follows mainly in order of the atomic number of the pertinent metal. However, in some cases when corresponding reactions of two metal centres (MCs) have been investigated the sub-section relates to both MCs.

Titanium

Titanium(IV) compounds of the general type $Ti(LL)_2X_2$, where LL is a bidentate anionic ligand and X is a halide or alkoxide, have been shown to possess antitumour activity.[166] The cyclopentadienyl compound $Ti(Cp)_2Cl_2$ has been studied and some kinetic characteristics established.[167] It is considered possible that the pharmacological activity resides in the Cp group, but other LL groups, e.g. the benzoylacetonato moiety in $Ti(bzac)_2(OEt)_2$, confers activity on this compound,[168] although there are some disadvantages in its application.[169] A search for other efficacious compounds focused on pyrones (see Scheme 1) and pyridinones, since anions of these ligands formed stable titanium(IV) complexes $Ti(LL)_2X_2$. (Pyrones with R = Me, Et, maltol and ethylmaltol are permitted as food additives.)

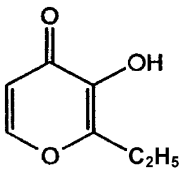

Scheme 1.

Solvolysis and substitution rates are known to be important for platinum antitumour agents,[170] and consequently these properties of titanium(IV) complexes containing pyronato and pyridinato ligands and halide or alkoxide leaving groups were examined.[171] Earlier studies on the kinetics of substitution at $Ti(Cp)_2Cl_2$[172] were extended to include the influence of hydrostatic pressure.[171] A wide-ranging kinetics study examined the effects of the non-leaving ligand, the leaving ligand and various entering (substituting) ligands on the rates for substitution at $Ti(LL)_2X_2$, where LLH = cyclopentadiene, the 4-pyrone ethylmaltol, several 4-pyridinones and related ligands with X = halide or alkoxide in acetonitrile, spectrophotometrically. Two reaction stages were observed and of sufficiently different rates that rate constants (first order for each, entering ligand in excess concentration) could be obtained. Analysis indicated a two-term rate law for each step consisting of a solvolysis pathway and a bimolecular attack. The stages refer to the successive removal of the departing ligands. The substitution reactions of NCS^- with $Ti(Cp)_2Cl_2$ and of H_2O with $Ti(Etmalt)_2Cl_2$ for the second stage were studied at pressures up to 100 MPa and derived activation volumes for bimolecular attack were –15 and –12 $cm^3\,mol^{-1}$, respectively. These values are of the magnitude expected for a bimolecular process in the absence of solvent effects.[11] Hydration effects have a significant impact on activation volumes for bimolecular inorganic reactions involving small hydrophilic anions such as hydroxide or cyanide in aqueous solution.[173,174] These effects can be attributed to extensive desolvation of the anionic nucleophile as it enters the transition state. In acetonitrile the situation will be very different since dipolar aprotic solvents solvate hydrophilic anions poorly. The transfer chemical potential of thiocyanate from water into acetonitrile of $+12\,kJ\,mol^{-1}$ or greater indicates that thiocyanate is essentially unsolvated in acetonitrile. [175] Therefore, in this situation a solvation contribution to the activation volumes for thiocyanate attack at these Ti(IV) species can be thought to be negligible, so that the negative values afford strong support for a bimolecular associative mechanism for that pathway.

Vanadium

In a partly parallel study to that reported for titanium(IV) above, the kinetics of substitution at vanadium(IV) in bis-cyclopentadienylvanadium dichloride by a range of anionic and uncharged nucleophiles (L) in acetonitrile have been investigated.[176] Such compounds were originally prepared over 50 years ago,[177] and some aspects of the kinetics of substitution have subsequently been studied.[167] As in the corresponding report on titanium(IV) compounds, by employing a wider range of incoming nucleophile concentrations, substitution of both chloro groups from $V(Cp)_2Cl_2$ could be observed, spectrophotometrically, and characterised. In an earlier report only one stage was detected.[172] Moreover, the two steps were sufficiently different in rate that rate constants could usually be determined accurately. Each of the two steps followed a two-term rate law, and in the first step the nucleophile concentration-independent rate constants are essentially identical as expected for a rate limiting solvolysis. For the second stage there is some variation in the solvolysis term, a finding to be expected since the substrate has progressed from $V(Cp)_2Cl_2$ to

$V(Cp)_2ClL$, where L has displaced Cl in the first stage. The rate constants for the nucleophile concentration-dependent part of the rate law for the first stage showed variation as expected for associative attack, and generally the variations were qualitatively consistent with expectations of relative nucleophilicity of the entering groups, and with a similar pattern as found for reactions of $Ti(Cp)_2Cl_2$. Both entering ligand and V(IV) species differ for the nucleophilic attack in the second stage. Therefore, it would be difficult to comment on the relative values of the second-order rate constants. High pressure kinetics measurements for the reaction of $V(Cp)_2Cl(NCS)$ with NCS^- yielded a value of $-12\,cm^3\,mol^{-1}$, supporting the associative nature of the reaction, and comparable to the value of $-15\,cm^3\,mol^{-1}$ for the corresponding reaction at Ti(IV). Reactions were slower at vanadium, and this was accounted for from Crystal Field considerations, d^1 (V) versus d^0 (Ti) ions.

Manganese

The reporting of a rhenium *fac*-tricarbonyl species containing two β-alanine ligands, functioning as unidentate ligands, and a bromo ligand, formed by reacting rhenium pentacarbonyl bromide with *β*-alanine,[178] was followed by a study of the analogous reaction between manganese pentacarbonyl bromide and *β*-alanine.[179] In the latter case the kinetics of the reaction in different solvents were studied and some activation parameters acquired. For the reaction in both 50% aqueous methanol and 50% aqueous dimethyl sulphoxide, two kinetically distinct steps were observed, the first-stage proceeding in the dark and the second-stage proceeding only in light. The entering β-alanine ligand, and in parallel experiments using glycine as the entering ligand, the amino acid was in excess over the concentration of the manganese species, in which case the kinetics were first order, and were monitored spectrophotometrically. In all cases, except for the first stage of the reaction of $Mn(CO)_5Br$ with *β*-alanine in 50% aqueous dimethyl sulphoxide, all first-order rate constants were independent of the concentration of entering amino acid concentration. A two-term rate law containing a solvolysis (dissociative) term and an associative pathway was indicated from the analysis of results for the first stage of the reaction of β-alanine with $Mn(CO)_5Br$ in 50% aqueous dimethyl sulphoxide. All other reaction steps were regarded as following a dissociative mechanism, although the difference of a factor of three for the rate constant (first stage) for reaction of *β*-alanine compared with glycine demonstrated that the dissociative mechanism was not entirely straightforward. For the second stage, first-order rate constants were independent of the concentrations of $Mn(CO)_5Br$, *β*-alanine or glycine, and independent of solvent suggesting a dissociative reaction mechanism. The difference in mechanisms for the first reaction stage was attributed to the markedly higher chemical potential of *β*-alanine in 50% aqueous dimethylsulphoxide. Activation parameters for reaction of $Mn(CO)_5Br + \beta$-alanine (first stage) were $121\,kJ\,mol^{-1}$, $+84\,J\,mol^{-1}\,K^{-1}$ and $-20\,cm^3\,mol^{-1}$ for $\Delta H^{\neq}$, $\Delta S^{\neq}$ and $\Delta V^{\neq}$, respectively. It was difficult to reconcile each of these values with a simple dissociative mechanism. A positive volume of activation would be expected for a dissocative mechanism. It was suggested that the amino acids (acting with different rates as referred to above) have specific but

different interactions with the manganese species. Drastic solvent reorganisation about the amino acid occurred as it went from a zwitterionic form in solution to a non-zwitterionic form in the pentacarbonyl manganese derivative. It was also proposed that the $Mn(CO)_5Br$-amino acid interaction is complete over the whole range of amino acid concentrations covered, but that the strength of the interaction depends on the nature of the amino acid involved. It was also pointed out that the entropy and volume of activation were not compatible with a correlation that might be expected.[180] Hence, although rationalisations for these results were provided, the magnitude and sign of the volume of activation remained puzzling.

A subsequent study[181] in which the kinetics of substitution of two CO molecules by bidentate ligands in $Mn(CO)_5X$ (X = Cl, Br) were monitored yielded distinctly positive volumes of activation. The ligands were dab (biacetyl bis(phenylimine) a diazabutadiene), dabCl (biacetyl bis(4-chlorophenylimine), dab-OCH_3 (biacetyl bis(4-methoxyphenylimine), phen (= 1,10-phenanthroline) and bpy. Toluene or dichloroethane were the solvents employed, solvents that are markedly less polar than those in the previously cited study. The rate constant for product ($Mn(CO)_3(LL)X$) formation was independent of the incoming ligand. In toluene the thermally derived activation parameters were very similar for the reactions of $Mn(CO)_5Cl$ and the bromo analogue with dab and for the reaction of the chloro compound with dab-OCH_3. For reaction of $Mn(CO)_5Cl$ with dab, a volume of activation of $+20.6\,cm^3\,mol^{-1}$ was obtained. All of these findings pointed towards a limiting D mechanism in which the rate constant represents the rate of dissociation of a *cis*-CO ligand from $Mn(CO)_5X$ to form a five-coordinate species. The product species $Mn(CO)_3(dab)Cl$ was confirmed to be a distorted octahedron with a facial arrangement of the three CO groups. It was also noted that the absence of a solvation contribution (no charge or significant polarity changes in the rate-determining step, and a non-polar solvent) means that the experimental volume of activation is virtually identical with $\Delta V^{\neq}_{intr}$. The chloro compound reacted about 10 times faster than the bromo compound, a fact related to the stronger electronegativity of the chloro ligand that reduced the electron density on Mn. Hence the extent of bond-stabilising π-back bonding to CO was also reduced. As could be predicted for a reaction not involving highly polar species, there was only a very modest decrease in rate when the reaction was conducted in the more polar dichloroethane.

Iron and molybdenum

The second-order term in the rate laws for reactions of low-spin iron(II)–diimine complexes with such nucleophiles as hydroxide and cyanide ions has been established as arising from a bimolecular reaction between complex and nucleophile.[182] Activation volumes that were obtained for reactions of CN^- and OH^- with $Fe(phen)_3^{2+}$ and $Fe(bpy)_3^{2+}$ were in the range of $+19.7$ to $+21.5\,cm^3\,mol^{-1}$.[183] Because these observations were not readily accounted for by an associative mechanism, a mechanism analogous to the Eigen–Wilkins mechanism of complex formation was introduced in which dissociative activation dominates in determining the observed activation volumes. However, subsequently it was shown that solvation

effects, specifically desolvation of the anionic nucleophile could play a large part in determining the sign and magnitude of the volume of activation in this type of reaction.[49] The approach that led to this proposal involved studying the kinetics of substitution reactions of iron(II)-tris-diimine complexes and of molydenum–diimine–tetracarbonyl complexes, in various solvents, at elevated pressures and made use of transfer chemical potential data of the relevant entering nucleophile (the cyanide ion).[49] In dimethylsulphoxide and methanol, respectively, the volumes of activation for reaction of cyanide with $Mo(bpy)(CO)_4$ were –9 and $+4\,cm^3\,mol^{-1}$. The same bimolecular mechanism would be expected for reaction of CN^- with $Fe(4\text{-}Me\text{-}phen)_3^{2+}$, yet for the reactions in a methanol water mixture and aqueous solution were $+13$ and $+10\,cm^3\,mol^{-1}$, respectively. Gibbs free energy of transfer of the cyanide ion from water into mixed and non-aqueous media suggest markedly lower solvation of the cyanide ion in methanol than in water and less solvation still in dimethyl sulphoxide. Thus the value of the volume of activation for reaction of cyanide with $Mo(bpy)(CO)_4$ is consistent with expectation for a bimolecular associative mechanism, and a small or negligible contribution in a positive direction from cyanide desolvation. The increasingly less negative to positive values of the volume of activation reflected qualitatively the increasing contributions to it of cyanide ion desolvation. Clearly other factors can assume some importance as there are differences in the value of $\Delta V^{\neq}$ for cyanide and hydroxide attack at similar iron (II)–diimine complexes. This issue has been addressed in later reports.[45,48] However, this early report highlights application of a combination of the volume of activation parameter and other thermodynamic quantities (transfer chemical potentials, $\delta_m\mu^{\theta}$) in a successful attempt to resolve mechanistic issues.[49]

Further employment of a combination of equilibrium and high-pressure-derived kinetic parameters enabled insight to be provided into the mechanism of cycloaddition of tetracyanoethene to tricarbonylcycloheptatrieneiron.[51] This reaction initially was reported to yield a 1,5-adduct,[184] but this was later shown to arise from isomerisation of a 1,3-adduct.[185] Interest in determining whether this cycloaddition reaction proceeds via a concerted or a stepwise dipolar mechanism has stimulated frontier orbital calculation predictions.[186] The finding of a lack of a significant solvent effect was significant[187] and the high dienophile dependence of the rate of addition was noted.[188] These studies pointed towards the concerted mechanism. In order to obtain direct information on the nature of the transition state, a study to determine the activation volumes in solvents of widely differing polarities, and to examine the effects of the same solvents on the initial and final states was undertaken.[51] The reaction had been established previously to be second order (first order in each reactant) in dichloromethane and acetone-d_6 at ambient pressure,[187,189] and the same rate law pertained for the reaction in acetonitrile. The volume of activation obtained from kinetics measurements by monitoring the reaction spectrophotometrically was statistically the same ($-31\,cm^3\,mol^{-1}$) in dichloromethane, acetone and acetonitrile. A highly ordered transition state could be inferred from the magnitudes of the entropy of activation (-165 to $-145\ J\,mol^{-1}\,K^{-1}$), similar to the values encountered in Diels–Alder reactions,[190] and indicated concerted bond formation. Closely similar values of the enthalpy of activation were obtained for the reaction in

each solvent. This would not be expected for a pathway involving a zwitterionic intermediate, since such a pathway would exhibit a spread of enthalpies of activation reflecting the changes in transition state solvation in the different solvents. From solubility measurements on both reactants and the product, transfer chemical potentials for transfer from the low polarity dichloromethane to acetone and acetonitrile could be calculated. Changes in the Gibbs energy of activation, calculated from the rate constants then permitted calculation of the transfer chemical potential for the transition state. The values of the transfer chemical potential for acetone and acetonitrile were intermediate between those for the initial state and the final state demonstrating that there is no increased solvation of the transition state that would have been anticipated for a dipolar transition state in polar solvents. Taken together, an analysis of the activation parameters and the transfer chemical potentials clearly provided support for a concerted mechanism.

Cobalt

There is substantial literature on cobalt-containing compounds in which a carbon–cobalt bond is in an axial position *trans* to usually an N-donor ligand, with the four equatorial positions occupied by N-donors too. This coordination arrangement is present in adenosylcobalamin (AdoCbl, coenzyme B_{12}) and in cyanocobalamin (CNCbl, vitamin B_{12}). The *trans* N-donor is dimethylbenzimidazole (DMBz) attached to a nucleotide (Scheme 2).

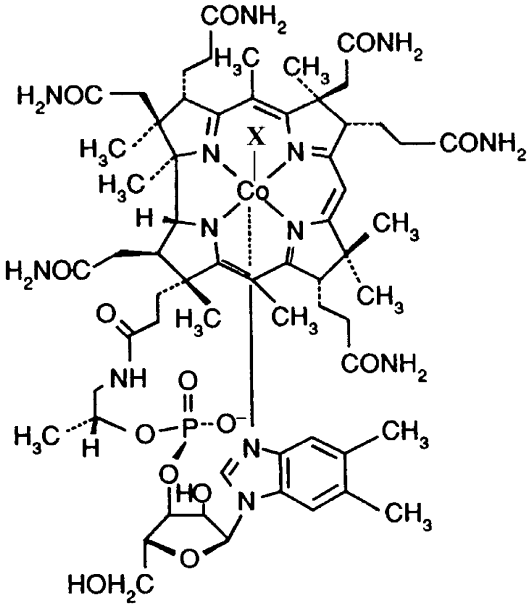

Scheme 2 Structure of cobalamin, where $X = CN^-$ for cyanocobalamin (vitamin B_{12}), $X = H_2O$ for aquacobalamin (vitamin B_{12a}) and X = 5′-deoxyadenosyl for coenzyme B_{12}.

Interest has been further stimulated by accounts of variable manipulation of axial ligation by different enzymes. Naturally the establishment of relevant kinetic and thermodynamic properties of processes that control cleavage of the cobalt–carbon bond and understanding the influence of the ligand *trans* to the bond are priorities, as well as is the development of correlations of such properties to structural characteristics. Investigations have taken several forms using the cited compounds themselves and analogues and model species. For example, a very recent investigation made use of a compound in which the DMBz moiety has been replaced by the less bulky imidazole in the compound cyanoimidazoylcobamide (CN(Im)Cbl).[191] One focus of some recent investigations is characterising the base-on/base-off equilibrium in which the axially coordinated DMBz- or Im-nucleotide is displaced by water and protonated.[192] In addition, the kinetics of axial ligand substitution in the case of vitamin B_{12} derivatives and model complexes have been examined in detail. These studies have benefitted in terms of mechanistic insight from application of high pressure techniques. An earlier lack of clarity in overall mechanistic understanding is being replaced by a more coherent understanding.[193] Mostly reports from the past few years will be highlighted.

The kinetics of substitution of coordinated water or methanol by three pyridine nucleophiles (pyridine itself and the 4-CN- and 4-NH_2-derivatives) in *trans*-$RCo(Hdmg)_2(H_2O)$ or *trans*-$RCo(Hdmg)_2(CH_3OH)$ ($R = C_6H_5CH_2$ or CF_3CH_2 and dmg = dimethylglyoxime), have been studied as a function of nucleophile concentration, temperature and pressure.[194] An analysis of the derived activation parameters led to the conclusion that the substitution mechanism varies with the R-substituent and solvent. Thus a limiting D mechanism was proposed when $R = C_6H_5CH_2$, reflecting a stronger donor property than when the substituent is CF_3CH_2 for which case an I_d mechanism was indicated for water substitution. The mechanism also varies in that the trend in $\Delta V^{\neq}$ values depended on the basicity of the nucleophile with progressively increasing positive $\Delta V^{\neq}$ values (4-CN- > H- > 4-NH_2-). An extension to this study used a wide range of different entering nucleophiles to displace the axial ligand in *trans*-[$Co(Hdmg)_2(R)S$] with R = Me and $PhCH_2$ and S = H_2O or CH_3OH, in order to determine the role of the nucleophilicity of the entering ligand and the nature of R on the reactivity of the Co(III) centre.[195] The entering ligands were imidazole, pyrazole, 1,2,4-triazole, *N*-acetylimidazole, 5-chloro-1-methylimidazole, NO_2^-, Ph_3P, Ph_3As and Ph_3Sb. The kinetics of substitution for all except the last two ligands showed through the absence of an intercept in plots of pseudo-first-order rate constants versus excess nucleophile concentration that a reverse or parallel reaction does not contribute. The presence of a significant intercept for corresponding plots for the last two ligands indicated that a reverse solvolysis reaction is significant in those substitution reactions. The forward second-order rate constants did not depend markedly on the ligand but the effect of solvent (H_2O or CH_3OH) was not insignificant. However, the character of the organic-R group has a strong influence on the lability of the system. From this study together with results from other studies, the order of the kinetic *trans* effect is $Et > PhCH_2 > Me > CH_2Cl > CF_3CH_2$, according to the donor properties of the organic group. The absence of a marked dependence on nucleophile of the substitution reaction rates is normally suggestive of a similar and

dissociative mechanism. An excellent isokinetic relationship obtained from the thermal activation parameters tends to confirm the former suggestion, while the values of the activation volumes support a dissociative interchange mechanism, since typical values were between $+3$ and $+7\,cm^3\,mol^{-1}$. In the case of substitution of MeOH by Ph_3As in *trans*-[$Co(Hdmg)_2(Me)MeOH$] the dependence on pressure of the rate constant for the reverse reaction (substitution of Ph_3As by MeOH) could be obtained leading to a volume of activation of $+15.9\,cm^3\,mol^{-1}$. For the forward direction the value of $\Delta V^{\neq}$ was determined to be $+10.6\,cm^3\,mol^{-1}$. These results permitted the drawing of a volume profile for the reaction (Fig. 10).

Obviously the reaction volume is negative. These volumes of activation were clearly much larger than those just cited above for other substituting ligands and would normally be thought to suggest the operation of a limiting D mechanism. The large value of $\Delta V^{\neq}$ for the reverse reaction was accounted for on the basis of the large partial molar volume of the leaving ligand Ph_3As. If the forward reaction actually proceeds by an I_d mechanism, the experimental volume of activation contains a term for the volume change for precursor formation as well as one for the interchange step itself. Thus the respective components are both unknown and thus complicating interpretation limiting any further detail to be introduced to the volume profile, and leaving the mechanism assignment less than unequivocal.

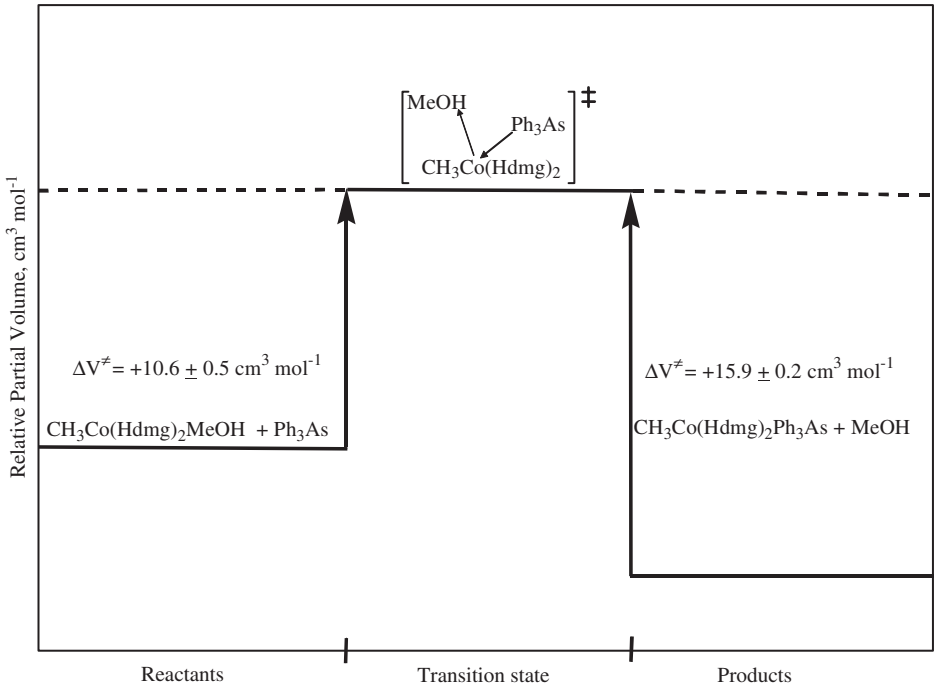

Fig. 10 Volume profile for the reversible reaction: *trans*-[$Co(Hdmg)_2(CH_3)MeOH$] + Ph_3As ⇄ *trans*-[$Co(Hdmg)(CH_3)AsPh_3$] + MeOH

The equilibria between the five- and six-coordinate species and possible adduct formation in Co(III)-corrinoids,[196] and the thermodynamic and kinetic properties of the base-on/base-off equilibration of alkyl cobalamins have been investigated.[197] In a closely related study the kinetics and thermodynamics of the corresponding equilibria and of the cyanation reaction in alkyl-13-epicobalamins have been examined.[198] In the first of these reports the pressure dependence of the UV/visible spectra of the five-coordinate (yellow)/six-coordinate (red) equilibrium for both methylcobalamin and vinylcobinamide was obtained.[196] Water is the additional ligand that gives rise to the five- to six-coordinate species conversion. The reaction volume could be obtained. It was identical for both equilibria ($\Delta V = -12.5 \pm 1.2$ and $-12.5 \pm 1.0\,cm^3\,mol^{-1}$ for the methyl and vinyl complexes, respectively). It was also remarkably close to the numerical value of –13 or $+13\,cm^3\,mol^{-1}$ advocated and generally accepted for limiting A or D mechanisms for the displacement of a water molecule.[199] Experiments with vinylcobinamide (five-coordinate) and dicyanocobinamide (six-coordinate) showed that adducts were formed with a selection of various added solutes, consistent with their places in the lyotropic series. It was suggested that these solute species are probably located in the hydrophobic cylinder surrounding the cobalt ion. The second report describes a study of the influence of the electronic nature of X on the base-on/base-off equilibration of a series of alkylcobalamins (XCbl). This is in effect a probe of the characteristic equilibrium property of cobalamins in which the axially coordinated DMBz is displaced by a water molecule (the base-off form) and protonated (Scheme 3).

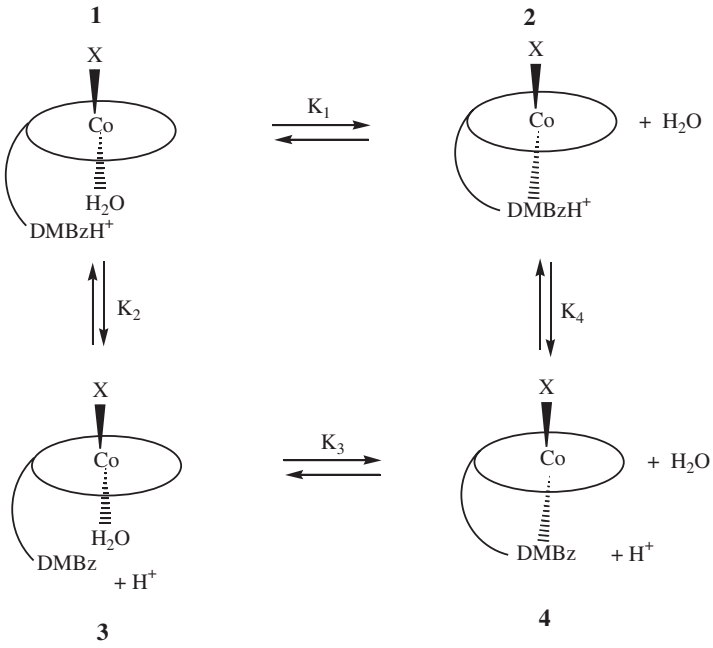

Scheme 3.

A combination of equilibrium and kinetic measurements as a function of temperature, pressure and acid concentration was analysed and indicated that the base-off form of different XCbl species can possess different coordination. AdoCbl and ethylcobalamin are mainly five-coordinate, whereas the CF_3-, CN- and H_2O-cobalamins have little base-off form and exist mainly as six-coordinate species. When $X = CH_3$, CH_2Br or CH_2CF_3 there is an equilibrium mixture of the five- and six-coordinate species. Evidence for an acid-catalysed dechelation (of DMBz) pathway was provided. Two derivatives ($NCCH_2$ and CN^-) of the epimer obtained by epimerisation at C13, in which the e-propionamide side chain adopts an upwardly axial configuration, have been the subject of an extensive study of the cyanation reaction.[198] From results obtained by varying the cyanide concentration, temperature and pressure, it was clear that epimerisation has a sensitive influence on the kinetics of displacement of the DMBz moiety, first by water and then by the cyanide ion. The rate of substitution was reduced compared with an alkylcobalamin. Displacement of DMBz at high cyanide concentration showed saturation kinetics, and the activation parameters, $\Delta S^{\neq}$ and $\Delta V^{\neq}$ for the limiting rate constant are $+77 \pm 4$ and $+82 \pm 4\,J\,mol^{-1}\,K^{-1}$, and $+13.3 \pm 1.0$ and $+14.8 \pm 1.2\,cm^3\,mol^{-1}$ for the $NCCH_2$ and CN^- epimers, respectively. These values were interpreted as evidence for a limiting D mechanism.

On the basis of significantly positive entropies and volumes of activation a limiting D mechanism was also proposed for the kinetics of displacement of DMBz by CN^- in XCbl where $X = \beta$-$NCCH_2$ or CN^-.[200] In these systems saturation kinetics were also observed at high cyanide ion concentrations. An overall appraisal of mechanistic features for these reactions was included as part of a reinvestigation into some of the apparent ambiguities in the literature. Further attempts to establish a consistent, comprehensive view of substitution reactions of Co(III) compounds that have analogy with the more direct bio-relevant compounds involved studying the kinetics of substitution reactions of various cobaloximes.[201] The kinetics of axial water substitution by cysteine in six different cobaloximes (*trans*-$RCo(Hdmg)_2(H_2O)$ with R = cyclo-C_5H_9, CH_3CH_2, CH_3, $C_6H_5CH_2$, C_6H_5 and CF_3CH_2) in aqueous solution, have been investigated. While five-coordinate species have been inferred from results of studies on coenzyme B_{12} in aqueous medium and on alkylcobaloximes in non-coordinating solvents, the evidence, largely on the basis of the magnitude of $\Delta V^{\neq}$, was that the mechanism is dissociative interchange, and implying the absence of five-coordinate species. The absence of a linear isokinetic plot suggested mechanistic variation and since the value obtained for $\Delta V^{\neq}$ for the CF_3CH_2 derivative was $0 \pm 1\,cm^3\ mol^{-1}$, it was concluded that an interchange mechanism operated in this case. It could also be concluded that the activation parameters are influenced by a combination of electronic and steric factors.

A perspective report emphasised the key role of the application of pressure in kinetic studies in bringing clarity to understanding the mechanism of substitution reactions of cobalamins.[193] The effect of various alkyl substituents in the *trans* position on the kinetic, thermodynamic and ground-state properties has been studied. Cobalamins featuring in these studies were cyanocobalamin (vitamin B_{12}), aquacobalamin and the complex formed when the cyano or water ligand is replaced

by the 3'-deoxyadenosyl moiety. This report recounted the use of $\Delta V^{\neq}$ in mechanistic diagnosis in this field. It also pointed out the role the effect of pressure on the UV/visible spectra of various cobalamins had in demonstrating the influence of the alkyl group in controlling the equilibrium between the five- and six-coordinate species, relating to these species potential participation in ligand substitution processes. It became clear that the nature of the cobalt–carbon bond and the character of the substituent supplying the carbon atom to that bond are vitally important. Applying UV/visible and ^{1}H NMR spectroscopies, including the determination of $\Delta V^{\neq}$ ($= -4.5\,cm^3\,mol^{-1}$) for the reaction of co-enzyme B_{12} with cyanide ion, indicated that the rate-determining step involves solvent assisted heterolytic cleavage of the cobalt–carbon bond.[202]

As noted above, the cobalamin analogue, in which DMBz has been replaced by imidazole (CN(Im)Cbl), has been prepared.[191] Experiments with this compound allow among other aspects a test of the effect of the steric bulk of the nucleotide base on the upward folding of the corrin ring. Furthermore, the properties of the system regarding substitution can be compared with those of similar systems. A systematic study of the kinetics of substitution of imidazole by cyanide was conducted, and the kinetics and thermodynamics of the acid–base chemistry of CN(Im)Cbl were investigated thoroughly. The cyanide ion substitutes imidazole in the α-position more slowly than it substitutes DMBz in cyanocobalamin. At high cyanide ion concentration saturation kinetics are exhibited yielding activation parameters, $\Delta H^{\neq} = 111 \pm 2\,kJ\,mol^{-1}$, $\Delta S^{\neq} = +97 \pm 6\,J\,mol^{-1}\,K^{-1}$ and $\Delta V^{\neq} = +9.3 \pm 0.3\,cm^3\,mol^{-1}$. The reverse reaction in which the coordinated cyanide is displaced by the dangling chelate is notably faster for CN(Im)Cbl, also consistent with an I_d mechanism. Spectrophotometric titrations led to the result that the $pK_{base-off}$ equilibrium is about one unit higher than the value determined earlier for cyanocobalamin. This has its origin in the different basicities of the nucleotide unit to which the Im and DMBz groups are attached. The kinetics of the base-on/base-off reaction indicated an acid catalysed pathway.

Contemporaneously, studies of ligand substitution of relevant organometallic model systems for coenzyme B_{12} were under investigation. As alluded to earlier, mechanistic clarity was sometimes absent and further studies on appropriate systems could usher in mechanistic transparency. Accordingly the kinetics of ligand substitution reactions of octahedral *trans*-$[Co(III)(en)_2(Me)H_2O]^{2+}$ (en = ethene 1,2-diamine) were studied.[203] The cyanide and imidazole (Im) nucleophiles (L) displaced the coordinated water molecule *trans* to the methyl group to form the six-coordinate complex *trans*-$[Co(en)_2(Me)L]$ (charge omitted). The reactions were rapid requiring employment of the s.f. method. Absorbance changes in the near UV and in the visible regions were used to monitor the substitution reactions spectrophotometrically. The kinetics of the reactions with cyanide ion and with ImH as a function of pressure gave rise to volumes of activation of +7 and $+4.7\,cm^3\,mol^{-1}$, respectively. These values were regarded as compatible with an I_d mechanism in which the entering ligand becomes weakly bound in the transition state. The stability constant for the reaction with cyanide was more than an order of magnitude higher than that for substitution of imidazole, a fact that made possible the determination of the

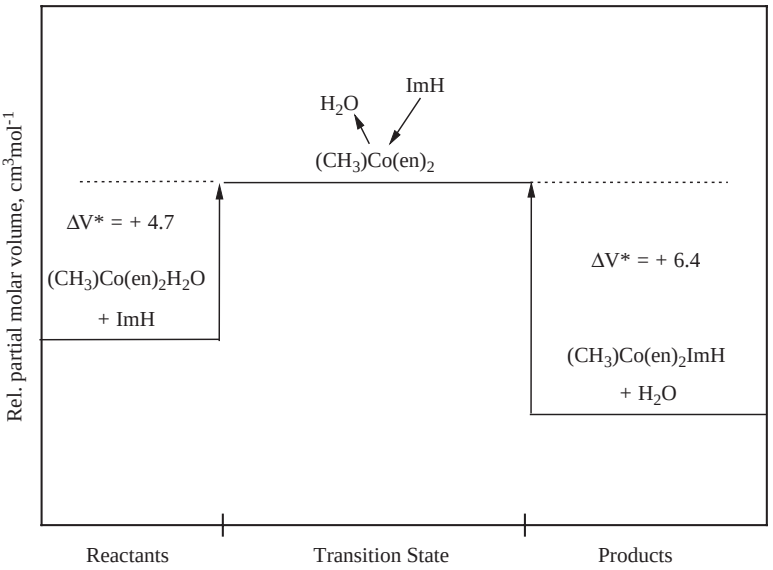

Fig. 11 Volume profile for the reaction of imidazole with *trans*-$[Co(en)_2(Me)H_2O]^{2+}$ in aqueous solution at 10 °C.

volume of activation for the reverse reaction in the latter case. The intercepts of plots of the observed first-order rate constants versus excess imidazole concentration at different pressures were utilised for that purpose. In turn the volume profile for the forward and reverse reactions of imidazole substitution could be constructed and is displayed in Fig. 11.

The dissociative nature of the reaction is evident from the magnitudes of the volumes of activation ($+6.4\,cm^3\,mol^{-1}$ for the substitution of ImH by H_2O). As in another report above the certainty of I_d character is clouded by the fact that the values of $\Delta V^{\neq}$ are composites of a precursor complex component and a contribution from the interchange step itself. A full D mechanism could not be categorically ruled out based on the properties of the system, and since the precursor formation step could contribute a negative volume term. Nevertheless a dissociative interchange mechanism was proposed as the more likely and a thorough discussion of mechanistic features, available at the time, of related systems was included.

In a following report equilibrium, kinetic and leaving group effects on ligand substitution in the same Co(III)-ethene 1,2-diamine complex and in the corresponding *trans*-$[Co(III)(en)_2(Me)NH_3]^{2+}$ were investigated.[204] The ligands employed were CN^-, SCN^-, N_3^- and NH_3, and these displace the coordinated water or ammonia molecules *trans* to the methyl group. The most important aspect of this report that is pertinent here is the reaction of NH_3 with the aqua complex, *trans*-$[Co(en)_2(Me)H_2O]^{2+}$, since kinetics experiments at elevated pressures were conducted. The kinetics results at ambient pressure established a second-order reaction, with the condition of NH_3 in excess, pseudo-first-order (k_{obs}) in practice. From the slope and intercept

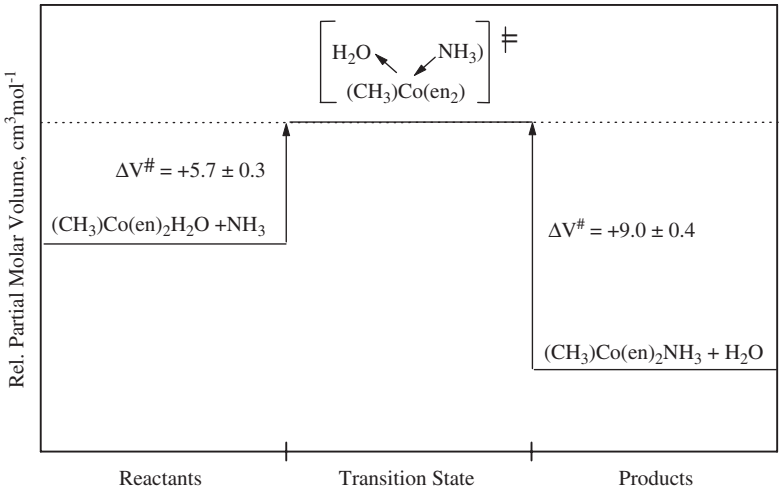

Fig. 12 Volume profile for the reaction of NH_3 with *trans*-$[Co(en)_2(Me)H_2O]^{2+}$ in aqueous solution at 5 °C.

of plots of k_{obs} versus $[NH_3]$ the rate constants of the forward and reverse reactions, respectively, could be acquired. Volumes of activation from the pressure dependence of kinetic parameters were $+5.7$ and $+9.0\,cm^3\,mol^{-1}$ for the substitution of H_2O, and the reverse aquation reaction, indicating a transition state of greater partial molar volume than reactant or product states. This is depicted in Fig. 12.

This volume profile is qualitatively similar to that in Fig. 11 and not very different quantitatively, indicating similarity in the mechanism, perhaps not unexpected for similar reactions. A potential advantage of the en model system, it was pointed out, was the two somewhat flexible chelate systems. It had been suggested that this property could be important for the biological activity of the coenzyme.[205] The substitution of NH_3 by SCN^-, N_3^- and CN^- in *trans*-$[Co(en)_2(Me)NH_3]^{2+}$ proceeded via the intermediate aqua complex such that aquation of the amine complex became the rate-determining step at high entering ligand concentration.

Rhodium and iridium

Substitution reactions of dimethylglyoximato complexes have also been studied for the transition metal second row analogue rhodium(III), specifically substitution of water in *trans*-$[Rh(Hdmg)_2R(H_2O)]$ where R is CH_3, CH_2Cl or CH_2CF_3.[206] These reactions had been studied earlier[207] at ambient pressure but a more definitive proposal for the mechanism was sought. The lability of the coordinated axial water molecule has been shown to be influenced by the nature of the R group and by the equatorial chelating ligands. The entering ligands were neutral (pyridine, thiourea (TU) or TMTU) or mono-anionic (I^-, SCN^- or N_3^-). It was established that the rate constant for the substitution reaction was not very sensitive to the nucleophilicity of the incoming ligand, and together with the values of the thermal activation parameters

suggested a dissociative interchange mechanism. Upon analysing the kinetics results, except for the iodide ion all incoming ligands provided no evidence of an observable back reaction. The dependence on pressure of the rate constants for the substitution reactions yielded positive values of the volume of activation for $R = CH_3$, py and TMTU as entering ligands, whereas the values for $R = CH_2Cl$ and CH_2CF_3 were negative (TU as the incoming ligand). The volume of activation for the aquation of the iodide complex species was also positive. The reason that the faster substitution reactions ($R = CH_3$) exhibit positive $\Delta V^{\neq}$ values while the slower reactions ($R = CH_2Cl$ or CH_2CF_3) proceeded with a rate acceleration with increasing pressure could have its origin in the *trans*-labilising effect on the Rh–O bond distance. For Rh–py complexes the bond lengths *trans* to the R group progressively decreases for $R = CH_3$, CH_2Cl, CH_2CF_3 and a parallel situation probably prevails for *trans*-$[Rh(Hdmg)_2R(H_2O)]$ species. Hence the mechanism is electronically tuned, changing from an I_d mechanism for the faster reactions to an I_a mechanism for the slower reactions. Other examples of substitution reactions in which a metal–carbon bond influences reactivity are covered in the section on platinum chemistry. A volume profile could be drawn for the reaction of the iodide ion and the reverse aquation reaction illustrating the increased volume of the transition state relative to reactant and product states (Fig. 13).

The more positive volume of activation ($+6.3\,cm^3\,mol^{-1}$) for the dissociative release of the iodide ion than for release of the water molecule ($+2.1\,cm^3\,mol^{-1}$) was considered to arise from the larger partial molar volume of the iodide ion and the reduction in electrostriction of the complex ion.

The lability of water molecules in the η^5-organometallic complexes $Cp^*Ir(H_2O)_3^{2+}$ and $Cp^*Rh(H_2O)_3^{2+}$ and the mechanism of water exchange with bulk solvent water molecules were discussed in the previous section.[159] A subsequent study in which the kinetics of substitution of a water molecule in these species by several ligands (L) at

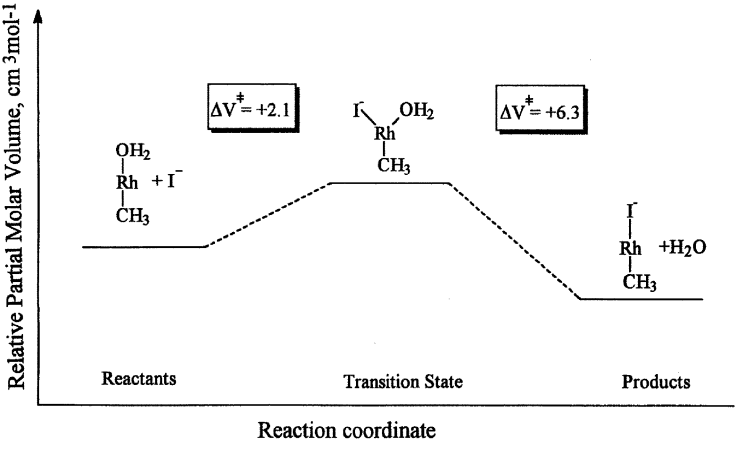

Fig. 13 Volume profile for the reaction of iodide ion with *trans*-$[Rh(Hdmg)_2Me(H_2O)]^{2+}$ in aqueous solution at 9 °C.

various concentrations, temperatures and pressures has brought insight into the mechanism of substitution and allowed the development of volume profiles.[208] The ligands were anionic (Cl^-, Br^-, I^-, SCN^-) or neutral (4-cyanopyridine, nicotinamide, pyridine, TU and dimethylsulphide (DMS)) which would allow the exploration of the significance, if any, of charge upon the entering ligand. The substitution reactions were monitored by s.f. spectrophotometry. Conditions for monitoring the kinetics could be selected since series of spectrophotometric, potentiometric and NMR pH titrations had been carried out to establish the species present in a range of conditions. For both anionic and neutral ligands the rhodium compound forms only mono-substituted complexes, $Cp^*Rh(H_2O)_2L^{2+/+}$ while both mono- and bisubstituted complexes are formed with the iridium compound when L is neutral. Stability constants that were determined were highest for two sulphur-containing neutral ligands. As noted earlier, coordination of the Cp^* ligand gives rise to extreme labilisation of the coordinated water relative to the corresponding hexa-aqua ions and this effect gives rise to rapid substitution reactions. The second-order rate constants for formation of the mono-substituted complexes are higher for the anionic ligands, but except for the SCN^- ligand range over little more than an order of magnitude, and are very similar for the rhodium and iridium species. A method of approach to determine the reaction mechanism involves correcting the second-order rate constant for outer-sphere complex formation and a statistical factor to yield the rate constant for the interchange (ligand for water) step. These rate constants were not highly dependent on the nature of L and were in the same general range as the rate constants for water exchange, thus suggesting an interchange mechanism of dissociative character. Although the second-order rate constants and the calculated interchange rate constants do not vary widely the variation of them was examined with respect to a scale of nucleophilicity for both the anionic and neutral ligands and also with the basicity of the pyridine ligands. The nucleophilicity discrimination factor was well below that found for typical associative mechanisms, and on this basis an associative mechanism of substitution could be excluded. Further mechanistic assignment could be inferred from the kinetic parameters derived from high pressure measurements. The volumes of activation for the forward substitution and reverse aquation reactions were determined, and thus the reaction volumes could be calculated and volume profiles developed for the mono-substitution process. In all cases the volume of the transition state was larger than that of the reactant state (triaqua species and the ground-state ligand), further supporting the proposal of a dissociative mode of activation. The reaction volumes for the charged ligands are positive since the anation reaction results in loss of electrostriction. The reverse (aquation) reaction is accompanied by charge creation, an increase in electrostriction, a volume change that surpasses the volume increase due to partial bond breakage since the volumes of activation are negative. It has also been noted that the volumes of activation in the forward direction are modest values. For example, when $L = Cl^-$ and Br^-, they are $+1.1$ and $+0.8\,cm^3\,mol^{-1}$ respectively, for the rhodium triaqua species, and that these could mask a volume contraction of the spectator water molecules around the small d^6 ion, that may occur as the transition state is reached. It was suggested further that the actual bond lengthening of the

M–OH_2 bond to reach a dissociative transition state is much smaller than would be the case for the ground-state labilisation arising from the effect of the presence of the Cp* moiety. Taken together these factors do not permit the exclusion of a limiting D mechanism. The volume profiles for reactions of chloride ion, bromide ion, 4-cyanopyridine (py-CN) and nicotinamide (py-nia) with $Cp^*Rh(H_2O)_3^{2+}$ are displayed in Fig. 14.

For the iridium compounds the volumes of activation for the anionic ligands are about $+4\,cm^3\,mol^{-1}$. When the ligands are neutral the reaction volumes are small and sometimes negative and sometimes positive (an exchange of one neutral ligand for another and absence of changes in electrostriction). But the volume of the transition state is always larger than that of the reactants or products, indicative of a dissociative mechanism. The sensitivity of the kinetic parameters to the nucleophilicity of the sulphur-containing ligands for the reaction with the iridium compound raised speculation that an associative activation mode occurs. However, the activation volume for the complex-formation reaction of SCN^- with $Cp^*Ir(H_2O)_3^{2+}$ was clearly positive, further supporting an I_d or even a D mechanism. Substitution of a second water molecule by a neutral ligand is slower by an order of magnitude indicating that the labilisation effect of Cp* is markedly reduced.

Subsequently a study of the kinetics and mechanism of water substitution on half-sandwich iridium(III) aqua cations, $Cp^*Ir(A\text{-}B)(H_2O)^{2+/+}$ (A-B = bidentate N,N or N,O ligand) by several monodentate ligands was reported.[209] The A-B ligands included the D/L proline anion, the picolinic acid anion, 2,2'-bipyridine and 1,10-phenanthroline. Monodentate entering ligands included pyridine, TU, DMS and the anions Br^-, I^-, SCN^-, N_3^- and NO_2^-. Second-order rate constants for substitution by pyridine in several aqua cations were sensitive to the nature of A-B with a range of values of over 500, with the singly charged cations reacting more rapidly than the doubly charged ones. Charge was found to be not the only rate-determining factor. When experimentally accessible the rate of the reverse, aquation reaction was not dramatically affected by the nature of A-B. Water substitution by TU and DMS at various cations is much faster for the singly charged cations than it is when A-B = phen. For a given cation the magnitude of the substitution rate constants follows the order TU > DMS > py. In general water substitution by anionic ligands is faster than it is for neutral ligands. Analysis of the data showed a rather weak dependence on the nucleophilicity of the entering ligand. The activation parameters obtained for the reactions of three monoaqua cations with TU were reasonably decisive in terms of mechanistic assignment. Specifically the modestly positive volumes of activation ($+2.3$ to $+7.4\,cm^3\,mol^{-1}$) point to a dissociatively controlled interchange mechanism. It was suggested that the increase in these values corresponded to an increase in the substitution rate constants; this may point to progressively more dissociative character. However, these values of $\Delta V^{\neq}$ are in line with those for the water substitution by ligands on the triaqua complex, $Cp^*Ir(H_2O)_3^{2+}$, also assigned an I_d mechanism. These reactions are all several orders of magnitude faster than water exchange and ligand substitution on hexa-aqua iridium(III) where the mechanism was assigned I_a based on the negative volumes of activation. However, the pronounced labilisation induced by the Cp* moiety stimulates a cautionary

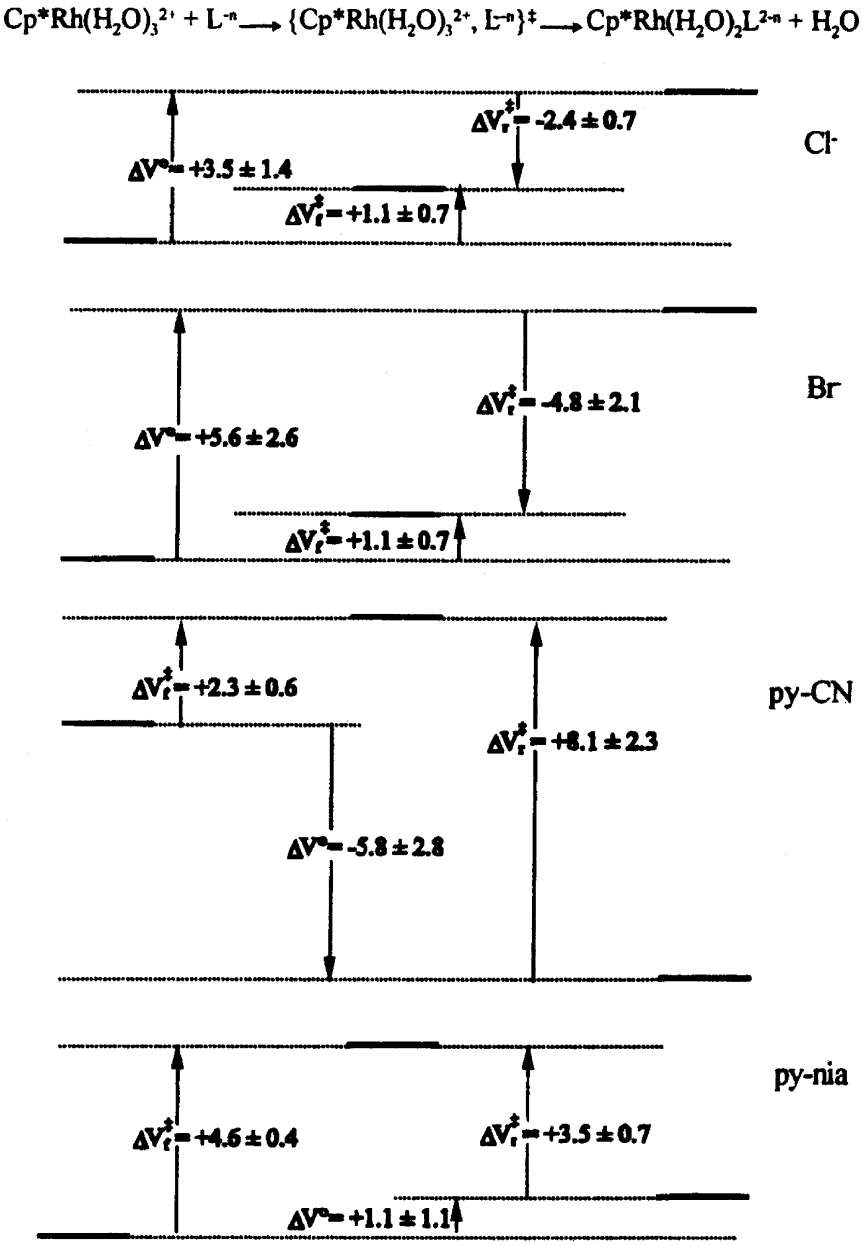

Fig. 14 Volume profiles for reactions of chloride ion, bromide ion, 4-cyanopyridine (py-CN) and nicotinamide (py-nia) with $Cp^*Rh(H_2O)_3^{2+}$ in aqueous solution at 25 °C.

note that since, as a consequence, ground-state lengthening of the Ir–OH_2 bond would be expected, then a lesser degree of bond breaking upon reaching the transition state would ensue in a substitution reaction. Hence a modest $\Delta V^{\neq}$ alone does not entirely rule out a D mechanism.

Tungsten

This section also includes reactions of organomolybdenum systems where these are related to comparable reactions of tungsten-based compounds. Several studies of substitution kinetics of Group 6 metal hexacarbonyls have shown that the reactions normally follow a two-term rate law representing parallel reaction pathways, one of which involves the incoming ligand in the transition state and the other does not.[210] The pathway involving associative attack provides the dominant path for Mo or W compounds.[211] Many pentacarbonyl derivatives [$M(CO)_5(L)$], including [$Mo(CO)_5$(py)], [$Mo(CO)_5$(4Mepy)], [$Mo(CO)_5$(4CNpy)] and [$W(CO)_5$(py)] also exhibited kinetic characteristics of a limiting D mechanism.[212,213] However, activation volumes for reactions of this type were smaller than might be expected, being in the range of 0 to $+5\,cm^3\,mol^{-1}$.[214] Substitution at tetracarbonyl derivatives [$Mo(CO)_4(L)_2$] and [$Mo(CO)_4$(LL)] (L = py, or 4Mepy, LL = bpy, phen or dab) was also considered to take place by a D mechanism, despite the small positive values of the volumes of activation. The entropies of activation were distinctly positive. The first-order rate constants were independent of the concentration of the entering bidentate ligand, a result that means either bond cleavage to produce a five-coordinate intermediate or ring closure of a ring opened product species was rate determining. Therefore all the evidence except the small positive volumes of activation pointed to a D mechanism. The explanation resided in two possibilities. It was noted that the rate of the rate-determining step was strongly dependent on solvent polarity in the series hexane, toluene, 1,2-dichloroethane. Solvent polarity increases with increasing pressure and this was argued to cause an increase in rate constant with pressure that reduces the actual rate retardation intrinsic to the reaction. This results in a volume of activation of $5\,cm^3\,mol^{-1}$ lower than it otherwise would be in the absence of the effect of pressure on solvent polarity. Alternatively, it was proposed that an internal rearragement of the five-coordinate intermediate might occur resulting in a volume collapse that is smaller than expected for a D mechanism.

In order to further extend this work to similar tungsten compounds, a study of the kinetics of substitution at *cis*-tetracarbonyl bis(4-methylpyridine)tungsten(0) in toluene was undertaken.[215] Incoming ligands employed were bpy, phen, 5-NO_2phen and bipym = 2,2′-bipyrimidine, and they were present in excess concentration over that of the tungsten compound. First-order rate constants were obtained from monitoring the appearance of [$W(CO)_4$(LL)] spectrophotometrically. Analysis of the dependence of rate constants on nucleophile concentration and on the rate retardation pattern when the leaving group was added to the reacting system led to the conclusion that a limiting D mechanism was in operation. Further kinetics experiments with phen as the entering ligand and applying pressure gave rise to an activation volume of $+8\,cm^3\,mol^{-1}$, thus supporting firmly a limiting dissociative mechanism.

Rhenium

Following the report cited above[165] that covered primarily the water exchange kinetics on *fac*-$[(CO)_3Re(H_2O)_3]^+$, an extensive study of the kinetics of ligand substitution of coordinated water by N- and S-donor ligands (pyrazine (pyz), tetrahydrothiophene (THT) and dimethylsulphide (DMS)) has been described.[216] To avoid complications that would ensue if the monohydroxy species of the tricarbonyl rhenium species were present, appropriate conditions of a range of acidity were chosen. The kinetics measurements were to be conducted at elevated pressures, therefore experiments (spectrophotometry and ^1H NMR spectroscopy) were performed to assess the effect of pressure upon the acidity constant of pyrazine. Depending on the ligand concentration the product of reaction was the monocomplex $[(CO)_3Re(H_2O)_2(pyz)]$ or in addition the binuclear complex $[(CO)_3(H_2O)_2Re(\mu\text{-pyz})Re(H_2O)_2(CO)_3]^{2+}$. The kinetics of the substitution reaction at variable pressure were studied under conditions where only one of the water molecules was substituted. Volumes of activation of $+5.4$ and $+7.9\,cm^3\,mol^{-1}$ were derived for the forward and reverse reactions, respectively. Corresponding experiments for substitution of water by THT yielded volumes of comparable magnitude but of opposite sign (-6.6 and $-6.2\,cm^3\,mol^{-1}$ for the forward and reverse reactions, respectively). All three water molecules of $[(CO)_3Re(H_2O)_3]^+$ can be displaced by DMS, and the equilibria and kinetics parameters have been obtained for each of the successive substitution reactions. Remarkably from the variable-pressure kinetics measurements the volumes of activation for each step have been derived enabling the development of a volume profile containing the volume change information for each reaction step. In all cases the volumes of activation were negative quantities (Fig. 15).

An initial attempt to assign the reaction mechanism for these complex-formation reactions was based on consideration of the nucleophilicity of the incoming ligands, three in this study and others reported earlier,[165] in terms of basicity and polarisability relative to the calculated interchange rate constant. It was debated whether the difference in solvation of the ligands (pyz is hydrophilic and THT and DMS are more hydrophobic) yielded a significant contribution to the volumes of activation. It was concluded from the reaction volumes that this was not a prominent factor, and mechanistic enlightenment emerged from deciding that the substitution could operate in dual modes. With hard nucleophiles, such as O- and N-donors an I_d mechanism prevails, whereas the affinity of soft S-nucleophiles for the soft rhenium centre leads these ligands to become part of an associative transition state, according to an I_a mechanism. The successive substitutions of the three DMS ligands show a progressive decrease in the rate constant, a trend related to increased steric hindrance on the MC. This is confirmation of an associatively activated substitution. At first sight the progressive increase in the equilibrium constant for each successive DMS ligand appears contradictory to the kinetics trend. Upon analysing data for formation of the corresponding TU complexes it was reasoned that the progressively increasing affinity arose from a softening of the MC by coordinated ligand(s).[220]

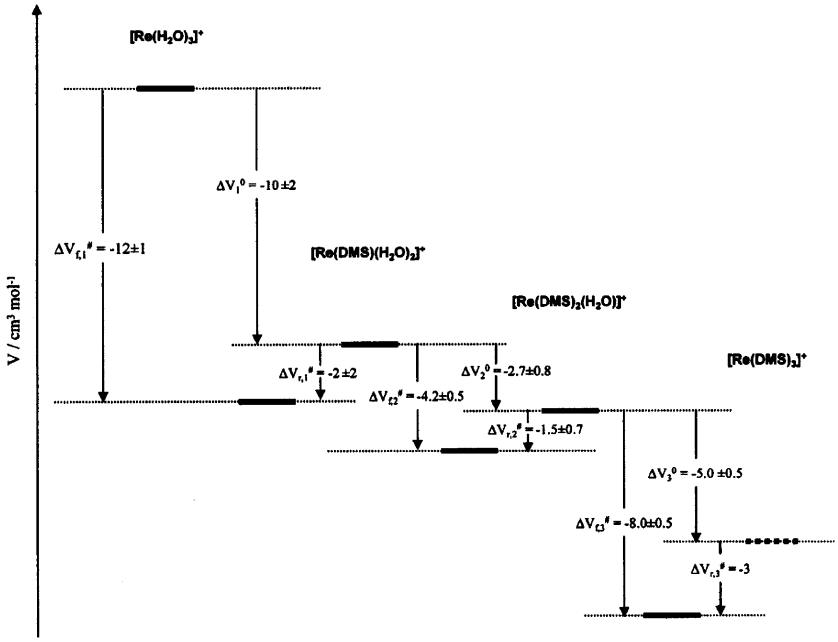

Fig. 15 Volume profile for the reaction of DMS with $[(CO)_3Re(H_2O)_3]^+$ in aqueous solution at 25 °C.

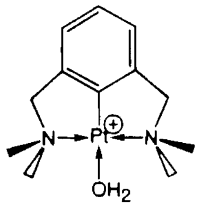

Scheme 4.

Platinum

Substitution reactions of platinum(II) complexes containing one or more metal carbon bond(s) have a long history.[217] Interest in such complexes and their reactivity is associated with their function as catalysts in synthetic procedures and in environmental applications. One important characteristic is the kinetic *trans* effect; this is ascribed to the labilisation of a *trans*-positioned group caused by a C-bonded ligand,[218] typically alkyl or aryl. In a mechanistic study in which kinetics measurements at elevated pressures were employed, cyclometallated Pt(II) complexes were used.[219] The complex shown in Scheme 4 is water-soluble permitting the kinetics of substitution by a wide range of nucleophiles to be studied in aqueous solution.

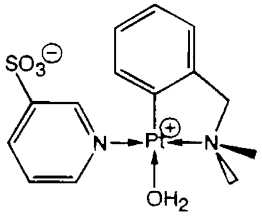

Scheme 5.

The reactions were rapid requiring s.f. techniques. Large negative values of the entropy and volume of activation were obtained for the reaction of TMTU with the cyclometallated compound, and were interpreted to indicate an associative substitution mechanism. The same conclusion had been reached in an earlier study of the substitution of the water molecule from the zwitterionic-Pt compound as shown in Scheme 5. [220]

The marked increase in lability of the former compound relative to the zwitterionic compound can be attributed to the σ-donicity of the second chelating dimethylamino group and/or the increased chelation effect of the terdentate ligand.

Some uncertainty arose regarding the mechanism of substitution reactions of complexes of the type *cis*-[PtR_2S_2] with R = Me, Ph and S = DMSO, thioether.[221] Substitution reactions for this type of Pt(II) complex have usually followed an associative pathway. However, convincing evidence for a dissociative mechanism was presented for reactions in which bidentate ligands functioned as the entering nucleophile. It was proposed that mechanistic clarity might follow if monodentate ligands were employed so that the successive substitution of the two labile solvent molecules could be monitored kinetically. Accordingly a kinetics study of the substitution reaction in which the pyridine ligand replaces DMSO in *cis*-[$PtMe_2(DMSO)_2$] was undertaken. The solvent was toluene and this allowed a systematic variation of the concentration of the leaving group by addition of DMSO. Analysis of the results revealed that in forming the monopyridine complex two reaction paths, one dissociative and one associative, were followed. The former was suppressed if the concentration of added DMSO was more than 40-fold in excess. The parallel path was supported in its associative nature by the volume of activation of $-11.4\,cm^3\,mol^{-1}$, at high saturating pyridine concentration. This value contains the volume change for the formation of the precursor complex and the substitution step itself, where substitution is the dominant contributor. Study of the entry of the second pyridine molecule indicated two parallel paths leading to the product. One involves the complete dissociation of the second DMSO molecule before the pyridine molecule binds and the second involves a synchronous substitution of pyridine for DMSO. The volume of activation determined for the formation of the bispyridine complex comprises contributions from both of these processes. For the former of the two steps the volume of activation must be distinctly positive, whereas for the latter step an associative activation mode can be expected contributing a negative component to the volume of activation. Therefore the measured value of $+1.9\,cm^3\,mol^{-1}$

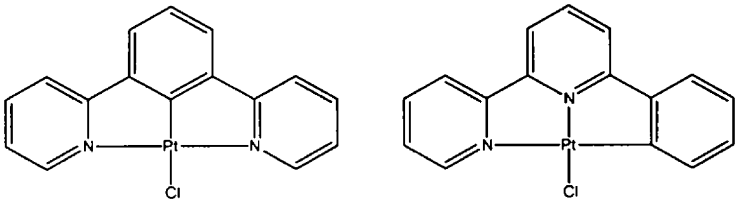

Scheme 6.

was said to represent a minimum value. The results were considered in terms of other reactions of Pt(II) complexes containing two *cis* metal–carbon bonds and also considering the *trans* effect on the lability of ligands. However, at the time of writing it was opined that the substitution mechanism of such complexes was not yet fully understood.

Since these earlier studies demonstrated the mechanistic diagnostic value of knowledge of the volume of activation, a wide-ranging study of several cyclometallated compounds analogues of platinum(II) terpyridine (terpy = 2,2′:6′,2″-terpyridine)/chloro complexes has been undertaken.[222] Structures were determined by crystallographic methods and reactivities were investigated by ligand substitution kinetics measurements. TU, DMTU and TMTU were employed to displace the chloro ligand from [Pt(N–N–C)Cl] and [Pt(N–C–N)Cl] where N–N–CH is 6-phenyl-2,2′-bipyridine and N–CH–N is 1,3-di(2-pyridyl)benzene. The complexes are illustrated in Scheme 6.

One principal objective in this and related studies is to examine the relationship between σ-donor and π-acceptor effects in Pt(II) chemistry. A much higher reactivity observed for the N–C–N compound was reflected in a $20\,kJ\,mol^{-1}$ lower enthalpy of activation than for the N–N–C compound. This was explained by citing the influence of the *trans* phenyl group in destabilising the ground state, thus facilitating cleavage of the leaving group to Pt bond. For the N–N–C compound the activation enthalpy trend was TMTU < DMTU ≈ TU whereas for the N–C–N compound the relationship was TMTU < DMTU < TU, a sequence not in accord with expected reactivity trends. It was concluded that differences in entropies of activation were responsible for the observed steric retardations. For each of the three TU entering ligands negative volumes of activation were obtained for both platinum compounds. A volume contraction occurs upon forming the transition state arising from the bond formation by the entering nucleophile, although this is partly offset by the geometry changing from square planar to trigonal bipyramidal. In the case of the N–C–N compound the platinum–ligand bonds of the entering and leaving ligands are longer owing to the *trans* influence. Thus the observed $\Delta V^{\neq}$ values were less negative for reaction of the N–C–N compound than for the reaction of the N–N–C compound reaction where the corresponding bonds are shorter. From these results and abundant literature on substitution reactions at Pt(II) it was concluded that the magnitude and direction of the *cis* effect (as compared to the *trans* effect of the same ligand) depend on the σ-donor strength, π-acceptor ability

and the steric property of the *cis* ligand. The relative magnitudes of these factors and their subtle interplay have consequences for reactivities of these and related compounds.

In a related investigation the roles of chelate substituents and the *cis* effect on the rate of ligand substitution at (Pt(N–N–N) and Pt(N–N–C) centres were explored in methanol solution.[223] The terdentate ligands were terpyridine, 4′-Ph-terpy, 4′-(2‴-CF_3–Ph)-terpy and 4′-(2‴-CF_3–Ph)-6-2,2′-bpy and the remaining position was occupied by a chloro ligand (Scheme 7).

The rates of substitution of the latter ligand by TU, DMTU and TMTU were followed as a function of nucleophile concentration, temperature and pressure by s.f. spectrophotometry. The reaction was first order in both platinum complex and nucleophile concentrations. From the form of the rate law and the negative entropies and volumes of activation it was concluded that the mechanism is an associatively activated substitution. It prevailed that substitution in the terpy parent ligand did not affect significantly the kinetic parameters. The reaction was slower when a carbon σ-donor was in the *cis* position than when an N σ-donor occupies this position, indicating a different situation from the effect of a Pt–C bond in the *trans* position.

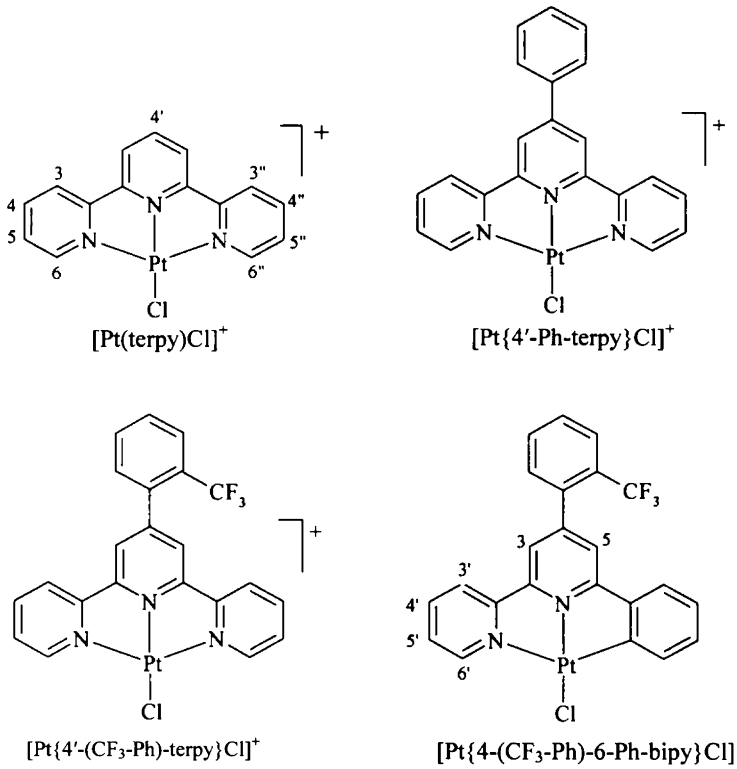

Scheme 7.

The subject of homogeneous hydrocarbon C–H bond activation and functionalisation with platinum compounds has been authoritatively reviewed, and the review contains literature reports up to and including most of 2003.[224] A noteworthy sample report from this account presented evidence for an associative mechanism for benzene substitution at a platinum(II) centre.[225] The mechanism specifically addressed was that for the first key step in the multistep catalytic cycle of a Shilov-type system.[226] The reaction of the platinum(II) methyl cation $[(N–N)Pt(CH_3)(solv)]^+$ (N–N = ArN = C(Me)C(Me) = NAr, Ar = 2,6-$(CH_3)_2C_6H_3$, solv = H_2O or TFE = CF_3CH_2OH), with benzene in TFE/H_2O mixtures afforded the platinum(II) phenyl cation $[(N–N)Pt(C_6H_5)(solv)]^+$. To resolve the mechanism of the mode of entry of benzene into the coordination sphere a high pressure kinetics study was undertaken, monitoring UV/visible absorbance changes. The reaction was accelerated by pressure yielding a negative volume of activation. This parameter contains a reaction volume term for displacement of the coordinated water by TFE and a second term for the volume of activation for the activation of benzene by the TFE–solvento complex. The latter term could be determined to be $-9.5\,cm^3\,mol^{-1}$, which together with the negative entropy of activation clearly supports the operation of an associative mechanism. A recent study provided mechanistic information on reductive elimination from cationic platinum(IV) complexes to form carbon–carbon bonds, and this is treated later in the appropriate section.

During a study of substitution reactions of dimethylhalo-platinum(IV) complexes in acetone, an intramolecular isomerisation was detected in two cases.[227] The complexes were *cis*-(CH_3/$S(CH_3)_2$) arranged dimethylhalo-platinum(IV) species in which PPh_3 substitutes the $S(CH_3)_2$ group. The isomerisation was monitored at low temperatures by ^1H and ^{31}P NMR spectroscopies and could be described as a very energetically demanding turnstile twist-type reorganisation of the molecule following a significant degree of dissociation of the ligand. The activation parameters were $\Delta H^{\neq}$ of about $100\,kJ\,mol^{-1}$, $\Delta S^{\neq} = +88\,J\,mol^{-1}\,K^{-1}$ and $\Delta V^{\neq} = +15$ and $+20\,cm^3\,mol^{-1}$. A substantial increase in volume in forming the transition state was therefore indicated. In other cases *mer*/*fac* ratio dispositions introduced complexities.

ISOMERISATION REACTIONS

As part of a comprehensive project aiming to develop metal-based reagents for the functionalisation of fluorocarbons, an unusual η^2-vinyl isomerisation process was uncovered.[228] As little information was available on the nature of the isomerisation of the tungsten(II)-based species, a detailed kinetics study was conducted.[229] The reaction under consideration is shown in Scheme 8.

The kinetics could be monitored by IR and UV/visible spectroscopies in toluene as solvent. In the absence of added ligand the loss of reactant was first order, with activation parameters, $\Delta H^{\neq} = 124\,kJ\,mol^{-1}$, $\Delta S^{\neq} = +48\,J\,mol^{-1}\,K^{-1}$ and $\Delta V^{\neq} = +15.6\,cm^3\,mol^{-1}$ at 60 °C. These parameters were interpreted as being in accord with a limiting dissociative mechanism. The dissociation of CO is rate determining, followed by rapid isomerisation and recombination of CO. The reaction was also

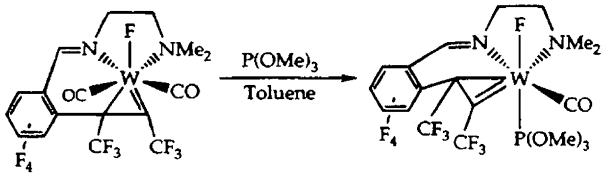

Scheme 8.

studied in the presence of ligands (CO or $P(OMe)_3$) serving to promote the rate of reaction. Carbon monoxide enhances the reaction rate which depends on p(CO). The enthalpy of activation is about $25\,kJ\,mol^{-1}$ lower than the non-promoted reaction value, suggesting formation of a transition state with less bond breaking and some bond formation. The volume of activation is a small positive value ($+3.9\,cm^3\,mol^{-1}$) which implied an intramolecular process with volume changes in an interchange mechanism almost mutually cancelling. The near zero entropy of activation was consistent with this proposal. Thus the attack by CO and subsequent release of coordinated CO were seen as a concerted process. In the case of the $P(OMe)_3$-promoted reaction, carried out in toluene at temperatures at or about room temperature, the product contains the $P(OMe)_3$ ligand coordinated to W *trans* to the coordinated fluorine and with the inserted acetylene moiety *cis* to the fluorine. The reaction is first order in the tungsten complex concentration and showed saturation kinetics at high [$P(OMe)_3$], a fact together with other evidence that indicated formation of an adduct before a step involving loss of CO. The activation parameters were obtained at both low and high ligand concentrations. This permitted extraction of both the volume change for formation of the precursor complex ($+10\,cm^3\,mol^{-1}$) and that for the rate-determining step ($+5.5\,cm^3\,mol^{-1}$). The former value was interpreted as arising from major rearrangement of the complex upon binding of $P(OMe)_3$, partially reflecting possibly the actual isomerisation process, for instance involving an η^2 to η^1 slippage. It was also acknowledged that desolvation of the entering ligand could make a contribution to the volume increase. The small value of the volume of activation for the rate-determining step is typical of values for a dissociative interchange ligand substitution mechanism (I_d). Steric congestion around the metal atom as a consequence of more W–CO bond lengthening than W–P bond shortening as the rigid η^3-[C,N,N'] imine chelate ligand and the 2-vinyl group rearranged upon forming the transition state was the explanatory argument.

REDOX REACTIONS

Cobalt complexes with 14-membered tetraazamacrocyclic ligands have been investigated and successfully employed as catalysts for electrochemical and photochemical reduction of CO_2 and H_2O.[230] One such complex low-spin $[Co(I)HMD]^+$ (HMD = 5,7,7,12,14,14,-hexamethyl-1,4,8,11-tetraazacyclotetradeca-4,11-diene (hexamethylcyclam)) reacts with CO_2 in H_2O and in CH_3CN to form the *N-rac*-$[CoHMD(CO_2)]^+$ species which is sufficiently stable in dry CH_3CN and in a CO_2

atmosphere to study the equilibrium between a purple five-coordinate form at room temperature and a yellow six-coordinate form at low temperatures:[231]

$$[\mathrm{CoHMD(CO_2)}]^+ + \mathrm{CH_3CN} \rightleftarrows [\mathrm{CoHMD(CO_2)(CH_3CN)}]^+ \quad (15)$$

The equilibrium system, in acetonitrile, has been studied by a variety of spectroscopic techniques, and after analysis it was concluded that the product could be interpreted as a Co(III)-CO_2 carboxylate complex,[232] meaning that the bound CO_2 has been reduced by a two electron transfer by the $[\mathrm{Co(I)HMD}]^+$ species. An additional perspective on the nature of this equilibrium was sought by application of pressure upon it in a pill-box cell, with spectrophotometric monitoring.[233] Previously, the entropy of reaction at 15 °C had been determined. It was about $-110\,\mathrm{J\,mol^{-1}\,K^{-1}}$, in accord with a highly ordered and compact six-coordinate species.[234] Therefore, a markedly negative reaction volume could be predicted and was found; it was $-17.7\,\mathrm{cm^3\,mol^{-1}}$ at the same temperature in CH_3CN. It was argued that this can be a result of both a volume reduction upon addition of a solvent molecule, but that a larger contribution arises from the volume collapse due to the intramolecular electron transfer process accompanied by a shortening of the Co–CO_2 bond length, and an increase in electrostriction. Bond length reduction had been observed earlier in XANES and EXFAS studies.[231] Knowledge of the temperature and pressure dependence of this equilibrium provides an opportunity that allows, through their variation, precise tuning of the electron density on the Co and CO_2 sites.

Determining the mechanism of self-exchange reactions of metallocenes is a considerable challenge.[235] Clarity has been brought to this subject following an investigation of the reaction between $[\eta^5\text{-}C_5(CH_3)_5)_2Fe^+]$ ($DmFc^+$) and $[\eta^5\text{-}C_5(CH_3)_5)_2Fe]$ ($DmFc^0$) in deuterated acetone, dichloromethane and acetonitrile.[236] The counter-ions were either hexafluorophosphate or tetrafluoroborate. Values of the exchange rate constant, k_{ex}, were obtained from ^{1}H NMR spectroscopic measurements at ambient and elevated pressures. Only very marginal effects of ion pairing were encountered. Values of $\Delta V^{\neq}$ were distinctly negative: –8.5 to $-8.9\,\mathrm{cm^3\,mol^{-1}}$ in $(CD_3)_2CO$ and –6.3 to $-7.2\,\mathrm{cm^3\,mol^{-1}}$ in CD_2Cl_2. Fully quantitative results for the self-exchange in CD_3CN were precluded owing to practical limitations. The small variations in values of the volumes of activation arise when different concentrations or counter-ions are used. The self-exchange reaction at elevated pressures was modelled through an extension of Marcus–Hush theory. Various contributions to $\Delta V^{\neq}$ were carefully examined particularly with appropriate reference to non-aqueous solvents. It was concluded that the results were entirely consistent with a two-sphere activation model and it was not necessary to invoke solvent dynamics in the explanation. This high pressure study enabled counter arguments to be made against the proposal that solvent dynamics are involved in this type of electron self-exchange.[237]

In a related study, the volume of reaction, the volume of activation for diffusion ($\Delta V^{\neq}_{diff}$), and the volume of activation obtained from the standard electrode reaction rate constant at various pressures, have been determined for the decamethylferrocene ($DmFc^{+/0}$) system, in several non-aqueous solvents.[238] The decamethylated ferrocene couple, rather than the unmethylated couple, was chosen. This

was because the large size of the former and low charge of the positive ion offer minimisation of complicating Coulombic interactions, such as ion-pairing. The unmethylated couple ($Fc^{+/0}$) is also less stable in the rigour of the electrochemical experimental conditions required. A further objective planned was a comparison of the pressure effects on the corresponding outer-sphere bimolecular electron transfer (self-exchange) rate constants in homogeneous solution with those on the non-aqueous electrode kinetics. The reaction volumes, ΔV_{cell} could be expressed as a linear function of the term Φ (the Drude–Nernst relation, $\Phi = (1/\varepsilon)\ (\delta \ln \varepsilon/\delta P)_T$ where ε is the solvent dielectric constant). $\Delta V^{\neq}_{diff}$ ranged from $+7$ to $+17\,cm^3\,mol^{-1}$ for the $DmFc^{+/0}$ system and generally increased with solvent viscosity. The values of $\Delta V^{\neq}_{el}$ for the electrode reaction of $DmFc^{+/0}$ were positive and within experimental uncertainty correspond to the relevant values of $\Delta V^{\neq}_{diff}$; this is in distinct contrast to the negative $\Delta V^{\neq}_{exp}$ values for the electron self-exchange in homogeneous solution. It was concluded that the electrode reactions were subject to solvent dynamical control. There was not a satisfactory relationship between the radii of the electro-active species obtained from the Drude–Nernst and Stokes–Einstein equations and radii related to crystallographic data; this discrepancy was discussed.

OXIDATIVE ADDITION AND REDUCTIVE ELIMINATION REACTIONS

Study of the catalytic oxidation of methane to methanol has witnessed a widespead use of Pt(II)/Pt(IV) complexes. A general scheme formulated on the basis of work by several investigators provided a level of understanding pertinent to about a decade ago.[239–243] It was as follows. A labile Pt(II) species bonds methane to give an η^2-methane complex which can interconvert to a five-coordinate methyl(hydrido)platinum(IV) complex. An additional ligand is required to stabilise the system. The additional ligand can be chloride or a nitrogen donor. Since both methane reductive elimination and methane activation pass through the same transition state the rationale was set for a study of methane elimination from a methyl(hydrido)platinum(IV) complex. The relevance for the mechanism of methane activation could then be accessed. Methane elimination from $[Pt(H)(CH_3)(BPMA)]^+$ where BPMA = bis(pyridylmethyl)amine could be monitored by NMR spectroscopic methods both at ambient and elevated pressures.[244] By judicious use of acid (HBF_4OEt_2 or F_3CSO_3H) at a particular concentration level, it was possible to obtain kinetic data for both the *cis* and *trans* isomeric forms where the position of the hydride relative to the amine nitrogen determines the isomer. Solvents employed were deuterated forms of methylene dichloride or acetone. The *trans* isomer eliminates methane by a factor of 20 slower than the *cis* isomer. Respective volume of activation values were $+6$ (*cis*) and $+8\,cm^3\,mol^{-1}$ (*trans*), values that were lower than anticipated based on earlier reports. These values could be accounted for given that the rate law from which these parameters were obtained was a composite one in which a five-coordinate complex was treated as a steady-state intermediate. This conclusion for the *cis* isomer was also based on elaboration of the mechanistic treatment by studying the rate and stereochemistry of deuterium incorporation into

one methyl group. The findings could be summarised in a reaction scheme illustrating the unimolecular reaction of the *cis* isomer and its deuterated analogue to form a five-coordinate Pt complex by ring opening of a pyridyl moiety (Scheme 9).

In the *trans* isomer the pyridyl residue is *trans* to the weaker σ-donor methyl rather than the hydride in the *cis* isomer accounting for the slower reacting *trans* isomer. Following the formation of the five-coordinate intermediate, two reaction paths were possible: formation of η^2-methane *cis* to the amine occupying position that then leads to elimination or formation of η^2-bound methane *trans* to the amine site that leads to deuterium/proton scrambling. Following the generation of this reaction coordinate diagram, implications for methane activation can be judged by viewing the diagram in the reverse direction. One conclusion is that the highest energy of activation is required for substitution of a strong donor ligand by methane. Subsequently, interconversion into the five-coordinate methyl(hydrido)platinum(IV) complex and ring closure to yield a stable six-coordinate complex are very facile processes.

A very recent report moves forward significantly understanding the mechanism of reductive elimination reactions to form carbon–carbon bonds from platinum(IV) complexes.[245] This report described the kinetics of reductive elimination from a cationic platinum(IV) complex as a function of solvent, of substituent character in a leaving group, of the potential effect of different spectator ligands and addressed whether there was a kinetic isotope effect. The reactions were studied also as a

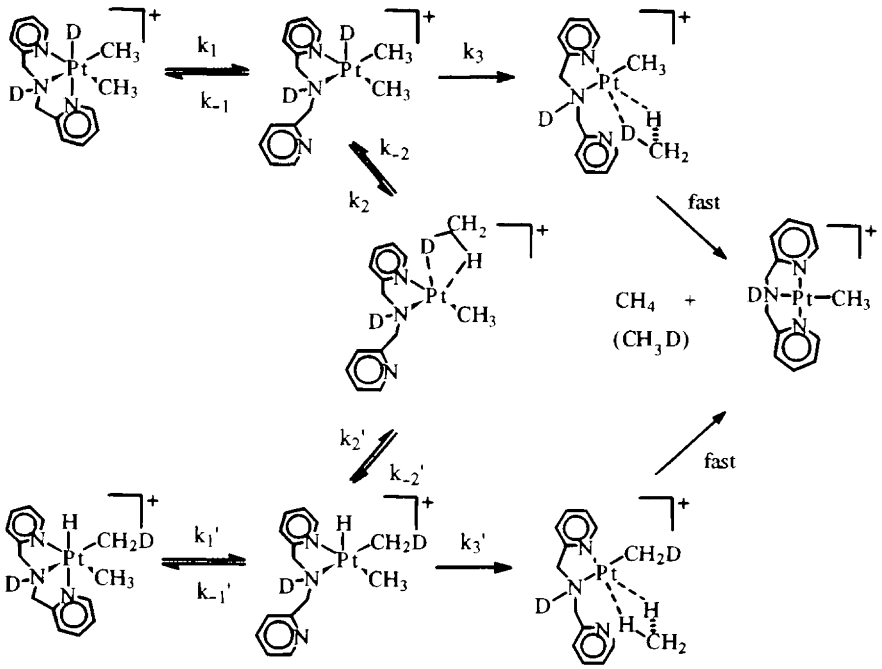

Scheme 9.

function of temperature and of hydrostatic pressure. Earlier neutral platinum(IV) complexes of the type *fac*-[$(L_2)PtMe_3X$], X = halide, carboxylate, aryloxide; L = a monodentate phosphine (PMe_2Ph, $PMePh_2$) or L_2 = a bidentate diphosphine (dppe = bis(diphenylphosphino)ethane, dppbz = o-bis(diphenylphosphino)benzene) were shown to undergo reductive elimination to form carbon–carbon and/or carbon–heteroatom bonds.[246–249] Kinetic studies on these complexes showed that for C–C and C–X reductive elimination reactions investigated, dissociation of a ligand occurred prior to the actual reductive coupling. The exact nature of the six-coordinate state to five-coordinate intermediate conversion depended on L, L_2 and X, but a five-coordinate intermediate could always be proposed if not based on actual, but on circumstantial evidence. Since electron withdrawing groups in X, addition of Lewis acids and solvent polarity changes all had influence upon the kinetic parameters, it was clear that variations among these reaction conditions could influence the extent of, or select for C–C or C–X coupling. Against this background and with a desire to form exclusively C–C coupled products, reductive elimination kinetic studies from cationic species *fac*-{[$(L_2)Pt(IV)Me_3$(pyr-X)][Otf]}, L_2 = dppe and dppbz, with pyr = pyridine and four-substituted derivatives NC_5H_4X (pyr-X) were undertaken.[245] Pre-equilibrium dissociation of the pyridine ligand from the Pt(IV) complex was shown to be responsible for the inverse dependence of the observed rate constant on the concentration of added pyridine. This implied that reductive elimination occurred from a five-coordinate cationic intermediate or from a six-coordinate solvento complex containing a weakly bound solvent molecule. The reaction rates were independent of solvent over a broad range of dielectric constant, compelling evidence for absence of a solvento six-coordinate intermediate and reinforced the view that elimination was from a cationic five-coordinate species. The dppe complex reacted about 3.5 times faster than the complex containing the dppbz spectator ligand, a moderate effect. The dppbz complex could bring about lower electron density on the MC, a property that may affect either or both of the reaction steps. A kinetic isotope of 1.1 for reaction of the deuterated pyr–d^5 complex was also consistent with the proposed mechanism of pyridine dissociation followed by carbon–carbon coupling (Scheme 10).

A linear free energy correlation based on four-substituted pyridine substituent constants yielded a value of ρ of 1.9; the reaction is considerably faster for more electron withdrawing substituents, i.e. better leaving groups. The proposed mechanism would signify that the value applies only to the first reaction step since the second does not involve pyridine(s). While cognisant of the difficulty of using substituent constants based on ionisation properties, nevertheless the value of ρ could be rationalised as reasonable. Activation parameters of $160\,kJ\,mol^{-1}$, $+180\,J\,mol^{-1}\,K^{-1}$ and $+16\,cm^3\,mol^{-1}$ for $\Delta H^{\neq}$, $\Delta S^{\neq}$ and $\Delta V^{\neq}$ were obtained, respectively. From the two-step mechanistic scheme and the derived rate law, subject to certain conditions, these parameters represent the change in the given property for the equilibrium relating to the first step of pyridine departure plus that for reaching the transition state of the second step. The thermal activation parameters were consistent with those obtained for reductive elimination from platinum(IV) neutral complexes,[246] and since more molecular disorder is occurring in both steps in reaction of the

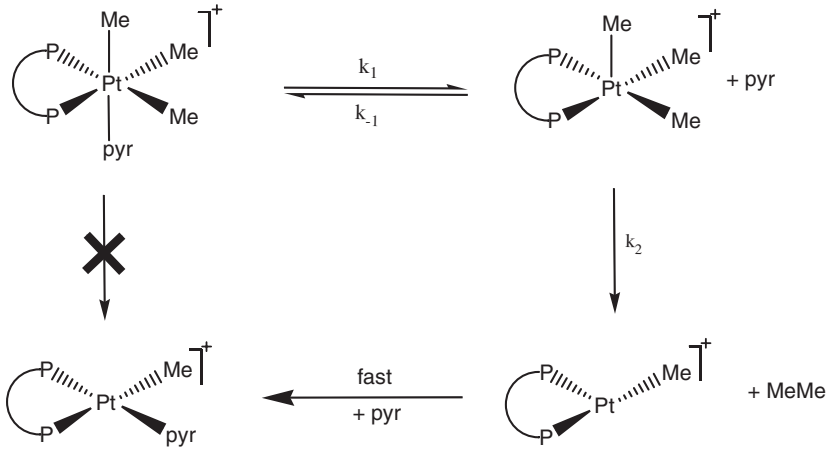

Scheme 10.

cationic complexes the large positive entropy is compatible with those events. Considering precedents for volume of activation values and the partial molar volume of ethane ($52.4\,cm^3\,mol^{-1}$), the significantly positive volume of activation that was determined supports the mechanistic scheme.

REACTIONS OF SMALL MOLECULES

There have been many studies in which the kinetics of dioxygen and carbon monoxide binding to myoglobins, haemoglobins and to porphyrin-based model complexes,[250–252] and also to some cobalt(II) complexes that bind dioxygen reversibly,[253] have been investigated and in which in some cases the pressure dependence of the kinetic parameters has been established. Iron(II) cyclidene compounds are non-porphyrin complexes that have been employed as functional mimics for binding of these small molecules.[254] The kinetics of the forward and reverse reactions of CO binding to the iron(II) cyclidene complex, Fe(II)(PhBzXy)]$(PF_6)_2$, have been monitored as a function of temperature and pressure in acetonitrile and an illustrative volume profile developed (Fig. 16).[255,256]

The complex Fe(II)(PhBzXy)$(PF_6)_2$ exists in solution as a five-coordinate species, (B)Fe(II)L, in which L is the macrocycle supplying four equatorial nitrogen donors and the fifth outside axial position is occupied by a coordinated solvent molecule (acetonitrile). Coordination of a sixth ligand, for example CO, was characterised as a bimolecular process, in the presence of a base molecule:[257]

$$(B)Fe(II)L + CO \rightleftarrows (B)Fe(II)L(CO) \quad k_{on}/k_{off} \tag{16}$$

The reaction volume could be obtained from the pressure dependence of the equilibrium constant as $-47.7\,cm^3\,mol^{-1}$, in excellent agreement with the value obtained from the kinetically determined value of $-48.3\,cm^3\,mol^{-1}$ (reaction

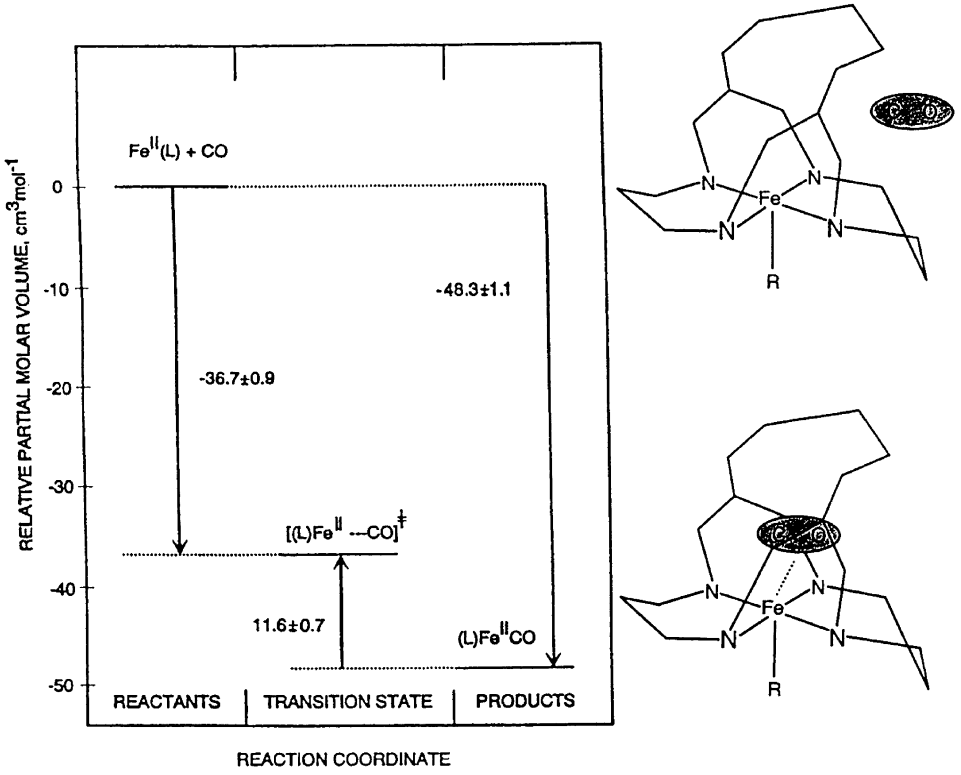

Fig. 16 Volume profile for the reversible binding of CO to a lacunar Fe(II) complex.

volume = $\Delta V^{\neq}_{on}$ ($-36.9\,cm^3\,mol^{-1}$) – $\Delta V^{\neq}_{off}$ ($+11.6\,cm^3\,mol^{-1}$)). The markedly negative value for the forward (on) reaction was taken to signify that CO is virtually enveloped within the structure of the iron complex. Indeed the reduction in volume is close to that of the partial molar volume of CO (33 and $44\,cm^3\,mol^{-1}$ in aqueous solution and 1,2-dichloroethane, respectively).[258,259] There is a spin change upon binding of CO from the high-spin five-coordinate species to the low-spin six-coordinate species. This factor was also considered in interpreting the activation volume as well as the fact that the iron that is out of the plane of the equatorial ligands in the former coordinate state but moves towards the plane upon forming a six-coordinate state. It was proposed that the spin change occurs after the transition state is reached in the forward direction meaning that the volume increase that occurred upon reaching the transition state in the reverse direction is attributable to the spin state change and also to the movement of iron(II) out of the ligand plane as partial bond breakage Fe–CO begins. Thus the transition state was envisaged as a high-spin iron (II)-CO species, late in the forward direction and early in the reverse direction. The large negative entropy of activation in the forward direction ($-108\,J\,mol^{-1}\,K^{-1}$) corresponded to the loss of degrees of freedom of CO. Weakening of the iron–CO bond and the spin state change accounted for the positive entropy of activation

($+30\,J\,mol^{-1}\,K^{-1}$) in the reverse direction. Free energy, entropy as well as volume profiles were presented. The thermodynamic parameters were similar to those found for binding of CO to myoglobin.

ADDITION REACTIONS

Cycloaddition reactions of derivatives of chromium and tungsten pentacarbonyl compounds

Addition reactions can be expected, in principle, to involve significant bond formation in the transition state, such that reaction acceleration would be anticipated at elevated pressures. Reactions of the type illustrated in Scheme 11, [2 + 2] cycloadditions, were significantly accelerated by pressure and there was almost no dependence on the polarity of the solvent.[260]

An average value of $\Delta V^{\neq}$ was $-16 \pm 1\,cm^3\,mol^{-1}$. This together with the reaction rates being independent of solvent suggested the reaction followed a non-polar concerted synchronous one-step mechanism. The insertion of dipropylcyanamide and 1-(diethylamino)propene into the metal–carbene bond of pentacarbonyl(methoxyphenylcarbene)chromium and tungsten had earlier been found also to yield significantly negative volumes of activation (-17 to $-25\,cm^3\,mol^{-1}$).[261]

Addition reactions of metal pentacarbonyl α, β-unsaturated Fischer carbene complexes

In acetonitrile all reactions of pyrrolidine addition exhibited $\Delta V^{\neq}$ values between -15 and $-17\,cm^3\,mol^{-1}$.[262] However, upon decreasing the solvent polarity, $\Delta V^{\neq}$ became markedly more negative and a good correlation with the solvent parameter q_p (i.e. the pressure derivative of q, the polarisability of the solvent) could be demonstrated. It was concluded that the addition of pyrrolidine followed a two-step process with a polar transition state leading to a zwitterionic intermediate. Addition of *para*-substituted anilines to a similar Fischer carbene complex in acetonitrile was characterised by more negative values of $\Delta V^{\neq}$ (-21 to $-27\,cm^3\,mol^{-1}$) than those for addition of pyrrolidine. [263] Second-order rate constants for the addition reaction exhibited an excellent correlation with the basicity of the aniline derivatives used. The trend in activation volumes could be correlated with an early or late transition state for the fast and slow addition reactions, respectively Scheme 12.

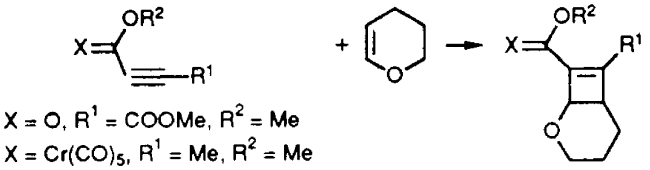

X = O, R^1 = COOMe, R^2 = Me
X = $Cr(CO)_5$, R^1 = Me, R^2 = Me
X = $W(CO)_5$, R^1 = Me , R^2 = Me
X = $W(CO)_5$, R^1 = Ph, R^2 = Et

Scheme 11.

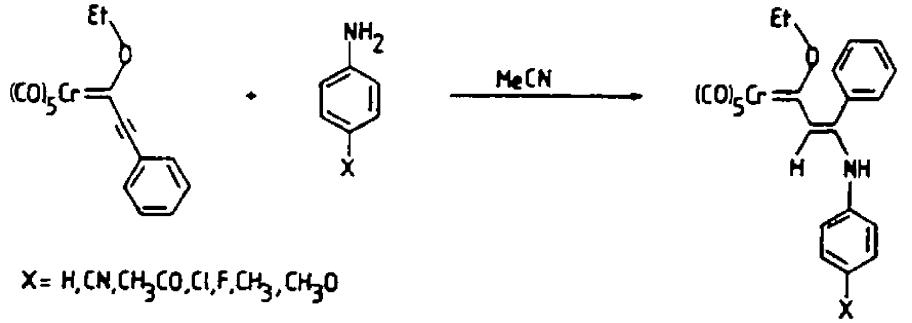

Scheme 12.

Addition to an osmium cluster

The unsaturated osmium hydrido carbonyl cluster $(\mu_2\text{-H})_2Os_3(CO)_{10}$ reacts with a wide variety of Lewis bases, L,[264] according to the following equation:

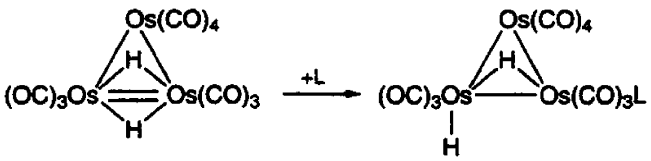

(17)

The addition of several P-donor ligands to the cluster in non-polar solvents was monitored spectrophotometrically. From the kinetics results clear, quantitative, electronic and steric profiles for the associative reaction based on the electronic and steric properties of the nucleophiles were provided.[265] The second-order rate constants could be correlated with the pK_a values of the ligands. The pK_a value is a property related to its σ-donicity. This aspect addresses the electronic effect of the added nucleophile. Potential steric effects upon the rate constant were addressed by considering both the cone angle and size of the nucleophile. An equation combining these principles was developed and with various parameters was able to correlate both electronic and steric effects. It was also pointed out that when the cone angle is lower than a critical threshold value, in the transition state the cluster provided a well-defined open space in the coordination sphere offering negligible repulsion to small entering donors. Notwithstanding this successful description of the reaction, a further comprehensive investigation of the reaction was undertaken in which 18 P-donor nucleophiles were employed.[266] The objective was to acquire the thermal- and pressure-derived activation parameters and determine whether similar correlations could be developed that could provide a further classification of the transition state, and indeed a novel and detailed picture of the transition state nature. The second-order rate constants for reactions in chlorobenzene, determined spectrophotometrically, followed the same empirical equation that had been developed for reactions in heptane. A term for the σ-donicity of the nucleophiles in non-polar solvents was applied for ligand electronic effects. Steric effects were not observed for ligands with a Tolman cone angle below the steric threshold of 147°. Larger ligands

have a significant effect upon the rate constant. Reaction of PPh_3 with the osmium cluster was characterised by a similar rate constant in heptane and nitrobenzene, but a slightly lower value when the solvent was chlorobenzene. These findings were taken to imply that the transition state for a given nucleophile remains essentially unchanged in different solvents. In all cases the entropies and volumes of activation were distinctly negative, the former typically in the range of –90 to –170 $J\,mol^{-1}\,K^{-1}$, and the latter almost all in the range of –12 to –26 $cm^3\,mol^{-1}$. A plot of $\Delta H^{\neq}$ versus $\Delta S^{\neq}$ could be interpreted to indicate the reaction rates are largely entropy controlled. The large negative values of $\Delta V^{\neq}$ (obtained in chlorobenzene) for the associative process are in accord with values for other associative reactions such as Michael addition, insertion reactions and [2 + 2]-cycloadditions. Values for isosteric ligands were invariant and since there was no dependence on σ-donicity, the volume reduction upon forming the transition state depended only on steric factors and not on nucleophile basicity. A geometrical model was developed based on the ligand cone angle and an equation formulated that could account for the observed volume of activation in terms of an intrinsic component and a volume term based on the volume of a ligand based on its cone angle. In fact this treatment is one of the most detailed analysis of volumes of activation in organometallic kinetics literature. The correlation of $\Delta V^{\neq}$ values with ligand cone angles was described as remarkable. For cone angles less than 160°, $\Delta V^{\neq}$ decreases linearly with a term that is a measure of the relative volume of the nucleophile. This suggested that the Os···P bond lengths in the transition state are the same for these nucleophiles, and enabled an estimate to be made of the penetration (ca. 24 pm) of the P-donor ligands inside the periphery of the cluster in the transition state. When the cone angle is 160° a new type of steric threshold appeared and above this value the volumes of activation become less negative, ligand penetration is lower and Os···P bond lengths become progressively longer. Practical limitations prevented determination of volume profiles. It is possible that these would have revealed evidence for early or late transition states. Nevertheless this report represents a landmark of thorough and valuable analysis and insight into the reaction mechanism.

OTHER REACTIONS

Metal exchange in heterobimetallic compounds

Interest in the coordination chemistry of thiophene and in model studies of the absorption process involved in hydrodesulfurisation in the petroleum industry led to the development of bimetallic and trimetallic complexes containing thiophene.[267] Of greater interest was the finding of irreversible exchange (σ and π) of coordination sites by metal fragments. An example of the reaction is shown in Scheme 13.

This finding was followed by a comprehensive preparative, structural characterisation and kinetics study of the conversions typified by the reaction above.[268] These reactions were accorded the term metal exchange reactions. The heterobimetallic complexes with σ, π bridging thiophene or selenophene ligands (η^1:η^5-$XCRCHCHCMn(CO)_5)Cr(CO)_3$ (X = S, R = H (**1**); R = Me (**2**); X = Se, R = H

Scheme 13.

(**3**) converted irreversibly at 0 °C in acetone into the complexes (η^1:η^5-XCRCHCHCCr(CO)$_5$)Mn(CO)$_3$ ((**4**), (**5**) and (**6**)), respectively. Changes in the UV/visible, IR and NMR spectra accompany these transformations. The kinetics of the reaction of (**2**)–(**5**) were monitored by UV/visible spectrophotometry; the first-order rate constant was essentially independent of the concentration of (**2**), and not significantly affected by variation of solvent employed. Solvents ranged from cyclohexane ($\varepsilon = 2.02$), tetrahydrofuran ($\varepsilon = 7.3$), dichloromethane ($\varepsilon = 8.9$) to acetone ($\varepsilon = 21$), and the rate constants were, respectively 11, 36, 26 and 38, all $\times 10^6\,s^{-1}$ at 15 °C. Comparable rate constants were determined for the reaction of (**2**)–(**5**) in d_6-acetone or d_2-dichloromethane by ^{1}H NMR spectroscopy, and no intermediates were observed. These findings indicated that solvent polarity does not play an important role in the metal exchange reaction and therefore direct participation of coordinated solvent molecules in the transition state could be ruled out. Thermal activation parameters were established for the conversions of compounds (**1**) and (**2**) and were 93 and 86 kJ mol^{-1} (enthalpies) and -16 ± 6 and -30 ± 11 J mol^{-1} K^{-1} (entropies), respectively. The former are values associated with covalent bond cleavage, while the latter are modest values and were considered to point to an intramolecular exchange process. A near zero (-0.6 ± 0.5 cm^3 mol^{-1}) volume of activation for the conversion of (**2**)–(**5**) substantiated this conclusion and excluded the possibility of an intermolecular arene displacement route. A scheme invoking bridging carbonyl ligands in which the MCs were η^1-bonded to the C2 of the thienyl ligand with the two bridging carbonyls occupying the free coordination sites was proposed. It could also be concluded that there were no measurable changes in electrostriction upon reaching the transition state (Scheme 14).

It was also noted that of the metal exchange reactions investigated the thermodynamically favoured product was always less polar than the starting material.

Monomerisation of dinuclear pallada- and platina-cycles

A complementary structural and kinetics characterisation study regarding the halogen cleavage reaction (by pyridines) in dimethylaminomethylphenyl-C^1,N pallada- and platina-cycles has been reported (see Scheme 15).[269] This work followed by 30 years a pioneering study of the kinetics of monomerisation of a dinuclear bromine-bridged platinum compound using pyridine.[270]

Reactions of this type are postulated as equilibria in synthetically important insertion reactions of alkenes, alkynes and other unsaturated molecules into the Pd–C bonds of dimeric palladacycles.[271,272] Further, this reaction can form the basis for

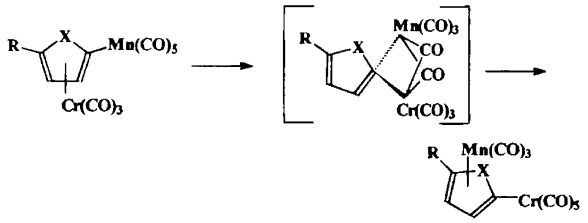

Scheme 14.

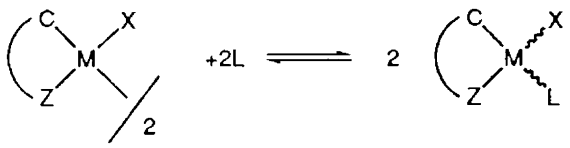

Scheme 15 M = Pd(II) and Pt(II), X = halogen bridge, Z = N, P, S, etc., and L = donor ligand.

synthesis of monomeric metallacycles from the corresponding dimers.[273] Specifically, the halogen-bridge cleavage reaction of $[\{M(o\text{-}C_6H_3RCH_2NMe_2)X\}_2]$ (M = Pd or Pt; R = H, 4-MeO, 5-Me, or 5-F; X = Cl or I) by a series of substituted pyridines in chloroform has been investigated as a function of concentration of excess pyridine, of temperature and when experimentally feasible as a function of hydrostatic pressure. The reactions were rapid and of second order, and showed strong steric rather than electronic demands, and there was no evidence of a reverse reaction confirming the essential irreversibility. Five dimeric Pd compounds reacted with essentially the same rates and thermal activation parameters with pyridine; the five included widely varying electron/donating/withdrawing groups (R) and change of Cl by I. This led to the conclusion that reaction rates demonstrated electronic insensitivity. However, varying the steric features of the pyridine nucleophiles (4-Me, 2,4-Me_2 and 2,6-Me_2) had a significant retarding effect, in that order. Steric hindrance in the vicinity of the donor centre was indicative of an associative mechanism. Further evidence for the associative nature of the bridge-cleavage reaction came from interpretation of the activation parameters. The enthalpies of activation were regarded as lower than would be compatible with incipient bond breakage as the transition state is formed in a dissociative mechanism. The $\Delta S^{\neq}$ values, in the range of -104 to $-158\,J\,mol^{-1}\,K^{-1}$, suggested the transition state is highly ordered, and included back donation from the metal into the apically coordinated pyridine ligand. In two cases the rates of monomerisation could be studied as a function of pressure. The compound with M = Pd, R = H and X = I upon reaction with 2,6-diMe_2py converted to the monomeric form with $\Delta V^{\neq} = -22.6\,cm^3\,mol^{-1}$, whereas the platinum compound with R = 4-MeO and X = Cl, upon reaction with 4-Mepy yielded $\Delta V^{\neq}$ of $-14.5\,cm^3\,mol^{-1}$. These distinctly negative values remove any doubt; these reactions are emphatically associative. The smaller volume change for the platinum compound reaction was thought to reflect partly the smaller entering group. Thus, a comprehensive kinetics study in which the

activation parameters were obtained has illuminated the reaction mechanism of a type of system first studied decades earlier.

Cyclometallation in dirhodium(II) compounds

Cyclometallation reactions of mononuclear compounds are well established,[274] but such reactions occurring on compounds having two MCs are not as well known. To address the lack of information regarding the mechanism of the latter reactions a systematic study of the reactivity of arylphosphines in dirhodium(II) compounds that give rise to cyclometallation was undertaken.[275] The compounds were $[Rh_2(O_2CMe)(\mu\text{-}O_2CMe)_2\{\mu\text{-}(XC_6H_3)P(C_6H_4X\text{-}p)_2\}\{P(C_6H_4X'\text{-}p)_3\}]$ (X = H, X′ = H or Me; X = Me, X′ = H or Me) and they underwent reaction to produce the corresponding doubly metallated compounds $[Rh_2(\mu\text{-}O_2CMe)_2\{\mu\text{-}(XC_6H_3)P(C_6H_4X\text{-}p)_2\}_2]$. The reactant possessed a metallated and an equatorial phosphine in a head-to-tail cisoid configuration (see Scheme 16).

The kinetics of the reaction have been studied under a multitude of variables and conditions, including toluene and glacial acetic acid as solvent, thermal, acid- and base-assisted conditions, different bases (PPh_3, $P(C_6H_4Me\text{-}p)_3$ or pyridine), and as a function of temperature, pressure and base concentration. Depending on the conditions, reaction paths differed such that a substitution path as well as metallation was revealed. The doubly metallated compounds were shown by ^{31}P NMR spectroscopy to retain the head-to-tail cisoid configuration. Activation parameters were acquired for several permutations of reactant variation and base variations for the spontaneous, acid- and base-assisted reactions. All values of the volume of activation were significantly negative: they were in the range of –23 to –37 $cm^3\,mol^{-1}$, –21 to –23 $cm^3\,mol^{-1}$ and –14 or –15 $cm^3\,mol^{-1}$, for the base-assisted, spontaneous and acid-assisted processes, respectively. This indicated that compression of the system as the transition state is reached in clearly important. The less negative values for the base-assisted reaction were observed when the base was pyridine. This was proposed to relate to smaller steric demands compared with the values when the base in question was PPh_3. Presumably owing to the complexity of the system, no detailed breakdown of contributions to the volumes of activation was offered. The entropies of activation mirrored the latter, supporting a measure of ordering in the transition state. The absence of electrostriction changes in forming the transition state could be inferred.

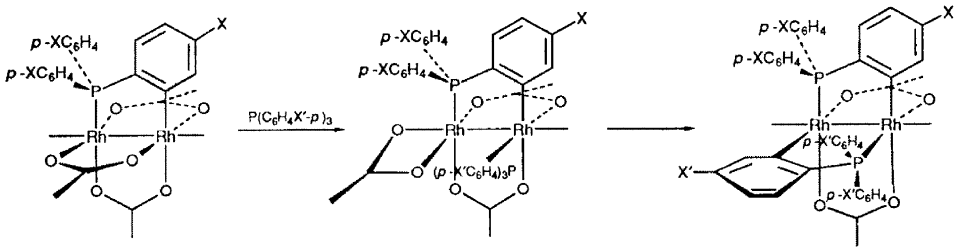

Scheme 16 Axial positions are occupied by any Lewis base present in solution. X, X″ = H or Me.

4 Volumes of activation for radiation-induced organometallic reactions

PHOTO-INDUCED REACTIONS

The photochemically induced substitution of one or more CO ligands in $M(CO)_4$(diimine), (M = Cr, Mo, W and diimine = phen or bpy) by an incoming nucleophile has been investigated with the purpose of understanding the reaction mechanism, over a considerable time period.[276] Using PEt_3 as the entering nucleophile it was shown that the mechanism of substitution on $M(CO)_4$(phen) in toluene could vary depending on whether excitation occurred through a low energy metal-to-ligand charge transfer (MLCT) band or via a ligand field (LF) wavelength.[277–279] In the latter case on the basis of analysis of quantum yields and the pressure dependence of the kinetics of the substitution the mechanism was assigned as dissociative. For substitution following MLCT excitation a mechanistic changeover to an associative one, when M = Mo, W, was proposed on the basis of results analysis. The changeover was explained by proposing that upon MLCT excitation electron density is transferred away from the MC onto the phen ligand, enabling an associative attack by the entering nucleophile at the more electrophilic MC. Whereas following LF excitation a lengthening of the metal–ligand bond occurs, promoting dissociative ligand substitution. When M = Cr the pressure dependence of the reaction progress indicated a less marked variation, a change from a D to an I_d mechanism. This finding could be rationalised on the basis of a smaller Cr centre, relatively to Mo and W, influencing the extent of bond formation in the MLCT excited state. A series of further pivotal studies in which nucleophiles and their respective concentrations, the irradiation wavelengths and hydrostatic pressure were all varied, was reported.[280–282] A systematic tuning of the photo-substitution mechanism was discerned by changes in the physical and chemical variables. A first report addressed the issue of how the mechanism might be affected by nucleophile bulk by using PMe_3 and PPh_3 as entering nucleophiles for photo-substitution on the chromium compound. The overall reaction is given in the following equation:

$$M(CO)_4(phen) + PR_3 + h\nu \rightarrow M(CO)_3(phen)(PR_3) + CO \quad (18)$$

A complete reaction scheme was presented based on the accumulated results including a possible step in which a solvent molecule is temporarily attached to the compound. LF photolysis is decelerated markedly upon pressure increase, consistent with a limiting D mechanism. Ligand substitution proceeds by a dissociative interchange mechanism following MLCT photolysis, and results for the two entering nucleophiles were rather similar demonstrating that relatively little bond formation occurs with the entering nucleophile. A second report describes a corresponding study upon the molybdenum and tungsten analogues. From the measurement of the pressure dependence of the quantum yield apparent volumes of activation could be determined at each irradiating wavelength, and could be analysed in terms of contributions arising from dissociative LF excitation and associative MLCT excitation.

Steric crowding caused by the PPh_3 nucleophile can hinder an associative ligand substitution process. Together these results for the different metals and different entering nucleophiles, including additional results for reaction when R = Bu^n were assessed and a scheme was presented that included the three possible pathways via D, I or A mechanisms for nucleophilic substitution from the excited state species $[M(CO)_4(phen)]^*$. A clear example of a mechanistic changeover was presented for the reaction of PBu^n_3 with $[W(CO)_4(phen)]$ for which the volume of activation for the quantum yield ranged from $+10.5$ to $-12.0\,cm^3\,mol^{-1}$ as the wavelength varied from 313 to 546 nm.A pattern of systematic variation in the mechanism of substitution could be extracted from results obtained by variation of the metal, entering nucleophile, nucleophile concentration, excitation wavelength and applied pressure. While analysis of ambient pressure results is fruitful, the key distinguishing feature regarding mechanism is the pressure dependence leading to the volume of activation.

The mechanism of reactions in which photolysis of $M(CO)_6$ (M = Cr, Mo, W) in the presence of a bidentate ligand in toluene leads to first a pentacarbonyl intermediate, followed by a mono-coordinated bidentate ligand and subsequent chelate ring closure with expulsion of a second CO ligand was thought to be understood.[283] That is for bidentate ligands phen, en and dab (en, dab = 1,4-diisopropyl-1,4-diazabutadiene), the volume of activation for the ring-closure step was significantly negative supporting the operation of an associatively activated chelation mechanism for M = Mo and W. When M = Cr the volume of activation value suggested a fine balance between the size of the MC and steric hindrance on the free end of the bidentate ligand as the transition state was approached. Hence for chromium complexes the chelation mechanism could proceed by an associative or dissociative mechanism. Subsequently it was shown that under certain conditions chromium binuclear bridged species and $Cr(CO)_5$(dab) could be isolated, raising concerns that other species may have (unknowingly) been present in the earlier ring-closure studies.[284] Accordingly, thermal ring-closure reactions of pentacarbonylchromium complexes with bidentate ligands dab (in *n*-heptane) and dmbpy (dmbpy = 4,4′-dimethyl-2,2′-bipyridine) (in toluene) were studied thoroughly. This was made possible by first isolating some of the monodentate pentacarbonyl chromium complexes. The kinetics were studied as a function of N–N (= dab or dmbpy) concentration, temperature and pressure.[283] The finding of a decrease in observed rate constant with increasing N–N concentration was interpreted in terms of competing reactions leading to the formation of $Cr(CO)_6$ and $Cr(CO)_4$(N–N). At high N–N the limiting rate constant represents only the chelation reaction for which activation volumes could be determined. These ranged from $+13$ to $+18\,cm^3\,mol^{-1}$ and strongly support the operation of a dissociatively activated chelation mechanism.

Since the molydenum compounds described above demonstrated mechanistic variation in photochemically initiated substitution reactions, the molybdenum dimetallacycle $[(CO)_4Mo(\mu\text{-}PMD)_2Mo(CO)_4]$ was selected for a study of the nature of the substitution mechanism associated with MC and MLCT excitation.[285] PMD is pentamethylenediazirine. The substituting ligands were bpy, phen and 1,2-bis(diphenylphosphino)ethane (dppe) for the reaction in toluene solution. For reaction with

bpy and phen (N–N) the irradiation leads to cleavage of the metal–diazirine bonds according to the following equation:

$$(CO)_4Mo(\mu\text{-PMD})_2Mo(CO)_4 + N - N + h\nu \rightarrow 2Mo(CO)_4(N - N) + 2PMD \quad (19)$$

Analysis of the results obtained by studying this reaction as a function of ligand concentration and pressure indicated that the photochemical reaction is in competition with a thermal reaction. For MC photolysis the photochemical reaction proceeds by a dissociative (D) route whereas the thermal reaction proceeds according to an associative (A) mechanism. This conclusion was reached primarily on the basis of the sign and magnitude of the volumes of activation extracted from the kinetic data. The reaction with dppe proceeds by displacing one bridging PMD ligand (Equation (20)), or by releasing CO to generate $Mo_2(\mu\text{-PMD})_2(\mu\text{-dppe})(CO)_6$:

$$Mo_2(\mu\text{-PMD})_2(CO)_8 + \text{dppe} + h\nu \rightarrow Mo_2(\mu\text{-PMD})(\mu\text{-dppe})(CO)_8 + PMD \quad (20)$$

Experimental results following MLCT excitation yielded significantly negative volumes of activation, indicating associative substitution mechanisms for both the MLCT initiated and thermal substitution processes. The concentration dependencies and magnitude of the activation volumes yielded no evidence for an interchange mechanism. A complete scheme indicating the photochemical, thermal, rate determining and rapid reaction steps was assembled.

Photo-induced homolysis reactions have been observed for a wide variety of metal–metal bonded complexes containing an α-diimine moiety.[286,287] The subsequent fate of the metal radicals has been investigated in detail for complexes such as $(CO)_5MnMn(CO)_3$(diimine).[288] In non-coordinating, non-viscous solvents the radicals diffuse from the solvent cage and dimerise, whereas in coordinating solvents this complex photodisproportionates, in the presence of an N- or P-donor ligand (L), into $Mn(CO)_5^-$ and $Mn(CO)_3(L)(\text{diimine})^+$. These interesting findings prompted a similar study on a metal triangular cluster, $Os_3(CO)_{10}$(diimine).[289] In acetonitrile and pyridine (S), zwitterions of the type $^-Os(CO)_4\text{–}Os(CO)_4\text{–}Os^+(S)(CO)_2$(diimine) were generated although the mechanism of formation was unclear. There was no evidence at this stage of biradical formation in any solvents investigated. A subsequent study established by electron paramagnetic resonance and nanosecond transient absorption spectroscopies, the formation of biradicals.[290] Conversion of the biradical species to zwitterions was also monitored. In order to clarify the mechanism of zwitterion formation, the osmium cluster containing the diimine, 2-acetylpyridine *N*-*n*-propylimine, in pyridine was irradiated in a pill-box cell, high pressure cell arrangement in the pressure range up to 150 MPa.The pressure dependence of the quantum yield afforded an apparent activation volume of $+7.5\,cm^3\,mol^{-1}$, a value that might not have been anticipated in view of the marked increase in electrostriction accompanying zwitterion formation and lower intrinsic volume arising from solvent coordination. The result was explained by invoking bond cleavage, the positive volume change for which is partly offset by the increase of electrostriction and coordination of pyridine.

Catalytic schemes for carbon monoxide activation required for methanol carbonylation to acetic acid and alkene hydroformylation often depend on a carbon

monoxide insertion into a metal alkyl bond in a critical carbon–carbon bond formation step.[291] Progress in elucidating reactivities and structures of intermediates in such processes is beset with difficulties owing to low concentrations of relevant species. One approach has been to generate potentially pertinent intermediates by flash photolysis and examine the properties of transient species by time-resolved optical and TRIR spectroscopies.[292,293] Reactions of the decarbonylated intermediate generated from the excited state of the photolysis of $CpFe(CO)_2(C(O)CH_3)$ in heptane have been studied in order to resolve the kinetic characteristics of a step in which the intermediate reacts with a ligand, rate constant, k_L, to yield $CpFe(CO)(C(O))(CH_3)(L) = A_L$ and another step, rate constant, k_m, in which the species formed is $CpFe(CO)_2(CH_3) = M$.[294] Measurements applying hydrostatic pressure were carried out and these resulted in clarification of mechanistic proposals made earlier. A detailed analysis of the derivation of volumes of activation for these steps from quantum yield measurements was presented, and use of the method yielded $\Delta V_L^{\neq} - \Delta V_m^{\neq} = -5\,cm^3\,mol^{-1}$. A similar value was established for the parallel reactions of the compound in which Cp is replaced by the indenyl (Ind) moiety. These $\Delta\Delta V^{\neq}$ values suggest transition states that are not dramatically different in character for the two pathways for each of the respective Cp and Ind compounds. One possible explanation suggested was that both pathways are concerted reactions involving a solvento species and it was argued that k_m would be independent of pressure thus attributing the numerical value of the difference entirely to the pressure dependence of k_L. The improved experimental approach applying FTIR enabled a mechanism, previously advanced, based on ring slippage, to be ruled out.

PULSE-RADIOLYSIS-INDUCED REACTIONS

Transition metal–carbon σ-bonds can be key intermediates in industrial processes, biochemical reactions, organic synthesis and in catalytic processes. The pulse radiolysis method can generate from the primary species formed in aqueous medium, secondary species depending on the solutes present. Aliphatic radicals, for example, can then react with metal-aqua ions or metal complexes to form complexes with metal–carbon σ-bonds. The subsequent reactivity of these species or the products can then be monitored, usually spectrophotometrically. The radicals are generated in sub-microsecond times, and very rapid processes ensue, requiring specialised methods. As cited earlier, two authoritative reviews have been published recently,[108,109] the former emphasising the application of high pressure methods in kinetics and mechanistic studies of species generated by pulse radiolysis. The second covers comprehensively the research conducted regarding kinetics and mechanistic studies over the past 30 years. This includes as well, accounts of the properties, spectra and acid dissociation constants, as appropriate, for complexes containing metal–carbon σ-bonds. A section on mechanistic features has 11 sub-sections, e.g. heterolysis and homolysis of metal–carbon σ-bonds, β-elimination reactions, CO insertion/methyl migration, bimolecular decomposition of the transient complexes and methyl transfer reactions, and such coverage cannot be repeated here and would

be beyond the scope of this contribution. Rather, here a selection of examples where use of hydrostatic pressure in kinetic studies enhances understanding of the mechanism will be presented.

In reactions of divalent transition metal ions with aliphatic free radicals, metal–carbon σ-bond formation is formally accompanied by oxidation of the MC:

$$M^n + R \rightarrow \left(M^{(n+1)} - R\right) \tag{21}$$

Cobalt(II) and nickel(II) species reacted with $^{X}CH_3$ to produce intermediate species containing metal–carbon σ-bonds, a process characterised by a small positive $\Delta V^{\neq}$, that indicated a dissociative interchange mechanism.[295,296] Similar reactions of aquated Cr(II) ions with a series of 10 different aliphatic radicals exhibited an average $\Delta V^{\neq}$ of $+4.3 \pm 1.0\,cm^3\,mol^{-1}$, also evidence for an I_d mechanism.[297]

Study of the formation and homolysis of (hedta)Fe(III)-CO_2^- and (hedta)Fe(III)-CH_3^- (hedta = $HOCH_2CH_2N(CH_2CO_2^-)CH_2CH_2N(CH_2CO_2^-)_2$) indicated three conclusions when these results were considered with other findings.[298] They were first:

$$M^nL_m + R \rightarrow L_{m-1}M^{n+1} - R + L \tag{22}$$

which proceeds by a ligand substitution mechanism. Second, homolysis of the metal–carbon bond follows the same mechanism, and third, $\Delta V^{\neq}$ for the homolysis reaction depends strongly on the nature of the central metal cation, i.e. the values are larger for M^{n+1} = Cr(III), Co(III), Ni(III) and smaller for Fe(III). It was also found that the volume of activation for the following reaction:

$$\text{(hedta)Fe(III)-}CO_2^{2-} + CO_2^{X-} + 2H^+ \rightarrow \text{Fe(II)(hedta)}(H_2O)^- + CO + CO_2 \tag{23}$$

upon analysis demonstrated the role of changes in the electronic environment in terms of the coordination number and spin state of the complex during the formation and dissociation of the metal–carbon σ-bonds.

Heterolysis of the metal–carbon σ-bond in transient complexes of the type L_mM^{n+1}-R produced as shown above can proceed by one of two alternative pathways in aqueous solution.[299,300] One pathway involves formally an overall oxidation of the MC and the other reduction of the MC occurs during the reaction:

$$L_mM^{n+} - R + H_2O \rightarrow M^{n+1}L_m + RH + OH^- \quad \text{Oxidation} \tag{24}$$

$$L_mM^{n+} - R + H_2O \rightarrow M^{n-1}L_m + ROH/R_{-H} + H_3O^+ \quad \text{Reduction} \tag{25}$$

The kinetics of the heterolysis of several species containing Cr(III)-C σ-bonds have been studied at ambient pressure and at elevated pressures. In general the pathway followed was consistent with the oxidation pathway. Under different conditions the reactions were acid or general base catalysed. Volumes of activation for each component of the rate laws could be determined.[301] A particular conclusion that emerged was that water molecule bond cleavage could play an important role in the transition state. In one case this conclusion was based on interpretation of the magnitude of the H/D solvent isotope effect. These early studies were followed by posing the question were the mechanistic conclusions reached for the chromium systems applicable for other metal–carbon σ-bonds? Accordingly, the kinetics of the

heterolysis of the copper–carbon σ-bond in a complex of the type $[LCu(II)\text{-}R]^{+}$ (L = 2,5,8,11-tetramethyl-2,5,8,11-tetraazadodecane; R = $CH_2CO_2^-$) were examined at elevated pressures.[298] Ambient pressure kinetics measurements earlier on this system had shown that the pathway followed is the oxidation pathway.[302,303] In addition corresponding experiments were conducted for the decomposition of $[(H_2O)_5Cu(III)\text{-}R]^{2+}$ (R = $CH_2CO_2^-$ or $CHCl_2^-$) systems which had been shown at ambient conditions to proceed by the reduction pathway.[304] The volumes of activation for heterolysis of the Cu(III)–C σ-bonds of the complexes $[Cu(III)\text{–}CH_2CO_2^-]^{+}$ and $[Cu(III)\text{–}CHCl_2]^{2+}$ were very different, –12.4 and +10.4 $cm^3\,mol^{-1}$, respectively. The observed rate constants were not very different but the widely different volumes of activation required separate interpretation of the heterolysis process. For the former complex after examining and rejecting other hypotheses the following explanation was given. Bond formation with a solvent molecule in reductive heterolysis gave a transition state in which a water molecule binds to the carbon atom (of the metal–carbon bond) and shifts the M–C σ-bond electrons towards the MC thus causing its reduction. In addition, charge was formed during the process and could provide a contribution to the negative volume of activation. In contrast, the positive value of $\Delta V^{\neq}$ found for heterolysis of the $[Cu(III)\text{-}CHCl_2]^{2+}$ species was also explained, in part, by binding of a water molecule to the carbon atom, and also by induction of cleavage of a C–Cl bond. It was argued that a late transition state in which considerable C–Cl and M–C bond cleavage had already occurred, then these positive volume contributions will more than compensate for the volume reduction associated with C–O bond formation.

The transient complex $[LCu(II)\text{–}CH_3]^{+}$ decomposed according to a second-order rate law, and the volume of activation for that process was determined to be –5 $cm^3\,mol^{-1}$. The reaction is:

$$2[LCu(II) - CH_3]^{+}(aq) \rightarrow 2LCu^{+}(aq) + C_2H_6 \qquad (26)$$

After considering and rejecting other interpretations it was suggested that the mechanism was one in which formation of the transition state involved a coherent, partial C–C bond formation that will be associated with a volume collapse and a stretching of the Cu–C bonds. It was further suggested that the latter process will partially offset the volume collapse, but the C–C bond formation dominates in volume terms, consistent with a modest negative volume of activation.

Copper(I) complexes catalyse a variety of organic reactions which are of synthetic and industrial importance.[305] In such processes that involve halide abstraction from aryl or alkyl halides, the abstraction step by a Cu(I) catalyst is believed to be the rate-determining step. In order to circumvent the property of facile disproportionation of Cu^{+}_{aq}, various methods of stabilising Cu(I) and influencing reaction rates were considered.[306] A kinetics study of ligand (L) effects on the reactivity of Cu(I)L complexes towards $Cl_3CCO_2^-$ was undertaken. The results indicated that the rate of the chlorine abstraction reaction was affected by several factors. These were the redox potential of the Cu(II/I)L couple, the hybridisation on Cu(I) in the Cu(I)L complex, steric hindrance, and electron density on the central Cu(I) cation at the binding site of the chlorine atom to be abstracted. The volume of activation,

distinctly negative, supported the expectation that the chlorine abstraction step proceeded by an associative mechanism.

5 Concluding remarks

Application of the hydrostatic pressure variable in a multitude of reaction kinetics studies leading to the volume of activation has been clearly demonstrated to be of inestimable value in mechanistic studies of organometallic chemistry reactions. Its relative simplicity of definition and precision of typical experimental values render the volume of activation to be of far superior mechanistic value than is the entropy of activation. The selection of reports described, a truly eclectic collection, illustrates that reactions of a wide range of metal-centred reactions have benefitted mechanistically from elevated pressure kinetics studies. Indeed in many cases the volume of activation adds that extra dimension to mechanistic elucidation. The breadth of techniques and variety of reaction monitoring methods described have added broader scope, interest and depth to this account.

Acknowledgements

We acknowledge the fact that several investigators have developed and applied high pressure technology in kinetics studies resulting in many interesting reports in this overall account. Colleagues who have contributed tirelessly to those reports from our own laboratories are also gratefully acknowledged. Financial support for the work performed in our laboratories came from the Deutsche Forschungsgemeinschaft and Fonds der Chemischen Industrie.

References

1. van t'Hoff, J.H. (1901). Vorlesungen über Theoretische und Physikalische Chemie, Vol. 1. Braunschweig
2. Arrhenius, S. (1889). *Z. Phys. Chem* **2**, 226
3. Pelzer, H. and Wigner, E. (1932). *Z. Phys. Chem* **B15**, 445
4. Eyring, H. (1935). *J. Chem. Phys* **3**, 107
5. Wynne-Jones, W.F.K. and Eyring, H. (1935). *J. Chem. Phys* **3**, 492
6. Glasstone, S., Laidler, K.J. and Eyring, H. (1941). *The Theory of Rate Processes*. McGraw-Hill Book Company, New York
7. Evans, M.G. and Polanyi, M. (1935). *Trans. Farad. Soc* **31**, 875;Evans, M.G. and M. Polanyi (1936). *Trans. Farad. Soc* **32**, 133
8. Evans, M.G. (1938). *Trans. Farad. Soc* **34**, 49
9. Perrin, M.W. (1938). *Trans. Farad. Soc* **34**, 144
10. Le Noble, W.J. (1988). *Organic High Pressure Chemistry*. Elsevier, Amsterdam
11. Asano, T. and le Noble, W.J. (1978). *Chem. Rev.* **78**, 407
12. van Eldik, R., Asano, T. and le Noble, W.J. (1989). *Chem. Rev.* **89**, 549
13. Whalley, E. (1959). *Trans. Farad. Soc.* **55**, 798
14. Stranks, D.R. (1974). *Pure Appl. Chem.* **38**, 303

15. Drljaca, A., Hubbard, C.D., van Eldik, R., Asano, T., Basilevsky, M.V. and le Noble, W.J. (1998). *Chem. Rev.* **98**, 2167
16. van Eldik, R. and Hubbard, C.D. (2005). *Application of high pressure in inorganic and bioinorganic chemistry. Chemistry at Extreme Conditions*, Riad Manaa, M. (ed.), Chapter 4. Elsevier, Amsterdam
17. *Comprehensive Organometallic Chemistry I* Wilkinson, G., Stone, F.G.A., Abel, E.W. (Eds). Elsevier, Amsterdam, 1982; *Comprehensive Organometallic Chemistry II*, Abel, E.W., Stone, F.G.A. and Wilkinson, G. (Eds). Elsevier, Amsterdam, 1995; *Comprehensive Organometallic Chemistry III*, Crabtree, R.H. and Mingos, D.M.P. (eds). Elsevier, Oxford, 2006, in press
18. van Eldik, R. et al., *Mechanisms of Inorganic and Organometallic Reactions*, Twigg, M.V. (Ed.). Plenum, New York, Vol. 3, 1985; Vol. 4, 1986; Vol. 5, 1988; Vol. 6, 1989; Vol. 7, 1991; Vol. 8, 1994. These volumes covered reports of high pressure studies from 1980 to mid-1991
19. Eckert, C.A. (1972). *Annu. Rev. Phys. Chem.* **23**, 239
20. Jenner, G. (1975). *Angew. Chem. Int. Edit.* **14**, 137
21. Jenner, G. (2002). *J. Phys. Org. Chem.* **15**, 1
22. van Eldik, R. (1986). *Inorganic High Pressure Chemistry. Kinetics and Mechanism*, van Eldik, R. (ed.), Chapter 1. Elsevier, Amsterdam
23. Hamann, S.D. (1957). *Physico-chemical Effects of Pressure*. Butterworths, London
24. Blandamer, M.J. (1992). *Chemical Equilibria in Solution. Dependence of Rate and Equilibrium Constants on Temperature and Pressure*. Ellis Horwood, Chichester
25. Isaacs, N.S. (1981). *Liquid Phase High Pressure Chemistry*. John Wiley and Sons, Inc., Chichester
26. Kotowski, M. and van Eldik, R. (1989). *Coordin. Chem. Rev.* **93**, 19
27. Hubbard, C.D. and van Eldik, R. (1995). *Instrum. Sci. Technol.* **23**, 1
28. *Chemistry Under Extreme or Non-classical Conditions*, van Eldik, R. and Hubbard, C.D. (Eds.), Chapters 2, 3 and 12. Wiley/Spektrum, New York/Heidelberg, 1996
29. *High Pressure Techniques in Chemistry and Physics. A Practical Approach*, Holzapfel, W.B. and Isaacs, N. (Eds). Oxford University Press, Oxford, 1997
30. van Eldik, R. and Hubbard, C.D. (2000). *S. Afr. J. Chem.* **53**, 139
31. *High Pressure Chemistry. Synthetic, Mechanistic and Supercritical Applications*, van Eldik, R. and Klärner, F.-G. (Eds), Chapters 1–11. Wiley-VCH, Weinheim, 2002
32. Helm, L. and Merbach, A.E. (2002). *J. Chem. Soc. Dalton Trans.* 633
33. Hubbard, C.D. and van Eldik, R. (2005). *High Pressure Chemistry, Kirk-Othmer Encyclopedia of Chemical Technology*. John Wiley and Sons, New York On-line version 13 May 2005
34. (a) Benson, S.W. (1960). *The Foundations of Chemical Kinetics*. McGraw-Hill, New York; (b) Frost, A.A. and Pearson, R.G. (1961). *Kinetics and Mechanism*. 2nd Edn John Wiley and Sons, New York; (c) Amdur, I. and Hammes, G.G. (1966). *Chemical Kinetics: Principles and Selected Topics*. McGraw-Hill, New York; (d) Laidler, K.J. (1987). *Chemical Kinetics*. 3rd Edn Harper Collins, New York
35. Katakis, D. and Gordon, G. (1987). *Mechanisms of Inorganic Reactions*. Wiley, New York
36. Wilkins, R.G. (1992). *Kinetics and Mechanism of Transition Metal Complexes*. 2nd Edn VCH, New York
37. Espenson, J.H. (1995). *Chemical Kinetics and Reaction Mechanisms*. 2nd Edn McGraw-Hill, New York
38. Atwood, J.D. (1997). *Inorganic and Organometallic Reaction Mechanisms*. VCH New York
39. Jordan, R.B. (1998). *Reaction Mechanisms of Inorganic and Organometallic Systems*. 2nd Edn Oxford University Press, New York

40. Tobe, M.L. and Burgess, J. (1999). *Inorganic Reaction Mechanisms*. Addison-Wesley-Longman, Harlow
41. Heaton, B.T., Strona, L., Jonas, J., Eguchi, T. and Hoffman, G.A. (1982). *J. Chem. Soc. Dalton Trans*. 1159
42. Iggo, J.A., Kawashima, Y., Liu. T.Hiyama, J. and Mozaki, K. (2003). *Organometallics* **22**, 5418
43. Liu, J., Heaton, B.T. and Iggo, J.A. (2004). Whyman. *R. Angew. Chem. Int. Edit.* **43**, 90
44. Hunt, H.R. and Taube, H.J. (1958). *Am. Chem. Soc.* **80**, 2642
45. Burgess, J. and Hubbard, C.D. (1984). *J. Am. Chem. Soc.* **106**, 1717
46. Burgess, J. and Hubbard, C.D. (1988). *Inorg. Chem.* **27**, 2548
47. Blandamer, M.J., Burgess, J., Fawcett, J., Guardado, P., Hubbard, C.D., Nuttall, S., Prouse, L.J.S., Radulovic, S. and Russell, D.R. (1991). *Inorg. Chem.* **31**, 1383
48. Burgess, J. and Hubbard, C.D. (1995). *Comment. Inorg. Chem.* **17**, 283
49. Burgess, J., Duffield, A.J. and Sherry, R. (1980). *J. Chem. Soc. Chem. Comm*. 350
50. Burgess, J. and Hubbard, C.D. (1982). *Inorg. Chim. Acta* **64**, L71
51. Hallinan, N., McCardle, P., Burgess, J. and Guardado, P. (1987). *J. Organomet. Chem.* **333**, 77
52. Le Noble, W.J. and Schlott, R. (1976). *Rev. Sci. Instrum.* **47**, 770
53. Alshehri, S., Burgess, J. and Hubbard, C.D. (1993). *Transit. Met. Chem.* **18**, 228
54. Kotowski, M. and Palmer, D.A. (1979). *H. Kelm Inorg. Chem.* **18**, 2555
55. Zahl, A., Igel, P., Weller, M., Koshtariya, D., Hamza, M.S.A. and van Eldik, R. (2003). *Rev. Sci. Instrum.* **74**, 3758
56. Hartridge, H. and Roughton, F.J.W. (1923). *Proc. Roy. Soc. A.* **104**, 376
57. Chance, B. (1940). *J. Franklin Inst*. 229, 455, 613, 737
58. Roughton, F.J.W. (1934). *Proc. Roy. Soc. B.* **115**, 473
59. Caldin, E.F. (1964). *Fast Reactions in Solution*. Blackwell, Oxford
60. Gibson, Q.H. (1952). *J. Physiol.* **117**, 49
61. Gibson, Q.H. and Greenwood, C. (1963). *Biochem. J.* **86**, 541
62. Gibson, Q.H. and Milnes, L. (1964). *Biochem. J.* **91**, 161
63. Haynes, A., Haslam, C.E., Bonnington, K.J., Parish, L., Adams, H., Spey, S.E., Marder, T.B. and Coventry, D.N. (2004). *Organometallics* **23**, 5907
64. van Eldik, R., Palmer, D.A., Schmidt, R. and Kelm, H. (1981). *Inorg. Chim. Acta* **50**, 131
65. Bugnon, P., Laurenczy, G., Ducommun, Y., Sauvageat, P.-Y., Merbach, A.E., Ith, R., Tschanz, R., Doludda, M., Bergbauer, R. and Grell, E. (1996). *Anal. Chem.* **68**, 3045
66. Heremans, K., Snauwaert, J. and Rijkenberg, J. (1980). *Rev. Sci. Instrum.* **51**, 806
67. Funahashi, S., Ishihara, K. and Tanaka, M. (1981). *Inorg. Chem.* **20**, 5
68. Ishihara, K., Funahashi, S. and Tanaka, M. (1982). *Rev. Sci. Instrum.* **53**, 1231
69. Nichols, P.J., Ducommun, Y. and Merbach, A.E. (1983). *Inorg. Chem.* **22**, 3993
70. Ducommun, Y., Nichols, P.J., Helm, L., Elding, L.I. and Merbach, A.E. (1984). *J. Phys.* **45C8**, 221
71. Balny, C., Saldana, J.L. and Dahan, N. (1984). *Anal. Biochem.* **139**, 178
72. van Eldik, R., Gaede, W., Wieland, S., Kraft, J., Spitzer, M. and Palmer, D.A. (1993). *Rev. Sci. Instrum.* **64**, 1355
73. Funahashi, S., Ishihara, K., Aizawa, S., Sugata, T., Ishii, M., Inada, Y. and Tanaka, M. (1993). *Rev. Sci. Instrum.* **64**, 130
74. Ishihara, K., Kondo, Y. and Koizumi, M. (1999). *Rev. Sci. Instrum.* **70**, 244
75. The Hi-Tech Scientific hpsf is now supplied by TgK Scientific Limited, 7, Long's Yard, St. Margarets Street, Bradford on Avon, Wiltshire, BA15 1DH, UK
76. Hikari High-Pressure Machinery Company. Ltd., 3-16-6 Nakahiro, Nish-ku, Hiroshima 733, Japan
77. Eigen, M. (1954). *Discuss. Farad. Soc.* **17**, 194

78. Eigen, M. and de Maeyer, L. (1963). *Investigations of Rates and Mechanisms of Reactions*, Friess, S.L., Lewis, E.S. and Weissberger, A. (eds), Part II, Chapter 18. Interscience, New York
79. Czerlinski, G. (1966). *Chemical Relaxation*. Marcel Dekker, New York
80. Hague, D.N. (1971). *Fast Reactions*. Wiley-Interscience, New York
81. Bernasconi, C.F. (1976). *Relaxation Kinetics*. Academic Press, New York
82. Strehlow, H. (1992). *Rapid Reactions in Solution*. VCH, Weinheim
83. Caldin, E.F. (2001). *The Mechanisms of Fast Reactions in Solution*. IOS Press, Oxford
84. Caldin, E.F., Grant, M.W., Hasinoff, B.B. and Tregloan, P.A. (1973). *J. Phys. E.* **6**, 349
85. Yu, A.D., Waissbluth, M.D. and Grieger, R.A. (1973). *Rev. Sci. Instrum.* **44**, 1390
86. Jost, A. (1974). *Ber. Bunsenges. Phys. Chem.* **78**, 300
87. Heremans, K. (1978). *High Pressure Chemistry*, Kelm, H. (ed.), p. 311. Reidel, Dordrecht
88. Doss, R., van Eldik, R. and Kelm, H. (1982). *Rev. Sci. Instrum.* **53**, 1592
89. Strehlow, H. and Becker, H. (1959). *Z. Elektrochem.* **63**, 457
90. Brower, K.R. (1968). *J. Am. Chem. Soc.* **90**, 5401
91. Inoue, T., Kojima, K. and Shimozawa, R. (1981). *Chem. Lett*. 259
92. Clegg, R.M. and Maxfield, B.M. (1976). *Rev. Sci. Instrum.* **47**, 1383
93. Heremans, K., Centerick, F. and Rijkenberg, J. (1980). *Rev. Sci. Instrum.* **51**, 252
94. Porter, G. (1963). *Investigations of Rates and Mechanisms of Reactions*, Weiss, S.L., Lewis, E.S. and Weissberger, A. (eds), Part II, Chapter 19. Interscience, New York
95. Brauer, H.-D., Schmidt, R. and Kelm. H. (1978). *High Pressure Chemistry*, Kelm, H. (ed.), p. 521. Reidel, Dordrecht
96. Drickamer, H.G. (1980). *Rev. Phys. Chem. Jpn.* **50**, 1
97. Weber, W., van Eldik, R., Kelm, H., DiBenedetto, J., Ducommun, Y., Offen, H. and Ford, P.C. (1983). *Inorg. Chem.* **22**, 623
98. McGarvey, J.J., Lawthers, I., Heremans, K. and Toftlund, H. (1984). *J. Chem. Soc. Chem. Commun*. 1575
99. DiBenedetto, J., Arkle, V., Goodwin, H.A. and Ford, P.C. (1985). *Inorg. Chem.* **24**, 455
100. Fetterolf, M.L. and Offen, H.W. (1985). *J. Phys. Chem.* **89**, 3320
101. Stochel, G. and van Eldik, R. (1997). *Coordin. Chem. Rev.* **159**, 153
102. van Eldik, R. and Ford, P.C. (1998). *Adv. Photochem.* **24**, 61
103. Wanat, A., Wolak, M., Urzel, L., Brindell, M., van Eldik, R. and Stochel, G. (2002). *Coordin. Chem. Rev.* **229**, 37
104. Chapter 6 in Ref. [31]
105. (a) Fleischmann, F.K., Conze, E.G., Stranks, D.R. and Kelm, H. (1974). *Rev. Sci. Instrum.* **45**, 1427; (b) Skibsted, L.H., Weber, W., van Eldik, R., Kelm, H. and Ford, P.C. (1983). *Inorg. Chem.* **22**, 541; (c) Wieland, S., van Eldik, R., Crane, D.R. and Ford, P.C. (1989). *Inorg. Chem.* **28**, 3663
106. Portius, P., Yang, J., Sun, X.-Z., Grills, D.C., Matousek, P., Parker, A.W., Towrie, M. and George, M.W. (2004). *J. Am. Chem. Soc.* **126**, 10713
107. Kayran, C., Richards, M. and Ford, P.C. (2004). *Inorg. Chim. Acta* **357**, 143
108. van Eldik, R. and Meyerstein, D. (2000). *Accounts Chem. Res.* **33**, 207
109. Masarwa, A. and Meyerstein, D. (2004). *Adv. Inorg. Chem.* **55**, 271
110. Chapter 1 in Ref. [31]
111. Tabata, Y. (1990). *Pulse Radiolysis*. CRC Press, Boca Raton, FL
112. For example: (a) Meier, M. and van Eldik, R. (1997). *Chem. Eur. J.* **3**, 39; (b) Ciosto, C., Bajaj, H.C., van Eldik, R. and Hubbard, C.D. (1999). *J. Chem. Soc. Dalton Trans*. 1503; (c) Hubbard, C.D., Gerhard, A. and van Eldik, R. (2001). *J. Chem. Soc. Dalton Trans*. 1069
113. Swaddle, T.W. (1986). *Inorganic High Pressure Chemistry. Kinetics and* Mechanism, van Eldik, R. (ed.), Chapter 5. Elsevier, Amsterdam

114. Swaddle, T.W. (2002). *High Pressure Chemistry. Synthetic, Mechanistic and Supercritical Applications*, van Eldik, R. and Klärner, F.-G. (eds), Chapter 5. Wiley-VCH, Heidelberg
115. Swaddle, T.W. (2005). *Chem. Rev.* **105**, 2573
116. Fu, Y. and Swaddle, T.W. (1997). *J. Am. Chem. Soc.* **119**, 737
117. Yu, B., Lever, A.P.B. and Swaddle, T.W. (2004). *Inorg. Chem.* **43**, 4496
118. Swaddle, T.W. and Tregloan, P.A. (1999). *Coordin. Chem. Rev.* **187**, 255
119. Akitt, J.W. (1983). *NMR and Chemistry*. 2nd Edn Chapman and Hall, London
120. Benedek, G.B. (1983). *Magnetic Resonance at High Pressure*. John Wiley and Sons New York
121. Voelkel, G., Lang, E. and Lüdemann, H.-D. (1979). *Ber. Bunsenges. Phys. Chem.* **83**, 722
122. Zahl, A., Igel, P., Weller, M. and van Eldik, R. (2004). *Rev. Sci. Instrum.* **75**, 3152
123. Sisley, M.J., Yano, Y. and Swaddle, T.W. (1982). *Inorg. Chem.* **21**, 1141
124. Moore, P. (1985). *Pure Appl. Chem.* **57**, 347
125. Merbach, A.E. (1987). *Pure Appl. Chem.* **59**, 161
126. Swift, T.J. and Connick, R.E. (1962). *J. Chem. Phys.* **37**, 307
127. Holyer, R.H., Hubbard, C.D., Kettle, S.F.A. and Wilkins, R.G. (1965). *Inorg. Chem.* **4**, 929
128. Eigen, M. and Wilkins, R.G. (1965). *Adv. Chem. Series,*. American Chemical Society, Washington, DC
129. Caldin, E.F., Grant, M.W. and Hasinoff, B.B. (1972). *J. Chem. Soc. Farad. Trans. I* **68**, 2247
130. Grant, M.W. (1973). *J. Chem. Soc. Farad. Trans. I* **69**, 560
131. Ishihara, K., Funahashi, S. and Tanaka, M. (1983). *Inorg. Chem.* **22**, 2564
132. van Eldik, R. and Mohr, R. (1985). *Inorg. Chem.* **24**, 3396
133. Dunand, F.A., Helm, L. and Merbach, A.E. (2003). *Adv. Inorg. Chem*. 54 van Eldik, R., and Hubbard, C.D. (eds), p. 1. Academic Press, San Diego, CA
134. Hepler, L.G. (1965). *J. Phys. Chem.* **69**, 965
135. Palmer, D.A. and Kelm, H. (1977). *Inorg. Chem.* **16**, 3139
136. Lawrance, G.A. and Suvachittanont, S. (1979). *Inorg. Chim. Acta* **32**, L13
137. Lincoln, S.F. and Merbach, A.E. (1995). *Adv. Inorg. Chem.* **42**, 1 (Table XIV)
138. Chapter 7 in Ref. [40]
139. Langford, C.H. and Gray, H.B. (1965). *Ligand Substitution Processes*. Benjamin, New York
140. Chapters 1 and 7 in Ref. [40]
141. Merbach, A.E. and van Eldik, R. (1992). *Comment. Inorg. Chem.* **12**, 341
142. Swaddle, T.W. (1983). *Inorg. Chem.* **22**, 2663
143. Lincoln, S.F. and Merbach, A.E. (1995). *Adv. Inorg. Chem.* **42**, 1
144. Powell, D.H., Merbach, A.E., Fábián, I., Schindler, S. and van Eldik, R. (1994). *Inorg. Chem.* **33**, 4468
145. Thaler, F., Hubbard, C.D., Heinemann, F.W., van Eldik, R., Schindler, S., Fábián, I., Dittler-Klingemann, A.M., Hahn, F.E. and Orvig, C. (1998). *Inorg. Chem.* **37** 4022
146. Neubrand, A., Thaler, F., Körner, M., Hubbard, C.D., Zahl, A. and van Eldik, R. (2002). *J. Chem. Soc. Dalton. Trans*. 957
147. Åkesson, R., Pettersson, L.G.M., Sandström, M. and Wahlgren, U. (1994). *J. Am. Chem. Soc.* **116**, 8691–8705
148. Rotzinger, F.P. (1996). *J. Am. Chem. Soc.* **118**, 6760
149. Rotzinger, F.P. (1997). *J. Am. Chem. Soc.* **119**, 5230
150. Hartman, M., Clark, T. and van Eldik, R. (1997). *J. Am. Chem. Soc.* **119**, 5867
151. deVito, D., Sidorenkova, H., Rotzinger, F.P., Weber, J. and Merbach, A.E. (2000). *Inorg. Chem.* **39**, 5547
152. deVito, D., Weber, J. and Merbach, A.E. (2004). *Inorg. Chem.* **43**, 858

153. Yerly, F., Hardcastle, K.L., Helm, L., Aime, S., Botta, M. and Merbach, A.E. (2002). *Chem. Eur. J.* **8**, 1031
154. Rapaport, I., Helm, L., Merbach, A.E., Bernhard, P. and Ludi, A. (1988). *Inorg. Chem.* **27**, 873
155. Stebler-Röthlisberger, M., Hummel, W., Pittet, P.-A., Bürgi, H.-B., Ludi, A. and Merbach, A.E. (1988). *Inorg. Chem.* **27**, 1358
156. Richens, D.T. (1997). *The Chemistry of Aquaions*. John Wiley, Chichester pp. 421–425
157. Cotton, S. (1997). *Chemistry of Precious Metals, p. 22*. Blackie Academic and Professional, Chapman Hall, London
158. Luginbühl, W., Zbinden, P., Pittet, P.A., Armbruster, T., Bürgi, H.-B., Merbach, A.E. and Ludi, A. (1991). *Inorg. Chem.* **30**, 2350
159. Dadci, L., Elias, H., Frey, U., Hörnig, A., Kölle, U., Merbach, A.E., Paulus, H. and Schneider, J.F. (1995). *Inorg. Chem.* **34**, 306
160. Frey, U., Li, Z.-W. and Matras, A. (1996). *Inorg. Chem.* **35**, 981
161. Kölle, U. (1994). *Coordin. Chem. Rev.* **134/135**, 623
162. Huber, F. and Barbieri, R. (1993). *Metal Complexes in Cancer Chemotherapy*, Keppler, B.K. (ed.), pp. 129–220. VCH, Weinheim
163. Aebischer, N., Sidorenkova, E., Ravera, M., Laurenczy, G., Osella, D., Weber, J. and Merbach, A.E. (1997). *Inorg. Chem.* **36**, 6009
164. Prinz, U., Koelle, U., Ulrich, S., Merbach, A.E., Maas, O. and Hegetschweiler, K. (2004). *Inorg. Chem.* **43**, 2387
165. Salignac, B., Grundler, P.V., Cayemittes, S., Frey, U., Scopelliti, R., Merbach, A.E., Hedinger, R., Hegetschweiler, K., Alberto, R., Prinz, U., Raabe, G., Kölle, U. and Hall, S. (2003). *Inorg. Chem.* **42**, 3516
166. Kopf, H. and Kopf-Maier, P. (1988). *Struct. Bond.* **70**, 103
167. Jensen, A. and Basolo, F. (1959). *J. Am. Chem. Soc.* **81**, 5312
168. Keppler, B.K., Diez, A. and Siegfried, V. (1985). *Arzneimittel Forsch* **35**, 12
169. Heim, M.H., Flechtner, H. and Keppler, B.K. (1989). *Prog. Clin. Biochem. Med.* **10**, 217
170. Romeo, R., Lanza, S., Minniti, D. and Tobe, M.L. (1978). *Inorg. Chem.* **17**, 2436
171. Burgess, J. and Parsons, S.A. (1993). *Appl. Organomet. Chem.* **7**, 343
172. Bin Ali, R., Burgess, J. and Casey, A.T. (1989). *J. Organomet. Chem.* **362**, 305
173. Burgess, J., Duffield, A.J. and Sherry, R. (1980). *J. Chem. Soc. Chem. Commun*. 350
174. Burgess, J., Galema, S.A. and Hubbard, C.D. (1991). *Polyhedron* **10**, 703
175. Barraque, C., Vedel, J. and Tremillon, R. (1968). *Bull. Soc. Chim. Fr*. 3421.
176. Alshehri, S., Burgess, J., Parsons, S.A. and Casey, A.T. (1997). *Int. J. Chem. Kinet*. **29**, 835
177. Wilkinson, G. and Birmingham, J.M. (1954). *J. Am. Chem. Soc.* **76**, 4281
178. Sladkov, A.M., Vasneva, N.A., Johansson, A.A. and Derunov, V.V. (1977). *Inorg. Chim. Acta* **25**, L97
179. Burgess, J. and Duffield, A.J. (1979). *J. Organomet. Chem.* **177**, 435
180. Twigg, M.V. (1977). *Inorg. Chim. Acta* **24**, L84
181. Schmidt, G., Paulus, H., van Eldik, R. and Elias, H. (1988). *Inorg. Chem.* **27**, 3211
182. Gillard, R.D. (1975). *Coordin. Chem. Rev.* **16**, 67
183. Lawrance, G.A., Stranks, D.R. and Suvachittanont, S. (1979). *Inorg. Chem.* **18**, 82
184. Hunt, D.F., Farrant, G.C. and Rodeheaver, G.T. (1972). *J. Organomet. Chem.* **38**, 349
185. Green, M., Heathcock, S.M., Turney, T.W. and Mingos, D.M.P. (1977). *J. Chem. Soc. Dalton Trans*. 204
186. Chopra, S.K., Moran, G. and McArdle, P. (1981). *J. Organomet. Chem.* **214**, C36
187. Chopra, S.K., Hynes, M.J. and McArdle, P. (1981). *J. Chem. Soc. Dalton Trans*. 586
188. McArdle, P. and Kavanagh, S. (1985). *J. Organomet. Chem.* **282**, C1
189. Goldschmidt, Z., Gottlieb, H.E. and Cohen, D. (1985). *J. Organomet. Chem.* **294**, 219
190. Brown, P. and Cookson, R.C. (1965). *Tetrahedron* **21**, 1977

191. Hamza, M.S.A., Zou, X., Banka, R., Brown, K.L. and van Eldik, R. (2005). *Dalton Trans*. 782
192. Hamza, M.S.A., Zou, X., Brown, K.L. and van Eldik, R. (2002). *Eur. J. Inorg. Chem*. 268
193. Hamza, M.S.A. and van Eldik, R. (2004). *J. Chem. Soc. Dalton Trans*. 1
194. Alzoubi, B.M., Hamza, M.S.A., Felluga, A., Randaccio, L., Tauzher, G. and van Eldik, R. (2004). *Eur. J. Inorg. Chem*. 653
195. Alzoubi, B.M., Liehr, G. and van Eldik, R. (2004). *Inorg. Chem.* **43**, 6093
196. Hamza, M.S.A., van Eldik, R., Harper, P.L.S., Pratt, J.M. and Betterton, E.A. (2002). *Eur. J. Inorg. Chem*. 580
197. Hamza, M.S.A., Zou, X., Brown, K.L. and van Eldik, R. (2003). *Eur. J. Inorg. Chem*. 268
198. Hamza, M.S.A., Zou, X., Brown., K.L. and van Eldik, R. (2003). *Dalton Trans*. 2986
199. Swaddle, T.W. (1980). *Rev. Phys. Chem. Jpn.* **50**, 230
200. Hamza, M.S.A., Zou, X., Brown, K.L. and van Eldik, R. (2003). *Dalton Trans*. 3832
201. Hamza, M.S.A., Felluga, A., Randaccio, L., Tauzher, G. and van Eldik, R. (2004). *Dalton Trans*. 287
202. Hamza, M.S.A., Gregan, A.G., Brasch, N.E. and van Eldik, R. (2003). *Dalton Trans*. 596
203. Hamza, M.S.A., Dücker-Benfer, C. and van Eldik, R. (2000). *Inorg. Chem.* **39**, 3777
204. Alzoubi, B.M., Hamza, M.S.A., Ducker-Benfer, C. and van Eldik, R. (2002). *Eur. J. Inorg. Chem*. 968
205. Hansen, L.M., Pavan Kumar, P.N.V. and Marynick, D.S. (1994). *Inorg. Chem.* **33**, 728
206. Dücker-Benfer, C., Dreos, R. and van Eldik, R. (1995). *Angew. Chem. Int. Edit. Engl.* **34**, 2245
207. Dandaccio, L., Geremia, S., Dreos-Gariatti, R., Tauzher, G., Asano, F. and Pelizet, G. (1992). *Inorg. Chim. Acta* **194**, 1
208. Cayemittes, S., Poth, T., Fernandez, M.J., Lye, P.G., Becker, M., Elias, H. and Merbach, A.E. (1999). *Inorg. Chem.* **38**, 4309
209. Poth, T., Paulus, H., Elias, H., Dücker-Benfer, C. and van Eldik, R. (2001). *Eur. J. Inorg. Chem*. 1361
210. Howell, A.A.S. and Burkinshaw, P.M. (1983). *Chem. Rev.* **83**, 557
211. Covey, W.D. and Brown, T.L. (1973). *Inorg. Chem.* **12**, 2820
212. Macholdt, H.-T. and Elias, H. (1984). *Inorg. Chem.* **23**, 4315
213. Abu-Gharib, E.A., Bin Ali, R., Blandamer, M.J. and Burgess, J. (1987). *Transit. Met. Chem.* **12**, 371
214. Macholdt, H.-T. and van Eldik, R. (1985). *Transit. Met. Chem.* **10**, 323
215. Burgess, J. and Smith, A.E. (1987). *Transit. Met. Chem.* **12**, 140
216. Grundler, P.V., Salignac, B., Cayemittes, S., Alberto, R. and Merbach, A.E. (2004). *Inorg. Chem.* **43**, 865
217. Basolo, F., Chatt, J., Gray, H.B., Pearson, R.G. and Shaw, B.L. (1961). *J. Chem. Soc*. 2207
218. Basolo, F. and Pearson, R.G. (1967). *Mechanisms of Inorganic Reactions: A Study of Metal Complexes in Solution*. 2nd Edn p. 351 John Wiley, New York
219. Schmülling, M., Grove, D.M., van Koten, G., van Eldik, R., Veldman, N. and Spek, A.L. (1996). *Organometallics* **15**, 1384
220. Schmülling, M., Ryabov, A.D. and van Eldik, R. (1995). *J. Chem. Soc. Dalton Trans*. 1357
221. Schmülling, M. and van Eldik, R. (1997). *Chem. Ber. Recl.* **130**, 1791
222. Hofmann, A., Dahlenberg, L. and van Eldik, R. (2003). *Inorg. Chem.* **42**, 6528
223. Jagyani, D., Reddy, D., Gertenbach, J.A., Hofmann, A. and van Eldik, R. (2004). *Dalton Trans*. 299
224. Fekl, U. and Goldberg, K.I. (2003). *Adv. Inorg. Chem.* **54**, 259

225. Procelewska, J., Zahl, A., van Eldik, R., Zhong, H.A., Labinger, J.A. and Bercaw, J.E. (2002). *Inorg. Chem.* **41**, 2808
226. Shilov, A.E. and Shul'pin, G.B. (2000). *Activation and Catalytic Reactions of Saturated Hydrocarbons in the Presence of Metal Complexes*. Kluwer, Boston, MA
227. Font-Bardia, M., Gallego, C., Gonzalez, G., Martinez, M., Merbach, A.E. and Solans, X. (2003). *Dalton Trans*. 1106
228. Kiplinger, J.L., King, M.A., Arif, A.M. and Richmond, T.G. (1993). *Organometallics* **12**, 3382
229. Kiplinger, J.L., Richmond, T.G., Arif, A.M., Dücker-Benfer, C. and van Eldik, R. (1996). *Organometallics* **15**, 1545
230. Ogata, T., Yanigada, S., Brunschwig, B.S. and Fujita, E. (1995). *J. Am. Chem. Soc.* **117**, 6708
231. Fujita, E., Furenlid, L.R. and Renner, M.W. (1997). *J. Am. Chem. Soc.* **119**, 4549
232. Sakaki, S. and Dedieu, A. (1987). *Inorg. Chem.* **26**, 3278
233. Fujita, E. and van Eldik, R. (1998). *Inorg. Chem.* **37**, 360
234. Fujita, E., Creutz, C., Sutin, N. and Brunschwig, B.S. (1993). *Inorg. Chem.* **32**, 2657
235. Kirchner, K., Dang, S.-Q., Stebler, M., Dodgen, H., Wherland, S. and Hunt, J.P. (1989). *Inorg. Chem.* **28**, 3604;Baik, M.-H., Crystal, J.B. and Friesner, R.A. (2002). *Inorg. Chem.* **41**, 5926
236. Zahl, A., van Eldik, R., Matsumoto, M. and Swaddle, T.W. (2003). *Inorg. Chem.* **42**, 3718
237. Nielson, R.M., McManis, G.E., Safford, L.K. and Weaver, M.J. (1989). *J. Phys. Chem.* **93**, 2152
238. Matsumoto, M. and Swaddle, T.W. (2004). *Inorg. Chem.* **43**, 2724
239. Stahl, S.S., Labinger, J.A. and Bercaw, J.E. (1996). *J. Am. Chem. Soc.* **118**, 5961
240. Canty, A.J., Dedieu, A., Jin, H., Milet, A. and Richmond, M.K. (1996). *Organometallics* **15**, 2845
241. O'Reilly, S.A., White, P.S. and Templeton, J.L. (1996). *J. Am. Chem. Soc.* **118**, 5684
242. Wick, D.D. and Goldberg, K.I. (1997). *J. Am. Chem. Soc.* **119**, 10235
243. Periana, R.A., Taube, D.J., Gamble, S., Taube, H., Satoh, T. and Fuji, H. (1998). *Science* **280**, 560
244. Fekl, U., Zahl, A. and van Eldik, R. (1999). *Organometallics* **18**, 4156
245. Procelewska, J., Zahl, A., Liehr, G., van Eldik, R., Smythe, N.A., Williams, B.S. and Goldberg, K.I. (2005). *Inorg. Chem.* **45**, 7732
246. Roy, S., Puddephatt, R.J. and Scott, J.D. (1989). *J. Chem. Soc. Dalton Trans*. 2121
247. Crumpton-Bregel, D.M. and Goldberg, K.I. (2003). *J. Am. Chem. Soc.* **125**, 9442
248. Williams, B.S. and Goldberg, K.I. (2001). *J. Am. Chem. Soc.* **123**, 2576
249. Williams, B.S., Holland, A.W. and Goldberg, K.I. (1999). *J. Am. Chem. Soc.* **121**, 252
250. Hasinoff, B.B. (1974). *Biochemistry* **13**, 1311
251. Unno, M., Ishimori, K. and Morishima, I. (1991). *Biochemistry* **30**, 10679
252. Taube, D.J., Projahn, H.-D., van Eldik, R., Magde, D. and Traylor, T.G. (1990). *J. Am. Chem. Soc.* **112**, 6880
253. Zhang, M., van Eldik, R., Espenson, J.H. and Bakać, A. (1994). *Inorg. Chem.* **33**, 130
254. Busch, D.H. and Alcock, N.W. (1994). *Chem. Rev.* **94**, 585
255. Busch, D.H., Zimmer, L.L., Grzybowski, J.J., Olszanski, D.J., Jackels, S.C., Callahan, R.W. and Christoph, G.G. (1981). *Proc. Natl. Acad. Sci. USA* **78**, 5919
256. Buchalova, M., Warburton, P.M., van Eldik, R. and Busch, D.H. (1997). *J. Am. Chem. Soc.* **119**, 5867
257. Buchalova, M., Busch, D.H. and van Eldik, R. (1998). *Inorg. Chem.* **37**, 1116
258. Projahn, H.-D. and van Eldik, R. (1991). *Inorg. Chem.* **30**, 3288
259. Schneider, K.J. and van Eldik, R. (1990). *Organometallics* **9**, 1235
260. Pipoh, R., van Eldik, R., Wang, S.L.B. and Wulff, W.D. (1992). *Organometallics* **11**, 490

261. Schneider, K.J., Neubrand, A., van Eldik, R. and Fischer, H. (1992). *Organometallics* **11**, 267
262. Pipoh, R., van Eldik, R. and Henkel, G. (1993). *Organometallics* **12**, 2236
263. Pipoh, R. and van Eldik, R. (1993). *Organometallics* **12**, 2668
264. Lavigne, G. (1990). *The Chemistry of Metal Cluster Complexes*, Shriver, D.F., Kaesz, H.D. and Adams, R.D. (eds), Chapter 2, VCH, New York
265. Hudson, R.H.E. and Poe, A.J. (1995). *Organometallics* **14**, 3238
266. Neubrand, A., Poe, A.J. and van Eldik, R. (1995). *Organometallics* **14**, 3249
267. Waldbach, T.A., van Rooyen, P.H. and Lotz, S. (1993). *Angew. Chem. Int. Edit. Engl.* **32**, 710
268. Waldbach, T.A., van Eldik, R., van Rooyen, P.H. and Lotz, S. (1997). *Organometallics* **16**, 4056
269. Ryabov, A.D., Kuz'mina, L.G., Polyakov, V.A., Kazankov, G.M., Ryabova, E.S., Pfeffer, M. and van Eldik, R. (1995). *J. Chem. Soc. Dalton Trans*. 999
270. Pearson, R.G. and Muir, M.M. (1966). *J. Am. Chem. Soc.* **88**, 2163
271. Ryabov, A.D. (1985). *Synthesis* 233
272. Ryabov, A.D., van Eldik, R., Le Borgne, G. and Pfeffer, M. (1993). *Organometallics* **12**, 1386
273. Evans, D.W. and Baker, G.R. (1989). *G.R. Newkome Coordin. Chem. Rev.* **93**, 155
274. Ref. [1] in Ref. [264]
275. Estevan, F., Gonzalez, G., Lahuerta, P., Martinez, M., Peris, E. and van Eldik, R. (1996). *J. Chem. Soc. Dalton Trans*. 1045
276. (a) Wrighton, M.S. and Morse, D.L. (1975). *J. Organomet. Chem.* **97**, 4405; (b) Rawlins, K.A. and Lees, A.J. (1983). *Inorg. Chem.* **28**, 1254; (c) Balk, R.W., Snoeck, T., Stufkens, D.J. and Oskram, A. (1980). *Inorg. Chem.* **19**, 3015
277. Wieland, S., Bal Reddy, K. and van Eldik, R. (1990). *Organometallics* **9**, 1802
278. Wieland, S. and van Eldik, R. (1989). *J. Chem. Soc. Chem. Commun*. 367
279. Wieland, S. and van Eldik, R. (1990). *Coordin. Chem. Rev.* **97**, 155
280. Wen-Fu, F. and van Eldik, R. (1996). *Inorg. Chim. Acta* **251**, 341
281. Wen-Fu, F. and van Eldik, R. (1997). *Organometallics* **16**, 572
282. Wen-Fu, F. and van Eldik, R. (1998). *Inorg. Chem.* **37**, 1044
283. Dücker-Benfer, C., Grevels, F.-W. and van Eldik, R. (1998). *Organometallics* **17**, 1669 and references loc. Cit
284. Grevels, F.-W., Kayran, C. and Ozkar, S. (1994). *Organometallics* **13**, 2937
285. Wen-Fu, F., Kisch, H. and van Eldik, R. (1997). *Organometallics* **16**, 3439
286. Stufkens, D.J. (1990). *Coordin. Chem. Rev.* **104**, 39
287. Stufkens, D.J. (1992). *Comment. Inorg. Chem.* **13**, 359
288. van der Graaf, T., Stufkens, D.J. and Oskam, A. (1991). *K. Goubitz Inorg. Chem.* **30**, 599
289. van Outersterp, J.W.M., Garriga Oostenbrink, M.T., Nieuwenhuis, H.A., Stufkens, D.J. and Hartl, F. (1995). *Inorg. Chem.* **34**, 6312
290. Nijhoff, J., Bakker, M.J., Hartl, F., Stufkens, D.J., Wen-Fu, F. and van Eldik, R. (1998). *Inorg. Chem.* **37**, 661
291. Parshall, G.W. and Itell, S.D. (1992). *Homogeneous Catalysis*. John Wiley and Sons, New York
292. Ryba, D.W. and van Eldik, R. (1993). *P.C. Ford Organometallics* **12**, 104
293. Boese, W.T., McFarlane, K.L., Lee, B., Rabor, J.G. and Ford, P.C. (1997). *Coordin. Chem. Rev.* **159**, 135
294. McFarlane, K.L., Lee, B., Wen-Fu, F., van Eldik, R. and Ford, P.C. (1998). *Organometallics* **17**, 1826
295. van Eldik, R., Cohen, H., Meshulam, A. and Meyerstein, D. (1990). *Inorg. Chem.* **29**, 4156
296. van Eldik, R., Cohen, H. and Meyerstein, D. (1991). *Angew. Chem. Int. Edit. Engl.* **30**, 1158

297. van Eldik, R., Gaede, W., Cohen, H. and Meyerstein, D. (1992). *Inorg. Chem.* **31**, 3695
298. Goldstein, S., Czapski, G., van Eldik, R., Shaham, N., Cohen, H. and Meyerstein, D. (2001). *Inorg. Chem.* **40**, 4966
299. Sisley, M.J., Rinderman, W., van Eldik, R. and Swaddle, T.W. (1984). *J. Am. Chem. Soc.* **106**, 7432
300. Cohen, H., van Eldik, R., Gaede, W., Gerhard, A., Goldstein, S., Czapski, G. and Meyerstein, D. (1994). *Inorg. Chim. Acta* **227**, 57
301. Gaede, W., van Eldik, R., Cohen, H. and Meyerstein, D. (1993). *Inorg. Chem.* **32**, 1997
302. Shaham, N., Cohen, H., van Eldik, R. and Meyerstein, D. (2000). *J. Chem. Soc. Dalton Trans*. 3356
303. Freiberg, M. and Meyerstein, D. (1980). *J. Chem. Soc. Farad. Trans. I* **76**, 1825
304. Navon, N., Golub, G., Cohen, H. and Meyerstein, D. (1995). *Organometallics* **14**, 5670
305. Bellus, D. (1985). *Pure Appl. Chem.* **57**, 1827
306. Navon, N., Burg, A., Cohen, H., van Eldik, R. and Meyerstein, D. (2002). *Eur. J. Inorg. Chem*. 423

Using kinetic isotope effects to determine the structure of the transition states of S_N2 reactions

KENNETH C. WESTAWAY

Department of Chemistry and Biochemistry, Laurentian University, Sudbury, Ont, P3E 2C6, Canada

1 Theory of kinetic isotope effects

In their 60-year history, kinetic isotope effects (KIEs) have been considered the most useful and sensitive tools for studying the mechanisms and determining the structure of the transition states of chemical and enzymatic reactions.[1,2] Since the goal of this chapter is to show how KIEs have been used to learn how various factors such as substituents, the solvent and ion pairing of the nucleophile affect the transition structures of S_N2 reactions:

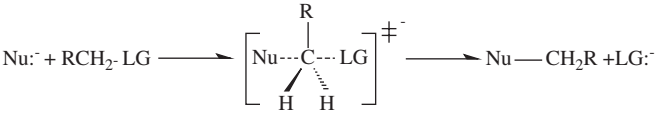

(1)

ADVANCES IN PHYSICAL ORGANIC CHEMISTRY
VOLUME 41 ISSN 0065-3160 DOI: 10.1016/S0065-3160(06)41004-2

where Nu:$^-$ is the nucleophile and LG:$^-$ is the leaving group and since several monographs[1,3,4] discuss heavy-atom and primary and secondary hydrogen–deuterium KIEs very well, only a brief introduction to the use of KIEs as a method of determining the mechanism and transition state structures of S_N2 reactions will be presented.

The Bigeleisen treatment,[5,6] which is based on Eyring and coworkers' absolute rate theory, assumes there is a single potential energy surface along which the reaction takes place, and that there is a potential energy barrier separating the reactants from the products. The reaction occurs along the minimum energy path between reactants and products with the transition state at the top of the barrier; i.e., at the energy maximum along the reaction coordinate but at an energy minimum in all other directions. The transition state is assumed to be in equilibrium with the reactants and products and have all the properties of a stable molecule except that one vibrational degree of freedom has become imaginary and that its energy is converted into motion along the reaction coordinate. The KIE for the reaction is:

$$k_L/k_H = (\kappa_L/\kappa_H)(Q_L^{\neq}/Q_H^{\neq})(Q_{AH}Q_{BH}/Q_{AL}Q_{BL}) \tag{2}$$

where the subscripts L and H refer to the molecules containing the lighter and heavier isotope(s), respectively, the κ terms are the transmission coefficients and the Qs and $Q^{\neq}$s are the complete partition functions for reactants A and B and the transition state, respectively:

$$Q_L/Q_H = (S_L/S_H)(I_{AH}I_{BH}I_{CH}/I_{AL}I_{BL}I_{CL})^{1/2}(M_H/M_L)^{3/2}\prod_i^{3n-6}[[(\upsilon_{Li}-\upsilon_{Hi})hc]/2kT]$$

$$[1-\exp(-hc\upsilon_{Li}/kT)]/[1-\exp(-hc\upsilon_{Hi}/kT)] \tag{3}$$

where s_L and s_H are the symmetry numbers of the respective molecules, the Ms are the molecular weights, the Is are the moments of inertia about the three principal axes of the n-atom molecules and the υs are the fundamental vibrational frequencies of the molecules in wave numbers. Using various approximations,[1] this complicated form of the KIE equation can be reduced to the product of three terms, a tunneling contribution to the KIE (KIE_T), a temperature-independent factor (TIF, the ratio of the imaginary frequency of the light and heavy transition states, respectively) and a temperature-dependent factor (TDF) that consists of the vibrational product (VP), the excitation (EXC) and the zero-point energy (ZPE) factors for the vibrations involving the isotopically labeled atom(s) in the reactants and transition state:

$$k_L/k_H = \underbrace{(k_L/k_H)_{Tunnel}}_{KIE_T}\ \underbrace{(\upsilon_L^{\neq}/\upsilon_H^{\neq})(VP)}_{TIF}\ \underbrace{(EXC)(ZPE)}_{TDF} \tag{4}$$

It has been assumed that the KIE_T and TIF are small in comparison to the TDF so the KIE, k_L/k_H, is primarily determined by the TDF in Equation (4). Also, since the EXC term is small for reactions at or near room temperature, the KIE to a first approximation is determined by the changes in the force constant that occur when the reactants are converted into the transition state. In simple terms, this means the

TDF term can be expressed as:

$$\mathrm{TDF} = [1 + \sum \mathrm{G(u_i)}\Delta \mathrm{u_i} - \sum \mathrm{G(u_i^{\neq})}\Delta \mathrm{u_i^{\neq}}] \quad (5)$$

where $G(u_i) = [1/2 - 1/(u_i) + 1/e^u i - 1)]$ and $\Delta u_i = hc/kT$ $(\Delta \upsilon_i)$. The terms h, c, k and T are Planck's constant, the speed of light, Boltzmann's constant and the absolute temperature, respectively. The $\Delta \upsilon_i$ and $\Delta \upsilon_{i\neq}$ terms represent the isotope effect on the vibrational frequencies of the reactant and transition state, respectively. If the bond to the isotopically labeled atom is broken in a reaction, but bond breaking has not occurred at the transition state of the rate-determining step of the overall reaction, there is no change in the force constants involving the isotopic atom (the second and third terms in Equation (5) will be equal) and the KIE, k_L/k_H, will be $= 1$. If there is a decrease in the force constants to the isotopically labeled atom(s) on going to the transition state of the rate-determining step of the reaction (the third term of Equation (5) is smaller than the second term) a normal KIE of >1.000 will be observed. Conversely, an increase in the force constants to the isotopically labeled atom(s) on going to the transition state of the rate-determining step of the reaction (the third term in Equation (5) is larger than the second term) can lead to an inverse (<1.000) KIE. Hence, KIEs are extremely useful for determining the mechanism of a reaction. Also, because the decrease (increase) in the force constants to the isotopically labeled atom(s) on going to the transition state of the rate-determining step of the reaction is thought to be related to the change in the length of bonds to the isotope(s), i.e., to the length of the bond(s) to the isotope(s) in the transition state, the magnitude of the KIE (normal or inverse) is the best way to determine the amount of bonding to the isotopically labeled atom(s) (the structure) of the transition state for the reaction. Finally, because this chapter only deals with the single step S_N2 reaction, the KIEs discussed below give detailed information about the transition state structure for the reaction.

PRIMARY KIES

A primary KIE is found when the bond to the isotopically labeled atom is breaking or forming in the transition state of the slow step of the reaction. Three basic relationships indicate how the magnitude of a primary KIE varies with transition state structure in S_N2 reactions.

Leaving group KIEs

A primary heavy-atom leaving group KIE is observed when the bond to the isotopic atom is breaking in the transition state. Typical examples are a nitrogen (k^{14}/k^{15}) KIE for the reactions of quaternary ammonium salts,[7] a sulfur (k^{32}/k^{34}) KIE for the reactions of sulfonium salts,[8] and chlorine (k^{35}/k^{37}),[4,9] and bromine (k^{79}/k^{81})[10] KIEs for the reactions of alkyl chlorides and bromides, respectively. A comprehensive review article on this type of KIE has been published by Shiner and Wilgis.[4] In the simple approach to these KIEs for S_N2 reactions, the bonding (the vibrational energy) to the isotopically labeled atom in the LG is reduced on going to the transition state

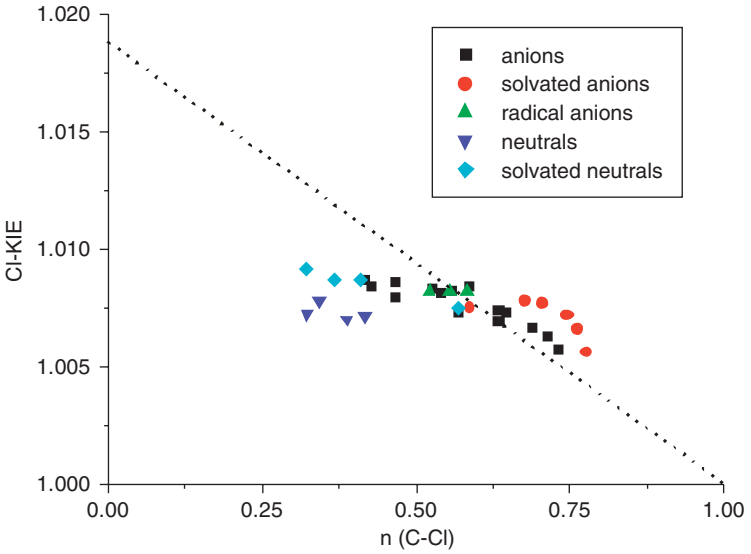

Fig. 1 The dependence of the chlorine KIE on the Wiberg C_α–Cl transition state bond order for the S_N2 reactions of methyl chloride with 26 different nucleophiles. The dashed line is the KIE estimated using the BEBOVIB approach. Reprinted with permission from Ref. [11]. Copyright (2004) American Chemical Society.

so the TDF (Equation (5)) and the KIE, will be >1.000. Since the magnitude of the isotope effect is directly related to the amount of C_α–LG bond rupture in the transition state, these KIEs should provide detailed information about the length (bond order) of the C_α–LG bond in the transition state, see the dotted line in Fig. 1.

Recently, however, this traditional interpretation of this type of KIE has been questioned.[11] The transition state structures and chlorine KIEs for the S_N2 reactions between 25 different nucleophiles (Nu:) and methyl chloride (Table 1) were calculated quantum mechanically at the B1LYP/aug-cc-pVDZ level of theory by Paneth, Westaway and Matsson and their coworkers, and plotted against the Wiberg C_α–Cl transition state bond order[12] (Fig. 1). The qualitative correlation based on the BEBOVIB method[13] (the dotted line in Fig. 1 representing the traditional method of interpreting a leaving group KIE) assumes the C_α–Cl force constant (the KIE) changes linearly with the C_α–Cl bond order in the transition state,[14] with no isotope effect when the transition state bond order approaches unity (reactant) and a maximum KIE of near 1.0190[15] for a reaction where the C_α–Cl bond is fully broken in the transition state. The calculated KIEs did not follow the BEBOVIB line but were almost identical ranging from 1.0056 to 1.0091 even though the C_α–Cl transition state bond order varied from 0.32 to 0.73 (the transition states varied from fairly reactant-like to very product-like) and covered a wide range from very weak neutral nucleophiles (water) to very strong (SH^-) anionic nucleophiles and even to radical anion nucleophiles. Clearly, the KIE does not change with the amount of C_α–Cl bond rupture in the transition state as had previously been thought.

Table 1 The transition structures and chlorine leaving group KIEs for the S_N2 reactions between methyl chloride and several different nucleophiles at 298°C

Nu	r(C–Cl)[a]	%(C–Cl)[b]	n(C–Cl)[c]	Charge–Cl[d]	r(C–Nu)[e]	n(C–Nu)[f]	Charge-Nu[g]	KIE[h]	TIF[i]	TDF[j]	Cl-KIE[k]	%KIET × TIF
Cl^-	2.364	30.61	0.467	−0.647	2.364	0.467	–0.647	1.0005	1.0021	1.0060	1.0086	30.2
F^-	2.076	14.70	0.713	–0.471	2.257	0.218	−0.824	1.0002	1.0014	1.0047	1.0063	25.4
F^- aq[l]	2.218	21.82	0.587	−0.588	2.026	0.285	−0.816	1.0008	1.0019	1.0048	1.0075	36.0
SH^-	2.229	23.15	0.559	−0.564	2.628	0.408	−0.678	1.0005	1.0020	1.0057	1.0082	30.5
CN^-	2.200	21.55	0.567	−0.560	2.462	0.380	−0.787	1.0005	1.0015	1.0053	1.0073	27.4
SCN^-	2.399	32.54	0.429	−0.640	2.384	0.495	−0.600	1.0005	1.0018	1.0061	1.0084	27.4
Br^-	2.428	34.14	0.418	−0.673	2.458	0.530	−0.547	1.0004	1.0020	1.0063	1.0087	27.6
BH_4^-	2.214	22.32	0.587	−0.554	1.702	0.230	−0.707	1.0010	1.0024	1.0050	1.0084	40.5
SeH^-	2.266	25.19	0.527	−0.576	2.709	0.445	−0.636	1.0004	1.0020	1.0059	1.0083	28.9
OCl^-	2.148	18.67	0.647	−0.518	2.158	0.282	−0.788	1.0004	1.0018	1.0051	1.0073	30.1
$S^{\bullet -}$	2.222	22.76	0.554	−0.562	2.630	0.422	−0.677	1.0005	1.0020	1.0057	1.0082	30.5
OBr^-	2.164	19.56	0.634	−0.526	2.136	0.294	−0.783	1.0005	1.0018	1.0051	1.0074	31.1
OF^-	2.094	15.69	0.688	−0.480	2.232	0.256	−0.825	1.0003	1.0015	1.0048	1.0066	27.3
$NHCl^-$	2.038	12.60	0.732	−0.436	2.483	0.233	−0.812	1.0001	1.0007	1.0049	1.0057	14.0
$NHCl^-$ aq[l]	2.068	14.23	0.704	−0.484	2.429	0.249	−0.809	1.0007	1.0021	1.0049	1.0077	36.4
NH_3	2.528	39.64	0.343	−0.681	1.788	0.581	0.132	1.0006	1.0019	1.0053	1.0078	32.1
NH_3 aq[l]	2.235	22.8	0.569	−0.601	2.180	0.338	0.019	1.0007	1.0017	1.0050	1.0075	32.0
OCF_3^-	2.386	31.82	0.466	−0.655	1.941	0.371	−0.737	1.0005	1.0016	1.0058	1.0079	26.6
N_3^-	2.274	25.64	0.541	−0.597	2.142	0.328	−0.761	1.0006	1.0019	1.0056	1.0081	30.9
$SO^{\bullet -}$	2.179	20.38	0.583	−0.520	2.669	0.361	−0.663	1.0004	1.0021	1.0057	1.0082	30.5
PH_3	2.532	39.87	0.323	−0.632	2.112	0.699	0.511	1.0002	1.0008	1.0062	1.0072	13.9
Pyridine	2.439	34.74	0.417	−0.625	1.859	0.486	0.129	1.0003	1.0009	1.0059	1.0071	16.9
4-Nitropyridine	2.470	36.49	0.387	−0.634	1.813	0.517	0.122	1.0003	1.0008	1.0059	1.0070	15.7
$C{\equiv}CH^-$	2.130	17.70	0.634	−0.518	2.433	0.318	−0.752	1.0004	1.0014	1.0051	1.0069	26.1
H_2O aq[l]	2.433	34.40	0.411	−0.709	1.906	0.405	0.190	1.0007	1.0020	1.0060	1.0087	31.1
H_2O THF	2.494	37.77	0.366	−0.733	1.845	0.445	0.201	1.0006	1.0020	1.0061	1.0087	29.9
H_2O ether	2.494	37.77	0.320	−0.711	1.845	0.486	0.191	1.0006	1.0022	1.0063	1.0091	30.8
NH_2^- aq[l]	2.024	11.84	0.741	−0.447	2.598	0.227	−0.868	1.0005	1.0019	1.0048	1.0072	33.3
NH_2^- DMSO	2.019	11.57	0.746	−0.443	2.602	0.223	−0.871	1.0005	1.0018	1.0048	1.0072	32.0
NH_2^- THF	2.005	10.80	0.761	−0.428	2.628	0.211	−0.876	1.0003	1.0015	1.0048	1.0066	27.3

(*Continued*)

Table 1 (*continued*)

Nu	r(C–Cl)[a]	%(C–Cl)[b]	n(C–Cl)[c]	Charge–Cl[d]	r(C–Nu)[e]	n(C–Nu)[f]	Charge-Nu[g]	KIE[h]	TIF[i]	TDF[j]	Cl-KIE[k]	%KIET × TIF
NH_2^- ether	1.991	9.98	0.776	−0.412	2.655	0.198	−0.883	1.0001	1.0009	1.0046	1.0056	17.9
OH^- aq[l]	2.106	16.35	0.676	−0.513	2.284	0.259	−0.824	1.0008	1.0020	1.0049	1.0078	35.9
$Se^{\bullet -}$	2.260	24.83	0.522	−0.576	2.713	0.458	−0.633	1.0004	1.0019	1.0059	1.0082	28.1

Reprinted with permission from Ref. [11]. Copyright (2004) American Chemical Society.

[a]The length of the C_α–Cl TS bond in angstroms.

[b]The % elongation of the C_α–Cl TS bond = 100 × (length of the C_α–Cl TS bond – length of the C_α–Cl bond in the reactant)/length of the C_α–Cl bond in the reactant.

[c]The Wiberg C_α–Cl TS bond order.

[d]The charge on the developing chloride ion in the TS.

[e]The length of the nucleophile—α-carbon bond in the TS in angstroms.

[f]The Wiberg Nu–C_α TS bond order.

[g]The charge on the nucleophile in the TS.

[h]The Wigner tunneling contribution to the chlorine KIE.

[i]The temperature-independent term or imaginary frequency contribution to the chlorine KIE.

[j]The temperature-dependent term or the vibrational energy contribution to the chlorine KIE.

[k]The chlorine leaving group KIE = $KIE_T \times TIF \times TDF$.

[l]Calculated using the PCM continuum solvent model with the conductor field model of electrostatic interactions (COSMO).

It is worth noting that adding water as the solvent with the PCM continuum solvent model[16] and the conductor field model of electrostatic interactions (COSMO)[17] or even specific water molecules to the calculations did not alter the chlorine KIEs, nor the conclusion, significantly. Also noteworthy is the observation that neither the method of calculating the transition state bond order nor anharmonicity affected the conclusions.

It was important to learn why the magnitude of the chlorine KIE is *not* related to the C_α–Cl bond order in the transition state. As expected, the plot of the percent extension of the C_α–Cl bond on going to the transition state varied linearly with the transition state bond order with a correlation coefficient of 0.994. This indicated that the transition state bond order is directly related to the percent extension of the C_α–Cl bond in the transition state even though the transition state bonds are much longer, and weaker, than normal bonds. An analysis of the tunneling contribution (KIE_T) the temperature-independent factor (TIF) and the temperature-dependent factor (TDF) for the KIE (Table 1) showed that the [$KIE_T \times TIF$] represents a significant portion (between 14% and 40%) of the KIE and that the [$KIE_T \times TIF$] term is not correlated with the chlorine KIE (Fig. 2). Since the product of the KIE_T and the TIF term does not vary with transition state structure in any obvious way and accounts for a significant portion of the chlorine KIE, it is this factor that leads to the unexpected results shown in Fig. 1; i.e., the simple theory (the TDF term) assumed the [$KIE_T \times TIF$] term was small and did not affect the magnitude of the KIE significantly and this is obviously not the case. As one would expect, however, the plot in Fig. 3 shows that the TDF is related to transition state structure and the

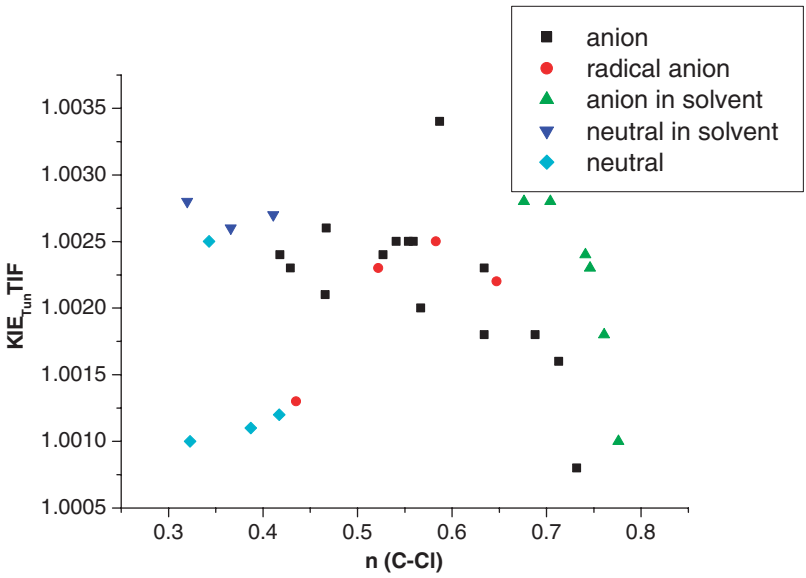

Fig. 2 The dependence of the [$KIE_T \times TIF$] on the C_α–Cl transition state bond order. Reprinted with permission from Ref. [11] Copyright (2004) American Chemical Society.

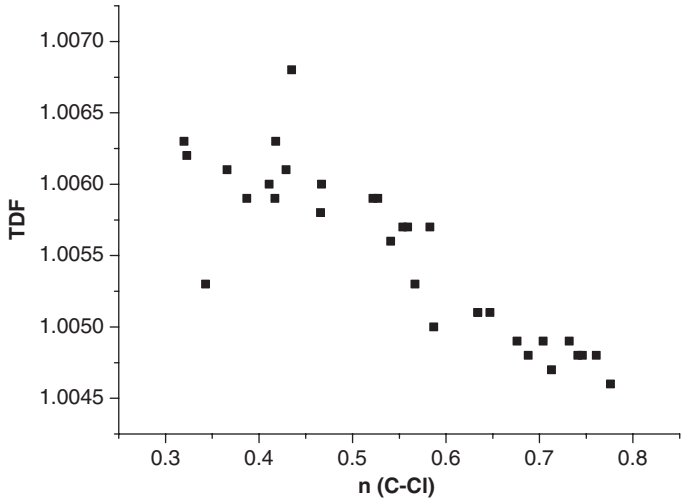

Fig. 3 The TDF term versus the Wiberg C_α–Cl transition state bond order for the S_N2 reactions between methyl chloride and 26 different nucleophiles. Reprinted with permission from Ref. [11] Copyright (2004) American Chemical Society.

magnitude of the leaving group KIE as the simple theory suggests. In fact, given the very wide range of nucleophiles used in this study, the agreement is unexpectedly good with a correlation coefficient of 0.926 when the outlier, NH_3, is discarded. This means the observed chlorine, and presumably other leaving group KIEs, could be used to determine the relative amount of C_α–LG bond rupture in the transition states of reactions if one calculated the transition structure and the KIE_T, the TIF and the TDF of the observed KIE and compared the TDF values. Finally, it is worth noting that the least squares (best) straight line through the data in Fig. 3 does not pass through either the maximum (1.014 for the TDF term) or minimum (1.000) value of the chlorine KIE suggesting the relationship between the TDF term of the KIE and the C_α–Cl transition state bond order must be curved at very small and very large C_α–Cl transition state bond orders.

Although the above work suggests that leaving group KIEs cannot be used to determine the relative transition state structure for different reactions, it is believed that the leaving group KIEs found for reactions where a para-substituent on a benzene ring has been altered or where the solvent has been changed, do reflect changes in transition state structure. This is because the $[KIE_T \times TIF]$ term is not altered significantly by either of these changes in a reaction. As a result, the KIE should change as the TDF term which is related to transition state structure. This is currently being tested both experimentally and with theory.[18] Also, an investigation of the chlorine KIE for the S_N2 reaction between cyanide ion and ethyl chloride in dimethyl sulfoxide (DMSO) and in tetrahydrofuran (THF) (*vide infra*) suggests that leaving group chlorine KIEs can be used to determine the effect of solvent on the relative amount of C_α–Cl bond rupture in the transition state.[19]

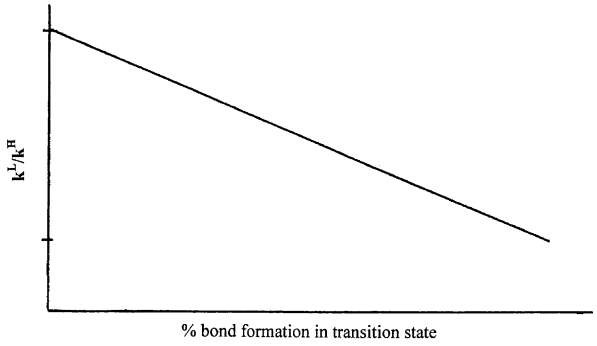

Fig. 4 The incoming group KIE versus the percent bond formation in the transition state.

Incoming group KIEs

A primary incoming group KIE is observed when the bond to the labeled atom is being formed in the transition state; i.e., when the isotope is the nucleophilic atom in an S_N2 reaction. Since there is no bonding between the nucleophile and the substrate in the initial state (the second term in Equation (5) is zero) but bonding in the transition state (the third term in Equation (5) is finite), the TDF is <1. The maximum value of these KIEs is >1.000 because the KIE_T and TIF are always >1.000. Finally, since the magnitude of the third term in Equation (5) is expected to increase with the amount of bonding between the nucleophile and the α-carbon in the transition state, the KIE decreases as the amount of Nu–C_α bonding in the transition state increases (Fig. 4), i.e., the negative TDF becomes larger than the normal $KIE_T \times TIF$ and the observed KIE is <1.000. This relationship between the magnitude of the incoming group KIE and transition state structure is currently being investigated experimentally and by theory.[18]

KIEs where the isotopically labeled atom is transferred between two atoms in the transition state

This type of primary KIE is observed when the α-carbon is labeled in an S_N2 reaction. α-carbon KIEs have been used extensively to determine the mechanism of S_N reactions.[20] Small α-carbon KIEs near 1% are indicative of a carbenium ion S_N (an S_N1) reaction while larger KIEs of up to 8% for a $^{12}C/^{13}C$ KIE,[21] 16% for a $^{12}C/^{14}C$ KIE[22] and 22% for an $^{11}C/^{14}C$ KIE[23] are indicative of an S_N2 mechanism.

The relationship between the magnitude of the KIE and transition state structure is different from the other primary KIEs because the isotopically labeled atom is being transferred between the nucleophile and the leaving group in the transition state. Westheimer[24] and Melander[25] independently pointed out that, because bond formation and bond breaking are occurring concurrently, new stretching vibrations in the transition state, that are not present in the reactants, must be considered. For instance, in the reaction

$$AH + B:^- \rightarrow [A \ldots H \ldots B]^{\neq} \rightarrow A:^- + HB \qquad (6)$$

Fig. 5 The symmetric and asymmetric stretching vibrations for a three atom system.

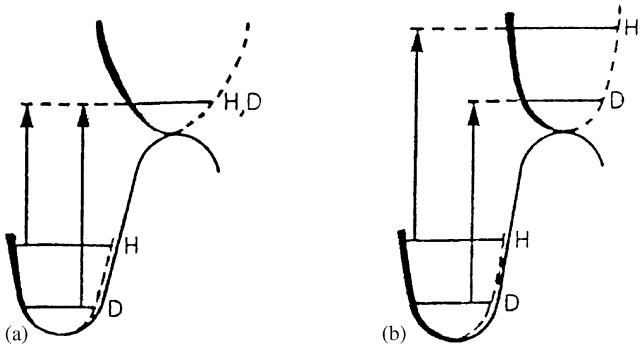

Fig. 6 The reaction coordinate diagram for the symmetric stretching vibration when the central atom is (a) symmetrically placed between atoms A and B (Fig. 5) and (b) closer to either atom A or B (Fig. 5).

where a proton is being transferred from one atom to another via a linear transition state, the transition state has two independent stretching vibrational modes (Fig. 5): the asymmetric vibrational mode represents translational motion in the transition state and has an imaginary force constant while the symmetric transition state vibration has a real force constant.[24–26] If the motion is truly symmetric, the central atom will be motionless in the vibration and the frequency of the vibration will not depend on the mass of this atom; i.e., the vibrational frequency will be the same for both isotopically substituted transition states (Fig. 6a). As a result, there will be no ZPE difference between the symmetric vibrations in the light and heavy isotopically labeled transition states. This means the difference in activation energy is the difference between the ZPE of the symmetric stretching vibrations in the initial state and a maximum KIE will be observed. In instances where bond breaking is either more or less advanced than bond formation, the central atom in the symmetric vibration is not motionless and the stretching frequency depends on the mass of the central atom (Fig. 6b). In these cases, there will be a ZPE difference for the vibrations of the isotopically substituted molecules at the transition state and a smaller KIE will be observed. This means the relationship between the magnitude of the KIE and the percent transfer of the central atom in the transition state is curved with a maximum KIE when the α-carbon is 50% transferred from the nucleophile to the leaving group in the transition state (the solid line in Fig. 7). It is worth noting that this curved relationship has been found experimentally by Yamataka and Ando for the S_N2

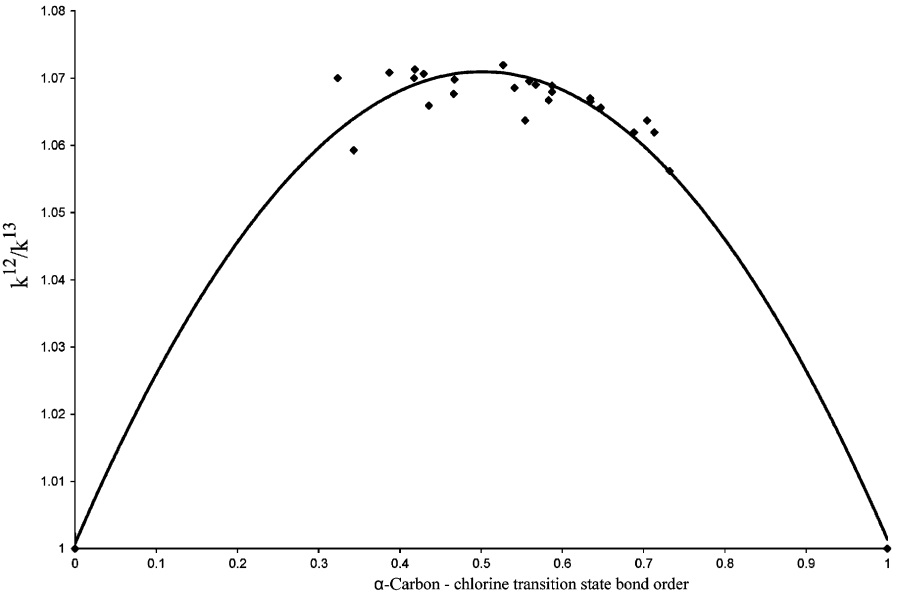

Fig. 7 The α-carbon KIE versus the C_α–Cl transition state bond order for the S_N2 reactions between methyl chloride and 22 different nucleophiles at 298°C. Reprinted with permission from Ref. [36]. Copyright (2005) American Chemical Society.

reactions between benzyl para-substituted benzenesulfonates and *N*,*N*-dimethyl-*p*-toluidine in acetone at 35°C[22] and also in several proton transfer reactions.

However, a review of the literature shows that almost all of the α-carbon KIEs reported for S_N2 reactions are near the experimental maximum KIE of ~8% for a $^{12}C/^{13}C$ KIE, 16% for a $^{12}C/^{14}C$ KIE and 22% for a $^{11}C/^{14}C$ KIE (Table 2).

Since the smallest α-carbon KIE reported for an S_N2 reaction is 80% of the largest-observed KIE, the qualitative conclusion would be that all these S_N2 reactions have symmetric or almost symmetric transition states. This is unreasonable, however, because the α-carbon KIEs that have been measured for S_N2 reactions with very different nucleophiles and leaving groups and in different solvents, Table 2, must have very different transition state structures. This problem led Matsson, Paneth and Westaway *et al*. to investigate the relationship between the magnitude of the α-carbon KIE and the structure of the S_N2 transition state.[36] The transition structure and the α-$^{12}C/^{13}C$ KIEs for 22 S_N2 reactions between different nucleophiles and methyl chloride were calculated at the B1LYP/aug-cc-pVDZ level of theory. The nucleophiles ranged in nucleophilicity from very weak (F^-) to very strong ($C{\equiv}N^-$ and SH^-) (Table 3), and included anionic, neutral and radical anion nucleophiles to cover a wide range of transition structures.

Aplot of the α-carbon KIEs versus the Wiberg C_α–Cl transition state bond order[12] (Fig. 7) shows that all of the calculated KIEs are within 1% of the largest KIE even though the C_α–Cl transition state bond orders vary from ~0.32 to 0.73, the C_α–Nu transition state bond orders vary from 0.21 to 0.70 and the transition states range

Table 2 The α-carbon KIEs measured for S_N2 reactions

k^L/k^H [a]	Reaction	Solvent	Temperature (°C)	Refs.
k^{12}/k^{13}				
1.071 ± 0.008	$CN^- + CH_3$–Cl	Water	31	27
1.071 ± 0.005	$CN^- + CH_3$–I	Water	31	28
1.082 ± 0.007	$CN^- + CH_3$–Br	Water	31	27
1.09 ± 0.05	3,4-Dihydroxyacetophenone + *S*-adenosyl-L-methionine	Water	37	29
1.08 ± 0.02	*S*-methyldibenzothiophenium ion + CH_3O^-	Methanol	25	30
k^{12}/k^{14}				
1.117 ± 0.011	*N*,*N*-dimethyl-*p*-toluidine + CH_3–I,	Methanol	48.5	31
1.120 ± 0.001	*N*,*N*-diethylaniline + CH_3–I	Methanol	62.7	31
1.134 ± 0.047	*N*,*N*-dimethyl-*o*-toluidine + CH_3–I	Methanol	62.7	31
1.119–1.162	Benzyl-*p*-substituted benzenesulfonates + *N*,*N*-dimethyl-*p*-toluidine	Acetone	35	32
1.137–1.151	*m*-bromobenzyl-*p*-substituted benzenesulfonates + *N*,*N*-dimethyl-*p*-toluidine	Acetone	35	32
1.140–1.148	Benzyl-*p*-substituted benzenesulfonates + *N*,*N*-dimethyl-*p*-methoxyaniline	Acetone	35	32
1.135–1.158	Benzyl-*p*-substituted benzenesulfonates + *N*,*N*-dimethylaniline	Acetone	35	32
1.129 ± 0.003	Benzyl-*p*-chlorobenzenesulfonate + *N*,*N*-dimethyl-*m*-toluidine	Acetone	35	32
1.117 ± 0.004	Benzyl-*p*-chlorobenzenesulfonate + *N*,*N*-dimethyl-*p*-bromoaniline	Acetone	35	32
1.127 ± 0.006	Benzyl-*m*-nitrobenzenesulfonate + *N*,*N*-dimethyl-*m*-nitroaniline	Acetone	35	32
k^{11}/k^{14}				
1.208 ± 0.019	$CN^- + CH_3CH_2$–Cl	DMSO	30	33
1.189 ± 0.012	2,4-Lutidine + CH_3–I	Acetonitrile	30	34
1.221 ± 0.006	Triethylamine + CH_3–I	Dimethoxymethane	15	34
1.192 ± 0.001	$OH^- + CH_3$–I	50% Dioxane-water	25	35

[a] k^L/k^H is either k^{12}/k^{13}, k^{12}/k^{14} or k^{11}/k^{14}.

Table 3 The transition state bond orders for the C_α–Nu and the C_α–Cl bonds and the α-carbon KIEs for the S_N2 reactions between methyl chloride and 22 different nucleophiles at 298°C

Nu	n(C–Cl)[a]	n(C–Nu)[b]	TIF[c]	KIE_T[d]	TDF[e]	^{13}C KIE[f]	Δn[g]	%[$KIE_T \times TIF$]
Cl^-	0.467	0.467	1.0342	1.0071	1.0271	1.0698	0.000	59.6
F^-	0.713	0.218	1.0313	1.0042	1.0254	1.0620	0.495	57.5
SH^-	0.559	0.408	1.0340	1.0069	1.0273	1.0695	0.151	59.1
$C{\equiv}N^-$	0.567	0.380	1.0330	1.0091	1.0256	1.0690	0.187	61.4
SCN^-	0.429	0.495	1.0343	1.0079	1.0271	1.0707	–0.066	60.1
Br^-	0.418	0.530	1.0358	1.0063	1.0278	1.0713	–0.112	59.4
BH_4^-	0.587	0.230	1.0314	1.0118	1.0233	1.0680	0.357	64.2
SeH^-	0.527	0.445	1.0359	1.0068	1.0278	1.0720	0.082	59.8
OCl^-	0.647	0.282	1.0327	1.0071	1.0246	1.0656	0.365	61.0
$S^{\bullet -}$	0.554	0.422	1.0339	1.0068	1.0219	1.0637	0.132	64.2
OBr^-	0.634	0.294	1.0332	1.0079	1.0246	1.0670	0.340	61.7
OF^-	0.688	0.256	1.0313	1.0042	1.0254	1.0620	0.432	57.5
$NHCl^-$	0.732	0.233	1.0281	1.0028	1.0246	1.0562	0.499	55.0
NH_3	0.343	0.581	1.0305	1.0077	1.0200	1.0593	–0.238	64.9
$NH_3^{\bullet -}$	0.435	0.359	1.0303	1.0085	1.0258	1.0659	0.076	59.3
OCF_3^-	0.466	0.371	1.0340	1.0101	1.0223	1.0677	0.095	65.6
N_3^-	0.541	0.328	1.0326	1.0092	1.0254	1.0685	0.213	61.5
$SO^{\bullet -}$	0.583	0.361	1.0325	1.0057	1.0272	1.0667	0.222	57.6
PH_3	0.323	0.699	1.0328	1.0089	1.0269	1.0700	–0.376	60.0
Pyridine	0.417	0.486	1.0362	1.0117	1.0207	1.0700	–0.069	69.0
4–NO_2 Pyr	0.387	0.517	1.0364	1.0130	1.0200	1.0708	–0.131	70.4
$C{\equiv}CH^-$	0.634	0.318	1.0324	1.0071	1.0257	1.0665	0.316	59.9
$NHCl^-{}_{aq}$[h]	0.704	0.249	1.0303	1.0090	1.0232	1.0637	0.455	62.1
$F^-{}_{aq}$[h]	0.587	0.285	1.0310	1.0131	1.0234	1.0689	0.303	64.6

Reprinted with permission from Ref. [36]. Copyright (2005) American Chemical Society.

[a]The Wiberg bond order of the C_α–Cl TS bond.

[b]The Wiberg bond order of the Nu–C_α TS bond.

[c]The temperature-independent term or the imaginary frequency contribution to the α-carbon KIE.

[d]The Wigner tunneling contribution to the α-carbon KIE.

[e]The temperature-dependent term or the vibrational energy contribution to the α-carbon KIE.

[f]The α-carbon KIE = $KIE_T \times TIF \times TDF$.

[g]$\Delta n = [(C_\alpha\text{–Cl})_{\text{TS bond order}} – (C_\alpha\text{–Nu})_{\text{TS bond order}}]$.

[h]Calculated using the PCM continuum solvent model with the conductor field model of electrostatic interactions (COSMO).

from very reactant-like to very product-like. Since large α-carbon KIEs are observed for transition states that are early, symmetric or late, the curved relationship in Fig. 7 has a very broad maximum. This, unfortunately, means that α-carbon KIEs are not useful in determining transition state structure. In spite of this, they remain an important tool for determining the mechanism of S_N reactions.

As was found for the chlorine KIEs, the tunneling contribution to the KIE (KIE_T) and the temperature-independent factor (TIF; Equation (4)) play a significant role in determining the magnitude of the KIE; i.e., the KIE_T ranges from 5.0% to 19.1% of the total KIE while the TIF term accounts for between 44.9% and 53.3% of the total KIE and the [$KIE_T \times TIF$] term represents between 55.0% and 70.4% of the

total KIE. As with the chlorine (leaving group) KIEs, none of the TIF, the KIE_T, or the product of the KIE_T and the TIF terms were related to the transition state structure. Finally, the TDF term versus the transition state bond C_α–Cl order does not show the bell-shaped curve, as the simple theory predicts. This probably is because the TDF values only vary over a very small range, i.e., from 1.0200 to 1.0278 (Table 3). It is worth noting that adding water as the solvent with the PCM continuum solvent model[16] and the conductor field model of electrostatic interactions (COSMO)[17] to the S_N2 reactions between fluoride ion or $NHCl^-$ and methyl chloride only increased the KIE slightly (by 0.0007) so solvent does not appear to be the reason for the observed lack of curvature in the KIE versus transition state structure curve. The unfortunate conclusion is that α-carbon KIEs are not useful for determining the structure of S_N2 transition states.

SECONDARY KIES

A secondary KIE is observed when the bond to the isotopically substituted atom is not being broken or formed in the transition state of the rate-determining step of the reaction. Since a secondary KIE is much smaller than a primary KIE, only two types of secondary KIEs, secondary α-deuterium and secondary β-deuterium KIEs, have been studied in any detail.

Secondary α-deuterium KIEs

Secondary α-deuterium KIEs arise when hydrogen(s) at the α- or reacting carbon are replaced by deuterium. Solvolysis reactions proceeding via a carbenium ion intermediate were found to have large normal isotope effects, (k_H/k_D)/α-D, of between 75% and 100% of the theoretical maximum values for each leaving group; i.e., 1.22 for fluoride, 1.15 for chloride, 1.13 for bromide, 1.09 for iodide, 1.19 for ammonia and 1.22 for benzenesulphonate.[37,38] Smaller α-deuterium KIEs, originally thought to be $\leqslant 1.04$/α-D for primary substrates,[39] were observed for reactions proceeding via the S_N2 mechanism. Two reviews discussing the origin and experimental values of this type of KIE are in Refs.[3,40]

Although the magnitude of these KIEs is affected slightly by steric and inductive effects,[3] the magnitude of these KIEs is primarily due to changes in the C_α–H(D) vibrations on going from the reactants to the transition state; i.e., they depend on the change in ZPE on going to the transition state. Smaller force constants for the C_α–H(D) bonds in the transition state than in the reactant leads to an isotope effect >1 (Fig. 8a). When the force constants are greater in the transition state than in the reactant, an isotope effect of <1 is observed (Fig. 8b).

Large α-deuterium KIEs were found for carbenium ion reactions and small KIEs for S_N2 reactions, and since the C_α–H(D) stretching vibration becomes stronger as the sp^3 hybridized substrate is converted into the sp^2 hybridized carbenium ion in an S_N1 reaction, an inverse KIE, not the large normal KIEs observed for S_N1 reactions, should be observed. Therefore, it was suggested that the magnitude of the KIE was

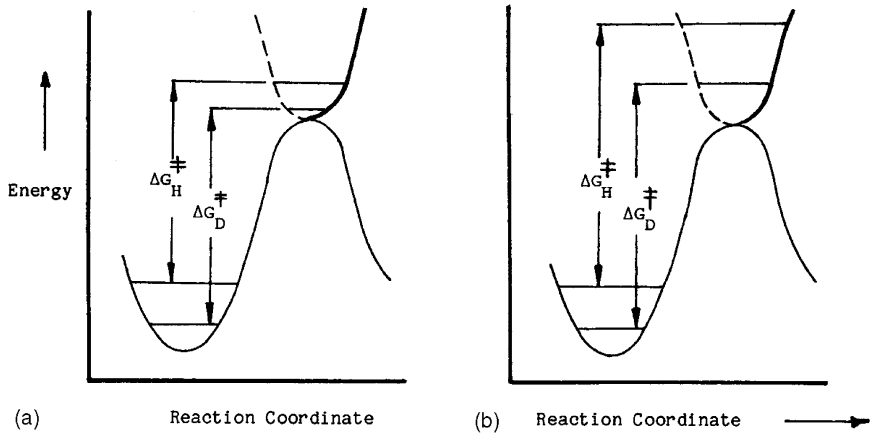

Fig. 8 The reaction coordinate diagram for the secondary α-deuterium KIE for an S_N2 reaction with (a) smaller force constants for the C_α–H(D) bonds in the transition state or for an S_N1 reaction and (b) greater force constants for the C_α–H(D) bonds in the transition state.

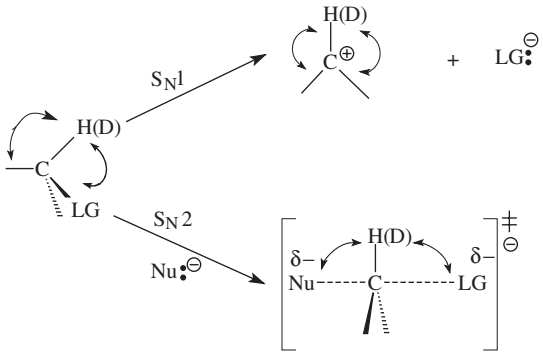

Fig. 9 The C_α–H(D) out-of-plane bending vibrations in the substrate and in the S_N1 and S_N2 transition states.

due to the change in the C_α–H(D) out-of-plane bending vibrations on going from the reactants to the transition state (Fig. 9).

A large normal KIE would be expected for an S_N1 reaction if the KIE was determined by the C_α–H(D) out-of-plane bending vibrations (Fig. 9) because the tetrahedral substrate is converted into the trigonal planar carbenium ion and the bond angle of the (D)H–C_α–H(D) bonds increases from ~109.5° in the substrate to nearly 120° in the transition state. This means the C_α–H(D) out-of-plane bending vibrations are easier (lower energy) in the transition state so a large KIE is observed (Fig. 8a). In an S_N2 reaction, the tetrahedral substrate is converted into a pentavalent transition state (Fig. 9). This would increase the energy of the C_α–H(D) out-of-plane bending vibrations and lead to the small normal or inverse KIEs that are observed for S_N2 reactions (Fig. 8b). This lead to the idea that the magnitude of

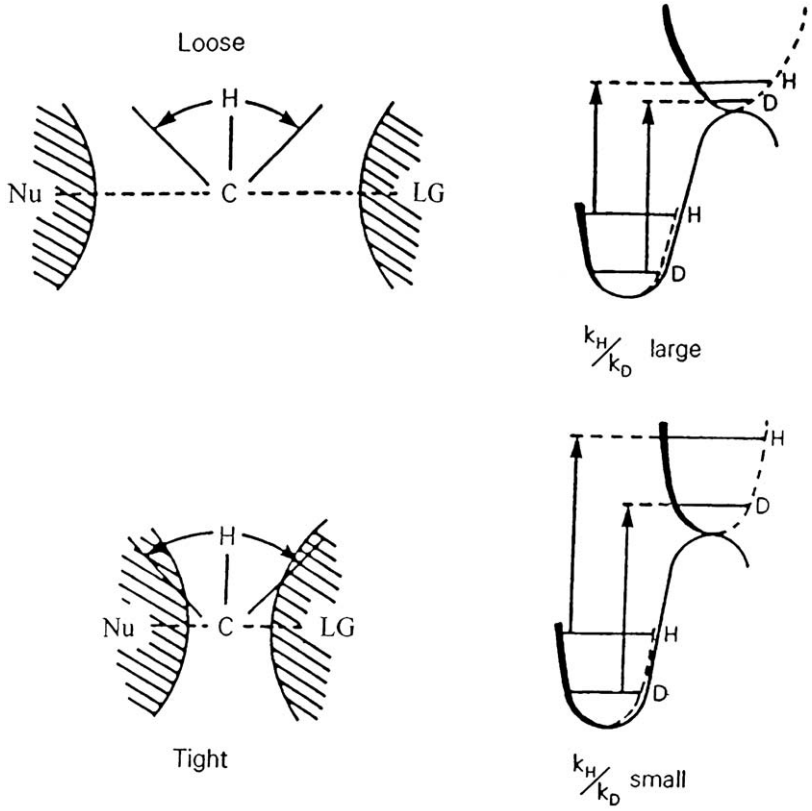

Fig. 10 The relationship between the looseness (the nucleophile–leaving group distance) of the S_N2 transition state and the magnitude of the secondary α-deuterium KIE as determined by the C_α–H(D) out-of-plane bending vibrations in the transition state. Reprinted with permission from Ref. [55]. Copyright (1997) American Chemical Society.

these KIEs was determined by the amount of steric crowding around the C_α–H(D) out-of-plane bending vibrations by the leaving group and/or the incoming nucleophile in the transition state; i.e., a smaller KIE would be found when the transition state was tighter with shorter C_α–Nu and/or C_α–LG bonds because the C_α–H(D) out-of-plane bending vibrations would be higher energy with a larger ZPE difference in the tighter transition state (Fig. 10). In fact, until recently, all of the secondary α-deuterium KIEs in S_N2 reactions have been interpreted by assuming that the magnitude of the KIE is primarily determined by the looseness (the lengths of the C_α–Nu and/or C_α–LG bonds) in the transition state.

Recently, however, this idea has been challenged. The first indication that interpreting these KIEs was more complicated than the simple theory suggested was theoretical calculations by Williams[41] and Truhlar and coworkers[42,43] who reported that the major contribution to the secondary α-deuterium KIE in S_N2 reactions was due to the C_α–H(D) stretching vibrations rather than the C_α–H(D) out-of-plane

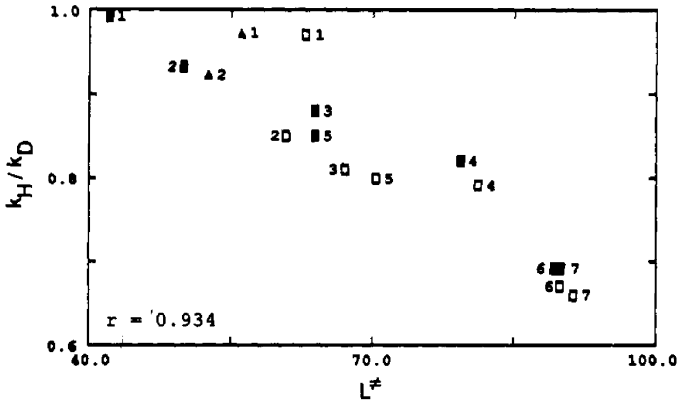

Fig. 11 The magnitude of the secondary α-deuterium KIE versus the looseness parameter $L^{\neq}$ for several identity S_N2 reactions of methyl substrates at different levels of theory. The filled squares were calculated at the 4-31G level, the open squares were calculated at the 6-31 + G* level and the triangles were calculated at the MP2/6-31 + G* level. The numbers refer to the reactions where the nucleophile and leaving group were: (1) Cl, (2) F, (3) OF, (4) CN, (5) MeO, (6) NC and (7) C≡CH, respectively. Reprinted with permission from Ref. [44]. Copyright (1991) American Chemical Society.

bending vibrations. This larger contribution of the stretching vibrations to the KIE was confirmed by Wolfe and Kim,[44] who calculated the transition state structure and the secondary α-deuterium KIE for five different identity (where the leaving group and the nucleophile are the same) S_N2 reactions at the 4-31G, the 6-31 + G* and the MP2/6-31 + G* levels of theory. Wolfe and Kim also defined a "looseness" parameter,

$$L^{\neq} = (\%C_\alpha\text{-Nu} + \%C_\alpha\text{-LG}) \tag{7}$$

where the percent increase in the length of the C_α–LG bond in going from the reactant to the transition state is

$$\%C_\alpha - LG = ((C_\alpha\text{-}LG^{\neq} - C_\alpha\text{-}LG_{react})/C_\alpha - LG_{react}) \times 100\% \tag{8}$$

and C_α–$LG^{\neq}$ and C_α–LG_{react} are the length of the C_α–LG bond in the transition state and reactant, respectively. A similar equation was used to calculate the $\%C_\alpha$–Nu for the Nu–C_α bond. A plot of the secondary α-deuterium KIE versus the $L^{\neq}$ for the five identity S_N2 reactions (Fig. 11) was inverse with a correlation coefficient of 0.943. This led Wolfe and Kim to conclude that the magnitude of the KIE was inversely related to the looseness of the transition state and that all of the secondary α-deuterium KIEs had been interpreted incorrectly! This suggestion obviously caused considerable anguish for those using secondary α-deuterium KIEs to determine transition state structure.

Wolfe and Kim also reported that the stretching vibration contribution to the KIE, effectively the KIE, was determined by the length of the C_α–H(D) bond in the substrate and not by the C_α–H(D) bonds in the S_N2 transition state because the

Table 4 The secondary α-deuterium KIEs for the S_N2 reactions between 3-X-, 5-Y-substituted pyridines and methyl iodide in 2-nitropropane at 25°C

3-X	5-Y	$(k_H/k_D)_\alpha$
CH_3	CH_3	0.908
CH_3	H	0.851
H	H	0.850
Cl	H	0.835
Cl	Cl	0.810

C_α–H(D) transition state bond lengths were identical in every reaction. This meant that the magnitude of the KIE did not depend on the structure of the transition state.

However, several experimental results suggested that Wolfe and Kim's conclusions were not correct. For instance, if Wolfe and Kim's suggestion that the KIE was primarily determined by the length of the C–H(D) bonds in the substrate were correct, secondary α-deuterium KIEs would be independent of the nucleophile used in an S_N2 reaction. Experimental evidence clearly showed that this was not the case. For example, Harris *et al.*[45] found that the secondary α-deuterium KIE varied markedly when the nucleophile was varied in the S_N2 reactions between 3,5-disubstituted pyridines and methyl iodide (Table 4) and in another study, Westaway and Lai[46] found that the secondary α-deuterium KIE changed from 1.13 to 1.03 when the nucleophile changed from a free ion to an ion pair in the S_N2 reaction between sodium thiophenoxide and *n*-butyl chloride in DMSO. Since neither of these changes in nucleophile affect the C_α–H(D) bonds of the substrate, the KIEs should not have changed if Wolfe and Kim were correct. A second argument against the proposal by Wolfe and Kim was that the secondary α-deuterium KIE for a unimolecular nucleophilic substitution (S_N1) reaction would be <1.00 if the C_α–H(D) stretching vibration contribution to the KIE was more important than the bending vibration contribution. This is because the C_α–H(D) bonds are shorter (stronger) in the carbenium ion-like transition state than in the reactant. However, the secondary α-deuterium KIEs found in S_N1 reactions are not inverse, but are large and normal, i.e., >1.07/α-D and can be as large as 1.25/α-D (*vide supra*). This suggests that the bending vibrations are more important than the stretching vibrations in determining the magnitude of the KIE. In fact, Wolfe and Kim's calculated equilibrium isotope effect (EIE) for the conversion of methyl chloride into the methyl carbenium ion and chloride ion supports this conclusion. The stretching vibration contribution to the EIE for this reaction was inverse at 0.93 whereas the bending vibration contribution was a large and normal 2.17 making the EIE large and normal.

These problems led Poirier *et al.*[47] to re-investigate the relationship between the magnitude of the secondary α-deuterium KIE and transition state structure in S_N2 reactions. The optimized geometries for the reactants and the transition structures for the S_N2 reactions where the nucleophile was F^-, Cl^-, OH^-, SH^-, NH_2^- or SCH_3^- and the substrate was either methyl fluoride or chloride were calculated at the HF/6-31 + G* level. Then, Sims' BEBOVIB-IV program was used to carry out a

Table 5 The HF/6-31+G* KIEs and the vibrational contributions to the KIEs for 11 S_N2 reactions of methyl fluoride and chloride with several different nucleophiles at 25°C

Nucleophile	$(k_H/k_D)_\alpha$	$(k_H/k_D)_{stretch}$	$(k_H/k_D)_{bend}$	$(k_H/k_D)_{vib}$	L_{TS}	R_{TS}
Methyl fluoride KIEs						
F^-	0.846	0.677	0.978	0.656	69.2	3.6930
OH^-	0.871	0.686	1.024	0.648	72.8	3.7845
NH_2^-	0.904	0.692	1.054	0.643	75.8	3.9055
Cl^-	1.002	0.665	1.157	0.762	74.5	4.2611
SH^-	1.010	0.663	1.215	0.701	72.4	4.3088
Methyl chloride KIEs						
F^-	0.882	0.705	1.098	0.711	74.5	4.2611
OH^-	0.907	0.714	1.128	0.704	79.7	4.3714
NH_2^-	0.897	0.716	1.112	0.665	80.2	4.4599
Cl^-	0.935	0.680	1.178	0.739	68.0	4.7880
SH^-	0.953	0.690	1.197	0.688	70.9	4.8844
SCH_3^-	0.953	0.701	1.221	0.552	70.1	4.8713

Reprinted with permission from Ref. [47]. Copyright (1994) American Chemical Society.

vibrational analysis and calculate the secondary α-deuterium KIEs at 25°C. In this study, the KIE was expressed as

$$(k_H/k_D) = (k_H/k_D)_{trans}(k_H/k_D)_{vib}(k_H/k_D)_{rot}(k_H/k_D)_T \quad (9)$$

where the tunneling term, $(k_H/k_D)_T$, was determined using the Wigner correction and the vibrational contribution to the KIE, $(k_H/k_D)_{vib}$, was factored into a stretching contribution, $(k_H/k_D)_{stretch}$, and a bending contribution, $(k_H/k_D)_{bend}$:

$$(k_H/k_D)_{vib} = (k_H/k_D)_{stretch}(k_H/k_D)_{bend} \quad (10)$$

The calculated total KIEs, the total vibrational contribution, and both the stretching and bending contributions to the KIE for 11 S_N2 reactions with methyl chloride and fluoride (Table 5) clearly showed that the stretching vibration contribution to the $(k_H/k_D)_\alpha s$ for all the methyl fluoride and chloride reactions was large and inverse as Williams, Truhlar *et al.* and Wolfe and Kim reported. The bending contributions to the KIE, on the other hand, were close to or greater than unity. The magnitude of $(k_H/k_D)_{stretch}$ is greater than $(k_H/k_D)_{bend}$, again, as Truhlar and Wolfe and Kim reported. As a result, the KIEs are inverse, or small and normal, as expected for the S_N2 reactions of methyl compounds. It is important to note that the KIEs in this study were in excellent agreement with those reported by Wolfe and Kim; i.e., 0.846 and 0.84 for the methyl fluoride identity reaction and 0.935 and 0.94 for the methyl chloride identity reaction even though Wolfe and Kim used the encounter complex rather than the reactants as the starting point for their calculations.

The results in Table 5 show the $(k_H/k_D)_{stretch}$ is effectively constant for each leaving group; i.e., it varies from 0.66 to 0.69 (by only 0.03) when the nucleophile changes from F^- to SH^- in the methyl fluoride reactions and from 0.68 to 0.72 (by only 0.04) when the nucleophile changes from F^- to SH^- in the methyl chloride reactions. $(k_H/k_D)_{bend}$, on the other hand, changes from 0.98 to 1.22, i.e., by 0.24 in

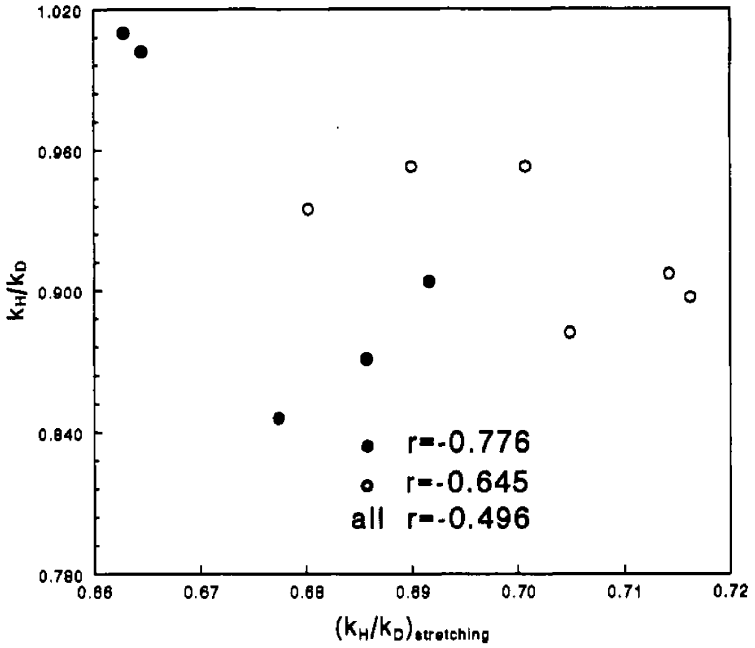

Fig. 12 The total KIE versus the stretching vibration contribution to the KIE for the S_N2 reactions of methyl chloride and fluoride in Table 5 with various nucleophiles. The open circles are for the methyl chloride reactions and the solid circles are for the methyl fluoride reactions. Reprinted with permission from Ref. [47]. Copyright (1994) American Chemical Society.

the methyl fluoride reactions, and by 0.12, i.e., from 1.10 to 1.22, in the methyl chloride reactions. Thus, the change in $(k_H/k_D)_{bend}$ is eight times greater than the change in $(k_H/k_D)_{stretch}$ for the methyl fluoride reactions and is three times greater for the methyl chloride reactions! Obviously, the bending vibration contributions to the KIE are much more sensitive to a change of nucleophile than the stretching vibration contribution in both the reactions. Since the $(k_H/k_D)_{stretch}$ is effectively constant, but different, for each leaving group, the change in $(k_H/k_D)_\alpha$ with a change in nucleophile is primarily determined by the change in $(k_H/k_D)_{bend}$. Plots of $(k_H/k_D)_\alpha$ versus $(k_H/k_D)_{stretch}$ and $(k_H/k_D)_{bend}$ (Figs. 12 and 13, respectively) illustrate this clearly. The correlation coefficients (r) were 0.985 for the methyl chloride reactions and 0.983 for the methyl fluoride reactions versus $(k_H/k_D)_{bend}$ whereas they were only 0.645 and 0.776, respectively, versus $(k_H/k_D)_{stretch}$. It is important to note that the KIEs for the identity reactions are included in these plots and, therefore, there is nothing unusual about the identity reactions. Since the changes in the bending vibration contribution to the KIE vary with the nucleophile, these vibrations must be responsible for the trends in the KIE and an S_N2 reaction with a looser transition state would be expected to have a larger KIE as the original relationship suggested. This was confirmed by the plots of the nucleophile–leaving group

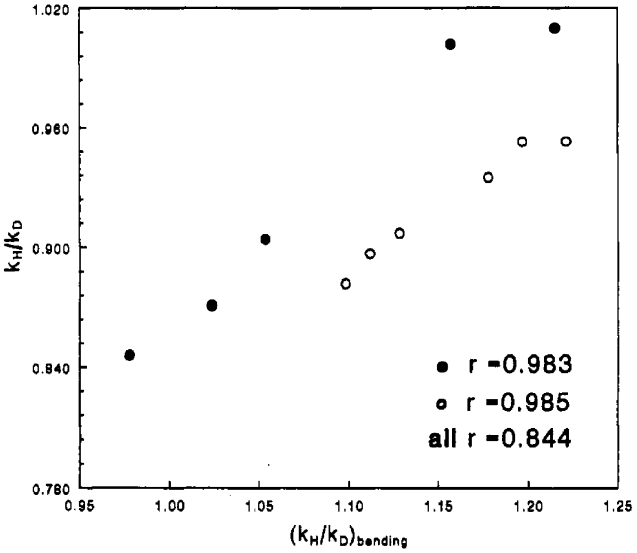

Fig. 13 The total KIE versus the bending vibration contribution to the KIE for the S_N2 reactions of methyl chloride and fluoride in Table 5 with various nucleophiles. The open circles are for the methyl chloride reactions and the solid circles are for the methyl fluoride reactions. Reprinted with permission from Ref. [47]. Copyright (1994) American Chemical Society.

(Nu⁻LG) distance in the S_N2 transition state, R_{TS}, where

$$R_{TS} = C_\alpha - Nu_{TS} + C_\alpha - LG_{TS} \tag{11}$$

and C_α–Nu_{TS} and C_α–LG_{TS} are the lengths of the C_α–Nu and C_α–LG transition state bonds, respectively, against $(k_H/k_D)_\alpha$ and $(k_H/k_D)_{bend}$ (Figs. 14 and 15). Both plots are linear with very high correlation coefficients. For instance, the plot of $(k_H/k_D)_\alpha$ and of $(k_H/k_D)_{bend}$ versus R_{TS}, Figs. 14 and 15, respectively, has correlation coefficients of 1.000 and 0.987, respectively, for the methyl fluoride reactions and 0.973 and 0.957, respectively, for the methyl chloride reactions. Thus, as R_{TS} increases (the transition state becomes looser), both the $(k_H/k_D)_{bend}$ and $(k_H/k_D)_\alpha$ increase as the bending vibration model predicts. Therefore, although the stretching vibration plays a significant role in determining the magnitude of the KIE for S_N2 reactions of a substrate *with a particular leaving group*, $(k_H/k_D)_{bend}$ and the trend in $(k_H/k_D)_\alpha$ are determined by the looseness of the S_N2 transition state. It is important to note that the R_{TS} model does not apply to identity reactions with different leaving groups because the large stretching contribution to the KIE is different for each leaving group. As a result, the major component of the KIE, i.e., the product of the stretching and bending vibration contribution to the total KIE, does not correlate with R_{TS}.

Poirier *et al.*[47] also found that plots of $L^{\neq}$ for the 11 S_N2 reactions in their study against the $(k_H/k_D)_\alpha$ had correlation coefficients of only 0.421 for the methyl fluoride

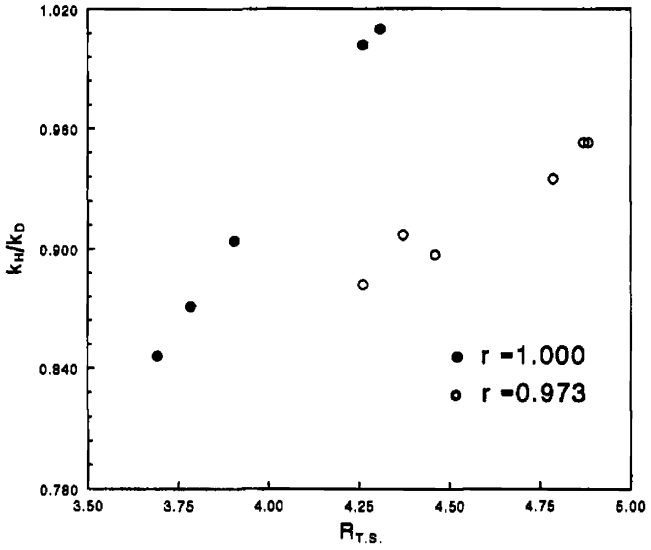

Fig. 14 The total KIE versus R_{TS} for the S_N2 reactions of methyl chloride and fluoride in Table 5 with various nucleophiles. The open circles are for the methyl chloride reactions and the solid circles are for the methyl fluoride reactions. Reprinted with permission from Ref. [47]. Copyright (1994) American Chemical Society.

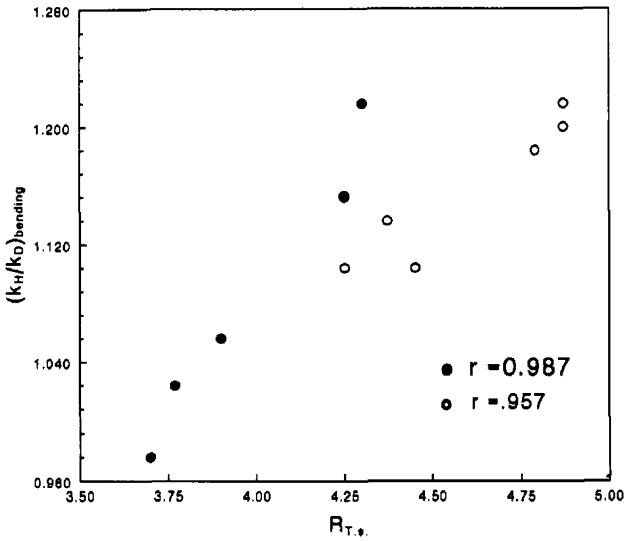

Fig. 15 The bending vibration contribution to the KIE versus R_{TS} for the S_N2 reactions of methyl chloride and fluoride in Table 5 with various nucleophiles. The open circles are for the methyl chloride reactions and the solid circles are for the methyl fluoride reactions. Reprinted with permission from Ref. [47]. Copyright (1994) American Chemical Society.

and 0.719 for the methyl chloride reactions. Clearly, there is no correlation between $L^{\neq}$ and the magnitude of the KIE. This may be because the energy required to increase the length of a bond by a certain percentage is different for each bond; i.e., it is determined by the strength of the bond and the curvature of its potential energy surface.

Finally, it is important to note that the $(k_H/k_D)_\alpha$ for the ethyl chloride and ethyl fluoride S_N2 reactions with several nucleophiles showed the same relationship between the α-deuterium KIE and transition state structure (R_{TS}). However, the (bending/stretching) contribution to the KIE is significantly greater for the S_N2 reactions of ethyl substrates; i.e., it increased from 0.48 for the methyl chloride reactions to 0.88 for the reactions of ethyl chloride and from 0.17 to 0.22 for the methyl and ethyl fluoride reactions. Thus, the bending vibrations play a greater role in determining the magnitude of the $(k_H/k_D)_\alpha$ for the reactions of more complex substrates. This accounts for the change from the inverse $(k_H/k_D)_\alpha$s often found for the methyl substrate S_N2 reactions to the normal $(k_H/k_D)_\alpha$s found for the S_N2 reactions of larger (more complex) substrates such as ethyl and benzyl.

Barnes and Williams[48] reached the same conclusion concerning the origin of these KIEs. These workers calculated the transition structure and the $(k_H/k_D)_\alpha$s for the S_N2 reactions of methyl, ethyl and isopropyl chlorides using the AM1 semiclassical level of theory. They found an almost constant inverse stretching vibration contribution to the KIE was accompanied by a normal bending vibration contribution to the KIE and that the $(k_H/k_D)_\alpha$ increased as the transition state became looser, in agreement with the findings of Poirier *et al.*

In another study, Glad and Jensen[49] calculated the transition structures and secondary α-deuterium KIEs for the S_N2 identity reactions of methyl fluoride, chloride and bromide at the MP2/6-31++G(d,p) level and analyzed the various contributions to the KIE. They reported that (i) the contribution from the C_α–H(D) stretching vibrations was important for determining the magnitude of the total KIE, (ii) the change in the KIE with transition state looseness was primarily due to the changes that occur in the (D)H–C_α–H(D) out-of-plane bending and umbrella bending vibrations and (iii) none of the other transition state vibrations nor the rotational or the translational contributions to the KIE have a significant effect on the magnitude of the KIE. They also found that neither Wolfe and Kim's $L^{\neq}$ nor Poirier *et al.*'s R_{TS} measurement of transition state looseness fit their data. The fit with R_{TS} fails because Glad and Jensen used reactions with different leaving groups and R_{TS} only applies to reactions with the same leaving group. However, they did find that the KIE was larger for a looser transition state with the same, almost linear, slope for the KIE versus $\Delta R_{CX} = 1/2\Delta R^{\neq}$ where

$$\Delta R^{\neq} = \Delta R^{\neq}_{CN_u} + \Delta R^{\neq}_{CL} \tag{12}$$

and $\Delta R^{\neq}_{CNu}$ and $\Delta R^{\neq}_{CL}$ are ($R^{\neq}_{CNu}$–$R_{prodCNu}$) and ($R^{\neq}_{CL}$–$R_{reactCL}$), respectively. This is in agreement with the findings of Poirier *et al.* However, it is interesting to note that Glad and Jensen's trend in the KIEs with leaving group for the methyl fluoride, chloride and bromide identity reactions differs from that calculated by Ruggiero and

Williams[50] (*vide infra*) so the Glad and Jensen definition of looseness may not be correct either.

In a recent publication, Ruggiero and Williams[50] calculated the secondary α-deuterium KIEs for several identity S_N2 reactions at the MP2/6-311 + G* level. Their secondary α-deuterium KIEs were attributed to both a steric factor (the bending vibrations) and the stretching vibration contribution to the KIE. They also found the C_α–H(D) stretching vibration contribution to the KIE was inverse but did not dominate the KIE and that there was no relationship between the stretching vibration component of the KIE and the KIE in agreement with the conclusions by Poirier *et al.* and Glad and Jensen. However, they also found there was no correlation with either Wolfe and Kim's $L^{\neq}$, Poirier *et al*'s R_{TS}, Jensen's ΔR_{CX} nor with the $\Delta\tau$ proposed by Albery and Kreevoy.[51] Thus, it appears that there is no good measure of transition state looseness to date that predicts the KIE for all S_N2 reactions, although R_{TS} seems to work for reactions with the same leaving group. In this regard, Bierbaum and coworkers[52] measured the secondary α-deuterium KIEs for the S_N2 reactions of methyl fluoride, chloride, bromide and iodide with several different nucleophiles in the gas phase. They also calculated the KIEs for these reactions using several levels of theory. All of the calculated KIEs and the experimental KIEs for the methyl fluoride and chloride S_N2 reactions correlated with the R_{TS} looseness parameter for each leaving group (Fig. 16). However, the KIE versus R_{TS} relationship failed for the experimental methyl bromide and iodide reactions (Fig. 16). The authors suggested the methyl bromide and iodide reactions may occur so rapidly in the gas phase that statistical thermodynamics and transition state theory do not apply to these reactions; i.e., they react so rapidly that the energy of the collision complex is not equilibrated so transition state theory does not apply and that this is the reason the KIEs for these two substrates do not fit the R_{TS} model. The important observation, however, is that there is evidence from both experiment and theory that indicates the R_{TS} model works for S_N2 reactions *with the same leaving group*.

Recently, work by Davico and Bierbaum has indicated that although the relationship with R_{TS} is basically correct, that it is not complete, and cannot account for magnitude of the secondary α-deuterium KIE in some S_N2 reactions. These workers suggest that crowdedness, rather than looseness, of the transition state is a better way of understanding the magnitude of a secondary α-deuterium KIE. This is because polyatomic nucleophiles and diatomic nucleophiles with two or more heavy atoms that are off the Nu–C_α–LG axis can sterically hinder the C_α–H(D) bending vibrations in the transition state. In these cases, the C_α–H(D) bending vibrations will be of higher energy than that expected for a particular R_{TS} (looseness of the transition state). This makes the C_α–H(D) transition state bending vibration contribution to the KIE, and the KIE, smaller than predicted by the R_{TS} model. Thus, monotomic and diatomic nucleophiles with a hydrogen atom, such as those used by Poirier *et al.*, follow the looseness or R_{TS} model while polyatomic or diatomic nucleophiles with two or more heavy atoms can affect the C_α–H(D) bending vibrations in the transition state and affect the magnitude of the KIE. It is worth noting that not all polyatomic or diatomic nucleophiles with two heavy atoms will

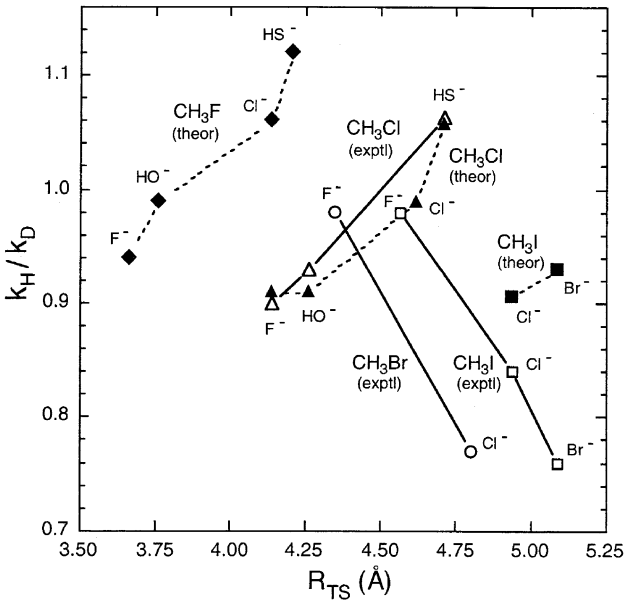

Fig. 16 The experimental (open symbols) and theoretical (closed symbols) secondary α-deuterium KIEs for the S_N2 reactions of methyl halides with various nucleophiles in the gas phase. The R_{TS} values were obtained from the theoretical calculations of the transition structure using transition state theory at the MP2/6-31 + + G*, MP2/6-31 + G(d), MP2/PDZ or MP2/PTZ level. Although R_{TS} varied with the level of theory, the correlations remained. Reprinted with permission from Ref. [52]. Copyright (2001) Elsevier.

affect the bending vibrations in the transition state. Only those where the other atoms affect the C_α–H(D) transition state bending vibrations will cause a reduction from the KIE predicted by the R_{TS} model.

Davico and Bierbaum[53] also reported that large nucleophiles affect the value of the rotational component of the KIE. The rotational component of the KIE is larger (~0.85) for small (monotomic and diatomic) nucleophiles but can be as low as 0.65 for large nucleophiles. However, this does not affect the KIE significantly because the product of the low-energy vibrational component, the translational component and the rotational component of the KIE is effectively constant for all nucleophiles.

Other theoretical calculations of the S_N2 reactions between fluoride ion and methyl fluoride at the B3LYP/6-31 + + G** (5d) level of theory by Hasanayn *et al.*[54] has suggested that the magnitude of secondary α-deuterium KIEs depends on the transition state Nu–C_α–LG bond angle. They found that the KIE is larger when the S_N2 reaction occurs with retention of configuration and a bent, rather than a linear, transition state. This suggests that a larger KIE will be found as the transition state Nu–C_α–LG bond angle is decreased from the expected 180° although it is not clear that small reductions in the Nu–C_α–LG bond angle will cause a reduction in the KIE. Finally, Ruggiero and Williams's[50] calculations have suggested that the magnitude of these KIEs is determined by the distance traveled by the methyl group on

going from the reactant complex to the product complex and the change in the C_α–LG force constant on going to the transition state. In fact, they found a "fair linear correlation" between the change in the C_α–LG bond stretching force constant on going from the reactant complex to the transition state and the KIE. It is interesting that this change in force constant must be related to looseness in some way. However, it is puzzling that the KIE does not seem to be influenced by the looseness of the Nu–C_α transition state bond.

Another suggestion was that the magnitude of a $(k_H/k_D)_\alpha$ was determined by the changes that occur in only the shorter of the reacting bonds in an unsymmetric S_N2 transition state; i.e., if one of the reacting bonds is short and the other is very long in an unsymmetric S_N2 transition state, a change in the length of the longer bond would not affect the C_α–H(D) bending vibrations in the transition state. As a result, the magnitude of the KIE would only be determined by changes in the length of the shorter reacting bond in the transition state (Fig. 17).

The first set of KIEs that suggested the magnitude of a secondary α-deuterium KIE might not be determined by the Nu–LG distance in the transition state was found for the S_N2 reactions between several para-substituted thiophenoxide ions and benzyldimethylphenylammonium ion in *N*,*N*-dimethyl formamide (DMF):[55]

$$\begin{aligned} &4\text{-Y-}C_6H_4S^- + C_6H_5CH_2\text{-}\overset{+}{N}(CH_3)_2C_6H_5 \\ &\rightarrow 4\text{-Y-}C_6H_4S\text{-}CH_2C_6H_5 + (CH_3)_2NC_6H_5 \end{aligned} \tag{13}$$

Both the nitrogen (leaving group) and secondary α-deuterium KIEs found for these reactions at 0°C in DMF at an ionic strength of 0.904 M (Table 6) are identical considering the experimental errors. The simplest interpretation of these identical KIEs would be that the transition state structure does not change when the substituent on the nucleophile is altered. This suggestion seemed highly unlikely, however, because (i) no one has observed this behavior in any study and (ii) it is unreasonable to conclude that a change in nucleophile, which changes the rate constant by a factor of 6.4, would not alter the energy and, therefore, the structure of the transition state. A second, and more likely, possibility is that the change in nucleophile alters the structure of the transition state but that the change in

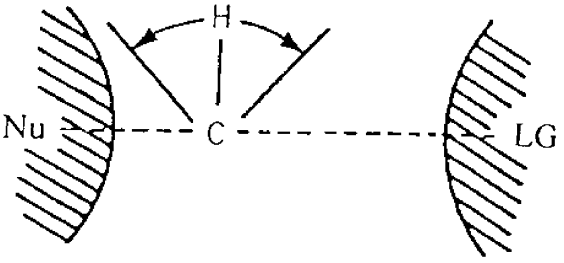

Fig. 17 The C_α–H(D) out-of-plane bending vibrations in an unsymmetric S_N2 transition state. Reprinted with permission from Ref. [55]. Copyright (1997) American Chemical Society.

Table 6 Nitrogen (leaving group) and secondary α-deuterium KIEs for the S_N2 reactions between several para-substituted sodium thiophenoxides and benzyldimethylphenylammonium nitrate in DMF at 0°C at an ionic strength of 0.940 M

Para-substituent on the thiophenoxide ion	k^{14}/k^{15}	$(k_H/k_D)_\alpha$
CH_3O	1.0162 ± 0.0007	1.221 ± 0.012
H	1.0166 ± 0.0004	1.215 ± 0.011
Cl	1.0166 ± 0.0005	1.215 ± 0.013

Table 7 The secondary α-deuterium and nitrogen leaving group KIEs and Hammett ρ values for the S_N2 reaction between sodium thiophenoxide and benzyldimethylphenylammonium nitrate at different ionic strengths in DMF at 0°C

Ionic strength (M)	k^{14}/k^{15}	$(k_H/k_D)_\alpha$	Hammett ρ
0.904	1.0166 ± 0.0004	1.215 ± 0.011	−1.62 ± 0.01
0.64	1.0200 ± 0.0007	1.179 ± 0.007	−1.76 ± 0.19

transition state structure does not cause a change in the secondary α-deuterium KIE. If one assumes that the nitrogen leaving group KIEs can be interpreted in the usual fashion; i.e., that the magnitude of the KIE increases with the percent C_α–N bond rupture in the transition state for these closely related S_N2 reactions only differing by the para-substituent on the nucleophile, then all three reactions have identical amounts of C_α–N bond rupture in the transition state. If this is the case, then interpreting the secondary α-deuterium KIEs must not be straightforward. The identical secondary α-deuterium KIEs were rationalized as follows. If the transition states were unsymmetric and the bonds to the reacting nucleophile (the S–C_α bonds) in the transition state were very long, the magnitude of the secondary α-deuterium KIE would only be determined by the shorter (C_α–N) reacting bond (Fig. 17) because the nucleophilic sulfur atom would be too far away to affect the C_α–H(D) bending vibrations in the transition state. So, if the C_α–N transition state bond that does not change with substituent was short and the S–$C_\alpha$transition state bond was long and changed with substituent, the magnitude of the secondary α-deuterium KIE would be determined by only changes that occur in the shorter C_α–N transition state reacting bond and identical secondary α-deuterium KIEs would be observed for the three reactions.

Several observations support the suggestion that the transition states for these reactions are unsymmetric with long S–C_α and short C_α–N bonds. A comparison of the nitrogen and secondary α-deuterium KIEs for the S_N2 reaction between benzyldimethylphenylammonium ion and thiophenoxide ion (Equation (13)) at two different ionic strengths[56] (Table 7) shows that the transition state for the 0.904 M ionic strength reaction is, indeed, unsymmetric with long S–C_α and short C_α–N bonds. The identical nitrogen KIEs of 1.0165 found at the high ionic strength (Table 6) were only approximately one-third of the theoretical maximum nitrogen KIE of 1.044[57] and are significantly smaller than the nitrogen KIE of 1.0200 found for the

same reaction at an ionic strength of 0.64 (Table 7). Therefore, C_α–N bond rupture is not well advanced in the transition states of the high ionic strength reactions and the C_α–N bonds must be reasonably short. The identical secondary α-deuterium KIEs of 1.22 for the high ionic strength reactions (Table 6) on the other hand, were the largest (~11%/α-D) that have been found for an S_N2 reaction of a quaternary ammonium ion and are significantly larger than the $(k_H/k_D)_\alpha = 1.179$ found for the same reaction at an ionic strength of 0.64 M (Table 7). Since the C_α–N bond is shorter and the secondary α-deuterium KIEs are larger in the high ionic strength reactions, the transition states for the high ionic strength reactions must be very loose with very long S–C_α bonds. Thus, the KIE data suggests the high ionic strength reactions with constant nitrogen and secondary α -deuterium KIEs have very reactant-like transition states with short C_α–N and very long S–C_α bonds.

The Hammett ρ values also suggest that the S–C_α transition state bond is very long in the high ionic strength reactions. Since a larger ρ value is observed when the change in charge on the sulfur atom on going from the reactants to the transition state is larger; i.e., when there is more S–C_α bond formation in the transition state, the smaller Hammett ρ value of –1.62 observed for the high ionic strength reaction (Table 7) indicates the S–C_α transition state bond is longer (less formed) in the high ionic strength reaction. Finally, since it was concluded the reaction at low ionic strength has a symmetric transition state,[7] the transition states in the reactions with the constant KIEs must be reactant-like with very long S–C_α and short C_α–N bonds.

Since the transition state is unsymmetric and very reactant-like, and since the change in substituent does not alter the short C_α–N transition state bond significantly, identical secondary α-deuterium KIEs are found for all three S_N2 reactions in Table 6. This occurs because the change in transition state structure with substituent is too far away to affect the C_α–H(D) bending vibrations in the transition state (the magnitude of the secondary α-deuterium KIE, Fig. 17).

Westaway's ''Bond Strength Hypothesis''[58] suggests that ''there will be a significant change in the weaker reacting bond but little or no change in the stronger reacting bond in an S_N2 transition state when a substituent in the nucleophile, the substrate or the leaving group is altered''. Since the C_α–S bond is weaker than the C_α–N bond in these S_N2 reactions, the ''Bond Strength Hypothesis'' predicts that adding an electron-withdrawing substituent to the nucleophile should not affect the C_α–N bond significantly but should lead to a significant change in the weaker S–C_α bond. These are the exact changes suggested on the basis of the KIEs. Finally, it is interesting that the stronger C_α–N bond is shorter than the weaker S–C_α bond in these unsymmetric S_N2 transition states.

The same phenomenon, i.e., that the secondary α-deuterium KIEs is only determined by the length of the shortest reacting bond rather than by the nucleophile–leaving group distance in the S_N2 transition state, has also been found in a series of S_N2 reactions between para-substituted benzyl chlorides and cyanide ion. Matsson, Westaway and coworkers[59] used $^{11}C/^{14}C$ incoming group, secondary α-deuterium and Hill and Fry's[60] chlorine leaving group KIEs to model the transition states for these reactions. The chlorine KIEs (Table 8) indicate that the C_α–Cl bond shortens significantly and the incoming nucleophile $^{11}C/^{14}C$ KIE suggests the

Table 8 The leaving group chlorine, the incoming group $^{11}C/^{14}C$ and the secondary α-deuterium KIEs for the S_N2 reactions between para-substituted benzyl chlorides and cyanide ion in 20% aqueous DMSO at 30°C

Para-substituent	k^{35}/k^{37}[a]	k^{11}/k^{14}[b]	$(k_H/k_D)_\alpha$[c]	Relative transition state structure
CH_3	1.0079 ± 0.0004	1.0104 ± 0.0001	1.008 ± 0.003	NC----C---------Cl
H	1.0072 ± 0.0003	1.0105 ± 0.002	1.011 ± 0.001	NC---C-----Cl
Cl	1.0060 ± 0.0002	1.0070 ± 0.001	1.002 ± 0.003	NC--C----Cl

[a]Measured in 20% aqueous dioxane at 30.0°C.[60]
[b]Measured at 30.00 ± 0.02°C.
[c]Measured at 30.000 ± 0.002°C.

NC–C_α bond shortens slightly when a more electron-withdrawing substituent is added to the benzene ring of the substrate. Therefore, the nucleophile–leaving group distance in these S_N2 transition states decreases when a more electron-withdrawing substituent is present. If the magnitude of the secondary α-deuterium KIEs were determined by the nucleophile–leaving group distance in the transition state, the secondary α-deuterium KIEs should decrease significantly when a more electron-withdrawing substituent is on the substrate. However, all the α-deuterium KIEs (Table 8) are small and normal and, moreover, do not change significantly with substituent. A comparison of the chlorine and the secondary α-deuterium KIEs in Table 8 shows that the magnitudes of these KIEs are clearly not related while the secondary α-deuterium and the incoming group k^{11}/k^{14} KIEs change in the same way with substituent; i.e., the largest KIEs are observed when the para-substituent is hydrogen and the smallest KIEs are found when the para-substituent is chlorine. This suggests that the NC–C_α bonds are short and that the C_α–Cl bonds are long in these transition states, i.e., that the transition states are unsymmetric and product-like. As a result, the changes that occur in the C_α–Cl bond when the para-substituent on the benzene ring is altered do not affect the C_α–H(D) bending vibrations significantly and the magnitude of the secondary α-deuterium KIE is only determined by the length of the shorter NC–C_α transition state bond. Again, the changes that occur in transition state structure are consistent with the "Bond Strength Hypothesis;"[58] i.e., the weaker C_α–Cl bond changes significantly and there is little or no change in the stronger NC–C_α bond when the substituent in the substrate changes. It is also worth noting that the weaker C_α–Cl reacting bond is long and the stronger NC–C_α reacting bond is short in these unsymmetric transition states. Thus, the behavior is identical to that observed in the ammonium salt reaction (*vide supra*) even though the change in substituent has been made in the substrate rather than in the nucleophile.

Another suggestion is that secondary α-deuterium KIEs can be used to determine the symmetry of an S_N2 transition state.[55] An examination of the secondary α-deuterium KIEs for several S_N2 reactions of benzyl substrates (Table 9) showed there were two different substituent effects on these KIEs. In some S_N2 reactions, the KIEs decrease markedly when a more electron-withdrawing substituent is

Table 9 The secondary α-deuterium KIEs for S_N2 reactions with symmetric transition states where the magnitude of the KIE varies with the nucleophile–leaving group distance and for unsymmetric transition states where the magnitude of the KIE is determined by the length of only the shortest, and strongest, reacting bond

Substrate/nucleophile	Para-substituent (Z) $((k_H/k_D)_\alpha)$						Δ KIE (%)	Reference
	CH_3O	CH_3	H	Cl	Br	NO_2		
S_N2 reactions with symmetric transition states								
Z–BzCl[a]/PhS^-	1.126	1.096	1.056	1.046		1.039	8.7	61
Z–BzCl/H_2O			1.096		1.032		6.3	62
Z–BzCl/H_2O in 10% aq CH_3CN			1.059		1.008		5.1	62
Z–BzOBs/H_2O in 90% aq EtOH			1.124			1.004	12.0	63
Z–BzCI/H_2O			1.092	1.061			3.1	64
Z–BzBr/$S_2O_3^=$			1.063			1.032	3.1	65
Z–BzBr/N_3^-			1.024			0.996	2.8	65
Z–BzBr/OH^-	1.028		0.984				4.4	65
4-Bz$\overset{+}{N}Me_2$Ph-Z/PhS^-	1.207		1.179	1.151			5.6	7
S_N2 Reactions with unsymmetric transition states								
Bz$\overset{+}{N}Me_2$Ph/Z-PhS^-	1.221		1.215	1.215			0.6	55
Z–BzCl/CN^-		1.008	1.011	1.002			0.99	55
4-$BzOSO_2$Ph–Z/4-MeOPhNH_2	1.096					1.102	0.6	66
4-$BzOSO_2$Ph–Z/3-NO_2PhNH_2	1.098					1.095	0.3	66
$MeOSO_2$Ph–Z/4-MeOPhNH_2	0.990					0.993	0.3	66
$MeOSO_2$Ph–Z/*m*-NO_2PhNH_2	0.971					0.974	0.3	66
$EtOSO_2$Ph–Z/4-MeOPhNH_2	0.981					0.984	0.3	66
$EtOSO_2$Ph–Z/*m*-NO_2PhNH_2	0.953					0.962	0.9	66
Secondary α-tritium KIEs								
4-$BzOSO_2$Ph–Cl/4-Z–PhNMe_2	1.061	1.055	1.042		1.048		1.9	32
m-BrBzOSO_2Ph–Cl/4-Z–PhNMe_2	1.033		1.026			1.033	0.7	32

Reprinted with permission from Ref. [55]. Copyright (1997) American Chemical Society.
[a]Bz = $-C_6H_4-CH_2$.

present while in other S_N2 reactions they are almost independent of substituent. This led Westaway *et al.* to propose that the reactions where the secondary α-deuterium KIE varies with substituent have reasonably tight, symmetric transition states while those where the KIE is independent of substituent have unsymmetric transition states where the strongest reacting bond is short and determines the magnitude of the KIE. In the S_N2 reactions with symmetric transition states the Nu–C_α and C_α–LG transition state bonds have comparable bond orders, the C_α–(H)D bending vibrations are affected by both the bond to the nucleophile and the bond to the leaving group, and the magnitude of the secondary α-deuterium KIE is determined by the Nu–LG distance in the transition state. In these reactions, the secondary α-deuterium KIEs decrease markedly (by between 2.8% and 12%) when a more electron-withdrawing substituent is added to the benzene ring on the α-carbon or the leaving group.

In S_N2 reactions with unsymmetric transition states, the C_α–H(D) bending vibrations, which are primarily responsible for the magnitude of the secondary α-deuterium KIE for the reactions of complex substrates, are only affected by the changes in the shortest reacting bond. In all the reactions with an unsymmetric transition state found to date, the stronger reacting bond is short and the weaker reacting bond is long. Since the "Bond Strength Hypothesis" predicts that little or no change will occur in the stronger (the shortest) reacting bond in an S_N2 transition state when a substituent on the nucleophile, the leaving group, or the substrate is altered, the secondary α-deuterium KIE should be insensitive to a change in substituent. In fact, the change in the secondary α-deuterium KIE with substituent is always $<1\%$ (the average change is 0.5%) even when the substituent is changed from strongly electron donating to strongly electron withdrawing. Finally, it is worth noting that this behavior has been observed for S_N2 reactions where the change in substituent is in the nucleophile, the leaving group, or the substrate so it appears to be a general phenomenon.

The magnitude of a secondary α-deuterium KIE in an S_N2 reaction can also be affected by the size of the leaving group. The influence of the size of the leaving group on the magnitude of these KIEs was first suggested by Westaway and Ali[7] who attributed the extremely large secondary α-deuterium KIEs of between 1.151 and 1.207 (1.073–1.099/α-D) found for the S_N2 reactions of benzyldimethyl-*p*-substituted phenylammonium ions and thiophenoxide ion (Equation (14)) to the relief of the steric crowding of the C_α–H(D) bending

$$C_6H_5S^- + C_6H_5CH_2\text{-}\overset{+}{N}(CH_3)_2C_6H_4\text{-}Z \rightarrow C_6H_5S\text{-}CH_2C_6H_5 + (CH_3)_2NC_6H_4\text{-}Z \quad (14)$$

vibrations in the substrate, on going to the transition state. This was reasonable because the fairly small Hammett ρ value of –1.70 found by changing the para-substituent on the thiophenoxide ion (the equilibrium ρ value for this reaction is –3.30)[67] indicated the S–C_α transition state bonds were long. The large nitrogen leaving group KIEs ranging from 1.0197 to 1.0202 (~50% of the theoretical maximum nitrogen KIE)[68] and a large Hammett ρ value of +2.04 found by varying the substituent on the leaving group (the equilibrium Hammett ρ value for this reaction would be ~ +4)[68] indicated that the C_α–N transition state bonds were also long.

Several other workers have found unusually large secondary α-deuterium KIEs in S_N2 reactions with a large leaving group. For instance, Ko and Leffek[69] reported secondary α-deuterium KIEs of 1.09 and 1.10/α-D for the S_N2 reactions of the same substrate with bromide and iodide ion, respectively. This rationale was also used to explain the very large secondary α-deuterium KIEs of 1.178 and 1.184/α-D for the S_N2 reactions of 1-phenylethyldimethylphenylammonium ion with bromide and iodide ion, respectively.[70] Craze *et al.*[71] also found very large KIEs ranging from 1.05 to 1.16/α-D for the S_N2 reactions of methoxymethoxy-2,4-dinitrobenzene (Equation (15)) which has a bulky leaving group:

$$Nu:^- + CH_3OCH_2\text{-}O\text{-}C_6H_3\text{-}(NO_2)_2 \rightarrow Nu\text{-}CH_3 + ^-:OCH_2\text{-}O\text{-}C_6H_3\text{-}(NO_2)_2 \quad (15)$$

Table 10 The chlorine leaving group and secondary α-deuterium KIEs and the Hammett ρ values for the S_N2 reactions between para-substituted benzyl chlorides and thiophenoxide ion in 0.250 M lithium methoxide in methanol at 20°C

Para-substituent	k^{35}/k^{37}[a]	$(k_H/k_D)_\alpha$[c]	ρ_{Nuc}
CH_3O	1.01012	1.126[c]	−0.283[e]
CH_3	1.00963	1.096–1.125[d]	−0.434
H	1.00976	1.056	−0.500
Cl	1.01013	1.046	−0.720
NO_2	1.00950	1.039	−0.961
	Average 1.00983 ± 0.00029[b]		

[a]Measured by Grimsrud.[76]
[b]Standard deviation.
[c]Measured at 0°C. The value at 20°C was estimated to be 1.096 from the temperature dependence of the KIE for the para-methylbenzyl chloride reaction.
[d]Measured at 0°C.
[e]The value at 0°C. The ρ value at 20°C was estimated to be –0.305 from the temperature dependence of the ρ value for the para-nitrobenzyl chloride reaction.

Unusually large secondary α-deuterium KIEs ranging from 1.18 to 1.07/α-D were also found for the S_N2 reactions of methoxymethoxy-*N*,*N*-dimethyl-*m*-nitroanilinium ion with the bulky $–OCH_2–N(CH_3)_2–m\text{-}C_6H_4–NO_2$ leaving group.[72] Finally, it has been suggested that the lone pairs of electrons on the oxygens of perchlorate and arenesulfonate leaving groups affect the C_α–H(D) bending vibrations and are responsible for the larger α-deuterium KIEs found in these S_N2 reactions.[73,74]

Finally, increasing the conjugation between the α-carbon and a benzene ring on the α-carbon reduces the magnitude of a secondary α-deuterium KIE.[75] The chlorine leaving group KIEs for the S_N2 reactions between para-substituted benzyl chlorides and thiophenoxide ion (Table 10) do not vary significantly with substituent; i.e., there is no trend in the KIEs and the standard deviation of the average KIE barely exceeds the error in the individual measurements, i.e., ±0.0002. Therefore, the best interpretation of these KIEs is that the C_α–Cl transition state bond lengths do not change significantly with substituent. The secondary α-deuterium KIEs for these S_N2 reactions increase for all but the para-methoxybenzyl chloride reaction when a more electron-donating substituent is added to the benzene ring on the α-carbon of the substrate. This suggests that the para-methyl benzyl chloride and the para-methoxybenzyl chloride reactions have the same S–C_α bond lengths in the transition state. However, the Hammett ρ values decrease for all substituents. Since a smaller ρ value is found when there is less S–C_α bond formation in the transition state, the S–C_α bond shortens for all reactions when a more electron-donating substituent is on the benzene ring of the substrate. Since the S–C_α transition state bond is longer for the reaction with the para-methoxy substituent, but the secondary α-deuterium KIE is the same as that for the reaction with the less electron-donating methyl substituent, the increased conjugation into the benzene ring that would be present with the more electron-donating methoxy substituent must decrease the magnitude

of the secondary α-deuterium KIE. This may occur because the increased conjugation increases the C_α–H(D) stretching frequency in the transition state.

In conclusion, although we do not know all the factors that determine the magnitude of a secondary α-deuterium KIE for S_N2 reactions, particularly those with different leaving groups, overwhelming evidence from theoretical calculations has shown that the KIE is primarily determined by contributions from an inverse C_α–H(D) stretching vibration that is effectively constant for each leaving group and an inverse, or normal, C_α–H(D) bending vibration contribution that seems to increase with transition states looseness (the steric crowding around C_α in the transition state). The stretching contribution to the total KIE is usually greater than the bending contribution for the S_N2 reactions of methyl substrates, so the KIEs are inverse or small and normal. However, the stretching contribution to the KIE becomes less important as the size of the substrate increases. Therefore, larger KIEs are found for the S_N2 reactions of larger substrates such as ethyl and benzyl where the normal $(k_H/k_D)_{bend}$ contribution plays a greater role in determining the magnitude of the KIE. Both experiment and theory suggests the R_{TS} model, based on the looseness of transition states with the same leaving group, seems to be valid for reactions with small nucleophiles. However, the R_{TS} model does not apply to reactions with large nucleophiles with heavy atoms off the Nu–C_α–LG axis. Here, the KIE is based on the crowdedness of the transition state although, unfortunately, it would seem to be impossible to estimate the effect of these off axis atoms on the magnitude of the KIE. Finally, theory has suggested that other factors such as the Nu–C_α–LG bond angle in the transition state and the change in the C_α–LG stretching force constant on going to the transition state also appear to affect the magnitude of these KIEs. Experimental evidence has suggested that (i) the secondary α-deuterium KIE in S_N2 reactions is determined by only the length of the shortest reacting bond in unsymmetric transition states, (ii) the symmetry of the transition state can be determined from the magnitude of the change in the KIE with substituent, (iii) a large, bulky leaving group increases the KIE significantly and (iv) increasing conjugation to a benzene ring on the α-carbon decreases the magnitude of these KIEs. While all these contributions to the magnitude of the KIE obviously make it difficult (impossible) to compare the structure of the transition states in different reactions based on the magnitude of a secondary α-deuterium KIE, it is believed that the magnitude of these KIEs can be used to determine the effect of substituents, a change in solvent and the effect of ion pairing on the structure of the transition state of an S_N2 reaction (*vide infra*). This is because these changes do not significantly affect factors such as the crowdedness, the Nu–C_α–LG bond angle or the leaving group in the reaction. As a result, the magnitude of the KIE should be related to the looseness of the transition state (R_{TS}) for the reaction.

Secondary β-deuterium KIEs

Secondary β-deuterium KIEs that arise when hydrogen(s) on the β-carbon are replaced by deuterium(s) have been extensively investigated by Shiner and coworkers. For instance, an elegant study by Shiner and Humphrey[40,77] showed that secondary β-deuterium KIEs are comprised of a steric KIE (the C_β–D bonds are shorter than

Table 11 Some secondary β-deuterium KIEs for S_N2 reactions

Substrate	Nucleophile	Temperature (°C)	(k_H/k_D)/β-D	Reference
CD_3CH_2–OTs	H_2O	60	1.006	78
CD_3CH_2–OMs	H_2O	60	1.009	78
CD_3CH_2–Br	H_2O	80	1.011	78
CD_3CH_2–I	H_2O	80	1.012	78
CD_3CH_2–OTf	TFE	25	1.03	79
CD_3CH_2–OTf	Acetic acid	25	1.04	80
CD_3CH_2–OTf	Formic acid	25	1.05	80
$CF_3C{\equiv}CCHCD_3$–OBs	50% Ethanol	45	1.018	81
$CF_3C{\equiv}CCHCD_3$–OBs	30% Ethanol	45	1.019	81
$HC{\equiv}CCHCD_3$–OBs	95% Ethanol	45	1.027	81
CD_3CH_2–Cl	CN^-/DMSO	30	1.005	33

the C_β–H bonds[74]), an inductive effect KIE (D is more electron donating than H[74]) and a hyperconjugative (the weaker C_β–H bonds stabilize the transition state more than C_β–D bonds via hyperconjugation[74]) KIE that is related to the amount of positive charge on the α-carbon in the transition state. The steric and inductive effect contributions to the KIE in S_N2 reactions are small because the deuterium(s) are not at the reaction center and inverse because the deuterated transition state is always less sterically crowded and there is usually a partial positive charge on C_α in the transition state. In fact, both the steric and inductive components of the KIE are $\leqslant 1\%$/β-D.[3,40] The hyperconjugative component of the KIE, on the other hand, is always normal and is invariably the largest contributor to the KIE. The hyperconjugative KIE, which varies with the amount of positive charge on C_α in the transition state, is large for a carbenium ion S_N reaction and small for an S_N2 reaction where the positive charge on C_α in the transition state is small. Therefore, a large, normal secondary β-deuterium KIE of $\geqslant 1.07$/β-D is expected for a carbenium ion S_N reaction and a small KIE of $\leqslant 1.05$/β-D is indicative of an S_N2 mechanism.[40] For example, the secondary β-deuterium KIE/β-D increases from ~1.02 for ethyl compounds (Table 11) which undoubtedly react by an S_N2 mechanism, to ~1.11 for a *t*-butyl compound that reacts by a limiting S_N1 mechanism.[40] Finally, the magnitude of these KIEs can be related to transition state structure because the hyperconjugative component to the KIE varies with the amount of positive charge on C_α in the transition state. This means that although small secondary β-deuterium KIEs are found for S_N2 reactions, reactions with a looser transition state will have a slightly larger KIE.

Several factors affect the magnitude of a secondary β-D KIE. For instance, the magnitude of these KIEs is strongly influenced by the stereochemistry of the carbenium ion. Shiner and coworkers[40,82,83] found that the magnitude of the KIE is reduced from 1.30/β-D when the dihedral angle between the C_β–H bond and the empty 2p atomic orbital on the α-carbon is 0°, to 1.07/β-D when the dihedral angle is 30°, to only 1.01/β-D when the dihedral angle is 60° and is inverse at 0.99 when the dihedral angle is 90°. Luckily, this is not a serious problem because small β-deuterium KIEs are only found in the carbenium ion reactions of bicyclic and other sterically crowded systems where free rotation about the C_α–C_β bonds is restricted.

Conjugation between the positive charge on the α-carbon of the carbenium ion and a strongly electron-donating group also reduces the magnitude of a secondary β-deuterium KIE significantly. For example, all but one of the β-deuterium KIEs for the hydrolyses of several 1-para-substituted phenylethyl chlorides (1.07–1.05/β-D) are between the values expected for a carbenium ion and an S_N2 mechanism and a very small KIE of 1.036/β-D is observed when the para-substituent is the methoxy group even though all these substrates react via a carbenium ion mechanism with the formation of the solvent-separated ion pair rate determining. The very small KIE is found for the para-methoxybenzyl chloride reaction because the highly conjugated (very stable) para-methoxybenzyl carbenium ion is not highly stabilized by hyperconjugation.[40]

Finally, strong solvation of the carbenium ion intermediate also causes a marked reduction in secondary β-deuterium KIE.[84] For example, the β-deuterium KIE in the solvolysis of isopropyl tosylate is reduced from 1.13/β-D in trifluoroethanol, which does not solvate the developing carbenium ion strongly, to 1.08/β-D in water where the carbenium ion is strongly solvated. Again, hyperconjugation is reduced because the solvent stabilizes the developing carbenium ion in the transition state.

2 Using KIEs to determine how substituents, the solvent, ion pairing and enzymes affect the structure of the S_N2 transition state

Unfortunately, most of the work investigating how substituents, ion pairing of the nucleophile, enzymes and the solvent affect the structure of S_N2 transition states has been done by measuring only one KIE. As a result, they do not indicate how the total transition state changes when the reactants and/or the solvent are altered. Only studies measuring more than one KIE or using KIEs in conjunction with other mechanistic criteria can indicate how the total transition state structure changes. Therefore, only a few selected examples illustrating how multiple KIEs have been used to determine how substituents, ion pairing and the solvent affect the structure of S_N2 reactions will be presented.

Changing the leaving group

In the one system where definitive results of the effect of changing the leaving group on transition state structure have been obtained, Westaway and Ali[7] used nitrogen leaving group and secondary α-deuterium KIEs and Hammett ρ values found by changing the substituent, Y, on the nucleophile of the S_N2 reactions between para-substituted phenylbenzyldimethylammonium ions and para-substituted thiophenoxide ions:

$$\begin{aligned} &4\text{-Y-C}_6\text{H}_4\text{-}S^- + \text{C}_6\text{H}_5\text{CH}_2\text{-}\overset{+}{\text{N}}(\text{CH}_3)_2\text{-4-C}_6\text{H}_4 - \text{Z} \\ &\rightarrow 4\text{-Y-C}_6\text{H}_4\text{-S-CH}_2\text{C}_6\text{H}_5 + (\text{CH}_3)_2\text{N-4-C}_6\text{H}_4\text{-Z} \end{aligned} \qquad (16)$$

to model the transition states. The primary nitrogen KIEs (Table 12) are all large; i.e., approximately half of the theoretical maximum nitrogen KIE of 1.044 at 0°C[57]

Table 12 The nitrogen and secondary α-deuterium KIEs and Hammett ρ values for the S_N2 reactions between para-substituted thiophenoxide ions and para-substituted phenylbenzyldimethylammonium ions in DMF at 0°C

Para-substituent on the leaving group	k^{14}/k^{15}	$(k_H/k_D)_\alpha$	Hammett ρ[a]	Relative transition state structure
CH_3O	1.0197	1.207	−1.54	S--------C------N
H	1.0200	1.179	−1.70	S----C------N
Cl	1.0202	1.151	−1.83	S--C------N

[a]The ρ values were determined by changing the substituent, Y, on the nucleophile.

indicating that there probably is substantial C_α–N bond rupture in the transition state of all three reactions. Although the nitrogen KIEs are not statistically different, they do increase in magnitude when a more electron-withdrawing substituent is added to the leaving group. Interpreting these KIEs is complicated because there is some C = N double bond formation between the nitrogen and the ipso carbon of the aniline ring in the transition state. The vibrational energy associated with this extra bonding to nitrogen in the transition state means that the magnitude of the observed KIE will be smaller than expected for a particular amount of C_α–N bond rupture in the transition state. This conjugation (bonding) will obviously be greater when a more electron-withdrawing substituent is in the leaving group. Therefore, since the nitrogen KIE increases very slightly and there is additional C = N bonding to the ipso carbon in the transition state when a more electron-withdrawing substituent is on the leaving group, the best explanation for these KIEs is that the C_α–N bond is slightly longer in the transition state with the better leaving group, i.e., when a more electron-withdrawing substituent is present.

The magnitude of the secondary α-deuterium KIE, on the other hand, decreases when there is a more electron-withdrawing substituent, Z, on the leaving group. Changing the substituent in the leaving group would not influence the C_α–H(D) bending vibrations in the substrate because the structural change is six bonds away from these bonds. Since the magnitude of these KIEs is directly related to the Nu–LG distance in these symmetric transition states,[7] the shortest S–N distance (the tightest transition state) is observed with the best leaving group, i.e., when Z is chlorine.

Combining the results from these two KIEs provides a detailed picture of the transition states for these reactions. Since the S–N distance decreases and the C_α–N transition state bond length increases slightly when a more electron-withdrawing substituent is added to the leaving group, changing to a better leaving group leads to a transition state with a slightly longer C_α–N bond and a much shorter S–C_α bond. It is worth noting that the magnitudes of the Hammett ρ values determined by changing the para-substituent, Y, on the nucleophile are consistent with a shorter S–C_α transition state bond when a more electron-withdrawing substituent is in the leaving group. When the S–C_α transition state bond is shorter, the change in charge on the sulfur atom when the reactants are converted into the transition state will be greater and a more negative ρ value will be observed. Finally, it is again interesting

Table 13 The incoming group $^{11}C/^{14}C$ carbon and secondary α-deuterium KIEs for the S_N2 reactions between meta-chlorobenzyl-para-substituted benzenesulfonates and cyanide ion in 0.5% aqueous acetonitrile at 0°C

Para-substituent on the leaving group	k^{11}/k^{14}	$(k_H/k_D)_\alpha$	Relative transition state structure
CH_3O	1.025		
CH_3	1.0119	1.028	NC-------C----------O
H	1.0111	1.012	NC-----C-----O
Cl	1.0096	1.009	NC----C---O

to note that the greatest change in bonding occurs in the weakest reacting bond in the transition state as the "Bond Strength Hypothesis"[58] suggests.

Another study utilizing more than one type of KIE to model the S_N2 transition states for reactions with a different leaving group was done using the reactions between meta-chlorobenzyl-para-substituted benzenesulfonates and cyanide ion:[85]

$$\begin{aligned} &CN{:}^- + m - Cl - C_6H_4 - CH_2 - OSO_2 - 4 - C_6H_4 - Z \\ &\rightarrow m - Cl - C_6H_4 - CH_2 - CN{+}^- : OSO_2 - 4 - C_6H_4 - Z \end{aligned} \quad (17)$$

The incoming group $^{11}C/^{14}C$ KIEs (Table 13) decrease slightly (the difference in the KIEs is greater than the experimental error in each KIE) indicating that the NC–C_α bond shortens slightly when a more electron-withdrawing substituent is on the leaving group. The secondary α-deuterium KIE also decreases when a more electron-withdrawing substituent is on the leaving group. However, the change in the KIE with substituent is very small suggesting that the transition states are unsymmetric.[55] Also, since the α-deuterium KIE changes in the same way as the incoming group KIE, it would appear that change in the NC–C_α bond is causing the variation in the secondary α-deuterium KIE. This suggests that the transition states must have short NC–C_α and long C_α–O bonds. The long C_α–O bond in these transition states has been confirmed by the large positive Hammett $\rho = +1.71$ found by changing the substituent on the leaving group. This conclusion is warranted because the ρ value of $+1.71$ is near the maximum Hammett ρ value found for the S_N2 reactions of benzenesulfonates; i.e., they vary from 0.76 to 2.13.[85] Also, since in the incoming group carbon KIE and the secondary α-deuterium KIE decrease when a more electron-withdrawing group is on the benzene ring, the NC–C_α bond must shorten slightly when a more electron-withdrawing substituent is used. Although the C_α–O bond must be long in these transition states, it is not known how it changes with substituent. However, the small change in the stronger NC–C_α bond is expected because the "Bond Strength Hypothesis" predicts the largest change with substituent will be in the weaker C_α–O bond. If the results obtained by Westaway and Ali (*vide supra*) can be applied to these reactions, one would expect the C_α–O bond to lengthen significantly when a more electron-withdrawing group is on the benzene ring of the leaving group.

The results from these two systems indicate that changing to a better leaving group in an S_N2 reaction leads to a tighter transition state with a shorter Nu–C_α bond. In one system, the C_α–LG transition state bond is longer when a better leaving group is present while in the second system the relative length of the C_α–LG transition state bond was undetermined. The results differ in that the greatest change in transition state structure occurs at different positions in the two systems; i.e., in the first study the greatest change occurred in the weaker S–C_α bond whereas it seems to be in the weaker C_α–O bond in the second system. It is worth noting that this is the result predicted by the "Bond Strength Hypothesis".

Changing the nucleophile

The effect of changing a substituent in the nucleophile on transition state structure is the most poorly studied of all of the substituent effects in S_N2 reactions. The problem is that in the many studies where only the secondary α-deuterium KIE has been measured, the KIEs suggest different changes in transition state structure when the nucleophile is changed.[86]

However, similar results were obtained in the two studies where the nucleophile was varied and more than one KIE was determined. In the Westaway and Jiang[87] study, the nitrogen leaving group KIEs for the S_N2 reactions between para-substituted thiophenoxide ions and benzyldimethylphenylammonium ion (Equation (13); Table 14) increase (the C_α–N bond is slightly longer) when a more electron-withdrawing substituent is on the nucleophile. The secondary α-deuterium KIEs, on the other hand, decrease significantly (the S–N distance in the transition state decreases) when a more electron-withdrawing substituent is on the nucleophile. Since the C_α–N bond becomes longer and the S–N distance shortens, the S–C_α bond must become significantly shorter when a more electron-withdrawing substituent is on the nucleophile. It is worth noting that the KIEs found for the same reactions, but where the nucleophile was the sodium thiophenoxide solvent-separated ion pair,[87] showed the same behavior; i.e., the S–C_α bond shortened significantly while the C_α–N bond lengthened slightly when a more electron-withdrawing group was on the nucleophile.

In the second study by Paneth and coworkers,[88] the nitrogen incoming group and the secondary α-deuterium KIEs were determined for the S_N2 reactions between three para-substituted *N*,*N*-dimethylanilines and methyl iodide. The incoming group nitrogen KIEs (Table 15) decreased when a poorer nucleophile was used. This is consistent with a shorter N–C_α bond in the transition states with the poorer

Table 14 The nitrogen leaving group and secondary α-deuterium KIEs for the S_N2 reactions between sodium para-substituted thiophenoxide ions and benzyldimethylphenylammonium ion in methanol at 20.000°C

Para-substituent on the nucleophile	k^{14}/k^{15}	$(k_H/k_D)_\alpha$	Relative transition state structure
CH_3O	1.0162	1.271	S---------C----N
CH_3	–	1.237	
H	1.0166	1.222	S-----C-----N
Cl	1.0169	1.121	S---C-----N

Table 15 The incoming group nitrogen and secondary α-deuterium KIEs for the S_N2 reactions between para-substituted *N*,*N*-dimethylanilines and methyl iodide in ethanol at 25°C

Para-substituent on the nucleophile	k^{14}/k^{15}	$(k_H/k_D)_\alpha$	Relative transition state structure
CH_3	1.0036	0.927	N-----C---I
H	1.0032	0.968	N----C-------I
$C(O)CH_3$	0.9989	1.143	N----C--------I

Table 16 The change in the secondary α-deuterium KIE for the S_N2 reactions of several para-substituted sodium thiophenoxides and *n*-butyl chloride in four solvents at 20.000 ± 0.002°C

	Free ion nucleophile		**Solvent-separated ion pair nucleophile**	
Solvent	Nucleophile concentration (M)	$(k_H/k_D)_\alpha$	Nucleophile concentration (M)	$(k_H/k_D)_\alpha$
DMSO	$<1.1 \times 10^{-2}$	1.116	$>2.5 \times 10^{-2}$	1.034
DMF	$<4.0 \times 10^{-3}$	1.129	$>8.6 \times 10^{-3}$	1.084
MeOH	$<7 \times 10^{-5}$	1.132	$>9 \times 10^{-5}$	1.100
Diglyme	–	–	$>1.0 \times 10^{-3}$[a]	1.14[a]

[a]The sodium thiophenoxide existed as the solvent-separated ion pair at all concentrations in diglyme.

nucleophile. The secondary α-deuterium KIE, on the other hand, increased when a more electron-withdrawing substituent was on the nucleophile. This suggested that the N–I distance increased when a poorer nucleophile was used in the reaction. Since the N–C_α bond shortens as the N–I distance increases, the C_α–I bond must be longer when a poorer nucleophile is used. Although the changes in transition state structure are in the same direction in these two studies, the greatest change in transition state structure in the Paneth study is in the C_α–LG bond whereas it was in the Nu–C_α bond in the Westaway–Jiang study. However, in both studies the greatest change in bonding is in the weakest reacting bond as the ''Bond Strength Hypothesis'' suggests.

Effect of ion pairing of the nucleophile

Westaway *et al.*[89] discovered that the secondary α-deuterium KIE varied with the concentration of the nucleophile in the S_N2 reaction between sodium thiophenoxide and *n*-butyl chloride. A combination of UV spectroscopy, conductivity studies and the effect of adding 15-crown-5 ether to the reaction mixture[90] was used to demonstrate that the source of the problem was a change in the form of the reacting nucleophile from a free ion to a solvent-separated ion pair. Examples of the change in the secondary α-deuterium KIE with the form of the reacting nucleophile are given in Table 16.[90] The smaller secondary α-deuterium KIEs found for the reaction with the solvent-separated ion pair suggests the transition state is tighter with shorter S–C_α and/or C_α–Cl bonds in each solvent. Although the change in the two reacting bonds cannot be deduced with certainly, the ''Bond Strength Hypothesis'' suggests that greatest change in transition state structure would occur in the weaker S–C_α bond

and that there would be little or no change in the stronger C_α–Cl bond. Therefore, it was concluded that changing the nucleophile from a free ion to a solvent-separated ion pair leads to a tighter transition state with a shorter S–C_α bond but does not affect the C_α–Cl bond significantly. The change to the shorter S–C_α bond for the solvent-separated ion pair reaction, i.e., the reaction with the poorer nucleophile, is identical to that found when changing to a poorer nucleophile (*vide supra*).

Finally, it is interesting that the smallest effect of ion pairing was found in methanol. This was attributed to the fact that the electron density on the sulfur of the free ion in methanol would be lower than that in DMSO and DMF because it is solvated by hydrogen bonding in methanol. This smaller negative charge on the sulfur atom in the free ion in methanol would approach that on the sulfur of the solvent-separated ion pair in DMSO and DMF. Since the change in the form of the reacting nucleophile on ion pairing is smaller in methanol than in DMSO and DMF, the change in the KIE on ion pairing is smaller in methanol.

The same change in KIE was observed when a solvent-separated ion pair was converted to a contact ion pair in the S_N2 reaction between lithium thiophenoxide and *n*-butyl chloride in diglyme.[91] Here, the secondary α-deuterium KIE changed from 1.131 ± 0.002 for the solvent-separated ion pair reaction to 1.070 ± 0.028 when the nucleophile was the contact ion pair. The smaller secondary α-deuterium KIEs found for the reaction with the contact ion pair and the "Bond Strength Hypothesis" suggest that changing to a contact ion pair leads to a tighter transition state with a shorter S–C_α bond but does not affect the stronger C_α–Cl bond significantly. The shorter S–C_α bond in the contact ion pair reaction was confirmed when a larger Hammett ρ value of -1.39 ± 0.1 was found by changing the para-substituent on the nucleophile in the contact ion pair reaction. The ρ value for the solvent-separated ion pair reaction was only -0.56 ± 0.04 indicating there was much less S–C_α bond formation in the transition state of the solvent-separated ion pair reaction. It is worth noting that this small ρ value confirmed that changing the form of the reacting nucleophile caused a large decrease in the S–C_α transition state bond.

The conclusions about the effect of ion pairing on transition state structure were confirmed by a study by Westaway and Jiang.[87] The nitrogen leaving group KIEs for the free ion and solvent-separated ion pair reactions (Table 17) are the same considering the experimental errors in the measurements. Therefore, the change in the nucleophile does not affect the stronger C_α–N bond significantly as the "Bond

Table 17 The nitrogen leaving group and secondary α-deuterium KIEs for the S_N2 reaction between the free thiophenoxide ion or solvent-separated sodium thiophenoxide and benzyldimethylphenylammonium nitrate in methanol at 20.000 ± 0.002°C

	Free ion KIEs		Solvent-separated ion pair KIEs	
Para-substituent	k^{14}/k^{15}	$(k_H/k_D)_\alpha$	K^{14}/k^{15}	$(k_H/k_D)_\alpha$
CH_3O	1.0162 ± 0.0005	1.271 ± 0.013	1.0161 ± 0.0005	1.216 ± 0.012
H	1.0166 ± 0.0008	1.222 ± 0.013	1.0162 ± 0.0010	1.207 ± 0.008
Cl	1.0169 ± 0.0005	1.121 ± 0.014	1.0166 ± 0.0003	1.150 ± 0.009

Table 18 The chlorine leaving group and secondary α-deuterium KIEs for the S_N2 reactions between the free phenoxide ion or the solvent-separated sodium phenoxide ion pair and benzyl or *n*-butyl chloride in several solvents at 20.000°C

	Free ion reaction		Solvent-separated ion pair reaction	
Substrate/solvent	k^{35}/k^{37}[a]	$(k_H/k_D)_\alpha$	k^{35}/k^{37}[a]	$(k_H/k_D)_\alpha$
Benzyl chloride/methanol	1.0826 ± 0.0001	1.022 ± 0.002	1.0831 ± 0.00005	1.021 ± 0.0002
n-butyl chloride/DMSO	1.0811 ± 0.00007	1.029 ± 0.008	1.0806 ± 0.00009	1.031 ± 0.012
Benzyl chloride/DMF	1.0822 ± 0.0001[b]	1.021 ± 0.0008	1.0819 ± 0.0009[b]	1.018 ± 0.011

[a]Measured in DMSO. Changing the solvent does not alter the chlorine KIE in these reactions.
[b]The nucleophile was sodium para-methoxyphenoxide.

Strength Hypothesis'' suggests. The secondary α-deuterium KIEs, however, are clearly smaller for the solvent-separated ion pair reactions. This means the transition states for the solvent-separated ion pair reactions are tighter with a shorter S–N distance than those for the free ion reactions. Since the C_α–N bonds are the same and the S–N distance is shorter for the solvent-separated ion pair reactions, the S–C_α bonds must be shorter in the solvent-separated ion pair reactions. Again, the shorter Nu–C_α transition state bond is found in the reaction with the poorer nucleophile, i.e., the ion pair.

Although the results showing that the form of the nucleophile has a significant effect on transition state structure causes concern for chemists studying reaction mechanisms, the results obtained in the following investigation suggest it is not as big a problem as one might think. Fang *et al.*[92] measured the chlorine leaving group and secondary α-deuterium KIEs for the S_N2 reactions between para-substituted sodium phenoxides and benzyl or *n*-butyl chloride in DMF, DMSO and methanol. They found neither the chlorine leaving group nor the secondary α-deuterium KIEs (Table 18) changed when the nucleophile changed from a free ion to a solvent-separated ion pair. These results suggest the effect of ion pairing is only important when soft nucleophiles are used in reactions and that one does not have to worry about this problem when hard (oxygen) nucleophiles are used. This may be because converting a free ion to an ion pair would have a much smaller effect on the electron density of an electronegative (oxygen) atom than on a less electronegative, more polarizable (sulfur) atom.

Changes at the α-carbon

A detailed study by Westaway and Waszczylo[61] used chlorine leaving group and secondary α-deuterium KIEs along with Hammett ρ values and activation parameters to demonstrate how the transition state is altered when a substituent on the benzene ring in the substrate is varied in the S_N2 reactions between para-substituted benzyl chlorides and thiophenoxide ions in 0.25 N lithium methoxide in methanol at 25°C (Equation (18)).

$$C_6H_5\text{-}S^- + 4\text{-}Z\text{-}C_6H_4CH_2\text{-}Cl \rightarrow 4\text{-}Z\text{-}C_6H_4CH_2\text{-}S\text{-}C_6H_5 + Cl^- \quad (18)$$

Table 19 The chlorine leaving group and secondary α-deuterium KIEs and Hammett ρ values for the S_N2 reactions between para-substituted benzyl chlorides and thiophenoxide ions in 0.25 N lithium methoxide in methanol at 25°C

Para-substituent on the substrate	k^{35}/k^{37}[a]	$(k_H/k_D)_\alpha$	ρ_{Nuc}	Relative transition state structure
CH_3O	1.01012	1.126[b]	−0.283[c]	S-------C-----Cl
CH_3	1.00963	1.096	−0.434	S-----C-----Cl
H	1.00976	1.056	−0.500	S---C-----Cl
Cl	1.01013	1.046	−0.720	S---C-----Cl
NO_2	1.00950	1.039	−0.961	S--C-----Cl
Average value	1.00983 ± 0.00029[d]			

[a]Measured by Grimsrud.[76]
[b]Measured at 0°C.
[c]Estimated at 20°C from the temperature dependence of the Hammett ρ value for the para-nitrobenzyl chloride reaction. The ρ value for the para-methoxybenzyl chloride reaction measured at 0°C was −0.26.
[d]The error in the individual KIE is ±0.00015.

The chlorine KIEs measured under the same conditions by Grimsrud[76] (Table 19) do not change significantly with substituent. In fact, there is no trend in the KIE with substituent and the standard deviation of the mean of these KIEs is barely outside the experimental error in the individual KIE. Therefore, the best interpretation of these KIEs is that changing the substituent on the benzene ring does not affect the C_α–Cl transition state bond significantly. Because the magnitude of the secondary α-deuterium KIEs is related to the S–Cl distance in the transition state (R_{TS}) and because the chlorine bonds are virtually the same length in all of the transition states, the magnitude of the secondary α-deuterium KIE is directly related to the length of the S–C_α transition state bond. The secondary α-deuterium KIEs decrease markedly when a more electron-withdrawing group is on the benzene ring indicating that the S–Cl distance and the S–C_α bond become significantly shorter with a more electron-withdrawing substituent. The Hammett ρ value found by changing the para-substituent on the nucleophile is larger (more negative) when a more electron-withdrawing substituent is on the benzene ring. This indicates that there is a greater change in charge on the sulfur atom of the nucleophile on going to the transition state and that the S–C_α bond is more completely formed (shorter) in the transition state with the more electron-withdrawing substituent. These results confirm the conclusions drawn on the basis of the secondary α-deuterium KIEs and one can safely conclude that adding a more electron-withdrawing substituent to the substrate leads to a transition state with a shorter S–C_α transition state bond but does not cause a significant change in the length of the C_α–Cl bond. It is worth noting that the greatest change in structure with the change in substituent is in the weaker S–C_α bond as the ''Bond Strength Hypothesis'' predicts. Finally, an analysis of the enthalpies of activation for these reactions suggested that the loss in bonding between the benzene ring and the α-carbon in the transition state that occurs when a more electron-withdrawing substituent is on the benzene ring, is replaced by increased bonding to the sulfur, i.e., due to the shorter S–C_α transition state bond.

Table 20 The chlorine leaving group, the primary hydrogen–deuterium and secondary α-deuterium KIEs and Hammett ρ values for the S_N2 reactions between para-substituted benzyl chlorides and borohydride ion in DMSO at $20.000 \pm 0.002°C$

Para-substituent on the substrate	k^{35}/k^{37}	$(k_H/k_D)_\alpha$	Primary k_H/k_D	Relative transition state structure
CH_3	1.0076	1.091	1.236	H-----C----------Cl
H	1.0074	1.089	1.250	H----C--------Cl
Cl	1.0078	1.092	1.239	H----C----Cl
NO_2	1.0036	1.085	1.257	H---C--Cl

The same general conclusion was reached in a study of the S_N2 reactions between borohydride ion and para-substituted benzyl chlorides (Equation (19)).[9]

$$BL_4{:}^- + 4\text{-Z-}C_6H_4CL_2\text{-Cl} \rightarrow BL_3 + 4\text{-Z-}C_6H_4CL_2\text{-L} + Cl{:}^- \qquad (19)$$

$$L = H, D$$

The chlorine leaving group KIEs (Table 20) decrease markedly when a more electron-withdrawing substituent is on the benzene ring of the substrate. This indicates that the weaker C_α–Cl bond shortens markedly as the electron-withdrawing ability of the substituent increases. The secondary α-deuterium and the primary hydrogen–deuterium KIE (for transfer of the hydrogen (deuterium) from borohydride ion to the α-carbon) do not change significantly with substituent; i.e., the changes in the secondary α-deuterium and the primary deuterium KIEs with substituent are $<1\%$. This suggests that there is little or no change in the H–C_α or the B–H transition state bonds with substituent. Since the secondary α-deuterium KIEs do not change with substituent, these transition states must be unsymmetric[55] and since there is a significant change in the chlorine KIEs but not in the secondary α-deuterium KIEs, it was concluded that these transition states were unsymmetric with short H–C_α and long C_α–Cl bonds.

In another study,[59] Matsson and Westaway and coworkers used secondary α-deuterium, incoming group carbon and chlorine leaving group KIEs to model the transition states for the S_N2 reactions between para-substituted benzyl chlorides and cyanide ion in 20% aqueous DMSO. The $^{11}C/^{14}C$ incoming group KIEs (Table 21) do not change significantly with substituent suggesting there is very little change in the stronger NC–C_α transition state bond. However, there is a marked decrease in Hill and Fry's chlorine KIEs[60] when a more electron-withdrawing substituent is added to the substrate. This indicates the C_α–Cl bond shortens significantly when there is a more electron-withdrawing substituent on the benzene ring. Finally, the secondary α-deuterium KIEs are small and do not change significantly with substituent. This suggests the transition states are unsymmetric.[55] Since the secondary α-deuterium KIEs change in the same way as the incoming group carbon KIEs, the authors suggested that the transition states were product-like with short NC–C_α bonds and long C_α–Cl bonds and that the transition states become tighter with shorter C_α–Cl bonds when a more electron-withdrawing group is present.

Table 21 The leaving group chlorine, the incoming group $^{11}C/^{14}C$ and the secondary α-deuterium KIEs for the S_N2 reactions between para-substituted benzyl chlorides and cyanide ion in 20% aqueous DMSO at 30°C

Para-substituent	k^{11}/k^{14a}	k^{35}/k^{37b}	$(k_H/k_D)_\alpha{}^c$	Relative transition state structure
CH_3	1.0104 ± 0.0001	1.0079 ± 0.0004	1.008 ± 0.003	NC----C-------Cl
H	1.0105 ± 0.002	1.0072 ± 0.0003	1.011 ± 0.001	NC---C----Cl
Cl	1.0070 ± 0.001	1.0060 ± 0.0002	1.002 ± 0.003	NC--C---Cl

[a]Measured at 30.00 ± 0.02°C.
[b]Measured in 20% aqueous dioxane at 30.0°C.[60]
[c]Measured at 30.000 ± 0.002°C.

Table 22 The nitrogen leaving group and secondary α-deuterium KIEs and Hammett ρ values for the S_N2 reaction between sodium thiophenoxide and benzyldimethylphenylammonium nitrate at different ionic strengths in DMF at 0°C

Ionic strength (M)	k^{14}/k^{15}	$(k_H/k_D)_\alpha$	Hammett ρ	Relative transition state structure
0.904	1.0166 ± 0.0004	1.215 ± 0.011	−1.62 ± 0.01	δ−δ+ S---------C----N
0.64	1.0200 ± 0.0007	1.179 ± 0.007	−1.76 ± 0.19	δδ–δδ+ S----C-----N

In all the above cases, the transition states become tighter when a more electron-withdrawing substituent is on the benzene ring of the substrate. Several other investigators have reported studies where only one KIE was measured for S_N2 reactions of para-substituted benzyl substrates. In all but one case, the changes in the KIE were consistent with the changes in transition state structure found in the above studies.[93] Finally, it is important to note that the weaker reacting bonds, i.e., the weaker S–C_α bond in the first reaction and the weaker C_α–Cl bond in the last two reactions, vary most with substituent as the "Bond Strength Hypothesis" predicts.

Solvent effects

One example of a large solvent effect on transition state structure of an S_N2 reaction was published by Pham and Westaway[56] who measured the leaving group nitrogen and secondary α-deuterium KIEs for the S_N2 reactions between benzyldimethylphenylammonium ion and thiophenoxide ion in DMF. The solvent was altered by adding different amounts of sodium nitrate to the solvent. Both the nitrogen and the secondary α-deuterium KIEs (Table 22) were different in the two solvents. The larger nitrogen KIE in the low ionic strength reaction indicates that there is more C_α–N bond rupture in the transition state in the less polar (ionic) solvent. The smaller secondary α-deuterium KIE in the low ionic strength reaction indicates the S–N distance is shorter in the S_N2 transition state in the less polar solvent. It is worth noting that the Hammett ρ values confirm that the S–C_α bond is shorter in the

Table 23 The secondary α-deuterium and leaving group nitrogen KIEs for the S_N2 reactions between the solvent-separated sodium thiophenoxide ion pair and benzyldimethylphenylammonium nitrate in DMF at 0°C and in methanol at 20.000 ± 0.002°C

Solvent	Temperature (°C)	$(k_H/k_D)_\alpha$	k^{14}/k^{15}	Hammett ρ[a]	Relative transition state structure
Methanol	20	1.207 ± 0.008	1.0162 ± 0.0010	−0.84 ± 0.1	δ–δ S-------C----N
DMF	0	1.179 ± 0.010	1.0200 ± 0.0007	−1.70 ± 0.05	δδ–δδ+ S----C-----N
DMF	20	1.17[b]	1.018[b]		

[a]The Hammett ρ value was obtained by changing the para-substituent on the nucleophile.
[b]This KIE was estimated at 20°C from the temperature dependence of the KIE (*vide infra*).

low ionic strength reaction. Since the C_α–N bond is longer but the S–N distance is shorter in the transition state for the low ionic strength reaction, the S–C_α bond must be much shorter in the transition state in the less ionic solvent. This means that a more ionic transition state with larger partial charges on the nitrogen and the sulfur is found in the more ionic solvent.

In another study, Westaway and Jiang[87] determined how changing the solvent from DMF to methanol affected the transition state of the S_N2 reaction between the solvent-separated sodium thiophenoxide ion pair and benzyldimethylphenylammonium ion. Unfortunately, the KIEs in methanol and in DMF (Table 23) were measured at different temperatures. However, the temperature dependence for both these KIEs is small. Applying the average temperature dependence of 0.008/20°C found for several S_N2 reactions[64,94] to the secondary α-deuterium KIE of 1.179 found at 0°C in DMF suggests that this KIE would be ~1.17 at 20°C. Therefore, the secondary α-deuterium KIE in methanol ($(k_H/k_D)_\alpha = 1.207$ at 20°C) is significantly larger than the $(k_H/k_D)_\alpha = 1.179$ at 0°C (~1.17 at 20°C) in DMF. No temperature effect has been reported for primary nitrogen leaving group KIEs. However, Turnquist *et al.*[95] reported that the chlorine leaving group KIE for the solvolysis of *t*-butyl chloride decreased from 1.01087 at 10°C to 1.01058 at 20°C and that the chlorine KIE for the S_N2 reaction between *n*-butyl chloride and sodium thiophenoxide in methanol decreased from 1.00964 at 0°C to 1.00895 at 20°C. Assuming the temperature dependence correction for a nitrogen KIE can he estimated from the temperature dependence of the chlorine KIE and the maximum chlorine and nitrogen KIEs of 1.0141 and 1.0436, respectively, at 25°C,[56] the leaving group nitrogen KIE of 1.0200 in DMF at 0°C would be ~0.0019 smaller or 1.018 in DMF at 20°C. This means the nitrogen KIE is significantly smaller in methanol than in DMF.

The larger secondary α-deuterium KIE of 1.207 in methanol ($(k_H/k_D)_\alpha = 1.17$ in DMF; Table 23) indicates that the S–N transition state distance is greater in methanol than it is in DMF. The nitrogen KIE, on the other hand, is smaller in methanol than in DMF. This indicates the C_α–N transition state bond is significantly shorter in methanol than in DMF. Because the transition state in methanol has a longer S–N distance but a shorter C_α–N bond, the S–C_α bond must be much longer in methanol than in DMF. Therefore, an earlier transition state, with a much longer S–C_α and a shorter C_α–N bond, is found in methanol.

The Hammett ρ values measured by changing the para-substituent on the nucleophile in DMF and methanol (Table 23) support this conclusion. The smaller magnitude of the ρ value in methanol indicates that the change in charge on the nucleophilic sulfur atom is smaller on going from the initial state to the transition state in methanol than it is in DMF. Therefore, S–C_α bond formation must be much less complete (the S–C_α bond is longer) in the transition state in methanol.

It is interesting to consider why the more ionic transition state is found in methanol. The earlier transition state in methanol may occur because the S_N2 transition state is solvated primarily at the partially charged sulfur atom (there would be little or no solvation of the α-carbon and the nitrogen atoms because these charges are sterically hindered to solvation). As a result, the transition state would be solvated by hydrogen bonding to the sulfur atom in methanol whereas it is only solvated by a much weaker ion–dipole interaction in DMF. This means the more ionic transition state found in methanol would be more stable in the methanol and a less ionic (a dipolar) transition state would be found in the dipolar aprotic solvent. This suggests the structure of the transition state depends on its stability in that solvent.

Finally, it is worth noting that the different transition state structures suggested by the secondary α-deuterium and nitrogen KIEs measured in methanol and in DMF are consistent with the "Solvation Rule for S_N2 Reactions"[96] which predicts that the transition state for this Type II S_N2 reaction will be very solvent dependent.

Using a combination of theory and experimental results to model the S_N2 transition state

Two different approaches have been used to estimate the structure of the transition state of a reaction. One of these is to use theory to calculate the transition structure of the reaction. This approach is limited to the gas phase and the effect of solvent has either been ignored or handled by crude approximations.[33] This is of particular concern for reactions where charges are being formed, delocalized or eliminated in the transition state, i.e., for S_N2 reactions. The other method of estimating transition state structure is by measuring and interpreting experimental KIEs. While this has the advantage that the data comes from the reaction where it occurs; i.e., in solution, interpreting KIEs have largely been done using qualitative relationships and there is no proof that this approach leads to the correct structure for the transition state of the reaction. One important study has compared these two approaches to determining transition state structure; i.e., compared the transition structures predicted by theory and by interpreting experimental KIEs. In this exhaustive study,[33] six different KIEs (Table 24) were measured for the simple S_N2 reaction between cyanide ion and ethyl chloride in DMSO at 30°C. The small secondary α-deuterium KIE indicated that the transition state was tight with either short NC–C_α and/or C_α–Cl bonds. The very small secondary β-deuterium KIE indicated there was very little positive charge developed on the α-carbon in the transition state; i.e., that the transition state was of the constant total bonding type with one or both of the partial bonds in the transition state short. The large α-carbon KIE was consistent with an S_N2 transition state but does not indicate whether the transition state was

Table 24 The KIEs found for the S_N2 reaction between ethyl chloride and cyanide in DMSO at 30°C

KIE	Experimental KIE
$(k_H/k_D)_{\alpha-D_2}$	0.990 ± 0.004
$(k_H/k_D)_{\beta-D_3}$	1.014 ± 0.003
k^{35}/k^{37}	1.0070 ± 0.0003
$(k^{11}/k^{14})_{\alpha}$	1.21 ± 0.02
$(k^{12}/k^{13})_{Nuc}$	1.0009 ± 0.0007
$(k^{14}/k^{15})_{Nuc}$	1.0002 ± 0.0006

reactant-like, central or product-like.[36] The chlorine leaving group KIE was fairly large at ~50% of the theoretical maximum KIE[57] so the authors interpreted this KIE as meaning there was significant C_α–Cl bond rupture in the transition state. Since the transition state was tight and of the constant bonding type as the secondary α- and β-deuterium KIEs suggested, it was concluded that the NC–C_α transition state bond must be short. This conclusion was supported by the small incoming group cyanide carbon KIE that was smaller (more inverse) than that measured in the benzyl-chloride–cyanide ion reactions where the NC–C_α bond was thought to be short.[59] As expected, the secondary nitrogen KIE was effectively 1.0000 indicating that there was little or no change in the bonding to the nitrogen on going to the transition state. Therefore, the best interpretation of the experimental KIEs using the traditional qualitative approach was that the transition state was product-like with a short NC–C_α bond and a long C_α–Cl bond.

The second part of this study involved using 42 different levels of theory ranging from semi-empirical, to Hartree Foch, to post Hartree Foch, to DFT methods to predict the transition structure and the KIEs for this reaction. A comparison of the adequacy of 42 different levels of theory for calculating the experimental KIEs for the ethyl-chloride–cyanide ion S_N2 reaction showed that the best results were obtained when B3LYP and B1LYP DFT functionals[16] were used in combination with the aug-cc-pVDZ basis set.[17] However, none of the theoretical methods were able to calculate all six experimental KIEs within the experimental error. More important was the discovery that while there was considerable variation between the theoretical methods tested, every method predicted that the transition state was reactant-like with a long NC–C_α bond and a short C_α–Cl bond. This meant that the transition state predicted for ethyl-chloride–cyanide ion reaction S_N2 reactions by interpreting experimental KIEs was at odds with the transition state predicted by theoretical calculations. This study was important because it indicated that one cannot use (i) interpreting the experimental KIEs or (ii) theory, or (iii) both methods to determine the correct structure for the transition state structure of even this simple reaction.

Two reasons seemed possible for the different transition structures found by interpreting the experimental KIEs and theory. One was that the experimental KIEs were measured in solution whereas the theoretical calculations were done for a gas-phase reaction. A second possibility was that the chlorine leaving group KIE was interpreted incorrectly. If one could not conclude the C_α–Cl transition state bond is

Table 25 The secondary α-deuterium, the secondary β-deuterium, the α-carbon $^{11}C/^{14}C$, the incoming group carbon $^{12}C/^{13}C$, the nucleophile nitrogen and the chlorine leaving group KIEs found for the S_N2 reaction between ethyl chloride and tetrabutylammonium cyanide in anhydrous DMSO and THF at 30°C

KIE	DMSO	THF
$(k_H/k_D)_{\alpha-D_2}$	0.990 ± 0.004	1.002 ± 0.003
$(k_H/k_D)_{\beta-D_3}$	1.014 ± 0.003	1.003 ± 0.001
$(k^{11}/k^{14})_{\alpha}$	1.208 ± 0.019	1.212 ± 0.021
$(k^{12}/k^{13})_{Nuc}$	1.0009 ± 0.0007	0.9990 ± 0.0007
$(k^{14}/k^{15})_{Nuc}$	1.0002 ± 0.0006	1.0014 ± 0.0003
k^{35}/k^{37}	1.00699 ± 0.00026	1.00659 ± 0.00012

long because of the reasonably large chlorine KIE; i.e., if the chlorine KIE of 1.0070 could be for a transition state with either a short or a long C_α–Cl bond, then the transition state could be reactant-like as theory suggested. These alternatives have recently been tested.

Unfortunately, it was not possible to measure the KIEs for this S_N2 reaction in the gas phase so one could not determine whether the lack of solvent in the calculations was responsible for the different transition states predicted by theory in the gas phase and the experimental KIEs in DMSO, directly. However, the six previously measured KIEs for the ethyl-chloride–cyanide ion S_N2 reaction could be measured in THF (dielectric constant, $\varepsilon, = 7.3$[97] as compared to DMSO which has an $\varepsilon = 49$).[97] THF was chosen because (i) it was the least polar solvent in which the reaction would occur and (ii) would not solvate the anions and transition state significantly thereby approaching the gas phase ($\varepsilon = 1.0$) as closely as one could experimentally; i.e., the reacting cyanide ion will have changed from being highly solvated in DMSO to a slightly solvated ion in THF approaching its form in the gas phase. Thus, the KIEs in THF should be closer to those expected in the gas phase, i.e., from theory.

An examination of the KIEs in Table 25 shows that only three of the KIEs, the secondary β-deuterium, the incoming group carbon and the chlorine leaving group KIEs, change significantly when the solvent is changed from DMSO to THF. The smaller secondary β-deuterium KIE suggests the transition state is tighter in THF with less positive charge on the α-carbon. The incoming group carbon KIE becomes inverse on going to THF indicating that NC–C_α bond formation is more advanced in the THF transition state.[59,85] The leaving group chlorine KIE decreases on going to THF indicating there is less C_α–Cl bond rupture in the transition state in THF. These changes in the KIE indicate there is a slightly tighter transition state in THF. The actual change in the NC–C_α and C_α–Cl transition state bonds was estimated by comparing the observed change in the KIE with the maximum possible change in the KIE. For the NC–C_α bond, the change in the KIE on going from DMSO to THF is $(0.19/5.3) \times 100\%$ or only 3.6%[98,99] while the corresponding change in the C_α–Cl bond is only $(0.040/1.90) \times 100\%$ or 2.1%.[11,100] Thus, the incoming group carbon and chlorine leaving group KIEs suggest the transition state is only very slightly tighter in THF. Only the change in the secondary α-deuterium KIE and in the

nucleophile nitrogen $^{14}N/^{15}N$ KIE is inconsistent with this interpretation; i.e., the secondary α-deuterium KIE should be smaller in THF where the transition state is tighter. Although this KIE is larger (it is normal rather than inverse) in THF than in DMSO, the KIEs are the same considering the experimental errors in the measurements and it appears that this KIE is not sensitive enough to detect the small change in transition state structure that occurred when the solvent was changed. The NC–C_α bond is slightly shorter in THF than in DMSO and since the vibrational energy of the N≡C bond increases in the reaction,[101] one would expect that shortening the NC–C_α bond in the transition state would also lead to some shortening of the N≡C bond and a smaller, not the larger, secondary nitrogen KIE that is observed in THF. However, the change in the very small nitrogen KIE of 0.1% is only 0.1% and probably does not represent a significant change in the KIE and transition state structure. Therefore, the best interpretation of the KIEs in the two solvents is that the both the NC–C_α and the C_α–Cl transition state bonds are very slightly shorter in THF. This change in transition state structure is expected on going from the highly polar DMSO ($\varepsilon = 49$) to the less solvating THF ($\varepsilon = 7.3$)[97] since a tighter, less ionic, transition state would be expected as the solvent's ability to stabilize the ionic transition state decreases.

The important discovery, however, was that changing the solvent only causes a slight tightening of the S_N2 transition state but does not cause the large shift required to change the transition state from product-like in DMSO to reactant-like in THF even though THF partially bridges the gap between the reaction in DMSO and the gas phase. Even though the solvation in THF is far from that in the gas phase,[102] the great difference in the polarity of the two solvents should show a trend toward an early transition state if it is mainly the absence of solvent in the gas-phase calculations that is primarily responsible for the difference in the transition states predicted by the two methods. Therefore, it is highly unlikely that the absence of solvent in the gas-phase calculations is responsible for the very different transition states that were predicted by interpreting the experimental KIEs found in DMSO and by the gas-phase calculations.

The second possible reason the transition states suggested by interpreting the experimental KIEs and theory differ was related to the interpretation of the chlorine leaving group KIE. This possibility was examined by calculating the chlorine KIEs for the reactions of 25 different nucleophiles with methyl chloride quantum mechanically at the B1LYP/aug-cc-pVDZ level of theory.[11] The results (Table 1; *vide supra*) showed that the magnitude of the chlorine leaving group KIE was not related to the amount of C_α–Cl bond rupture in the transition state as had been previously believed. Given this new information, the transition state based on the experimental KIEs could be reactant-like with a long NC–C_α and a short C_α–Cl bond as theory predicted. Certainly, the experimental α-deuterium, the β-deuterium, the α-carbon, the nucleophile carbon and the nucleophile nitrogen KIEs are all consistent with a reactant-like transition state and since the chlorine KIE of 1.0070 could be found for a reactant-like transition state, there is no good reason to conclude that the transition state is product-like. Although this does not prove the transition state is reactant-like, it could be reactant-like resolving the discrepancy between transition

states predicted by theory and interpreting the experimental KIEs using the traditional relationships.

While these results do not identify the reason the two methods of determining transition state structure predict very different transition states for the ethyl chloride–cyanide ion reaction, they do suggest that theory gives the more accurate transition state structure for the reaction. The following arguments support this view.

The first reason for suggesting the transition state predicted by theory is correct is that the difference between the best set of KIEs calculated from the transition structures and the experimental values,[33] although outside experimental error, are small; i.e., the differences $\Delta(KIE_{calc} - KIE_{exp})$ are 0.004 for the secondary α-deuterium, 0.009 for the secondary β-deuterium, 0.04 for the α-carbon, 0.008 for the nucleophile carbon, 0.0001 for the nucleophile nitrogen and 0.0000 leaving group chlorine KIE. In this regard, it is worth noting that the KIEs calculated by theory for several other S_N2 reactions have been close to the KIEs found experimentally.[103] This means theory reproduces the experimental KIEs fairly well. The fact that the gas-phase calculated transition state and KIEs are in good agreement with the KIEs found experimentally, suggests that solvent does not affect transition state structure of this reaction significantly. This obviously supports the results from the DMSO–THF investigation.

A second result which suggests that the theory gives the better model for the transition state is that the experimental $\Delta H^{\ddagger}$ (18.7 kcal mol^{-1}) for the reaction in DMSO was very well reproduced using several continuum solvent models.[33] For example, SM5.42/HF/6-31G(d) calculated the $\Delta H^{\ddagger}$ exactly, while COSMO/PM3 calculated it within 0.4 kcal mol^{-1}, and several other models gave values that were within 4 kcal mol^{-1} of the experimental value. Also, calculations at a different level by Almerindo and Pliego[104] gave the free energy of activation and a transition state structure in good agreement with those published previously; i.e., the $\Delta G^{\ddagger}$ in DMSO which was within 1.5 kcal mol^{-1} of the experimental $\Delta G^{\ddagger}$ if one uses the experimental $\Delta S^{\ddagger}$[33] and the transition state bonds in the best calculated results from the original study[33] and in the Almerindo–Pliego study were 2.341 and 2.156 Å for the NC–C_α bond and 2.291 and 2.134 Å for the C_α–Cl bond, respectively.

It is worth noting that the very small change in transition state structure found in the experimental investigation of the ethyl chloride–cyanide ion S_N2 reaction is consistent with the "Solvation Rule for S_N2 Reactions"[96] which predicts that a change in solvent will not affect the structure of a Type I transition state (where the nucleophile and leaving group have the same change) significantly. The change in solvent from DMSO to THF only changes the reacting bond by $<4\%$. It is interesting that the change in solvent had so little effect on the transition state for this reaction because when the "Solvation Rule" was proposed, it was suggested that Type I transition states with very different nucleophiles, e.g., the S_N2 reaction between fluoride ion and methyl iodide, might be sensitive to change in solvent. This was because the solvation of the two nucleophiles in the transition state would be very different so a change in solvent could result in a very different effect on the solvation energy of each nucleophile. This would change the relative nucleophilicity of the nucleophiles and lead to a shift in transition state structure. The cyanide

ion–ethyl chloride reaction with its very small cyanide ion carbon atom and the, in comparison, larger and more diffuse charge on the chloride ion in the transition state might be expected to be susceptible to the change of solvent from DMSO to THF. However, this is not observed.

Finally, it is worth noting that this lack of change in transition state structure with a significant change in solvent is supported by theoretical calculations. For instance, Yamataka and Aida[105] showed that changing the solvating water molecules from three to thirteen for the S_N2 reaction between water and methyl chloride and changing the $\Delta G^{\ddagger}$ by 13.5 kcal mol^{-1} did not change the transition structure significantly; i.e., the change in the C_α–O transition state bond was only 0.18 Å while that in the C_α–Cl transition state bond was only 0.074 Å.This very small change in transition state structure with the change in solvation is surprising because this is a Type II (where the charges on the nucleophile and leaving group are different) S_N2 reaction where Saunders and coworkers[8] and Westaway and Jiang[87] found the transition state was altered significantly by a change in solvent. In another study of the Type I S_N2 reaction between chloride ion and methyl chloride, Mohamed and Jensen[106] found that microsolvation by four water molecules did not affect the transition state structure significantly although it changed the $\Delta G^{\ddagger}$ for the reaction (the rate constant) by ~16 kcal mol^{-1}. Thus, both the experimental results and the theory suggest that a significant change in solvent does not alter the transition state structure for a Type I S_N2 reaction significantly and gives some assurance that the results of the above calculations are also correct. It is worth noting that both the above theoretical results and experimental results suggest that the lack of solvent modeling is not the reason the transition state structure predicted by theory and by interpreting the experimental KIEs using the traditional method differ.

Although the recently observed discrepancy between the transition state structure predicted by theory and by interpreting the experimental KIEs using the traditional methods appears to favor the transition state structure predicted by theory, it is worth noting that none of the 39 theoretical methods calculated all six KIEs that were measured for the ethyl chloride–cyanide ion reaction within the experimental error. Obviously there is a need for further investigations of the relationship between observed KIEs and transition state structure.

The effect of enzyme catalysis on transition state structure

An extremely interesting application of KIEs and theory has been elucidating the effect of enzyme catalysis on the structure of the S_N2 transition state. Schowen and coworkers[29,30] measured the secondary α-deuterium and α-carbon $^{12}C/^{13}C$ KIEs for the enzyme-catalyzed S_N2 methyl transfer reaction between *S*-adenosylmethionine (Fig. 18) and 3,4-dihydroxyacetophenone in the presence of the rat-liver enzyme catechol O-methyltransferase (COMT) at 37°C (Fig. 19) and for the closely related, uncatalyzed S_N2 reaction between methoxide ion and *S*-methyldibenzothiophenium ion in methanol at 25°C (Fig. 20). The near maximum α-carbon KIEs of 1.09 ± 0.02 for the enzyme-catalyzed S_N2 reaction and 1.08 ± 0.01 for the uncatalyzed S_N2 reaction were taken as evidence that both transition states were symmetric. However,

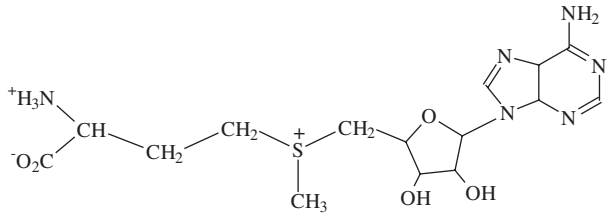

Fig. 18 *S*-adenosylmethionine.

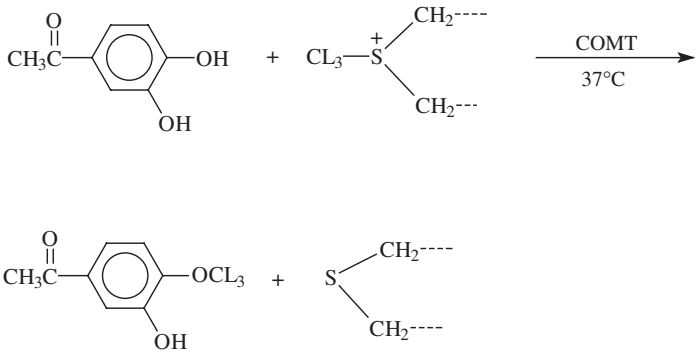

Fig. 19 The enzyme-catalyzed S_N2 methyl transfer reaction between 3,4-dihydroxyacetophenone and *S*-adenosylmethionine in the presence of the rat-liver enzyme COMT. The *S*-adenosylmethionine structure has been abbreviated.

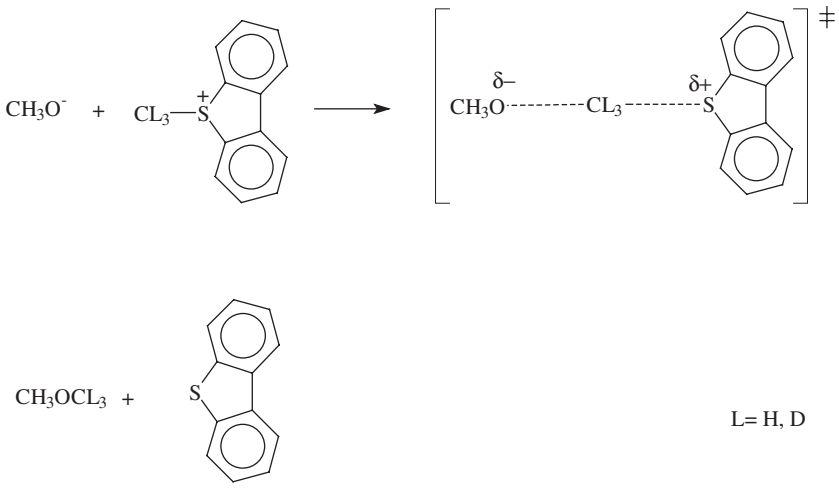

Fig. 20 The uncatalyzed S_N2 reaction between methoxide ion and *S*-methyldibenzothiophenium ion.

subsequent research[36] has shown that these conclusions were not warranted; i.e., the transition states could be reactant-like, symmetric or product-like, although plots of the KIEs versus the S_N2 transition state structure generated from BEBOVIB-IV calculations suggested the transition states for both the enzyme-catalyzed and the enzyme-uncatalyzed reactions are near symmetric but slightly product-like.[107]

A secondary α-deuterium KIE of 0.83 ± 0.05 was found for the enzyme-catalyzed S_N2 methyl transfer reaction while a KIE of 0.975 ± 0.02 was found for the closely related uncatalyzed S_N2 reaction.[29,30] The much smaller KIE in the enzyme-catalyzed reaction was taken as evidence that the transition state is much tighter; i.e., the S–O distance is significantly shorter in the enzyme-catalyzed S_N2 methyl transfer reaction than in the uncatalyzed S_N2 reaction. The BEBOVIB-IV calculations[107] suggested the uncatalyzed reactions had a looser transition state with O–C_α and C_α–S transition state bonds between 0.03 and 0.29 Å longer than those of the enzymatic reaction.

These results led Schowen and coworkers to suggest that the catalytic effect of the enzyme arose because it compressed the transition state. This suggestion was initially supported by Williams ab initio calculations.[108] Williams calculated the energies of the reactants, the encounter complex and the transition states for the S_N2 methyl transfer reaction between methylammonium ion and ammonia. The calculations showed that the catalytic effect of the enzyme arose because compression of the transition state by the enzyme is less costly in terms of energy than compression of the reactant–encounter complex. In fact, the calculations suggest that compression by the enzyme stabilizes the encounter complex by 15.6 kcal mol^{-1} and the transition state by 21.2 kcal mol^{-1}. Thus, the enzyme catalyzes the reaction by reducing the free energy of activation by 5.6 kcal mol^{-1}. Williams also calculated the free energies of the reactant–encounter complex and transition state when they were stabilized by point charges but not compressed. The point charges alone reduced the free energy of the encounter complex by 38.8 kcal mol^{-1} and the transition state by 34.7 kcal mol^{-1}. Thus, when there is no compression, the free energy of activation for the reaction is 4.1 kcal mol^{-1} greater than that for the compressed (the catalyzed) reaction. Since the free energy of activation for the S_N2 methyl transfer reaction is only lower when the reactants and transition state are compressed by the enzyme, the catalytic effect of the enzyme must arise from the compression by the enzyme as Schowen and coworkers suggested. Once the calculations had shown that the catalysis was caused by compression by the enzyme, Williams went on to demonstrate the immense effect compression has on the enzyme's ability to catalyze S_N2 reactions. He found that shortening the enzyme cavity for the reaction from 8.00 to 7.55 Å, i.e., compressing the enzyme cavity by only 6%, increased the catalytic power of the enzyme 3300 times. Finally, it is interesting to speculate on the reason the compression of the transition state is less costly in terms of energy. This may occur because it is easier to compress the partial (weak) bonds of the transition state than the full bonds of the reactants.

Subsequent calculations by Moliner and Williams[109] at the HF/6-31G, the HF/6-31G*, the B3LYP/6-31G and the B3LYP/6-31G* levels of theory tested the compression theory in an elegant study. They calculated the energies and transition

structures for the methyl transfer S_N2 reaction between tetramethylammonium ion and trimethylamine for both a normal S_N2 reaction and for the same reaction compressed within bicyclic cage structures. They found smaller secondary α-deuterium KIEs at the B3LYP level of theory for the cage reactions where the Nu–LG distances in the transition state were shorter. It is worth noting that in every calculation, the component of the KIE that included the bending vibration contribution to the KIE was smaller for the reactions with the tighter transition state, i.e., with the shorter Nu–LG distance in the transition state. The B3LYP calculations clearly supported Schowen's compression theory and his interpretation of the secondary α-deuterium KIEs.

Other calculations at high levels of theory by Boyd and Wolfe and coworkers[110] and by Williams and Ruggiero and coworkers[50,111] have argued against Schowen's compression theory. In another study, calculations by Williams and coworkers[112] have identified several steps in the enzymatic reaction that affect the energetics of the reaction significantly. Finally, the latest, and most advanced QM/MM calculations of the enzyme reaction by Williams and Ruggiero[113] suggest that the Schowen theory is correct. In any case, the much smaller secondary α-deuterium KIE found in the enzyme-catalyzed reaction certainly indicates the enzyme causes a significant change in the S_N2 transition state. However, whether the smaller KIE is due to a much tighter transition state caused by compression of the enzyme is still an open question. One other possibility is that the enzyme causes a reduction in the secondary α-deuterium KIE by sterically hindering the C_α–H(D) bending vibrations by altering the crowdedness[53] of the transition state. How long it will be before theoretical calculations can be used with certainty, especially in very complicated systems such as enzyme-catalyzed reactions, remains to be seen.

In conclusion, KIEs still remain one of the most convincing probes of transition state structure and reaction mechanism, especially when applied at several positions in a reaction. Although the recently observed discrepancy[33] between the transition states predicted by theory and the interpretation of the experimental KIEs using the traditional qualitative relationships is disturbing, and although the need for further investigations of the relationship between observed KIEs and transition state structure is obvious, it seems the interplay of theory and experimental results will play an important role in understanding how KIEs are related to transition state structure and reaction mechanism for some time to come.

Acknowledgment

I would like to thank Prof. Olle Matsson for helpful discussions and for proof reading the manuscript.

References

1. Melander, L. and Saunders, W.H.Jr. (1980). *Reaction Rates of Isotopic Molecules*. Wiley, New York

2. Cook, P.F. (ed.), (1991). *Isotope Effects in Enzyme Reactions*. CRC Press, Boca Raton, FL
3. Westaway, K.C. (1987). Buncel, E. and Lee, C.C. (eds), *Isotopes in Organic Chemistry* Vol. 7 pp. 275–392, Elsevier, New York
4. Shiner, V.J. and Wilgis, F.P. (1992). Buncel, E. and Saunders, W.H.Jr. (eds), *Isotopes in Organic Chemistry* Vol. 8 pp. 239–335, Elsevier, New York
5. Bigeleisen, J. (1949). *J. Chem Phys.* **8**, 675
6. Bigeleisen, J. and Wolfsberg, M. (1958). *Adv. Chem. Phys.* **1**, 15
7. Westaway, K.C. and Ali, S.F. (1979). *Can. J. Chem.* **57**, 1354–1367
8. Hargreaves, R.T., Katz, A.M. and Saunders, W.H.Jr. (1976). *J. Am. Chem. Soc.* **98**, 2614–2617
9. Koerner, T., Fang, Y-R. and Westaway, K.C. (2000). *J. Am. Chem. Soc.* **122**, 7342–7350
10. Willey, J.F. and Taylor, J.W. (1980). *J. Am. Chem. Soc.* **102**, 2387–2391
11. Dybala-Defratyka, A., Rostkowski, M., Matsson, O., Westaway, K.C. and Paneth, P. (2004). *J. Org. Chem.* **69**, 4900–4905
12. Bochicchio, R.C., Lain, L. and Torre, A. (2003). *Chem. Phys. Lett.* **374**, 567
13. Sims, L.B. and Lewis, E.D. (1985). Buncel, E. and Lee, C.C. (eds), *Isotopes in Organic Chemistry* Vol. 6. Elsevier, Amsterdam Chapter 4
14. Pauling, L. (1947). *J. Am. Chem. Soc.* **69**, 542
15. Paneth, P. (1992). Buncel, E. and Saunders, W.H.Jr. (eds), *Isotopes in Organic Chemistry* Vol. 8. Elsevier, New York Chapter 2
16. (a) Mennucci, B. and Tomasi, J. (1977). *J. Chem. Phys.* **106**, 5151; (b) Barone, V. and Cossi, M. (1998). *J. Phys. Chem. A* **102**, 1995
17. Eckert, F. and Klamt, A. (2002). *Aiche J* **48**, 369
18. Westaway, K.C., Matsson, O. and Poirier, R.A., Private Communication.
19. Fang, Y., MacMillar, S., Eriksson, J., Koldziejska-Huben, M., Dybala-Defratyka, A., Paneth, P., Matsson, O. and Westaway, K.C. (2006). *J. Org. Chem.* **71**, 4742–4747
20. Shiner, V.J.Jr. and Wilgis, F.P. (1992). In: Buncel, E. and Saunders, W.H.Jr. (eds), *Isotopes in Organic Chemistry* Vol. 8. Elsevier, New York pp. 245, 246, 309–315
21. Willi, A.V. (1977). *Isot. Org. Chem.* **3**, 237
22. Yamataka, H. and Ando, T. (1975). *Tetrahedron. Lett*. 1059
23. Axelsson, B.S., Matsson, O. and Langstrom, B. (1990). *J. Am. Chem. Soc.* **112**, 6661
24. Westheimer, F.H. (1961). *Chem. Rev.* **61**, 265
25. Melander, L. (1960). *Isotope Effects on Reaction Rates*. Ronald Press, New York
26. More O'Farrell (1970). *J. Chem. Soc. B* 785.
27. Lynn, K.R. and Yankwich, P.E. (1961). *J. Am. Chem. Soc.* **83**, 3220
28. Lynn, K.R. and Yankwich, P.F. (1961). *J. Am. Chem. Soc.* **83**, 790
29. Hegazi, M.F., Borchardt, R.T. and Schowen, R.L. (1979). *J. Am. Chem. Soc.* **101**, 4359
30. Gray, C.H., Coward, J.K., Schowen, K.B. and Schowen, R.L. (1979). *J. Am. Chem. Soc.* **101**, 4351
31. Buist, G.J. and Bender, M.L. (1958). *J. Am. Chem. Soc.* **80**, 4308
32. Ando, T., Tanabe, H. and Yamataka, H. (1984). *J. Am. Chem. Soc.* **106**, 2084
33. Fang, Y., Gao, Y., Ryberg, P., Eriksson, J., Kolodziejska-Huben, M., Dybala-Defratyka, A., Madhavan, S., Danielsson, R., Paneth, P., Matsson, O. and Westaway, K.C. (2003). *Chem. Eur. J.* **9**, 2696–2709
34. Persson, J., Berg, U. and Matsson, O. (1995). *J. Org. Chem.* **60**, 5037
35. Axelsson, B.S., Matsson, O. and Langstrom, B. (1990). *J. Am. Chem. Soc.* **112**, 6661
36. Matsson, O., Dybala-Defratyka, A., Rostkowaski, M., Paneth, P. and Westaway, K.C. (2005). *J. Org. Chem.* **70**, 4022–4027
37. Westaway, K.C. (1975). *Tetrahedron Lett.* 4229–4232
38. Hartshorn, S.R. and Shiner, V.J.Jr. (1972). *J. Am. Chem. Soc.* **94**, 9002
39. Humski, H., Sendijarevic, V. and Shiner, V.J.Jr. (1974). *J. Am. Chem. Soc.* **96**, 6187
40. Shiner, V.J.Jr. (1970). Collins, C.J. and Bowman, N.S. (eds), *Isotopes in Chemical Reactions, Am. Chem. Soc. Monograph 167*, pp. 90–159, Van Nostrand Rheinhold, New York

41. Williams, I.H. (1984). *J. Am. Chem. Soc.* **106**, 7206
42. Zhao, X.G., Tucker, S.C. and Truhlar, D.G. (1991). *J. Am. Chem. Soc.* **113**, 826–832
43. Viggiano, A.A., Paschkewitz, J.S., Morris, R.A., Paulson, J.F., Gonzalez-Lafont, A. and Truhlar, D.G. (1991). *J. Am. Chem. Soc.* **113**, 9404–9405
44. Wolfe, S. and Kim, C-K. (1991). *J. Am. Chem. Soc*. **113**, 8056–8061
45. Harris, J.M., Paley, M.S. and Prasthofer, T.W. (1981). *J. Am. Chem. Soc.* **103**, 5915
46. Westaway, K.C. and Lai, Z.-G. (1989). *Can. J. Chem.* **67**, 345
47. Poirier, R.A., Wang, Y. and Westaway, K.C. (1994). *J. Am. Chem. Soc.* **116**, 2526–2533
48. Barnes, J.A. and Williams, I.H. (1993). *J. Chem. Soc. Chem. Commun*. 1286
49. Glad, S.S. and Jensen, F. (1997). *J. Am. Chem. Soc.* **119**, 227
50. Ruggiero, G.D. and Williams, I.H. (2002). *J. Chem Soc. Perk. Trans 2*. 591–597.
51. Albery, W.J. and Kreevoy, M.M. (1978). *Adv. Phys. Org. Chem.* **15**, 87
52. Kato, S., Davico, G.E., Lee, H.S., DePuy, C.H. and Bierbaum, V.M. (2001). *Int. J. Mass Spectrom.* **210/211**, 223
53. Davico, G.E. and Bierbaum, V.M. (2000). *J. Am. Chem. Soc.* **122**, 1740–1748
54. Hasanayn, F., Stretwieser, A. and Al-Rifai, R. (2005). *J. Am. Chem. Soc.* **127**, 2249–2255
55. Westaway, K.C., Pham, T.V. and Fung, Y. (1997). *J. Am. Chem. Soc.* **119**, 3670–3676
56. Pham, T.V. and Westaway, K.C. (1996). *Can. J. Chem.* **74**, 2528–2530
57. Maccoll, A. (1974). *Annu. Rep. A Chem. Soc.* **71**, 77–101
58. Westaway, K.C. (1993). *Can. J. Chem.* **71**, 2084–2094
59. Matsson, O., Persson, J., Axelsson, B.S., Langstrom, B., Fang, Y. and Westaway, K.C. (1996). *J. Am. Chem. Soc.* **118**, 6350–6354
60. Hill, J.W. and Fry, A. (1962). *J. Am. Chem. Soc.* **84**, 2763
61. Westaway, K.C. and Waszczylo, Z. (1982). *Can. J. Chem.* **60**, 2500–2520
62. Ashan, M., Robertson, R.E., Blandamer, M.J. and Scott, J.M.W. (1980). *Can. J. Chem.* **58**, 2142
63. Shiner, V.J.Jr., Rapp, M.W. and Pinnick, H.R.Jr. (1970). *J. Am. Chem. Soc.* **92**, 232
64. Koshy, K.M. and Robertson, R.E. (1974). *J. Am. Chem. Soc.* **96**, 914
65. Vitullo, V.P., Grabowski, J. and Sridharan, S. (1980). *J. Am. Chem. Soc.* **102**, 6463
66. Lee, I., Koh, H.J., Lee, B.-S., Sohn, D.S. and Lere, B.C. (1991). *J. Chem. Soc. Perk. Trans 2*. 1741.
67. Westaway, K.C. and Ali, S.F. (1979). *Can. J. Chem.* **64**, 1089–1097
68. Westaway, K.C. and Poirier, R.A. (1975). *Can. J. Chem.* **53**, 3216–3226
69. Ko, E.C.F. and Leffek, K.T. (1971). *Can. J. Chem.* **49**, 129
70. Joly, H.A. and Westaway, K.C. (1986). *Can. J. Chem.* **64**, 1206–1214
71. Craze, G.A., Kirby, A.J. and Osborne, R. (1978). *J. Chem. Soc. Perk. 2*. 357.
72. Knier, B.L. and Jencks, W.P. (1980). *J. Am. Chem. Soc.* **102**, 6789
73. Abraham, M.H. and McLennan, D.J. (1977). *J. Chem Soc. Perk. 2*. 873.
74. Westaway, K.C. (1987). Buncel, E. and Lee, C.C. (eds), *Isotopes in Organic Chemistry* Vol. 7 pp. 355–357, Elsevier, New York
75. Waszczylo, Z. and Westaway, K.C. (1982). *Tetrahedron Lett*. **23**, 143–146.
76. Grimsrud, E.P. (1971). Ph.D. Dissertation, University of Wisconsin, Madison, WI
77. Shiner, V.J.Jr. and Humphrey, J.S.Jr. (1963). *J. Am. Chem. Soc.* **85**, 2416
78. Shiner, V.J.Jr. and Jewett, J.G. (1964). *J. Am. Chem. Soc.* **86**, 945
79. Dafforn, G.A. and Streitwieser Jr., A. (1970). *Tetrahedron Lett*. 3159.
80. Streitwieser, A.Jr., Wilkins, C.L. and Kiehlman, E. (1968). *J. Am. Chem. Soc.* **90**, 1598
81. Shiner, V.J.Jr. (1970). Collins, C.J. and Bowman, N.S. (eds), *Isotopes in Chemical Reactions, J. Am. Chem. Soc. Monograph 167*, pp. 118, Van Nostrand Rheinhold, New York
82. Fisher, R.D., Seib, R.C., Shiner, V.J.Jr., Szele, I., Tomic, M. and Sunko, D.E. (1975). *J. Am. Chem. Soc.* **97**, 2408
83. Shiner, V.J.Jr., Murr, B.L. and Heinemann, G. (1963). *J. Am. Chem. Soc.* **85**, 2413
84. Streitwieser Jr., A. and Dafforn, G.A. (1969). *Tetrahedron Lett*. 1263.

85. Westaway, K.C., Fang, Y., Persson, J. and Matsson, O. (1998). *J. Am. Chem. Soc.* **120**, 3340–3344
86. Westaway, K.C. (1987). Buncel, E. and Lee, C.C. (eds), *Isotopes in Organic Chemistry* Vol. 7 pp. 342–353, Elsevier, New York
87. Westaway, K.C. and Jiang, W. (1999). *Can. J. Chem.* **77**, 879–889
88. Szylhabel-Godala, A., Madhavan, S., Rudzinski, J., O'Leary, M.H. and Paneth, P. (1996). *J. Phys. Org. Chem.* **9**, 35–40
89. Westaway, K.C., Waszczylo, Z., Smith, P.J. and Rangappa, K.S. (1985). *Tetrahedron Lett* **26**, 25
90. Westaway, K.C. and Lai, Z.-G. (1988). *Can. J. Chem.* **66**, 1263–1271
91. Fang, Y.-r. and Westaway, K.C. (1991). *Can. J. Chem.* **69**, 1017–1021
92. Fang, Y.-r., Lai, Z.-G. and Westaway, K.C. (1998). *Can. J. Chem.* **76**, 758–764
93. Westaway, K.C. (1987). Buncel, E. and Lee, C.C. (eds), *Isotopes in Organic Chemistry* Vol. 7 pp. 332–342, Elsevier, New York
94. Shiner, V.J.Jr., Dowd, W., Fisher, R.D., Hartshorn, S.R., Kessik, M.A., Milakofsky, L. and Rapp, M.W. (1969). *J. Am. Chem. Soc.* **91**, 4838
95. Turnquist, C.R., Taylor, J.W., Grimsrud, E.P. and Williams, R.C. (1973). *J. Am. Chem. Soc.* **95**, 4133–4338
96. Westaway, K.C. (1978). *Can. J. Chem.* **56**, 2691–2699
97. Gordon, A.J. and Ford, R.A. (1972). In *The Chemist's Companion*. John Wiley & Sons, New York pp. 6–7.
98. The maximum change in the incoming group $^{12}C/^{13}C$ KIE has been estimated by adjusting the nucleophile $^{11}C/^{14}C$ KIE calculated by Matsson et al.[59] for the different masses of the isotopes, to be 5.0%. This agrees very well with the maximum $^{12}C/^{13}C$ KIE of 5.5% and 5.4% suggested by Maccoll[57] and Buddenbaum and Shiner,[99] respectively. The average of these values (5.3%) was used in calculating the change in the incoming group carbon KIE with solvent
99. Buddenbaum, W.E. and Shiner, V.J.Jr. (1977). Cleland, W.W., O'Leary, M.H. and Northrop, D.B. (eds), *Isotope Effects on Enzyme-Catalyzed Reactions*. University Park Press, London p. 18
100. Paneth, P. (1992). Buncel, E. and Saunders, W.H.Jr. (eds), *Isotopes in Organic Chemistry* Vol. 8. Elsevier, New York Chapter 2
101. Jobe, D.J. and Westaway, K.C. (1993). *Can. J. Chem.* **71**, 1353–1361
102. Bogdanov, B. and McMahon, T.B. (2005). *Int. J. Mass Spectrom.* **241**, 205
103. Davico, G.E. and Bierbaum, V.M. (2000). *J. Am. Chem. Soc.* **122**, 1740–1748
104. Almerindo, G.I. and Pliego, J.R.Jr. (2005). *Org. Lett.* **7**, 1821–1823
105. Yamataka, H. and Aida, M. (1998). *Chem. Phys. Lett.* **289**, 105–109
106. Mohamed, A.A. and Jensen, F. (2001). *J. Phys. Chem. A* **105**, 3259–3268
107. Rodgers, J., Femec, D.A. and Schowen, R.L. (1982). *J. Am. Chem. Soc.* **104**, 3263
108. Williams, I.H. (1984). *J. Am. Chem. Soc.* **106**, 7206
109. Moliner, V. and Williams, I.H. (2000). *J. Am. Chem. Soc.* **122**, 10895–10902
110. Boyd, R.J., Kim, C.-K., Shi, Z., Weinberg, N. and Wolfe, S. (1993). *J. Am. Chem. Soc.* **115**, 10147
111. Ruggiero, D.G., Williams, I.H., Roca, M., Moliner, V. and Tunon, I. (2004). *J. Am. Chem. Soc.* **126**, 8634–8635
112. Roca, M., Marti, S., Andres, J., Moliner, V., Tunon, I., Bertran, J. and Williams, I.H. (2003). *J. Am. Chem. Soc.* **125**, 7726–7737
113. Williams, I.H. and Ruggiero, D.G. (2005). *Isotopes 2005 Bath – An International Conference*, June 27 to July 1, Bath, England